

AD-760 026

**AIRCRAFT PERFORMANCE - PREDICTION
METHODS AND OPTIMIZATION**

John Williams

**Advisory Group for Aerospace Research
and Development
Paris, France**

March 1973

DISTRIBUTED BY:

NTIS

**National Technical Information Service
U. S. DEPARTMENT OF COMMERCE
5285 Port Royal Road, Springfield Va. 22151**

**Best
Available
Copy**

AGARD-LS-56

AGARD-LS-56

AD 760026

AGARD

ADVISORY GROUP FOR AEROSPACE RESEARCH & DEVELOPMENT

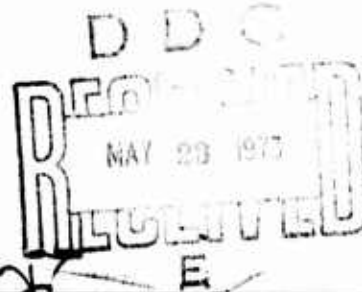
7 RUE ANCELLE 92200 NEUILLY SUR SEINE FRANCE

AGARD LECTURE SERIES No. 56

on

Aircraft Performance — Prediction Methods and Optimization

Edited by
J. Williams



NORTH ATLANTIC TREATY ORGANIZATION



Approved by
NATIONAL TECHNICAL
INFORMATION SERVICE
1200 KENT ROAD
ANN ARBOR MI 48106

DISTRIBUTION AND AVAILABILITY
ON BACK COVER

Approved for release
Unlimited

**NORTH ATLANTIC TREATY ORGANIZATION
ADVISORY GROUP FOR AEROSPACE RESEARCH AND DEVELOPMENT
(ORGANISATION DU TRAITE DE L'ATLANTIQUE NORD)**

**AGARD Lecture Series No.56
AIRCRAFT PERFORMANCE – PREDICTION METHODS AND OPTIMIZATION**

**J.Williams
P.Colin**

Lecture Series Directors

Editor – J.Williams

These papers were presented at a Lecture Series jointly sponsored by the Fluid Dynamics Panel of AGARD and the von Kármán Institute, Rhode-Saint-Genese, Belgium, 24–28 April 1972.

THE MISSION OF AGARD

The mission of AGARD is to bring together the leading personalities of the NATO nations in the fields of science and technology relating to aerospace for the following purposes:

- Exchanging of scientific and technical information;
- Continuously stimulating advances in the aerospace sciences relevant to strengthening the common defence posture;
- Improving the co-operation among member nations in aerospace research and development;
- Providing scientific and technical advice and assistance to the North Atlantic Military Committee in the field of aerospace research and development;
- Rendering scientific and technical assistance, as requested, to other NATO bodies and to member nations in connection with research and development problems in the aerospace field;
- Providing assistance to member nations for the purpose of increasing their scientific and technical potential;
- Recommending effective ways for the member nations to use their research and development capabilities for the common benefit of the NATO community.

The highest authority within AGARD is the National Delegates Board consisting of officially appointed senior representatives from each member nation. The mission of AGARD is carried out through the Panels which are composed of experts appointed by the National Delegates, the Consultant and Exchange Program and the Aerospace Applications Studies Program. The results of AGARD work are reported to the member nations and the NATO Authorities through the AGARD series of publications of which this is one.

Participation in AGARD activities is by invitation only and is normally limited to citizens of the NATO nations.

Published March 1973

533.6.015.8



*Printed by Technical Editing and Reproduction Ltd
Harford House, 7-9 Charlotte St, London. W1P 1HD*

PREFACE

This publication contains edited versions of the prepared Lecture Notes and supplementary Seminar Contributions from the AGARD-VKI Lecture Series on "Aircraft Performance Prediction Methods and Optimisation", at the von Kármán Institute for Fluid Dynamics during the week 24–28 April 1972.

The aim of this Lecture Series was to provide an up-to-date account and appraisal of performance prediction methods and their practical utilisation for subsonic and supersonic aircraft. The basic topics comprised range/radius, airfield and flight-manoeuve performance aspects related to both combat and transport aircraft. Special reviews were added on problems of aerodynamic prediction, aircraft mass estimation, and engine selection. Parametric and optimisation techniques for aircraft design synthesis were also discussed.

The Course was well supported as regards both the number of attendees and their technical quality. The organization was carried out under the auspices and with the support of AGARD, in collaboration with the von Kármán Institute who had the responsibility for the general administration and local organization. Professor Paul E. Colin (Associate Director of the VKI) deserves particular commendation for his extensive efforts towards the success of the Course, in his capacity as its Chief Administrator and Joint Technical-Director.

A special tribute must be paid to the Lecturers for the quality of their presentations, the valuable analysis contained in their lecture notes provided for distribution during the Course, and their participation in the discussions. Various supplementary contributions to these discussions and the concluding Seminar are also gratefully appreciated, particularly in respect of attendees who provided appropriate texts subsequently for publication here. Finally, our acknowledgements are due to the official and private organizations through whose helpful cooperation and courtesy it was possible to offer such technical experts as lecturers and contributors.

John Williams (RAE, UK)
Editor and Joint Technical-Director of Course

LIST OF SPEAKERS

Lecturers

Mr J.F.Dugan
Head of Propulsion Section, Mission Analysis Branch
National Aeronautics and Space Administration
Lewis Research Center
Cleveland, Ohio 44135, USA

Dr H.Friedel
Head, Flight Mechanics Dept.
Dornier A.G.
799 Friedrichshafen
Postfach 317, Germany

Mr C.Lievens
Service Technique Aeronautique
Section Etudes Generales
4, avenue de la Port d'Issy
75 Paris 15eme, France

Mr R.K.Page
Project Performance Analysis, Section 1
Procurement Executive,
Ministry of Defence
1-13 St.Giles High Street
London WC2H 8LD, UK

Mr C.Vivier
Service Technique Aeronautique
Section Etudes Generales
4, avenue de la Port d'Issy
75 Paris 15eme, France

Mr P.Cormier
Service Technique Aeronautique
Section Etudes Generales
4, avenue de la Port d'Issy
75 Paris 15eme, France

Mr R.Wallace
Aerodynamics Staff, Product Development
Commercial Airplane Division
The Boeing Company
P.O. Box 3707
Seattle, Washington 98124, USA

Dr J.Williams
Deputy Chief Scientific Officer
Aerodynamics Department
Royal Aircraft Establishment
Farnborough, Hants, UK

Seminar Contributions

Mr Gérard Dumas
Chef de Service Performance
Dept. Aérodynamique
Société Nationale Industrielle Aérospatiale
31 Toulouse-Blagnac, France

Mr E.Torenbeek
Research Associate
Dept. of Aeronautics
Delft University of Technology
Delft, Netherlands

Dipl. Ing. P.Foerster
Dornier A.G.
799 Friedrichshafen
Postfach 317, Germany

Mr P. Middleton
Operational Analyst
Future Projects Department
Hawker Siddeley Aviation Ltd
Brough, UK

Mr D.L.I.Kirkpatrick
Senior Scientific Officer
Aerodynamics Department
Project Division
Royal Aircraft Establishment
Farnborough, Hants, UK

CONTENTS

PREFACE

by John Williams (Editor)

Page

iii

Reference

LECTURES

RANGE AND RADIUS OF ACTION PERFORMANCE PREDICTION FOR TRANSPORT AND COMBAT AIRCRAFT

by Robert K. Page (UK)

1

AIRFIELD PERFORMANCE PREDICTION METHODS FOR TRANSPORT AND COMBAT AIRCRAFT

by John Williams (UK)

2

FLIGHT-MANOEUVRE AND CLIMB-PERFORMANCE PREDICTION

by Heribert Friedel (Germany)

3

L'ESTIMATION DES COEFFICIENTS AERODYNAMIQUES NECESSAIRES AU CALCUL DES PERFORMANCES

par C. Lievens (France)

4

MASSE D'UN AVION

par C. Vivier et P. Cormier (France)

5

ENGINE SELECTION FOR TRANSPORT AND COMBAT AIRCRAFT

by James F. Dugan (USA)

6

PARAMETRIC AND OPTIMISATION TECHNIQUES FOR AIRPLANE DESIGN SYNTHESIS

by Richard E. Wallace (USA)

7

SEMINAR CONTRIBUTIONS

DISCREPANCY BETWEEN APPROVAL AND MODERNISM

by Gérard Dumas (France)

8

AN ANALYTICAL EXPRESSION FOR THE BALANCED FIELD LENGTH

by Egbert Torenbeek (Netherlands)

9

SUPPLEMENTARY NOTE TO "MANOEUVRE AND CLIMB PERFORMANCE PREDICTION"

by Peter Foerster (Germany)

10

MINIMUM TIME TRAJECTORY COMPUTATION - DEVELOPMENT OF THE BALAKRISHNAN METHOD

by Peter Middleton (UK)

11

REVIEW OF TWO METHODS OF OPTIMISING AIRCRAFT DESIGN

by David L.I. Kirkpatrick (UK)

12

**RANGE AND RADIUS-OF-ACTION PERFORMANCE PREDICTION FOR
TRANSPORT AND COMBAT AIRCRAFT**

by

Robert K. Page

**Project Performance Analysis Section
Ministry of Defence (PE), London, UK**

CONTENTS

	Page
1. INTRODUCTION: DEFINITIONS	1-1
2. THE PLACE OF THE RANGE/RADIUS SECTORS IN THE TOTAL MISSION OR SORTIE PROFILE	1-1
3. DATA REQUIRED FOR THE PREDICTION PROCESS	1-2
4. CHOICE OF METHODS APPROPRIATE TO THE STATE OF THE PROJECT	1-2
5. OPTIMUM CRUISING SPEEDS AND SPECIFIC RANGES	1-3
5.1 Climb	1-3
5.2 Specific Range	1-3
5.3 Cruise Height Schedules and Integrated Range	1-9
5.4 Effect of Various Aircraft and Engine Characteristics	1-14
5.5 Descent	1-15
5.6 Allowances	1-15
6. USE OF FUEL AND DISTANCE DIAGRAM	1-16
7. OPTIMISATION	1-16
REFERENCES	1-17
FIGURES	1-18

RANGE AND RADIUS-OF-ACTION PERFORMANCE PREDICTION FOR TRANSPORT AND COMBAT AIRCRAFT

Robert K. Page

1. INTRODUCTION: DEFINITIONS

To explain the double descriptive term in the title of this section of the Course: with the emphasis in the NATO context of operational military aircraft the purely technical term 'range', meaning the distance an aircraft can fly between take off and landing as limited by its fuel capacity often has to be given a special qualification, in that instead of taking off from A, flying to B and landing there, the aircraft will return from 'overhead' B and land again at A. In the first case the air and ground ranges are identical and equal to the straight line distance AB, in the second case the air range will be $AB + BA = 2 \times AB$, but the operational interest is in the ground distance AB, which is then termed the 'Radius-of-Action' and is thus equal to half the air range capability of the aircraft. In certain cases, e.g. for search and rescue, combat air patrol or maritime reconnaissance operating the time, rather than distance will be the parameter of interest, either alone or in conjunction with a specified radius-of-action, but, of course, the two are simply related as

$$\text{time} = \frac{\text{distance}}{\text{cruise speed}}$$

'Duration' and 'Endurance' are alternative terms for the time the aircraft can spend at a specified condition of speed and height.

It is usual, when predicting the performance of an aircraft for assessment to assume still air, i.e. zero wind conditions. Similarly, for comparative purposes ISA temperature conditions only are adequate, but in some specialised instances (such as combat aircraft with appreciable periods at specified engine ratings) calculations may have to be done at some specified non-standard ambient temperatures.

2. THE PLACE OF THE RANGE/RADIUS SECTORS IN THE TOTAL MISSION OR SORTIE PROFILE

The justification for including this section originates from the primarily military, and especially combat emphasis in the Course. In contrast, for civil airline transport operations, range flying (especially if, as is usual, the distances covered in climb and descent are credited to the total range) makes virtually the whole of the total flight apart from the take off and landing circuits. The only 'allowances' are those made for possible diversion to an alternate destination, and 'loiter' or 'stacking' whilst awaiting ATC permission to land, and even these are from the technical viewpoint of performance prediction equally range and duration operations. For combat aircraft on the other hand there will commonly be operational requirements for 'combat' or 'target area attack' phases, as well as diversion and pre-landing loiter, that not only are NOT reckoned as contributing to the operational range/radius, but in total may be the same order of magnitude in their final requirements, and hence must be dealt with to the same order of accuracy.

Figures 1-3 show the expenditure of fuel for the various segments of the total sorties for some combat aircraft. Figure 4 shows for comparison similar information applicable to a bomber or a medium-range transport. The points to notice are

- (i) the proportions of the total fuel used that are consumed in range flying and in fixed allowances,
- (ii) for the combat aircraft, even some of the range fuel is consumed whilst flying under precisely specified conditions of speed and height.

On the diagrams, the parts marked with a heavy line are 'pure' cruising, where height and speed may be chosen to optimise the results, those with a broken line have height or speed (or both) restrained to prescribed values.

In Example 1 (a subsonic low-level strike sortie), rather less than half is used for cruising at best economy conditions (though at a fixed height) and about $\frac{1}{3}$ for a high-speed cruise or 'dash' for which both height and speed are fixed. A variation on this type of sortie is the Hi Lo Lo Hi where the economic cruise is made at altitude in which case rather more than $\frac{1}{3}$ of the total (allowing for two climbs) would be pure cruising.

Example 2 is a special type of Hi Lo Lo Hi strike sortie, in which the aircraft when within a certain distance from the target on the run-in is required to be below the line of sight of a radar beam at or near the target; and in the particular example this actually prohibits any initial high-level cruise at all, so that the only unrestricted cruise is on the return, amounting to $\frac{1}{3}$ of the total fuel requirement. The third example is a different type of mission, a Combat Air Patrol at a fixed distance from base at a height probably loosely defined as 'high', 'medium' or 'low' level, at a speed optimised for endurance. Because of the relatively very high fuel consumption during the supersonic attack phase, cruising accounts for only about half the total fuel requirement, and more than half of this will be restricted to a particular height level.

The fourth example is a high-altitude bomber (which for the present purpose is regarded as a transport on which the effect of dropping the load half-way is to slightly reduce the fuel requirement for the return leg). For this example $\frac{2}{3}$ of the fuel is used in pure cruising – or $\frac{4}{5}$ if the diversion is included (though this latter may be restricted in height or speed by ATC).

The conclusion to be drawn from these examples is that the degree of sophistication of methods justified for optimising cruising conditions and estimating fuel consumed will be judged against the kind of mission being studied, that is whether cruising is likely to account for the major or only a small proportion of the total fuel used.

3. DATA REQUIRED FOR THE PREDICTION PROCESS

In this section the data required will be listed; the methods by which those items not likely to be directly available may have to be calculated or estimated is dealt with in other lectures in the course.

The data can be grouped as follows:

- 1 Airframe:
 - 1.1 Weight
 - 1.2 Lift and Drag
 - 1.3 Fuel capacity
- 2 Engine:
 - 2.1 Thrust (or power) ratings
 - 2.2 Thrust and fuel consumption variations with forward speed and height
 - 2.3 Variation of fuel consumption with thrust at all appropriate speed and height combinations
 - 2.4 Installation arrangements in multi-engined aircraft as affecting possibility of cruising with some engines shut down.

Commenting on each of these:—

- 1.1 *Weight* is all-important, primarily because, as will be shown in a later section, a 'limiting case' for cruising (to which various conditions approach more or less closely) is the speed for maximum L/D ratio, at which the thrust required, and to a first approximation, the fuel consumption are directly proportional to the aircraft total weight.

For range calculations, the weight data required are the weight less usable fuel, the usable internal fuel, the weight of any drop-tanks and their contents, and the weight of any weapons or other stores released in flight.

- 1.2 *Drag* is required as a function of lift coefficient over the range of Mach numbers relevant to the level flight envelope, and also for the total height band, to take account of Reynolds number variations. Also, limiting values of lift coefficient from buffet onset considerations may be relevant to high altitude cruising.

For analytical purposes, and in general unless and until wind-tunnel tests show the contrary, it is usual to assume a lift drag relationship of the form:

$$C_D = C_{D0} + \frac{K}{\pi A} C_L^2.$$

4. CHOICE OF METHODS APPROPRIATE TO THE STATE OF THE PROJECT

We have seen, in Section 2, how the proportion of the total fuel usage that is accounted for in the cruise phases of a flight varies considerably with the type of mission considered. When the proportion is relatively small (say less than one half) and in addition we are dealing with the preliminary 'feasibility' phase of a project, it would be unnecessary and inappropriate to use methods incorporating such detail of refinement and accuracy as are desirable when an aircraft has been more closely defined and when (as for the transport or strategic bomber) the cruising phase is predominant.

As examples of areas where some degrees of approximation or simplification resulting from alternative methods can be introduced:—

- (i) Fuel consumption can be calculated for a mean weight (that can be checked from the result of the calculation and re-approximated if necessary), rather than doing a step-by-step process or integration depending on the variation of aircraft weight as fuel is used.
- (ii) Omission of the acceleration and deceleration phases between successive legs of the sortie that are flown at different speeds.
- (iii) Similarly to (ii), where there are large changes of height between successive stages, as in a Hi Lo strike sortie, the total change in 'energy height' (which includes the accompanying change in cruise speed with height) can be calculated with the value of rate-of-change corresponding to some mean height, instead of doing a step-by-step summation.
- (iv) When, from previous experience, it is known that the variation of fuel consumption (or fuel per unit distance) will have a fairly 'flat' optimum and also the final choice of speed will in the final analysis be influenced by considerations of vulnerability as well as by fuel economy, some 'second order' factors affecting the result can be omitted.

5. OPTIMUM CRUISING SPEEDS AND SPECIFIC RANGES

This aspect of the subject has been extensively treated in the literature of aircraft performance. It comprises:— the selection of the speed and height to give the best range and the variation from the 'best' value if external influences, e.g. ATC requirements force deviations from the optimum speed or height, the way in which the optima vary as the aircraft weight is reduced when fuel is consumed, and finally the integration of the 'specific' ranges (or instantaneous rate of change of distance with fuel consumption) to give the total distance flown for a given amount of fuel. The treatment to be given here was developed by Peckham¹ a former colleague of the present author when a member of Projects Division of Aerodynamics Department of the RAE at Farnborough; this assistance and advice is gratefully acknowledged.

Before starting on the detailed analysis of this part of the problem it should be pointed out that any analytical treatment in which a fairly large number of parameters is involved can be made tractable only if reasonably simple expressions can be formulated for the variables, which will involve some approximations, e.g. the assumption of constant values for those that vary only to a very small extent, or the neglect of 2nd order terms. Whilst such procedures necessarily result in some degree of inaccuracy in the results, the resulting analysis is none the less valuable in giving an insight into at least the qualitative relationships between the primary parameters, and so is particularly suited to preliminary 'parametric' project studies.

Two assumptions in particular will be noted:—

- (i) The relationship between drag and lift is taken as a simple quadratic expression; this is usually true in practice, the conditions in which it does not hold are dealt with in the detailed discussion later.
- (ii) 'The engine specific fuel consumption is constant during the flight.'

This statement is true only to a certain limited extent.

5.1 Climb

For turbine-engined aircraft even the initial optimum cruise height (when very little of a possibly large fuel load has yet been used) is likely to be at least in the region of 25,000-35,000 ft so that, unless some much lower level is chosen for operational reasons, the cruise phase will be preceded by a fairly prolonged climb, and in general the distance covered during this phase will be credited to the range or radius. Because (as will be shown later) cruise economy improves markedly with height, it will generally pay to climb as quickly as possible, i.e. to use the highest engine rating permissible, so long as this does not entail a very large increase in sfc, e.g. by the use of maximum reheat. Climb optimisation is a subject in itself; but for most purposes, where the climb segment is short compared with the cruise, considerable simplifications can be made in the interests of pilot work-load, e.g. fixing climbing speed as at a constant Mach number.

5.2 Specific Range

5.2.1 Estimation of specific range is described in Section 5.2.2 and the theory for the particular case of a parabolic drag polar is discussed in Section 5.2.3. Section 5.2.4 deals with optimum specific range in general, and Section 5.2.5 with optimum specific range for the particular case of a parabolic drag polar. All theory in the above sections is based on the assumption that the specific fuel consumption remains essentially constant along the cruise trajectory considered (this is *not* in general exactly true but otherwise the algebra would be intractable). Integration of specific range, over a change of aircraft weight equal to the weight of fuel consumed, gives the range; this is discussed in detail in Section 5.3.

5.2.2 Estimation of Specific Range

The rate of change of aircraft weight, being equal to the rate at which fuel is consumed, is given by

$$\frac{dW}{dt} = -cT, \quad (1)$$

where
 c = specific fuel consumption (sfc)
 t = time
 T = thrust
 W = aircraft weight.

The instantaneous value of range in still air is then given by

$$dR = Vdt = -\frac{V}{cT}dW, \quad (2)$$

where
 R = range
 V = cruise true airspeed.

Now in cruising flight, because the incidence is small, it can be assumed that lift is equal to weight, and that thrust is equal to drag, so the expression for specific range becomes

$$-\frac{dR}{dW} = \frac{V}{cT} = \frac{1}{W} \frac{V}{c} \frac{L}{D} \quad (3)$$

which, for speed in knots, sfc in lb/lb/h, and aircraft weight in pounds has the units of nautical miles per pound of fuel.

In some theoretical studies, it is more convenient to work in terms of an overall efficiency of the powerplant, η_p , defined as

$$\eta_p = \frac{V}{cH}, \quad (4)$$

where H = the calorific value of the fuel.

The expression for specific range then becomes

$$-\frac{dR}{dW} = \frac{\eta_p H}{T} = \eta_p \frac{H}{W} \frac{L}{D}. \quad (5)$$

The calorific value of kerosene is 18,550 Btu/lb. For use in a range equation, H needs to be expressed in appropriate length units. Thus it should be noted that

$$\begin{aligned} 18,550 \text{ Btu/lb} &= 18,550 \times 778 \text{ ft lb/lb} = 14.43 \times 10^6 \text{ ft} \\ 14.43 \times 10^6 \text{ ft} &= 4398 \text{ m} \\ &= 2733 \text{ mile (statute)} \\ &= 2373 \text{ n mile (UK)} \\ &= 2373 \text{ n mile (international)}. \end{aligned}$$

5.2.3 Specific Range Based on a Parabolic Drag Polar

The simplest expression for the total drag coefficient of an aircraft, and one which accords very closely with actual drag characteristics for a wide range of aircraft types is

$$C_D = C_{D0} + C_{Di} = C_{D0} + \frac{K}{\pi A} C_L^2, \quad (6)$$

where

C_{D0} = drag coefficient at zero lift*

C_{Di} = lift-dependent drag coefficient

K = lift-dependent drag factor

A = aspect ratio

C_L = lift coefficient = $L/\frac{1}{2}\rho V^2 S = W/qS$

ρ = air density

S = wing area.

Thus the ratio of drag to lift is then

$$\frac{D}{L} = \frac{C_D}{C_L} = \frac{C_{D0}}{C_L} + \frac{K}{\pi A} C_L, \quad (7a)$$

which on substitution for C_L gives

$$\frac{D}{L} = \frac{1}{2}\rho C_{D0} \frac{V^2}{W/S} + \frac{2K}{\pi \rho A} \frac{W/S}{V^2} \quad (7b)$$

or

$$\begin{aligned} &= \frac{2K}{\pi \rho} \frac{W}{b^2} \frac{1}{V^2} \\ &= C_{D0} \left(\frac{q}{w} \right) + K \left(\frac{w}{q} \right). \end{aligned}$$

Thus the lift-to-drag ratio, required for use in Equation (3), can be obtained by taking the reciprocal of D/L in Equations (7a) or (7b), depending on which is the most convenient form to use.

When a number of results are required, over a range of speeds for example, a convenient method is to base the calculation on conditions for minimum drag. Differentiation of Equation (7a) with respect to C_L gives the conditions for minimum drag (and maximum lift-to-drag ratio) as

$$C_{D0} = \frac{K}{\pi A} C_{Lmd}^2 \quad \text{and} \quad C_{Dmd} = 2C_{D0}. \quad (8)$$

It follows that

$$C_{Lmd} = \left(\frac{\pi A C_{D0}}{K} \right)^{1/2} \quad (9)$$

$$\left(\frac{L}{D} \right)_{\max} = \frac{1}{2} \left(\frac{\pi A}{K C_{D0}} \right)^{1/2} \quad (10)$$

and

$$V_{md} = \left(\frac{2W}{\rho S} \right)^{1/2} \left(\frac{K}{\pi A C_{D0}} \right)^{1/4}. \quad (11)$$

Substituting Equation (10) into Equation (7a) gives

$$\frac{D}{D_{\min}} = \left(\frac{1}{2} \frac{C_{Lmd}}{C_L} + \frac{C_L}{C_{Lmd}} \right) = \frac{1}{2} \left[\left(\frac{V}{V_{md}} \right)^2 + \left(\frac{V_{md}}{V} \right)^2 \right] = \frac{1}{2} \left(m^2 + \frac{1}{m^2} \right), \quad (12)$$

where $m = V/V_{md}$.

* It must be admitted that, for a cambered wing, the term "drag coefficient at zero lift" is not very meaningful. For the purpose of performance computation, however, Equation (6) can be used as a "best fit" over the range of lift coefficients which are of interest.

Equation (12) is a perfectly general function that applies to any aircraft whose drag characteristics can be represented by Equation (6). The variation of lift-to-drag ratio with speed is tabulated below and shown in Figure 5.

$m = V/V_{md}$	0.9	1.0	1.1	1.2	1.3	1.4	1.5	2.0	2.5
$\frac{D_{min}}{D} = (L/D)/(L/D)_{max}$	0.9782	1.0	0.9821	0.9370	0.8765	0.8096	0.7423	0.471	0.312
or D/D_{min}	1.02	1.0	1.018	1.068	1.14	1.24	1.35	2.125	3.285

Using such values, specific range can be obtained from the expression

$$-\frac{dR}{dW} = \frac{V}{cW} \frac{L}{D} = \frac{V}{cW} \frac{2(L/D)_{max}}{m^2 + 1/m^2} \quad (13)$$

Numerical Example

For an altitude of 30,000 ft ($\sigma = \rho/\rho_0 = 0.3747$), and a speed range from 400 knots to 500 knots ($M = 0.675-0.85$) estimate the specific range of an aircraft with the following characteristics:

$$W = 30,000 \text{ lb}, \quad S = 300 \text{ ft}^2, \quad \frac{A}{K} = 20, \quad C_{D0} = 0.02, \quad c = 0.7 \text{ lb/lb/h}, \quad W/S = 100 \text{ lb/ft}^2.$$

In addition, calculate the speed and specific range for a thrust of 2000 lb.

From Equation (11),

$$V_{md} = \left(\frac{2 \times 30,000}{0.00238 \times 0.3747 \times 300} \right)^{1/2} \times \left(\frac{1}{20 \times 0.02} \right)^{1/4} = 595.5 \text{ ft/s} = 352.6 \text{ knots.} \quad (14)$$

Thus the speed range of 400 knots to 500 knots is covered by a range of m from 1.1 to 1.4.

From Equation (10),

$$\left(\frac{L}{D} \right)_{max} = \frac{1}{2} \left(\frac{20}{0.02} \right)^{1/2} = 15.811.$$

Therefore

$$\frac{1}{cW} \left(\frac{L}{D} \right)_{max} = \frac{15.811}{0.7 \times 30,000} = 75.29 \times 10^{-6} \text{ h/lb}.$$

m	1.1	1.2	1.3	1.4	1.5
V knots	388	423	458	494	530
$(L/D)/(L/D)_{max}$	0.9821	0.9370	0.8765	0.8096	0.7423
$\frac{V}{cW} \frac{L}{D}$ (n mile/lb)	0.0287	0.0298	0.0303	0.0301	0.296

$$D_{min} = \frac{W}{(L/D)_{max}} = \frac{30,000}{15.811} = 1897 \text{ lb}.$$

Thus for 2000 lb thrust,

$$\frac{V^2}{V_{md}^2} = \frac{2000}{1897} \left[1 + \sqrt{1 - \left(\frac{1897}{2000} \right)^2} \right] = 1.3874, \quad \frac{V}{V_{md}} = 1.1779. \quad (15)$$

$$\frac{D_{min}}{D} = \frac{1897}{2000} = 0.9485 \text{ and, from Figure 5,}$$

$$V = 1.78 \times 352.6 = 415 \text{ knots.}$$

$$\text{Specific range} = \frac{V}{cW} \frac{L}{D} = \frac{415.3}{0.7 \times 30,000} \left(\frac{2 \times 15.811}{1.1779^2 + 1.1779^{-2}} \right) = 0.297 \text{ n mile/lb.}$$

5.2.4 Optimum Specific Range Performance

Maximum specific range, at a given aircraft weight, will occur when $(V/c)(L/D)$ is a maximum, and different values will be obtained depending on the cruise condition specified, i.e. whether constant speed, constant engine setting, or constant altitude. (As weight is reduced by consumption of fuel for a constant engine setting, either height or speed or both will increase).

On the assumption that engine specific fuel consumption does *not* vary along the cruise trajectory for each of these cruise techniques, (the justification for making this assumption is that only small changes are considered) the relationships between lift and drag to obtain maximum specific range are derived below, *and it is shown that these relationships are independent of the way in which drag varies with lift.*

5.2.4.1 Constant speed

For cruise at a constant true airspeed, it follows directly from Equation (3) that maximum specific range will occur when drag is a minimum (i.e. when the ratio of lift to drag is a maximum). The same is also true for cruise at a constant Mach number in the stratosphere, where the temperature and speed of sound are constant. That is, the height should be that where the V_{md} becomes equal to the chosen speed.

5.2.4.2 Constant engine setting

At a given engine rpm, engine performance in the stratosphere (where temperature is constant) is such that thrust is directly proportional to air density, and specific fuel consumption remains constant. Usually, also, thrust may be considered independent of speed (at subsonic speeds) over a limited speed band. For these conditions a simple relationship between lift and drag to obtain best specific range can be derived, provided that there is sufficient thrust at the maximum cruise rating of the engines for flight in the stratosphere to be attained. The required relationship can be obtained by substituting in Equation (3),

$$V = \left(\frac{2D}{\rho S C_D} \right)^{1/2} = \left(\frac{2T}{\rho S C_D} \right)^{1/2} \quad (16)$$

and it follows that

$$-\frac{dR}{dW} = \frac{1}{cW} \left(\frac{2T}{\rho S} \right)^{1/2} \frac{C_L}{C_D^{3/2}}. \quad (17)$$

This is the condition for maximum specific range in the stratosphere, at a given engine setting, occurs when $(\text{lift})/(\text{drag})^{3/2}$ is a maximum, or $(\text{lift})^{2/3}/(\text{drag})$ is a maximum.

5.2.4.3 Constant altitude

To obtain the relationship between lift and drag for maximum specific range at a constant cruise altitude, V in Equation (3) can be eliminated by substituting

$$V = \left(\frac{2W}{\rho S C_L} \right)^{1/2}, \quad (18)$$

giving

$$-\frac{dR}{dW} = \frac{1}{c} \left(\frac{2}{\rho S W} \right)^{1/2} \frac{C_L^2}{C_D} \quad (19)$$

Thus the condition for maximum specific range at a given altitude (ρ constant) occurs when $(\text{lift})^{1/2}/(\text{drag})$ is a maximum.

5.2.4.4 Summary of conditions for maximum specific range

In the three previous sections it has been shown that maximum specific range in the following cruise conditions is obtained when:

For constant speed	—	L/D is a maximum
For constant engine setting	—	$L^{2/3}/D$ is a maximum
For constant altitude	—	$L^{1/2}/D$ is a maximum.

It is emphasised, once again, that these conditions have been derived without making any assumptions in regard to the way in which lift and drag vary with speed. However, they apply only to the case of specific fuel consumption constant.

It should be noted that $\rho^{1/2}$ appears in the denominators of the expressions for specific range and this is one fundamental reason why high cruising altitudes are chosen for jet aircraft when good range performance is required.

5.2.5 Optimum Specific Range Performance with a Parabolic Drag Polar

The relationships between lift and drag for maximum specific range, obtained in Section 4, are now used with the theory of Section 3, to obtain optimum specific range relationships for the case where an aircraft's drag characteristics can be represented by Equation (6).

5.2.5.1 Constant speed

From Section 4.1, we have that maximum specific range at a constant speed occurs when drag is a minimum, and Equations (9), (10) and (11) then apply. In particular, we get from Equation (11) that

$$V_{md} \sqrt{\sigma} = \left(\frac{2W}{\rho_0 S} \right)^{1/2} \left(\frac{K}{AC_{D0}} \right)^{1/4} = (V_e)_{md} \quad (20)$$

is a constant for a given aircraft at a given weight, where $(V_e)_{md}$ is the minimum drag speed in EAS ($V_e = V \sqrt{\sigma}$), and σ is the air density relative to sea level conditions.

Hence the maximum specific range condition for any required true airspeed is obtained at an altitude defined by

$$\sqrt{\sigma} = \frac{(V_e)_{md}}{V_{reqd}} \quad (21)$$

5.2.5.2 Constant engine setting

Maximum specific range in this case is obtained when $L^{2/3}/D$ is a maximum, and Equation (7a) gives

$$\frac{D}{L^{2/3}} = \frac{C_{D0}}{C_L^{2/3}} + \frac{K}{\pi A} C_L^{4/3},$$

which, on differentiation, gives

$$C_{D0} = \frac{2K}{\pi A} C_{Les}^2, \quad \text{i.e.} \quad C_{Des} = \frac{3}{2} C_{D0}, \quad (22)$$

where the suffix *es* refers to conditions at a constant engine setting.

It follows that

$$C_{L,es} = \left(\frac{AC_{D0}}{2K} \right)^{1/2} = \frac{1}{\sqrt{2}} C_{L,md} = 0.707 C_{L,md} \quad (23)$$

$$\left(\frac{C_L}{C_D} \right)_{es} = \frac{\sqrt{2}}{3} \left(\frac{A}{KC_{D0}} \right)^{1/2} = \frac{2\sqrt{2}}{3} \left(\frac{L}{D} \right)_{\max} = 0.943 \left(\frac{L}{D} \right)_{\max} \quad (24)$$

$$V_{es} = \left(\frac{2W}{\rho S C_{L,es}} \right)^{1/2} = 2^{1/4} V_{md} = 1.189 V_{md} \quad (25)$$

5.2.5.3 Constant altitude

Maximum specific range in this case is obtained when $L^{1/2}/D$ is a maximum, and Equation (7a) gives

$$\frac{D}{L^{1/2}} = \frac{C_{D0}}{C_L^{1/2}} + \frac{K}{\pi A} C_L^{3/2}$$

which, on differentiation, gives

$$C_{D0} = \frac{3K}{\pi A} C_{Lh}^2, \quad \text{i.e. } C_{Dh} = \frac{4}{3} C_{D0} \quad (26)$$

where the suffix *h* refers to conditions at a constant altitude.

It follows that

$$C_{Lh} = \left(\frac{\pi A C_{D0}}{3K} \right)^{1/2} = \frac{1}{\sqrt{3}} C_{L,md} = 0.577 C_{L,md} \quad (27)$$

$$\left(\frac{L}{D} \right)_h = \frac{\sqrt{3}}{4} \left(\frac{\pi A}{K C_{D0}} \right)^{1/2} = \frac{\sqrt{3}}{2} \left(\frac{L}{D} \right)_{\max} = 0.866 \left(\frac{L}{D} \right)_{\max} \quad (28)$$

$$V_h = \left(\frac{2W}{\rho S C_{Lh}} \right)^{1/2} = 3^{1/4} V_{md} = 1.316 V_{md} \quad (29)$$

Equations (21), (25) and (29) are collected on Figure 6.

5.2.5.4 Numerical examples

For the aircraft characteristics used as an example in Section 5.2.3, calculate the maximum specific range (and thrust requirements) for the following cases:

- (i) A Mach number of 0.8 (in the stratosphere).
- (ii) An engine setting as in (i).
- (iii) Cruise at 30,000 ft ($\sigma = 0.3747$).

The results of the calculations are shown on Figure 7.

5.3 Cruise Height Schedules and Integrated Range

5.3.1

This section collects together, with some extensions, the classical theory of range performance of jet aircraft in cruising flight, for conditions where engine specific fuel consumption can be assumed to remain essentially constant during the flight. Most of the theory can be found scattered amongst standard text-books on aerodynamics in the references cited in 5.3.6, but is summarised here for convenience to the user, together with some worked examples.

5.3.2

The distance covered during cruising flight (in still air) is obtained by integration of the "specific range" (i.e. the distance flown per unit quantity of fuel consumed) over a change of aircraft weight equal to the weight of fuel consumed.

$$\text{i.e. cruise range} \quad R = \int_{W_i}^{W_i - W_F} \left(\frac{dR}{dW} \right) dW \quad (1a)$$

$$\text{and} \quad dW = dW_F, \quad (1b)$$

$$\text{where} \quad -\frac{dP}{dW} = \frac{V}{cT} = \text{specific range}$$

V = cruise speed

c = specific fuel consumption

T = thrust

W_i = aircraft weight at start of cruise

W_F = weight of fuel consumed.

For short ranges it is often sufficiently accurate to obtain cruise range by multiplying a mean specific range by the weight of fuel consumed, since the variation of specific range with weight is usually close to linear.

Thus we have, approximately, that

$$\text{either} \quad R = \left(\frac{dR}{dW} \right)_{W_i - W_F/2} W_F \quad (2)$$

$$\text{or} \quad R = \frac{1}{2} \left[\left(\frac{dR}{dW} \right)_i + \left(\frac{dR}{dW} \right)_f \right] W_F, \quad (3)$$

where the subscripts i and f refer to initial and final conditions, respectively.

For instance, in the example from an aircraft performance manual given in Figure 8, for an initial cruise weight of 26,000 lb and 8000 lb of fuel consumed, we get

Method	Mean (dR/dW) (n mile/lb)	Range (n mile)	Error (%)
Integration	0.380	3040	—
Equation (2)	0.382	2056	+ 0.5
Equation (3)	0.377	3016	— 0.8

However, for theoretical work and early project studies, it is often more convenient to obtain cruise range from direct integration of Equation (1a) over a chosen cruise trajectory. In some cases, it then is necessary to assume a law for the variation of aircraft drag with speed such as* the single parabolic law:

$$D = \frac{1}{2} \rho S V^2 \left(C_{D0} + \frac{K}{A\pi} C_L^2 \right) = qS \left(C_{D0} + \frac{K}{A\pi} C_L^2 \right). \quad (4)$$

Also, it is necessary to express the equation for specific range in the form

$$-\frac{dR}{dW} = \frac{V}{cT} = \frac{V}{cD} = \frac{1}{W} \frac{V}{c} \frac{L}{D} \quad (\text{Equation (3) of Section 5.2.2}). \quad (5)$$

The integration of this equation is discussed in the next section.

* Theoretically, it may not always be justifiable to express the drag in this way, e.g. for an aircraft with a twisted wing such that minimum drag does not occur at zero lift; in such a situation, it may nevertheless be good enough to use Equation (4) as a "best-fit" to the C_L - C_D polar over the range of lift coefficients likely to be used during cruise.

5.3.3 Range Equations

5.3.3.1 General remarks

It can be seen from inspection of Equation (5) that one class (simple from the analytical point of view) of cruise trajectories that can be considered, are those where speed and/or the ratio of lift to drag are kept constant throughout the flight. Keeping the ratio of lift to drag constant also means that the aircraft incidence and lift coefficient will remain constant.

Examination of the basic equation

$$L = W = C_L q S = C_L \frac{1}{2} \rho V^2 S \quad (6)$$

shows that flight at constant lift coefficient can be achieved in the following ways:

- (i) *Speed constant.* This requires the cruise altitude of the aircraft to be steadily increased as fuel is consumed, in a way such that air density is proportional to the weight of the aircraft.
- or (ii) *Altitude constant.* This requires the speed of the aircraft to be steadily reduced as fuel is consumed, in a way such that V^2 is proportional to the weight of the aircraft.
- or (iii) *Dynamic pressure proportional to the weight of the aircraft.* However, an infinite variety of combinations of ρ and V is possible, and this case is not amenable to a general theoretical approach.

Case (i) above is generally referred to as the *Breguet "cruise-climb"* technique; it may not be acceptable in many situations because of the requirements of Air Traffic Control. Case (ii) which requires a steady decrease in speed during the cruise is unlikely to be acceptable to airlines as a normal operational procedure. The more practical procedures from the operational point of view, of cruising at constant altitude with either speed or engine thrust kept constant, are considered in Sections 5.3.3.3.1 and 5.3.3.3.2 respectively.

Also in these sub-sections each of the equations derived for various methods of cruising at constant altitude are compared with the Breguet equation for a cruise-climb, for the same initial conditions of aircraft weight, speed, altitude and fuel fraction. Values of the "ratios of range" so obtained are plotted. This has been done in order to show the loss of range relative to the Breguet cruise-climb technique, and also to simplify computation. Thus, once a Breguet range has been obtained, for given initial cruise conditions, the range using other cruise techniques can quickly be found by application of the appropriate "ratio of range" rather than having to substitute values into each range equation in turn.

A typical variation of specific range with aircraft weight and speed is shown in Figure 9, with cross-plots showing the various types of cruise trajectory, at constant altitude, that have been considered. The worked examples in Section 4 are based on this figure.

5.3.3.2 Cruising with incidence, lift coefficient, and lift-to-drag ratio constant

5.3.3.2.1 Speed constant, altitude increasing ($\rho \propto W$; both decrease together).

Integration of Equation (5) gives the Breguet equation

$$R_{Br} = \frac{V}{c} \frac{L}{D} \log_e \frac{W_i}{W_f} \quad (7a)$$

$$\text{i.e.} \quad R_{Br} = \frac{V}{c} \frac{L}{D} \log_e \frac{1}{1 - W_f/W_i} \quad (7b)$$

5.3.3.3 Cruising at constant altitude with lift coefficient and lift-to-drag ratio free to vary

5.3.3.3.1 Speed constant ($C_L \propto W$)

For this method of cruising, the aircraft incidence has to be steadily decreased as fuel is consumed, in such a way that the lift coefficient is proportional to the aircraft weight. In addition, the engine thrust will need to be steadily decreased during the course of the flight. An example of such a cruise trajectory is shown by the line AC in Figure 9.

From Equations (4) and (5), for the same conditions at start of cruise, the ratio of the cruise ranges is given by

$$\frac{\text{Range at constant speed and altitude}}{\text{Breguet range}} = \frac{(m_i^2 + 1/m_i^2) \tan^{-1} \left[\frac{W_F/W_i}{m_i^2 + (1 - W_F/W_i)/m_i^2} \right]}{\log_e \left(\frac{1}{1 - W_F/W_i} \right)} \quad (8)$$

The above ratio of ranges is plotted in Figure 10 and it can be seen that, for the same conditions at start of cruise, cruising at constant speed and altitude always results in a loss of range relative to the Breguet cruise-climb technique.

5.3.3.3.2 Thrust constant

The method of cruising described in Section 5.3.3.3.1 above, requires that the engine thrust be steadily reduced during the course of the flight. A possibly more convenient method from the operational point of view is to leave thrust constant, and to allow the aircraft speed to increase steadily during the course of the flight.

For the same conditions at start of cruise, the ratio of the cruise ranges is given by

$$\frac{\text{Range at constant thrust and altitude}}{\text{Breguet range}} = \frac{V_{\text{mean}}}{V_i} \frac{W_F/W_i}{\log_e \left(\frac{1}{1 - W_F/W_i} \right)} \quad (9)$$

The ratio V_{mean}/V_i is plotted in Figure 11, and the ratio of ranges in Figure 12. In general, there is a loss of range relative to the Breguet technique, except at low values of m_i and W_F/W_i . Comparison of Figures 10 and 12 shows that, at the higher values of m_i and W_F/W_i , there is very little difference in range between the constant-speed and constant-thrust techniques (for the same initial cruise conditions).

5.3.4 Initial Cruise Conditions for Maximum Range

All the "ratio of ranges" given so far have been based on the same initial cruise conditions of aircraft weight, speed and altitude. In many circumstances, this is a fair basis of comparison, but on occasions it may be more realistic to make comparisons on the basis of initial cruise conditions which give *maximum* range.

For the cruise techniques in which the lift coefficient is held constant throughout the flight, maximum range will be obtained when VL/D is a maximum. From Equation (29) of 5.2.5 we have that $(VL/D)_{\text{max}}$ is obtained when

$$m = \frac{V}{V_{\text{md}}} = 3^{1/4} = 1.316$$

and, since

$$\frac{VL}{D} \propto \frac{m}{m^2 + 1/m^2}$$

we obtain that

m_i	1.0	1.1	1.2	1.3	1.316	1.4	1.5	1.75	2.0
$\frac{\text{Breguet range}}{(\text{Breguet range})_{\text{max}}}$	0.8774	0.9479	0.9865	0.9998	1.000	0.9996	0.9769	0.906	0.825

Thus the ratios of (range obtained by cruising at constant speed or constant thrust) to maximum Breguet range, can be found by multiplying the "ratios of range" from Equations (8) and (9), respectively, by the ratio of Breguet range to *maximum* Breguet range given above.

For example, for cruising at constant thrust and $W_F/W_i = 0.2$, we get

m_i	R/R_{Br} (same V_i)	$R_{Br}/R_{Br \max}$	$R/R_{Br \max}$
1.0	1.062	0.8774	0.932
1.1	0.989	0.9479	0.937
1.2	0.953	0.9865	0.940
1.3	0.934	0.9998	0.934
1.4	0.922	0.9996	0.922
1.5	0.915	0.9769	0.894

The above table also shows that the initial speed to give maximum range, using the constant-thrust technique, is about $1.2 V_{md}$ in this particular case.

5.3.5 Example of Range Calculation

For the purpose of these examples, an aircraft with the following characteristics is assumed:—

$$\begin{aligned}
 \text{Initial cruise weight} &= 30,000 \text{ lb} \\
 \text{Final cruise weight} &= 20,000 \text{ lb} \\
 \text{Initial (or constant) cruise height} &= 30,000 \text{ ft } (\sigma = 0.3747) \\
 \text{Wing reference area} &= 300 \text{ ft}^2 \\
 C_{D0} = 0.02; \frac{\pi A}{K} &= 20; c = 0.07 \text{ lb/lb/h.}
 \end{aligned}$$

Thus we have

$$\begin{aligned}
 \left(\frac{L}{D}\right)_{\max} &= \frac{1}{2} \left(\frac{A}{K C_{D0}}\right)^{1/2} = \frac{1}{2} \left(\frac{20}{0.02}\right) = 15.811 \\
 C_{Lmd} &= \left(\frac{\pi A C_{D0}}{K}\right)^{1/2} = (20 \times 0.02)^{1/2} = 0.6325 \\
 (V_{md})_i &= \left(\frac{2W}{\sigma \rho_0 S C_{Lmd}}\right)^{1/2} = \left(\frac{200}{0.000891 \times 0.6325}\right)^{1/2} = 595.7 \text{ ft/s} \\
 &= 353 \text{ knots.}
 \end{aligned}$$

Thus, the initial speed for maximum Breguet range is

$$3^{1/4} (V_{md})_i = 1.316 \times 353 = 464 \text{ kt.}$$

The specific range performance of this aircraft, for an altitude of 30,000 ft, is plotted in Figure 9. The constant- C_L trajectory is shown by the line AB, the constant-speed trajectory by the line AC, and the constant-thrust trajectory by the line AD, all for an initial cruise speed of 464 knots, as calculated above.

(a) Breguet cruise-climb

From Equation (7b)

$$R_{Br} = \frac{V}{c} \frac{L}{D} \log_e \left(\frac{1}{1 - W_F/W_i} \right)$$

i.e.
$$R_{Br} = \frac{464.2}{0.7} \times 13.693 \log_e \left(\frac{1}{1 - 0.333} \right) = 3682 \text{ n mile.}$$

Since W/σ is constant,

$$\sigma_f = (W_f/W_i) \sigma_i = \frac{2}{3} \times 0.3747 = 0.2498 \text{ giving } h_f = 39,800 \text{ ft.}$$

It should be noted that there is a difference between a cruise-climb schedule and those flown at constant height; the former requires work to be done against gravity as well as against drag; in the example,

$$\frac{\text{work done against gravity}}{\text{work done against drag}} \times 100\% = \frac{W \times 9000 \times 100}{(W/13.7) \times 3682 \times 6020} = 0.6\%$$

Correcting for this, range = $3682 (1 - 0.006) = 3660$ n miles ,

small, but not quite negligible!

(b) *Constant V and h*

From Figure 10,

$$R = 0.890 \times R_{Br} = 3277 \text{ n mile.}$$

From Figure 12,

$$R = 0.849 R_{Br} = 3200 \text{ n mile.}$$

5.3.6 Bibliography

The theory of range performance is partially covered in a number of text-books, articles, etc. For a deeper study of the question References 2-6 are recommended.

5.4 Effect of Various Aircraft and Engine Characteristics

5.4.1

In the development of any simple analytical treatment, such as those for cruise speed height and range outlined above it is tacitly assumed that any relationships between parameters hold good over the ranges of values that need to be considered, i.e. there will be no discontinuities in the functions. In particular, it is assumed that (for the aircraft) drag is a continuous (in the mathematical sense) function of lift, and of speed, and for the engine, fuel consumption and thrust are continuing functions of 'pilots demand' (i.e. throttle position) forward speed and height. None of these assumptions can be justified unreservedly and without limit. The simple parabolic law connecting drag with lift, $C_D = C_{D0} + K_1 C_L^2$, holds good only up to $C_L = C_{Lcrit}$, after which a further term $K_2 (C_L - C_{Lcrit})^2$ must be added. Profile drag C_{D0} varies as V^2 only up to a value of V corresponding to an often ill-defined Mach number M_{crit} , at which the value of C_{D0} is no longer (approximately) constant, but increases sharply. For practical purposes these two effects may be dealt with by assuming that the speeds corresponding to the critical values represent points at which the fuel consumption in lb/nm will increase sharply, and so they are effective boundary conditions. For the engine, discontinuities occur when some engineering design parameter such as TET, compressor total pressure, or r.p.m. that respond to external conditions, reach a limiting value, or some modified mode of operation such as the action of compressor blow-off valves (e.g. Figure 17) comes into effect. The effect of these on the aircraft performance is usually only progressive, and of course, it can only be allowed for empirically.

5.4.2

It is instructive to examine the extent to which the basic assumption of the preceding sections — that the sfc is constant over the cruise phase — is borne out in practice, and the effect on the cruise performance of any deviations that occur.

In fact, sfc for a turbo-reaction engine (jet or fan) in general varies with

- (i) r.p.m. (or more directly of interest in the aircraft performance context, with thrust)
- (ii) forward speed,
- (iii) height (or more correctly, with ambient temperature), i.e. the variation occurs only below the tropopause. (Above the tropopause there may be a minor variation resulting from blading Reynolds number effects, but this is usually only of consequence in extreme cases.)

(ii) and (iii) are significant in all cases, though the magnitude of the rate of change depends on the characteristics of a particular engine.

(ii) is (one suspects) a source of occasional confusion, in that when (as in modern high temperature and high compression engines), there is very little change in sfc at a constant forward speed over the working range of thrust, this is just when the variation of sfc with forward speed in level flight at constant weight when installed in an aircraft, is greatest. This apparent anomaly is best explained graphically – see Figures 13 to 16, which show sfc plotted against thrust for a range of speeds (Mach number) for four different types of engine:—

1. a low pressure ratio and moderate temperature (TET) turbo-jet, Figure 13,
2. a moderately high pr, high TET turbo-jet, Figure 14,
3. a high pr, high TET low by-pass ratio turbo-fan, Figure 15,
4. a high pr, fairly high TET, high bpr turbo-fan, Figure 16.

The curve super-imposed on all these is the thrust required (= drag) for the level flight of an aircraft of aspect-ratio 7 cruising at low altitude (this latter chosen so that a wide variation in speed can be shown).

Comparing the four sets of curves it will be seen that there is in fact an appreciable variation of sfc with speed, particularly in the region of V_m for the turbo-fan engines.

The effect on specific range is shown in Figures 17 and 18, where it is plotted against speed for the four engines, and compared with the values obtained with constant sfc. The important point to note is the variation in the speed for optimum specific range from the value of $1.316 V_m$ given by the simple analytical treatment.

N.B. Except that the general order of progression from engines (1 to 4) is correct, the curves should not, NOT, be taken as a measure of the exact differences in specific range obtained by installing engines of different characteristics in a given aircraft. These will depend on how the engines are 'matched', e.g. for same take-off thrust, same maximum speed, or to give the same range. (In the Figure, for convenience they are matched at the same thrust at the same maximum speed). The matching involves a whole host of parameters such as installed weight and drag, and is another major subject in itself!

Figure 18, for cruise at the tropopause illustrates the condition (for engine 1) where the optimum speed is not reached at all, as it would be above V_{max} which is assumed to be determined by drag rise at $M = 0.9$. There would be a similar but even more abrupt increase in slope of the curves where $C_L = C_{Lcrit}$, if this occurs before the drag rise.

5.5 Descent

As with climb, so can the descent from a high-altitude cruise to ground level often be a segment contributing to the total range distance. Whether it does so or not is usually a matter for operational consideration. For military aircraft returning to base, or attacking a target after a surprise approach at altitude, a rapid descent will be permissible or desirable, often with engine throttled back and air brakes in operation; the distance covered and the fuel actually consumed are both small and it is an acceptable simplification to assume that the aircraft continues to cruise until overhead base, and ignore the descent completely.

At the other extreme are civil passenger aircraft for which both the rate of descent (actual increase in cabin pressure) and attitude must be kept to low values, and so the descent (at some prescribed Mach number or CAS – height schedule) will cover an appreciable distance, comparable to the climb segment, and must be dealt with in a similar way, by stages. A technically similar condition exists for combat aircraft for which an 'under the radar beam' approach to a target is required. (In passing, one may perhaps be allowed a facetious comment that in treating this special condition, actually that of following a target to the earth's surface, it seems to be a common, if heretical, practice to regard it as a curved path above a flat earth!)

5.6 Allowances

This term is used to cover secondary (though by no means always second-order in terms of fuel usage) phases or segments of the total flight plan, after the main distance contributions of cruise and the associated climb and descent. They include phases where the aircraft is changing speed between major phases, e.g. climb and fast cruise, combat or attack phases for military aircraft, diversions from the intended destination to an alternate and stand-off or loiter before receiving permission to land.

As the amounts of acceleration and deceleration expressed as speed changes must always in total be equal and opposite in the course of a flight, one might be tempted to ignore them and assume that the speed changes are made over zero distances flown. Although the amounts of fuel concerned are usually small they are not equal; (a) because the acceleration phase takes longer, the net force being $T - D$, which may often be small towards the end of the phase, whereas for deceleration it is Drag minus idling thrust (which may well be negative at low r.p.m., i.e. momentum drag > gross thrust); (b) the deceleration will occur later in the flight, when the aircraft weight has been reduced; (c) as it is not practical to shut down the engines entirely, fuel is still being consumed at an appreciable rate to produce unwanted thrust.

'Combat' attack or 'dash' phases for military aircraft may sometimes be specified as not being considered as contributory to distance but, if they are to be included, the fuel used at (usually) maximum-rating conditions may well be comparable with that used on the true cruise phases, even though the distance is small.

'Diversion' can of course, be treated as just another set of cruise conditions but, as they may in practice have to be started from low level and be comparatively short, it may not be possible to attain anywhere near the optimum cruise height; but even so it will often be more economical to follow a climb-descent path, with no level cruise segment at all, than to fly the whole distance at low level. This will be illustrated by means of a fuel-distance diagram, in the final section (Fig.26).

Loiter, or stand-off is, in a sense, a type of cruise flight, but in contrast to range cruising, the object is to maximise time flown (rather than distance) for a given fuel quantity. It is fairly obvious that this will be achieved by flying at the speed requiring minimum thrust: i.e. V_{md} if sfc is constant, or in the practical case, the slightly higher speed at which $sfc/(L/D)$ is a minimum.

Fuel consumed will usually be reduced by flying higher, but true speed will then increase, which may not be desirable; in any event the height will often be specified for operational reasons.

6. USE OF FUEL AND DISTANCE DIAGRAMS

There are two ways in which this type of diagram is useful, first as a graphical presentation of the calculated results of range of radius together with the other components of a complete sortie, i.e. the total flight plan; and secondly it is often an easier method in practice of arriving at the total operational range of radius or duration when the separate specific ranges and allowances have been found, than the alternative of formulating and solving a possibly complex and cumbersome equation.

Figure 19 shows such a diagram, with the essential features annotated. The slope of the various curves equals $1/\text{specific range}$ (and thus for no-distance allowances specific range is zero). Where (and this in general is the case) specific range is varying, this will show up as a curve, but if intermediate points are of no interest in a particular case the diagram can be simplified by drawing straight lines between the terminal points.

The second use of the diagram is illustrated by Figure 20 by drawing the part of the diagram containing the descent, attack and re-climb phases on a transparent sheet and placing it over the out and return cruise curves so that the end points of the descent and re-climb phases coincide with the cruise curves. The procedure enables the radius for the sortie to be found very much more easily than by an analytical solution when the allowances (as in the example) are complex, and the cruise lines non-linear, and when no computer program is available.

Figures 21, 22, 23 and 24 show diagrams corresponding to the block diagrams of fuel usage for various types of sortie with which we started in Figure 1 of the paper. Figure 24, for a high-level range flight, has been chosen to show another use of the diagram; the additional range obtainable by in-flight refuelling. In Figure 25, note that two types of solution are obtained, according to whether or not the limitation due to observing a 'point of no return' before refuelling is to be complied with or not. Possible deviations from the required cruise conditions necessary during the refuelling process affect only the amount of fuel dispersed by the tanker, *except* for an additional fuel used during a re-climb from refuelling to cruise height, though this can in practice be allowed for by implicitly assuming (as in the figure) that the refuelling takes place at constant range, whereas it will normally be done whilst continuing on course.

Figure 26 shows how the fuel for a diversion that is started from low level, may be minimised by climbing to a cruise height appropriate to the diversion distance. For example, for the diversion range R_{D3} , less fuel will be used by cruising at the height H_2 than by continuing to H_3 , because the extra climb fuel would outweigh the better specific range at the greater height for the very short cruise distance involved.

7. OPTIMISATION

We mean by 'optimisation' of range or radius-of-action, something more than for example the selection of a cruise regime (i.e. height, speed and engine setting) to give the greatest distance when the aircraft is otherwise completely defined.

Optimisation in the fullest sense means designing the complete aircraft – wing geometry, type and location of engines, body proportions – to give the best range performance for a given cost (which may include R & D, initial unit cost and also subsequent operating costs) or, alternatively the minimum cost for a given range.

Because weights, aerodynamics parameters and engine performance are so inter-dependent (as is shown in R.Wallace's paper), it is hardly conceivable that, except in the simplest cases, when some arbitrary constraints reduce the number of variables, any simple formulae or set of equations can be written to give a direct answer. Rather, a

complete 'parametric study' must be done, using where appropriate, the methods and rules for cruising developed in this lecture to give 'families' of aircraft for which varying cruising performance levels can be matched against other performance parameters, e.g. airfield performance. The different sizes of aircraft to give these performance levels can be evaluated, from their airframe weight and engine outputs, on a cost basis, and thence yield the information from which an optimum choice can be made in terms of whatever 'cost-effectiveness' criteria are deemed appropriate.

REFERENCES

1. Peckham, D.H. Range Performance in Cruising Flight. RAE Tech. Report to be issued.
2. Edwards, A.D. Performance Estimation of Civil Jet Aircraft. Aircraft Engineering, April 1950, p.95.
3. Dommasch, D.O.
et al. Airplane Aerodynamics. Pitman, London.
4. Perkins, C.D.
Hage, R.E. Airplane Performance, Stability and Control. Wiley, London.
5. — Estimation of Range. Royal Aero Soc. Data Sheet EG4/1.
6. Miele, A. Flight Mechanics, Vol. I. Pergamon, London.

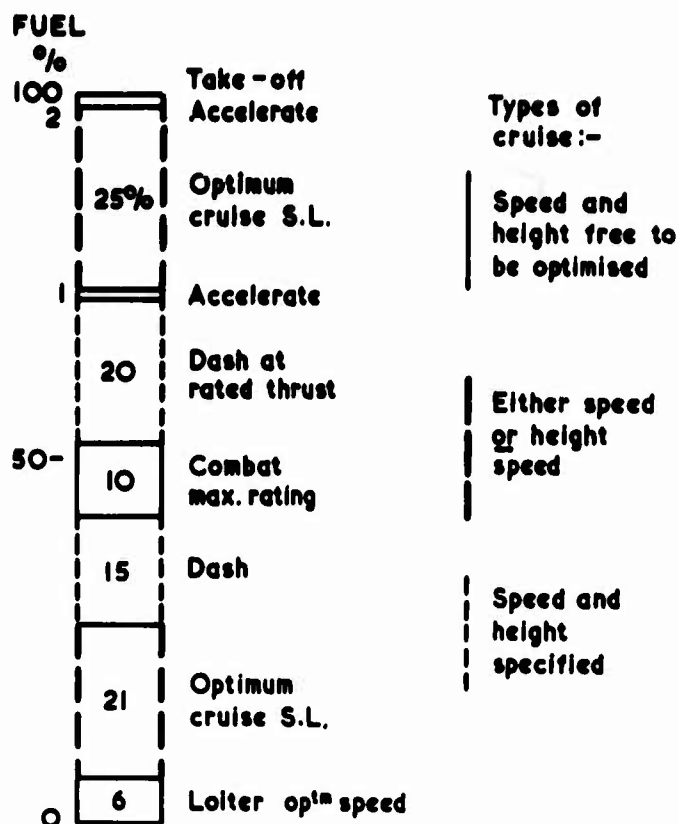


Fig.1 Subsonic low-level tactical sortie

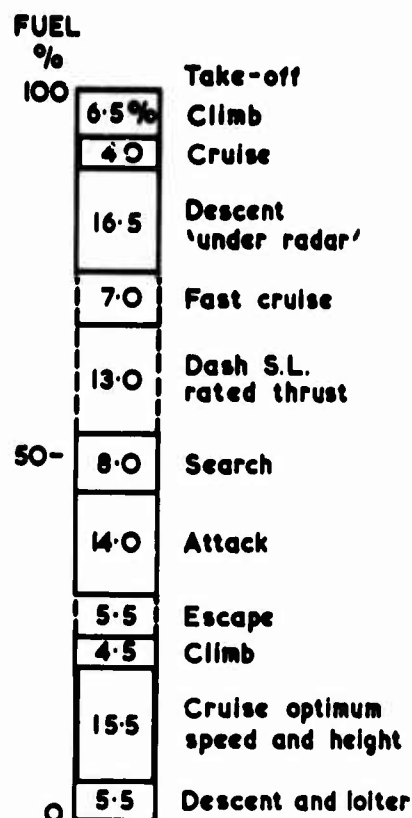


Fig.2 Subsonic Hi Lo Lo Hi attack sortie

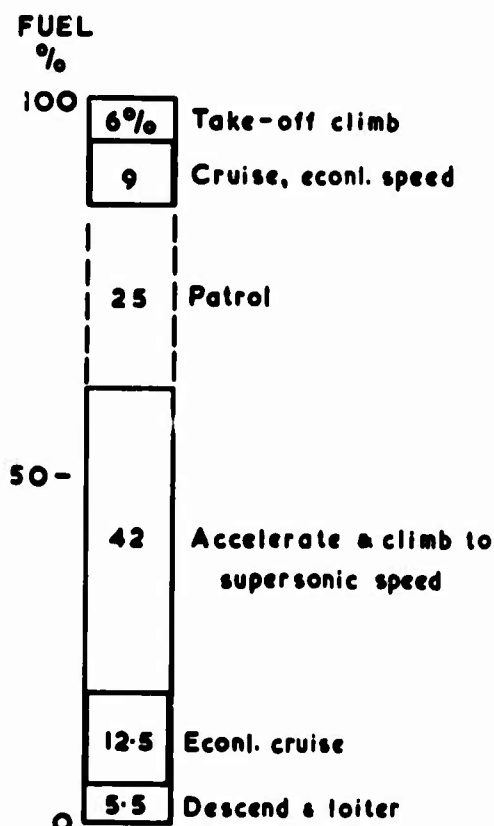


Fig.3 Combat air patrol supersonic interception

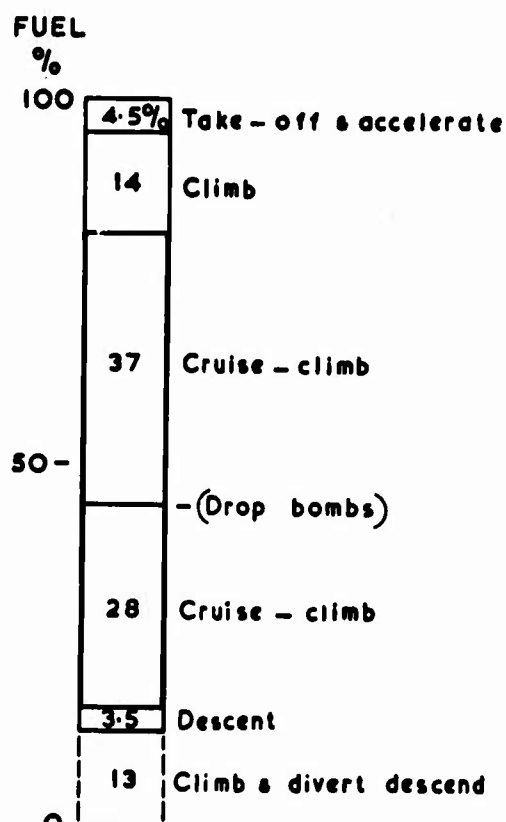


Fig.4 High-altitude transport (or bomber)

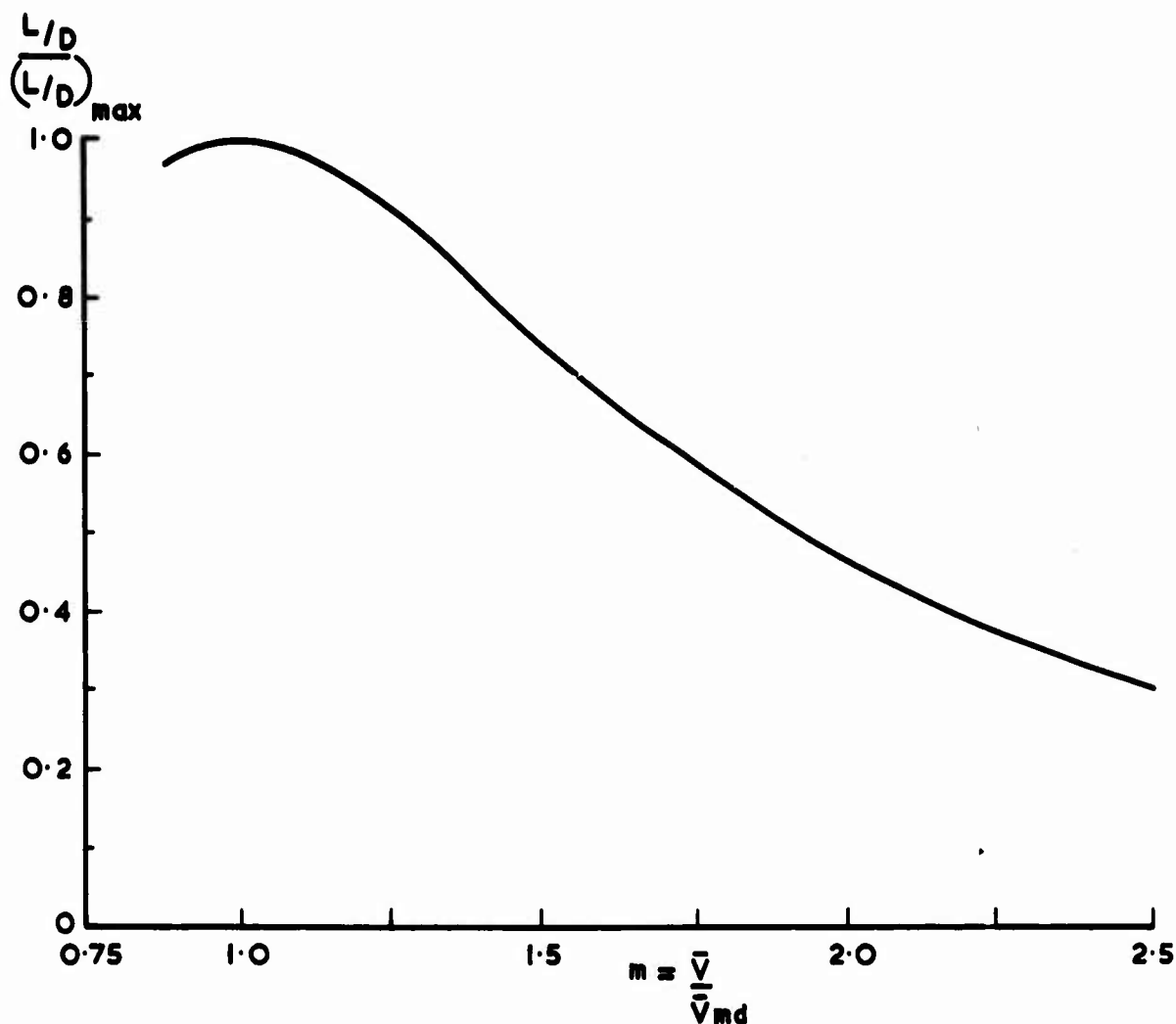


Figure 5

EXAMPLE

MAXIMUM SPECIFIC RANGE FOR:-

1. Constant speed

$$\sqrt{\sigma} = \frac{(\bar{V}_e)_{m_d}}{(\bar{V}_e)_{\text{required}}}$$

2. Constant engine setting

$$\bar{V}_{e_s} = 1.189(\bar{V})_{m_d}$$

3. Constant height

$$\bar{V}_h = 1.316(\bar{V})_{m_d}$$

1. Constant speed
- $M = 0.8$
- ,
- $\bar{V} = 460$
- kt

Height = 42200 ft

$$\underline{0.345 \text{ nm/lb}} \quad T/\rho = 36 \times 10^4 \text{ ft}^4/\text{sec}^2$$

$$T = 18975 \text{ lb}$$

2. Engine setting
- $T/\rho = 36 \times 10^4$
- ,

 $T = 20120$ lb at height 41100 ft

$$\bar{V} = 530 \text{ kt} \quad \underline{0.376 \text{ nm/lb}}$$

3. Height = 30000 ft

$$\bar{V} = 464 \text{ kt} \quad \underline{0.302 \text{ nm/lb}}$$

Figure 6

Figure 7

SPECIFIC RANGE
n mile / lb

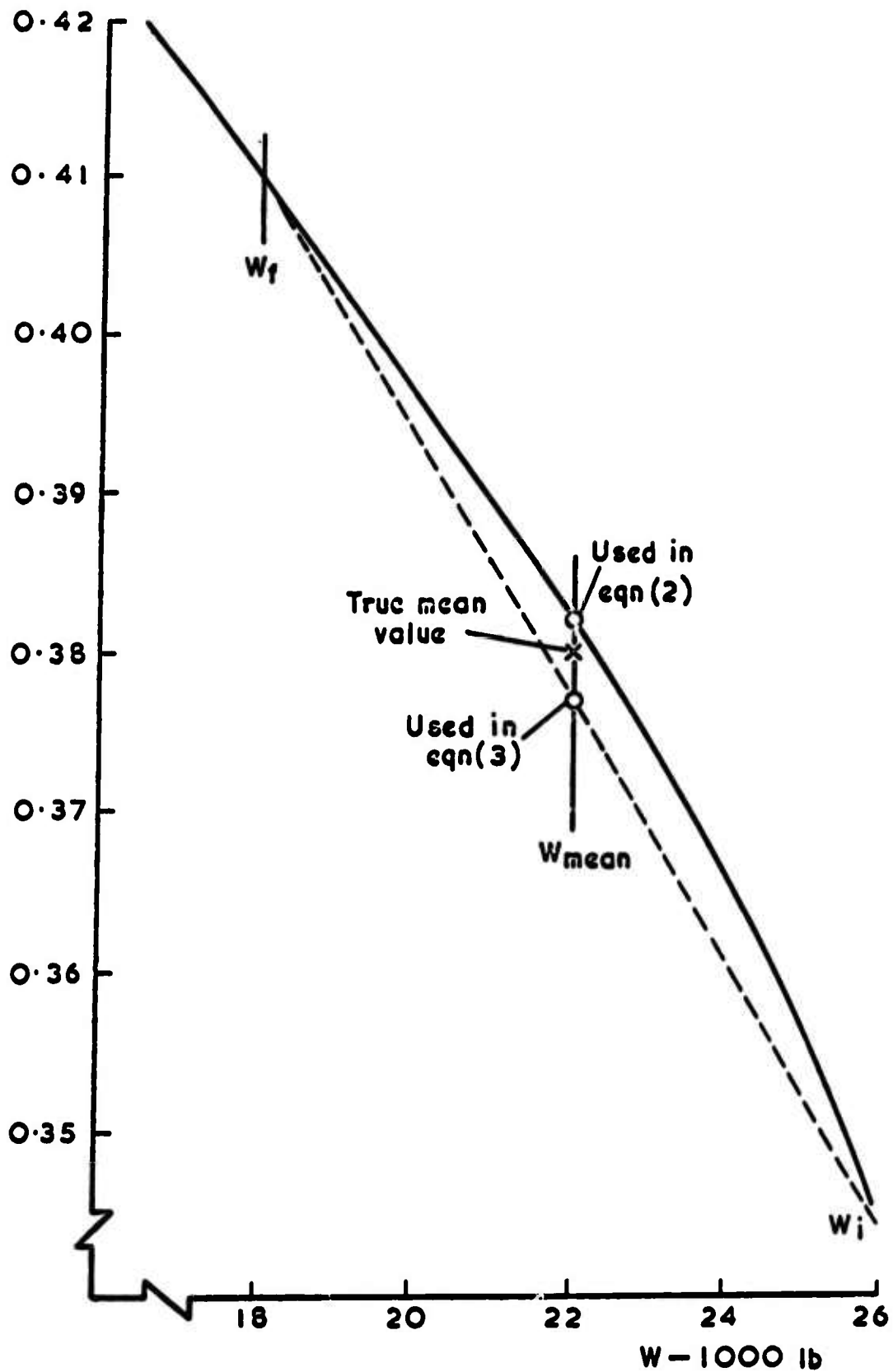


Fig.8 Typical variation of specific range with weight, at constant speed and altitude

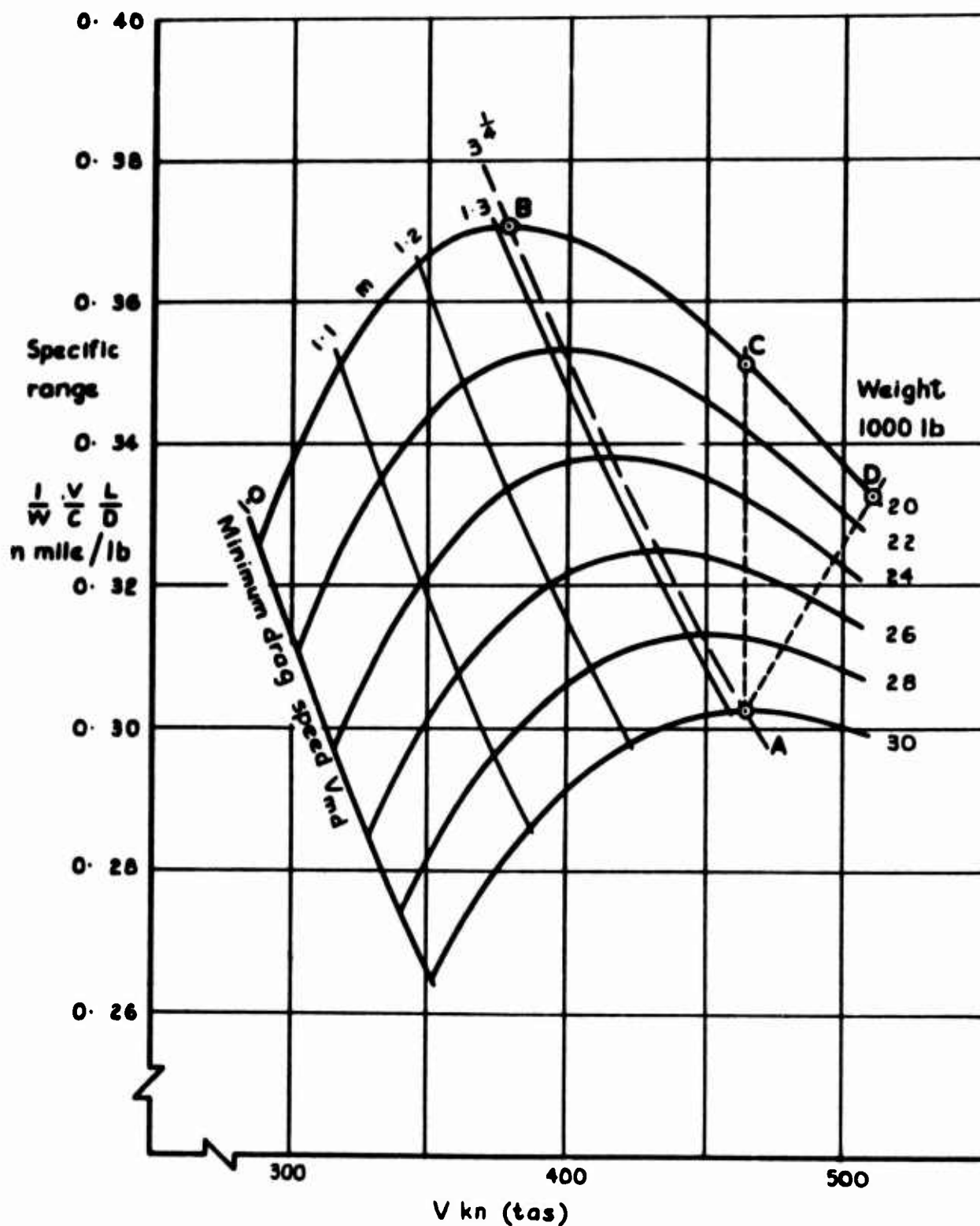


Fig.9 Typical specific range performance (30,000 ft). $C_D = 0.02 + 0.05C_L^2$; $S = 300 \text{ ft}^2$; $c = 0.7 \text{ lb/lb/hr}$

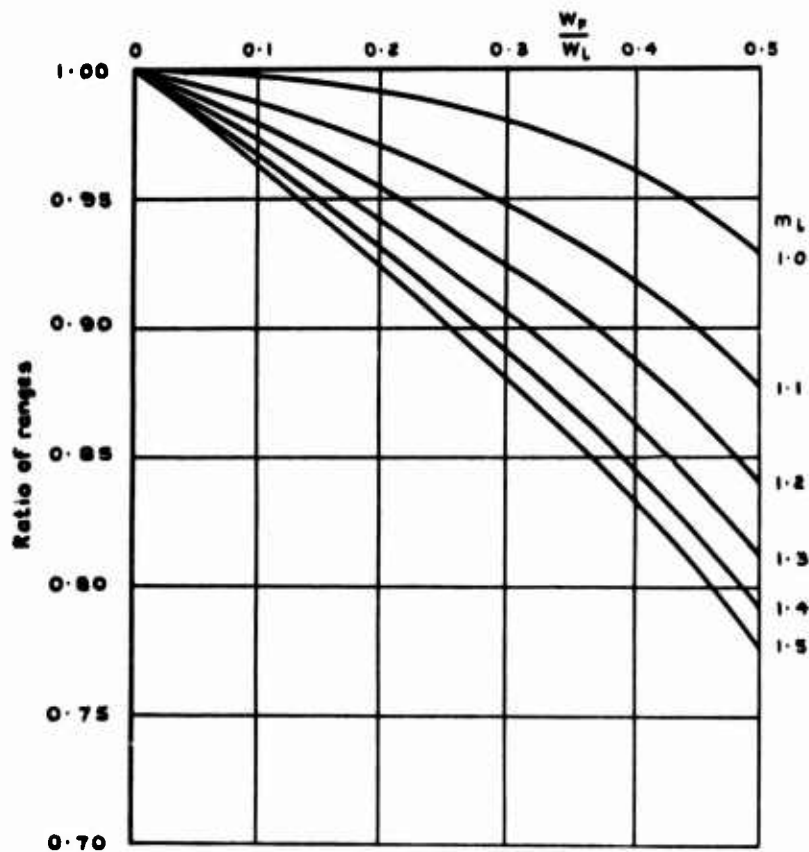


Fig.10 Ratio of range at constant *speed* and altitude to Breguet range, for the same conditions at start of cruise

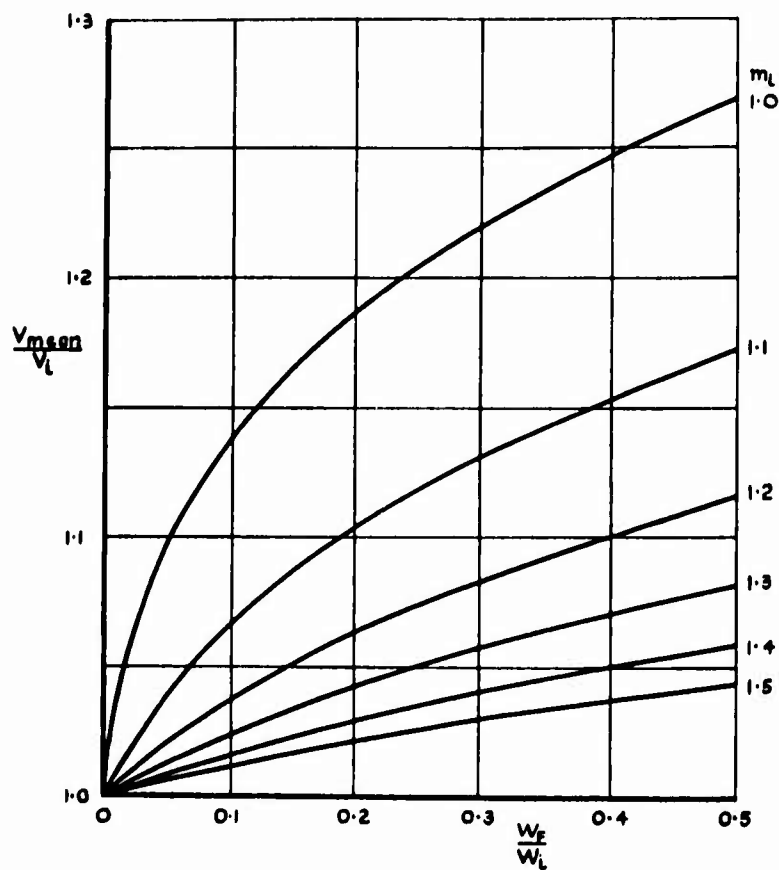


Fig.11 Ratio of mean speed to initial speed for cruise at constant *thrust* and altitude

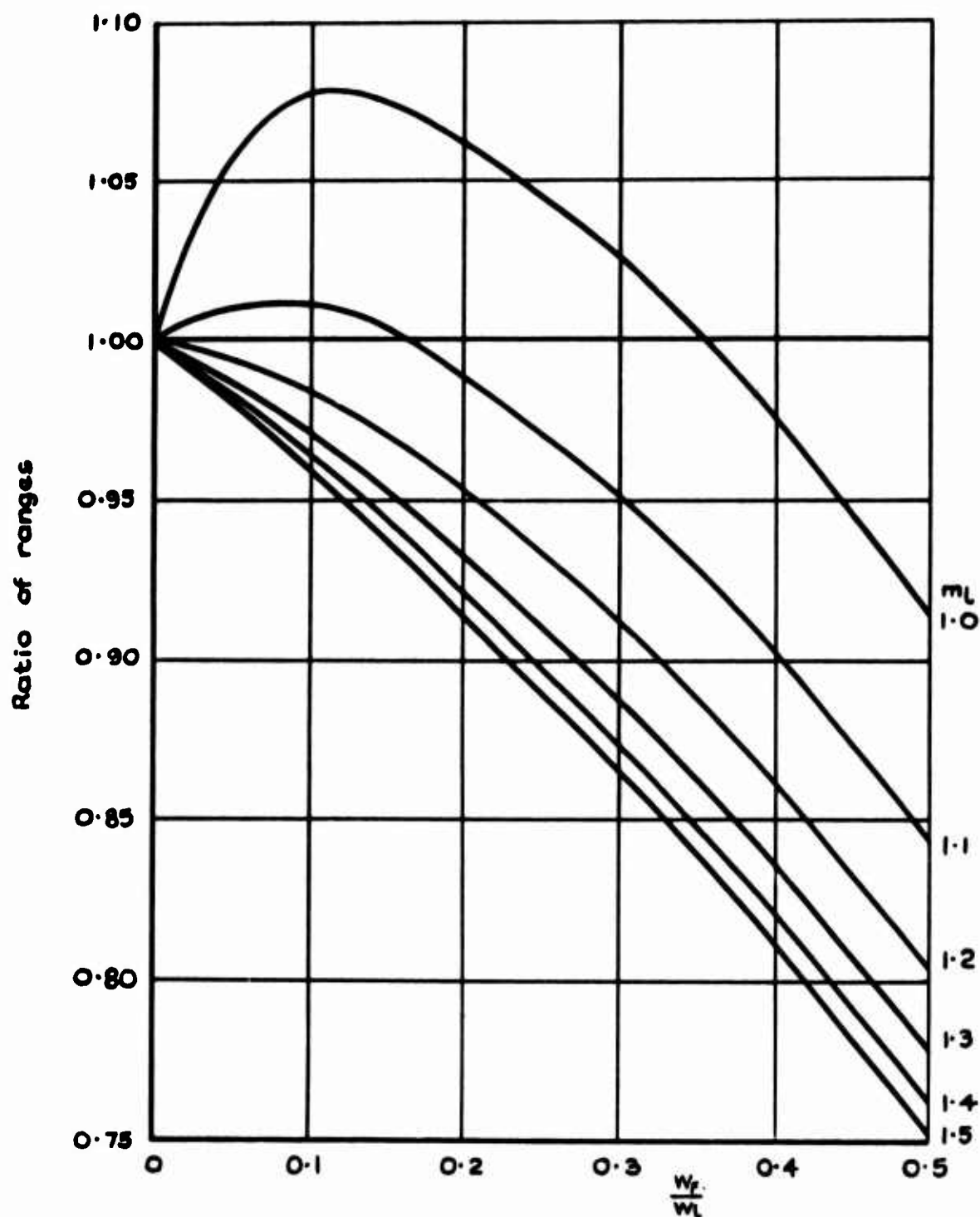


Fig.12 Ratio of range at constant *thrust* and altitude to Breguet range, for the same conditions at start of cruise

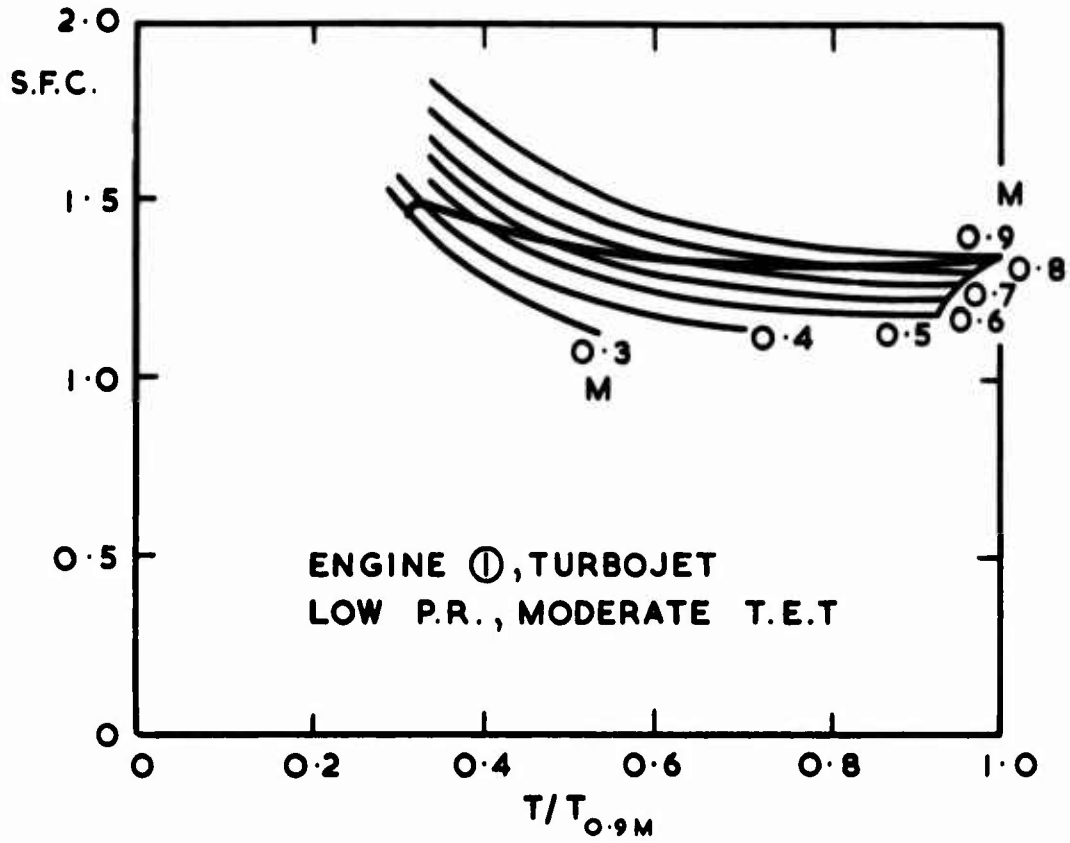


Figure 13

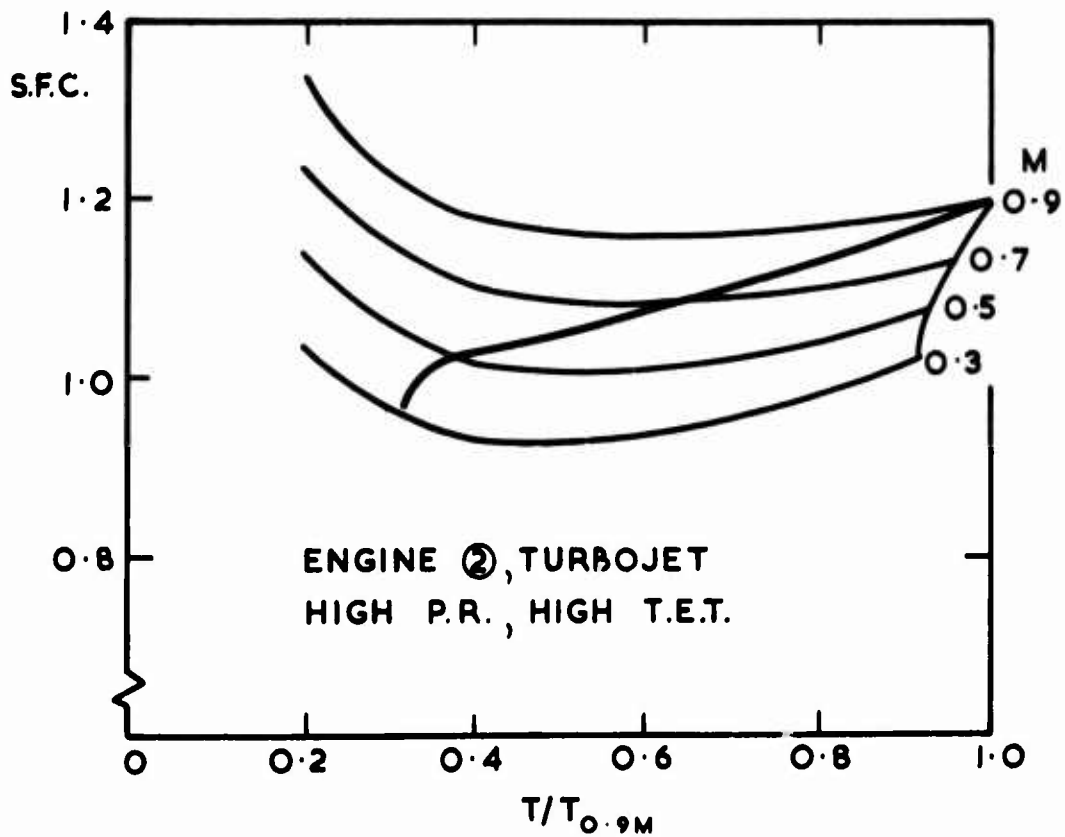


Figure 14

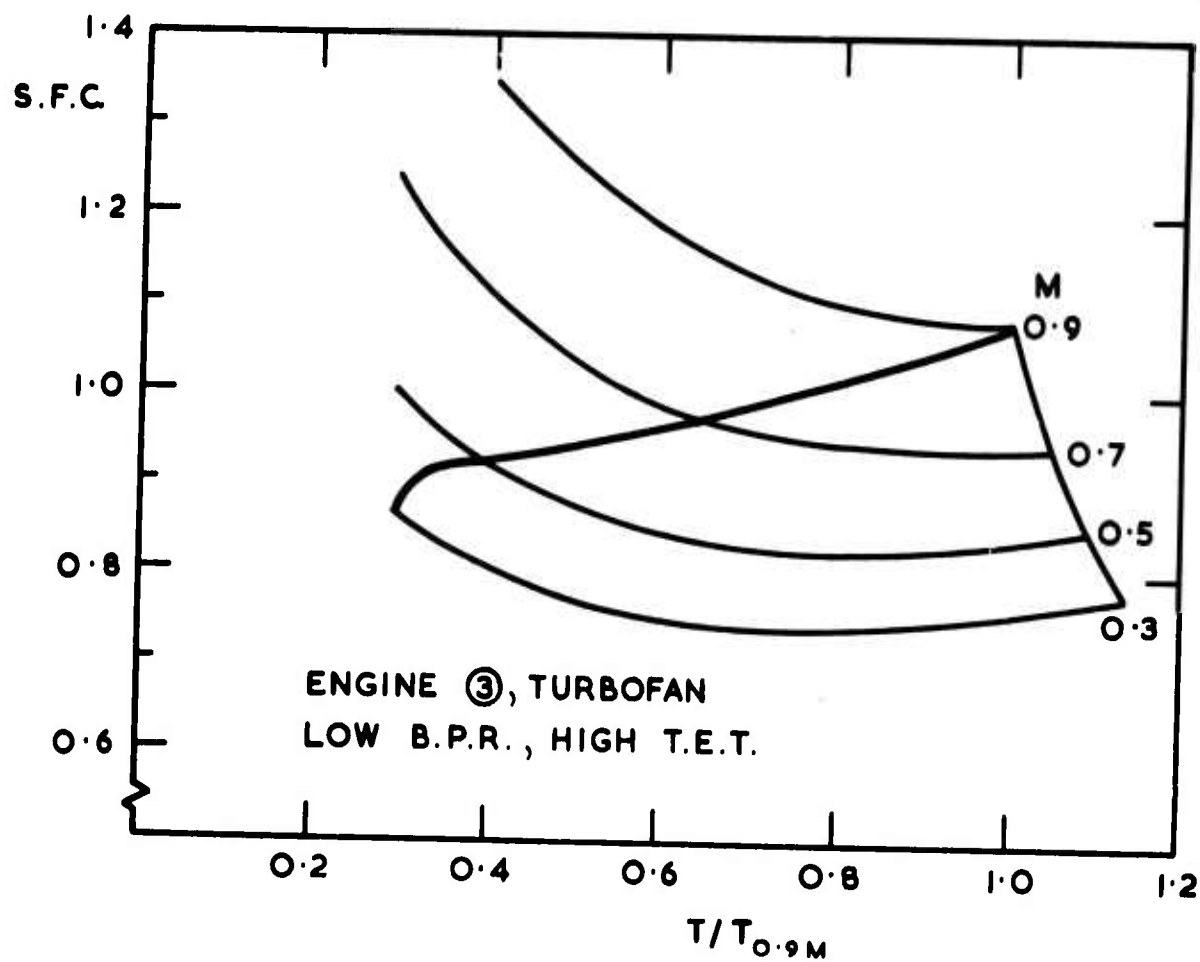


Figure 15

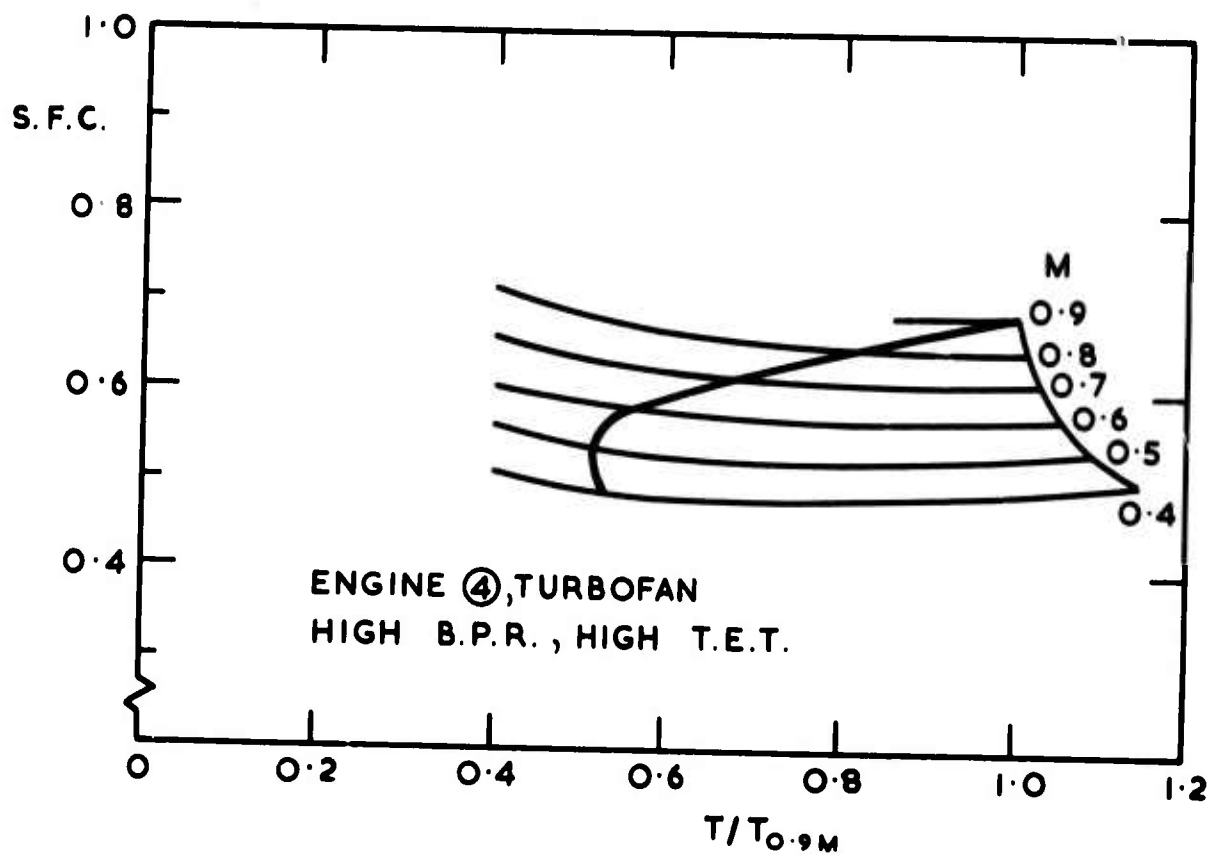


Figure 16

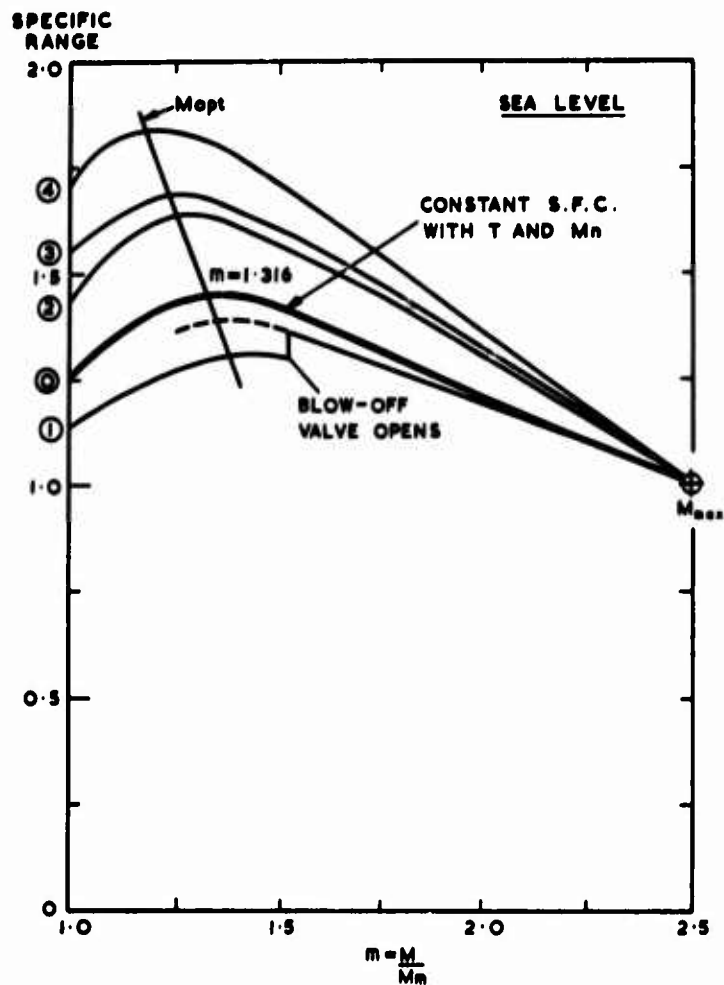


Figure 17

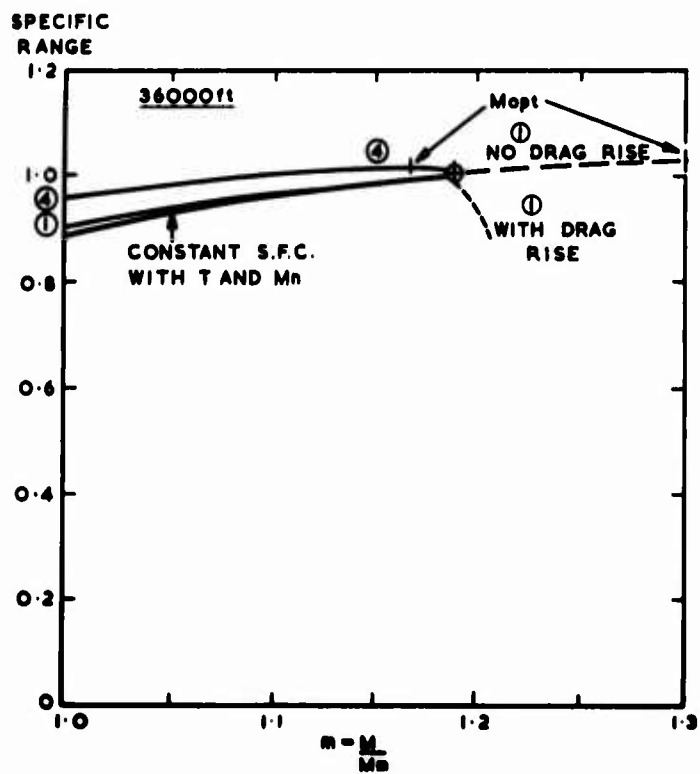


Figure 18

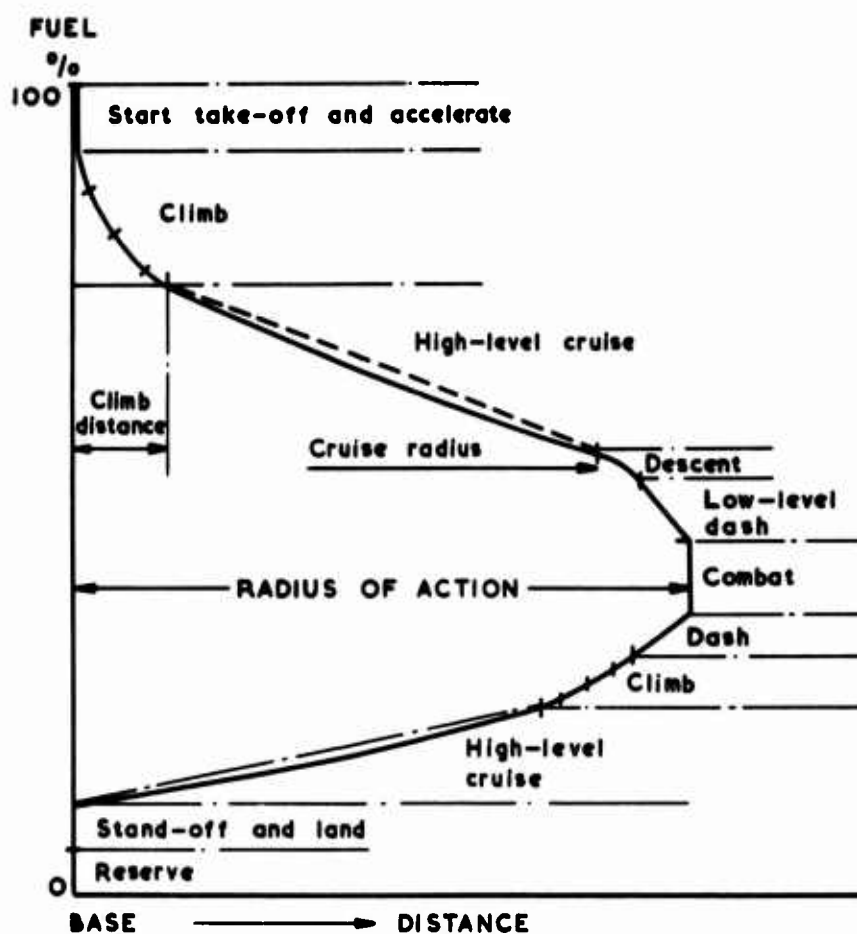
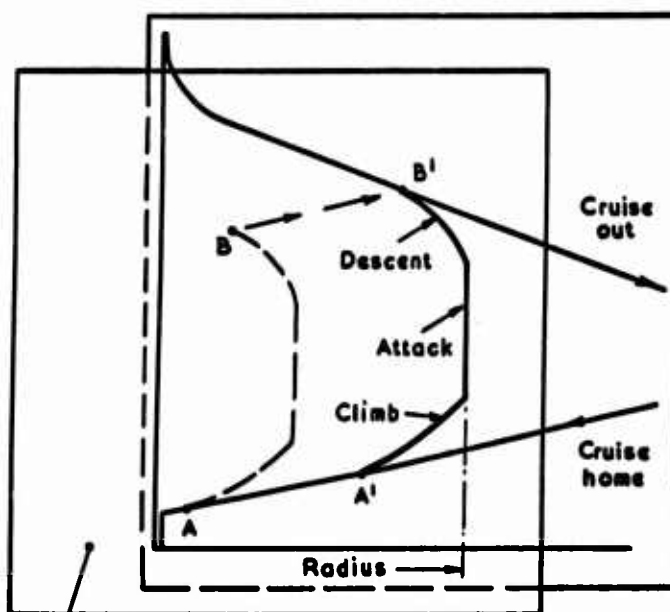


Figure 19



Transparent sheet with Descent - Attack - Climb profile : placed with point A on 'Cruise Home' curve and moved until point B lies on cruise out curve

Fig.20 Graphical determination of radius

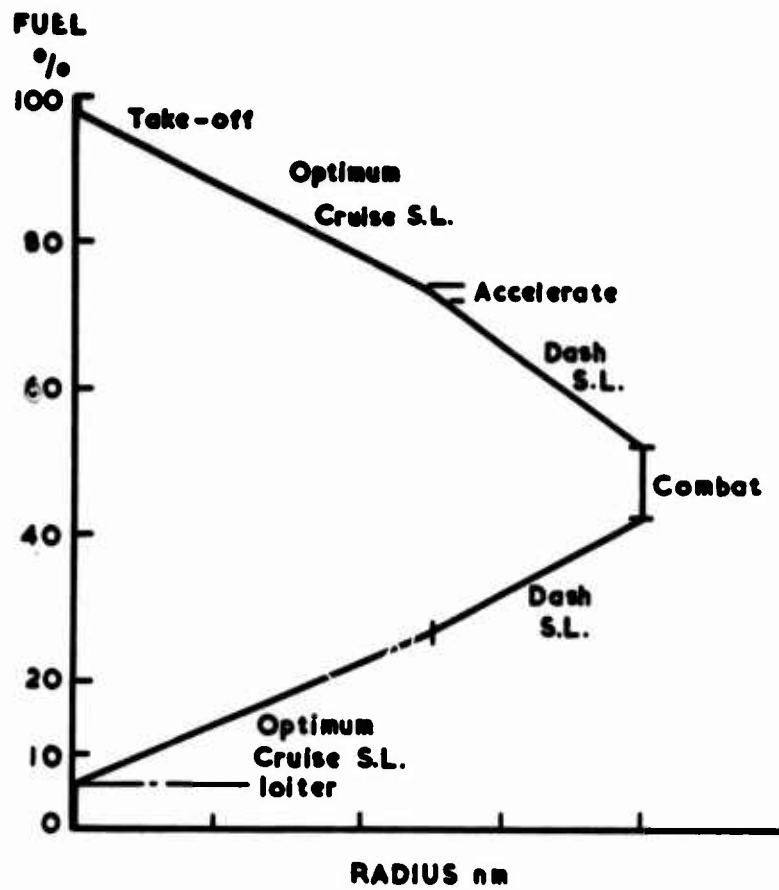


Fig. 21 Subsonic low-level tactical sortie

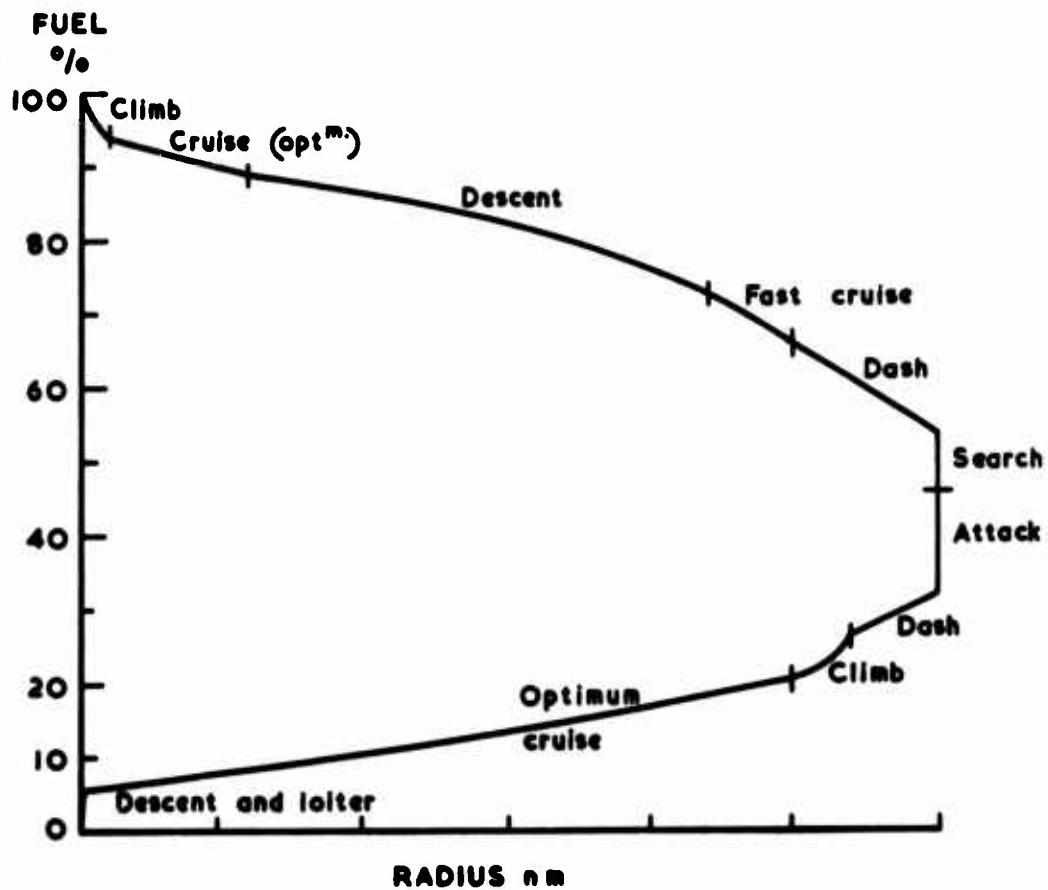


Fig. 22 Hi Lo Lo Hi attack sortie

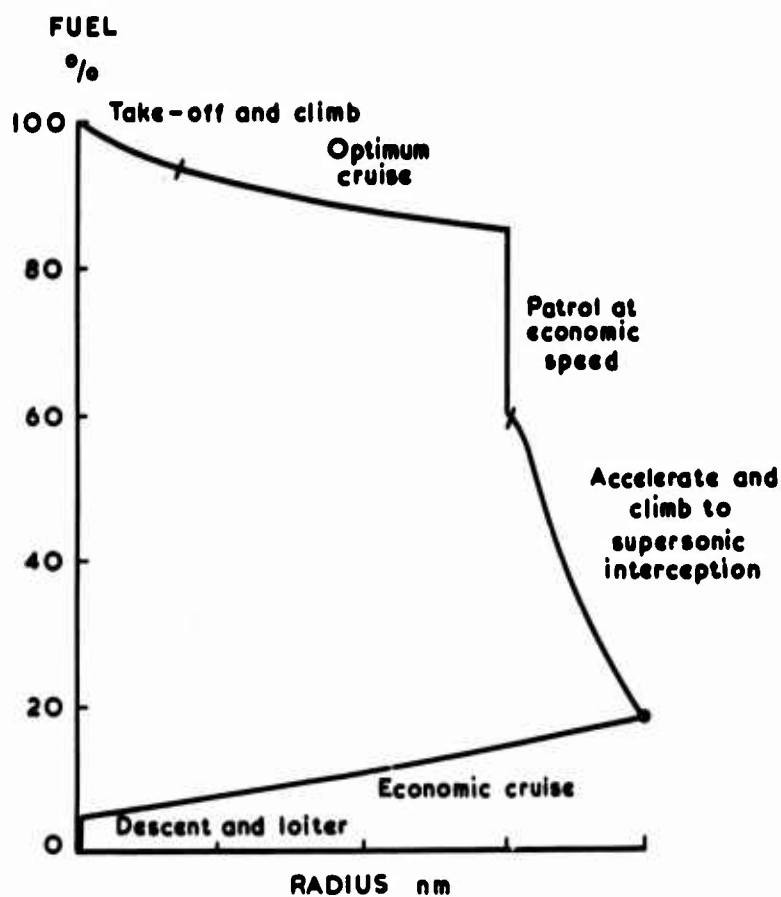


Fig. 23 Combat air patrol with supersonic interception

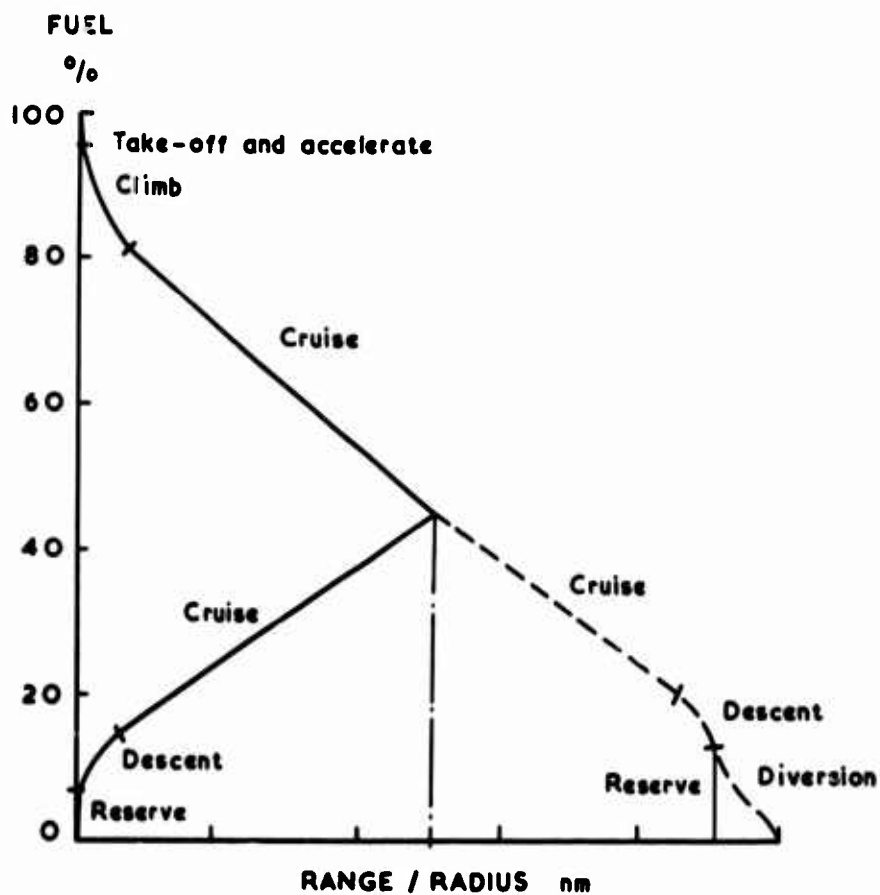


Fig. 24 High-altitude bomber (or transport)

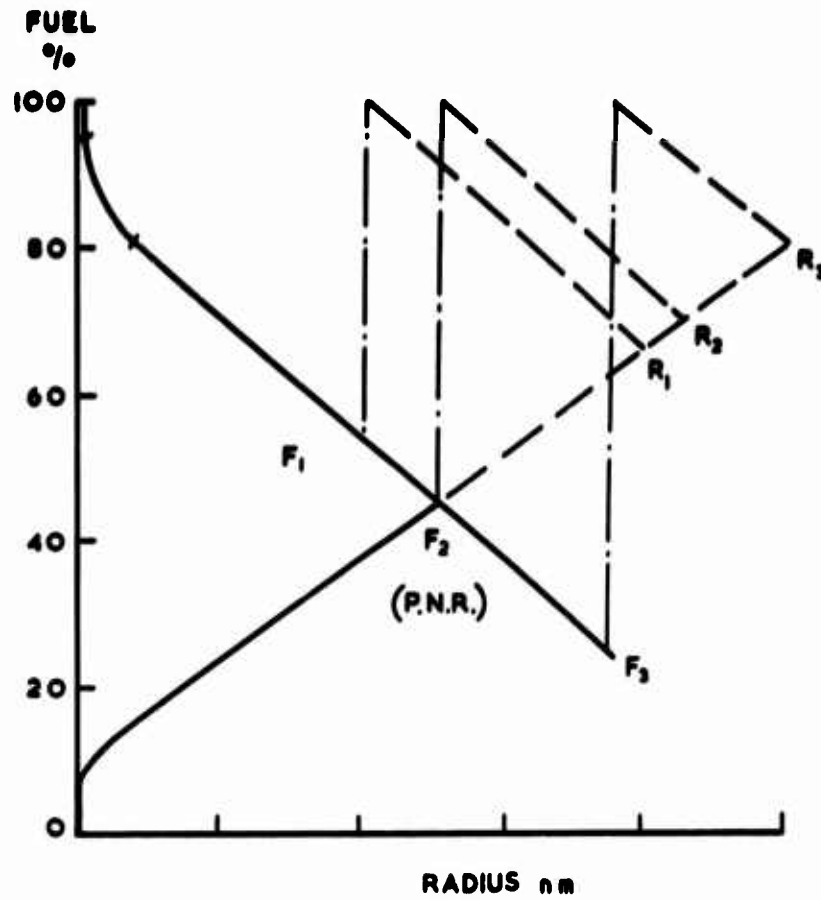


Fig.25 Bomber with in-flight refuelling

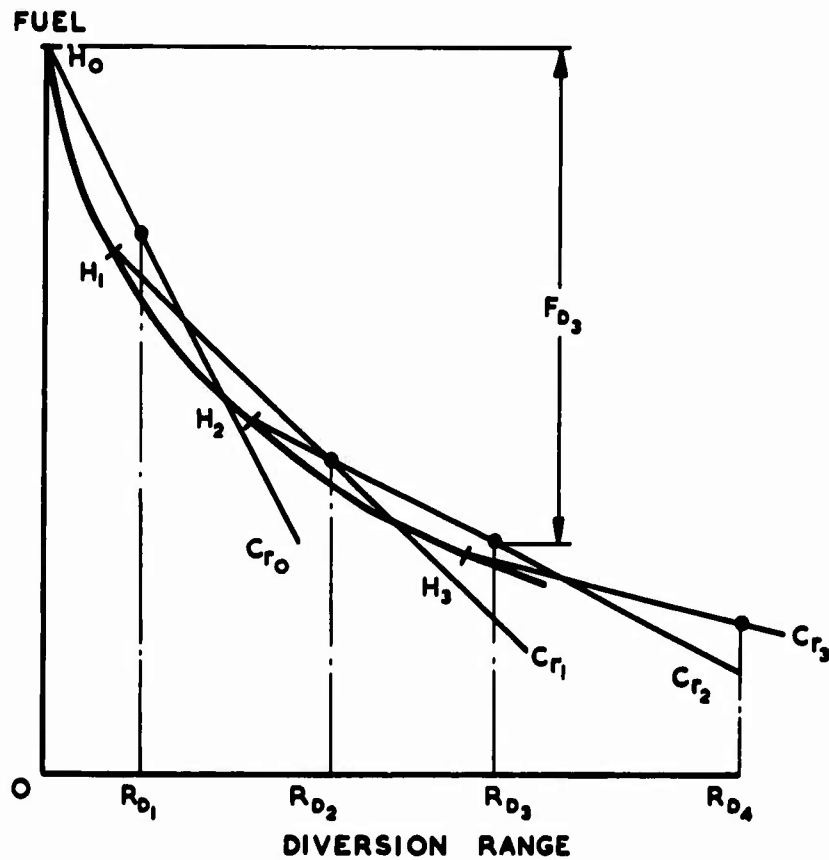


Fig.26 Fuel for diversions

**AIRFIELD PERFORMANCE PREDICTION METHODS FOR
TRANSPORT AND COMBAT AIRCRAFT**

by

John Williams

**Deputy Chief Scientific Officer
Aerodynamics Department
Royal Aircraft Establishment
Farnborough, Hampshire, UK**

CONTENTS

<u>PART I – INTRODUCTION AND BASIC CONCEPTS</u>		Page
1. INTRODUCTION		2-1
2. BASIC AIRFIELD PERFORMANCE CONCEPTS		2-1
2.1 Take-Off		2-1
2.2 Landing		2-3
2.3 Operational Safety and Certification Aspects		2-4
 <u>PART II – TAKE-OFF AND LANDING FACTORS</u>		
3. TAKE-OFF FACTORS FOR CONVENTIONAL AIRCRAFT		2-6
3.1 Take-Off Speeds		2-6
3.2 Airfield Take-Off Distances		2-7
3.3 Take-Off Climb Gradients		2-8
4. SPECIAL TAKE-OFF FACTORS		2-9
4.1 Slender Wing Aircraft		2-9
4.2 STOL Aircraft		2-10
4.3 Combat Aircraft		2-11
5. LANDING FACTORS FOR CONVENTIONAL AIRCRAFT		2-12
5.1 General Background		2-12
5.2 Landing Speeds: Reference Method		2-13
5.3 Airfield Landing Distances		2-14
5.4 Climb-Out Gradients		2-15
6. SPECIAL LANDING FACTORS		2-15
6.1 Slender Wing Aircraft		2-15
6.2 STOL Aircraft		2-16
6.3 Combat Aircraft		2-16
 <u>PART III – SPECIFIC PREDICTION TECHNIQUES</u>		
7. SIMPLE CORRELATION OF AIRFIELD PERFORMANCE		2-17
7.1 Take-Off Distance		2-17
7.2 Landing Distance		2-17
8. TAKE-OFF GROUND-RUN PREDICTION		2-17
8.1 Basic Formulation and Force Contributions		2-17
8.2 Simplified Distance Integration with Thrust Variation		2-17
8.3 Equivalent Mean-Acceleration Approximation		2-18
8.4 Rotation to Lift-Off Attitude		2-18
8.5 Generalised Ground-Run Equations (Powered Lift) and Step-by-Step Integration		2-18
9. TAKE-OFF AIRBORNE PATH PREDICTION		2-18
9.1 Basic Formulation		2-18
9.2 Circular-Arc Flare-Up and Empirical Correlation		2-18
9.3 Constant C_L Flare-Up and Empirical Correlation		2-19
9.4 Constant Pitch-Rate Flare-Up		2-19
9.5 Generalised Airborne-Path Equations (Powered Lift) and Step-by-Step Integration		2-20
10. LANDING GROUND-RUN PREDICTION		2-20
10.1 Basic Formulation		2-20
10.2 Simplified Distance Integration		2-20
10.3 Generalised Ground-Run Equations (Powered Lift) and Step-by-Step Integration		2-21

	Page
11. LANDING AIRBORNE PATH PREDICTION	2-21
11.1 Basic Formulation	2-21
11.2 Circular-Arc Flare and Speed Loss Estimation	2-21
11.3 Distance and Touch-Down Speed Meeting BCAR Requirement	2-21
11.4 NASA Three-Phase Model for Airborne Manoeuvre	2-21
11.5 Generalised Equations (Powered Lift) and Step-by-Step Integration	2-22
12. CONCLUDING REMARKS	2-22
REFERENCES	2-23
FIGURES	2-25

AIRFIELD PERFORMANCE PREDICTION METHODS FOR TRANSPORT AND COMBAT AIRCRAFT

John Williams

PART I – INTRODUCTION AND BASIC CONCEPTS

1. INTRODUCTION

This paper is intended to analyse and synthesise some essential background for the evaluation and prediction of the airfield performance of turbo-jet and turbo-fan aircraft projects designed for CTOL/RTOL or STOL operation (Fig.1). Relevant aircraft configurations (Fig.2) include^{7,8} those incorporating conventional wings with moderate values of sweep, thickness-chord ratio and aspect ratio; slender wings with highly-swept thin wings of low aspect-ratio; and powered wing-lift augmentation or direct engine-lift for STOL at least. While turbo-jet and turbo-fan types of aircraft are mainly treated here, some of the discussion is of interest also for propeller and rotary-wing aircraft.

In Part I, basic airfield performance concepts and frameworks are first clarified with respect to the major individual segments of normal take-off and landing operations, comprising: –

Accelerating and decelerating ground run;
Rotation to lift-off and from touchdown;
Airborne flare, up and out;
Climb-up and descent-approach.

Operational safety and certification aspects are then introduced, not only by reference to current regulations based largely on extrapolation from existing experience, but also by outlining possible novel treatments now envisaged in terms of forward estimation of "probability-levels" for "failures" and deficiencies" with new projects.

In Part II, the complex factors involved in airfield performance prediction are formulated separately for take-off and landing. Special attention has to be paid to the nature and magnitude of performance margins likely to arise from typical handling/airworthiness/certification demands, especially as regards operational restraints on relevant aircraft speeds and attitudes, airfield distances and climb gradients; proper specification of mandatory official requirements is of course not intended. The various factors are illustrated first by consideration of conventional CTOL transport aircraft for preciseness, most of the fundamental aspects at least being also of some significance for other aircraft types. Clarification of special features peculiar to new slender-wing CTOL aircraft and to STOL aircraft with lift-augmentation is then attempted, as well as of the simpler treatments often tolerated currently for project studies on combat aircraft as distinct from transports.

In Part III, specific prediction techniques are set down in "notebook form", with critical comments on diagrams showing the primary features. Firstly, a brief appraisal is made of simple correlation treatments for the rough estimation of overall take-off and landing distances. Possible analytical treatments of the individual segments of take-off and landing operations are then examined in more detail. Particular attention is devoted to the assumptions necessary for the provision of tractable theoretical models and to the empirical factors inherently involved for satisfactory practical prediction. The sensitivity of airfield performance comparisons to the specific choice of technical and operational assumptions is also illustrated. Finally, attention is drawn to some relevant aspects not analysed here, in particular the evaluation of aircraft noise and its implications on airfield performance capabilities.

2. BASIC AIRFIELD PERFORMANCE CONCEPTS

2.1 Take-Off

Nature of Take-Off Path

"Horizontal" take-offs, proceeding from rest at one end of an airstrip to clear a screen/barrier at the other, can be introduced conveniently by reference to Figure 3, where variations of aircraft height, pitch angle and speed with horizontal distance are illustrated qualitatively.

The *ground-run distance* comprises:

- (i) The primary ground-run during which the aircraft accelerates from rest to its "rotational speed" V_R , i.e. normally maintaining its ground attitude unchanged.
- (ii) The secondary ground-run during which conventionally the aircraft rotates to a higher wing incidence, or more generally generates lift-augmentation by other means, while still accelerating slightly to the "lift-off" speed V_{LO} .

The *airborne distance* comprises:

- (i) The flare-up when airborne, with the aircraft possibly still rotating and/or accelerating to provide excess lift normal to the local flight path. Sometimes, the screen may be cleared before the flare is completed.
- (ii) A further short steady climb, if the flare is completed before reaching the screen, in order to clear the appropriate height with adequately safe speed V_2 . For certification or comparative purposes the screen height is usually prescribed as 10.5 m (35 ft) or 15 m (50 ft) with civil or military specifications respectively.

Ground-Run

For conventional runway operation, only some 10% to 20% of the propulsive energy is dissipated by rolling friction or aerodynamic drag during the ground run. Thus, from the simplest first-order considerations (Fig.6) relating:-

the mean accelerating-thrust T (during the ground-run distance S_G) to the aircraft terminal energy $\frac{1}{2}(W/g)V_{LO}^2$ at lift-off,

$$S_G \approx \frac{1}{2}(W/g)V_{LO}^2(1/T),$$

i.e.
$$S_G \approx (W/S)(W/T)(1/C_{L,LO}) \frac{1}{g\rho}.$$

The advantages of high installed thrust/weight ratio (T/W), high aircraft lift-coefficient at lift-off ($C_{L,LO}$), and low wing-loading (W/S) are immediately apparent as regards minimisation of ground-run distance. For long-range conventional transport aircraft, intended for CTOL operation with $T/W \approx 0.2$, the take-off ground run and the time required may typically exceed 1500 m (5000 ft) and 50 sec respectively. In contrast, for short-range aircraft intended for STOL operation with $T/W \approx 0.6$, the take-off ground run and the time required could be reduced to say about one-sixth and one-quarter respectively, taking also into account the relevant increase in $C_{L,LO}$ and decrease in W/S .

Flare-Up

The "flare-up" tends to present conditions not so amenable to trivial first-order analysis, even for conventional aircraft, since piloting techniques can play a major role and can vary widely with the aircraft type as well as the pilot. The crudest assumption, that the steady climb angle γ_c (away from ground) is achieved immediately and maintained, usually underestimates significantly the airborne distance S_a from lift-off to the screen height h_s . Thus (Fig.6),

$$S_a > h_s/(\tan \gamma_c) \approx h_s/\gamma_c,$$

where
$$\gamma_c = \sin^{-1}[(T - D)/W] \approx (T/W) - (D/L) \text{ rad}.$$

Simple-arc flare paths (concave upwards) can represent more reasonable approximations, as discussed more fully later (Section 9.2). For example, an elementary circular-arc path tangential to the ground at lift-off and to the steady-climb path at the screen (Fig.6), gives simply

$$S_a \approx (2h_s/\gamma_c).$$

Although crude, such arguments can demonstrate forcibly the significance of high lift/drag ratio (L/D) along with high lift conditions at and following lift-off, as well as of high thrust/weight ratio (T/W). They illustrate also the demand for capability of generating appreciable excess lift coefficient and/or speed rise during the flare, to provide the required normal (centripetal) acceleration.

Climb

Climb capability after completion of the flare is significant also for reasons other than clearance of the "regulatory" screen height. These include safe and acceptable clearance of surrounding terrain or obstacles, and more recently the compliance with noise restrictions. Reference will be made later (Section 3.3) to different segments of the climb path, for various conditions of the aircraft configuration, including engine failure. To ensure good climb capability over the various segments, the advantages of high L/D are again obvious for the relevant climb configurations, as well as high T/W commensurate with environmental noise constraints. Such demands for maximum L/D to meet climb-angle requirements, or even to reduce airborne-path distance, can conflict of course with the preference for very high lift-coefficients at lift-off speed to reduce the ground-run distance.

Engine Failure

In the event of an engine failure, the nett available T/W for aircraft acceleration and/or balancing the drag at high lift can become especially critical. Then, not only does a significant reduction in thrust occur – even with the other engine powers raised to emergency rating – but also noticeable drag increases can arise from wind-milling of the dead engine and from trimming out the asymmetric thrust. This leads naturally later to the formulation of a variety of possible safety criteria as regards minimum speeds, distances and climb gradients to be attainable with a critical engine failure. This includes also a requirement for abandoning the take-off during the ground run, by decelerating to rest, if engine failure occurs before a critical Decision Speed (V_1) is reached.

2.2 Landing

Nature of Landing Path

“Horizontal” landings, proceeding from a steady descending approach so as to clear the screen/threshold at one end of the airstrip and come to rest before the other, are illustrated qualitatively in Figure 5. While the variations of aircraft height and speed with horizontal distance during landing may appear broadly similar in character to those for take-off in reverse, the variations of pitch angle tend to be substantially different in the airborne phase.

The *airborne distance* can again comprise:

- (i) The final part of the steady descent, typically 3° from the horizontal for CTOL. But this contribution may not arise with very steep descents (e.g. STOL), if the flare has to be started before reaching the screen to preclude the need for excessive normal accelerations. For certification or comparative purposes, the landing threshold height is usually taken as 9 metres (30 ft) and sometimes 15 m (50 ft).
- (ii) The flare distance, to ensure a tolerable vertical velocity at touchdown, typically 0.6 m/sec (2 ft/sec) for CTOL, often with appreciable reduction of the horizontal speed at touchdown (V_{td}) to below that at the threshold (V_{AT}).

The *ground-run distance* comprises:

- (i) The initial ground-run from touchdown when conventionally the aircraft rotates down to ground attitude (all wheels touching), or more generally any special lift-augmentation is cancelled, during which period some deceleration occurs and braking is initiated.
- (ii) The major ground-run with the aircraft at ground attitude, where rapid deceleration is obtained from wheel brakes, air brakes and thrust reversal, or possibly even by drag-parachute deployment in the case of military aircraft and prototype testing.

Airborne Phase

The landing airborne distance typically accounts for one-third to one-quarter of the overall landing distance, but the nature of the flare is of course highly relevant. Neglecting any possible “float” period before touchdown and referring simply again to steady-descent or to tangential circular-arc paths from threshold to touchdown, the airborne-distance might crudely be expected to satisfy the relation (Fig.6)

$$h_s/\gamma_a \leq S_a \leq 2h_s/\gamma_a,$$

where

$$\gamma_a \approx (D/L) - (T/W).$$

In the absence of reverse thrust during the airborne phase, this implies the generation of a large enough drag (low L/D) to provide the required γ_a and to reduce the airspeed during the flare, while still maintaining a high C_L to ensure adequate excess lift in the flare for checking the vertical velocity and for appropriate manoeuvrability.

Ground Run

For the landing ground-run distance, the concept of a sensibly constant deceleration d_G , can again be employed, leading to the simple relation

$$S_G \approx \frac{1}{2} d_G V_{td}^2$$

where $d_G \approx 0.35 g$ for conventional transports.

However, this tends to be rather inadequate because of the complexity of the retardation process with modern aircraft. In particular, different time delays can arise between touchdown and full application of the various possible braking devices, while some distinction may be necessary between wet and dry runway operations.

Climb-Out

Even with landing, climb-out capability becomes of special interest for the emergency cases of a discontinued approach – just before reaching the threshold or a baulked landing – after passing the threshold. Although there arise here broadly similar considerations to the take-off climb, the starting conditions tend to be rather different at the climb-out decision point during landing, when the engines are at low thrust and the aircraft at high drag until appropriate changes can be made.

2.3 Operational Safety and Certification Aspects

Current Airworthiness Requirements

Present safety and certification criteria for conventional aircraft are based largely on qualitative extrapolation of past experience. Moreover, even for conventional civil transport aircraft, an internationally-recognised set of certification requirements has not yet been agreed world-wide, though the collaboration between western countries is steadily improving, particularly as regards compatibility and future improvements.

For conventional *civil transport* aircraft, the two sets of requirements most frequently cited are:

- (i) BCAR (Section D):– British Civil Airworthiness Requirements produced by the Air Registration Board¹¹.
- (ii) FAR (Part 25):– United States Federal Aviation Requirements produced by the Federal Aviation Agency¹².

Light aircraft, broadly with take-off mass below 5700 kg (12,500 lb), are required to satisfy slightly less stringent requirements defined by BCAR (Section K) and FAR (Part 23), but will not be referred to again specifically here.

As regards conventional *military transport* aircraft, civil standards are usually adopted for normal peacetime operations in general passenger and freight roles, but higher risk standards may be tolerated for a particular role or for operation in military emergency conditions. More generally, there exist formal sets of requirements also published for all military aircraft, for example:–

- (i) UK Av P 970 (Parts 6 and 9):– Design Requirements for Service Aircraft¹³.
- (ii) US AF Mil-F-008785:– Flying Qualities of Piloted Airplanes¹⁴.

Revision Demands

Such airworthiness requirements are lengthy and involved, with much cross-referencing and qualification as properly appropriate to mandatory certification terminology. Changes can and must be undertaken continually in the light of operational experience and to cover new operational techniques or fresh hazards. Complete revisions also become necessary when novel types of aircraft are to be introduced, such as presently being undertaken for supersonic transports^{15,16} and STOL transports^{17,18}. The main purpose of such requirements could be regarded as to ensure reduction of the risks to passenger and to public safety down to acceptable levels, without making flying costs unnecessarily prohibitive. Some progress is now being made towards more quantitative analytical treatments of likely risks and effects in the formulation of new safety and certification criteria, as exemplified already from their application by ARB to new concepts involved with Autoland and Concorde. Such treatments naturally involve safety analyses relating statistically the probability of occurrences to the effects they may produce, so that essential ingredients comprise numerical specification of safety targets and reasonable allocation of risks among the various possible causes.

As regards overall safety targets for future civil transport aircraft, these should surely be at least as good as for current jet transports. Figure 7 shows some representative data¹⁷ over the decade 1959-1969 for the annual variation of the number of aircraft flying hours and the number of fatal accidents (one or more persons killed in an aircraft); together, these give the annual accident rate which is seen to be levelling off at about one per 10⁶ hrs. Thus, for example on the assumption that only about one-fifth of such accidents should arise from airworthiness causes and that only about one-half should be attributed to airfield operation (take-off and landing), the average probability of a fatal accident from airworthiness causes during airfield operation would become

$$1 \times \frac{1}{5} \times \frac{1}{2} \text{ per } 10^6 \text{ flying hours}$$

i.e. this particular safety target should not exceed 10⁻⁷ per flying hour, or perhaps 10⁻⁷ per take-off + landing.

Next, as regards airworthiness risks, about ten broad categories of appropriate qualities might be listed as in Figure 8 and, for our crude illustration, we might allocate rationally an even distribution of risks to these categories. Then, the safety target for the average probability of a fatal accident during airfield operation from one of these categories, e.g. performance aspects, should be at least

$$10^{-8} \text{ per take-off + landing.}$$

Furthermore, in performance analysis, certain critical conditions have to be considered and accounted for, e.g. when the aircraft take-off mass is limited to satisfy an airfield runway length restriction. Provided such "critical conditions" are not a regular occurrence, the relevant probability might then perhaps be allowed to deteriorate, say by a factor of 10 (to 10^{-7} per TO + L). Again, flight may take place under "critical conditions" at the same time as other non-accountable factors are also at their declared limits (e.g. maximum permitted crosswind). Under such occasional "minimum conditions", the relevant probability might perhaps be allowed to deteriorate further, again say by a factor of 10 (to 10^{-6} per TO + L).

For new projects, Manufacturers with the aid of Airworthiness Authorities and R & D Establishments have naturally had to make extensive studies of variables (both accountable and non-accountable) which can affect the aircraft performance, handling and other qualities. However, in future, additional reference will be necessary to "probability level objectives" similar to but more sophisticated than those crudely illustrated above.

Scope of Present Analysis

The further discussions of safety and certification considerations here certainly cannot attempt formulation in probability terms at this time. They are intended to clarify and interpret some existing and possible new requirements of direct relevance to practical methods of estimation of airfield performance. Moreover, the particular arguments developed for this purpose must not be taken to agree necessarily or precisely with specific official airworthiness requirements.

PART II – TAKE-OFF AND LANDING FACTORS

3. TAKE-OFF FACTORS FOR CONVENTIONAL AIRCRAFT

3.1 Take-Off Speeds (Fig.9)

There are a large variety of aircraft speed conditions during the take-off phase which have become significant for reference in airfield performance calculations, operational monitoring, or certification codes^{11,12}. Figure 9 lists some of these in the normal order of magnitude, with quotation of some relative values which are currently considered advisable for conventional CTOL transports at least. The following discussion serves to illustrate the significance of such reference speeds and their inter-relationships, as background for performance estimation methods.

The *Decision Speed* V_1 provides a basic reference for a piloting decision as to whether to abandon or continue the take-off ($V < V_1$ or $V > V_1$) in the event of an engine-failure recognition at speed V . More particularly, from our viewpoint, it serves to define a "balanced field length" so that an engine failure can be dealt with safely at any stage of the take-off; by appropriately braking to a stop ($V < V_1$) or continuing on the remaining engines ($V > V_1$), as discussed in Section 3.2. Usually,

$$V_1 > V_{MCG}, \quad \text{the minimum control speed on or near the ground, beyond which it is possible to maintain adequate aircraft control (primarily by aerodynamic means) for take-off in the event of an engine failure.}$$

The *Take-Off Safety Speed* V_2 is essentially referenced as the lowest speed, as achieved by proper rotation and lift-off procedures, at which the aircraft must reach the screen height to ensure an adequate safe climb-out with a critical engine failure. Conventionally, its minimum acceptable value is prescribed by

$$V_2 > 1.1 \times V_{MCA}, \quad \text{the minimum control speed in free air with an engine failed,}$$

$$V_2 > 1.2 \times V_{S,1g}, \quad \text{the minimum speed in the free-air stall under 1 g conditions with power off or perhaps at a minimum.}$$

Essentially, these two simple requirements are intended to ensure five vital safeguards during take-off:—

- (i) Some reduction below target speed can be tolerated, still maintaining positive climb (see also Section 3.3).
- (ii) Some speed reduction due to atmospheric disturbance or pilot error can be accepted while still maintaining control.
- (iii) Lift margins are available for aircraft manoeuvres to climb, turn, etc.
- (iv) Incidence margins are available to preclude stall or loss of control from an up-gust.
- (v) With an engine-failure, possibly accompanied by speed errors, control can be maintained.

Later on, for STOL aircraft using powered lift augmentation, the difficulty of finding only *two* simple criteria to satisfy adequately these five safeguards will become apparent.

The *Rotation Speed* V_R is naturally the reference speed for the pilot to begin rotation of the aircraft from its normal ground attitude towards its lift-off condition, a typical mean rate of rotation being about 3°/sec for CTOL transports. The minimum acceptable value of V_R is specified conventionally by the following criteria:

$$V_R > 1.05 \times V_{MCA}$$

$$V_R > 1.1 \times V_{MLO}, \quad \text{the minimum lift-off speed all-engines}$$

$$\text{or } 1.05 \times V_{MLO}, \quad \text{if rotation is limited by lack of tail power or by the tail hitting the ground.}$$

Also, V_R must permit the take-off safety speed V_2 (with engine failure) to be reached at the screen, as already defined.

The *All-Engines Screen Speed* V_3 is also of interest since not only should this provide a more substantial safety margin appropriate to normal operation but also, as regards distance certification, the all-engines case can be more critical sometimes than the engine-failure case when taking into account the respective safety factors (see Section 3.2).

$$\text{Typically} \quad V_3 \simeq V_2 + 10 \text{ kn.}$$

The *Lift-Off Speed* V_{LO} , or more particularly the *Minimum Lift-Off Speed* V_{MLO} , is prescribed directly by conventional airworthiness requirements only insofar as V_R may in some instances be defined by it. However, the safety margins are intended to ensure that the normal V_{LO} exceeds V_{MLO} by an adequate amount, so that the stalling speed on or near the ground is not too closely approached, nor does slight over-rotation prove troublesome. Otherwise rapid degradation of Lift/Drag ratio and handling characteristics could then arise, preventing the safe attainment of V_2 or V_3 .

The *Minimum Stalling Speed* V_{MS} in free air is sometimes quoted for reference instead of $V_{S,1g}$, where the former is obtained by steadily decreasing flight speed – typically by 1 kn/sec. instead of under 1 g stalling conditions as implied by the latter; conventionally, both are determined power-off or at minimum power setting. The distinction between the two speeds is not necessarily trivial and has produced some misunderstandings in the past. Typically, V_{MS} may be as low as $0.94 V_{S,1g}$, so that the corresponding “maximum lift coefficient” C_{LMS} may be quoted at a value some 13% higher than the C_{Lmax} condition normally referenced for aerodynamic analysis.

Practical derivation (or demonstration) of the values for the speeds V_2 , V_R , etc. which meet the respective airworthiness certification requirements may necessitate some iteration procedures, to ensure that these values remain compatible with other aspects of practical and safe airborne manoeuvres with the specific aircraft during take-off. For example, starting with the minimum allowable rotation speed (from handling and airworthiness considerations), the resulting speed at screen height then may work out at a value higher than the minimum allowable value of V_2 ; this represents an acceptable take-off procedure. Otherwise, the calculations must be repeated with higher rotation speeds until a satisfactory screen speed is achieved. A thorough design study or the preparation of a flight operations manual will require these and allied studies to cover the whole operations envelope envisaged for the aircraft, including different take-off weights and configuration changes, as well as various environmental conditions.

3.2 Airfield Take-Off Distances (Figs.4, 12 and 13)

General Considerations

The minimum take-off distances needed for specific aircraft vary of course with the aircraft configuration and gross weight at take-off, the ambient temperature, altitude, wind, runway slope and runway condition. Relevant distances provided at a specific airfield may be defined conveniently as in Figure 4.

- (i) The “*take-off ground-run*” available is the length of *runway*, having a hard prepared surface compatible with the aircraft weight and undercarriage design.
- (ii) The “*take-off emergency distance*” available is the length of *runway* + *stopway*, where the stopway has a surface capable of supporting the aircraft with little damage, and possibly contains a specially-roughened strip or arresting device (e.g. for military use).
- (iii) The “*total take-off distance*” available is the length of *runway* + *stopway* + *clearway*, where the clearway is essentially free of large obstacles, thus permitting fly-over with little ground clearance, but does not necessarily have a solid surface (e.g. water).

In scheduling reference take-off distances for the certification of a specific aircraft and the preparation of an operations manual (or for project estimates), flight demonstration distances (or predictions) are required under representative conditions for both the all-engines case and the single-engine failure case, satisfying reference-speed safety rules as illustrated in the preceding section. To allow for general flying inaccuracies and random variations in everyday operation, different safety factors are then applied to the all-engines and engine-failure distances, as appropriate to acceptable normal operation and emergency operation respectively. The scheduled minimum distance requirements for the specific aircraft configuration and the particular environmental conditions are then taken as the worst of these. For other available airfield distances and different ambient conditions, the aircraft limiting weights (and speeds) are derived by careful analysis of a range of such flight checks (or estimates) covering the planned operations, the Flight Manual data being usually presented in graphical form to facilitate interpolation by the airline/service pilots for routine operations.

All-Engines Reference Distances

Conventionally, for transport aircraft, the minimum acceptable values of all-engine take-off distance may be quoted in two forms:

- (i) Factored total take-off distance = $(S_G + S_a) \times 1.15$
- (ii) Factored take-off run = $(S_G + \frac{1}{3} S_a) \times 1.15$.

Here, S_G and S_a represent respectively the demonstrated ground run distance (from start to lift-off) and airborne distance (from lift-off to screen height) satisfying other safety requirements, while there is incorporated a distance safety margin of 15%. This does not of course imply that inaccurate flying or neglect of changes in aircraft condition and environment can be tolerated. To the contrary, modern jet aircraft can be even more sensitive to abuse than their propeller-driven predecessors. For example, an increase of some 10% in the speeds used for lift-off or reached at screen height could more than absorb the distance safety margins, unless accompanied by corresponding increases in acceleration and climb capability.

Emergency (Engine-Failure) Reference Distance

This so-called "*Balanced Field-Length*" concept is intended to ensure that a single engine-failure at any stage of the take-off can be handled safely for the particular aircraft and environmental conditions, by alternative actions according as to whether engine-failure recognition occurs before or after a declared *Critical Decision Speed* V_1 is reached. This speed is prescribed so that, with a single engine failure there (Fig.12), the total acceleration-stop distance from rest to rest becomes identical with the total take-off distance to safely reach screen height, namely the balanced field-length. Thus,

- (i) Braking to a stop with engine-failure at $V < V_1$ provides a total acceleration-stop distance which is less than the balanced field-length.
- (ii) Continuation to screen height with engine failure at $V > V_1$ provides a take-off complete distance also less than the balanced field-length.

In current BCAR regulations for conventional CTOL transport aircraft¹¹, the *unfactored* balanced field-length is accepted as the emergency (engine-failure) reference distance. Reverse thrust (safely applied) may also be used in establishing the distance, but a 10% increase is then put on the measured stopping distance. For wet runway conditions the Decision Speed V_1 may be recommended to be somewhat less (\approx by 10 kn) than for dry conditions to ensure that the same accelerate-stop distance can be achieved. But there is then a risk period of a few seconds (≈ 4) after V_1 , during which engine-failure would imply clearance of a screen height reduced to about 4.5 m (15 ft).

Applicability

The scheduled take-off distances are usually determined by the emergency engine-failure reference distance (i.e. the unfactored balanced field length) for twin-engined aircraft, but by the factored all-engines distance for aircraft with more than two engines (Fig.13). It must be re-emphasised that, while these distances are intended to embrace the expected take-off performance of the aircraft including some safety margins to account for variability in routine service, other major operational factors have to be accounted for specifically in the aircraft flight-performance manual. These include, for example, changes in aircraft weight, airfield altitude, ambient temperatures, wind and runway accountability; to cover the flight operations scope planned for the aircraft.

3.3 Take-Off Climb Gradients (Figs.14 and 15)

The ability of an aircraft to maintain an adequate climb gradient $\gamma [\approx (T/W) - (D/L)]$, at speeds high enough to ensure acceptable handling characteristics, represents an important take-off consideration apart from the ground-run and flare-up distances involved. Conditions are of course particularly critical when an engine fails during take-off, tending to become especially important for twin-engined aircraft where about half the thrust is lost, and to become catastrophic for the single-engine aircraft! It should be noted that the speed for maximum rate-of-climb $(V_\gamma)_{\max}$ is normally above the take-off safety speed V_2 defining the minimum acceptable speed but, under critical conditions, acceleration to the higher speed is only warranted under exceptional conditions.

For the analysis and certification of CTOL transport aircraft at least, it is common practice to divide the take-off climb into a number of nominally distinct segments (Fig.14). These include:—

- (i) A *first segment* shortly after lift-off, while the undercarriage and high-lift flaps are still extended — with consequent drag penalty, and with the generally favourable effects of ground proximity excluded.
- (ii) A *second segment*, typically extending to a height of about 120 m (400 ft), during which the undercarriage is retracted but the high-lift devices may still not be altered from their take-off setting.
- (iii) A *third segment*, further extending to a height of about 450 m (1500 ft), during which different settings can be selected for the high-lift devices.

Beyond this, the aircraft cruise-climb phase is usually considered to begin, with appropriate crediting of the further horizontal distance to range or radius-of-action, the aircraft configuration and climb path being optimised commensurate with local demands as regards terminal airspace control and noise-abatement procedures.

The specific minimum climb-gradients to be achieved (BCAR) in each of the three segments, with one engine failed and the appropriate aircraft configuration, are listed in Figure 14 for conventional transports with 2, 3 and 4-engined installations. The second segment requirement nearly always provides the critical design case as regards climb gradients. Here, a nett 2% gradient (from the screen height) is considered to be essential to clear obstacles and terrain along the take-off path, plus some margin above this to account for variations in operation, e.g. 1% for 4-engined aircraft; giving the mandatory gross gradients quoted for rectilinear flight, e.g. 3% for 4-engined aircraft. There is a small but noticeable alleviation of climb-gradient requirements as the number of installed engines is decreased from 4 to 2, which presumably reflects the associated halving of the probability of an engine failure. While the performance of all engines generally becomes superior, in view of the relatively higher installed thrust required with 2 engines (Fig.15), the risk of twin-engined failure must also become negligible.

4. SPECIAL TAKE-OFF FACTORS

4.1 Slender Wing Aircraft

General Background

Slender wing aircraft intended for cruise flight at supersonic speeds have thin wings of low aspect-ratio with highly swept leading-edges; e.g. $t/c \approx 0.05$; $A \approx 1.5$, $\Lambda_{LE} \approx 65^\circ$. Their low speed aerodynamic characteristics differ significantly in several respects from those of conventional aircraft⁷ because of the markedly different flow characteristics through the incidence range.

In particular:

- (i) Stalling in the sense of a significant lift loss arising from flow breakdown at high incidences is often ill-defined for slender wings and in any case can occur well outside any practically usable value of incidence; e.g. $\alpha \approx 30^\circ$ at zero sideslip. This demands a new reference speed to replace $V_{S,lg}$.
- (ii) The combination of low aspect-ratio with leading-edge vortex flow leads to high induced drag at high incidences, the lift acting effectively normal to the wing plane. This leads not only to the low L/D ratios (e.g. $L/D \approx 3$ at $\alpha = 20^\circ$) which is fortunately counterbalanced by the high T/W , but also to relatively high minimum drag speeds (aggravated further by the absence usually of part-span trailing-edge flaps); so that take-off occurs well below minimum drag speed.
- (iii) The lift-incidence curve is decidedly non-linear and often accompanied by a nose-up pitching moment at very high incidences.
- (iv) The favourable ground effect on lift can be significant, so that its loss as the aircraft climbs away has to be made up by further increase of wing incidence, and of course vice versa.

Take-Off Speeds (Fig.10)

In many respects, conventional transport rules may be expected to apply but, to preclude difficulties in defining a practical stall speed and to allow for the increased significance of drag, two new reference speeds have been suggested¹⁵, replacing the conventional $V_{S,lg}$:

- (i) V_{MIN} , the minimum demonstrated flight speed in steady rectilinear flight; sometimes chosen as the maximum of measurements made with the engines at minimum thrust or at 75% maximum appropriate thrust. Typically, it is recommended that the take-off safety speed

$$V_2 \geq 1.25 V_{MIN}.$$

- (ii) V_{ZRC} , the zero-rate-of-climb speed (one engine failed). Recent simulator studies at NASA¹⁶, in conjunction with British/French experience on Concorde development and an FAA flight test programme on an F102, have suggested the further restraint

$$V_2 \geq 1.125 V_{ZRC}.$$

More generally, speed considerations become intimately related with the probability of speed errors in regular operations, along with their effects on take-off distances and climb gradients as will be discussed later.

Airfield Take-Off Distances (Fig.13)

Here again, the conventional transport rules may be largely retained. However, the higher thrust/weight ratios and lower lift-coefficients of slender aircraft imply larger accelerations in the ground run and higher take-off speeds, which together lead to greater sensitivity of take-off distances (and speeds) to piloting variations such as time leads and lags. Moreover, greater difficulties can arise in ensuring good speed holding and good control characteristics. Thus more error/abuse predictions (or demonstrations) should be added for slender aircraft; typically including early or late rotations (say by ± 3 sec or $\pm 5\% V_R$) and more rapid rotations, without exceeding the otherwise scheduled distances while maintaining an acceptable flight path.

Take-Off Climb Gradients (Figs.14 and 16)

The sensitivity of climb-out performance to speed variations is well illustrated by Figure 16 (from NASA¹⁶); where a speed abuse of only 6 kn from V_2 for a slender wing SST could absorb the conventional 1% safety margin over the nett second-segment gradient of 2%, while a speed abuse of about twice this could correspondingly be tolerated for a conventional swept-wing subsonic transport. The situation can be further aggravated with slender-wing aircraft because, in the all-engines condition, a critical piloting task may arise to avoid lift-off much below V_2 and to avoid speed loss during the flare-up. For example, rotation as little as 1 sec early can cause lift-off about 5kn early, while the large spread between V_R and V_2 makes rotation-rate critical, and excessive g (normal acceleration) during the flare causes rapid speed deterioration. Fortunately, with the provision of good handling characteristics and good attitude information, speed control on slender wing aircraft can be maintained to the same level as on current conventional transports.

Thus, it seems reasonable to accept the same nett climb gradient for slender wing transports as for conventional, e.g. 2% nett at V_2 during the second-segment climb for critical engine failure on a 4-engined aircraft. However the margin between the nett and mandatory gross gradient, to allow for normal speed errors, should effectively be greater on slender-wing than conventional aircraft.

Some *alternative* procedures for specifying rationally appropriate climb requirements, while still retaining compatibility with existing regulations for conventional transports, are illustrated below for second-segment conditions (engine-failed, undercarriage retracted) with 4-engined aircraft.

- (i) The most direct approach logically would be to require the standard nett gradient to be achievable with a prescribed speed error from the declared V_2 ;

e.g. $\gamma(\text{nett}) = 2\% , \text{ at (say) } V_2 - 10 \text{ kn} .$

- (ii) The major contributory factor, the induced drag (D_i), could be introduced analytically into the specification of the gross gradient to be achievable for the particular aircraft;

e.g. $\gamma(\text{gross}) = 1.8\% + (D_i/W) \times 13\% , \text{ at } V_2 .$

This yields typically $\gamma(\text{gross})$ of 4½% for current SST designs, and was originally proposed in relation to Concorde¹⁵ (1969), but appears to have been dropped because of possible controversial arguments concerning the specification of induced drag for general certification purposes.

- (iii) The induced drag characteristics could be allowed for indirectly by requiring the standard nett gradient to be achievable at a higher lift, as demanded in a coordinated turn, instead of at a reduced speed;

e.g. $\gamma(\text{nett}) = 2\% , \text{ at } V_2 , \text{ in an } 18^\circ \text{ banked turn} .$

Typical degradations of climb gradients with bank angle are illustrated in Figure 16, where the gradient loss from 18° bank for conventional transport is seen to be compatible with the presently incorporated margin of 1% (gross gradient 3%), while the loss for slender wing SST is compatible with the margin of 2% to 2½% expected from (ii).

Some possible revisions of second-segment and third-segment requirements along these lines are included for interest in Figure 14, to cover the cases of 2, 3 and 4-engined aircraft.

4.2 STOL Aircraft

General Background

Consideration of STOL aircraft with powered wing-lift augmentation systems, direct engine-lift (vectored thrust or vertical mounting), or thrust augmentation/reversal schemes, introduces many new aspects on safety and certification as well as on prediction of the take-off and landing performance. These include:—

- (i) The applied thrust (or power) can affect directly the total lift achieved, not merely indirectly through the conventional thrust-drag balance. Thus powerplant failure can cause not only thrust loss but also substantial lift losses, trim changes, and probably stability/control degradations.
- (ii) Configuration changes become especially attractive for lift-off and in the climb segments, to supplement or even replace conventional wing attitude changes; these could improve safety provided the appropriate mechanisms (e.g. thrust vectoring or flap deflection) were installed as "primary controls".
- (iii) While the lower speeds associated with STOL operation in themselves can reduce risks, there are many related factors which could become more troublesome, such as gust response, cross-wind effects, speed errors, the lower airframe loads compared with engine forces, and inertial forces, or unusual aerodynamic derivatives. Special precautions may be needed, possibly involving automatic control and control-power augmentation in some degrees of freedom.
- (iv) Ground proximity can generate large and novel effects, peculiar to the particular STOL aircraft configuration and mode of operation.
- (v) Higher accelerations (or decelerations) are demanded, both longitudinal and normal to the flight trajectory, and possibly up to passenger toleration limits — say up to 0.5 g depending on the duration. The effects of the time delays and manoeuvre deficiencies thus become of even greater significance.

For all STOL transport projects, the specification of adequate safety margins and certification procedures continues to be the subject of much debate; particularly in view of the large variety of possible STOL types and the small experience with sizable STOL transport aircraft at this stage. In fact, precise regulations for the certification of airfield performance with STOL aircraft are still not formally agreed, even within one country alone. Here, we shall attempt to highlight only some possible essential modifications to the safety margin considerations already formulated for conventional transports, again primarily as background for STOL airfield performance estimation.

Take-Off Speeds (Fig. 11)

At the lower speeds associated with STOL airfield operation, the five vital safeguards listed already in Section 3.1 cannot all be adequately satisfied for STOL aircraft by merely prescribing percentage safety margins for V_2 and V_R (or V_{LO}) over V_{MCA} and $V_{S,1g}$.

Firstly, possible aircraft speed deviations sensibly *independent* of the reference speed, due either to pilot variability or to atmospheric disturbances, can become more important than those proportional to reference speed. Thus, to ensure adequately safe speeds from lift-off to the screen, we might reasonably now complement or supersede the earlier conventional percentage margins by true speed differentials, e.g.

$$V_2 \geq V_{MCA} + 10 \text{ kn}$$

$$V_2 \geq V_{S,1g} + 15 \text{ kn}$$

with

$$V_R \text{ (or } V_{LO}) \geq V_{MCA} + 5 \text{ kn}$$

$$V_{LO} \geq V_{S,1g} + 10 \text{ kn}.$$

Here, *all* speeds sensibly could be associated for our purposes with the critical engine failure condition (propulsion, wing-lift augmentor, or direct lift), taking into account stability/control deterioration as well as lift and thrust loss. For certification purposes at least, it might again seem justified to replace the 1g stalling speed $V_{S,1g}$ by the minimum demonstrated flight speed V_{MIN} in rectilinear flight.

Secondly, the aircraft manoeuvre capability in the flare (incorporating an appropriate safety margin) may not be adequately covered by such speed criteria, so reference should be made to the maximum normal-acceleration capability $(n_{max} - 1)g$ in the flare from aerodynamic + engine lift; e.g.

$$n_{max} - 1 \geq 0.5,$$

or

$$n_{max} - n_{flare} \geq 0.2 \quad (\text{assuming say up to } 0.3g \text{ normal acceleration is usually pulled in the flare}).$$

Thirdly, to ensure adequate allowance for vertical upgusts and for pilot variability in controlling incidence, a stalling incidence or maximum incidence α_{max} permitting controlled flight must provide a sufficient margin; e.g.

$$\alpha_{max} - \alpha_{flare} \geq 10^\circ \text{ (say).}$$

Alternatively, there might be required to be no significant buffet, no loss of control, nor significant loss of height, in the event of a gust (from any direction) of specified average strength (≈ 10 m/sec) of specified duration (≈ 3 sec), and with suitable gust alleviation factor.

Finally, it could be argued what combination of the speed, manoeuvre and gust margins should be covered simultaneously by the aircraft capability, and whether the critical engine-failure case should apply to them all; bearing in mind the desire for all-weather operation in urban environments, but taking account also of the probably higher levels of automatic stabilisation and guidance.

Take-Off Distances and Climb Gradients (Figs. 13 and 14)

With the likelihood of larger proportional errors in times and speeds for STOL airfield operation as compared with CTOL, some error/abuse cases should be checked along similar lines to those already postulated for slender-wing aircraft. Thus, as regards scheduled take-off distances, these should be adequate to cover early or late rotations (e.g. by ± 2 sec or ± 5 kn) while maintaining an acceptable flight path, possibly also incorporating a small incremental factor on the achieved distance; see Figure 13. Again, the take-off climb gradients in the various segments should achieve certain prescribed nett values with critical engine failure for a speed below V_2 in rectilinear flight (e.g. at $V_2 - 5$ kn); see Figure 14.

It must be stressed that the topic of STOL safety margins is still under debate, so the present discussion is included only to indicate some of the major factors involved, and the numerical values are quoted only to illustrate relevant orders of magnitude.

4.3 Combat Aircraft

General Background

Military transport aircraft can for our purpose be regarded as being required to satisfy civil standard safety and certification standards, except during times of military emergency when special operational risks may be allowed.

However for combat aircraft, where at most twin-engined and two-man crew considerations are usually appropriate, lower than civil safety levels tend to be tolerated even for everyday service operation. Some compensating features can be included of course, at least as far as crew safety is concerned; for example by installing ejector seats in the aircraft and stop-barriers on the airstrip. The certification aspects tend to be considered and applied more directly towards clearance for a particular combat aircraft project, since the Military test agency concerns itself simultaneously with both airworthiness aspects and operational usefulness. The trial results are assessed against standards of acceptability based on past experience up-dated by flight explorations with the particular new type, ultimately qualified by examination of the average behaviour and the variability of the aircraft under test with special reference to its particular role. Naturally, with radical new types of civil transports, this latter type of procedure can arise too in the development of appropriate certification regulations to cover novel aircraft handling features and new modes of operation.

Basically, the combat aircraft performance data derived from clearance trials at the Military Test Establishment is analysed for presentation in an ODM (Operations Data Manual), usually in a manner to represent the *average* achievable by a good Service Pilot under reasonably good environmental conditions. Because of the special need for the Service to vary their operational risk, some freedom must be left to the operator to apply appropriate safety factors to cover scatter and variation from this "average standard" due to operational conditions. However, the ODM can recommend at least a safety factor on take-off distance to allow for general random variations in flying and to take some account of engine-failure; while also including some advice as to special operational limitations, e.g. with respect to particular handling deficiencies or unusual environmental constraints.

Simplified Safety Margins (Fig.17)

For take-off performance prediction with combat aircraft, at least in the project stage, it appears usual to accept safety constraints in much simpler forms than with transport aircraft. Typical restraints on speed and attitude may simply be:

$$V_{LO} \approx 1.12 V_{S,lg}; \quad C_L \leq 0.8 C_{L,max} \quad (\text{all engines}).$$

$$\text{Mean rotation rate} \leq 5^\circ/\text{sec}.$$

Of course, combat aircraft typically have high thrust/weight ratios ($> \frac{1}{2}$), so that the resulting vertical lift contribution at high take-off incidence ($\approx 15^\circ$) can be significant even without thrust vectoring, thus supplementing the foregoing aerodynamic margins.

Scheduled runway distances may be defined also by simple factoring, e.g.

$$K \times (\text{distance from "brakes-off" to 15 m height}); \quad K \approx 1.25 \text{ to } 1.5;$$

in terms of the "average" distance capability quoted in the ODM for the particular airfield conditions – altitude, temperature, runway slope, wind. An additional safety criteria for single-engine failure on a twin-engined aircraft may be that the climb-rate at screen height (15 m) over the end of the runway must then exceed a certain minimum, e.g. 5 m/sec (1000 ft/min). Note that, in the absence of further safety margins, such conditions can imply that there may be accepted a critical period of two or three seconds during the take-off run in which neither safe take-off nor stopping within the runway length could be guaranteed in the event of engine failure, i.e. the balanced field length concept does not apply here. A runway safety barrier or arresting device is sometimes installed, particularly as an emergency provision against all-engine failure (in the ground run), but of course the entry speed, weight and configuration of the aircraft must be compatible with the particular arresting device provided.

5. LANDING FACTORS FOR CONVENTIONAL AIRCRAFT

5.1 General Background

Many of the basic aspects already introduced regarding aircraft speed, distance and climb-out considerations for conventional take-offs have also some relevance for conventional approach and landing, and will not be repeated except when essential for clarity. The approach technique is conventionally envisaged as comprising a descent with a gradient not exceeding 5% (or $\gamma \leq 3^\circ$), at a final steady approach speed V_{APP} from about 300 m height (1000 ft) down to decision height at about 60 m (200 ft), followed by a gradual deceleration to the target threshold speed V_{AT} . However, as regards landing certification at least, some distinction needs to be made at the outset between the concepts of two radically different treatments which currently can apply for transport aircraft (Fig.18).

Arbitrary Landing Distance Method

This classic treatment, which is still used generally in the USA¹² and sometimes still employed for propeller-driven aircraft in the UK¹¹, formulates speed safety margins very simply through prescribing a minimum approach speed V_{APP} in terms of the minimum stalling speed $V_{MS,L}$ (power-off) with landing flap setting; e.g.

$$V_{APP} > V_{AT} > 1.3 V_{MS,L}.$$

Additionally, if there is a different flap setting for the approach, the minimum stalling speed $V_{MS,A}$ (power-off) with the approach flap setting may be further constrained in relation to that with landing flap, e.g.

$$V_{MS,A} \leq 1.1 V_{MS,L}.$$

There could be other speed restraints of course from climb-out considerations, following on a discontinued approach or baulked landing, as will be discussed later. But otherwise, few direct restrictions appear to be placed on the landing techniques themselves.

Then, the shortest possible landing distance $(S_a + S_G)_{\min}$ demonstrated under relatively ideal conditions by "test pilots" may be used as a datum (for factoring), subject only to the foregoing speed constraints, avoidance of excessive tyre wear or damage, and usually non-application of reverse thrust in this demonstration on a dry runway. However, a substantial factor is then applied to this datum distance for the particular aircraft and environmental conditions, to take care of possible deviations (e.g. excess speeds) in everyday commercial operations. Thus, the minimum scheduled landing distance is then given for example by

$$\text{Total "Arbitrary Landing Distance"} = 1.67 \times (S_a + S_G)_{\min}.$$

For wet runway operation, it has become usual to apply an additional factor, (e.g. 1.15) so giving an appreciably higher overall factor (e.g. 1.92) under these conditions. The threshold/screen height is chosen usually about 15 m (50 ft) with this method.

"Reference Landing Distance Method"

This more elaborate approach was first introduced into British Civil Airworthiness Requirements over ten years ago, in an attempt to reduce the dependence on large empirical distance factors and to relate the landing manoeuvre used in certification more directly to those encountered in actual commercial operations. The landing manoeuvre constraints are intended to represent the worst threshold conditions from which a commercial pilot should attempt to complete a landing rather than select to overshoot, so that only small factors need then be applied to the associated landing distance to allow for other in-service degradations. The threshold/screen height is currently chosen as about 9 m (30 ft), apparently combining a typical practical threshold height of about 6 m (20 ft) with a margin of about 3 m (10 ft) based on statistical correlation between excessive speed and height at the threshold occurring together. Apart from obvious certification interests, the "Reference Landing Distance" concepts are worth further elaboration because they reveal naturally some operational aspects directly relevant to the formulation of realistic prediction methods.

The five vital safeguards listed in Section 3.1 for take-off are also worth recalling, since with slight obvious revisions they are equally significant for landing.

5.2 Landing Speeds: Reference Method (Fig.19)

There are a variety of safety and manoeuvrability constraints which, as in the case of conventional take-offs, can be expressed simply in terms of relative values of appropriate reference speeds along the lines illustrated in Figure 19.

Target Threshold Speed V_{AT}

This represents the normal speed at the threshold which should guarantee an adequate margin from the stalling speed together with sufficient manoeuvrability and control effectiveness to achieve a safe landing in relatively good conditions. Typical requirements are:

- (i) $V_{AT} \geq 1.3 V_{MS}$, i.e. a proportional speed margin, where V_{MS} may strictly be appropriate to the landing configuration, with the engines at low power;
- or
- (ii) $V_{AT} \geq V_{MS} + 22 \text{ kn}$, i.e. a discrete speed margin, where V_{MS} may strictly be appropriate to the approach configuration, with the engines at low power;

whichever is the lesser. Also,

- (iii) $V_{AT} \geq 1.16 V_{S,lg}$, i.e. a manoeuvre margin, which should strictly be $n_{\max} \geq 1.35 g$ at $V = V_{AT}$; as presented here it assumes $C_{L,\max}$ does not vary between the two speeds and that the engine thrust contribution can be ignored.

The distinction between landing and approach settings for the flaps can usually be ignored with conventional jet transports. These three constraints then tend to predominate respectively in turn for aircraft falling in different ranges of stalling speeds, roughly

- (i) below 75 kn, (ii) 75 kn to 100 kn, (iii) above 100 kn.

Furthermore, on the assumption that V_{MS} takes the maximum value $0.94 V_{S,1g}$ which can normally be credited, the following single expression satisfies simply all three constraints

$$V_{AT} \geq 1.08 V_{S,1g} + 10 \text{ kn} \quad (\text{for } 60 \text{ kn} < V_{AT} < 140 \text{ kn}).$$

Some additional possible constraints on target threshold speed V_{AT} are also included in Figure 19 arising from

- V_b the pre-stall buffet speed (all engines) in the landing configuration.
- V_{MCL} the minimum control speed (critical engine failed) in the landing configuration.
- V_A the steady final approach speed.
- V_{Tmin} the minimum demonstrated threshold speed for safe landing in calm conditions.

Maximum Threshold Speed V_{Tmax}

This essentially defines the largest speed excursion allowed (above V_{AT}) from which landing may be attempted, distance limited, where the scheduled distances are based on safe landing demonstrations from this speed. Thus, in regular service operations, an overshoot is called for if the actual threshold speed exceeds the prescribed V_{Tmax} appropriate to the particular landing weight and airfield conditions. Typically,

$$V_{Tmax} - V_{AT} \approx 15 \text{ kn}.$$

But there can and should exist regulatory provisions for employment of a smaller differential when more precise control of landing approach than usual is fitted. Naturally, the allowed difference also includes some compromise between accepting too low a value with unreasonably high frequency of baulked landings, and too high a value with an unwarrantably large value of certificated landing distance or excessive risk of overrun.

For emergency landings with a critical power unit inoperative, there exist other similar requirements in respect of the relevant target threshold speed $V_{AT,1}$ and maximum threshold speed $V_{Tmax,1}$; also for the target threshold speed $V_{AT,2}$ with two critical engines inoperative. These could become more especially significant with regard to allied requirements for powered lift aircraft.

5.3 Airfield Landing Distances (Fig.18)

General Distance Considerations

The available total landing distance at a specific airfield comprises the length of runway extending from the location of the threshold/screen height, usually all of which has a hard prepared surface compatible with the aircraft landing weight and undercarriage design (Fig.4). Close to the threshold, possibly for about the first 100 m (300 ft) where touchdown should occur only under exceptional circumstances, a poorer hard surface may be tolerated, but such touchdowns should nevertheless be possible with only minor damage. Beyond the end of the normal runway, some overrun distance may also be provided as an extra stopway for exceptional emergencies, again possibly containing a specially roughened strip or arresting device – at least for military use.

Scheduled landing distances as determined by the classic "Arbitrary Distance Method" have already been discussed (Section 5.1, Figure 18). Effectively the best demonstrated landing distance is employed, with the landing technique constrained only by a simple safety margin (above the stall) placed on threshold speed. Then a simple but large empirical safety margin on distance is applied to account for the more adverse circumstances encountered during regular operations. In contrast, the "Reference Distance Method" discussed below depends on determining the landing distance under fairly adverse conditions, but then applying a much smaller extra safety margin. Analysis from a range of such flight checks, at different aircraft weights and ambient conditions, can then provide the scheduled distances for reference over the planned service operations, using either method.

Landing Distances: Reference Method

For the derivation of scheduled landing distance by the "Reference Method" (Fig.18) the test threshold speed V_T is taken as the maximum permitted threshold speed V_{Tmax} allowed for completion of the landing, as already defined, i.e.

$$V_T \equiv V_{Tmax} = V_{AT} + 15 \text{ kn}.$$

Moreover, possible advantages from adopting unrepresentative flare and touchdown techniques are precluded by specification of a minimum value for the time interval t_a between passing the threshold and touchdown. Typically,

$$t_a \approx 7 \text{ sec} \quad \text{for conventional jet transports}.$$

More specifically (BCAR),

$$t_a \geq (13 - 0.045 V_{Tmax}) \text{ sec, where } V_{Tmax} \text{ is in knots.}$$

The demonstrated distance is then determined for a *wet* runway, though in principle all reliable safe means of retardation can be employed. Thus, for example, selection of the idling reverse thrust condition while airborne may be accepted and reverse thrust during the ground run permitted, provided there are no unsafe trim changes arising from these actions or from malfunction of one of the thrust units.

The scheduled distance, for a particular aircraft configuration and airfield ambient conditions, is then taken as the maximum of the demonstrated distances $(S_a + S_G)_L$, all-engines and critical-engine failed, applying small and slightly different safety margins in the two cases to cover other possible degradations. Such field length factors can be derived from statistical examination of the variability in landing distance which might occur in service, due to random variations in such features as threshold speeds, braking coefficients, time delays, etc. Typically:-

$$\left. \begin{array}{l} \text{Factored total} \\ \text{Landing distance} \end{array} \right\} = (S_a + S_G)_L \times \left\{ \begin{array}{l} 1.11 \text{ all-engines} \\ 1.08 \text{ critical engine failed.} \end{array} \right.$$

More specifically (BCAR), the field length factors to be applied to the demonstrated landing distances depend slightly on the particular aircraft characteristics¹¹. These factors tend to diminish from some maximum values (1.24 or 1.19) with increases in the ratio of ground-borne to airborne retardation, until the overriding minima quoted above are reached; roughly when the ground-borne retardation in excess of that from wheel braking becomes more than half the airborne retardation. This latter condition is likely to be satisfied by any aircraft having auxiliary means of ground-borne retardation, such as reverse thrust.

5.4 Climb-Out Gradients (Fig.23)

The ability of an aircraft to maintain an adequate climb gradient $\gamma_c [\simeq (T/W) - (D/L)]$, at speeds high enough to ensure acceptable handling characteristics, represents an important consideration not only for take-off but also to cope safely with a discontinued final landing approach (before threshold) or a baulked landing (after threshold). Usually, there is a natural conflict between the desire for low drag to improve such climb-out capabilities and that for higher drag associated with landing descent and ground deceleration requirements, particularly since time considerations may preclude credit for favourable configuration changes in an emergency.

For the analysis and certification of CTOL transport aircraft at least, it is the usual practice to distinguish between the discontinued approach and baulked landing conditions, with appropriate specifications of minima to be achieved or exceeded in respect of operational speeds and climb gradients, together with restraints on permissible configuration changes both as regards time allowed and change of stalling speed involved. Some typical requirements are listed in Figure 23 for conventional transports. The minimum climb gradients for the discontinued approach are assumed to refer to a critical engine failed condition, with the other engines at maximum contingency rating; the required values are about half those usually specified for the take-off second segment, but again with some alleviation as the number of installed engines reduces from 4 to 2. The baulked landing requirements refer to all-engines operating condition; the maximum take-off ratings are allowed provided these are attainable within an appropriate time – typically less than 8 seconds.

6. SPECIAL LANDING FACTORS

6.1 Slender Wing Aircraft (Fig.20)

Relevant general background, on the novel aerodynamic characteristics of slender-wing aircraft and on the significance of such characteristics as regards reference conditions or performance sensitivities, has already been given in Section 4.1 so need not be presented here.

The *landing reference speeds* may be determined for project prediction purposes by following similar arguments to those for conventional transport aircraft. However, to preclude difficulties in defining a practical stall speed for slender wing aircraft, the minimum demonstrated flight speed V_{MIN} in steady rectilinear flight under appropriate aircraft conditions is again chosen to replace V_{MS} and $V_{S,1g}$ (Section 4.1). Moreover, the possible greater sensitivity to speed errors with slender-wing aircraft requires even more careful restrictions on possible speed excursions. Some typical values are illustrated in Figure 20 for the all-engines landing, though it must be noted that these represent only a selection from the reference speeds involved in certification regulations. Likewise, speed margins have also to be defined in respect of emergency landings with at least one critical engine inoperative.

The *scheduled landing distance* definitions may reasonably be chosen the same as in the "Reference Method" for Conventional Aircraft (Section 5.3, Figure 18), subject of course to the different constraints as regards landing speeds.

The *climb-out gradients* after discontinued or baulked landing may likewise be conveniently specified as those for conventional aircraft (Section 5.4, Figure 23). However, in view of the extra sensitivity to speed errors, some reference to nett values achieved under appropriate abuse conditions may need to be introduced as discussed for take-off (Section 4.1).

6.2 STOL Aircraft (Fig.21)

The general background on the new aspects of airfield performance prediction introduced by powered wing-lift augmentation systems or direct engine-lift has already been given in Section 4.2. Also, the discussion there on particular reference speeds, distances and climb gradients for take-off has raised principles which are equally relevant to landing considerations.

Some typical *landing reference speeds* for the all-engines condition are correspondingly listed in Figure 21, again along with possible requirements for incidence margins and maximum normal-acceleration capability during the flare. Further margins also need to be assumed for the emergency landing case with at least one critical engine inoperative. The touch-down speed V_{td} has been included because of its increased significance with respect to aircraft control and accurate touch-downs, in the presence of strong ground proximity effects.

The scheduled *landing distances* may be defined at this stage similarly to those in the "Reference Method" for Conventional Aircraft (Section 5.3, Figure 18). However, new features will be involved in STOL operation particularly in view of the larger descent angles and the more severe time/space limitations. Thus, for STOL, clear identification of a touch-down zone and a specific operational drill for the flare/touch-down may be essential. Then, the touch-down zone could become the final decision point (rather than the threshold) as regards committal or overshoot, necessitating a somewhat modified approach to landing distance certification and also to the conventional *climb-out* requirements (Section 5.4, Figure 23).

Moreover, at least for certification purposes, the steep descent and flare capabilities may require special attention in view of the possible tendency for flight-path control and flare pull-up abilities to deteriorate with increasing descent angle.

6.3 Combat Aircraft (Fig.22)

The general background on certification/clearance of combat aircraft, already given in Section 4.3, is equally relevant here. Again, it must be stressed that the safety margins relating to airfield performance prediction for combat aircraft are usually specified much more simply and flexibly than those for transports. Some typical values are listed in Figure 22, with respect to:

- Approach speed V_A and touch-down speed V_{td} .
- Incidence rotation rate ($d\alpha/dt$).
- Distance margin over "average" ODM capability.
- Climb after discontinued or baulked approach.

PART III – SPECIFIC PREDICTION TECHNIQUES

7. SIMPLE CORRELATION OF AIRFIELD PERFORMANCE

7.1 Take-Off Distance (Figs.6 and 24)

Elementary kinematic relations have already been introduced in Section 2.1 (Fig.6) for ground-run and flare-up distances.

Scheduled take-off distances to screen height, as prescribed in flight manuals available for some conventional transports and combat aircraft, are correlated crudely in Figure 24 against the take-off values for a simple classical parameter (see also References 1, 21, 24, 25); namely⁴

$$(W/S)(W/T_0)(1/C_{LMS})(1/\sigma).$$

Here, T_0 is chosen for convenience as the static thrust from the engine-manufacturers specification; C_{LMS} is the lift-coefficient corresponding to the minimum speed during stalling tests (see Section 3.1), i.e. somewhat higher than for the 1 g stall; σ is the relative air-density.

7.2 Landing Distance (Figs.25 and 26)

Elementary kinematic relations have already been introduced in Section 2.2 for the airborne phase and ground run.

Some representative mean decelerations related to the overall landing distances are listed in Figure 25⁴².

Some scheduled landing distances for conventional transport aircraft are correlated crudely in Figure 26⁴ against the landing values for the simple classical parameter

$$(W/S)(1/C_{LMS})(1/\sigma).$$

Reference is essential to the relevant distance safety factor (f_s) applied and to the corresponding braking methods assumed, with FAA and BCAR requirements.

8. TAKE-OFF GROUND-RUN PREDICTION

8.1 Basic Formulation and Force Contributions (Figs.27, 28 and 29)

The framework for ground-run calculations in terms of one-dimensional arguments is illustrated in Figure 27, together with the relative significance of the various contributions to the nett accelerating force and of typical variations with speed.

The major factors influencing ground-rolling resistance³⁶ are listed in Figure 28 and some conventional mean values for rolling resistance coefficients are also tabulated.

Some representative engine-thrust variations with forward speed are shown in Figure 29⁴, illustrating the marked lapse in thrust with increasing speed and its aggravation by higher bypass-ratio. Typical polynomial forms for thrust variation with speed are also mentioned to facilitate algebraical treatments for ground-run estimation.

8.2 Simplified Distance Integration with Thrust Variation (Fig.30)

With thrust changes proportional to (speed)², i.e. $T/T_0 = (1 + K_2 V^2)$, an elementary expression follows for the ground run S_{GR} (Fig.30) by assuming that the coefficients of lift C_{LG} , drag C_{DG} , and rolling-friction μ_R all remain sensibly constant. The logarithmic term involving these variables can be further simplified of course by series expansion neglecting say the second and higher-order terms. Alternatively, extending a treatment proposed by Kettle²⁶, a carpet-chart can be prepared for $S_{GR}\{(g\rho C_{L,LO})/(W/S)\}$ in terms of the two parametric variables:

$$(T_0/W - \mu_R) \quad \text{and} \quad \{C_{DG} - \mu_R C_{LG} - (K_2 T_0 / \frac{1}{2} \rho S)\} / C_{L,LO}.$$

Other algebraic solutions are of course feasible, including those for thrust varying linearly with speed ($T/T_0 = 1 + K_1 V$), as in Reference 27; and thrust varying as a quadratic function of speed ($T/T_0 = 1 + K_1 V + K_2 V^2$), as in Reference 45.

8.3 Equivalent Mean-Acceleration Approximation (Fig.31)

A first approximation for the ground-run distance is often obtained without integration, at least from start to rotation speed $V = V_R$, by assuming a constant equivalent-mean acceleration $a = \bar{a}$, throughout the ground-run. The speed condition $V = V$ at which \bar{a} should strictly be derived is shown in Figure 31 as a function of the ratio of the true acceleration $a_R(V = V_R)$ at rotation speed to the starting value $a_0(V = 0)$, for representative variations^{2,28} of a with V . The relevance of the classical choice $V \approx 0.7V_R$ is apparent.

8.4 Rotation to Lift-Off Attitude

Angular rotations may range from 1 or 2° for old straight-wing aircraft to more than 5° for modern swept-wing aircraft, and even beyond 10° for some slender-wing and STOL aircraft.

For corresponding ground-run distance estimation, a simple approximation is to assume that the rotation takes a fixed time deduced from experience with relevant types; e.g. about 3 sec for modern swept-wing aircraft. Then assume constant forward-acceleration during rotation as the mean of true end-values at $V = V_R$ and $V = V_{LO}$.

If large rotations are involved, the alternative simple assumption of constant rate-of-rotation may be preferable; e.g. $d\alpha/dt \approx 3^\circ/\text{sec}$.

8.5 Generalised Ground-Run Equations (Powered Lift) and Step-by-Step Integration (Figs.32, 33 and 34)

Basic representative equations for accelerating ground-runs during take-off, and for deceleration (with braking) in an emergency stop, are set down in Figure 32. Here, the i^{th} propulsive unit with gross thrust T_{Gi} and intake momentum drag D_{Ei} can have its thrust deflected at an angle θ_i downwards – here defined relative to the reference axis giving the aircraft attitude α to the horizontal; $|\alpha + \theta_i| > 90^\circ$ implies reverse thrust. The airframe lift L_A and drag D_A can include engine-airflow interference effects on the airframe aerodynamics (favourable or unfavourable); e.g. may be a function of the engine location and of its airflow characteristics relative to the main-stream (forward speed) condition.

The simplified flow diagram in Figure 33 illustrates a step-by-step timewise integration procedure for evaluating the ground-run distance to lift-off ($V = V_{LO}$) or to an emergency stop. A variety of methods can be adopted of course for iterations and integrations over the intervals, employing standard computational techniques. If time itself is of no consequence as a variable, then distance s could be introduced directly as the independent variable, writing the acceleration $(dV/dt) = V(dV/ds)$, with step-by-step integration using selected distance intervals δs .

Precise definition is important of the acceptable take-off procedures such as rotation characteristics and thrust/flap deflection during the ground run, which may differ for civil and military certification. Pilot action and time delays become specially important for the calculation of acceleration-stop distances, as illustrated in Figure 34 by the emergency-stop schedule for a typical conventional transport. Relevant braking characteristics are discussed later for convenience, in relation to landing.

9. TAKE-OFF AIRBORNE PATH PREDICTION

9.1 Basic Formulation

The nature of the airborne manoeuvre from lift-off to screen height is associated largely with piloting techniques employed for specific types of aircraft, particularly as regards flare-up (Fig.3). Often the choice of treatment has to depend more on the form in which relevant data is given or required, rather than on the choice of best theoretical model, unless a particular type of aircraft has already been well explored as regards take-off handling characteristics.

Various simplifying assumptions are commonly adopted to permit elementary algebraical treatments for the estimation of airborne distance S_a , at least for conventional aircraft with fixed flap setting and without thrust deflection. Typically these may specify either:

- The geometry of the flare; e.g. circular arc.
- The lift condition (incidence) during the flare; e.g. $C_L = C_{LO}$ when the excess lift for the flare results from speed increase alone.
- The aircraft attitude variation characteristics during the flare; e.g. constant pitch-rate.

9.2 Circular-Arc Flare-Up and Empirical Correlation (Figs.35, 36 and 37)

From a first-order analysis, the circular-arc flare of radius R at speed V , with $C_L = (W/\frac{1}{2}\rho V^2 S) + \Delta C_L$ and with normal load factor n implies (Fig.35)

$$V^2/(n-1)g \equiv (2W/S)/(\rho g \Delta C_L) \equiv R = \text{constant}.$$

For the estimation of the horizontal distance S_a from lift-off to screen height, two conditions relating to either transition uncompleted at the screen or completed before the screen are illustrated in Figure 35.

For estimation purposes, empirical values of the mean "constant" ΔC_L used in practice are of interest. Some typical results for maximum effort take-offs of a twin-jet fighter²⁹ are plotted on Figure 36 in terms of the ratio V_M/V_S of measured mean-speed in the flare to the 1g stalling speed. A generalised correlation formula for ΔC_L (maximum effort) in terms of (V_M/V_S) and C_{Lmax} is quoted and plotted also in Figure 36, being derived²⁹ from flight measurements for several aircraft. Note that a "normal-effort" take-off may give only half these values, e.g.

$$\Delta C_L \approx 0.15 \text{ for } V_M/V_S \approx 1.2 \text{ and } C_{Lmax} \approx 2.$$

Some corresponding curves of S_a for circular-arc flares to 10.7 m (35 ft) screen-height, are plotted in Figure 37⁴ against W/S at prescribed ΔC_L -values, with ρ taken as SL/ISA condition.

9.3 Constant C_L Flare-Up and Empirical Correlation (Figs.38 and 39)

The basic equations of motion, normal and along an element δl of the flare path at local angle γ to the horizontal, are set down in Figure 38 for conventional flight. In the *simple accelerating case* with $C_L \equiv C_{L,LO}$, i.e. lift increase resulting from speed rise only, linearisation of the differential equations and algebraical integration becomes possible by assuming that γ and speed-changes $\delta V/V_{LO}$ are small compared with unity and by prescribing $(T - D)/W \approx \text{constant}$. The resulting motion represents a segment of a phugoid, starting at $\gamma = 0$ and stopping at the steady climb gradient $\gamma = \gamma_c$; see the equation for γ in Figure 38. Note that distance relations are given separately when the flare-up is completed before the screen and when uncompleted.

A classical empirical relation³¹ for the distance to the screen in the completed-flare case is

$$S_a \approx (k_1 V_{LO}^2/g) + (h_s/\gamma_c),$$

where $k_1 = 0.707$ on the preceding theoretical arguments. Some empirical values for k_1 suggested by Ewans³¹ and by Edwards³³ are listed in Figure 39, along with the equivalent values for the normal acceleration $(n - 1)g$ which would correspond to a circular-arc flare with $\gamma_c = 0.1$. Some recent ARB data for normal accelerations achieved with conventional transports³⁴ suggests a peak value of 0.12 for $(n - 1)$, i.e. a sinusoidal mean of 0.076; this tends to support a value of k_1 not far from the theoretical.

More general algebraical solutions can also be formulated for a flare with constant $C_L > C_{L,LO}$ and allowing speed variation³⁰, but the assumption $(T - D)/W \approx \text{constant}$ and the rejection of some second-order terms are often incorporated to reduce complexity^{29,2,32}. If the steady climb angle is reached before the screen, the extra airborne distance may be simply taken as $(h_s - h_F)/\gamma_c$ if an abrupt change in aircraft flight condition is allowed at the end of the transition, or alternatively some smoothing procedure can be incorporated³².

9.4 Constant Pitch-Rate Flare-Up (Fig.40)

It has been argued that³⁵ the variable most directly under the pilot's control during flare-up is the time rate-of-pitch $\dot{\theta}(t)$. With the simplifying assumptions,

$$\dot{\theta} = \text{constant}; (T - D)/W = \text{constant},$$

Perry's analysis²² in terms of non-dimensional time variable $\tau = gt/V_{LO}$ then gives a non-dimensional flight-path angle F_γ and non-dimensional height parameter F_h . These are defined in Figure 40 and plotted against τ for constant prescribed values of the non-dimensional lift-incidence slope parameter $n_\alpha \equiv (dC_L/d\alpha)/C_{L,LO}$.

The non-dimensional speed increment $\delta V/V_{LO}$ is then defined (Fig.40) by the energy-height relation, and the distance S_a specified approximately by the product of the mean speed $(V_{LO} + \frac{1}{2}\delta V)$ and the time t_s to reach height h_s . Thus to find S_a with $\dot{\theta}$, n_α , $(T - D)/W$, V_{LO} prescribed:—

- F_h is first evaluated at appropriate height h ;
- Corresponding τ value is read off from the appropriate n curve;
- δV is then calculated at τ -value, using energy-height relation;
- S_a is obtained from product of mean-speed and time.

The F_γ curve can be used to check that steady-climb angle is not exceeded before $h = h_s$.

Mean $\dot{\theta}$ -values deduced from flight measurements on some transport aircraft have ranged from

$$0.009 \text{ rad/sec } (\frac{1}{2}^\circ/\text{sec}) \text{ to } 0.017 \text{ rad/sec } (1^\circ/\text{sec}).$$

For conventional transport aircraft $\dot{\theta} \approx 0.013 \text{ rad/sec (0.075}^\circ/\text{sec)}$ might tentatively be assumed. For combat aircraft and STOL aircraft much higher rates may be envisaged, typically $\dot{\theta} \approx 0.09 \text{ rad/sec (5}^\circ/\text{sec)}$, with perhaps as much as twice this if maximum effort take-offs are allowed.

9.5 Generalised Airborne-Path Equations (Powered Lift) and Step-by-Step Integration (Figs.41 and 42)

Basic equations of motion along the local flight direction and normal to the local flight direction are set down in Figure 41. Here, the individual force and angle definitions are as in Section 8.5, with the additions of the local climb angle γ to the horizontal and of course the climb height h . In general, the pitch angles α , $(\alpha + \gamma)$ and θ_i are specified by the pilot/automatic inputs or airworthiness/geometry constraints. The space coordinates (s, h) can follow from the time integrals of the forward speed $V \cos \gamma$ and climb speed $V \sin \gamma$ respectively.

The simplified flow diagram in Figure 42 illustrates a step-by-step timewise integration procedure for evaluating the airborne path from lift-off ($V = V_{LO}$) to the screen height $h = h_s$. A variety of methods can again be devised for iterations and integrations over the intervals. Some typical limit stops associated with possible airworthiness requirements have been included as examples, but of course the optimum airborne path is not necessarily achieved by continuing with a limiting value once this has been reached.

Alternatively, if time itself is of no significance as a variable, then airborne path length l could be introduced directly; writing again $d/dt = V(dV/dl)$, with step-by-step integration using selected airborne-distance intervals. The space coordinates (s, h) follow naturally from the integration of the horizontal and vertical projections ($\delta l \cos \gamma$, $\delta l \sin \gamma$) of the local path length, while the time elapsed can likewise be evaluated by integration of the corresponding time intervals $\delta t \equiv (\delta l/V)$. In the absence of an abrupt change at or near lift-off, the equation of motion normal to the flight path may be ill-conditioned for linear step-by-step integration at the start, but this may be overcome by considering second-order terms.

10. LANDING GROUND-RUN PREDICTION

10.1 Basic Formulation (Fig.43)

The basic equations and analysis are naturally similar to those for the take-off run (Figs.27, 30). The major differences in methods of solution arise primarily from changes in relative importance of some of the variables. In particular the braking friction coefficient for landing becomes a factor of major significance, whereas the rolling friction coefficient for take-off is of relatively minor importance except for rough or soft ground operation.

The variation of tyre-friction coefficient with forward speed is illustrated in Figure 43 for wet and dry runways, according to ICAO reference standards. Note that the available wheel braking is further restricted by the necessity to keep inadequately below the skidding point and to limit the applied wheel-braking torque from energy-dissipation considerations.

10.2 Simplified Distance Integration (Figs.44 and 45)

With the thrust assumed constant $T = T_L$ during the landing ground-run, as well as the coefficients of lift C_{LG} , drag C_{DG} , and braking friction μ , an elementary expression follows for the ground-run distance S_{GR} (Fig.44). The logarithmic term can again be further simplified by series expansion, neglecting the second-order terms if $(\mu - T_L/W)$ is large compared with $(C_{DG} - \mu C_{LG})/C_{L,td}$, where the suffix td denotes the value just before touch-down.

Alternatively, as a first approximation, the landing ground-run distance may be obtained without integration by assuming an equivalent mean deceleration (Fig.44), complementary to the equivalent mean acceleration concept used for the take-off case (Section 8.3, Figure 31). Representative levels of deceleration are listed in Figure 45.

More accurately, algebraic solutions are of course feasible over selected intervals of the landing ground-run, using simple polynomial expressions in V for the variables (or locally constant values) as in the analysis for the take-off ground-run (Section 8.2); see for example Reference 45. But substantial discrete changes must be allowed between some intervals to account for sequential operation of the various devices, e.g. wheel brake operation, spoiler operation (lift dumpers and aerodynamic braking), reverse thrust operation. Some typical time-delays between initial touch-down and the operation of such devices are quoted in Figure 45 for present-day transports, though for future projects some reduction in times may be anticipated with the trends towards automatic actuation and advance signalling.

10.3 Generalised Ground-Run Equations (Powered Lift) and Step-by-Step Integration (Figs.32, 33 and 45)

Basic equations for the landing run are represented by the decelerating equations of motion already quoted for the emergency-stop during take-off (Fig.32). The step-by-step integration may be carried out similarly (Fig.33) with respect to either time or distance as the dependent variable. But the step intervals used just after touch-down may need to be quite short, say 1 sec during the first 10 sec. In addition to the delay times already referred to (Fig.45), other factors which may need to be taken into account include:

Variation of allowable wheel-braking torque with actual energy being absorbed.

Variation of incidence due to Oleo compression as well as force aircraft-attitude changes.

Effect of thrust reversal and lift dumping on aerodynamic C_D and C_L .

11. LANDING AIRBORNE PATH PREDICTION

11.1 Basic Formulation

Conventionally, the airborne path for landing from the threshold to touch-down (Fig.5) comprises a final part of the steady descent, followed by a flare-out to reduce the vertical velocity w_{td} at touch-down to a target mean of the order of 0.6 m/sec (2 ft/sec). The undercarriage design is intended to permit a reasonably large scatter to cope with misjudgements or difficult flying conditions, say $w_{td} \leq 2$ m/sec (6 ft/sec). Typical flight speed decelerations in the flare are of the order 0.07 g to 0.10 g, but much smaller values can occur if throttle closure is not permitted, or much larger (say 0.2 g) if in-flight thrust reversal is allowed.

Naval-carrier landings are usually of the fly-on type without flare, so the undercarriage is designed accordingly with a weight penalty for this and for the need to cope with a heaving/pitching deck. Although STOL aircraft usually have much lower approach speeds than CTOL, higher descent angles are employed, so the flare may have to be started *before* the statutory threshold height is reached to ensure that a tolerable vertical velocity may be achieved without risk or discomfort. Alternatively, the degree of flare may in some cases be limited to reduce scatter in the touch-down position.

Thus, the particular flare characteristics to be employed (or assumed) and their repeatability under various operational conditions become especially significant for the reliable prediction of airborne landing distances.

11.2 Circular-Arc Flare and Speed Loss Estimation (Figs.35 and 46)

A landing manoeuvre in which the flare is sensibly a circular arc, tangential to the ground at the touch-down point, is amenable to a simple analysis like that in Section 9.2 and Figure 35 (for take-off) and corresponding expressions result for the airborne distance from the threshold to touch-down. The loss of flight speed in the flare, from approach speed V_A to touch-down speed V_{td} , is additionally of special significance. A simple iterative process for its determination may be devised⁴⁴ (Fig.46) by introducing the energy equation relating these speeds to the horizontal distance S_F covered in the flare, the corresponding reduction in vertical height h_F , and the approach descent angle $\gamma_F \approx (D - T)/W$.

11.3 Distance and Touch-Down Speed Meeting BCAR Requirement (Figs.18 and 47)

The "Reference Landing Distance" requirements proposed by BCAR, already discussed in Section 5 and Figure 18, specify the landing techniques precisely as regards minimum acceptable airborne time t_a from threshold to touch-down and maximum acceptable threshold speed V_{Tmax} . On this basis, a simple iterative procedure can be devised (Fig.47) for the determination of the touch-down speed V_{td} and the airborne distance S_a in terms of the mean deceleration $a_{ag} [\approx (D - T)g/W]$, the V_{Tmax} and the screen height h_s .

11.4 NASA Three-Phase Model for Airborne Manoeuvre (Fig.48)

This analytical model proposed by White⁴⁷ for transport landings is of special interest in that it allows for some inaccuracy in the flare, by specifying three phases:—

- (i) An initial flare.
- (ii) A float period.
- (iii) A touch-down period.

For the estimation of landing distance, it is convenient to consider these three phases in the reverse order and several empirical values need to be introduced (Fig.48).

11.5 Generalised Equations (Powered Lift) and Step-by-Step Integration

The basic equations for the airborne part of the landing are of course identical to those set down for take-off (Fig.41), but with a descent angle $\gamma' (\equiv -\gamma)$ introduced. Again, the pitch angles α , $(\alpha - \gamma')$ and θ_i are specified by pilot/automatic inputs and relevant airworthiness/geometry constants, while the space coordinates (s, h) can follow from the timewise integration of the forward speed $V \cos \gamma'$ and descent speed $V \sin \gamma'$ respectively.

Step-by-step integration procedures for the equations can be formulated similar to those in the take-off flow-diagram of Figure 42, including the introduction of appropriate limit stops to satisfy landing operational restraints. Likewise, if time itself is of no significance as a variable, the airborne path length can itself be introduced and used instead (Section 9.5), when again a possible ill-conditioned state of the first step in the flare-out may need to be watched.

12. CONCLUDING REMARKS

Although the foregoing discussion of airfield performance prediction methods is extensive (see list of contents), several aspects have had to be left out in limiting the scope of this paper. Some involve natural extensions of the ideas and methods already presented, e.g.

- (i) algebraical treatments of ground-run and airborne-path equations for powered lift systems;
- (ii) application of special airfield devices, such as catapult-launchers and arrester-gears;
- (iii) effects of natural wind, such as from headwinds or tailwinds, wind shear, cross-winds and gusts;
- (iv) influence of weather categories and automatic landing/take-off devices.

However, from my own viewpoint at least, the most significant related topic not discussed here is the prediction of aircraft noise, during airfield operations and associated climb-out/descent-approach paths. Nowadays, the aircraft designer is faced with the problem of predicting, assessing and guaranteeing the noise field from future transport aircraft projects to a much greater accuracy than hitherto, while at the same time achieving much lower noise levels and improved airfield performance, as well as employing novel airframe/engine schemes. During the next decade, predictions to within ± 1 or ± 2 dB may have to be attained, along with about 20 dB reduction in noise levels at airport boundaries (e.g. 110 PNdB to 90 PNdB) and in the surrounding populated areas. Similar reductions are also desirable for some military operations; not merely for transports but also for low-level search, reconnaissance, and rescue aircraft. Moreover, such improvements are required with minimum penalties on aerodynamic, structural and propulsive efficiency. Many of these demands tend to make the resultant noise field from the engines much more sensitive to aircraft configuration, powerplant installation and flight conditions.

Naturally, some standard methods have already been developed for aircraft noise prediction, but the complexity required for comprehensive reliable treatments can be appreciated from the simplified breakdown illustrated in Figure 49. Firstly, there exist difficulties in the evaluation of noise source characteristics (engine and airframe) and of the associated noise field, even under static conditions and with only conventional meteorological effects included. Furthermore, uncertainty in the predictions of far-field sound pressure levels and spectra can arise from poor knowledge of the forward-speed flow-field effects on engine noise and its diffraction by the airframe, together with the noise arising directly from airframe aerodynamics – including the wing lift augmentation devices. In turn, such effects influence some of the radiation factors (directivity and atmospheric attenuation) and ultimately some subjective factors (e.g. through broadband spectra and pure tones) required in the calculation of far-field annoyance.

REFERENCES

General

1. Perkins, C.D., Hage, R.E. *Airplane Performance, Stability and Control*. John Wiley, 1949.
2. Dekker, F.E.D., Lean, D. *Take-Off and Landing Performance*. AGARD Flight Test Manual, Vol. I, Chapter 8, Pergamon Press, 1962.
3. Davies, D.P. *Handling the Big Jets: 2nd Edition*. Air Registration Board, 1968.
4. Perry, D.H. *A Review of Methods for Estimating the Airfield Performance of Conventional Fixed-Wing Aircraft*. RAE Unpublished Work.
5. Overesch, E. *The Problems of Exact Calculation of Take-Off and Landing Characteristics of Conventional Transport Aircraft*. AGARD Report 417, 1963.
6. Taylor, J. *Manual on Aircraft Loads*. AGARDograph 83, 1965.
7. Williams, J., Ross, A.J. *Some Airframe Aerodynamic Problems at Low Speeds*. Annals NY Acad. Sc., Vol. 154, November 1968, pp.264-305.
8. Williams, J., (Editors) Colin, P. *Assessment of Lift-Augmentation Devices*. AGARD Lecture Series LS-43-71, 1971.
9. Brooks, P.W. *The World's Airlines*. Putnam, London, 1962.

Airworthiness and Certification

11. ARB *British Civil Airworthiness Requirements Section D (Issue 8) and Section K (Issue 3)*. Air Registration Board, 1966 and 1969.
12. FAA *Federal Aviation Regulations Part 25 and Part 23*. US Federal Aviation Agency, 1965.
13. - *Design Requirements for Service Aircraft*. Aviation Publication 970, Vol.1, Chapter 607, British Government Publication, 1956.
14. - *Flying Qualities of Piloted Airplanes*. US Military Specifications Mil-F-8785.
15. - *Concorde TSS Standards 2-1*. Issue 3, 1969.
16. Snyder, C.T., et al. *Simulation Studies for Development of Safety Criteria Applicable to SST Take-Off*. Paper 21, NASA SP 270, 1971.
17. Hall, L.J.W., Meiklem, P. *Safety Level and STOL Performance*. BALPA Symposium on V/STOL in Civil Aviation, London, 1970.
18. Holzhauser, C.A., Innis, R.C. *Safety Considerations for Powered Lift STOL Aircraft*. Paper 17, NASA SP 270, 1971.

Take-Off Prediction

21. Perry, D.H. *An Analysis of Some Major Factors Involved in Normal Take-Off Performance*. ARC Current Paper 1034, RAE TR 67314, 1967.
22. Perry, D.H. *The Airborne Path During Take-Off for Constant Rate-of-Pitch Manoeuvres*. ARC Current Paper 1042, RAE TR 68071, 1968.
23. Perry, D.H. *Exchange Rates Between Some Design Variables for an Aircraft Just Satisfying Take-Off Distance and Climb Requirements*. RAE TR 69167, 1969.
24. Nilakantan, P., Krishnamurthy, T.S. *Take-Off Ground Run of Aeroplanes*. J. Aero Soc. of India, Vol.4 (4), 1952, pp.119-131.

25. Krenkel, A.R.,
Salzman, A. *Take-Off Performance of Jet-Propelled Conventional and Vectored-Thrust STOL Aircraft.* Journal of Aircraft, Vol.5 (5), 1968, pp.429-436.
26. Kettle, D.J. *Ground Performance at Take-Off and Landing.* Aircraft Engineering, Vol.30, 1958; RAE TM Aero 481.
27. John, G. *A Further Development in Calculating the "Take-Off to 50 ft" Distance of an Aeroplane.* Aircraft Engineering, Vol.20, 1948, pp.98-101.
28. — *Estimation of Take-Off Distance.* Royal Aeronautical Society Data Sheet Perf. EG 5/1, 1952.
29. Buckingham, W.R.,
Lean, D. *Analysis of Flight Measurements on the Airborne Path During Take-Off.* ARC Current Paper 156; RAE TN Aero 2191, 1952.
30. Buckingham, W.R. *A Theoretical Analysis of the Airborne Path During Take-Off.* Aircraft Engineering, Vol.30, 1958, pp.5-8.
31. Ewans, J.R.,
Jufton, P.A. *Note on a Method of Calculating Take-Off Distance.* RAE TN Aero 880, 1940.
32. Rogerson, G.E. *Estimation of Take-Off and Landing Airborne Paths.* Aircraft Engineering, Vol.32, 1960, pp.328-331.
33. Edwards, A.D. *Performance Estimation of Civil Jet Aircraft.* Aircraft Engineering, Vol.22, 1950, pp.70-75.
34. — *Civil Aircraft Airworthiness Data Recording Programme "Stall Margins During the Take-Off Manoeuvre".* ARB Technical Note 94, 1968.
35. Tomlinson, B.N.,
Judd, M. *Some Calculations of the Take-Off Behaviour of a Slender Wing Supersonic Transport Design Constrained to Follow a Specific Pitch-Attitude Time History.* ARC R & M 3493; RAE TR 65174, 1965.
36. Collingbourne, J. *A Survey of the Available Data on the Value of Rolling Resistance on Hard Runways.* RAE Unpublished Work.

Landing Prediction

41. Perry, D.H. *A First-Order Analysis of Landing Performance Based on Current British Civil Airworthiness Requirements.* RAE Unpublished Work.
42. — *A First Approximation to the Total Landing Distance from 50 ft Height.* Royal Aeronautical Society Data Sheet Perf. EG 6/1, 1960.
43. — *Estimation of Approach Speed.* Royal Aeronautical Society Data Sheet Perf. EG 6/2, 1959.
44. — *Estimation of Airborne Distance During Landing.* Royal Aeronautical Society Data Sheet Perf. EG 6/3, 1960.
45. — *Estimation of Ground-Run During Landing.* Royal Aeronautical Society Data Sheet Perf. EG 6/4, 1960.
46. Cook, P.H.,
Thorne, R.G. *The Landing Flare.* RAE Unpublished Work.
47. White, M.D. *Proposed Analytical Model for the Final Stages of a Landing of a Transport Airplane.* NASA TN D-4438, 1968.
48. Yager, J.T. *A Comparison of Aircraft and Ground Vehicle Stopping Performance on Dry, Wet, Flooded, Slush, Snow and Ice-Covered Runways.* NASA TN D-6098, 1970.

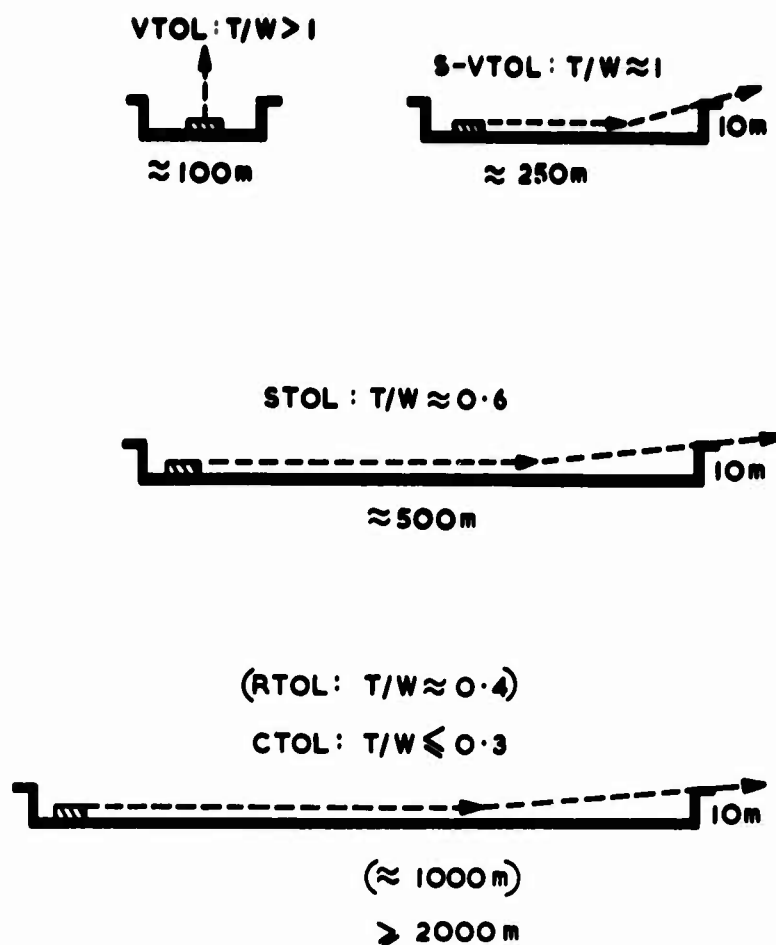


Fig.1 Spectrum of airfield capabilities

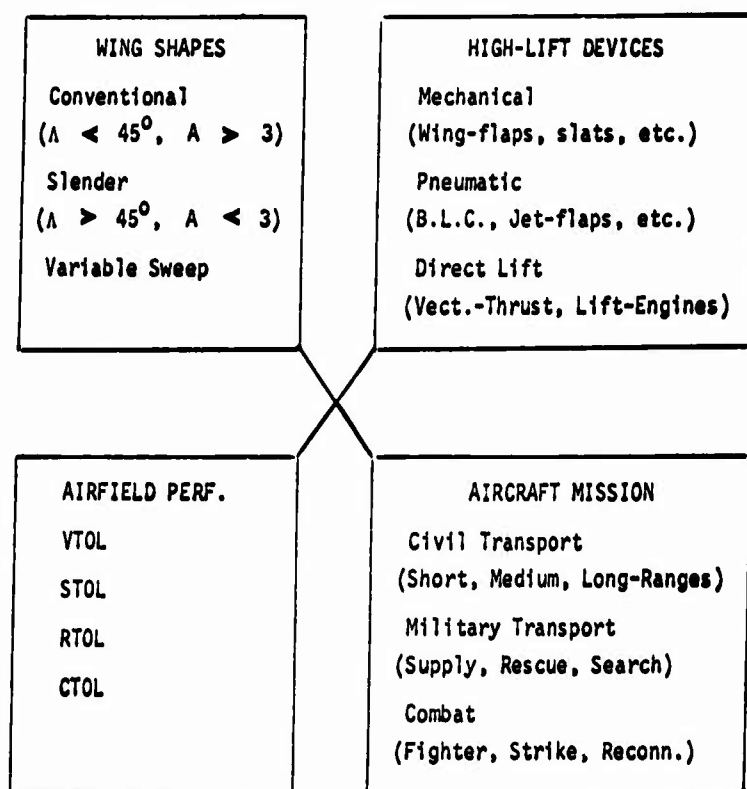


Fig.2 Broad spectrum of aircraft configurations and utilisation

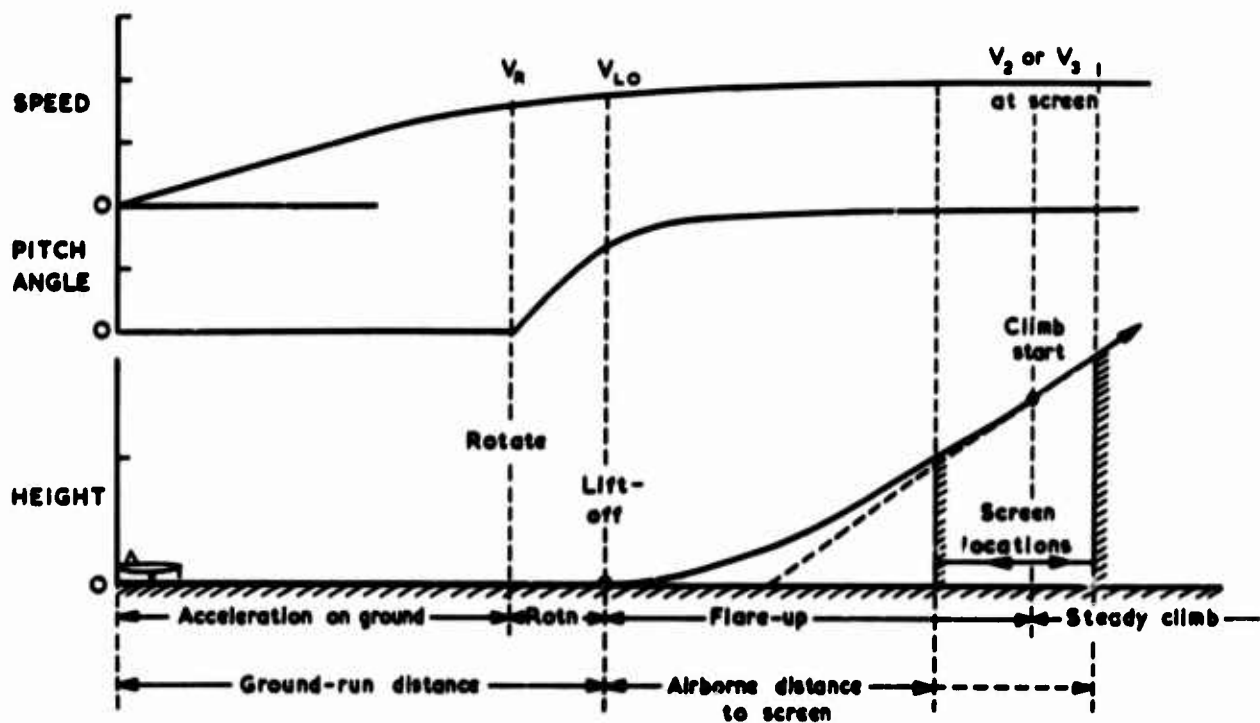


Fig.3 Basic take-off framework

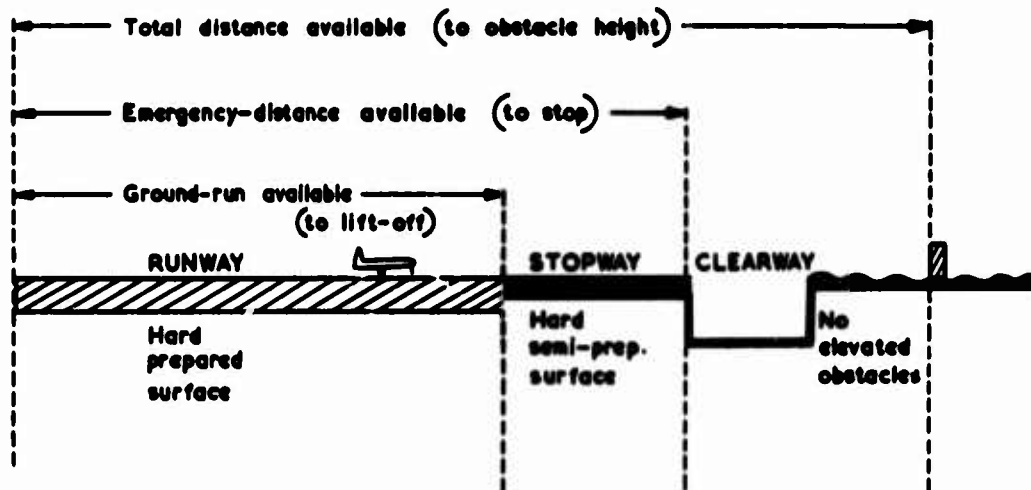


Fig.4 Take-off airstrip utilisation

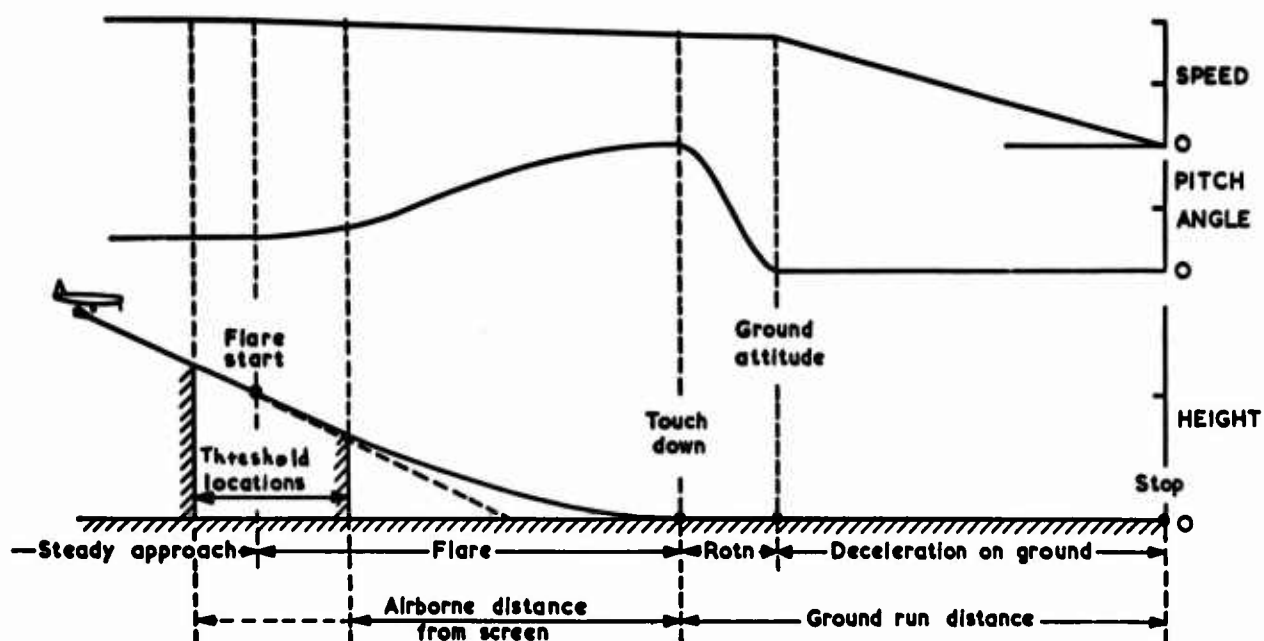


Fig.5 Basic landing framework

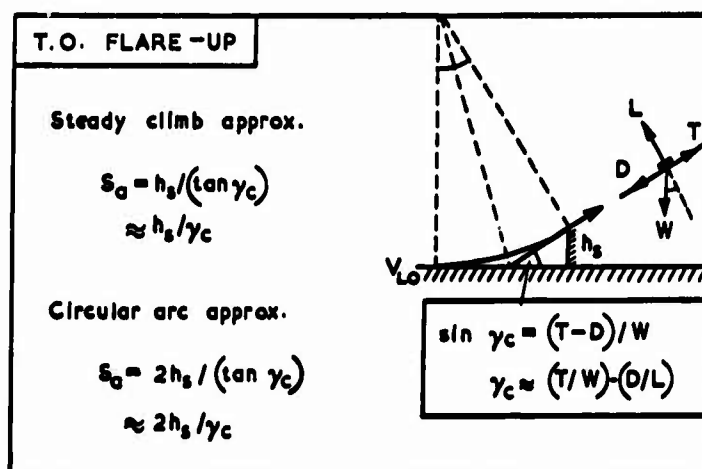
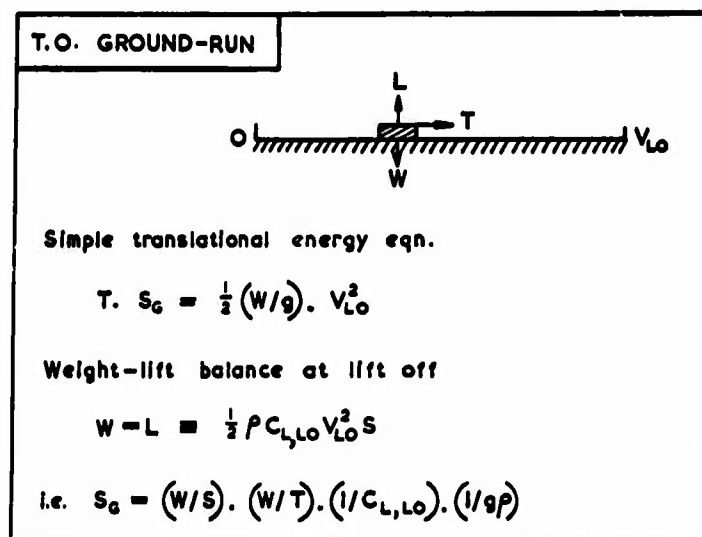


Fig.6 Crude take-off models

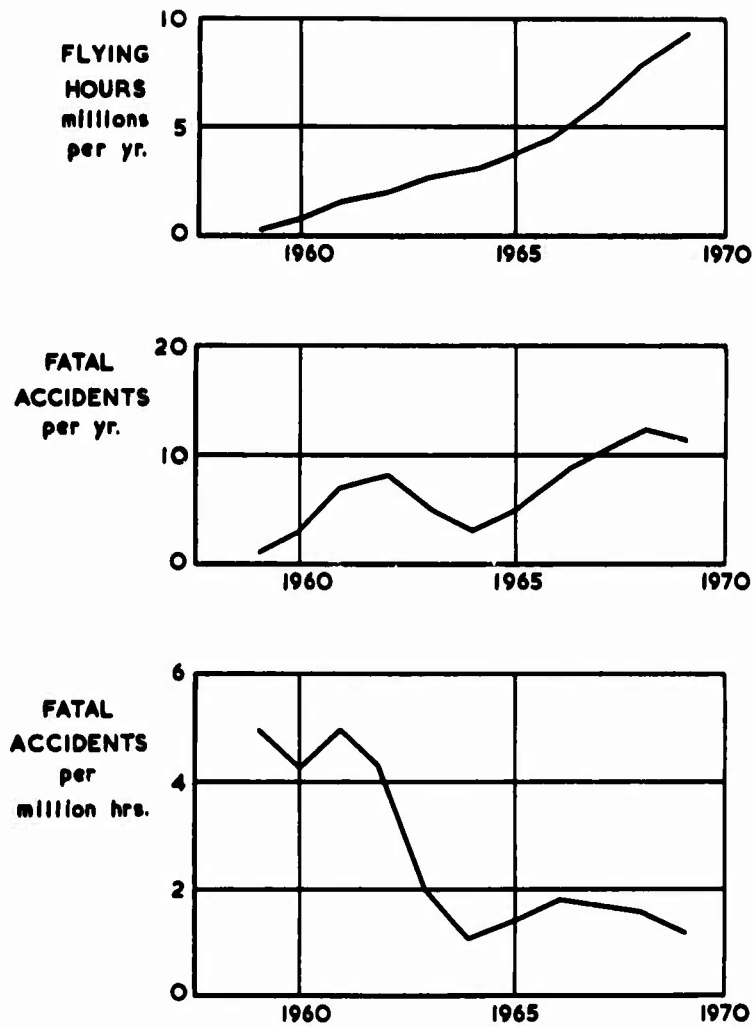


Fig.7 Conventional jet transports (revenue operations)

Performance
 Stability & Controllability
 Structural Integrity
 Powerplant Integrity
 Systems Integrity
 Fire Safety
 Cabin Environment
 Navigational Information
 (position & environment)

Fig.8 General safety factors

[...]	Signifies ratio of upper reference speed to lower
(ae)	Denotes all-engines condition
(fe)	Denotes critical engine failure condition
(me)	Denotes minimum engine power condition

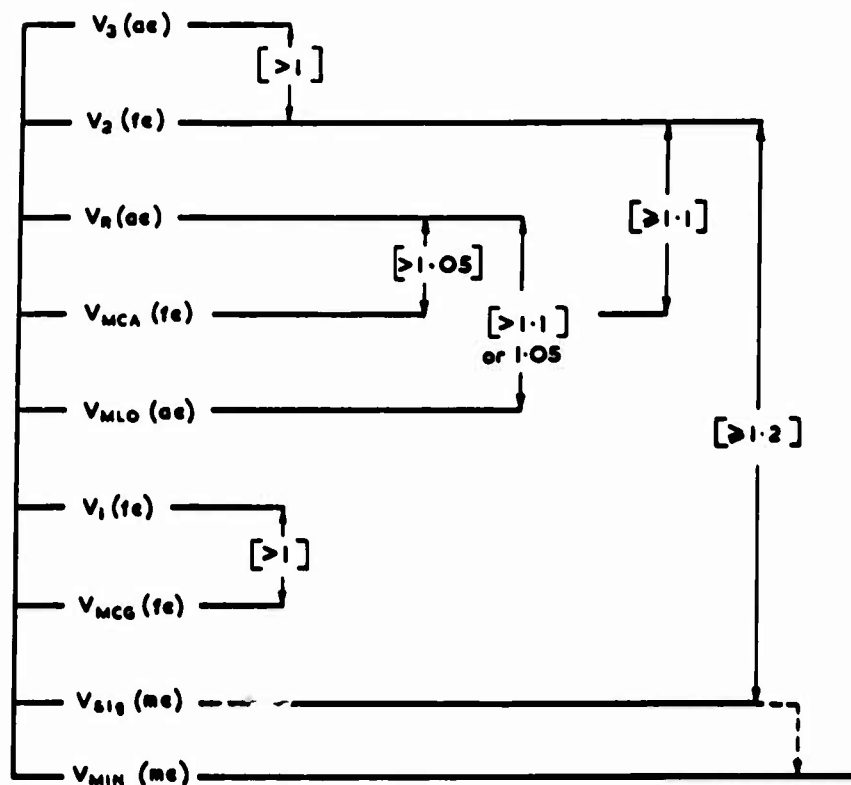


Fig.9 Typical take-off reference speeds. Conventional transport

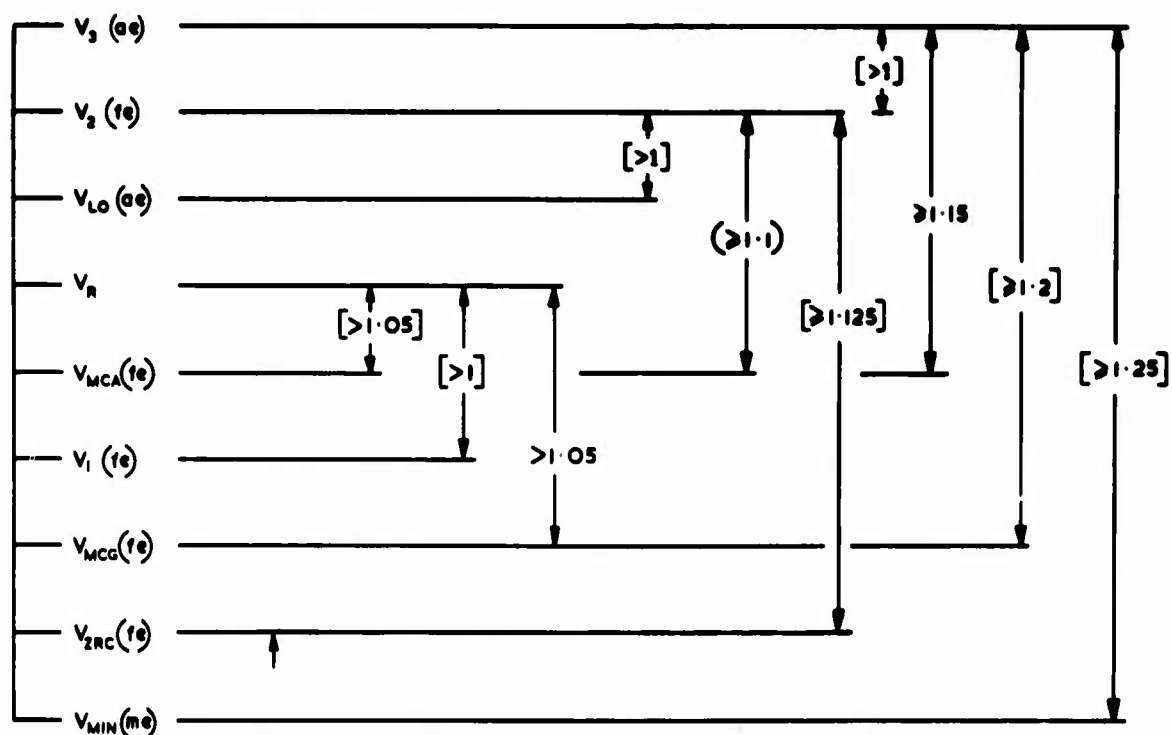


Fig.10 Typical take-off reference speeds. Slender transport

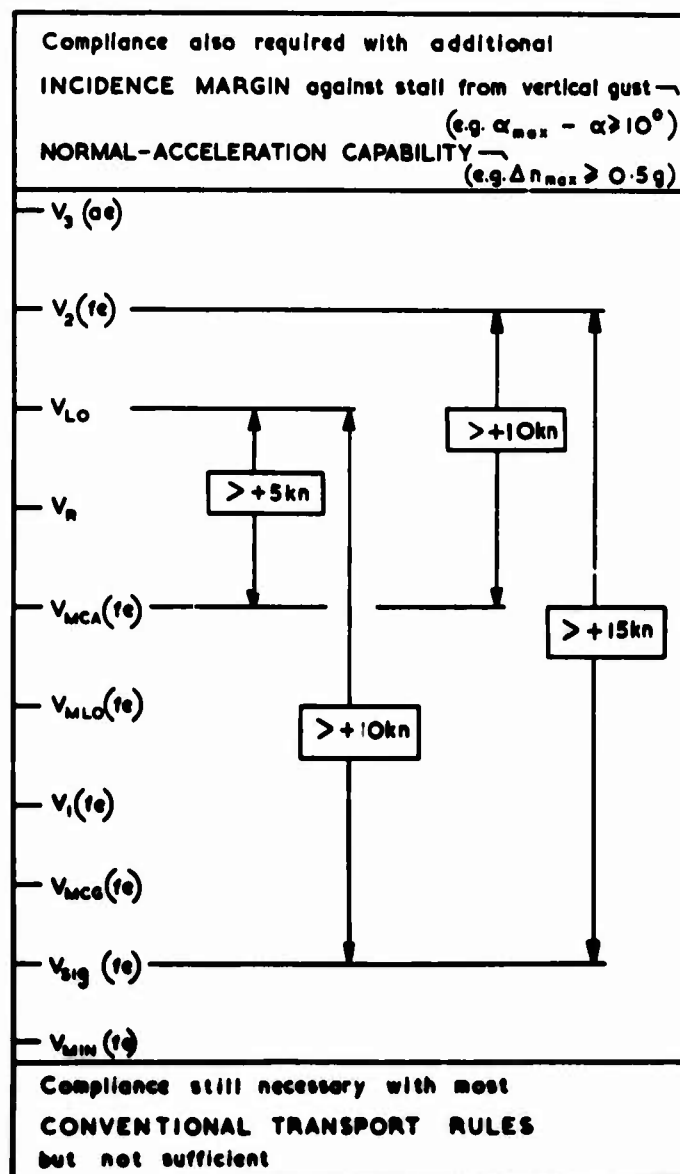
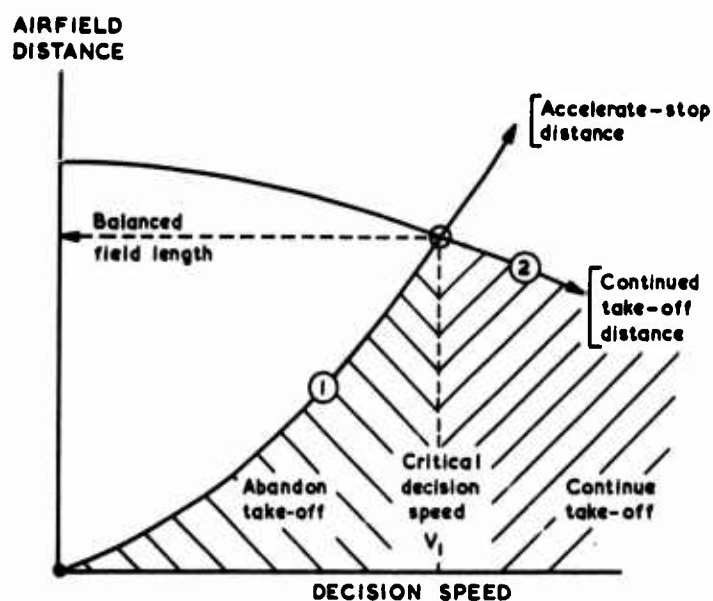


Fig. 11 Possible take-off reference speeds. STOL transport



① Brake to stop if $V_{fe} < V_1$

② Continue take-off if $V_{fe} > V_1$

Fig.12 Balanced field-length concept

TYPICAL FOR CONVENTIONAL TRANSPORTS	
FACTORED ALL-ENGINES DISTANCE to 35ft height	$1.15 \times [S_G + S_A]_{00, 35}$
EMERGENCY DISTANCE (DRY RUNWAY) to 35ft height or stop: critical engine failure.	$[S_G + S_A]_{10, 35}$ $\approx [S_G + S_{S, DRY}]_{10}$
EMERGENCY DISTANCE (WET RUNWAY) to 15ft height or stop: critical engine failure.	$[S_G + S_A]_{10, 15}$ $\approx [S_G + S_{S, WET}]_{10}$
FACTORED ALL-ENGINES GROUND-RUN	$1.15 \times [S_G + \frac{1}{2} S_A]_{00, 35}$
EMERGENCY GROUND-RUN critical engine failure	$[S_G + \frac{1}{2} S_A]_{10, 35}$
EMERGENCY DISTANCE (EARLY-ROTATION) to 35ft height: critical engine failure V_R (actual) $\approx V_R$ (ref) - 5kn or $0.95 V_R$ (ref)	$[S'_G + S'_A]_{10, 35}$

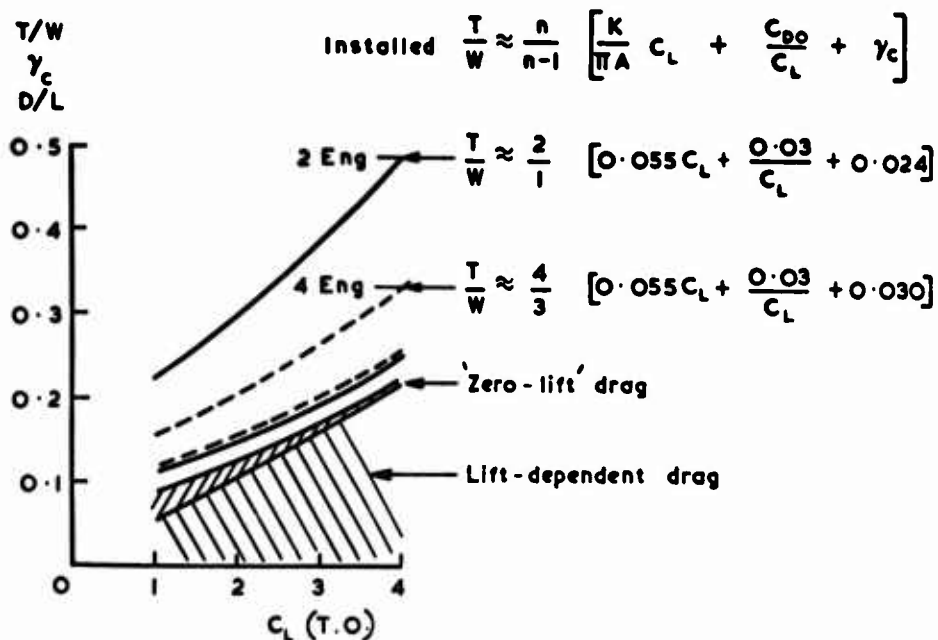
POSSIBLE ADDITIONS FOR SLENDER OR STOL	
ALL-ENGINES DISTANCES WITH EARLY OR LATE ROTATION: to 35ft height (e.g. ± 3 secs relative to $V = V_R$ for slender)	$1.05 \text{ or } 1.0 \times [S'_G + S'_A]_{00, 35}$

Fig.13 Take-off reference distances

TYPICAL FOR CONVENTIONAL TRANSPORTS (Critical engine failure)			
INSTALLED ENGINES	2 Eng	3 Eng	4 Eng
CLIMB SEGMENT			
1st Seg (U/C down)	0%	0.3%	0.5%
2nd Seg (U/C up)	2.4%	2.7%	3.0%
3rd Seg (U/C up; Flaps reset)	1.2%	1.5%	1.7%

POSSIBLE ADDITIONS FOR SLENDER (Critical engine failure)			
Climb segments with $\left\{ \begin{array}{l} V = V_2 - 10 \text{ kn in rectilinear flight} \\ \text{or } 18^\circ \text{ Bank angle and } V = V_2 \end{array} \right.$			
	2 Eng	3 Eng	4 Eng
2nd Seg (U/C up)	1.6%	1.8%	2.0%
3rd Seg (U/C up; Flaps reset)	0.4%	0.6%	0.7%

Fig.14 Take-off climb gradients

Fig.15 Comparative breakdown of installed T/W for take-off climb

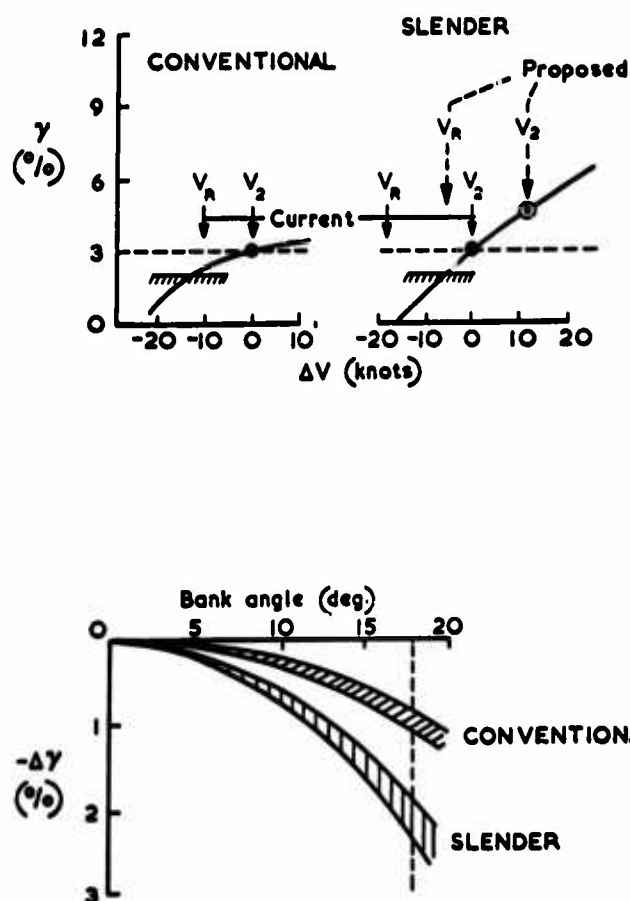


Fig.16 Take-off climb gradients (1 of 4 engines failed). Comparison of conventional and slender transports

Speed and Lift Margins

$$V_{LO} \approx 1.12 V_{s,1g}; C_L < 0.8 C_{L_{max}}$$

Rotation Rate Limitation

$$d\alpha/dt < 50^\circ/s$$

Scheduled T.O. Distance: All-Engines

$$\text{Runway length} > K(S_G + S_a)_{ae,50'}$$

$$\text{with } K \approx 1.25 \text{ to } 1.5$$

Climb-Rate at Screen: 1 of 2 Eng. Failed

$$dh/dt > 5 \text{ m/s (1000 ft/min)}$$

Fig.17 Typical simplified take-off margins. Combat aircraft

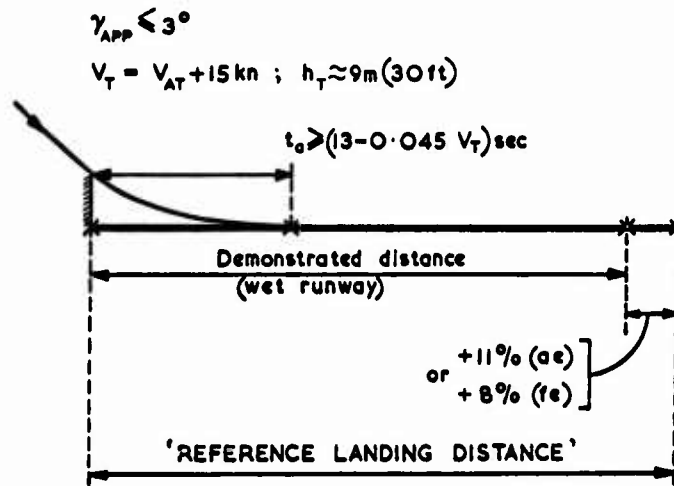
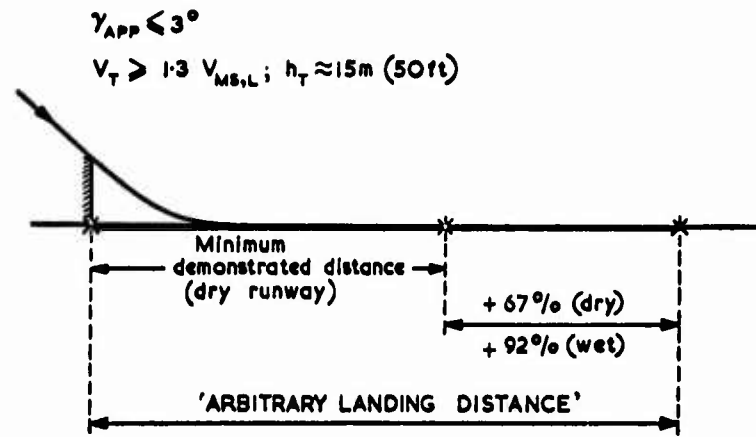


Figure 18

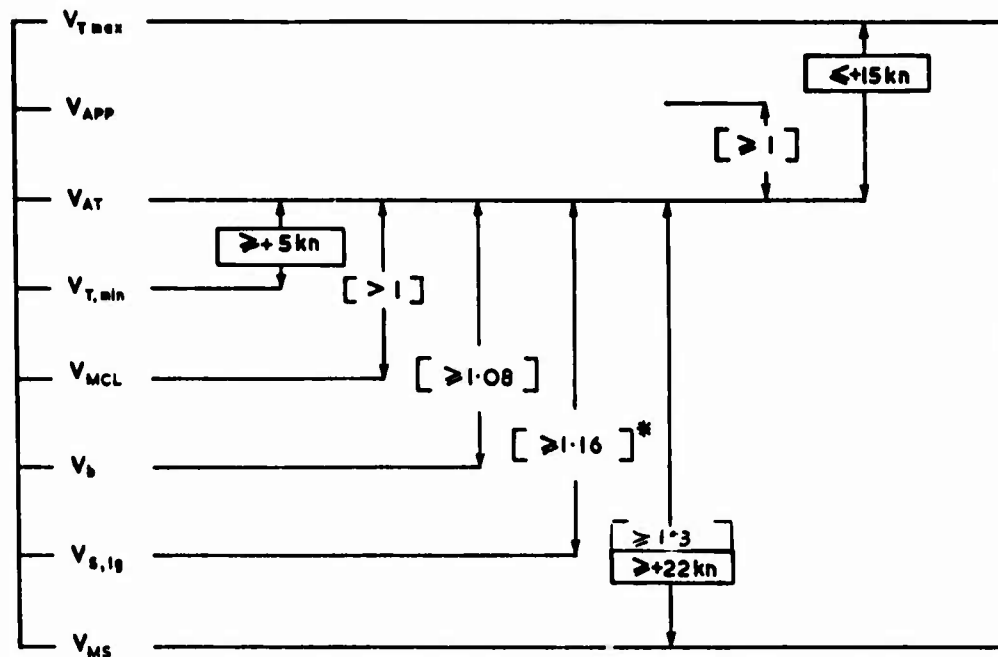


Fig.19 Typical landing reference speeds. Conventional transport

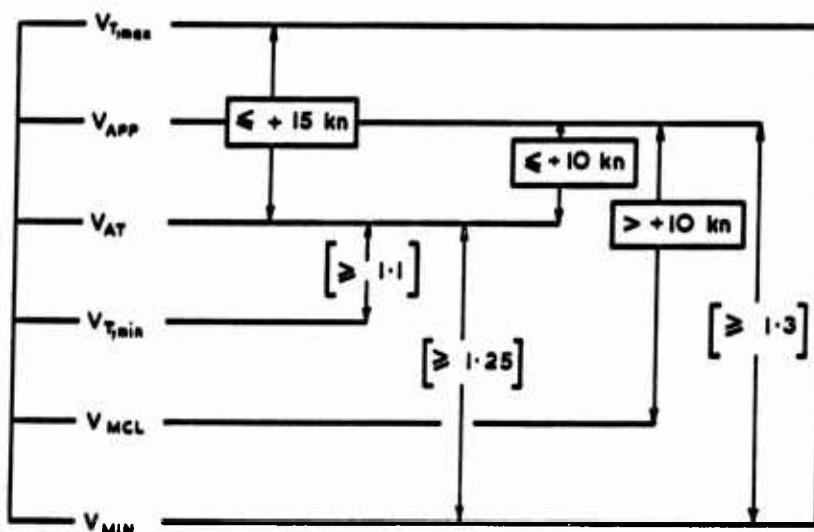


Fig.20 Typical landing reference speeds. Slender transport

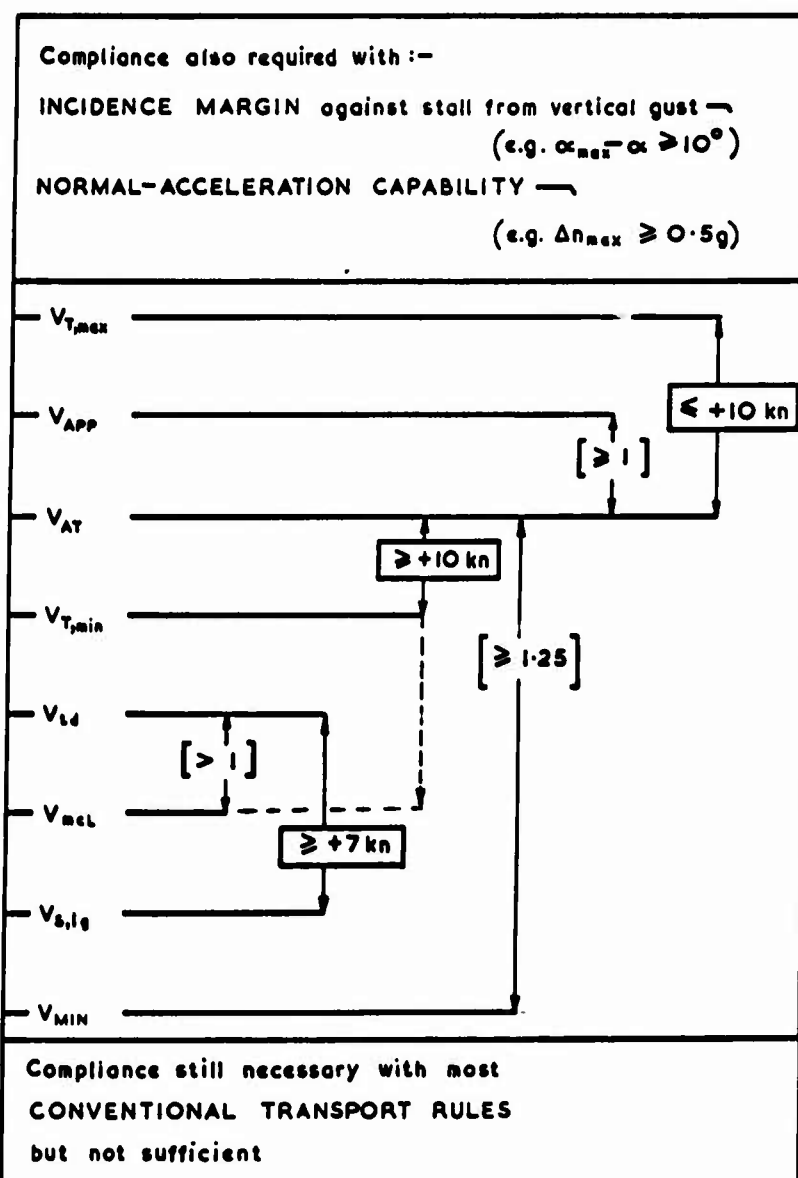


Fig.21 Possible landing reference speeds. STOL transport

Speed Margins

$$V_A > \begin{cases} 1.2 V_{s,lg} & \text{for Visual Approach} \\ 1.3 V_{s,lg} & \text{for Instrument Approach} \\ 1.15 V_{s,lg} & \text{for No-Flare Approach} \end{cases}$$

$$V_{td} > 1.10 V_{s,lg}$$

Rotation Rate Limitation

$$d\alpha/dt < 50^\circ/s$$

Scheduled Landing Distance

$$\text{Runway Length} > K(S_G + S_a)_{50'}$$

$$\text{with } K \approx 1.25 \text{ to } 1.5$$

Climb after Discontinued or Baulked Approach

$$\gamma_c > \begin{cases} 0 & \text{if 1 of 2 Eng. Failed.} \\ 2.5\% & \text{All Eng. Operating.} \end{cases}$$

after 5 s from select full-power and close airbrakes, with U/C down and approach flaps.

Fig.22 Typical simplified landing margins. Combat aircraft

DISCONTINUED FINAL APPROACH	
$V > \begin{cases} 1.2 \times V_{s,lg} \\ V_{MCL} + 5 \text{ kn} \\ V_{APP} \end{cases}$	$\gamma_c > \begin{cases} 1.1\% & \text{for 2 eng. instal.} \\ 1.3\% & \text{for 3 eng. instal.} \\ 1.4\% & \text{for 4 eng. instal.} \end{cases}$
<p>(i) Speed and gradients correspond to one engine failed and others at max. contingency</p> <p>(ii) Any configuration change must be completed within 10 secs</p> <p>Any reduction of associated stalling speeds $\leq 5\%$</p>	
BAULKED LANDING	
$V > \begin{cases} 1.2 \times V_{s,lg} \\ V_{MCL} \\ V_{AT} \end{cases}$	$\gamma_c > 3.2\%$
<p>(i) All-engines at max. T.O. rating if attainable within 8 secs</p> <p>(ii) Any configuration change must be completed within 5 secs</p>	

Fig.23 Typical climb demands for conventional transport

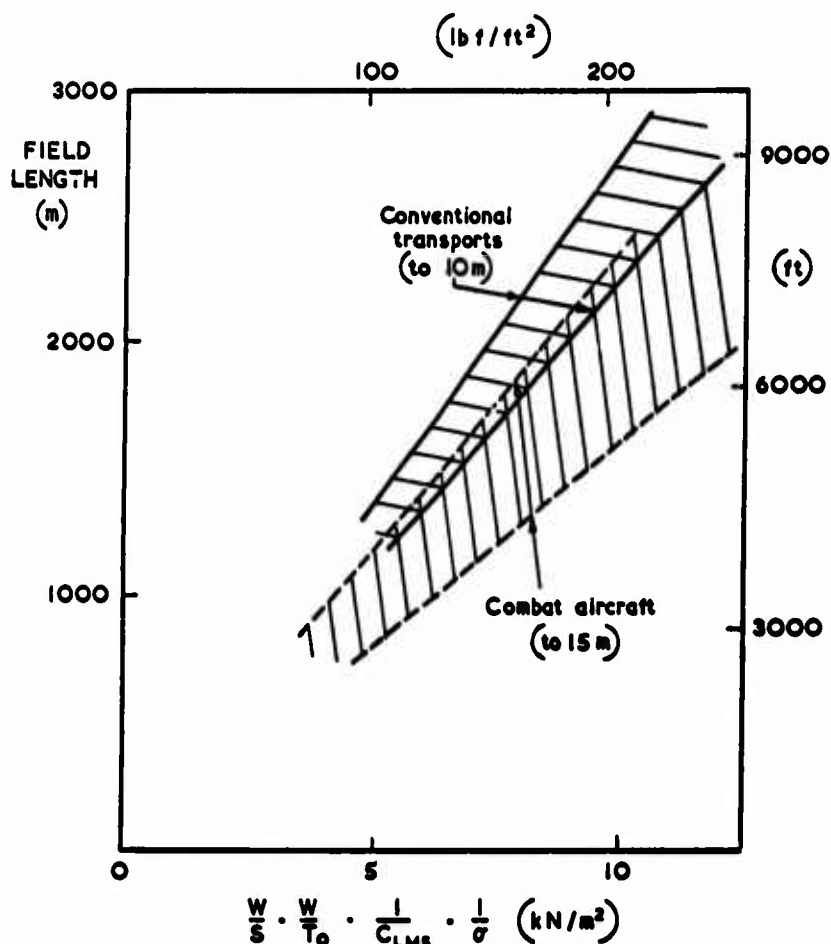


Fig.24 Take-off distance to screen. Semi-empirical correlation

Elementary Kinematic Relations

Assume Overall Mean deceleration d

$$\begin{aligned} \text{i.e. } S_{Ldg} &\approx \frac{1}{2} d V_A^2 = \frac{1}{2} d (K V_{S,lg})^2 \\ &= d K^2 \cdot (W/S) \cdot (1/\rho C_{Lmax}) \end{aligned}$$

where $K \approx 1.3$ typically.

Representative Mean Decelerations

Elementary Braking Systems	1.2 m/s ² (4 ft/s ²)
Average Techniques but No Automatic Braking	1.5 m/s ² (5 ft/s ²)
Modern Braking with Automatic Control	1.8 m/s ² (6 ft/s ²)
Modern Braking with Lift-Dumping and Reverse Thrust	2.1 m/s ² (7 ft/s ²)

Fig.25 Overall landing distance. Crude estimation method

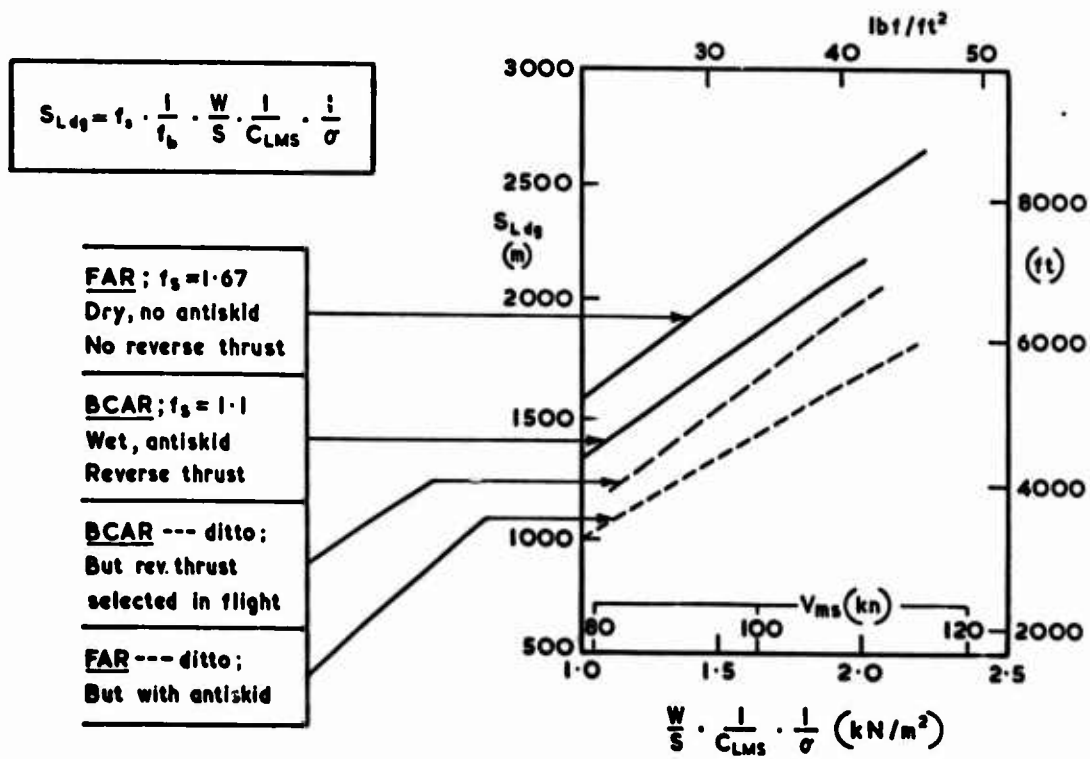


Fig.26 Landing distance correlation. Conventional transports

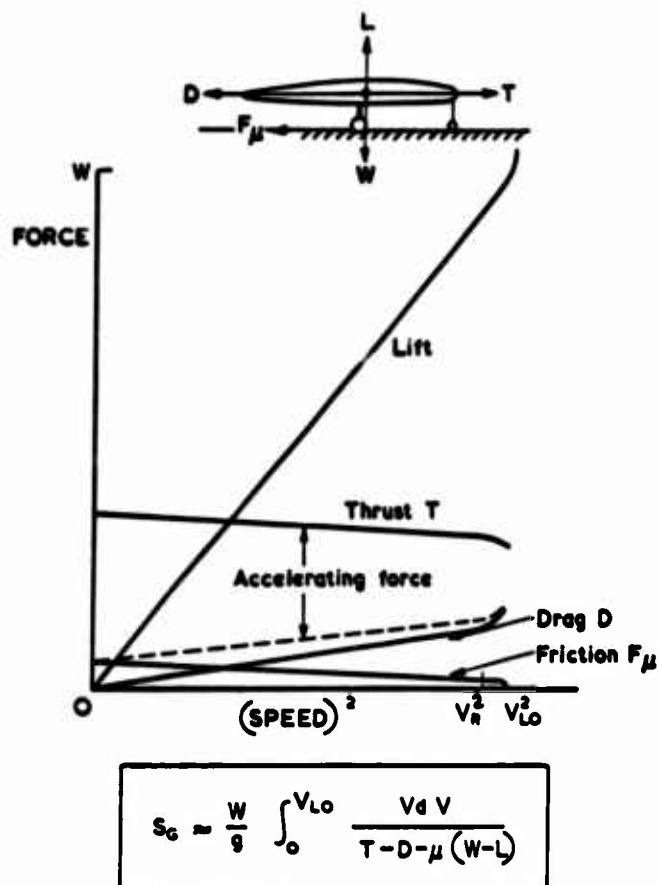


Fig.27 Take-off ground-run framework

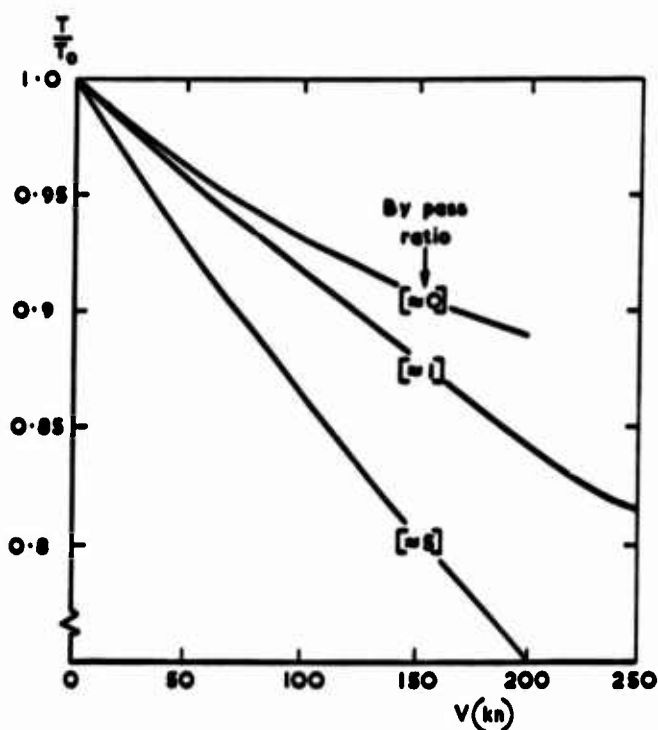
Hard Runway	0.025
Hard Turf	0.04
Short Grass	0.05
Long Grass	0.10
Soft Ground	0.10 to 0.3

CONVENTIONAL ROLLING RESISTANCE COEFFICIENTS

TYRE	AIRCRAFT	RUNWAY
Tread/Wear	Forward Speed	Surface
Material	Vertical Load	Contamination
Pressure	Yawed Rolling	
Heating	U/C Type	
Tyre Footprint		

GROUND ROLLING RESISTANCE FACTORS

Fig.28 Rolling resistance



TYPICAL POLYNOMIAL APPROXIMATIONS

$$\frac{T}{T_0} \begin{cases} = K_0: & (0 < K_0 \leq 1) \\ = K_0 + K_1 V: & (K_0 = 1, K_1 < 0) \\ = K_0 + K_2 V^2: & (K_0 = 1, K_2 < 0) \\ = K_0 + K_1 V + K_2 V^2: & (K_1 < 0, K_2 > 0) \end{cases}$$

Fig.29 Take-off engine-thrust variation

Force Model (T.O.)

$$D = C_{DG}qS, \quad L = C_{LG}qS,$$

$$T = T_0(1 + k_2 V^2), \quad F_\mu = \mu_R(W - L).$$

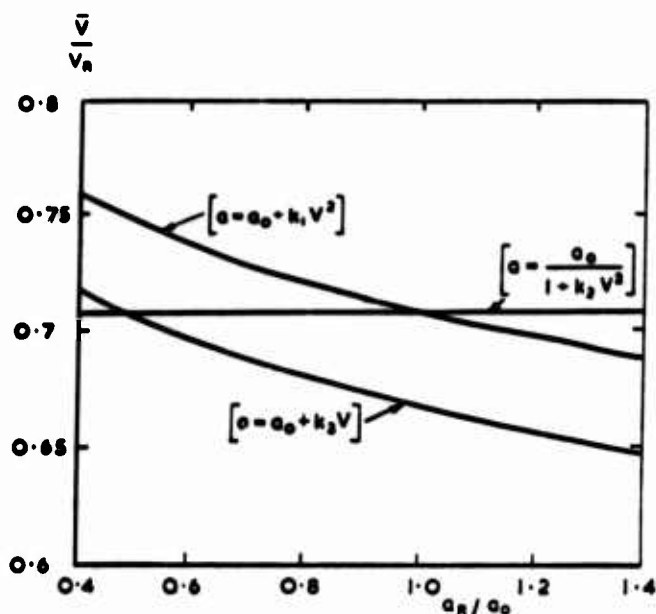
$$C_{DG} = \mu_R C_{LG}, \quad \mu_R, \quad T_0, \quad k_2 \quad \text{all constant}$$

Distance Integral (T.O.)

$$\begin{aligned} S_{GR} &= \frac{W}{g\rho} \int_0^{L_0} dq / \{(T - D) - \mu_R(W - L)\} \\ &= -\frac{W/S}{g\rho K_R} \log_e \left[1 - \frac{(K_R/C_{L,LO})}{(T_0/W) - \mu_R} \right] \end{aligned}$$

where $K_R \equiv \{C_{DG} - \mu_R C_{LG} - (k_2 T_0 / \rho S)\}$, $C_{L,LO} \equiv W / q_{LO} S$

Fig.30 Take-off ground run. Simplified integration



$$\begin{array}{c} C_{DG}qS \leftarrow \boxed{} \rightarrow T : a = \frac{dV}{dt} \\ \mu(W - C_{LG}qS) \leftarrow \end{array}$$

$$S_{GR} = \int_0^R \left\{ \frac{V dV}{\bar{a}} \right\} = \frac{V_R^2}{2\bar{a}}$$

Where \bar{a} then given by identity :-

$$\frac{\bar{a}}{g} = \left[\frac{T}{W} - \mu - \frac{S}{W} \{C_{DG} - \mu C_{LG}\} \right]_{V=\bar{V}}$$

Fig.31 Take-off ground run. Equivalent mean acceleration concept

Accn. Eqn. of Motion

$$\frac{W}{g} \frac{dV}{dt} = \sum_i \{ T_{Gi} \cos (\alpha + \theta_i) - D_{Ei} \} - D_A$$

$$- \mu_r \left[W - L_A - \sum_i \{ T_{Gi} \sin (\alpha + \theta_i) \} \right]$$

where T_{Gi} and D_{Ei} are Fns. of Throttle and V , p .

$$D_A = \frac{1}{2} \rho V^2 C_D(\alpha; \theta_i, h) S$$

$$L_A = \frac{1}{2} \rho V^2 C_L(\alpha; \theta_i, h) S$$

$$\mu_r \approx \text{Constant or Fn. of } V$$

α and $\theta_i \approx \text{Constant for } V < V_R$

α or $\theta_i \dots \text{Rapid Varn. for } V \geq V_R$.

Decn. Eqn. of Motion

$$- \frac{W}{g} \frac{dV}{dt} = \mu \left[W - L_A - \sum_i \{ T_{Gi} \sin (\alpha + \theta_i) \} \right]$$

$$+ D_A + \sum_i \{ D_{Ei} - T_{Gi} \cos (\alpha + \theta_i) \}.$$

Due to Pilot Action and Time Delays

C_D , C_L , T_{Gi} , D_{Ei} , θ_i and μ are

subject to Discontinuous or Rapid Varn.

Fig.32 Ground run. Powered lift

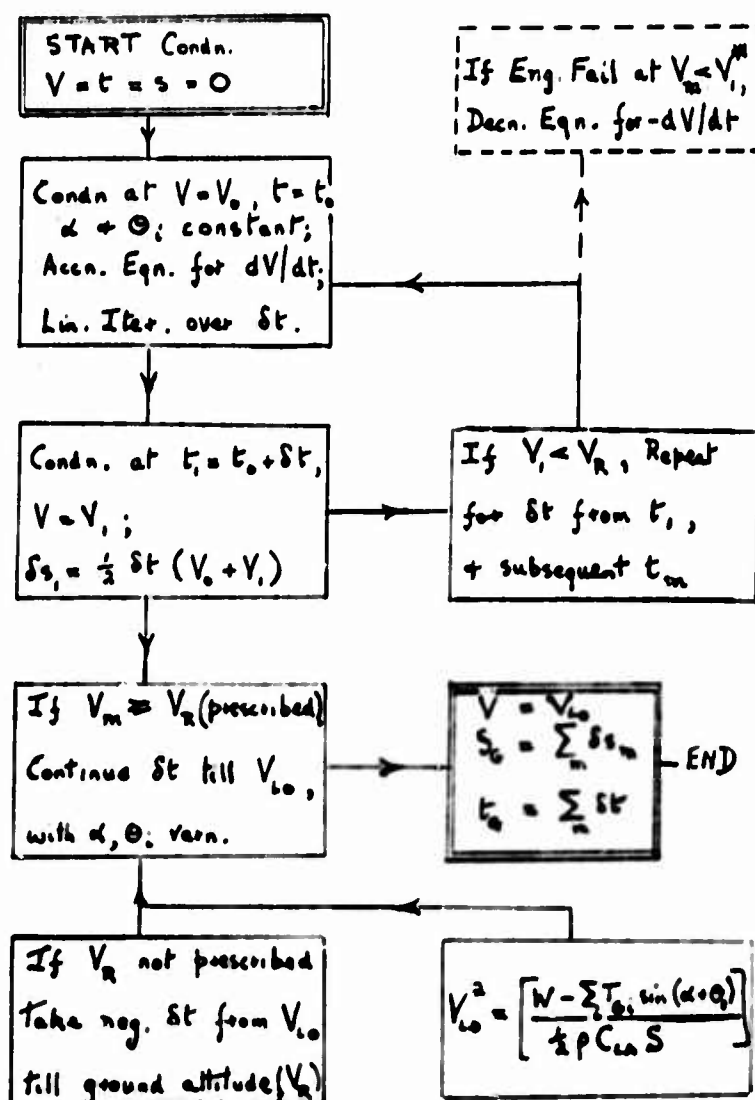


Fig.33 Take-off ground run. Step integration

Decision to Abandon T.O.

2 s -

Wheel Braking Effective

½ s -

Engine Throttles Closed

1 s -

Airbrakes Selected

1 s -

Airbrakes Effective

½ s -

Reverse Thrust Selected

2 s -

Reverse Thrust Effective
(cancel at 50-25 kn)

Transition uncompleted at screen

$$\gamma_s < \gamma_c$$

$$\begin{aligned}\gamma_s &= 2 \sin^{-1} \{h_s / 2R\}^{\frac{1}{2}} \\ &= (2h_s / R)^{\frac{1}{2}}\end{aligned}$$

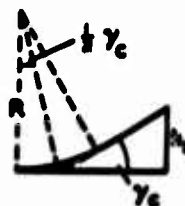
$$\begin{aligned}s_s &= (2R h_s - h_s^2)^{\frac{1}{2}} \\ &\approx (2R h_s)^{\frac{1}{2}}\end{aligned}$$



Transition completed before screen

$$\gamma_s = \gamma_c = \sin^{-1} \{(T-Q)/W\}$$

$$\begin{aligned}s_s &= R \tan (\gamma_c / 2) + h_s / (\tan \gamma_c) \\ &\approx (R \gamma_c / 2) + (h_s / \gamma_c)\end{aligned}$$



Radius and radial force

$$WV^2/gR = W(n - \cos \gamma) \text{ or } (C_L - C_{L,0}) g s$$

$$\text{i.e. } R = V^2 / (n-1)g \text{ or } (2W/S) / (\rho g \Delta C_L)$$

Fig.35 Circular-arc transition path

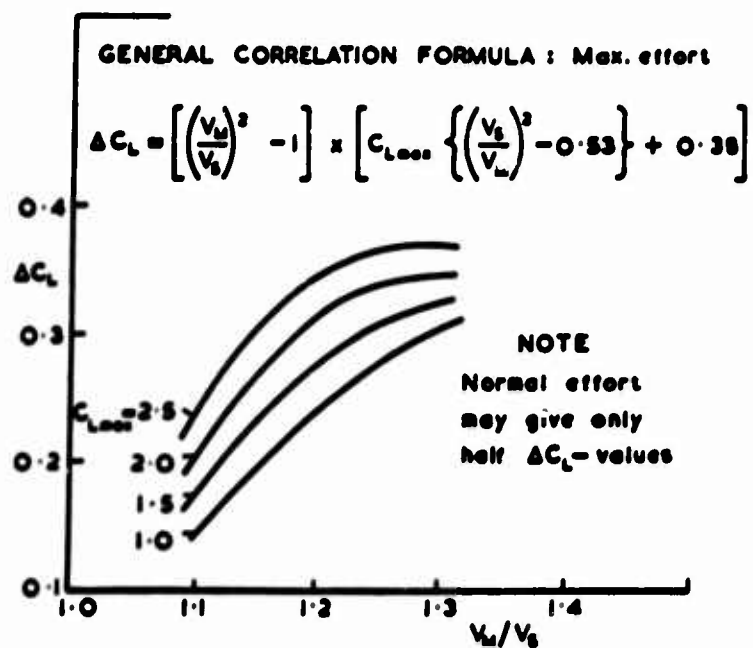
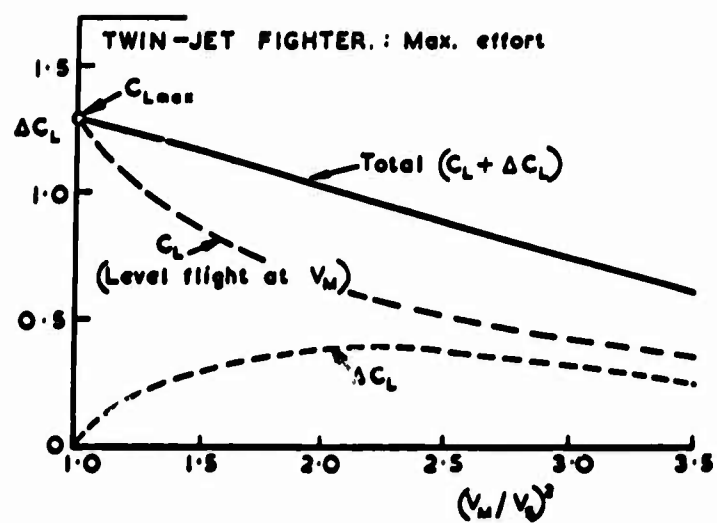


Fig.36 Take-off flare. Empirical mean ΔC_L

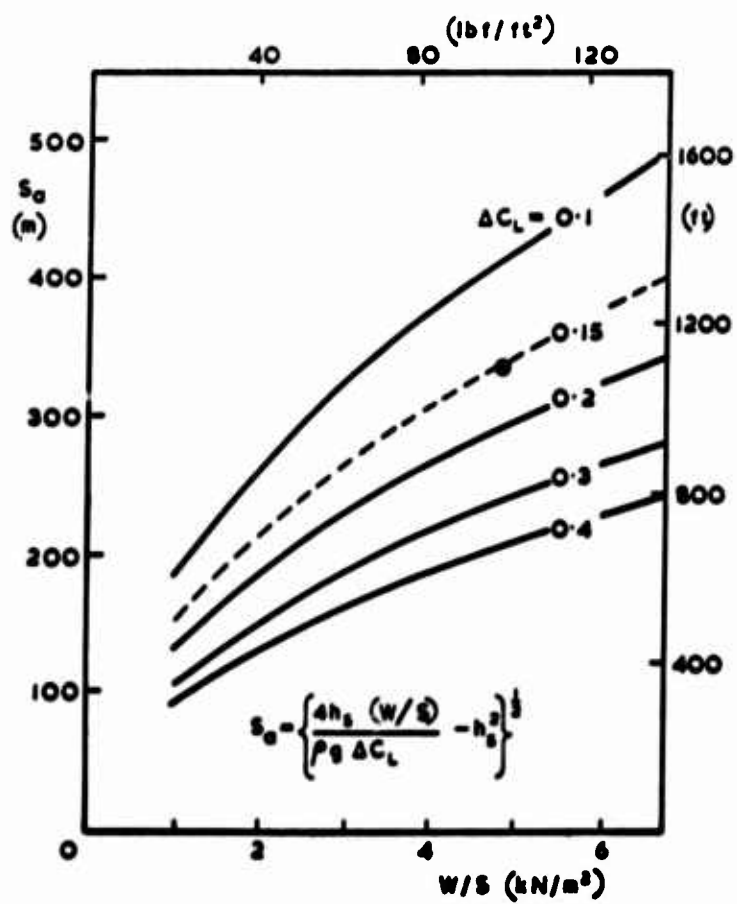


Fig.3? Take-off airborne distance, ISA/SL. Circular arc to 10.7 m (35 ft)

Basic Flare-up Equations

Along normal and tangent to element δl of flight path at angle γ to horizontal.

$$(W/g)V^2(d\gamma/dl) = L - W \cos \gamma$$

$$\frac{1}{2}(W/g)(dV^2/dl) = (T - D) - W \sin \gamma .$$

Flare-Path Equations

Assuming γ and $\delta V/V_{L0}$ small c.f. unity.

$$(T - D)/W \approx \gamma_c \text{ constant} ,$$

$$\gamma = \gamma_c \{1 - \cos (s/k)\} \text{ with } k = V_{L0}^2 / \sqrt{2}g .$$

$$\text{When } \gamma = \gamma_c ; s_c = (\pi/2)k, h_c = \gamma_c k \{(\pi/2) - 1\} .$$

Uncompleted Flare ($\gamma_s < \gamma_c$)

$$h = \gamma_c k \{(s/k) - \sin (s/k)\}$$

$$h_s / \gamma_c k = (s_s / k) - \sin (s_s / k)$$

$$V/V_{L0} = \{\sqrt{2}\gamma_c \sin (s/k) + 1\}^{\frac{1}{2}} .$$

Completed Flare ($\gamma_s \equiv \gamma_c$)

$$h = h_c + \gamma_c (s - s_c) = \gamma_c (s - k)$$

$$s_s = (h_s / \gamma_c) + k$$

$$V_c / V_{L0} = \{1 + \sqrt{2}\gamma_c\}^{\frac{1}{2}} .$$

Fig.38 Take-off flare. Accelerating with $C_L \equiv C_{L,L0}$

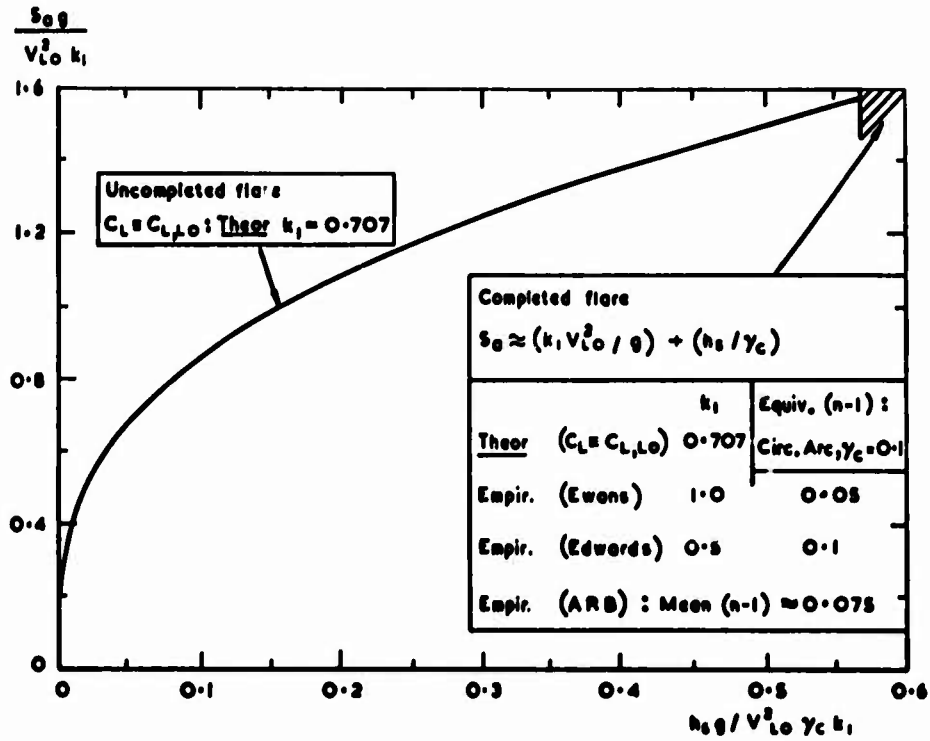


Fig.39 Take-off airborne distance to screen height

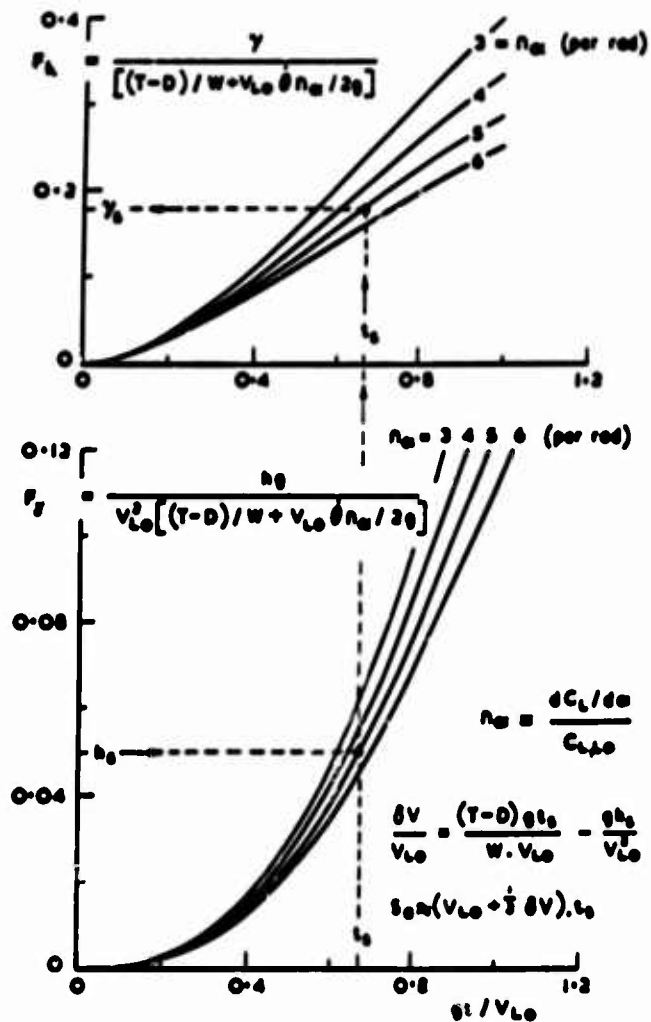
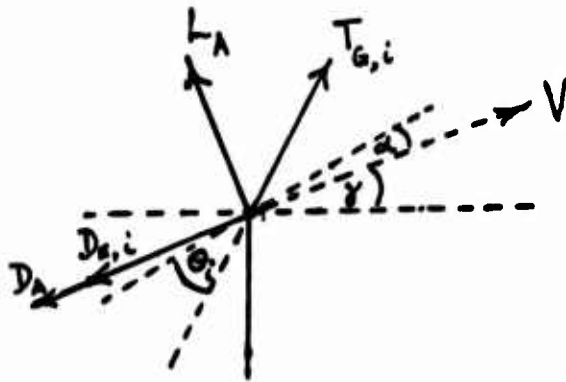


Fig.40 Take-off airborne path. Constant pitch-rate



Along Local Flight Direction

$$\frac{W}{g} \frac{dV}{dt} = \sum_i \{ T_{G_i} \cos (\alpha + \theta_i) - D_{E_i} \} - D_A - W \sin \gamma .$$

Normal to Local Flight Direction

$$\frac{W}{g} V \frac{d\gamma}{dt} = \sum_i \{ T_{G_i} \sin (\alpha + \theta_i) \} + L_A - W \cos \gamma .$$

Pitch Angles

α or $(\alpha + \gamma)$ and θ_i specified by Pilot Input and Constraints .

Space Coordinates

$$\frac{dh}{dt} = V \sin \gamma ; \quad \frac{ds}{dt} = V \cos \gamma .$$

Fig.41 Take-off airborne path. Powered lift

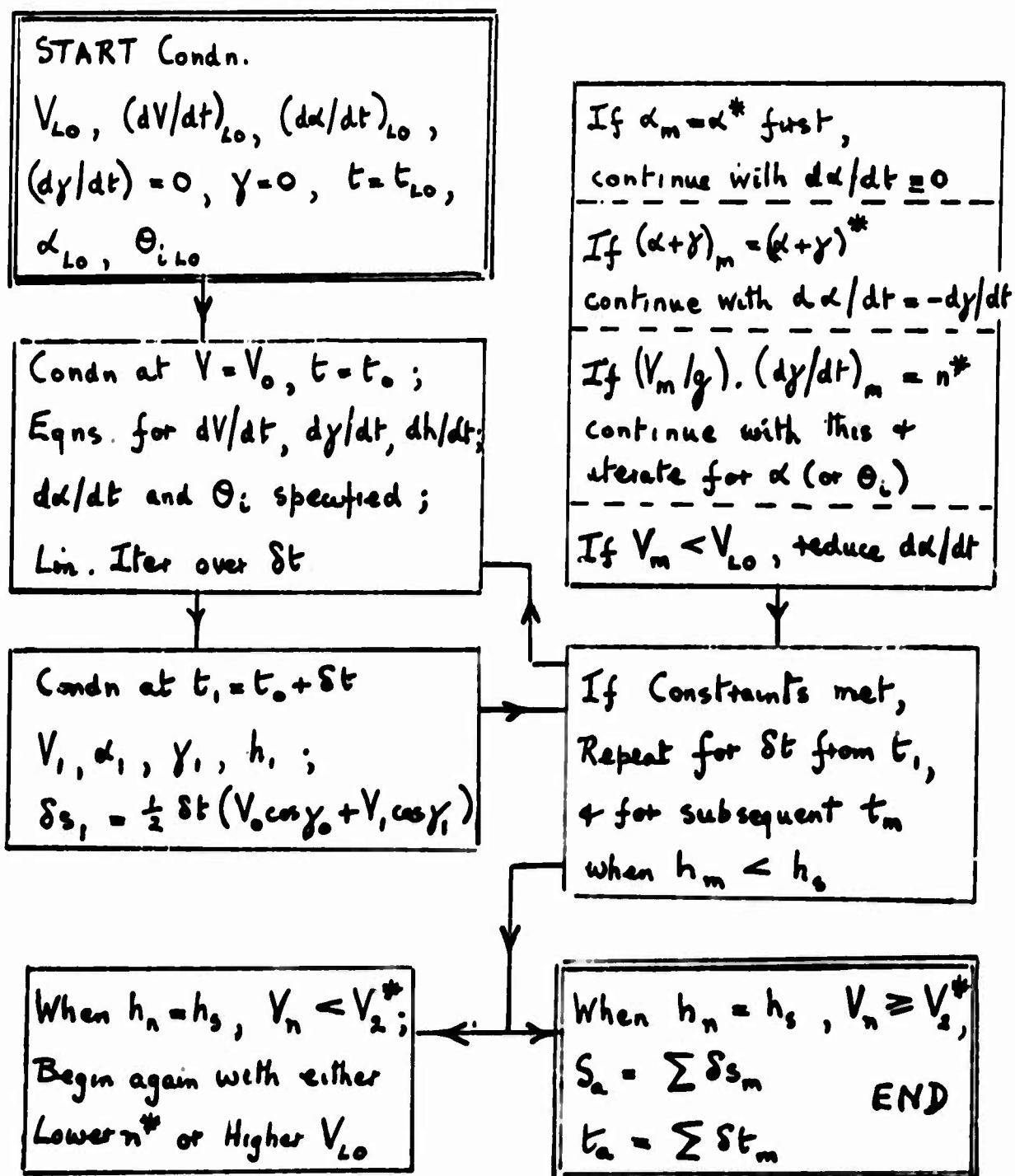


Fig.42 Take-off airborne path. Step integration

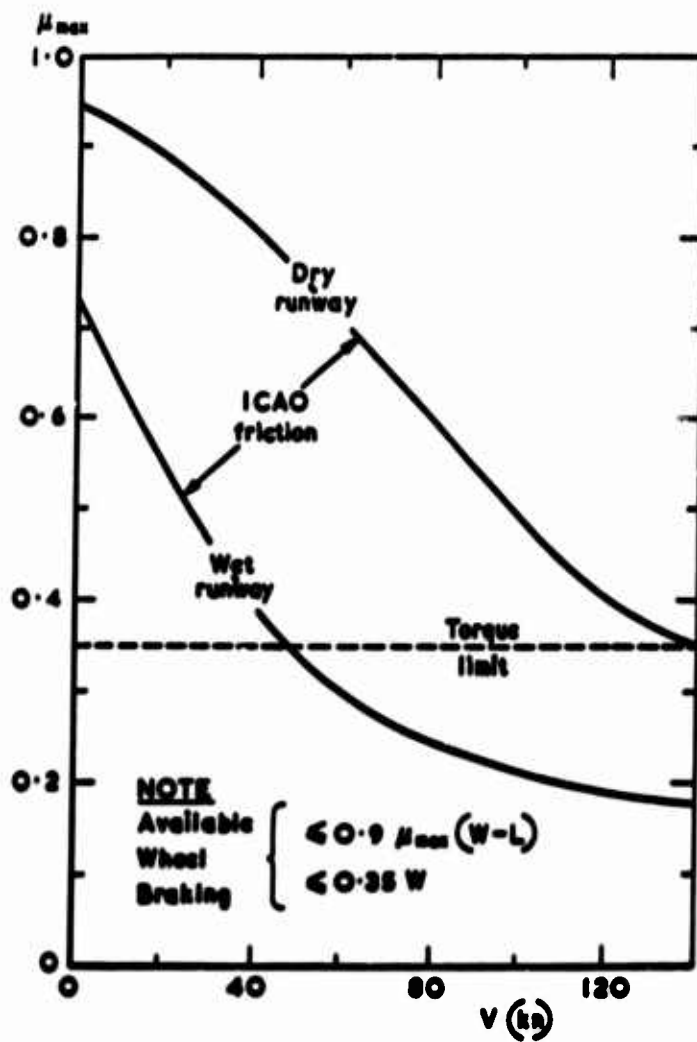


Fig.43 ICAO reference standards for maximum tyre-friction coefficient (wheel on point of skidding)

Force Model (Ldg)

$$D = C_{DG}qS, \quad L = C_{LG}qS$$

$$T = T_L, \quad F_\mu = \mu(W - L)$$

$$C_{DG} - \mu C_{LG}, \quad \mu, \quad T_L \quad \text{all assumed constant.}$$

Distance Integral (Ldg)

$$\begin{aligned} S_{GR} &= \frac{W}{g\rho} \int_0^{t_d} dq / \{(D - T_L) + \mu(W - L)\} \\ &= \frac{W/S}{g\rho K} \log_e \left[1 + \frac{(K/C_{L,t_d})}{\mu - (T_L/W)} \right] \end{aligned}$$

$$\text{where } K \equiv \{C_{DG} - \mu C_{LG}\}, \quad C_{L,t_d} \equiv W/q_{t_d}S$$

Distance from Equivalent Mean Deceleration (Ldg)

$$S_{GR} = v_{td}^2 / (2\bar{d})$$

$$\text{with } \frac{\bar{d}}{g} = \left[\mu - \frac{T_L}{W} + q \frac{S}{W} \{C_{DG} - \mu C_{LG}\} \right] v = \bar{v}$$

$$\text{where } \bar{v} \approx 0.7v_{td}.$$

Fig.44 Landing ground run. Simplified integration

Time Delays

- 2 s - Touchdown to Brake Operation.
- 3½ s - Touchdown to Spoilers Effective.
- 7 s - Touchdown to Reverse Thrust Effective (cancellation to rev. thr. at 50 kn).

Ground Speed Deceleration

- 0.15 g - Wet Runway, Simple Braking;
or Flooded Runway, Reverse Thrust.
- 0.35 g - Wet Runway, Modern Braking,
with anti-skid, lift-dumpers, rev. thr.
- 0.55 g - Dry Runway, Maximum Effort, ignoring
passenger tolerance.

Fig.45 Typical landing operations. Conventional transport

From Energy Equation with $ds = dl$, $(D - T)/W = \gamma_F$ constant,

$$S_F \approx [(V_A^2 - V_{td}^2)/2g + h_F]/\gamma_F$$

$$\text{or } -\Delta V \equiv (V_A - V_{td}) = g[\gamma_F S_F - h_F]/V_F,$$

$$\text{where } V_F = \frac{1}{2}(V_A + V_{td}).$$

For Circ. Arc Flare, with $\{V^2/(n-1)\}$ constant

$$S_F \approx \gamma_A \{V^2/(n-1)g\}, \quad h_F \approx \frac{1}{2}\gamma_A^2 \{V^2/(n-1)g\}.$$

Iteration for Speed Loss

Assign $V_F \approx 0.95V_A$, $(n-1) = 0.1$ at $V = V_A$, $\gamma_F = \gamma_A$.

Evaluate S_F , h_F , $-\Delta V(1)$.

Adjust V_F value to $\{V_A - \frac{1}{2}\Delta V(1)\}$.

Iterate for $-\Delta V$.

More Specifically

$$\gamma_F = \{(C_{D0}/C_{L,A}) + (Kn^2 C_{L,A}/\pi A) - (T/W)\}.$$

Fig.46 Landing flare distance and speed loss. Simplified estimation

Min. Airborne Time from Threshold to Touchdown

$$t_a = c_1 - c_2 V_{Tmax}$$

$$\text{Min. } S_a \approx \frac{1}{2}(V_{Tmax} + V_{td})(c_1 - c_2 V_{Tmax}).$$

At Max. Mean Deceleration $d_a g$.

$$\text{Min. } S_a \approx \left[\frac{1}{2}(V_{Tmax} + V_{td})(V_{Tmax} - V_{td}) + h_a g \right] / d_a g.$$

Eliminating S_a and Substituting $V_m \equiv \frac{1}{2}(V_{Tmax} + V_{td})$.

$$V_{td} = V_{Tmax} + (gh_a/V_m) - (c_1 - c_2 V_{Tmax})gd_a.$$

or Quadratic in V_{td} .

Evaluate simply by approx. $V_m \approx V_{Tmax}$ or $0.95 V_{Tmax}$.

Fig.47 Landing airborne-distance and touchdown-speed. Time and threshold-speed specified

Initial flare over time t_a , with starting speed V_A ,
from $\gamma = \gamma_A$ to $\gamma = 0$ descending to 'set-down height' (≈ 2 m),
assuming load factor $n \approx n_a$ constant and thrust $T \approx T_a$ constant.

Float period over time t_b about 5 s, with starting speed V_B ,
assuming aircraft eased downwards towards touchdown point,
with $n \approx 1$ and $T \approx 0$.

Touchdown effected at V_{td} ,
assuming normal acceleration $(n - 1)g \approx 0.1 g$ available.

Calculation Procedure. (Phases considered in reverse order)

$$V_{td} = \{2n(W/S)/\rho C_{L \max}\}^{1/2}, \text{ with } n = 1.1$$

$$V_B = V_{td} + gt_b/(L/D)_b, \text{ with } t_b = 5 \text{ s}$$

$$V_A = V_B + \{V_A^2 \gamma_a / 2(n_a - 1)\} + \{V_A \gamma_a / (\partial C_L / \partial C_D)_a\}$$

with $V_a \approx V_B$ and iteration

$$t_a = \{V_a \gamma_A / (n_a - 1)g\}$$

Distances obtained from product of mean speeds and times.

Fig.48 NASA three-phase model for landing airborne manoeuvre

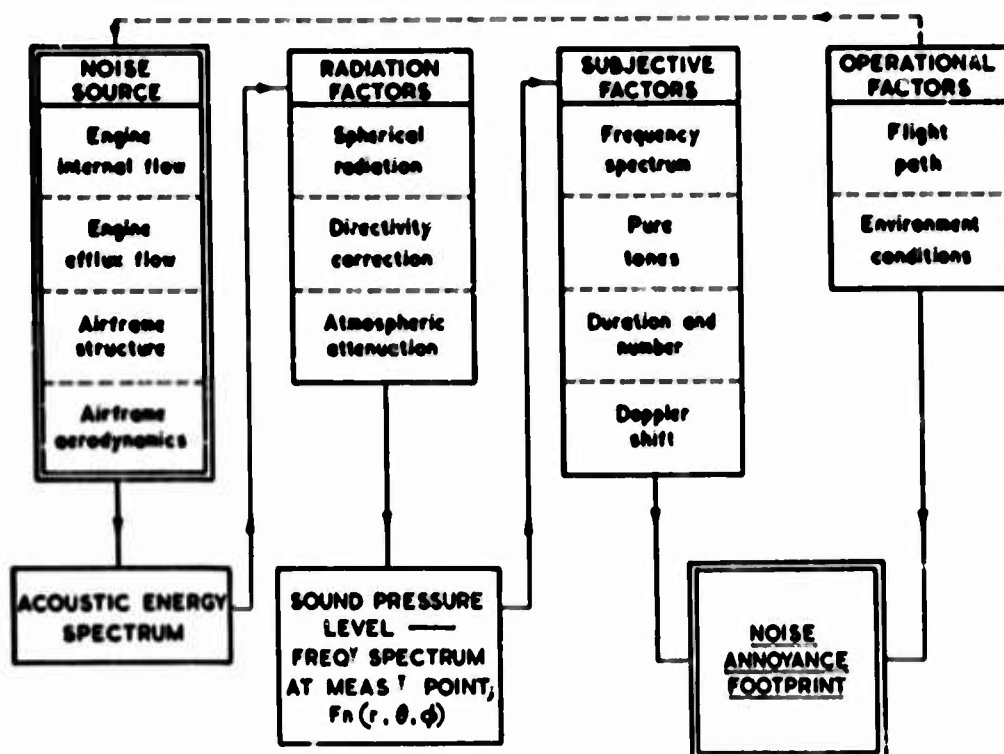


Figure 49

FLIGHT-MANOEUVRE AND CLIMB-PERFORMANCE PREDICTION

by

Heribert Friedel

**Head of Flight Mechanics Department
Dornier A.G., Friedrichshafen, Germany**

SUMMARY

As an introduction to the field of flight-manoeuve and climb-performance prediction, the basic equations of motion in a vertical and in a horizontal plane are given, with some brief remarks about the usual representation of aerodynamic and engine performance data.

In the main section, the problems concerning the prediction of the so-called point-performance values are explained. The relationship between specific excess power and load factor and their influence on climb and turn performance are discussed in detail; attention is drawn to the effects of thrust inclination. In this case, the basic performance relations contain the angle of attack and the Mach number in an implicit form. In practice, therefore, iterative methods must be applied. A description of such methods is given for the evaluation of the Mach-dependent performance values and for the related optimum values.

In the last section, the prediction of the most usual integral-performance values in climbing and turning flight are explained briefly.

As a supplement, the calculation of optimum climbing flight paths with the aid of R.Bellman's "Principle of Optimality" is given in an Appendix.

CONTENTS

	Page
SUMMARY	3
NOTATION	3
1. INTRODUCTION	3-1
2. BASIC RELATIONS	3-1
2.1 Equations of Motion	3-1
2.2 Aircraft Characteristics	3-4
3. POINT-PERFORMANCE PREDICTIONS	3-6
3.1 "Specific Excess Power" and "Specific Excess Acceleration"	3-6
3.2 Steady Climb Angle and Steady Rate of Climb	3-8
3.3 Steady Turn Performance	3-10
3.4 Aircraft with Constant Thrust and with a Parabolic Polar	3-12
3.5 Aircraft with Constant Power and with a Parabolic Polar	3-12
4. NUMERICAL PROCEDURES FOR EVALUATION OF THE POINT-PERFORMANCE VALUES	3-12
4.1 Basic Relations	3-12
4.2 Evaluation of the "Specific Excess Acceleration" SEA for a Given Load Factor n	3-13
4.3 Evaluation of the Steady Climb Performances	3-16
4.4 Evaluation of the Steady Turn Performance	3-17
5. INTEGRAL-PERFORMANCE PREDICTION	3-18
5.1 Climbing Flight	3-18
5.2 Unsteady Horizontal Turn	3-20
5.3 Unsteady Vertical Turn	3-21
REFERENCES	3-21
TABLES	3-22
APPENDIX A – Calculation of Optimum Climbing Flight Paths with the Aid of the "Principle of Optimality" by R.Bellman	3-30
FIGURES	3-36

NOTATION

a	sonic speed
A_0, A_1, A_2	constants, see Equations (4.13) to (4.15c)
c_D	drag coefficient = $D/(qS)$
c_{D0}	drag coefficient for $c_L = 0$
c_{Dmin}	minimum drag coefficient
c_L	lift coefficient
c_{Lcrit}	critical lift coefficient where separation first occurs
C	$= \frac{\rho}{2} - \frac{S}{W} a^2 = \frac{1}{M_R^2}$
C_F	fuel consumption
D	drag
ΔD	jet induced drag increment
D_M	intake momentum drag
$f()$	function of ()
g	gravity acceleration
h, H	altitude
h_E	energy altitude = $\frac{V^2}{2g} + h$
k, k^*	factor in the formula for the parabolic polar curve
L	lift
ΔL	jet-induced lift increment
m	airplane mass
\dot{m}	air mass flow
M	Mach number
M_R	reference Mach number (corresponding to $c_L = 1.0$)
M_R^*	reference Mach number (corresponding to $c_{L \epsilon min}$)
n	load factor
q	dynamic pressure = $\frac{\rho}{2} V^2$
R	turn radius
S	airplane reference area = wing area
t, T	time
T	thrust
T_G	gross thrust

T_N	net thrust
T_n	normal thrust component (perpendicular to the flight path direction)
T_t	tangential thrust component (in flight path direction)
V	flight velocity (in flight path direction)
V_R	reference velocity (corresponding to $c_L = 1.0$)
v	$= V/V_R =$ dimensionless velocity
V_R^*	reference velocity (corresponding to $c_{L \epsilon \min}$)
w	rate of climb
w_s	sinking speed
W	airplane weight
x	horizontal distance coordinate
X	integrated horizontal coordinate
y	lateral distance coordinate
Y	integrated lateral coordinate
z	vertical distance coordinate
Z	integrated vertical coordinate
z_T	dimensionless thrust
z_P	dimensionless power
α	angle of attack
$\Delta\alpha$	angle of attack correction ($\Delta\alpha = \text{rad}$)
γ	flight path angle (positive for climb)
σ	gross thrust deflection angle
δ_F	angle of flap deflection
ϵ	$= c_D/c_L =$ glide angle
ϵ_a	measure of accuracy in angle of attack iteration
ϵ_M	measure of accuracy in Mach number iteration
ρ	air density
τ	$= T/W =$ thrust/weight ratio
ϕ	bank angle
ψ	yaw angle

Abbreviations

c.g.	centre of gravity
rpm	"rotations per minute" of engine

3

SEA "specific excess acceleration"

SEP "specific excess power"

Indices

∞ free stream

f final

i initial

j jet

FLIGHT-MANOEUVRE AND CLIMB-PERFORMANCE PREDICTION*

Heribert Friedel

1. INTRODUCTION

Flight-maneuvre and climb-performance are the most critical aircraft performance values. Their accurate prediction is therefore a pre-eminent task in the aircraft optimization procedure.

First, the basic equation of motion for general manoeuvring flight and for climbing and horizontal turning flight are given, with some remarks about the representation of aerodynamic and engine performance data.

In the next sections the whole class of performance is split into the class of steady and quasi-steady point-performances and the class of integral-performance values.

Most attention is focused on the first class because it represents the basis for the second class. Firstly the relationships between specific excess power and load factor are discussed; the most general case of an aircraft with inclined thrust and the special cases of an aircraft with the thrust acting in the direction of the flight path and/or with constant thrust and parabolic polar curve are considered. Further, the relationships between specific excess power and climb and turn performances are explained.

In the next section the problems of satisfying the various conditions which arise in practice are considered, where the usual simplifications of constant thrust and parabolic polar are no longer valid. In computational practice there is a need to apply effective iteration procedures. Some methods of such iterations are discussed.

In the last section the main problems in the evaluation of the integral-performance values due to climbing and turning flight are explained briefly.

The calculation of optimum climbing flight paths with the aid of R.Bellman's "Principle of Optimality" are explained in some detail in an Appendix.

2. BASIC RELATIONS

2.1 Equations of Motion

2.1.1 General Equations

In this section, a trajectory flown in a three-dimensional space is considered. Further the following assumptions are employed:

- flat earth
- constant acceleration of gravity
- aircraft considered as a mass point
- atmospheric properties are known functions of altitude
- sideslip angle is zero (this means that the velocity vector, the resultant aerodynamic force and the resultant thrust force are contained in the plane of symmetry of the aircraft).

In the light of these hypotheses and with the definitions of Figure 1, the basic equations of motion are written in the form of:

- Equilibrium of forces per unit weight in direction of the flight path:

$$\left(\frac{1}{g} \frac{dV}{dt} + \sin \gamma \right) = \frac{T_t - D}{mg} \quad (2.1)$$

* See also Paper 10 of this volume.

- Equilibrium of forces per unit weight normal to the direction of the flight path and in the plane of symmetry of the aircraft:

$$\cos \phi \cos \gamma + \frac{V}{g} \left(\frac{d\psi}{dt} \sin \phi \cos \gamma + \frac{d\gamma}{dt} \cos \phi \right) = \frac{T_n + L}{mg} . \quad (2.2)$$

- Equilibrium of forces per unit weight normal to the direction of the flight path and normal to the plane of symmetry of the aircraft:

$$\sin \phi \cos \gamma + \frac{V}{g} \left(-\frac{d\psi}{dt} \cos \phi \cos \gamma + \frac{d\gamma}{dt} \sin \phi \right) = 0 . \quad (2.3)$$

- Velocity components with respect to an earth-fixed coordinate system:

$$\frac{dx}{dt} = V \cos \gamma \cos \psi . \quad (2.4)$$

$$\frac{dy}{dt} = V \cos \gamma \sin \psi . \quad (2.5)$$

$$\frac{dz}{dt} = -V \sin \gamma = -\frac{dh}{dt} . \quad (2.6)$$

- Mass change due to fuel consumption:

$$\frac{dm}{dt} = -C_F ; \quad (2.7)$$

where

- x, y, z = Cartesian coordinates, earth fixed
 h = $-z$, altitude
 V = flight velocity
 t = time
 γ = flight path angle
 ϕ = roll angle
 ψ = yaw angle
 m = aircraft mass
 g = acceleration of gravity
 W = mg , aircraft weight
 D = aerodynamic drag
 L = aerodynamic lift
 T_t = thrust component, tangential to flight path direction
 T_n = thrust component, normal to flight path direction
 C_F = fuel flow.

Equation (2.1) multiplied by the velocity V represents the change of *energy height* with respect to time,

$$\frac{dh_E}{dt} = V \left(\frac{T_t - D}{mg} \right) . \quad (2.8)$$

In Equation (2.2) the right member represents the *load factor*,

$$n = \frac{T_n + L}{mg} . \quad (2.9)$$

Equations (2.4) to (2.6) are the kinematical relationships in the x , y , and z directions.

2.1.2 Flight in a Vertical Plane

The main properties of the climbing flight are well described by the flight in a vertical plane. In this case the roll angle ϕ and the yaw angle ψ are zero. Introducing these conditions, the general equations of motion, Equations (2.1) to (2.6), reduce to the following simplified set of equations (see Figure 2):

– Tangential force equilibrium:

$$\left(\frac{1}{g} \frac{dV}{dt} + \sin \gamma \right) = \frac{T_t - D}{W} = \frac{1}{V} \frac{dh_E}{dt} . \quad (2.10)$$

– Normal force equilibrium:

$$\left(\frac{V}{g} \frac{d\gamma}{dt} + \cos \gamma \right) = \frac{T_n + L}{W} = n . \quad (2.11)$$

– Flight path change in x direction:

$$\frac{dx}{dt} = V \cos \gamma . \quad (2.12)$$

– Flight path change in the negative z direction:

$$\frac{dh}{dt} = V \sin \gamma = -\frac{dz}{dt} . \quad (2.13)$$

– Mass change due to fuel consumption:

$$\frac{dm}{dt} = -C_F . \quad (2.14)$$

2.1.3 Flight in a Horizontal Plane

The main properties of the turning flight are well described by the flight in a horizontal plane. In this case the height is constant and the flight path angle is zero. Introducing these conditions into the set of general equations of motion, Equations (2.1) to (2.7), we obtain the following simplified set of equations (see Figure 3):

– Tangential force equilibrium:

$$\frac{1}{g} \frac{dV}{dt} = \frac{T_t - D}{W} = \frac{1}{V} \frac{dh_E}{dt} . \quad (2.15)$$

– Normal force equilibrium in the plane of symmetry:

$$\cos \phi + \frac{V}{g} \frac{d\psi}{dt} \sin \phi = \frac{T_n + L}{W} = n . \quad (2.16)$$

– Normal force equilibrium normal to the plane of symmetry:

$$\sin \phi - \frac{V}{g} \frac{d\psi}{dt} \cos \phi = 0 . \quad (2.17)$$

– Flight path change in x direction:

$$\frac{dx}{dt} = V \cos \psi . \quad (2.18)$$

– Flight path change in y direction:

$$\frac{dy}{dt} = V \sin \psi . \quad (2.19)$$

– Mass change due to fuel consumption:

$$\frac{dm}{dt} = -C_F . \quad (2.20)$$

Adding Equation (2.16) multiplied by $\sin \phi$ and Equation (2.17) multiplied by $(-\cos \phi)$ yields for the

– Normal force equilibrium in horizontal direction:

$$\frac{V}{g} \frac{d\psi}{dt} = \left(\frac{T_n + L}{W} \right) \sin \phi . \quad (2.21)$$

Adding Equation (2.16) multiplied by $\cos \phi$ and Equation (2.17) multiplied by $\sin \phi$ yields for the

– Normal force equilibrium in vertical direction:

$$0 = \left(\frac{T_n + L}{W} \right) \cos \phi - 1 = n \cos \phi - 1 . \quad (2.22)$$

2.2 Aircraft Characteristics

2.2.1 Aerodynamic Forces

In performance calculations the essential aerodynamic forces are:

Aerodynamic lift:

$$L = c_L \frac{\rho}{2} V^2 S . \quad (2.23)$$

Aerodynamic drag:

$$D = c_D \frac{\rho}{2} V^2 S . \quad (2.24)$$

where

- c_L = lift coefficient
- c_D = drag coefficient
- ρ = air density
- S = reference wing area.

The lift and drag coefficients are in general dependent on:

- Reynolds number Re
- Mach number M
- angle of attack α
- angle of flap deflection δ_F
- trim conditions (e.g. position).

In most of the cases considered later, the c.g. position and the flap deflection or the Mach number are fixed. Further, the Reynolds number in a given altitude is only a function of the Mach number, so that the lift drag coefficients are in the high-speed regime only dependent on angle of attack α and Mach number M (as shown in Figure 4),

$$c_L = c_L(\alpha, M) \quad (2.25a)$$

$$c_D = c_D(\alpha, M) . \quad (2.25b)$$

In the low-speed regime, they are only dependent on angle of attack α and flap deflection angle δ_F (see Figure 5),

$$c_L = c_L(\alpha, \delta_F) \quad (2.26a)$$

$$c_D = c_D(\alpha, \delta_F) . \quad (2.26b)$$

In practice these curves are mostly evaluated by calculations with semi-empirical methods and/or by investigations of wind-tunnel test data. In most of the cases the dependence on α , M and δ_F is only given in the form of tabulated numerical values.

Parabolic polar curves

In the case of subcritical Mach numbers ($M < 0.6$) where no shocks occur, the drag depends on lift quadratically. For aircraft with symmetrical profiles on untwisted wings, the following parabolic relation holds in the separation-free lift region:

$$c_D = c_{D0} + k c_L^2 \quad \text{for } c_L < c_{Lcrit} . \quad (2.27a)$$

For aircraft with twisted and cambered wings and with inclined fuselages an improved approximation of the drag polar is given by

$$c_D = c_{Dmin} + k^*(c_L - c_{Lopt})^2 \quad \text{for } c_L < c_{Lcrit} . \quad (2.27b)$$

In practice the difference between these two approximation formulae may be not so important if the low c_L region is not to be considered (see Figure 6).

2.2.2 Thrust Forces

In general, the thrust vector acting on an aircraft can be defined as the vectorial sum of the intake momentum loss (or momentum drag) D_M and the gross thrust T_G . The various definitions of both are defined in Reference 2. Further information is given in References 3 and 4. If we propose an inclination σ of the exit nozzle of the engine relative to the x -axis of the aircraft (see Figure 7), the thrust components are:

– Tangential to the flight path:

$$T_t = T_G \cos(\alpha + \sigma) - D_M . \quad (2.28)$$

– Normal to the flight path:

$$T_n = T_G \sin(\alpha + \sigma) , \quad (2.29)$$

where the *momentum drag* is defined as

$$D_M = \dot{m} V \quad (2.30)$$

and \dot{m} denotes the mass flow of the engine.

The gross thrust T_G and the mass flow are in general functions of

- engine power setting (rpm, percent maximum available thrust)
- atmospheric condition (pressure, temperature)
- Mach number
- Reynolds number.

Since most of the climbing and manoeuvring flight are flown with maximum power settings, the engine data are mostly only functions of Mach number M and altitude H :

$$T_G = T_G(M, H) \quad (2.31)$$

$$\dot{m} = \dot{m}(M, H) . \quad (2.32)$$

If the thrust is acting only in the flight direction, the tangential thrust component of Equation (2.28) reduces to the net thrust

$$T_N = T_t(\alpha + \sigma = 0) = T_G - D_M , \quad (2.33)$$

while the normal thrust component vanishes.

The relation (2.33) must be applied in the evaluation of the gross thrust from such engine brochures where only the net thrust and the mass flow are given.

Assumption of constant thrust or constant power

The assumptions of "constant thrust" or "constant power" respectively are often used for single flow turbojet aircraft or for aircraft with piston engines and propellers. In both cases, the above assumptions are only useful simplifications to show the differences for the main performance values in an analytical manner.

2.2.3 Jet-Induced Interference Effects

In the above definitions of the aerodynamic forces and of the thrust forces the jet-induced interference effects are not included. They are often defined in the following form:

$$\frac{\Delta L}{T_G} = f \left[\left(\frac{\rho_j V_j^2}{\rho_\infty V_\infty^2} \right), \alpha, \sigma, M \right] \quad (2.34)$$

$$\frac{\Delta D}{T_G} = f \left[\left(\frac{\rho_j V_j^2}{\rho_\infty V_\infty^2} \right), \alpha, \sigma, M \right], \quad (2.35)$$

where $[(\rho_j V_j^2)/(\rho_\infty V_\infty^2)]$ denotes the ratio of the momentum per unit mass of the jet and of the free-stream. The square root of it is often called the effective velocity ratio. It represents the most important parameter due to jet-interference effects.

The above lift and drag increments are mostly given in form of measured curves and seldom in form of analytical expressions. In practice the values ΔL and ΔD are small compared with the forces defined in Sections 2.2.1 and 2.2.2. However, they are seldom negligible, especially the afterbody drag near the thrust nozzles of conventional aircraft and the jet-induced lift loss in the transition flight regime of V/STOL aircraft. Since these lift and drag increments are only corrective ones, the principle character of the climb and manoeuvre performance with respect to the angle of attack does not change. Therefore in the following sections the performance prediction methods are explained without jet-induced interference effects. However, it may be noted that these effects may easily be taken into consideration in an iterative manner.

3. POINT-PERFORMANCE PREDICTIONS

The most interesting point-performances in climbing and manoeuvring flight are:

- the specific excess power SEP
 - the specific excess acceleration SEA
 - the steady rate of climb
 - the steady angle of climb
 - the steady load factor
 - the steady angle of bank
 - the steady turn rate
 - the radius of curvature
- } in a steady horizontal turn.

3.1 "Specific Excess Power" and "Specific Excess Acceleration"

3.1.1 Relationship between SEP and n

The previous section has shown that the whole influence of the aircraft data to the equations of motion are concentrated in the "specific excess power" SEP and in the "load factor" n . [See Equations (2.1), (2.2), (2.8), (2.9), (2.10), (2.11), (2.15) and (2.16)]. Introducing the lift and drag definitions from Section 2.2.1 and the thrust definitions from Section 2.2.2 and neglecting possible jet-induced interference effects, we get the following relations:

- Specific excess power SEP:

$$SEP = Ma(H) \left[\frac{T_G(M, H)}{W} \cos(\alpha + \sigma) - \frac{\dot{m}(M, H)}{W} Ma(H) - c_D(\alpha, M) \frac{\rho(H)}{2} M^2 a(H)^2 \frac{S}{W} \right]. \quad (3.1)$$

$$SEP = f_1(\alpha, M, H). \quad (3.1a)$$

– Load factor n :

$$n = \left[\frac{T_G(M, H)}{W} \sin(\alpha + \sigma) + c_L(\alpha, M) \frac{\rho(H)}{2} M^2 a(H)^2 \frac{S}{W} \right] \quad (3.2)$$

$$n = f_2(\alpha, M, H) . \quad (3.2a)$$

If we consider flight at a given altitude H , the above relations are only functions of Mach number M and angle of attack α . If we prescribe further the load factor n , one of the two variables α or M is no longer independent. From Equation (3.2a) we get then

$$\alpha = f_2^*(n, M) \quad (3.3a)$$

or

$$M = f_2^{**}(n, \alpha) . \quad (3.3b)$$

Introducing Equation (3.3a) or Equation (3.3b) in Equation (3.1a) leads to the following functional relationship for the specific excess power:

$$SEP = Ma \left[\frac{T_G(M)}{W} \cos[\alpha(n, M) + \sigma] - \frac{\dot{m}(M)}{W} Ma - c_D[\alpha(n, M), M] \frac{\rho}{2} M^2 a^2 \frac{S}{W} \right] . \quad (3.4)$$

$$SEP = Ma \left[\frac{T_t(n, M)}{W} - \frac{D(n, M)}{W} \right] . \quad (3.4a)$$

$$SEP = f_1(n, M) . \quad (3.4b)$$

Figure 8 shows this relationship for a typical subsonic trainer aircraft in two different forms.

3.1.2 Pénau Diagram

If we draw the thrust-to-weight curve $T_t(M)/W$ and the drag-to-weight curve $D(M)/W$ in one diagram, we get the so-called Pénau diagram, from which the available specific excess acceleration SEA may be found as the difference between the appropriate T_t/W and D/W curves. Figure 9 shows the influence of various thrust levels and load factors in the case of a typical subsonic aircraft.

3.1.3 Influence of Angle of Attack α and Gross Thrust Deflection Angle δ_F on the Specific Excess Acceleration SEA

As pointed out above the evaluation of specific excess power SEP and of the specific excess acceleration needs first the evaluation of the appropriate Mach number or appropriate angle of attack from Equation (3.2), which can only be done in an iterative process. If however we assume a thrust acting in direction to the flight path and a linear relationship between lift coefficient c_L and angle of attack α , the appropriate lift coefficient $c_L(n, M)$ or angle of attack $\alpha(n, M)$ may be expressed explicitly:

$$c_L(n, M) = \frac{n}{\frac{\rho}{2} \frac{S}{W} a^2 M^2} \quad (3.5a)$$

or

$$\alpha(n, M) = \alpha_0(M) + \frac{c_L(n, M)}{c_{L\alpha}} . \quad (3.5b)$$

If we further assume the parabolic polar of Equation (2.27a), the "specific excess acceleration" SEA (and the "specific excess power" SEP) also may be expressed explicitly:

$$SEA = \frac{T_N(M)}{W} - \left[c_{D0} \left(\frac{2}{\rho a^2} \frac{W}{S} \right) + \left(\frac{2}{\rho a^2} \frac{W}{S} \right) k \frac{n^2}{M^2} \right] . \quad (3.6)$$

The numerical evaluation of this equation is very simple. Figure 10, however, shows that Equation (3.6) leads to significant errors in the low-speed region, if the thrust-to-weight ratio is large. The reasons for these errors are

- the cosine effect in Equation (3.4)
- the less effective weight in Equation (3.2), which leads to a smaller lift coefficient and therefore to a smaller induced drag, which shifts the drag curve in the Pénau diagram to smaller Mach numbers.

In the case where the thrust is acting in zero lift direction, a significant difference between the accurate solution [Eqn (3.1)] and the approximate solution [Equations (3.5a) and (3.6)] occurs only in the low-speed region. In the case where the thrust is inclined relative to the zero-lift direction, significant differences occur in the high-speed region too. The reason for this behaviour lies in the loss of propulsive thrust due to the cosine effect.

Figure 11 shows the influence of the thrust inclination $(\alpha + \sigma)$ on the curves for the specific excess power in the height-Mach number diagram for a typical subsonic fighter aircraft with small thrust inclination. It may be seen that differences between the two calculation methods occur only in the high-speed region below the compressible drag rise. Further they are only significant at low altitude where the thrust-to-weight ratio is high.

3.2 Steady Climb Angle and Steady Rate of Climb

In the case of the steady climbing flight, where the tangential and the normal acceleration are zero, the basic Equations (2.10) and (2.11) are reduced to

$$\sin \gamma = \frac{T_t - D}{W} = f_1(\alpha, M) \quad (3.7)$$

and

$$\cos \gamma = \frac{T_n + L}{W} = f_2(\alpha, M), \quad (3.8)$$

where the terms on the right are the specific excess acceleration SEA and the loadfactor n respectively, which are both functions of the angle of attack α and of the Mach number M (see also Section 3.1.1). Together with the angle of climb γ we have now three variables from which only two are independent. If we want to evaluate the available angle of climb γ one of the other two variables must be prescribed. If we choose the Mach number M as a parameter, we get two equations in which the angle of climb is expressed as a function of the angle of attack only. Thus, in the most general case, we have two transcendental equations with two unknowns which can only be solved graphically or by an iteration process. The description of an effective iteration process is given later on.

3.2.1 Special Cases. Aircraft with Thrust Acting only in the Flight Path Direction

If the thrust is acting only in the flight path direction, Equations (3.7) and (3.8) take the form

$$\sin \gamma = \frac{T_N}{W} - c_D \frac{\rho a^2}{2} \frac{S}{W} M^2 \quad (3.9)$$

and

$$\cos \gamma = c_L \frac{\rho a^2}{2} \frac{S}{W} M^2, \quad (3.10)$$

respectively, where T_N denotes the net thrust defined in Equation (2.33).

Combining Equation (3.9) with Equation (3.10) yields

$$\sin \gamma = \frac{T_N}{W} - \frac{c_D}{c_L} \cos \gamma \quad (3.11)$$

or

$$\sin \gamma = r_N - \epsilon \cos \gamma, \quad (3.11a)$$

where r_N denotes the net thrust-to-weight ratio and ϵ is the so-called glide angle which is the reciprocal of the lift-to-drag ratio.

3.2.2 Simplified Analysis

If the square of the flight path inclination is assumed to be negligible with respect to unity, the sine of the flight angle γ may be replaced by γ itself and the cosine by unity. With these assumptions we get the following simplified climb performances:

– Angle of climb γ :

$$\gamma = r - \epsilon \quad (3.12)$$

– Rate of climb w_s :

$$\frac{w_s}{V_R} = \frac{1}{\sqrt{c_L}} (r - \epsilon). \quad (3.13)$$

- Speed and Mach number in climbing flight:

$$\frac{V}{V_R} = \frac{M}{M_R} = \frac{1}{\sqrt{c_L}} \quad (3.14)$$

where the reference velocity V_R and the reference Mach number M_R respectively are defined by

$$V_R = \sqrt{\frac{2W}{\rho S}} \quad (3.15)$$

and

$$M_R = \sqrt{\frac{2W}{\rho a^2 S}} \quad (3.16)$$

3.2.3 Exact Analysis

The above simplifications are no longer valid if the thrust-to-weight ratio is large. Setting $\gamma = \sqrt{1 - \sin^2 \gamma}$ in Equation (3.11a), we get after some rearrangements the quadratic equation:

$$(1 + e^2) \sin^2 \gamma - 2r \sin \gamma + (r^2 - e^2) = 0, \quad (3.17)$$

with the solution for the flight path inclination:

$$\sin \gamma = \frac{1}{(1 + e^2)} \left[r^{(\pm)} \sqrt{(1 + e^2) - r^2} \right], \quad (3.18)$$

where the lower sign is to be exclusively employed for $r < 1$, while both signs may yield physically possible solutions for $r > 1$. Furthermore we get for the

- Rate of climb $w_s = V \sin \gamma$

$$\frac{w_s}{V_R} = \frac{1}{\sqrt{c_L}} \frac{1}{(1 + e^2)^{3/2}} \left\{ \left[\sqrt{e r^{(\pm)} \sqrt{(1 + e^2) - r^2}} \right] \left[r^{(\pm)} e \sqrt{(1 + e^2) - r^2} \right] \right\}. \quad (3.19)$$

- Speed and Mach number in climbing flight:

$$\frac{V}{V_R} = \frac{M}{M_R} = \frac{1}{\sqrt{c_L}} \sqrt{\frac{e r^{(\pm)} \sqrt{(1 + e^2) - r^2}}{(1 + e^2)}} \quad (3.20)$$

Relations (3.18) to (3.20) are the most general solution for climbing flight in a vertical plane in terms of the lift coefficient c_L and of the thrust-to-weight ratio r . However, we must pay attention to the fact that the glide angle e (inverse lift-to-drag ratio) is not always independent from the Mach number M , so that Equation (3.20) must be solved iteratively. A comparison between the simplified and the exact solution is shown in Table 1.

3.2.4 Gliding Flight

Introducing the gliding condition

$$r = 0, \quad (3.21)$$

the climbing performances of Equations (3.18), (3.19), (3.20) and (3.12), (3.13), (3.14) respectively reduce to the gliding performances shown in Table 2:

Since e is defined as the inverse lift-to-drag ratio, the gliding performances are functions only of the lift coefficient c_L .

Optimum gliding performance

Differentiating the exact solution for the gliding angle of Table 2 with respect to the lift coefficient c_L and setting zero yields the condition for the minimum gliding angle γ_{\min} (flattest glide).

$$\left(\frac{d \sin \gamma}{d c_L} \right)_e = - \frac{1}{(1 + e^2)^{3/2}} \frac{d e}{d c_L} = 0. \quad (3.22)$$

This condition is identical with that obtained from the simplified solution:

$$\left(\frac{d \sin \gamma}{d c_L} \right)_s = - \frac{d e}{d c_L} = 0. \quad (3.23)$$

The minimum sinking speed w_{smin} occurs if the condition

$$\frac{d(w_s/V_R)}{dc_L} = \frac{\frac{1}{2}[(1 + e^2)e - c_L(2 - e^2)(de/dc_L)]}{(1 + e^2)^{7/4}} = 0 \quad (3.24)$$

is satisfied. This is the case for the lift coefficient due to

$$\frac{de}{dc_L} = \left(\frac{1 + e^2}{2 + e^2} \right) \frac{e}{c_L} \quad (\text{exact solution}) \quad (3.25a)$$

or

$$\frac{de}{dc_L} = \frac{1}{2} \frac{e}{c_L} \quad (\text{simplified solution}) \quad (3.25b)$$

Gliding aircraft with parabolic polar

Assuming the parabolic polar of Equation (2.27), the simplified solutions of the gliding flight as shown in Table 2 may be written in the form of the first row of Table 3. The appropriate optimum solutions for the flattest glide and for the gliding flight with minimum sinking speed are also shown in Table 3.

Introducing the optimum lift coefficients into Equation (2.27) for the parabolic drag curve shows us that the induced drag is equal to the zero lift drag in the case of the flattest glide and three times the zero lift drag in the case of the minimum sinking speed.

3.3 Steady Turn Performance

3.3.1 General Solution

The basic relations for the turn in a horizontal plane are given in Equation (2.15) to Equation (2.21). In the case of the steady turn, Equation (2.15) must be set zero. This means the same as setting the specific excess acceleration of Equation (3.1) zero. Since the turn should occur in a horizontal plane, the right member of Equation (3.1) is dependent only on the angle of attack α and on the Mach number M . In the general case this function $f_1(\alpha, M)$ contains both variables in an implicit form. If one prescribes one of the two variables, the other must be evaluated from the relation

$$f_1(\alpha, M) = 0. \quad (3.26)$$

In the most general case this can only be done iteratively (see Section 4.3). Once the solution $\alpha(M)$ or $M(\alpha)$ is computed the interesting steady turn performance values can be computed from the following relations (see also Table 6):

- Load factor n :

$$n = f_2[\alpha(M), M] \quad (3.27a)$$

$$n = f_2[\alpha, M(\alpha)] \quad (3.27b)$$

where $f_2(\alpha, M)$ is given in Equation (3.2).

- Angle of bank ϕ :

$$\tan \phi = \sqrt{n^2 - 1}. \quad (3.28)$$

- Turn rate $(d\psi/dt)$:

$$\frac{d\psi}{dt} = \frac{g}{V} \sqrt{n^2 - 1} = \frac{g}{V} \tan \phi. \quad (3.29)$$

- Radius of curvature R :

$$R = \frac{V^2}{g} \frac{1}{\sqrt{n^2 - 1}} = \frac{V^2}{g} \cot \phi. \quad (3.30)$$

Figure 12 shows for example the dependence of the steady load factor n on Mach number M and altitude h for a typical subsonic aircraft. In the low-speed region, the load factor is limited by the maximum usable lift-coefficient, while in the high-speed region it is limited by the maximum available thrust.

3.3.2 Aircraft with Thrust Acting in Direction of Flight Path

In this case the angle of attack α influences only the aerodynamic drag, so that the function $f_1(\alpha, M)$ takes the form

$$f_1(\alpha, M) = \left[\frac{T_N(M)}{W} - c_D(\alpha, M) \frac{\rho}{2} \frac{S}{W} u^2 M^2 \right] = 0; \quad (3.31)$$

or if the angle of attack is replaced by the lift coefficient c_L :

$$f_1(c_L, M) = \left[\frac{T_N(M)}{W} - c_D(c_L, M) \frac{\rho}{2} \frac{S}{W} u^2 M^2 \right] = 0. \quad (3.32)$$

On the other side, the relation $f_2(\alpha, M)$ for the load factor may now be written in the form

$$n = f_2(c_L, M) = c_L \frac{\rho}{2} \frac{S}{W} u^2 M^2. \quad (3.33)$$

Eliminating $(\rho/2)(S/W)u^2 M^2$ from Equation (3.32) and (3.33), we get

$$\left[\frac{T_N(M)}{W} - \frac{c_D}{c_L} [c_L(M, n), M] n \right] = 0. \quad (3.34)$$

Assuming constant Mach number, we have an implicit expression with respect to the load factor n which can only be solved iteratively as long as the drag polar depends on Mach number. If however the polar does not depend on Mach number, relation (3.34) delivers an explicit expression for the load factor

$$n = \left(\frac{T_N}{W} \right) \frac{c_L}{c_D} = \frac{\tau_N}{\epsilon} = \frac{\tau}{\epsilon}. \quad (3.35)$$

The other related turn performances are given in Table 4.

Maximum values

The maximum load factor and the maximum angle of bank occur at the lift coefficient $c_{Lopt\epsilon}$ where the lift-to-drag ratio reaches its maximum value.

$$n_{max} = \frac{\tau}{\epsilon_{min}} = \tau(L/D)_{max} \quad (3.36)$$

$$\tan \phi_{max} = \sqrt{[\tau(L/D)_{max}]^2 - 1}. \quad (3.37)$$

where

$$\left(\frac{V}{V_R} \right)_{opt, n max} = \sqrt{\frac{\tau}{c_{D opt, \epsilon min}}}. \quad (3.38)$$

The maximum turn rate occurs at the polar point where the condition

$$\frac{c_L}{c_D} \frac{dc_D}{dc_L} = \frac{2\tau^2}{\tau^2 + (c_D/c_L)^2} \quad (3.39a)$$

or

$$\frac{c_L}{\epsilon} \frac{d\epsilon}{dc_L} = \frac{\tau^2 - \epsilon^2}{\tau^2 + \epsilon^2} \quad (3.39b)$$

holds, while the *minimum radius of curvature* is given by the condition

$$\frac{c_L}{c_D} \frac{dc_D}{dc_L} = \left(\tau \frac{c_L}{c_D} \right)^2 \quad (3.40a)$$

or

$$\frac{c_L}{\epsilon} \frac{d\epsilon}{dc_L} = \frac{\tau^2 - \epsilon^2}{\epsilon^2}. \quad (3.40b)$$

Special case. Large thrust-to-weight ratios

Assuming the thrust-to-weight ratio τ is large with respect to the inverse lift-to-drag ratio ϵ , the turn rate and the radius of curvature may be approximated by

$$\frac{d\psi}{dt} \approx \frac{g}{V_R} c_l \sqrt{\frac{\tau}{c_D}} \quad (3.41)$$

and

$$R \approx \frac{V_R^2}{g} \frac{1}{c_l} \quad (3.42)$$

respectively.

3.4 Aircraft with Constant Thrust and with a Parabolic Polar

Assuming constant thrust and parabolic polar, all the point-performance values of the previous section can be expressed in an explicit form which is shown in Reference 1. Introducing a reference speed V_R^* ,

$$V_R^* = \sqrt{\frac{T}{\rho S}} \sqrt{\frac{k}{c_{D0}}} = V_R \sqrt{\frac{k}{c_{D0}}} \quad (3.43)$$

the dimensionless thrust τ_1 ,

$$\tau_1 = \frac{T}{W} \left(\frac{L}{D} \right)_{\max} = \frac{\tau}{\epsilon_{\min}} \quad (3.44)$$

and the dimensionless speed v ,

$$v = \frac{V}{V_R^*} \quad (3.45)$$

we can show the performance values in a dimensionless form as seen in Table 5 for the non-optimum climb performance values and in Table 7 for the non-optimum horizontal turn performance values. Assuming small thrust-to-weight ratios and high lift-to-drag ratios (simplified solution is applicable) the maximum performance values may be easily computed from the formulae given in Table 8 (see also Reference 1). Figure 13 shows their dependence on the dimensionless thrust.

3.5 Aircraft with Constant Power and with a Parabolic Polar

Assuming a constant power P , a constant propeller efficiency η , and a parabolic polar, all the point-performance values may be expressed also in an explicit form. Introducing the reference speed V_R^* from Equation (3.43), the dimensionless speed v from Equation (3.45) and the

dimensionless power,

$$\tau_P = \frac{\eta P}{W V_R^*} \frac{1}{\epsilon_{\min}} \quad (3.46)$$

we can show the performance values in a dimensionless form as seen in Table 6 for the non-optimum climb performances and in Table 7 for the non-optimum steady horizontal turn performances. Assuming small power-to-weight ratios and high lift-to-drag ratios the formulae for the maximum performance values are also very simple (see Table 8).

4. NUMERICAL PROCEDURES FOR EVALUATION OF THE POINT-PERFORMANCE VALUES**4.1 Basic Relations**

In the previous section it was shown that the basic relations which describe the point-performance in manoeuvring and in climbing flight respectively have the same form in the equilibrium of forces.

- Tangential to the direction of the flight path:

$$SEA = f_1(\alpha, M) \quad (4.1a)$$

or

$$\sin \gamma = f_1(\alpha, M) \quad (4.1b)$$

where

$$f_1(\alpha, M) = \frac{T_1 - D}{W} \quad (4.2)$$

$$= \left[\frac{T_G(M)}{W} \cos(\alpha + \sigma) - \frac{m(M)}{W} aM - c_D(\alpha, M) \frac{\rho}{2} \frac{S}{W} a^2 M^2 \right]^0.$$

Normal to the direction of the flight path:

$$n = f_1(\alpha, M) \quad (4.3a)$$

or

$$\cos \gamma = f_1(\alpha, M), \quad (4.3b)$$

where

$$f_2(\alpha, M) = \frac{T_R + L}{W} \quad (4.4)$$

$$= \left[\frac{T_G(M)}{W} \sin(\alpha + \sigma) + c_L(\alpha, M) \frac{\rho}{2} \frac{S}{W} a^2 M^2 \right]^0.$$

In most cases of practical interest the functions f_1 and f_2 are only dependent on angle of attack α and Mach number M , which is shown in Equation (4.3) and (4.4). Furthermore, the engine brochures contain the engine data in form of tables or diagrams which cannot be represented in an analytical form. The same is true for the aerodynamic data, so that in our computational practice we have almost only tabulated data sets, which must be interpolated by appropriate methods.

4.2 Evaluation of the "Specific Excess Acceleration" SEA for a Given Load Factor n

4.2.1 Iteration Procedure in the Case of Conventional Aircraft

If we want to calculate the dependence of SEA on the flight Mach number M for a given load factor n , at first we have to find the angle of attack α_n which is necessary to fulfil the condition (4.3a). Since Equations (4.3a) and (4.4) contain the angle of attack α only in implicit form we must apply an adequate iterative process, for example the Newtonian iteration procedure according to

$$\alpha_{\text{new}} = \alpha_{\text{old}} - \frac{(f_2(\alpha_{\text{old}}) - n)}{\left(\frac{df_2(\alpha_{\text{old}})}{d\alpha}\right)} = \alpha_{\text{old}} + \Delta\alpha. \quad (4.5)$$

where $df_2/d\alpha$ follows from Equation (4.4) by partial differentiation:

$$\frac{df_2}{d\alpha} = \frac{\partial f_2}{\partial \alpha} = \left[\frac{T_G(M)}{W} \cos(\alpha + \sigma) + \frac{\partial c_L(\alpha, M)}{\partial \alpha} \frac{\rho}{2} \frac{S}{W} a^2 M^2 \right]. \quad (4.6)$$

The iteration process itself is shown in Table 9. It works well as long as the second term in Equation (4.4) dominates. This is always true in the case of a conventional aircraft with small thrust deflections.

4.2.2 Iteration Procedure in the Case of V/STOL Aircraft

In the case of V/STOL aircraft with large thrust deflections, especially in the speed range from hovering up to about half the conversion speed, the above iteration does not converge because $df_2/d\alpha$ becomes small if the thrust is directed nearly to the vertical.

In the case where this occurs a better iteration will be done in the following way:

If we assume that a better value of α can be calculated from the relation

$$\alpha = \alpha_{\text{old}} + \Delta\alpha, \quad (4.7)$$

as above, the basic Equation (4.4) takes the form

$$f_2(\alpha, M) = \left[\frac{T_G(M)}{W} \sin(\alpha_{\text{old}} + \Delta\alpha + \sigma) + c_L(\alpha_{\text{old}} + \Delta\alpha, M) \frac{\rho}{2} \frac{S}{W} a^2 M^2 \right]. \quad (4.8)$$

* Jet-induced interference effects are neglected.

Now we can replace $\sin(\alpha_{old} + \Delta\alpha + \sigma)$ by the well-known relation

$$\sin(\alpha_{old} + \Delta\alpha + \sigma) = [\sin \Delta\alpha \cos(\alpha_{old} + \sigma) + \cos \Delta\alpha \sin(\alpha_{old} + \sigma)] \quad (4.9)$$

which may be arranged in the following way before introducing in Equation (4.8)

$$\sin(\alpha_{old} + \Delta\alpha + \sigma) = \left[\begin{aligned} &+ \cos(\alpha_{old} + \sigma) \Delta\alpha + \cos(\alpha_{old} + \sigma)(\sin \Delta\alpha - \Delta\alpha) - \\ &- \sin(\alpha_{old} + \sigma) \frac{\Delta\alpha^2}{2} + \sin(\alpha_{old} + \sigma) \left(\cos \Delta\alpha + \frac{\Delta\alpha^2}{2} \right) \end{aligned} \right] \quad (4.9a)$$

Further, we represent $c_L(\alpha_{old} + \Delta\alpha, M)$ by

$$c_L(\alpha_{old} + \Delta\alpha, M) = c_L(\alpha_{old}, M) + \frac{\partial c_L(\alpha_{old}, M)}{\partial \alpha} \Delta\alpha \quad (4.10)$$

Doing this, Equation (4.8) takes the form of a quadratic equation with respect to the correction $\Delta\alpha$:

$$f_2(\alpha_{old}, \Delta\alpha, M) = \left\{ \begin{aligned} &\frac{T_G(M)}{W} \left[+ \cos(\alpha_{old} + \sigma)(\sin \Delta\alpha - \Delta\alpha) + \sin(\alpha_{old} + \sigma) \left(\cos \Delta\alpha + \frac{\Delta\alpha^2}{2} \right) \right] + \\ &+ c_L(\alpha_{old}, M) \frac{\rho}{2} \frac{S}{W} a^2 M^2 + \left[+ \frac{T_G(M)}{W} \cos(\alpha_{old} + \sigma) + \frac{\partial c_L(\alpha_{old}, M)}{\partial \alpha} \frac{\rho}{2} \frac{S}{W} a^2 M^2 \right] \Delta\alpha - \\ &- \frac{1}{2} \frac{T_G(M)}{W} \sin(\alpha_{old} + \sigma) \Delta\alpha^2 \end{aligned} \right\} \quad (4.11)$$

Assuming $\Delta\alpha$ is small the expression $(\sin \Delta\alpha - \Delta\alpha)$ is negligible while the expression $(\cos \Delta\alpha + \Delta\alpha^2/2)$ may be replaced by unity. Under these conditions, the first two terms of Equation (4.11) represent the well-known function $f_2(\alpha_{old}, M)$ of Equation (4.4). The third term in Equation (4.11) however is identical with the derivation $df_2/d(\alpha_{opt}, M)$ from Equation (4.6) multiplied by $\Delta\alpha$. Taking into account these facts we are able to write Equation (4.11) in the following reduced form:

$$f_2(\alpha_{old}, \Delta\alpha, M) = \left[f_2(\alpha_{old}, M) + \frac{\partial f_2(\alpha_{old}, M)}{\partial \alpha} \Delta\alpha - \frac{1}{2} \frac{T_G(M)}{W} \sin(\alpha_{old} + \sigma_M) \Delta\alpha^2 \right] \quad (4.12)$$

Setting $f_2(\alpha_{old}, \Delta\alpha, M) = n$, we get a better relation for the determination of the correction $\Delta\alpha$ in the form

$$\Lambda_0 + \Lambda_1 \Delta\alpha + \Lambda_2 \Delta\alpha^2 = 0 \quad (4.13)$$

with the solutions

$$\Delta\alpha = -\frac{1}{2} \frac{\Lambda_1}{\Lambda_2} \pm \sqrt{\left(\frac{\Lambda_1}{\Lambda_2} \right)^2 - \frac{\Lambda_0}{\Lambda_2}} \quad (4.14)$$

where

$$\Lambda_0 = f_2(\alpha_{old}, M) - n \quad (4.15a)$$

$$\Lambda_1 = \frac{\partial f_2(\alpha_{old}, M)}{\partial \alpha} \quad (4.15b)$$

$$\Lambda_2 = -\frac{1}{2} \frac{T_G(M)}{W} \sin(\alpha_{old} + \sigma) \quad (4.15c)$$

If the thrust level is high enough, the two solutions (4.14) are real. One of these must be chosen for the further iteration. The lower of these applies normally to the accelerated flight, the higher to the decelerated flight. However, if Equation (4.13) yields only a complex solution one should choose first of all the real part for the next iteration step, since it may be possible that nevertheless a solution does exist.

The improved iteration process differs from the original iteration process described in Table 9 only thereby that in step 1 Equation (4.5) must be replaced by Equation (4.14) and (4.15).

The final value of the "specific excess acceleration" can now be computed from Equation (4.2) with the last value $\alpha(n, M)$.

4.2.3 Evaluation of the Maximum Specific Excess Acceleration SEA_{\max} for a Given Load Factor n

With the procedure described above, we are able to compute the specific excess acceleration as a function of the Mach number M and of the load factor n :

$$SEA = f_1[\alpha(n, M), M] . \quad (4.16)$$

The condition for the maximum excess acceleration is defined by

$$\frac{df_1[\alpha(n, M), M]}{dM} = 0 , \quad (4.17)$$

which in general cannot be solved analytically, so that we must apply an iterative process again.

Let us now consider the total changes of f_1 and f_2 respectively:

$$df_1 = \frac{\partial f_1}{\partial \alpha} d\alpha + \frac{\partial f_1}{\partial M} dM \quad (4.18a)$$

$$df_2 = \frac{\partial f_2}{\partial \alpha} d\alpha + \frac{\partial f_2}{\partial M} dM . \quad (4.18b)$$

Dividing Equation (4.18) by dM yields:

$$\frac{df_1}{dM} = \frac{\partial f_1}{\partial \alpha} \frac{d\alpha}{dM} + \frac{\partial f_1}{\partial M} . \quad (4.19)$$

If we further take into account the fact that $\alpha(n, M)$ is a solution of Equation (4.3a) for a given n and M , we can state the total change of f_2 must vanish since n is constant. From Equation (4.18b) we get then:

$$\frac{d\alpha}{dM} = - \frac{\partial f_2 / \partial M}{\partial f_2 / \partial \alpha} . \quad (4.20)$$

Introducing this in Equation (4.19) and taking into account the condition (4.17) we get the relation

$$\frac{df_1}{dM} = \frac{\partial f_1}{\partial M} - \frac{\partial f_2 / \partial M}{\partial f_2 / \partial \alpha} \frac{\partial f_1}{\partial \alpha} = f_1(M_{\text{opt}}) \stackrel{!}{=} 0 . \quad (4.21)$$

which must be solved by an iterative procedure like that described in Table 11. The partial derivatives $\partial f_1 / \partial \alpha, \dots, \partial f_2 / \partial M$ follow from Equation (4.2) and (4.4):

$$\frac{\partial f_1}{\partial \alpha} = - \left[\frac{T_G(M)}{W} \sin(\alpha + \sigma) - \frac{\partial c_D(\alpha, M)}{\partial \alpha} CM^2 \right] \quad (4.22a)$$

$$\frac{\partial f_1}{\partial M} = \left[\frac{\partial \left(\frac{T_G(M)}{W} \right)}{\partial M} \cos(\alpha + \sigma) - \frac{\partial \left(\frac{\rho(M)}{W} \right)}{\partial M} aM - \frac{\rho(M)}{W} a - \frac{\partial c_D(\alpha, M)}{\partial M} CM^2 - 2c_D(\alpha, M)CM \right] \quad (4.22b)$$

$$\frac{\partial f_2}{\partial \alpha} = \frac{T_G(M)}{W} \cos(\alpha + \sigma) + \frac{\partial c_L(\alpha, M)}{\partial \alpha} CM^2 \quad (4.23a)$$

$$\frac{\partial f_2}{\partial M} = \left[\frac{\partial \left(\frac{T_G(M)}{W} \right)}{\partial M} \sin(\alpha + \sigma) + \frac{\partial c_L(\alpha, M)}{\partial M} CM^2 + 2c_L(\alpha, M)CM \right] . \quad (4.23b)$$

with

$$C = \frac{\rho}{2} \frac{S}{W} a^2 = \frac{1}{M_R^2} .$$

4.3 Evaluation of the Steady Climb Performances

4.3.1 Iteration Procedure for a Given Mach Number M

Assuming the Mach number M is given, the basic relations in climbing flight Equation (4.1b) and (4.3b) reduce to

$$\sin \gamma = f_1(\alpha) \quad (4.24)$$

$$\cos \gamma = f_2(\alpha) \quad (4.25)$$

which in the most general case must be solved iteratively in the following manner, which may be shown only briefly in Table 11.

4.3.2 Iteration Procedure for Calculating the Maximum Angle of Climb γ_{\max}

The condition for the evaluation of the maximum angle of climb is given by

$$\frac{d \sin \gamma}{d\alpha} = 0 \quad (4.26a)$$

or

$$\frac{d \sin \gamma}{dM} = 0 \quad (4.26b)$$

where Equation (4.3b) must be satisfied.

The conditions of the steady climbing flight may be written in the following form:

$$f_1^*(\alpha, M, \gamma) = f_1(\alpha, M) - \sin \gamma = 0 \quad (4.27)$$

and

$$f_2^*(\alpha, M, \gamma) = f_2(\alpha, M) - \cos \gamma = 0 \quad (4.28)$$

with the total changes

$$df_1^* = \frac{\partial f_1^*}{\partial \alpha} d\alpha + \frac{\partial f_1^*}{\partial M} dM + \frac{\partial f_1^*}{\partial \sin \gamma} d \sin \gamma = 0 \quad (4.29)$$

and

$$df_2^* = \frac{\partial f_2^*}{\partial \alpha} d\alpha + \frac{\partial f_2^*}{\partial M} dM + \frac{\partial f_2^*}{\partial \sin \gamma} d \sin \gamma = 0 \quad (4.30)$$

where the partial derivatives $\partial f_1^*/\partial \alpha$, $\partial f_1^*/\partial M$, $\partial f_2^*/\partial \alpha$ and $\partial f_2^*/\partial M$ are identical with those of the functions f_1 and f_2 as given in Equations (4.22) and (4.33), while $\partial f_1^*/\partial(\sin \gamma)$ and $\partial f_2^*/\partial(\sin \gamma)$ are

$$\frac{\partial f_1^*}{\partial \sin \gamma} = -1 \quad (4.31)$$

and

$$\frac{\partial f_2^*}{\partial \sin \gamma} = \tan \gamma \quad (4.32)$$

respectively.

If we divide df_1^* and df_2^* by dM , we get the following relations:

$$\frac{df_1^*}{dM} = \frac{\partial f_1^*}{\partial \alpha} \frac{d\alpha}{dM} + \frac{\partial f_1^*}{\partial M} + \frac{\partial f_1^*}{\partial \sin \gamma} \frac{d \sin \gamma}{dM} \quad (4.33)$$

$$\frac{df_2^*}{dM} = \frac{\partial f_2^*}{\partial \alpha} \frac{d\alpha}{dM} + \frac{\partial f_2^*}{\partial M} + \frac{\partial f_2^*}{\partial \sin \gamma} \frac{d \sin \gamma}{dM} \quad (4.34)$$

which represents a system of two linear equations with the unknown $d\alpha/dM$ and $d(\sin \gamma)/dM$ whose solutions are given by the relations

$$\frac{d\alpha}{dM} = \frac{\frac{\partial r_2^*}{\partial M} + \tan \gamma \frac{d \sin \gamma}{dM}}{\frac{\partial r_2^*}{\partial \alpha}} \quad (4.35)$$

and

$$\frac{d \sin \gamma}{dM} = \frac{\frac{\partial r_2^*}{\partial M} \frac{\partial r_1^*}{\partial \alpha} - \frac{\partial r_1^*}{\partial \alpha} \frac{\partial r_2^*}{\partial M}}{\frac{\partial r_2^*}{\partial \alpha} - \tan \gamma \frac{\partial r_1^*}{\partial \alpha}} = f_3(M_{opt}) = 0. \quad (4.36)$$

Equation (4.36) represents the slope of the sine of the angle of climb with respect to the Mach number if the angle of attack is always set to that value which satisfies the condition (4.25). Taking into account the condition (4.26b) for the maximum angle of climb Equation (4.36) enables us to construct an iteration procedure for calculating the maximum angle of climb γ_{max} like that in Table 11 for calculating the maximum excess acceleration.

4.3.3 Iteration Procedure for Calculating the Maximum Rate of Climb

The condition for maximum rate of climb is defined by

$$\frac{dw_z}{dM} = \frac{d(V \sin \gamma)}{dM} = a \frac{d(M \sin \gamma)}{dM} = 0 \quad (4.37a)$$

or

$$f_3(M) = \sin \gamma + M \frac{d \sin \gamma}{dM} = 0. \quad (4.37b)$$

If we introduce this condition in the iteration scheme of Table 10 instead of Equation (4.21), we get the iteration procedure for calculating the maximum rate of climb.

4.4 Evaluation of the Steady Turn Performance

4.4.1 Iteration Procedure for a Given Mach Number

The condition for the steady horizontal turn as given in Equation (3.39) states that the specific excess power must be zero. Equation (3.1) shows that the function f_1 contains the angle of attack in an implicit form. The nature of Equation (3.1) is near quadratic, so that we can hope that a quadratic approximation of Equation (3.1) may be a reasonable basis to construct an iteration procedure for calculation of the appropriate angle of attack at a given Mach number.

Developing Equation (3.1) in a Taylor series about point α up to the quadratic term, we get a quadratic relation

$$f_1(\alpha + \Delta\alpha) = f_1(\alpha) + \frac{df_1(\alpha)}{d\alpha} \Delta\alpha + \frac{d^2f_1(\alpha)}{d\alpha^2} \frac{\Delta\alpha^2}{2}, \quad (4.38)$$

which may be used (in the same way as described in Section 4.2.2) to correct the angle of attack by successive corrections $\Delta\alpha$ until the condition $f_1 = 0$ is satisfied. Taking into account Equation (3.1), the derivatives $df_1/d\alpha$ and $d^2f_1/d\alpha^2$ are defined by the partial derivatives

$$\frac{df_1}{d\alpha} = \frac{\partial f_1}{\partial \alpha} = - \left[\frac{T_G(M)}{W} \sin(\alpha + \sigma) + \frac{\partial c_D(\alpha, M)}{\partial \alpha} \frac{\rho}{2} \frac{S}{W} a^2 M^2 \right] \quad (4.39)$$

and

$$\frac{d^2f_1}{d\alpha^2} = \frac{\partial^2 f_1}{\partial \alpha^2} = \left[\frac{T_G(M)}{W} \cos(\alpha + \sigma) + \frac{\partial^2 c_D(\alpha, M)}{\partial \alpha^2} \frac{\rho}{2} \frac{S}{W} a^2 M^2 \right]. \quad (4.40)$$

The iteration procedure for calculating the angle of attack due to a steady turn at a given Mach number has the same scheme as described in Section 4.2.2.

4.4.2 Iteration Procedure for Calculating the Maximum Steady Turn Load Factor

In this case the additional condition is given by

$$\frac{df_2[\alpha(M), M]}{dM} = 0 = f_3(M_{opt}), \quad (4.41)$$

where $\alpha(M)$ is the solution of $f_1(\alpha) = 0$ at constant Mach number as described in Section 4.2.1.

Recognizing the relations of Section 4.2.3, we find that our problem is solved automatically if we change the indices 1 and 2 in the Equations (4.17) up to (4.21).

4.4.3 Iteration Procedure for Calculating the Maximum Steady Turn Rate

Respecting Equation (3.42), the additional condition for this case is given by

$$\frac{d(d\psi/dt)}{dM} = \frac{a}{g} \frac{d\left(\frac{\sqrt{n^2-1}}{M}\right)}{dM} = 0 \quad (4.42)$$

or

$$f_3(M) = \left[(n^2 - 1) - Mn \frac{dn}{dM} \right] = 0 \quad (4.43a)$$

or

$$f_3(M_{opt}) = \left[(f_2^2 - 1) - Mf_2 \frac{df_2}{dM} \right] = 0. \quad (4.43b)$$

4.4.4 Iteration Procedure for Calculating the Minimum Steady Radius of Curvature in a Horizontal Turn

Respecting Equation (3.43), the additional condition for this case is given by

$$\frac{dR}{dM} = \frac{a^2}{g} \frac{d\left(\frac{M^2}{\sqrt{n^2-1}}\right)}{dM} = 0 \quad (4.44)$$

or

$$f_3(M) = \left[2(n^2 - 1) - Mn \frac{dn}{dM} \right] = 0 \quad (4.45a)$$

or

$$f_3(M_{opt}) = \left[2(f_2^2 - 1) - Mf_2 \frac{df_2}{dM} \right] = 0. \quad (4.45b)$$

5. INTEGRAL-PERFORMANCE PREDICTION

5.1 Climbing Flight

5.1.1 Definitions

The interesting integral-performance values in climbing flight are

- the time T
- the horizontal distance X
- the fuel consumption W_F ,

during a climb from an initial height h_i to a final height h_f . The integrals for these performances are defined as follows:

$$T(h_f) = \int_{h_i}^{h_f} \frac{dt}{dh}(h) dh = \int_{h_i}^{h_f} \frac{dh}{V(h) \sin \gamma(h)} = \int_{h_i}^{h_f} \frac{dh}{w(h)} \quad (5.1)$$

$$X(h_f) = \int_{h_i}^{h_f} \frac{dx}{dt}(h) \frac{dt}{dh}(h) dh = \int_{h_i}^{h_f} \cot \gamma(h) dh \quad (5.2)$$

$$\Delta W_F(h_f) = \int_{h_i}^{h_f} C_F(h) \frac{dt}{dh}(h) dh = \int_{h_i}^{h_f} \frac{C_F(h)}{w(h)} dh. \quad (5.3)$$

In the most general case these integrals must be solved with the aid of numerical methods. The final results depend on the "law of climb" that we want to use. There are different way to define such laws.

5.1.2 Fastest Climb

In general, the fastest climb is a climbing flight where the time between the initial height h_i and the final height h_f should be a minimum. If we prescribe further the speed V and the flight path angle γ at the initial and final flight points, we have to solve an optimization problem which must be carried out with the Calculus of Variations. However, if we prescribe only the height, we can choose that law where the change of potential energy is a maximum. This is as pointed out in Sections 3.2 and 4.3.3 as the flight with maximum rate of climb.

Kinetic energy correction

In Section 4.3.3 the maximum rate of climb was analyzed from a quasi-steady point of view, that means, that the acceleration terms $(dV/dt)/g$ and $(Vd\gamma/dt)/g$ in Equation (2.10) and (2.11) respectively were assumed to be zero. This is not true in a real climbing flight since the speed V and the angle of climb γ where the maximum rate of climb occurs vary with the altitude. However, if we consider the fact that the change of energy height can be expressed in the form

$$\frac{dh_E}{dt} = V \sin \gamma + \frac{V}{g} \frac{dV}{dh} \frac{dh}{dt} \quad (5.4)$$

$$\frac{dh_E}{dt} = \frac{dh}{dt} \left(1 + \frac{V}{g} \frac{dV}{dh} \right) = \frac{dh}{dt} \left(1 + \frac{d(V^2/2)}{d(gh)} \right), \quad (5.4a)$$

we get a formula for correcting the quasi-steady rate of climb (subscript s) – which is identical with the specific excess power for $n = \cos \gamma_s$ – to the accelerated rate of climb (subscript a).

$$\left(\frac{dh}{dt} \right)_a = \frac{\left(\frac{dh}{dt} \right)_s}{\left[1 + \frac{d(V^2/2)}{d(gh)} \right]}. \quad (5.5)$$

It may be noted that only the tangential acceleration, and not the normal acceleration, is considered here.

The use of this correction formula may be demonstrated in Figure 15. The dashed line in the diagram on the left shows the steady maximum rate of climb without kinetic energy correction, the full line with kinetic energy correction. The full line in the right diagram shows the optimum climbing speed. In the high altitude region one can see the influence of the transonic drag rise.

5.1.3 Further Climb Laws

Steepest climb

The law of the steepest climb is that of the flight with maximum angle of climb according to Section 4.3.2.

Most economic climb

The most economic climb is defined by the condition for minimum fuel consumption per unit step increase in height:

$$\frac{d\left(\frac{dW_F}{dh}\right)}{dM} = \frac{d\left(\frac{dW_F}{dt} \frac{dt}{dh}\right)}{dM} = \frac{d\left(\frac{C_F}{w_s}\right)}{dM} = 0. \quad (5.6)$$

Climb with constant calibrated airspeed

This represents a climbing flight with constant dynamic pressure and constant c_L . In the case of a subcritical parabolic drag polar and of aircraft with constant thrust, this climb procedure enables optimum climbing flights such as fastest climb and steepest climb.

Climb with constant Mach number

This climb procedure is approximately realized at high altitudes where the flight Mach number is so high that the transonic drag-rise boundary is reached.

Figures 15(a) and (b) show the effect of the last two climb procedures in comparison with the fastest climb procedure. In the lower altitude region, the constant CAS-climb has a less rate of climb because the kinetic energy correction is nearly twice of that of the fastest climb. At the higher altitudes where the constant Mach number procedure is applied, the rate of climb is a little higher. At $H = 7500$ m a step occurs in the curve for the rate of climb because the airspeed changes abruptly.

Figures 15(c) and (d) show the time history and total fuel consumption of the fastest climb from Figures 15(a) and (b).

5.2 Unsteady Horizontal Turn

5.2.1 Definitions

The interesting integral performance values for the unsteady horizontal turn are

- the time T
- the flight path coordinates x and y
- the flight velocity.

Further we are interested in the time history of

- the load factor
- the angle of bank,

which depend on the prescribed "turn law".

The definitions of the integrals are:

$$T(\psi_f) = \int_{\psi_i}^{\psi_f} \frac{d\psi}{\frac{d\psi}{dt}(\psi)} \quad (5.7)$$

$$V(\psi_f) = \int_{\psi_i}^{\psi_f} \frac{\frac{dV}{dt}(\psi)}{\frac{d\psi}{dt}(\psi)} d\psi \quad (5.8)$$

$$X(\psi_f) = \int_{\psi_i}^{\psi_f} \frac{V(\psi) \cos \psi}{\frac{d\psi}{dt}(\psi)} d\psi \quad (5.9)$$

$$Y(\psi_f) = \int_{\psi_i}^{\psi_f} \frac{V(\psi) \sin \psi}{\frac{d\psi}{dt}(\psi)} d\psi, \quad (5.10)$$

where

$$\frac{d\psi}{dt}(\psi) = \frac{g}{V(\psi)} \sqrt{n(\psi)^2 - 1}, \quad (5.11)$$

which depends on the prescribed turn law.

The results are further a function of the given initial flight velocity V_i .

5.2.2 Turn Laws

There are several turn laws which may be used with maximum power settings:

- Turn with constant load factor

$$n(\psi) = \text{constant} . \quad (5.12)$$

- Turn with constant angle of bank

$$n(\psi) = \frac{1}{\cos \phi} = \text{constant} . \quad (5.13)$$

- Turn with constant rate of turn $d\psi/dt$

$$n(\psi) = \sqrt{1 + \left[\frac{V(\psi)}{g} \left(\frac{d\psi}{dt} \right) \right]^2} . \quad (5.14)$$

- Turn with constant radius of curvature R

$$n(\psi) = \sqrt{1 + \left[\frac{V(\psi)}{gR} \right]^2} . \quad (5.15)$$

In all of these cases the angle of attack α and the tangential acceleration dv/dt alter. Attention must be drawn here to the possibility that the angle of attack may reach its maximum value. If this occurs, the prescribed law no longer holds and must be replaced by the law for the steady turn with maximum available angle of attack.

5.3 Unsteady Vertical Turn

In this case the yaw angle ψ and the coordinate y are replaced by the flight path angle γ and the height h respectively. Further, attention must be drawn to the fact that the specific excess power and the load factor are now functions of the altitude h .

ACKNOWLEDGEMENTS

The author thanks Mr Rudolph Matecki for his welcome help in the preparation of the lecture notes, especially in preparation of the drawings for the illustrations, in reading the corrections of the text, and for his helpful discussions of the subject; also Mr Wolfgang Häberle for carrying out some numerical calculations; Mrs I.Schmidt and Miss H.Schatz for typing the text, and Mrs I.Sikora and Miss G.Pfister for drawing the diagrams.

REFERENCES

1. Miele, A. Flight Mechanics, Volume 1, Theory of Flight Paths, Pergamon Press, London-Paris: 1962.
2. — Introduction to the Measurement of Thrust in Flight. Eng. Sc. Data Item No.69006 Engineering Sciences, Data Unit; London, 1969.
3. — The Determination of Gross Thrust and Mass Flow in Flight. Eng. Sc. Data Item No. 69007 Engineering Sciences, Data Unit; London 1969.
4. — Curves for Use in the Determination of Gross Thrust and Mass Flow in Flight. Eng. Sc. Data Item No. 69008 Engineering Sciences, Data Unit, London 1969.

TABLE 1

Comparison of Climb Performance Formulae for Aircraft with Thrust Acting in Flight Path Direction

	<i>Simplified Analysis</i>	<i>Exact Analysis</i>
Angle of climb: $\sin \gamma$	$\tau - \epsilon$	$\frac{1}{(1 + \epsilon^2)} \tau^{(+)} \sqrt{(1 + \epsilon^2) - \tau^2}$
Rate of climb: $\frac{w_s}{V_R}$	$\frac{\tau - \epsilon}{\sqrt{c_L}}$	$\frac{1}{\sqrt{c_L}} \frac{1}{(1 + \epsilon^2)^{3/2}} \left\{ \left[\sqrt{\epsilon \tau^{(-)} \sqrt{(1 + \epsilon^2) - \tau^2}} \right] \left[\tau^{(+)} \epsilon \sqrt{(1 + \epsilon^2) - \tau^2} \right] \right\}$
Climbing velocity: $\frac{V}{V_R} = \frac{M}{M_R}$	$\frac{1}{\sqrt{c_L}}$	$\frac{1}{\sqrt{c_L}} \sqrt{\frac{\epsilon \tau^{(-)} \sqrt{(1 + \epsilon^2) - \tau^2}}{(1 + \epsilon^2)}}$
where $\tau = \frac{T_N}{W}$; $\epsilon = \frac{c_D}{c_L}$; $V_R = \sqrt{\frac{2}{\rho} \frac{W}{S}}$; $M_R = \frac{V_R}{a}$.		

TABLE 2

Comparison of Gliding Performance Formulae

	<i>Simplified Analysis</i>	<i>Exact Analysis</i>
Gliding angle: $\sin \gamma$	$-\epsilon$	$-\frac{\epsilon}{\sqrt{1 + \epsilon^2}}$
Sinking speed: $\frac{w_s}{V_R}$	$-\frac{\epsilon}{\sqrt{c_L}}$	$-\frac{\epsilon}{\sqrt{c_L} (1 + \epsilon^2)^{3/4}}$
Gliding speed: $\frac{V}{V_R}$	$\frac{1}{\sqrt{c_L}}$	$\frac{1}{\sqrt{c_L} (1 + \epsilon^2)^{1/4}}$
where $\epsilon = \frac{c_D}{c_L}$; $V_R = \sqrt{\frac{2}{\rho} \frac{W}{S}}$		

TABLE 3

Simplified Solution of Gliding Performance for Aircraft with
Parabolic Polars of the Form $c_D = c_{D0} + kc_L^2$

	Non-optimum gliding performance	Optimum gliding performance	
		Flattest glide	Glide with minimum sinking speed
Gliding angle: $\sin \gamma$	$-\left(\frac{c_{D0}}{c_L} + kc_L\right)$	$-2\sqrt{kc_{D0}}$	$-\frac{4}{\sqrt{3}}\sqrt{kc_{D0}}$
Sinking speed: $\frac{w_s}{V_R}$	$-\frac{c_{D0}}{\sqrt{c_L^3}} + k\sqrt{c_L}$	$-2\sqrt[4]{k^3 c_{D0}}$	$-\frac{4}{3}\sqrt[4]{3k^3 c_{D0}}$
Lift coefficient:	c_L	$\sqrt{\frac{c_{D0}}{k}}$	$\sqrt{3}\sqrt{\frac{c_{D0}}{k}}$
Gliding speed: $v = \frac{V}{V_R}$	$\sqrt{\frac{1}{c_L}}$	$\sqrt[4]{\frac{k}{c_{D0}}}$	$\frac{1}{\sqrt[4]{3}}\sqrt[4]{\frac{k}{c_{D0}}}$
where $V_R^* = \sqrt[4]{\frac{k}{c_{D0}}} V_R$; $V_R = \sqrt{\frac{2}{\rho} \frac{W}{S}}$			

TABLE 4

Formulae for Steady Horizontal Turn Performance

Load factor:	$n = \frac{\tau}{\epsilon(c_L)} = \frac{c_L}{c_D(c_L)} \tau$
Flight speed:	$\frac{V}{V_R} = \sqrt{\frac{\tau}{c_L \epsilon(c_L)}} = \sqrt{\frac{\tau}{c_D(c_L)}}$
Angle of bank:	$\tan \phi = \sqrt{\left[\frac{\tau}{\epsilon(c_L)}\right]^2 - 1} = \sqrt{\left[\frac{c_L \tau}{c_D(c_L)}\right]^2 - 1}$
Turn rate:	$\frac{V_R}{g} \left(\frac{d\psi}{dt}\right) = \sqrt{\frac{c_D(c_L)}{\tau} \left[\left[\frac{\tau c_L}{c_D(c_L)}\right]^2 - 1\right]} = \sqrt{c_L^2 \frac{\tau}{c_D(c_L)} - \frac{c_D(c_L)}{\tau}}$
Radius of curvature:	$\frac{g}{V_R^2} R = \frac{1}{\sqrt{c_L^2 - \left[\frac{c_D(c_L)}{\tau}\right]^2}}$
where	$V_R = \sqrt{\frac{2}{\rho} \frac{W}{S}}; \quad \tau = \frac{T_N}{W}$

TABLE 5

Non-optimum Climb Performance. Constant Thrust Acting in Flight Path Direction.
Parabolic Polar $c_D = c_{D0} + kc_L^2$

	<i>Simplified solution</i>	<i>Exact solution</i>
Angle of climb: $\frac{\sin \gamma}{\epsilon_{\min}} =$	$z_T - \frac{1}{2} \left(v^2 + \frac{1}{v^2} \right)$	$\frac{1}{\epsilon_{\min}} \left(\frac{v^2}{\epsilon_{\min}} \right) \left[1 \pm \sqrt{1 - \frac{2z_T v^2 - 1 - v^4}{\left(\frac{v^2}{\epsilon_{\min}} \right)^2}} \right]$
Rate of climb: $\frac{1}{\epsilon_{\min}} \frac{w_s}{V_R^*} =$	$z_T - \frac{1}{2} \left(v^3 + \frac{1}{v} \right)$	$\frac{v}{\epsilon_{\min}} \left(\frac{v^2}{\epsilon_{\min}} \right) \left[1 \pm \sqrt{1 - \frac{2z_T v^2 - 1 - v^4}{\left(\frac{v^2}{\epsilon_{\min}} \right)^2}} \right]$
where $v = \frac{V}{V_R^*}$; $V_R^* = \sqrt[4]{\frac{k}{c_{D0}}} \sqrt{\frac{2W}{\rho S}}$; $\epsilon_{\min} = 2\sqrt{kc_{D0}}$; $z_T = \frac{T}{W} \frac{1}{\epsilon_{\min}}$		

TABLE 6

Non-optimum Climb Performance. Constant Power Acting in Flight Path Direction.
Parabolic Polar $c_D = c_{D0} + kc_L^2$

	<i>Simplified solution</i>	<i>Exact solution</i>
Angle of climb: $\frac{\sin \gamma}{\epsilon_{\min}} =$	$\frac{z_P^*}{v} - \frac{1}{2} \left(v^2 + \frac{1}{v^2} \right)$	$\frac{1}{\epsilon_{\min}} \left(\frac{v^2}{\epsilon_{\min}} \right) \left[1 \pm \sqrt{1 - \frac{2z_P^* v - 1 - v^4}{\left(\frac{v^2}{\epsilon_{\min}} \right)^2}} \right]$
Rate of climb: $\frac{1}{\epsilon_{\min}} \frac{w_s}{V_R^*} =$	$z_P^* - \frac{1}{2} \left(v^3 + \frac{1}{v} \right)$	$\frac{v}{\epsilon_{\min}} \left(\frac{v^2}{\epsilon_{\min}} \right) \left[1 \pm \sqrt{1 - \frac{2z_P^* v - 1 - v^4}{\left(\frac{v^2}{\epsilon_{\min}} \right)^2}} \right]$
where $v = \frac{V}{V_R^*}$; $V_R^* = \sqrt[4]{\frac{k}{c_{D0}}} \sqrt{\frac{2W}{\rho S}}$; $\epsilon_{\min} = 2\sqrt{kc_{D0}}$; $z_P^* = \frac{\pi^*}{\epsilon_{\min}}$; $\pi^* = \frac{\eta P}{W V_R^*}$		

TABLE 7

Non-optimum Steady Horizontal Turn Performance. Comparison between Constant Thrust and Constant Power Aircraft with Parabolic Polar $c_D = c_{D0} + kc_L^2$

Physical magnitude	Constant thrust	Constant power
Required lift coefficient: $\frac{c_L}{c_L^*} = \frac{n}{v^2}$	$\sqrt{2\frac{z_T}{v^2} - 1}$	$\sqrt{2\frac{z_P}{v^3} - 1}$
Load factor: n	$v\sqrt{2z_T - 1}$	$\sqrt{v(2z_P - v^3)}$
Angle of bank: $\cos \phi = \frac{1}{n}$	$\frac{1}{v\sqrt{2z_T - 1}}$	$\frac{1}{\sqrt{v(2z_P - v^3)}}$
Turn rate: $\frac{V_R^*}{g} \left(\frac{d\psi}{dt} \right)$	$\sqrt{2z_T - v^2 - \frac{1}{v^2}}$	$\sqrt{2\frac{z_P}{v} - v^2 - \frac{1}{v^2}}$
Radius of curvature: $\frac{g}{V_R^{*2}} R = \frac{v}{\frac{V_R^*}{g} \left(\frac{d\psi}{dt} \right)}$	$\frac{1}{\sqrt{2\frac{z_T}{v^2} - 1 - \frac{1}{v^4}}}$	$\frac{1}{\sqrt{2\frac{z_P}{v^3} - 1 - \frac{1}{v^4}}}$
where $c_L^* = \sqrt{\frac{c_{D0}}{k}} = (c_L)_{\epsilon \min}$; $\epsilon_{\min} = 2\sqrt{kc_{D0}}$; $V_R^* = \sqrt[4]{\frac{k}{c_{D0}}} \sqrt{\frac{2W}{\rho S}}$; $z_T = \frac{\tau}{\epsilon_{\min}}$; $\tau = \frac{T}{W}$; $z_P = \frac{\pi^*}{\epsilon_{\min}}$; $\pi^* = \frac{\eta P}{V_R^* W}$		

TABLE 8

Optimum Steady Climb and Horizontal Turn Performance.
Comparison between Constant Thrust and Constant Power Aircraft with
Parabolic Polar $c_D = c_{D0} + kc_L^2$

		Constant thrust	Constant power
	Optimum steady climb performances		
Steepest climb	$\frac{\sin \gamma_{\max}}{\epsilon_{\min}}$	$z_T - 1$	$\frac{1}{2} \left(\frac{1}{v_{\text{opt}}^2} - 3v_{\text{opt}}^2 \right)$
	$(v_{\text{opt}})_{\gamma \max}$	1	$v_{\text{opt}}^4 + z_P v_{\text{opt}} - 1 = 0$
Fastest climb	$\left(\frac{w_s}{V_R^*} \frac{1}{\epsilon_{\min}} \right)_{\max}$	$\frac{2}{3\sqrt{3}} \left[\sqrt{z_T + \sqrt{z_T^2 + 3}} (2z_T - \sqrt{z_T^2 + 3}) \right]$	$z_P - \frac{2}{3} \sqrt[3]{3}$
	$(v_{\text{opt}})_{w_s \max}$	$\frac{1}{\sqrt{3}} \sqrt{z_T + \sqrt{z_T^2 + 3}}$	$\frac{1}{\sqrt[3]{3}}$
	Optimum steady horizontal turn performances		
Maximum load factor Maximum bank angle	n_{\max}	z_T	$\sqrt[3]{3} \left(\frac{z_P}{2} \right)^{2/3}$
	$\cos \phi_{\max}$	$\frac{1}{z_T}$	$\frac{1}{\sqrt[3]{3}} \left(\frac{2}{z_P} \right)^{2/3}$
	$(v_{\text{opt}})_{n \max} = (v_{\text{opt}})_{\phi \max}$	$\sqrt{z_T}$	$\sqrt[3]{\frac{z_P}{2}}$
Max. turn rate	$\frac{V_R^*}{g} \left(\frac{d\psi}{dt} \right)_{\max}$	$\sqrt{2(z_T - 1)}$	$\frac{1}{v_{\text{opt}}^2} - 3v_{\text{opt}}^2$
	$(v_{\text{opt}})_{(d\psi/dt) \max}$	1	$v_{\text{opt}}^4 + z_P v_{\text{opt}} - 1 = 0$
Minimum radius of curvature	$\frac{g}{V_R^*} R_{\min}$	$\frac{1}{\sqrt{z_T^2 - 1}}$	$\frac{1}{\sqrt{\frac{4}{3} \left(\frac{3z_P}{2} \right)^4 - 1}}$
	$(v_{\text{opt}})_{R \min}$	$\frac{1}{\sqrt{z_T}}$	$\frac{2}{3z_P}$

TABLE 9

Iteration Procedure for Finding the Appropriate Angle of Attack α
from the Relation $f_2(\alpha, M) - n = 0$ for a Given Mach number M
and a Given Load Factor n

<i>Given</i>	n, M and W, S, σ , atmospheric conditions and tabulated curves for: $T_G(M)$, $c_L(\alpha, M)$, accuracy ϵ_α .
<i>Step 0</i>	<p>Determine: $\rho, a, T_G(M)$</p> <p>Compute: $T_G/W(M)$; $C = \frac{\rho}{2} \frac{S}{W} a^2 M^2$</p> <p>Estimate: A suitable value for α</p> <p>(Set: Iteration counting number $i = 0, i_{\max}$).</p>
<i>Step 1</i>	<p>Determine: $c_L(\alpha, M)$, $\frac{\partial c_L}{\partial \alpha}(\alpha, M)$</p> <p>Compute: $f_2(\alpha, M)$ from Equation (4.4)</p> <p>$\frac{df_2}{d\alpha}(\alpha, M)$ from Equation (4.6)</p> <p>$\Delta\alpha$ from Equation (4.5)</p> <p>$\alpha_{\text{new}} = \alpha_{\text{old}} + \Delta\alpha$</p> <p>$i = i + 1$</p>
<i>Step 2</i>	<p>Accuracy check:</p> <p>If $\Delta\alpha > \epsilon_\alpha$: Repeat step 1.</p> <p>If $\Delta\alpha \leq \epsilon_\alpha$: End of iteration, write results.</p>

TABLE 10

Iteration Process for Finding the Maximum Specific Excess Acceleration
SEA for a Given Load Factor n (see also Figure 14)

<i>Given</i>	n, W, S, σ , atmospheric conditions and tabulated curves for $T_G(M), \dot{m}(M), c_L(\alpha, M), c_D(\alpha, M)$, accuracy ϵ_M .
<i>Step 0</i>	<p>Determine: ρ, a</p> <p>Compute: $C = \frac{\rho}{2} \frac{S}{W} a^2$</p> <p>Estimate: A suitable Mach number</p> <p>Set: Iteration counting number $k = 0; k_{\max}$.</p>
<i>Step 1</i>	Execute iteration procedure of Table 9 with given values for n and M .
<i>Step 2</i>	<p>Set: $M_{\text{old}} = M; k = k + 1$</p> <p>Determine: $c_L(\alpha, M); \frac{\partial c_L(\alpha, M)}{\partial \alpha}; \frac{\partial c_L(\alpha, M)}{\partial M};$ $c_D(\alpha, M); \frac{\partial c_D(\alpha, M)}{\partial \alpha}; \frac{\partial c_D(\alpha, M)}{\partial M};$ $T_G(M); \frac{\partial T_G(M)}{\partial M}; \dot{m}(M); \frac{\partial \dot{m}(M)}{\partial M}$</p> <p>Compute: $\frac{\partial f_1(\alpha, M)}{\partial \alpha}; \frac{\partial f_1(\alpha, M)}{\partial M}; \frac{\partial f_2(\alpha, M)}{\partial \alpha}; \frac{\partial f_2(\alpha, M)}{\partial M}; f_3(M)$</p>
<i>Step 3</i>	<p>If $k = 1$ Set: $\Delta M = \text{sign}(f_3) 0.05$; go to Step 4.</p> <p>If $k > 1$: Compute: $\Delta M = -\frac{f_3 \Delta M}{f_3 - f_{3\text{old}}}$; go to Step 4.</p>
<i>Step 4</i>	Set: $M = M_{\text{old}} + \Delta M; f_{3\text{old}} = f_3, M = M_{\text{old}}$.
<i>Step 5</i>	<p>Accuracy check:</p> <p>If $\Delta M \leq \epsilon_M$: End of iteration: go to Step 6.</p> <p>If $\Delta M > \epsilon_M$: go to Step 5.</p>
<i>Step 6</i>	<p>Compute f_1 from Equation (4.2)</p> <p>Write: $n, M_{\text{opt}}, \alpha_{\text{opt}}, \text{SEA}_{\max}$.</p>

TABLE 11

Iteration Process for Finding the Steady Angle of Climb γ for a
Given Mach Number M

Step 0	Set:	Angle of climb $\gamma = 0$.
	Estimate:	An appropriate value for the angle of attack α .
Step 1	Apply iteration procedure of Table 9 to evaluate that angle of attack which satisfies Equation (4.25) for the last given value of γ_{old} .	
Step 2	Compute:	γ_{new} from Equation (4.24)
		$\Delta\gamma = \gamma_{new} - \gamma_{old}$.
	Set:	$\gamma_{old} = \gamma_{new}$.
Step 3	Accuracy check:	
	If $ \Delta\gamma > \epsilon_\gamma$: Repeat Step 1.	
	If $ \Delta\gamma \leq \epsilon_\gamma$: End of iteration.	

APPENDIX A

Calculation of Optimum Climbing Flight Paths with the Aid of the
"Principle of Optimality" by R.Bellman

A1. BASIC RELATIONS

A1.1 Equations of Motion

Let us consider a climbing flight in a vertical plane as shown in the Height-Velocity diagram of Figure A-1. Introducing the well-known relation for the energy height,

$$h_E = h + \frac{v^2}{2g}, \quad (A1)$$

the basic equations of motion as given in Section 2.1.2 of the main part take the following form:

Specific excess acceleration:

$$\frac{1}{v} \frac{dh_E}{dt} = \frac{T_t - D}{W} = \left[\frac{1}{g} \frac{dv}{dt} + \sin \gamma \right] = f_1(\alpha, v, h). \quad (A2)$$

Load factor n :

$$n = \frac{T_n + L}{W} = \left[\frac{v}{g} \frac{d\gamma}{dt} + \cos \gamma \right] = f_2(\alpha, v, h). \quad (A3)$$

Change of the angle of climb γ :

$$\frac{d\gamma}{dh_E} = \frac{n - \cos \gamma}{\left(\frac{v^2}{g}\right) f_1}. \quad (A4)$$

Change of the vertical distance h (altitude):

$$\frac{dh}{dh_E} = \frac{\sin \gamma}{f_1}. \quad (A5)$$

Change of the horizontal distance x :

$$\frac{dx}{dh_E} = \frac{\cos \gamma}{f_1}. \quad (A6)$$

Change of the fuel consumption m :

$$\frac{dm}{dh_E} = - \frac{C_1}{vf_1}. \quad (A7)$$

A1.2 Principle of Optimality by R.Bellman

Let us consider all points $P_\nu(v_\rho)$ on the curve of constant energy height $(h_E)_\nu$ and assume that we know the minimum time $T_\nu(v_\rho)$ (or minimum fuel in the case of finding the minimum fuel) from each point $P_\nu(v_\rho)$ to the final point P_f (see Figure A-2). The Principle of Optimality by R.Bellman (see Reference 1) states the minimum time $T_{\nu-1}(v_\mu)$ between a point $P_{\nu-1}(v_\mu)$ and the final point P_f may be found by the relation

$$T_{\nu-1}(v_\mu) = \text{Min}_{\{v_\rho\}} [\Delta t_{\mu\rho} + T_\nu(v_\rho)]. \quad (A8)$$

in which $\Delta t_{\mu\rho}$ represents the flight time from point $P_{\nu-1}(v_\mu)$ to point $P_\nu(v_\rho)$. The notation $\{v_\rho\}$ denotes the available velocity range of the curve $(h_E)_\nu = \text{constant}$ in which the minimum time is sought. Further, Equation (A8) represents a recursive formula which enables us to construct a procedure for finding the minimum time between the initial point P_i and the final point P_f by successive calculations of the dependence on velocity of the minimum time to the final point P_f for the successive decreasing energy height levels.

A2. CALCULATION OF THE TIME INCREMENT $\Delta t_{\mu\rho}$

In the height-velocity diagram the flight from point $P_{\nu-1}(v_\mu)$ to point $P_\nu(v_\rho)$ is essentially characterized by the prescribed values of the energy height h_E and of the flight velocity v . The altitude h belonging to it is defined by Equation (A1) and therefore also known. The further state of flight, namely the angles of climb γ and their change $d\gamma/dh_E$, is only known at point $P_\nu(v_\rho)$ from the foregoing optimization step. At point $P_{\nu-1}(v_\mu)$ it is for the present unknown and defined by the condition that the altitude change defined by Equation (A5) must be equal to the altitude difference $\Delta h = h_\rho - h_\mu$ prescribed.

To evaluate this we write the differential equations of motion in form of difference equations.

Assuming a small increment Δh_E of the energy height according to

$$\Delta h_E = (h_E)_\nu - (h_E)_{\nu-1}, \quad (A9)$$

the altitude change Δh and the change $\Delta\gamma$ of the angle of climb may be expressed by

$$\Delta h = h_\rho - h_\mu = \left[\left(\frac{dh}{dh_E} \right)_\nu + \left(\frac{dh}{dh_E} \right)_{\nu-1} \right] \frac{\Delta h_E}{2} \quad (A10)$$

and

$$\Delta\gamma = \gamma_\rho - \gamma_\mu = \left[\left(\frac{d\gamma}{dh_E} \right)_\nu + \left(\frac{d\gamma}{dh_E} \right)_{\nu-1} \right] \frac{\Delta h_E}{2} \quad (A11)$$

respectively.

In Equations (A10) and (A11) the values of Δh , Δh_E , $(dh/dh_E)_\nu$ and $(d\gamma/dh_E)_\nu$ are known while $(dh/dh_E)_{\nu-1}$ and $(d\gamma/dh_E)_{\nu-1}$ are unknown but defined by Equations (A5) and (A4) respectively. Introducing Equation (A5) in Equation (A10) and rearranging, we get a relation for the required angle of climb γ_μ at point $P_{\nu-1}(v_\mu)$ which satisfies the altitude change condition:

$$\sin(\gamma_\mu)_{\text{req}} = \left[2 \frac{\Delta h}{\Delta h_E} - \left(\frac{dh}{dh_E} \right)_\nu \right] f_1(\alpha_\mu, v_\mu, h_\mu). \quad (A12)$$

The required change of the angle of climb thus is given by

$$(\Delta\gamma)_{\text{req}} = \arcsin(\gamma_\mu)_{\text{req}} - \arcsin \gamma_\rho. \quad (A13)$$

Introducing this relation in Equation (A11) and taking into account Equation (A4), we finally get a relation between the required load factor at point $P_{\nu-1}(v_\mu)$ and the altitude change prescribed.

$$n_{\text{req}} = \left[2 \frac{(\Delta\gamma)_{\text{req}}}{\Delta h_E} - \left(\frac{d\gamma}{dh_E} \right)_\nu \right] \left(f_1 \frac{v_\mu^2}{g} \right)_{\nu-1} - \cos \gamma_\mu. \quad (A14)$$

On the other side n_{req} must satisfy Equation (A3) according to

$$n_{\text{req}} - f_2(\alpha_\mu, v_\mu, h_\mu) = 0, \quad (A15)$$

in which the angle of attack α_μ is the only free control variable which allows us to adjust the load factor to the required one. Since the system of Equations (A12) to (A15) contains α_μ in an implicit form, the calculation of $(\alpha_\mu)_{\text{req}}$ must be done by an iterative procedure like that in Section 4.2.1 of the main text.

Once $(\alpha_\mu)_{\text{req}}$ is calculated, we are able to compute the time increment $\Delta t_{\mu\rho}$ by

$$\Delta t_{\mu\rho} = \left[\left(\frac{dt}{dh_E} \right)_\nu + \left(\frac{dt}{dh_E} \right)_{\nu-1} \right] \frac{\Delta h_E}{2} \quad (A16)$$

or

$$\Delta t_{\mu\rho} = \left[\frac{1}{v_\rho(f_1)_\nu} + \frac{1}{v_\mu(f_1)_{\nu-1}} \right] \frac{\Delta h_E}{2}. \quad (A16a)$$

Equation (A16a) is accurate enough if the difference of the products $v_\rho(f_1)_\nu$ and $v_\mu(f_1)_{\nu-1}$ is small compared with their mean value, as can always be reached by setting a suitable energy height increment Δh_E . In the case of optimization of transition flight paths of V/STOL aircraft which begins normally at the initial point with zero speed

Equation (A16a) may lead to significant errors if equidistant energy height steps are used. In this case, a better approximation of the time integral will be obtained by approximation of the energy height integral in the following manner:

$$\Delta h_E = \int_0^{\Delta t} \frac{dh_E}{dt} dt = \int_0^{\Delta t} v(t) f_1(t) dt. \quad (A17)$$

Assuming $v(t)$ and $f_1(t)$ are both linear functions of time according to

$$v(t) = v_l + \frac{v_u - v_l}{\Delta t} t \quad (A18a)$$

$$f_1(t) = f_l + \frac{f_u - f_l}{\Delta t} t, \quad (A18b)$$

the evaluation of the integral (A17) yields the following relation between the energy height increment Δh_E and the time increment Δt :

$$\Delta h_E = \frac{1}{2} [v_u f_u + (v_u f_l + v_l f_u) + v_l f_l] \Delta t \quad (A19)$$

or, in the notation of Equation (A16a),

$$\Delta t_{\mu\rho} = \frac{3\Delta h_E}{\{v_\rho(f_1)_\nu + \frac{1}{2}[v_\rho(f_1)_{\nu-1} + v_\mu(f_1)_\nu] + v_\mu(f_1)_{\nu-1}\}}. \quad (A20)$$

A3. DESCRIPTION OF THE OPTIMIZATION PROCEDURE

The optimization procedure may be split into two main parts.

A3.1 Calculation of the Optimum Functions

In the first part the dependence of the minimum time on the velocity v is to be calculated for each energy height level beginning with the highest one, by using the recursive formula Equation (A8) and applying the calculation routine for the time increment $\Delta t_{\mu\rho}$ described in Section A2. Attention must be drawn to the various end conditions which may be prescribed at the final point P_f (see below). The calculation yields for each energy height level $(h_E)_\nu$ a table of the following functions depending on the velocity v :

- $T_\nu(v)$ = minimum time for the optimum flight, between the point $P_\nu(v)$ on the curve of $(h_E)_\nu = \text{constant}$ to the final point P_f
- $v_{\nu+1}(v)$ = optimum velocity for $(h_E)_{\nu+1} = \text{constant}$ at v
- $h_\nu(v)$ = altitude corresponding to v and h_E
- $\gamma_\nu(v)$ = optimum angle of climb
- $\left[\frac{dh}{dh_E}(v) \right]_\nu$ = optimum change of the altitude
- $\left[\frac{d\gamma}{dh_E}(v) \right]_\nu$ = optimum change of the angle of climb
- $[f_1(v)]_\nu$ = optimum specific excess acceleration
- $[f_2(v)]_\nu$ = optimum load factor.

The last two or the two before need not necessarily be stored because they may be calculated always from the other two by applying Equations (A4) and (A5).

A3.2 Finding the Optimum Flight Path

Once all tables of the optimum functions described above are calculated the optimum flight path from an arbitrary point P_i on the curve $(h_E)_i = (h_E)_0 = \text{constant}$ may be found by successive interpolations in the tables for the optimum velocity $v_{\nu+1}(v)$ according to

$$(v_{opt})_{\nu+1} = v_{\nu+1} [(v_{opt})_{\nu}] . \quad (A21)$$

The time history of the optimum flight path and the optimum flight parameters belonging to it may also be found by interpolations in the corresponding tables.

$$\begin{aligned} T_{min}[(h_E)_{\nu}] &= T_{\nu}[(v_{opt})_{\nu}] \\ \vdots \\ n_{opt}[(h_E)_{\nu}] &= \{f_2[(v_{opt})_{\nu}]\}_{\nu} . \end{aligned} \quad (A22)$$

A3.3 End Conditions at the Final Point P_f

A3.3.1 Angle of Climb γ_f Prescribed

Prescribing γ_f there exists the additional possibility to prescribe the time derivative $(d\gamma/dt)_f$ at point $P_f = P_n$. If we do this (for example: $(d\gamma/dt)_f = 0$), the load factor n_f at point P_f is absolutely defined by the system of Equations (A2) to (A4). The tables of optimum functions described in Section A3.1 contain therefore only one value, namely that for the velocity v_f . The available velocity range $\{v_{\rho}\}$ in the optimization formula (A8) is therefore shrunk to a velocity point, so that all flight path elements which connect the points $P_{n-1}(v_{\mu})$ on the curve $(h_E)_{n-1} = \text{constant}$ with the final point P_f are optimum ones.

If we do not prescribe $(d\gamma/dt)_f$, we may assume that $(d\gamma/dt)_f$ or the load factor n_f or the angle of attack α_f at point P_f is always equal to that at the connecting point $P_{n-1}(v_{\mu})$ on the curve $(h_E)_{n-1} = \text{constant}$. These assumptions lead to some modifications in the computation scheme of Section A2.

The actual difference between these two assumptions may not be very important. In both cases the actual optimization process Equation (A8) begins only in the second step from curve $(h_E)_{n-2} = \text{constant}$ to curve $(h_E)_{n-1} = \text{constant}$.

A3.3.2 Angle of Climb γ_f Free

In this case there are many ways to fly from a definite point $P_{n-1}(v_{\mu})$ to the final point P_f which differ from each other only by the angle of climb γ_f . In the first optimization step we must find the minimum time $\Delta t_{\mu\rho}$ according to

$$T_{n-1}(v_{\mu}) = \min_{\{\gamma_{\rho}\}} [\Delta t(v_{\mu}, \gamma_{\rho})] . \quad (A23)$$

The table of optimum functions for the energy height level $(h_E)_{n-1}$ now contains the function $\gamma_n(v_{\mu})$ instead of $v_n(v_{\mu})$.

The two possibilities, to prescribe $(d\gamma/dt)_f$ at the final point P_f , do also exist here. Their influence on the optimization process is the same as in Section A3.3.1.

A3.4 Conditions at the Initial Point P_i

A3.4.1 Angle of Climb γ_i Prescribed

If we prescribe the angle of climb γ_i at the initial point $P_i = P_0$ our task is to find that point $P_1(v_1)$ on the curve $(h_E)_1 = \text{constant}$ which gives a connecting flight path element that satisfies the approximated equations of motion. Since the altitude $h_1(v_1)$ and the angle of climb $\gamma_1(v_1)$ on $(h_E)_1 = \text{constant}$ are both dependent on v_1 , we must satisfy the two conditions

$$h_1(v_1) - h_i = \left[\left[\frac{dh}{dh_E}(v_1) \right]_1 + \left(\frac{dh}{dh_E} \right)_i \right] \frac{\Delta h_E}{2} \quad (A24)$$

and

$$\gamma_1(v_1) - \gamma_i = \left[\left[\frac{d\gamma}{dh_E}(v_1) \right]_1 + \left(\frac{d\gamma}{dh_E} \right)_i \right] \frac{\Delta h_E}{2} . \quad (A25)$$

Introducing Equations (A4) and (A5) we get

$$h_1(v_1) - h_i = \left[\frac{\sin \gamma_1(v_1)}{[f_1(v_1)]_1} + \frac{\sin \gamma_i}{[f_1(\alpha_i)]_i} \right] \frac{\Delta h_E}{2} \quad (A24a)$$

and

$$\gamma_i(v_i) - \gamma_i = \left\{ \frac{n_i(v_i) - \cos \gamma_i(v_i)}{|f_i(v_i)|_i \left(\frac{v_i^2}{g}\right)} + \frac{n_i(\alpha_i) - \cos \gamma_i}{|f_i(\alpha_i)|_i \left(\frac{v_i^2}{g}\right)} \right\} \frac{\Delta h_E}{2}, \quad (A25a)$$

which is a system of two equations with the two unknowns v_i and α_i which must be solved iteratively. The flight path element described by this system of equations is the only one which connects the point P_i with the energy height level $(h_E)_1$. It is therefore the optimum one. Further, Equation (A25a) shows that the load factor n_i is not allowed to be prescribed. Once $(v_1)_{opt}$ is found, $(v_\nu)_{opt}$ ($\nu = 2, 3 \dots n$) may be found by interpolations according to Equation (A21).

A3.4.2 Angle of Climb γ_i Free

If the angle of climb γ_i is not prescribed, we may prescribe the initial load factor n_i or not. If we do the first, the angle of attack α_i is defined by Equation (A3). The system of Equations (A24a) and (A25a) may then be combined to one equation with the only unknown v_i . The solution of this equation gives the optimum velocity for the energy height level $(h_E)_1$.

However, if we do not prescribe the load factor n_i , we must seek the optimum one by applying the optimization formula

$$T_i = T_0 = \min_{\{n_i\}} \{ \Delta t(n_i) + T_1[v_i(n_i)] \}, \quad (A26)$$

where $v_i(n_i)$ must be calculated as above.

A4. SOME REMARKS ABOUT NUMERICAL PROBLEMS

In the optimization procedure described above there are three numerical tasks which must be done with great care, namely

- to find zeros by iterations
- to interpolate tabulated functions
- to find the minimum or maximum of non-analytical functions.

The latter represents the main problem of the optimization procedure. It may be done successfully only if the first two tasks are carried out without producing jumps and waves in the progress of the function to be minimized. Therefore, all iterations should be done with a fixed number of iteration steps to avoid small jumps due to truncation errors. The number of iteration steps itself should only be as high as it is necessary to guarantee a sufficient accuracy to avoid high rounding errors. Further, the interpolation method should have some smoothing character.

A5. SOME REMARKS ABOUT THE APPLICABILITY OF THE METHOD

The optimization procedure described above allows us also to calculate the optimum climbing flight path with respect to minimum fuel if the time in the optimization formulae (A8), (A23) and (A26) is replaced by the fuel consumption.

Further, it should be mentioned that the tables of the optimum functions represent the whole field of optimum climbing flight paths which satisfy the one prescribed final flight condition. Once these tables are known, we are able to find very rapidly the optimum flight path for another initial flight condition.

Furthermore, the method is also applicable in the field of calculating the optimum transition flight paths of V/STOL aircraft which have mostly more than one control variable (above we have introduced for simplicity only one control variable, namely the angle of attack α) if we introduce an auxiliary control variable, for example the load factor n , and determine the dependence of the optimum control variables (with respect to minimum time per unit energy height increase) on the auxiliary control variable before applying the above optimization procedure. This may be done either analytically or numerically. However, the programming of such a procedure must be made very carefully because these optimum control functions may be unsteady.

APPENDIX REFERENCES

- A1. Bellman, Richard E. Dynamic programming. Princeton University Press; 1957.
- A2. Bellman, Richard E. Applied dynamic programming. Princeton University Press; 1962.
Dreyfus, Stuart E.

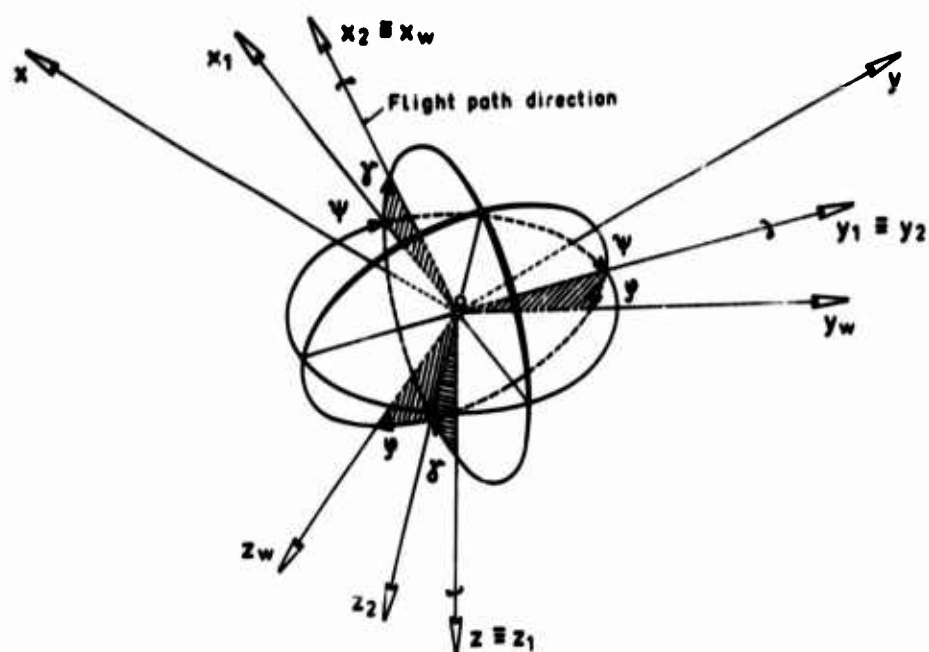


Fig.1 Definition of the coordinate systems

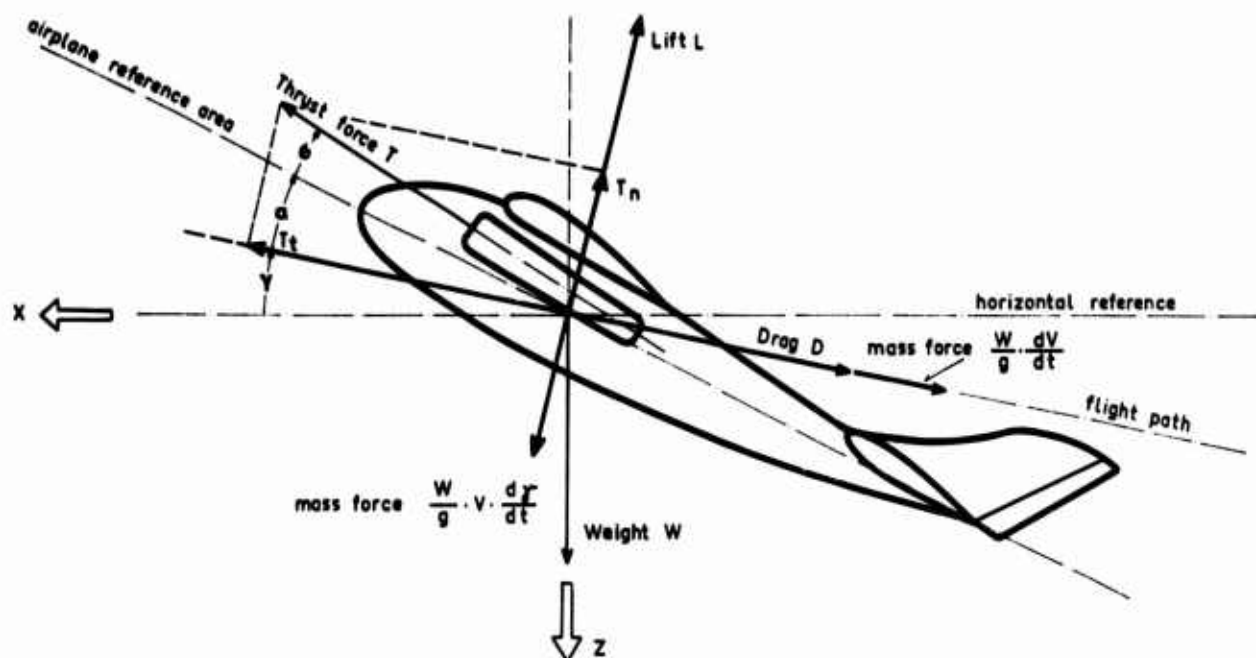


Fig.2 Definition of forces for flight in a vertical plane

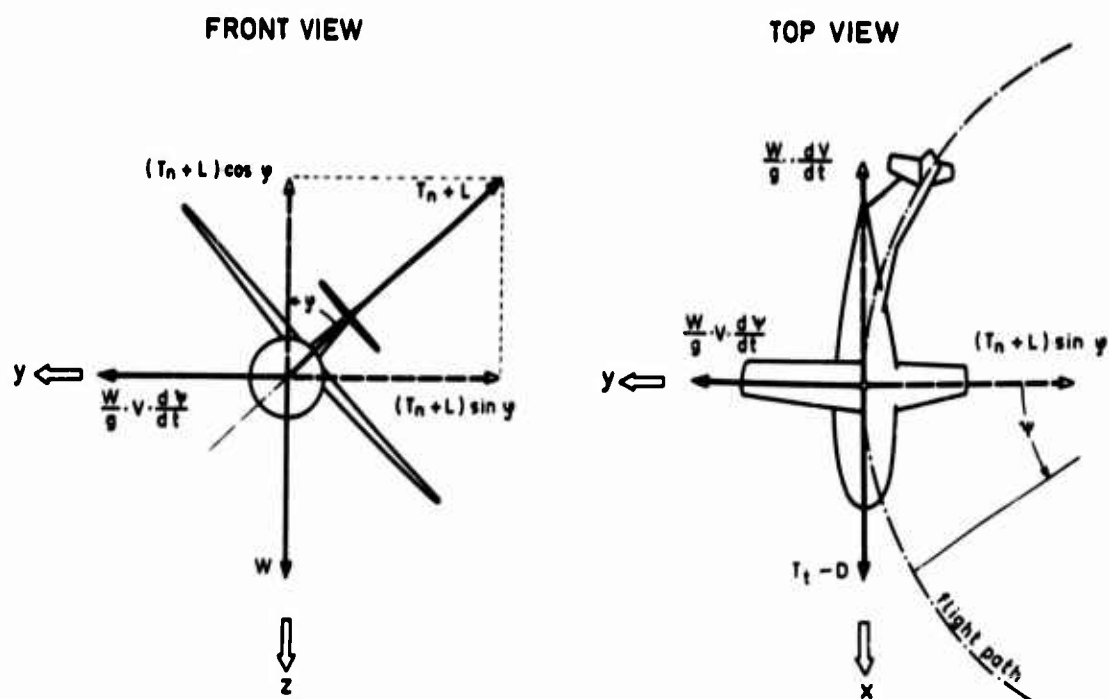
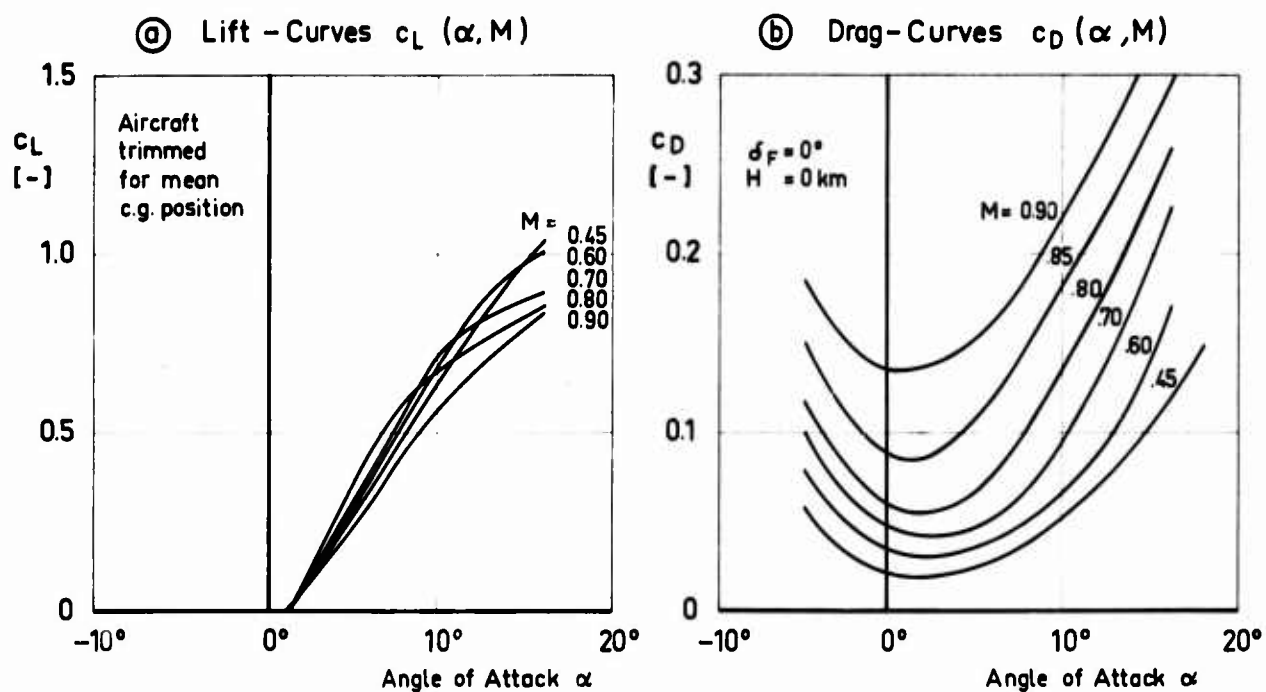


Fig.3 Definition of forces for flight in a horizontal plane

Fig.4 Typical influence of angle of attack α and Mach number M on lift coefficient c_L and drag coefficient c_D .

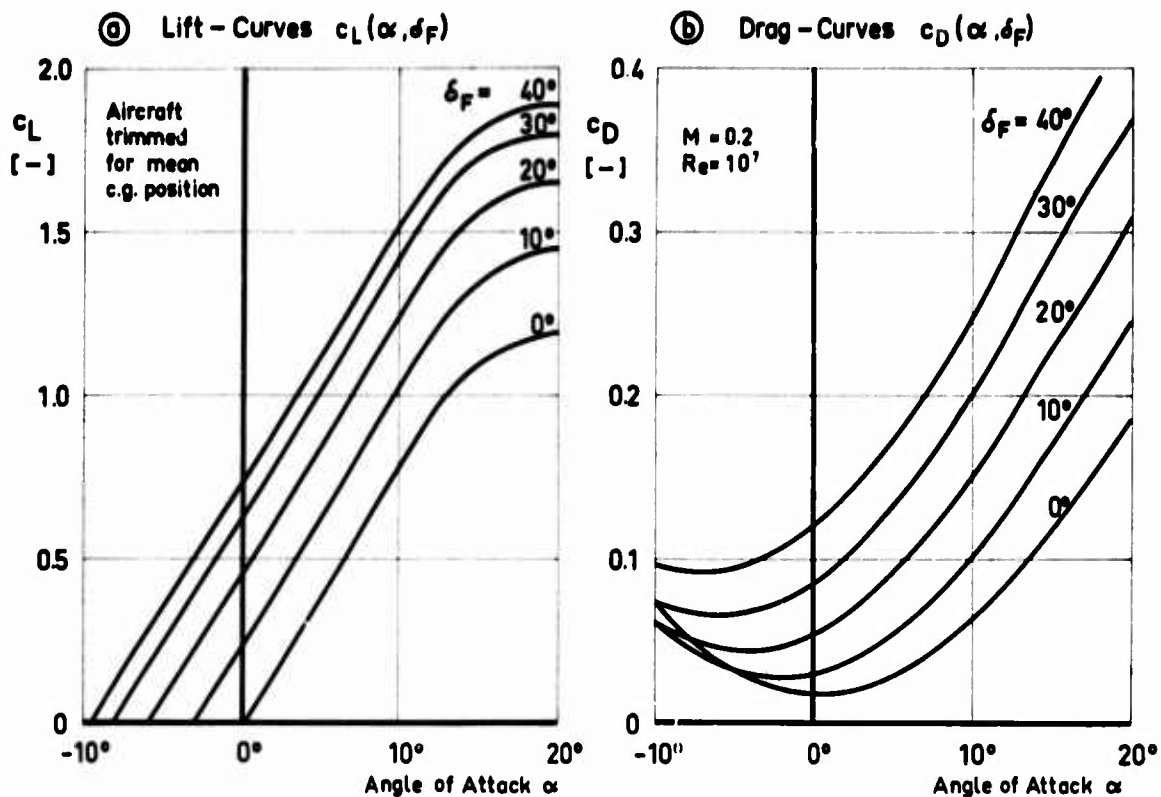


Fig.5 Typical influence of angle of attack α and flap setting δ_F on lift coefficient c_L and drag coefficient c_D

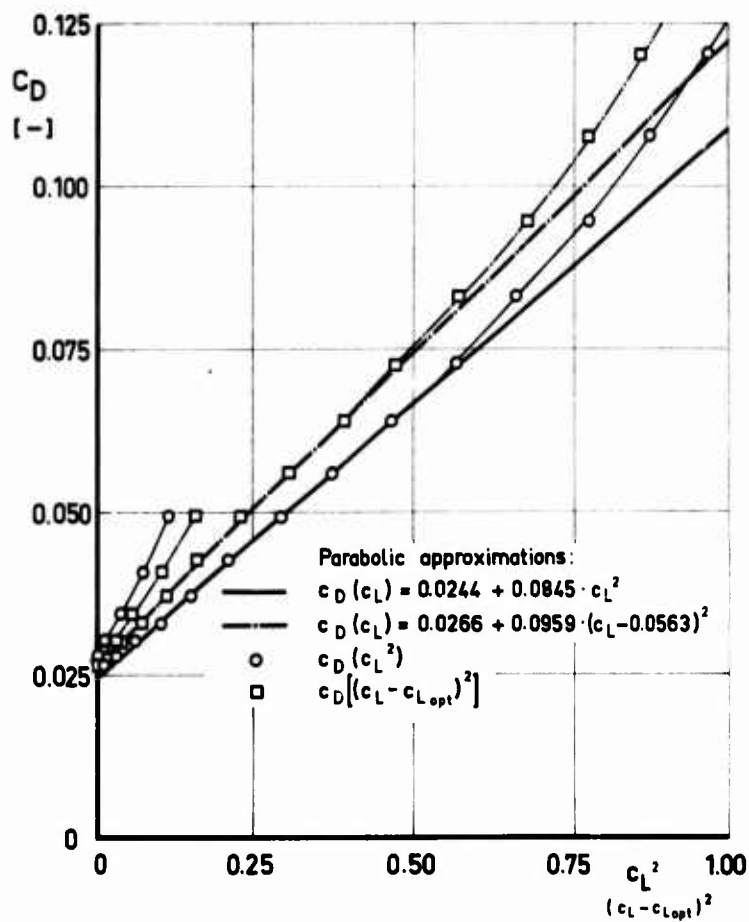


Fig.6 Typical approximation of a subcritical drag polar by parabolas according to equations (2.27a) and (2.27b)

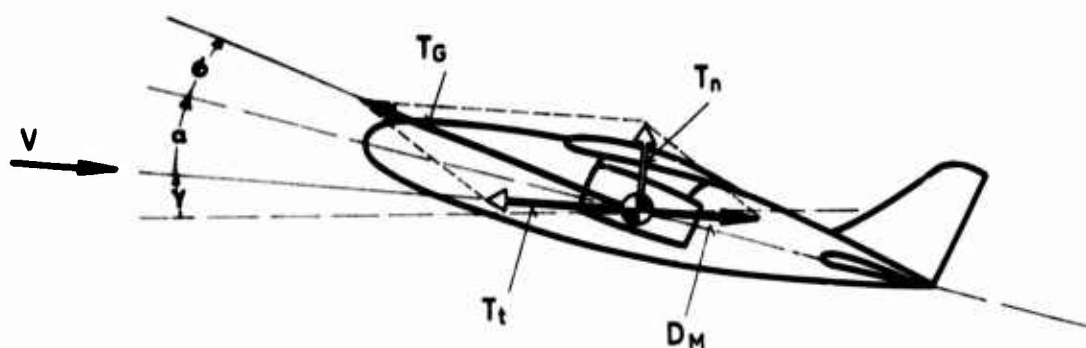


Fig.7 Definitions of the thrust components

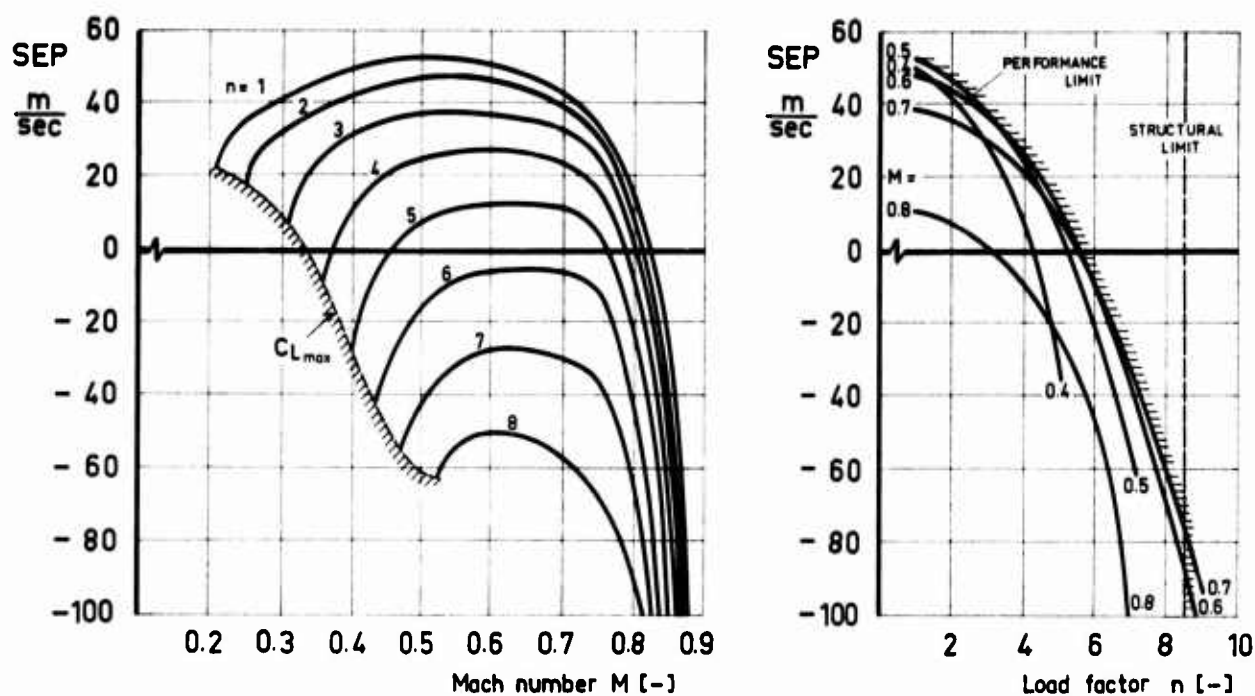
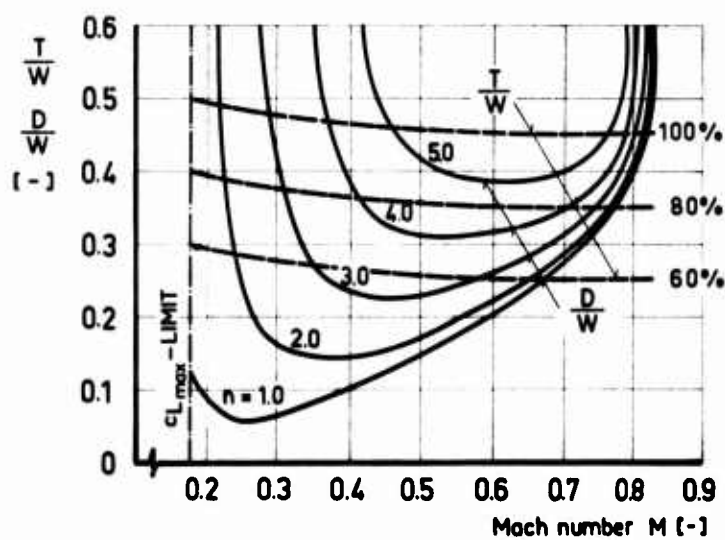
Fig.8 Influence of load factor n and Mach number M on available specific excess power SEP.

Fig.9 Pénaud diagram. The difference between thrust-to-weight curve and drag-to-weight curve represents the available specific excess acceleration SEA.

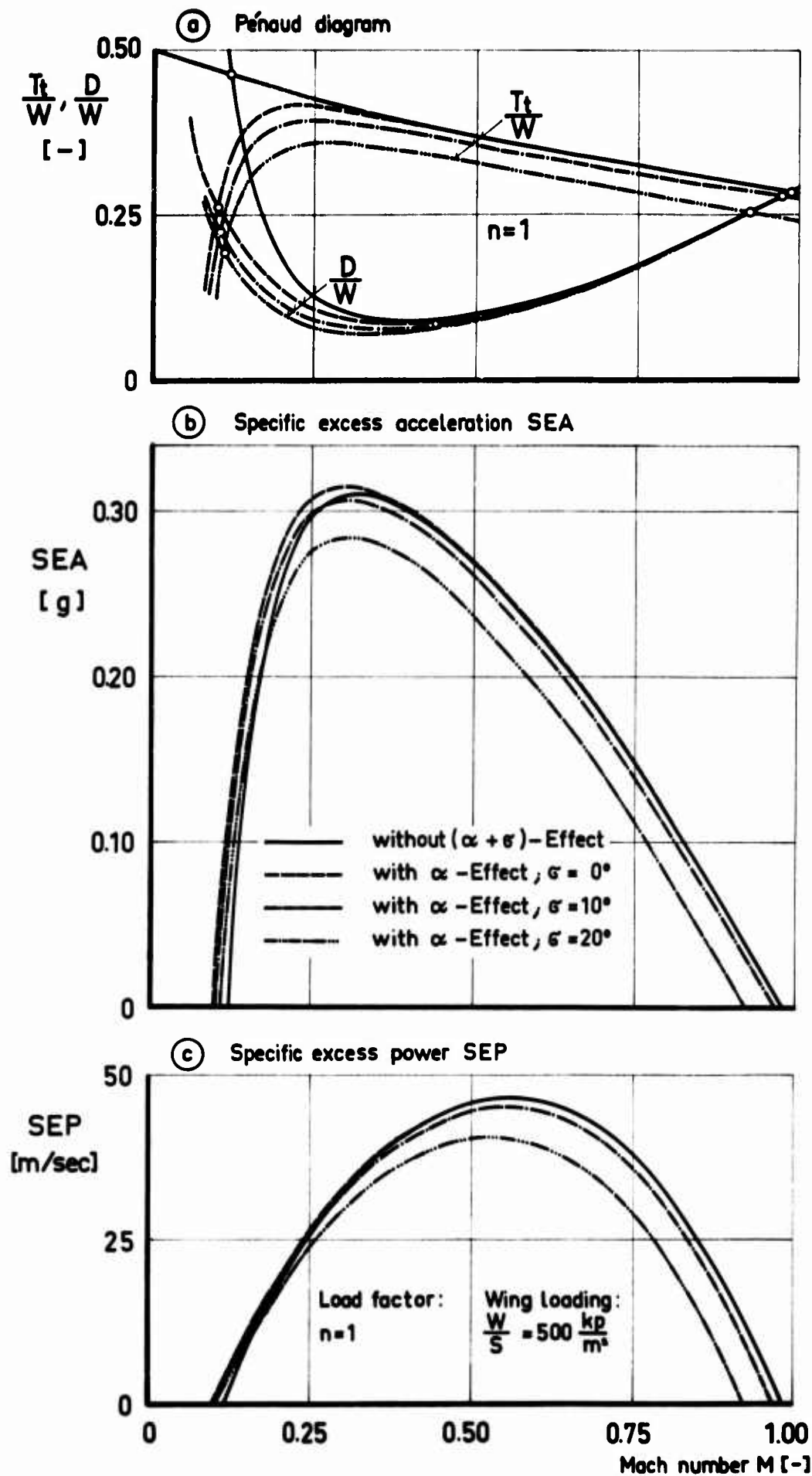


Fig.10 Influence of angle of attack and thrust inclination σ on specific excess acceleration SEA and specific excess power SEP.

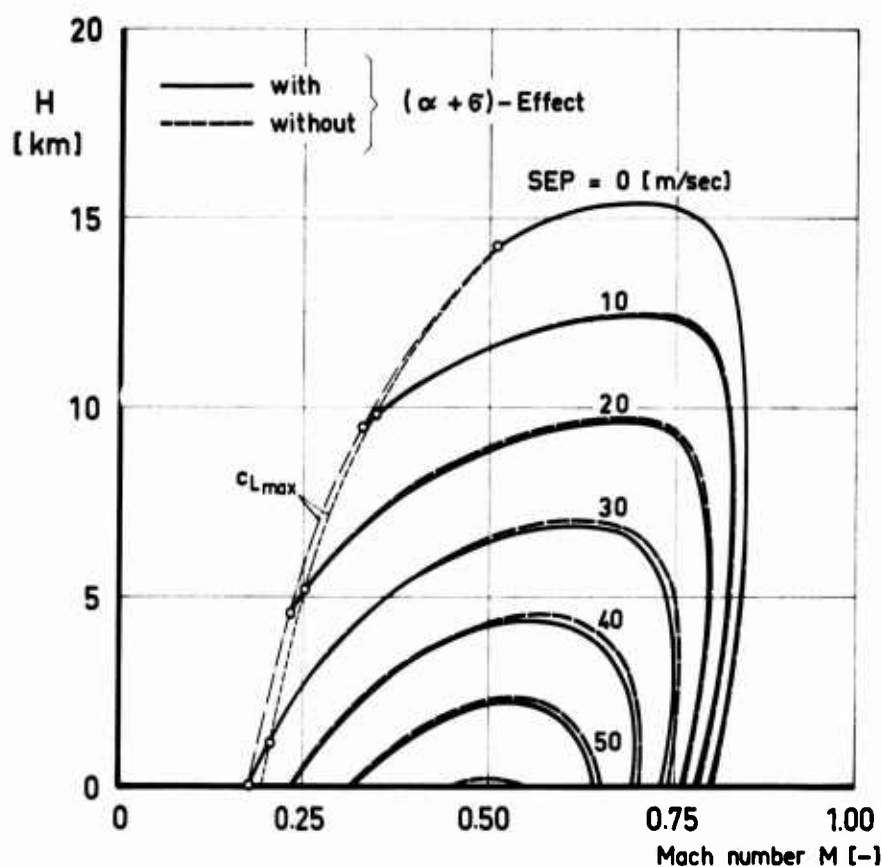


Fig.11 Influence of thrust inclination $(\alpha + \delta)$ on the curves of constant SEP in the height-velocity diagram for a typical subsonic aircraft ($\delta = 5^\circ$)

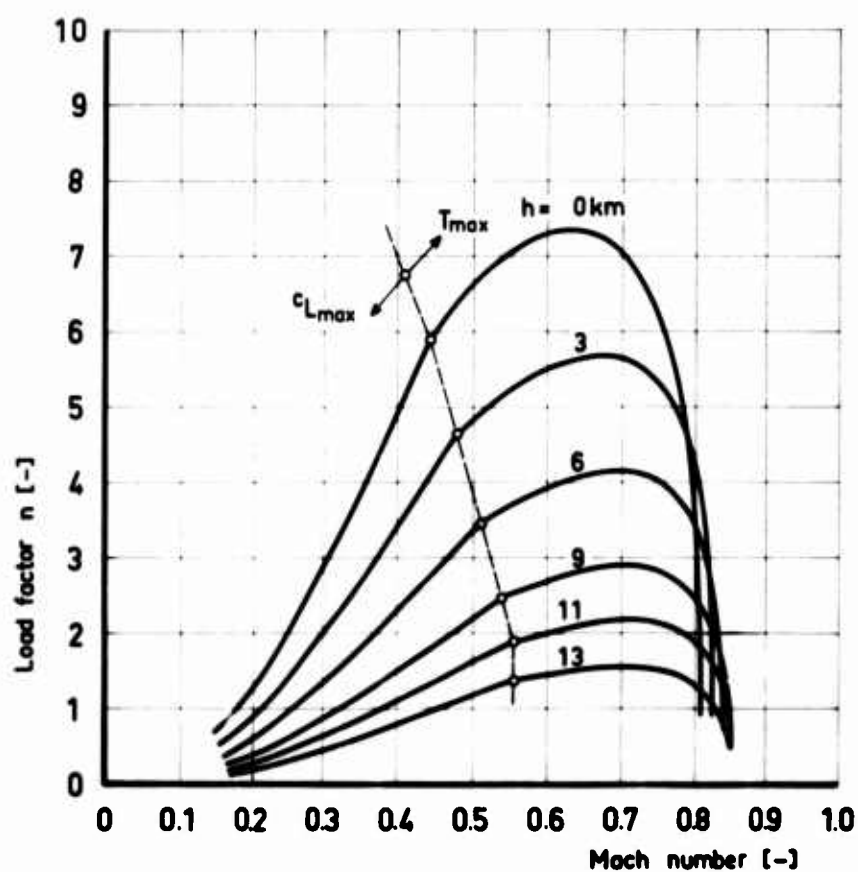


Fig.12 Influence of altitude h and Mach number M on the available steady load factor n for a typical subsonic aircraft

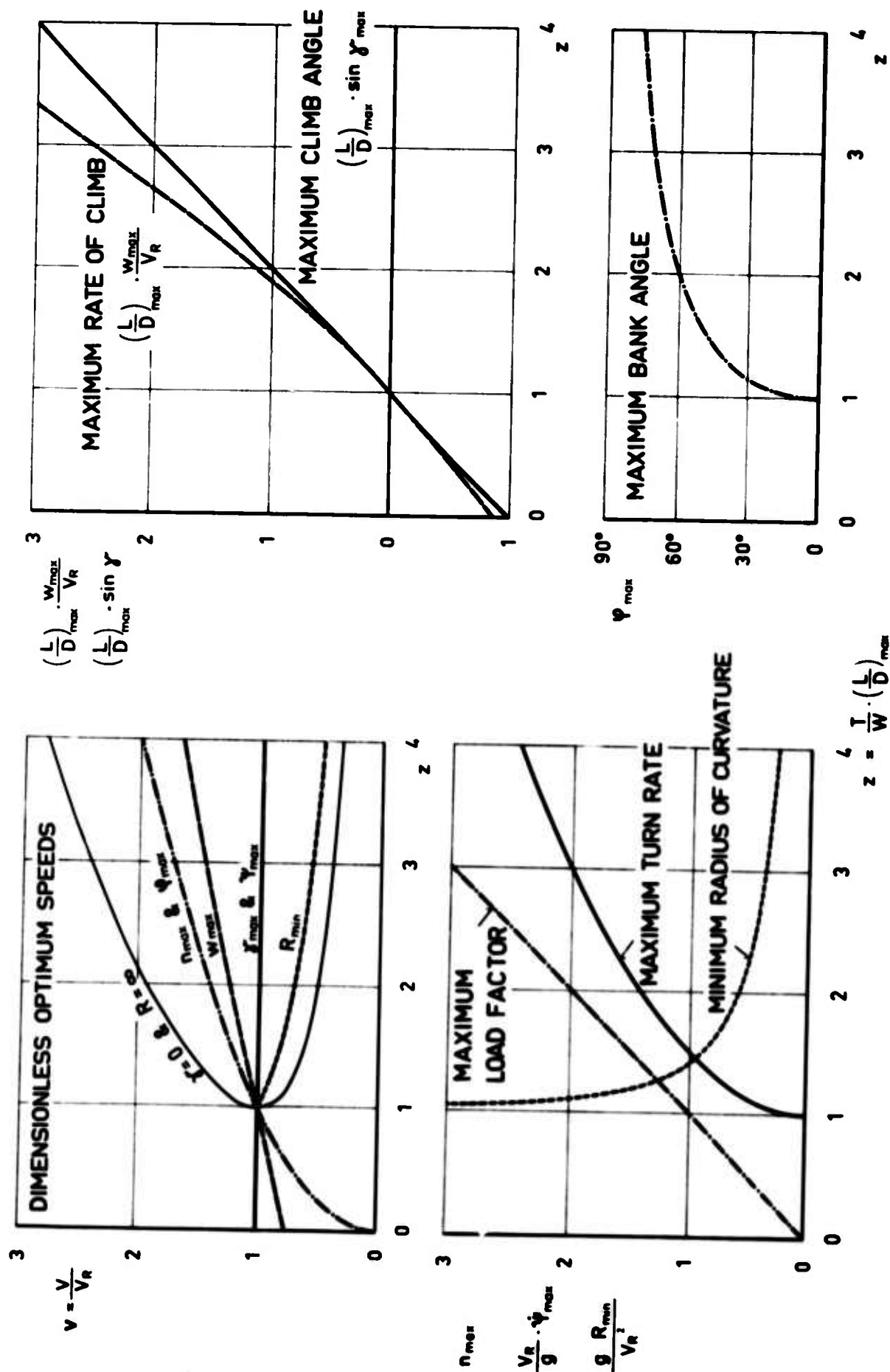


Fig. 13 Dimensionless optimum climb and manoeuvre performance for aircraft with constant thrust and parabolic polar

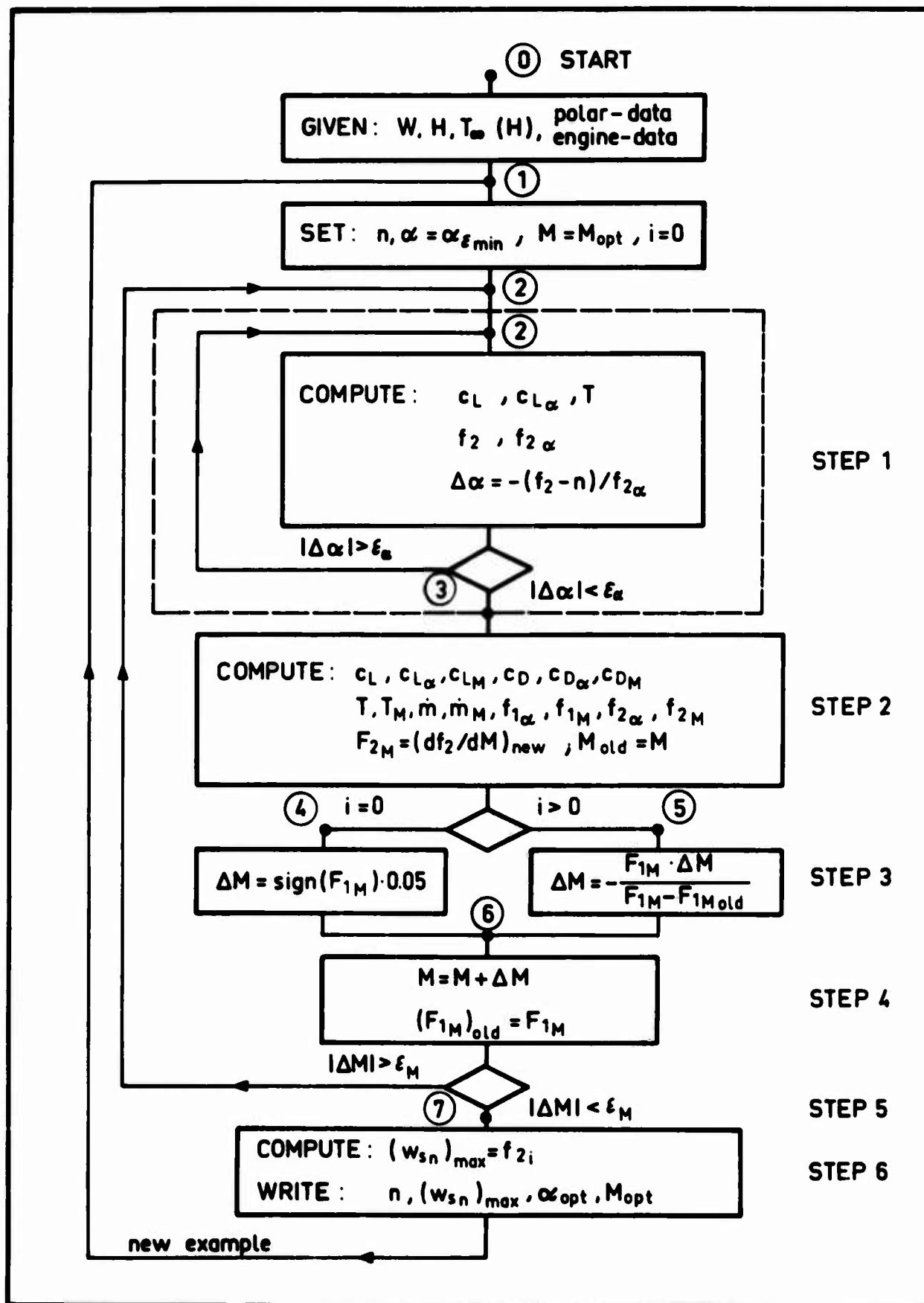


Fig.14 Flow diagram of the iteration process for finding the maximum specific excess acceleration SEA for a given load factor n

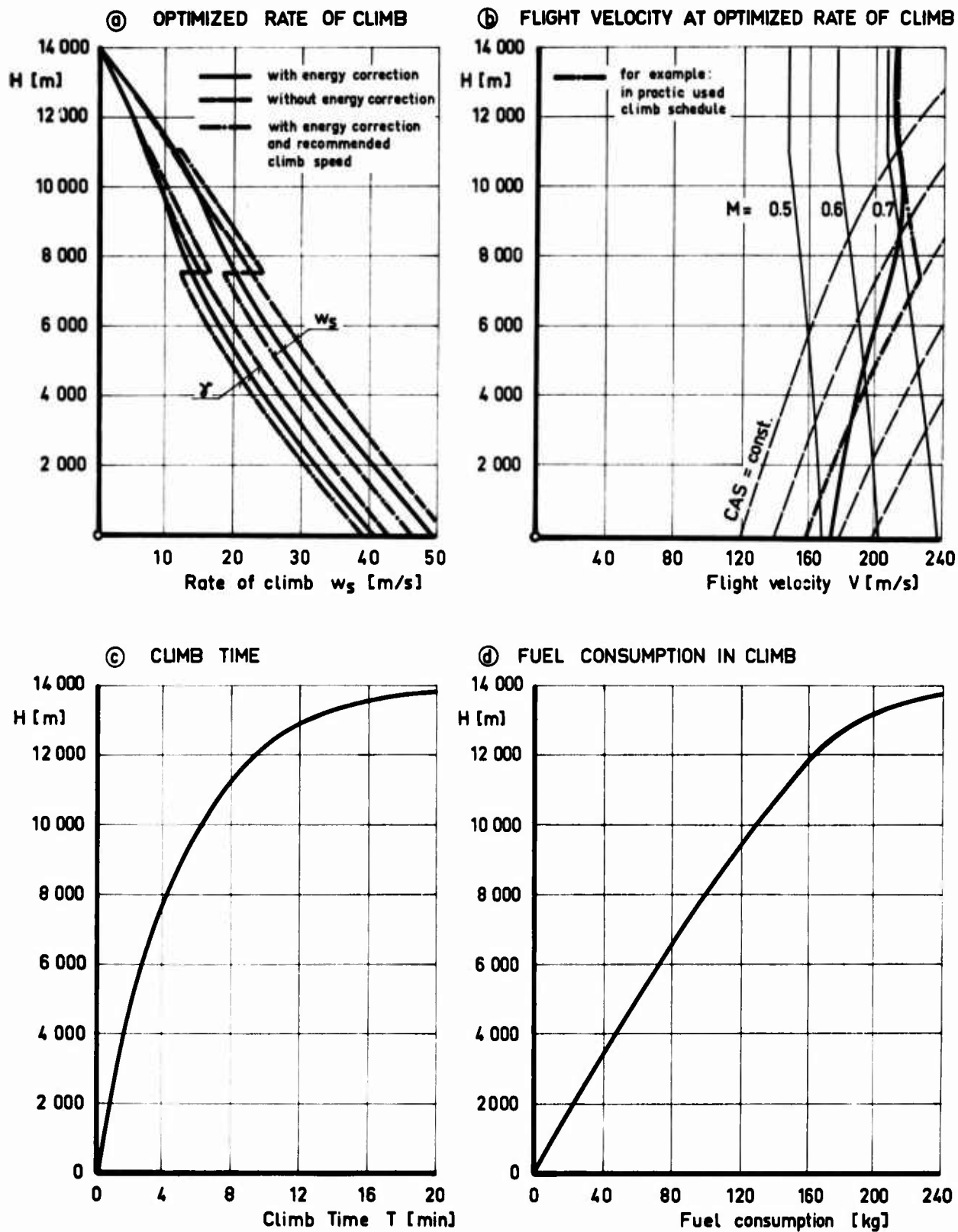


Fig.15 Typical result of the calculation of climbing flight with maximum rate of climb

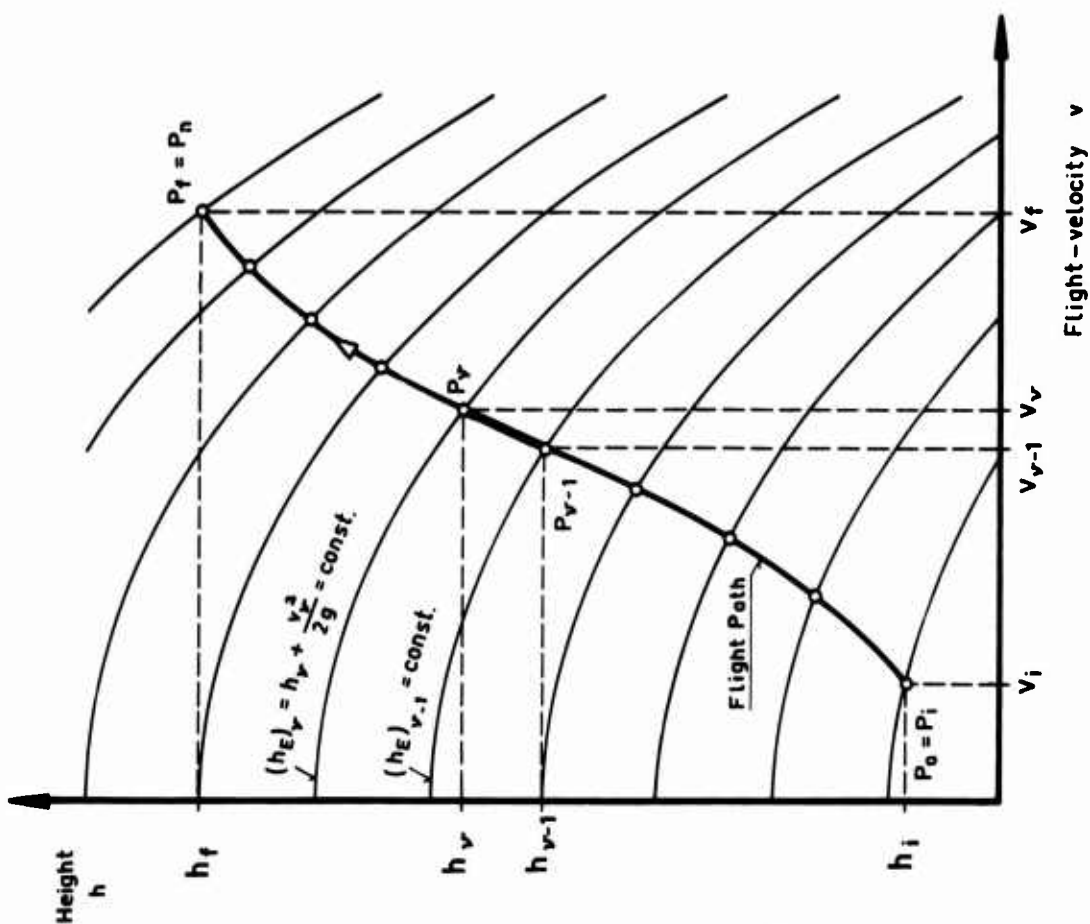


Fig.A-1 Height-velocity diagram. Subdividing the climbing flight path into n flight path elements

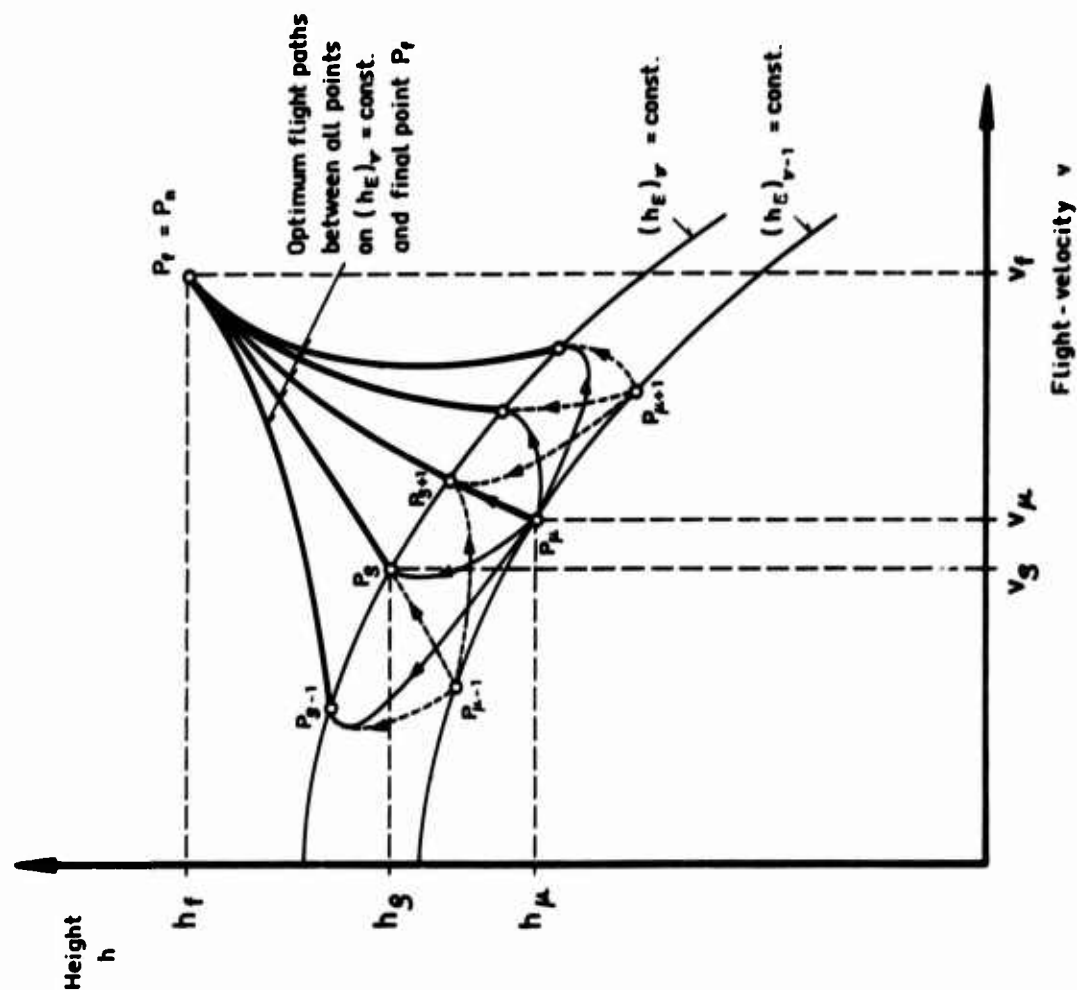


Fig.A-2 Definition of the possible flight path elements between the curves $(h_E)_{v-1} = \text{constant}$ and $(h_E)_v = \text{constant}$

**L'ESTIMATION DES COEFFICIENTS AERODYNAMIQUES NECESSAIRES
AU CALCUL DES PERFORMANCES**

(The Estimation of Aerodynamic Coefficients Necessary for Performance Calculations)

par

C.Lievens

**Ingénieur Principal de l'Armement
Section Etudes Générales, Service Technique Aéronautique
Paris, France**

CONTENTS

	Page
GENERALITES	4-1
<u>SECTION I – L'EFFET D'ECHELLE</u>	
INTRODUCTION	4-3
1. LA COUCHE LIMITE PRES DU BORD D'ATTAQUE	4-3
1.1 La transition de la couche limite	4-3
1.2 Les phénomènes de décrochage	4-4
2. L'INTERACTION ONDE DE CHOC COUCHE LIMITE	4-5
3. DECOLLEMENTS DUS AUX GRADIENTS DE PRESSION	4-6
4. L'INTERACTION AVEC L'ECOULEMENT EXTERNE	4-7
FIGURES	4-9
<u>SECTION II – FIGURATION DES FUSEAUX REACTEURS</u>	
1. INTRODUCTION	4-16
2. TRANSPOSITION SOUFFLERIE VOL.	4-18
3. REALISATION PRATIQUE	4-19
4. MESURE SUR MAQUETTE DE TUYERE ISOLEE	4-20
FIGURES	4-22
<u>SECTION III – L'UTILISATION DES CALCULS</u>	
1. INTRODUCTION	4-23
2. ECOULEMENTS NON VISQUEUX	4-23
3. ECOULEMENT VISQUEUX	4-24
4. PERSPECTIVES	4-25
FIGURES	4-26

L'ESTIMATION DES COEFFICIENTS AERODYNAMIQUES NECESSAIRES AU CALCUL DES PERFORMANCES

C. Lievens

GENERALITES

Le domaine que concerne le présent document est si vaste qu'il serait vain de le traiter d'une manière complète. Nous nous limiterons volontairement à quelques points qui, eu égard aux questions les plus fréquemment discutées, paraissent revêtir aujourd'hui une importance particulière.

Il convient d'abord de remarquer le rôle que peuvent jouer les contraintes diverses pesant sur un programme. Dans le cas d'un appareil de transport supersonique destiné par exemple au trajet Paris-New York, une erreur relative de 1% sur la traînée de frottement risque de compromettre le succès du projet. Dans de nombreuses autres circonstances, heureusement, une incertitude de cet ordre, dommageable certes sur le plan économique ou technique, pouvait être compensée par d'autres éléments et n'aboutissait pas, jusqu'à maintenant, à une condamnation systématique du programme. L'industriel doit donc, dès les premières phases de l'avant-projet, recenser l'ensemble des contraintes et juger de leur niveau de sévérité. La répartition des efforts entre les diverses tâches nécessaires au développement tiendra le plus grand compte de ce jugement.

Toutefois, la sévérité croissante de la concurrence internationale dans le domaine civil, l'importance attachée à certaines missions dans le domaine militaire (notamment dans un contexte de dissuasion) donnent à l'aspect performances un poids sans cesse croissant. Les exigences de précision dans l'évaluation des coefficients aérodynamiques en sont rendues plus sévères. Le problème à mesure qu'il prend de l'importance est aussi rendu plus difficile

- par l'accroissement de la taille des appareils et l'entrée dans de nouveaux domaines de vol,
- par l'adoption de nouveaux concepts aérodynamiques (profils supercritiques, hypersustentations très sophistiquées, . . .)

Les données aérodynamiques du planeur utilisées dans le calcul des performances peuvent en général se diviser en sept parties principales:

- (a) Données de référence: elles sont issues du calcul et des résultats d'essais en soufflerie et sont relatives à la configuration suivante:—
 - la traînée de frottement-soufflerie (toujours calculée) a été déduite;
 - les entrées d'air fonctionnent à un débit de référence bien déterminé;
 - l'état de surface est celui de la maquette;
 - les gouvernes sont braquées à 0°;
 - le train d'atterrissage est rentré;
 - les aérofreins sont rentrés;
 - l'appareil est hors effet de sol.
- (b) Trainée de frottement: elle est calculée (par exemple par la loi de Michel) suivant différentes conditions de vol et pour l'état de surface équivalent à celui de la maquette.
- (c) Influence du coefficient de débit: elle est calculée ou déduite des essais en soufflerie et s'évalue par rapport au coefficient de débit de référence déjà évoqué.
- (d) Influence du braquage des gouvernes: elle correspond au passage de la situation "braquage nul des gouvernes" à la situation "moment de tangage nul".
- (e) Trainée parasite externe, incluant le supplément de traînée de frottement et de forme dues aux différentes aspérités, cavités, etc., qu'il est impossible (ou inusuel) de représenter sur la maquette. Cette traînée parasite est toujours calculée par une méthode assez globale.

- (f) Influence de la sortie du train d'atterrissage, déduite le plus souvent des essais en soufflerie.
- (g) Influence de l'effet de sol par rapport à la position hors effet de sol, déduite le plus souvent des essais en soufflerie.

Il est certain que, pour les programmes en cours de développement, le rôle des essais en soufflerie est très largement prépondérant. Seule aujourd'hui la traînée de frottement fait l'objet d'une investigation presque systématique par le calcul. En soufflerie, les efforts sont en général mesurés à l'aide d'une balance interne classique, à six composantes; les caractéristiques du jet naturel traversant les fuseaux peuvent être déterminées.

- soit par un sondage de pressions totales et statiques à la sortie des fuseaux grâce à un peigne rotatif;
- soit par la technique du col sonique avec mesure de pression statique interne dans la chambre de tranquillisation;
- soit par la technique du col sonique avec mesure de débit par un débitmètre.

Enfin, nous constaterons plus loin qu'il est nécessaire, dans tous les cas difficiles, d'effectuer en plus une analyse fine de l'écoulement, afin de caractériser les phénomènes aérodynamiques réels.

Le passage des grandeurs mesurées en soufflerie aux données aérodynamiques comporte les étapes suivantes:—

- corrections dues aux montages en soufflerie,
- lissage des résultats corrigés de plusieurs essais relatifs à la même configuration,
- élimination de la traînée de frottement soufflerie (par exemple suivant la loi de Michel),
- élimination de la traînée de captation des fuseaux,
- élimination de la poussée brute du jet interne des fuseaux (et de l'effort de culot s'il y a lieu),
- correction, si on est en supersonique et s'il y a lieu, relative à la hauteur de couche limite captée par le déviateur.

Mais quelle crédibilité peut-on accorder aux essais en soufflerie, même en admettant que les diverses corrections relatives aux montages et aux souffleries aient été correctement évaluées? Autrement dit, quelles sont les conséquences de l'effet d'échelle lié aux différences de taille entre la maquette et l'avion? Ce problème fera l'objet de la première partie de l'exposé.

Il ne suffit pas de connaître les données aérodynamiques du planeur sans l'installation des fuseaux; il faut encore introduire l'ensemble des données relatives aux entrées d'air et aux tuyères. Si on utilise pour cela les essais en soufflerie, il se pose le problème de la figuration des fuseaux réacteurs qui fera l'objet de la seconde partie de l'exposé.

Enfin, l'industrie commence à utiliser des moyens de calcul extrêmement puissants pour évaluer les coefficients aérodynamiques nécessaires au calcul des performances. Quelles sont les difficultés sur lesquelles buttent ces calculs? Que peut-on en attendre à court terme et à long terme? Telles seront les questions dont nous discuterons dans la troisième et dernière partie.

Section I

L'EFFET D'ECHELLE

INTRODUCTION

Le problème de l'effet d'échelle résulte de la divergence entre l'évolution de la couche limite sur maquette en soufflerie, et celle qui sera obtenue à l'échelle avion. Le nombre de Reynolds conditionne très largement le point de transition de la couche limite et ses caractéristiques à abscisse relative donnée.

- Il peut donc déterminer aux grandes incidences l'existence de bulbes de bord d'attaque et influencer plus ou moins largement la valeur maximale et l'évolution du coefficient de portance;
- Dans les écoulements avec choc, il y a interaction entre l'onde de choc et la couche limite, avec apparition de phénomènes qui dépendent de la structure initiale de la couche limite, donc du nombre de Reynolds;
- La structure de la couche limite conditionne l'apparition de décollements (qu'il s'agisse de décollements au pied du choc et plus généralement dans des zones de fort gradient de pression);
- Enfin, lorsqu'il y a des décollements, l'interaction entre la couche limite et l'écoulement externe (qui intègre tous les phénomènes qui viennent d'être mentionnés et dépend donc du nombre de Reynolds) peut être importante.

L'énoncé de ces divers phénomènes laisse pressentir que c'est dans le domaine transsonique – et également en incompressible aux grandes incidences – que l'effet d'échelle peut être critique.

Dans ces domaines, il est certain que l'effet d'échelle laisse planer un doute sur la validité des coefficients aérodynamiques nécessaires au calcul des performances. Cette incertitude s'avère parfois grave

- pour les appareils de transport croisant en subsonique élevé,
- pour les appareils supersoniques où les performances en transsonique ont une importance notable,
- pour les formules très hypersustentées.

On voit qu'il n'y a guère de programme moderne où le problème de l'effet d'échelle ne se pose; mais à notre sens l'extrapolation au vol des résultats en soufflerie doit se faire à partir d'une interprétation très physique des phénomènes qui se produisent aux échelles correspondantes. C'est pourquoi nous envisagerons successivement:

- la couche limite près du bord d'attaque,
- l'interaction onde de choc-couche limite,
- le décollement au bord de fuite,
- l'interaction couche limite-écoulement externe.

1. LA COUCHE LIMITE PRES DU BORD D'ATTAQUE

1.1 La transition de la couche limite

Sur une aile en flèche par exemple, la couche limite demeure laminaire tant que le nombre de Reynolds, $R_\theta \equiv V\theta/\nu$, basé sur l'épaisseur de quantité de mouvement θ , demeure inférieur à une valeur qui se situe aux environs de 100. En pratique, cela signifie que, même à l'échelle avion, lorsque les gradients de pression le permettent on peut trouver des cas où la couche limite demeure laminaire sur une longueur non négligeable à proximité du bord d'attaque. Avec les approximations usuellement retenues, on peut considérer que la couche limite laminaire a une structure indépendante du nombre de Reynolds. Dans ce cas donc, le point de décollement du bulbe éventuel est correctement représenté par la soufflerie.

Mais le point de transition de la couche limite (que ce soit ou non après un bulbe de décollement) dépend du nombre de Reynolds; il se situe, à l'échelle avion, très près du bord d'attaque, mais peut avoir en soufflerie une position extrêmement variable en fonction du nombre de Reynolds. Encore convient-il de rappeler qu'il n'y a pas de passage brutal de la structure laminaire à la structure turbulente, mais qu'il existe une couche limite transitionnelle, dont les propriétés, encore mal connues, dépendent aussi du nombre de Reynolds. L'influence de cet état intermédiaire n'est pas toujours négligeable, surtout dans des souffleries de dimension relativement modeste.

Enfin, lorsque la couche limite est pleinement turbulente, l'influence du nombre de Reynolds peut être considérée comme modeste tant que n'interviennent pas des phénomènes de décollement. Ce qui explique la validité de la méthode classique de déclenchement de transition en soufflerie pour la plupart des essais habituels. Il est néanmoins impossible de reproduire par les procédés utilisés jusqu'à maintenant une structure valable de la couche limite au

moment du déclenchement. Le déclenchement de la transition ne permet donc pas une étude pleinement satisfaisante des phénomènes avec décollements qui seront évoqués plus loin.

1.2 Les phénomènes de décrochage

Les divers types de décrochages sur un profil peuvent être classés en fonction de la manière dont se produisent les décollements sur la partie supérieure du profil. Trois classes sont à envisager, correspondant à trois formes particulières des courbes coefficient de portance-incidence (voir Figure I-1).

- (a) Certains profils épais conduisent à des distributions de pression relativement arrondies avec un maximum assez prononcé à 10% de la corde, puis des gradients de pression relativement modérés. A partir d'une certaine incidence, la couche limite turbulente décolle au voisinage du bord de fuite; au fur et à mesure que l'incidence croît, le coefficient de portance augmente, les gradients de pression s'accroissent, le point de décollement se déplace vers l'avant, la courbe $C_z(\alpha)$ a l'allure la plus classique. Supposons qu'à incidence constante le nombre de Reynolds s'accroisse; l'état de dégénérescence de la couche limite turbulente est réduit, le décollement est reculé, le coefficient de portance maximum est accru, et la courbe $C_z(\alpha)$ garde relativement la même allure.
- (b) Pour des profils minces, la couche limite laminaire est susceptible de décoller avant la transition; cette dernière se produit dans la zone décollée et la couche limite recolte en turbulent pour former un bulbe long (d'environ 2 à 3% de la corde) qui apparaît dès les faibles incidences. Lorsque l'incidence croît, le bulbe se développe vers l'arrière jusqu'au delà du bord de fuite; au cours de cette évolution $C_{2\alpha}$ décroît constamment et la courbe $C_z(\alpha)$ est assez plate autour du maximum.
- (c) Pour des profils modérément épais, le décollement laminaire peut encore intervenir, mais la couche limite recolte sur une très courte distance (inférieure à 1% de la corde) formant ainsi un bulbe court. Lorsque l'incidence s'accroît, la pression diminue dans le bulbe, la courbure augmente, le bulbe se raccourcit; et il éclate pour une certaine valeur du coefficient de portance. La couche limite turbulente ne recolte plus, si bien que la courbe $C_z(\alpha)$ a un maximum très pointu.

Il convient de noter que certains profils d'épaisseur moyenne peuvent changer leurs caractéristiques de décrochage en fonction du nombre de Reynolds et passer — lorsque celui-ci s'accroît — d'un décrochage de bord d'attaque (avec bulbe court) à un décrochage de bord de fuite (avec décollement turbulent). De plus, sur certaines gammes de nombre de Reynolds, les caractéristiques de ces deux types de décrochage (décollement laminaire avec bulbe court au bord d'attaque, et décollement turbulent qui remonte du bord de fuite et dont le déplacement est accéléré par l'épaississement de la couche limite turbulente à cause de l'existence du bulbe court). En conclusion, on peut dire que la valeur maximum et l'évolution du coefficient de portance en bidimensionnel dépendent du nombre de Reynolds, mais qu'il n'existe aucune loi universelle et que la tendance globale ne peut être pressentie que par une analyse assez fine des phénomènes.

Dans le cas d'un profil avec volet, le développement de la couche limite est représenté sur la Figure I-2. Il apparaît ici un bulbe de décollement sur la partie inférieure de l'aile à proximité de son bord de fuite et dont la longueur dépend de la forme de l'intrados volet sorti. Ce bulbe ne disparaît pas, malgré tous les moyens utilisés pour éliminer les discontinuités de pente. Mais sa présence n'a pas, en général, une influence considérable sur le mécanisme du décrochage. Il y a de plus interaction et mélange entre le sillage de l'aile et la couche limite de la partie supérieure du volet. D'après certains expérimentateurs, l'optimum des performances correspondrait à une interaction très faible et une absence de mélange entre sillage et couche limite. Dans ce cas, le développement de la couche limite sur le volet, donc le décollement, varie relativement peu avec l'incidence; par conséquent, le décrochage résulte d'un éclatement de l'écoulement sur la partie supérieure de l'aile et on en revient au mécanisme déjà décrit à propos d'un simple profil; toutefois, la présence du volet tend à augmenter les gradients de pression après le pic: le décrochage de bord d'attaque semble devenir relativement plus probable que celui de bord de fuite. Dans le cas d'un profil hypersustenté avec becs et volets, il apparaît encore un bulbe de décollement sur la surface inférieure de la voilure à proximité du bord de fuite et une interaction sillage de voilure — couche limite de volet. Mais ici plusieurs auteurs estiment que la configuration optimale implique qu'il y ait un mélange complet entre l'un et l'autre. La présence du bec induit une notable réduction du pic de pression (Figure I-3). En ce cas le décrochage peut résulter d'un éclatement de l'écoulement soit au bord d'attaque du bec, soit au bord d'attaque de l'aile, soit au bord de fuite de l'aile; mais il semble que la présence d'un sillage turbulent en aval du bec avance la transition de la couche limite de l'aile et réduit d'autant la probabilité d'avoir un décrochage de bord d'attaque de la voilure. Naturellement, l'occurrence du décrochage par bulbe au bord d'attaque du bec ou par décollement de la couche limite turbulente sur l'aile dépend du nombre de Reynolds.

Sur une aile en flèche d'allongement infini, les gradients de pression transversaux influenceraient les caractéristiques de la couche limite et susciteraient une diminution du coefficient de portance maximum par rapport au bidimensionnel. Néanmoins, le mécanisme fondamental du décrochage n'est pas modifié par l'existence d'une flèche. Considérons maintenant le cas d'une aile en flèche d'allongement fini; on constate que c'est à l'extrémité de la voilure que la portance locale est la plus élevée et que les gradients de pression en aval du pic sont les plus forts; il y aurait donc tendance au décollement en extrémité de voilure avec apparition d'un bulbe court. Néanmoins, aux nombres de Reynolds qui permettraient l'existence de ce bulbe court, le décollement au bord d'attaque

semble générer un tourbillon qui prend naissance à l'apex de l'aile et traverserait le bord de fuite à environ 70% de la demi-envergure, accroissant ainsi notablement la hauteur du pic vers l'intérieur de la voilure. D'où une différence notable:—

- d'une part entre le bidimensionnel et le tridimensionnel. (La tendance au bulbe court en bidimensionnel tendant à se transformer en un décollement turbulent en tridimensionnel);
- d'autre part entre la soufflerie et le vol.

Si nous nous référons, à titre purement indicatif à un avion de transport relativement récent, (Trident), nous constatons

- en vol, un décrochage qui commence aux environs de 40% d'envergure, positionné vers l'arrière;
- en soufflerie (compte tenu de la plus faible épaisseur relative de la couche limite aux environs du bord de fuite) un décrochage de bord d'attaque à 60% d'envergure qui progresse à la fois vers l'intérieur et l'extérieur.

On constate ainsi que les phénomènes liés au décrochage dépendent dans une très large mesure du nombre de Reynolds. Il sera souvent difficile d'extrapoler au vol les résultats obtenus en soufflerie; mais une telle transposition devra, en tout état de cause, tenir compte du mécanisme de décrochage en soufflerie et de ceux susceptibles d'intervenir en vol.

2. L'INTERACTION ONDE DE CHOC COUCHE LIMITE

Lorsqu'on accroît le nombre de Mach ou l'incidence d'un profil supercritique, le régime supersonique à l'extrados se développe et se termine par un choc normal d'intensité croissante. La Figure I-4 schématise l'interaction entre une couche limite turbulente et une onde de choc normal en tridimensionnel dans le cas où le choc n'est pas assez intense pour entraîner le décollement. Il conduit néanmoins à un épaississement de la couche limite, déforme son profil de vitesse, celui-ci ne reprenant une allure normale qu'à une dizaine d'épaisseurs de couche limite après le choc. Le résultat de cette interaction est un adoucissement de l'effet du choc, de telle sorte que le saut de pression sur le profil n'est pas brusque, mais qu'il s'étend sur une longueur de deux à trois épaisseurs de couche limite. L'écoulement extérieur est progressivement défléchi, d'où existence d'ondes de compression en avant du choc. Tant qu'il n'y a pas de décollement, il n'y a pas de variation notable de la position du choc, l'effet sur les coefficients aérodynamiques est quasi-négligeable. Cependant, le comportement ultérieur de la couche limite dépend de l'épaississement qu'elle a subi et présente une tendance plus marquée au décollement, d'où un effet important possible sur l'ensemble de l'écoulement. Sur les voilures en flèche, en l'absence de décollement, les phénomènes ne diffèrent pas notablement de ce qu'ils sont sur les profils. L'écoulement tridimensionnel a évidemment une structure plus complexe (Figure I-5); le saut de pression le plus important se produit à travers le choc extérieur et si alors la couche limite ne décolle pas en soufflerie à la suite de cette interaction, on peut penser qu'il n'y aura de décollement nulle part et que le résultat en soufflerie sera représentatif du vol.

A partir de certaines valeurs du nombre de Mach et de l'incidence, le saut de pression est assez fort pour faire décoller la couche limite. Depuis bien longtemps les auteurs ont remarqué qu'il existait une grande différence suivant le caractère laminaire ou turbulent (voire transitionnel) de la couche limite. L'effet sur une couche limite laminaire se propage beaucoup plus loin vers l'amont. D'où le risque qu'il existe un effet d'échelle considérable si la couche limite est laminaire sur la maquette (voir Figure I-5a), d'où l'habitude de déclencher la couche limite pour avoir une représentation plus correcte des phénomènes apparaissant sur l'avion. C'est pourquoi nous n'étudierons l'interaction avec décollement que d'une onde de choc avec une couche limite turbulente (Figure I-6). Le couplage est beaucoup plus marqué que lorsqu'il n'y a pas de décollement; l'existence même du bulbe correspondant aggrave l'effet de compression de l'écoulement extérieur. Il est difficile, faute de méthodes, et même de données satisfaisantes, de prévoir l'apparition du décollement. Citons néanmoins le critère d'Alber: tant que la vitesse du son peut être atteinte sans que l'écoulement tourne d'un angle supérieur à $6,6^\circ$, il n'y a pas de décollement; l'interaction forte apparaît à des nombres de Mach tels que la compression de Prandtl-Meyer de $6,6^\circ$ soit possible sans que l'écoulement devienne sonique; au delà, le décollement se produit suivant un angle de $6,6^\circ$.

L'une des rares études suffisamment fines d'un tel écoulement a été réalisée par Seddon à $M = 1,47$ sur une plaque plane. Il apparaissait un bulbe de décollement (Figure I-7) dont la longueur était de l'ordre de dix épaisseurs de couche limite. On remarquera aussi l'épaississement de la couche avant le décollement, les ondes de compression conduisant à un choc en λ . Mais les vitesses de l'écoulement diffèrent suivant que l'on est derrière la partie supérieure ou la partie inférieure du λ , d'où l'apparition d'une feuille de tourbillons à la jonction des deux écoulements. Il est surprenant de trouver derrière le choc une zone supersonique dont la recompression jusqu'au subsonique est isentropique. Le profil de vitesse de la couche limite est rendu anormal pendant cinquante épaisseurs de couche limite environ.

L'effet du nombre de Reynolds sur ce type d'interaction est assez mal connu. A partir de quel nombre de Reynolds, d'abord, apparaît un tel décollement? C'est un point sur lequel les opinions des différents auteurs divergent; certains pensent que l'influence n'est pas négligeable. Nous donnons ainsi Figure I-8 l'évolution

qualitative du saut de pression nécessaire pour qu'apparaisse le décollement, ceci en fonction du nombre de Reynolds R_θ basé sur l'épaisseur de couche limite. Il s'agit d'une hypothèse dont J.E.Green (RAE) pense qu'elle est valable aux environs de $M = 1,5$.

- Aux R_θ élevés, la couche limite est très turbulente; la résistance au décollement s'accroîtrait avec le nombre de Reynolds.
- A des R_θ un peu moins élevés (de l'ordre de 10^{-3} à 10^{-4}), l'évolution du profil de vitesse de la couche limite serait inversée et le décollement se produirait plus tôt lorsque le nombre de Reynolds s'accroîtrait.
- A des R_θ faibles, la couche limite est transitionnelle et la résistance au décollement semblerait s'accroître avec le nombre de Reynolds. (Ce cas peut se rencontrer en soufflerie et même en vol dans le cas de chocs proches du bord d'attaque.)

Faute d'une masse suffisante d'informations on ne peut accorder à un tel schéma une crédibilité absolue. S'il était valable on pourrait certes contester la validité de certains essais en soufflerie. Pour une voilure ayant en transsonique un choc à 40% de la corde, des essais d'une part, dans une soufflerie permettant un nombre de Reynolds modéré (disons 2×10^6), d'autre part en vol, pourraient conduire pour R_θ à des valeurs qui se situeraient aux deux bornes de l'intervalle où le saut de pression nécessaire au décollement décroît. D'où une sensibilité importante du phénomène d'apparition du décollement.

Néanmoins, la plupart des spécialistes ne sont pas aussi pessimistes et pensent que l'influence du nombre de Reynolds sur ce phénomène est toujours faible. En tout état de cause, lorsqu'une interaction onde de choc-couche limite est apparue, accompagnée d'un décollement, l'évolution du bulbe est relativement indépendante de l'échelle. Ainsi, lorsque le décollement existe à la fois en vol et sur la maquette (par exemple en transition déclenchée), et qu'il est le seul phénomène à jouer un rôle, les essais en soufflerie seront parfaitement représentatifs de la réalité. En aval du choc, il existe toujours un gradient de pression positif vers le bord de fuite, les tubes du courant supersonique se contractent et la tendance au recollement du bulbe est réduite. Si on accroît alors le nombre de Mach ou l'incidence, le bulbe s'accroît très rapidement, jusqu'à ce qu'il atteigne le bord de fuite (ceci est schématisé Figure I-9); l'écoulement est alors complètement décollé à partir du pied du choc. On a affaire dans ce cas à un écoulement dit de type A (Pearcey).

La croissance du bulbe est toujours si rapide qu'il faut un très faible accroissement du nombre de Mach pour passer de l'apparition du bulbe au décollement complet. Ainsi, on pourra conclure, dans l'état actuel des connaissances

- qu'il y a un accord en général satisfaisant entre la soufflerie et le vol dans le cas de l'interaction onde de choc-couche limite, à condition que la couche limite sur la maquette soit turbulente;
- que les limites de buffeting peuvent être estimées avec une assez bonne confiance à partir des essais en soufflerie tant que l'on a affaire à un écoulement de type A.

3. DECOLLEMENTS DUS AUX GRADIENTS DE PRESSION

La tendance moderne vers la conception de voilures d'avion plus chargées aérodynamiquement a introduit de tels gradients de pression sur la surface que les couches limites sont largement susceptibles de décoller. Ces décollements ne sont pas de nature très différente suivant qu'ils apparaissent en transsonique ou aux basses vitesses: ils dépendent du nombre de Reynolds et peuvent survenir dans n'importe laquelle des régions où les gradients de pression sont défavorables (recompression supersonique ou partie arrière de certains profils). Le cas du décollement de bord de fuite des voilures modernes est sans doute l'un des plus critiques effets d'échelle auxquels on se trouve confronté aujourd'hui.

Dans cette étude du décollement de bord de fuite on peut évidemment se limiter au cas où la couche limite est turbulente. Il est souvent admis que c'est la valeur de $(\theta/\rho_e U_e^2) dp/dx$ qui détermine le décollement,

- θ est l'épaisseur de quantité de mouvement,
- ρ_e est la masse volumique au bord de la couche limite,
- U_e est la vitesse au bord de la couche limite,
- dp/dx est le gradient de pression le long de la surface.

(En incompressible il y a décollement si $(\theta/\rho_e U_e^2) dp/dx \geq 0,0035$.)

Cette expression peut être rendue sans dimension

$$\frac{\theta}{c} \frac{d(p/q)}{d(x/c)}$$

c étant le corde de référence, q la pression dynamique à l'infini.

Elle illustre la cause des effets de l'échelle lors du décollement au bord de fuite. Avec ces voilures modernes, $d(p/q)/d(x/c)$ s'est accru à cause de l'épaississement des profils et de l'accroissement des charges arrières. De plus (θ/c) montre l'importance de l'épaisseur relative de quantité de mouvement de la couche-limite; cette épaisseur relative étant beaucoup plus élevée en soufflerie qu'en vol, la couche limite tend à décoller prématurément sur la maquette, ce qui peut entraîner de notables effets d'échelle.

Les écoulements qui conduisent à un décollement au bord de fuite ont été nommés écoulements de type B (Thomas), par opposition au type A précédemment décrit. Un schéma de ce type d'écoulement et de décollement est présenté – Figure I-10: le décollement prend naissance près du bord de fuite puis lorsque l'incidence ou le nombre de Mach s'accroissent, le point de décollement remonte vers l'amont jusqu'à ce qu'il atteigne le pied du choc. Ce schéma est un peu simplifié et la dichotomie type A – type B est trop schématique. Plusieurs variantes doivent être envisagées:

- cas d'un décollement arrière provoqué par le bulbe au pied du choc: ce bulbe ne suscite pas le décollement par lui-même; mais il accroît l'épaisseur de quantité de mouvement de la couche limite de telle sorte que θ/c devienne trop élevé. Alors l'écoulement "éclate" au bord de fuite; la pression de bord de fuite en est modifiée, la circulation change le long du profil, suscitant un déplacement du choc vers l'avant.
- cas d'un décollement arrière provoqué par le choc lui-même: c'est le même cas que précédemment, mais dans lequel l'interaction onde de choc-couche limite était trop faible pour créer le décollement au pied du choc.
- cas d'un décollement arrière préexistant: le décollement arrière existe en l'absence de choc sur le profil, mais il est aggravé soit par l'interaction faible onde de choc-couche limite soit par l'existence du bulbe.

On peut s'attendre, dans tous ces cas, à l'existence d'effets d'échelle notables. Des variations dans le nombre de Reynolds peuvent parfois modifier l'importance relative des deux décollements de type A ou de type B ou éliminer l'un de ces deux types, changeant l'aspect quantitatif des résultats. Le seul moyen de lever le doute consiste en des calculs de couche limite avec des méthodes suffisamment bien éprouvées. Mais pour chercher la position du décollement il importe d'utiliser une distribution de pression correcte: en particulier il pourrait être absurde de rechercher l'évolution de la couche limite avec le champ de pression extérieur qui correspond à un écoulement non décollé: il faut tenir compte de l'influence du décollement sur la répartition de pression extérieure.

La remontée du point de décollement vers le pied du choc se produit d'une manière relativement progressive lorsque le nombre de Mach ou l'incidence augmentent. A ce sujet on pourra comparer (Figure I-11) les vitesses de propagation du décollement d'une part dans le cas d'un profil conduisant à un écoulement de type A (NPL 4111, $\rho/l = 9,45\%$) d'autre part dans le cas d'un profil conduisant à un écoulement du type B (RAE 103, $\rho/l = 12\%$). Dans le premier cas, il est extrêmement facile de connaître le Mach d'apparition du buffeting, et l'extrapolation de la soufflerie au vol est d'autant plus aisée que ce type d'écoulement serait peu sensible à l'effet d'échelle. Dans le deuxième cas, le premier problème est de déterminer quand apparaît le buffeting, le second d'extrapoler de la soufflerie au vol:

- plusieurs praticiens s'accordent à reconnaître que le buffeting apparaît lorsque le début du décollement atteint 90% de la corde;
- quant aux effets d'échelle, nous avons dit à quel point il était difficile d'en tenir compte pour un tel écoulement de type B.

En conclusion, la finesse de prévision du buffeting en soufflerie dépend essentiellement du type de l'écoulement à considérer.

4. L'INTERACTION AVEC L'ÉCOULEMENT EXTERNE

Cette interaction est faible tant que l'écoulement ne présente pas de décollement. Dans ce cas l'estimation en soufflerie des coefficients de portance et de moment de tangage est à peu près correcte. Bien entendu, il est nécessaire de faire la correction de couche limite (calcul de son évolution dans les conditions de la soufflerie d'une part, dans les conditions du vol d'autre part) si on veut évaluer correctement les trainées. Mais ce calcul peut être fait en utilisant le champ de pression tel qu'il apparaît en soufflerie dans l'écoulement externe.

Il en est différemment si on doit faire face à un écoulement qui comporte des décollements notables (que ce soit au bord d'attaque, au bord de fuite ou au pied de l'onde de choc). Les frontières de l'écoulement externe sont tellement modifiées que le champ des pressions ne pourra plus être considéré comme réaliste. Il sera nécessaire de mettre en oeuvre un processus d'itération:

champ de pression observé en soufflerie → calcul de couches limites et des décollements → correction du champ de pression externe → nouveau calcul des couches limites et des décollements, etc. . . .

La convergence d'un tel processus n'est pas évidente dans tous les cas.

L'estimations des C_m et des C_z en sera rendue plus difficile. Il est en particulier exclu, dans cette démarche, de se limiter à des mesures globales de coefficients de moment ou de portance. Il devient indispensable de procéder à une analyse suffisamment fine de l'écoulement pour:

- caractériser les couches limites et les sillages,
- localiser les décollements,
- repérer le type d'écoulement qui conduit à ce que la couche limite décolle.

L'effet global peut être très important, ainsi que le révèlent les Figures I-12 et I-13 représentant le déplacement du choc, résultat de toutes ces interactions. On notera en particulier que des essais effectués par Lockheed sur une maquette de C-141 à des nombres de Reynolds élevés ($8,5 \times 10^6$) donnent des résultats assez différents de ce qui a été observé en vol (Figure I-13). Cette constatation nous conduit à la remarque suivante: il n'existe pas de nombre de Reynolds magique à partir duquel la soufflerie est parfaitement représentative du vol. Aussi loin que l'on puisse aller maintenant dans la sophistication des moyens d'essais, on a la certitude que ceux-ci ne seront même pas en mesure de reproduire parfaitement les phénomènes sur lesquels les praticiens s'interrogent aujourd'hui.

Les remarques que j'ai fait jusqu'à présent sembleraient pessimistes vis à vis de la soufflerie; en réalité, dans l'état actuel des choses, les services de la soufflerie demeurent considérables. Et je crois qu'on a commis davantage d'erreurs en appliquant aux résultats de soufflerie des corrections de Reynolds inadaptées qu'en leur accordant une crédibilité excessive. La plupart des phénomènes peuvent être très correctement étudiés à des nombres de Reynolds modérés.

On parle beaucoup des souffleries à grands nombres de Reynolds, et je voudrais à ce sujet faire les remarques suivantes:

- les nouveaux moyens d'essais permettront l'investigation de phénomènes mal connus et importants; ils permettront en particulier de développer des modèles de calcul valables et de mettre en évidence des critères assez simples et assez réalistes pour qu'ils satisfassent l'ingénieur. Ceci démontre l'importance de souffleries de recherche à grands nombres de Reynolds;
- mais ces nouveaux moyens seront coûteux, parfois même d'un maniement industriel délicat (cf durée de rafales), et s'ils ont effectivement un rôle dans le développement des programmes, ils n'éclipseront vraisemblablement pas les moyens actuellement existants;
- il n'existe pas de nombre de Reynolds magique à partir duquel on puisse affirmer que l'écoulement est représentatif de la réalité; il va de soi que la construction de souffleries à grands Reynolds permettra un progrès, mais l'extrapolation au vol demeurera dans certains domaines hasardeux.

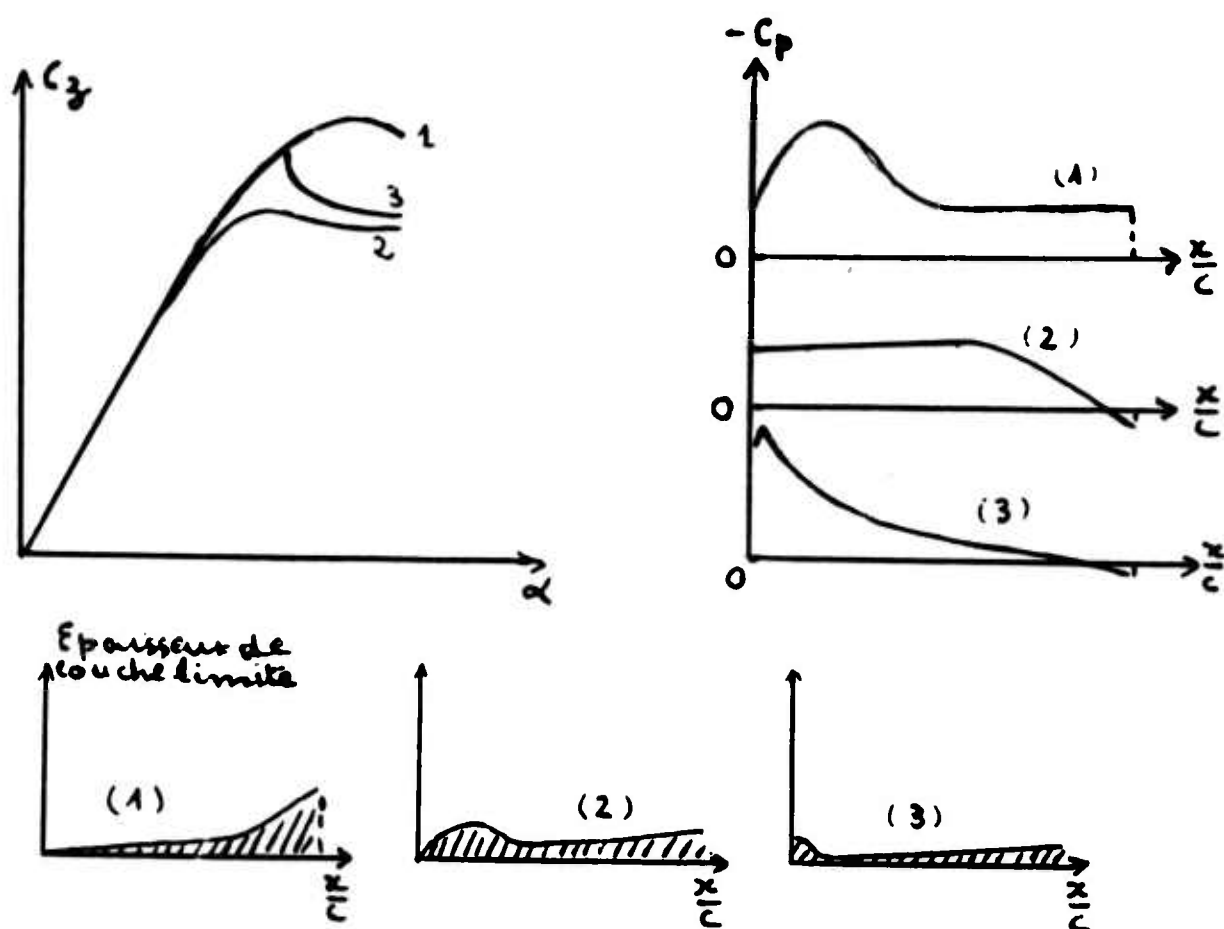


Figure I-1

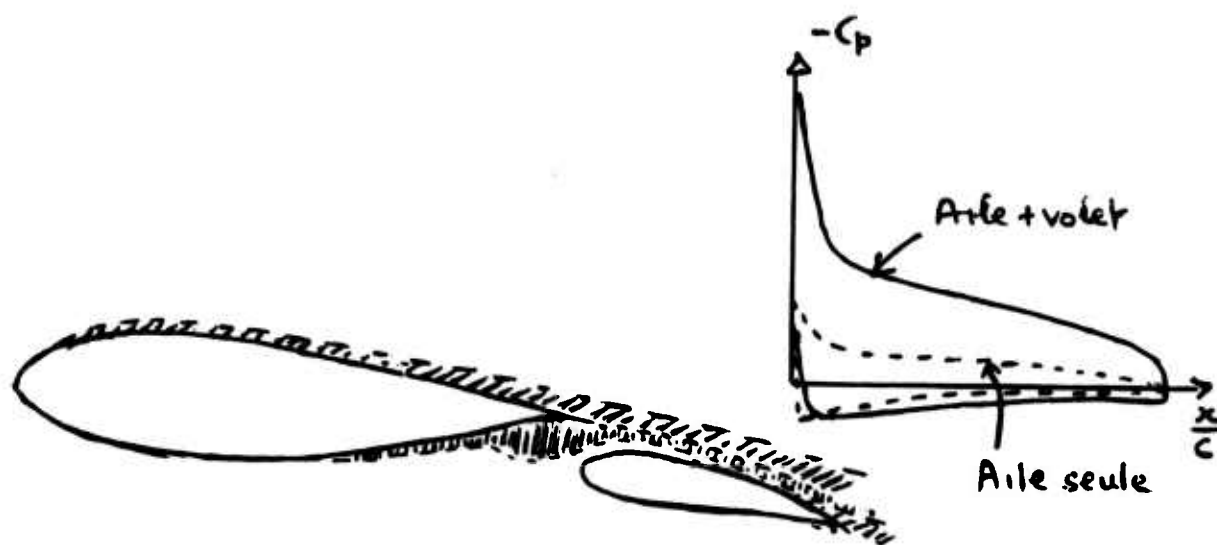


Figure I-2

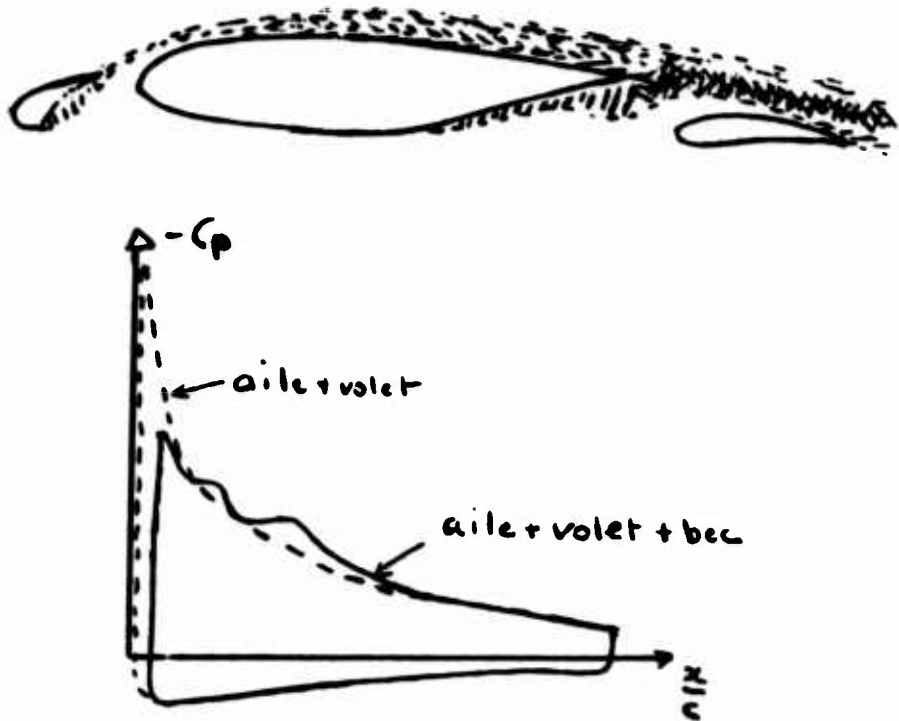


Figure 1-3

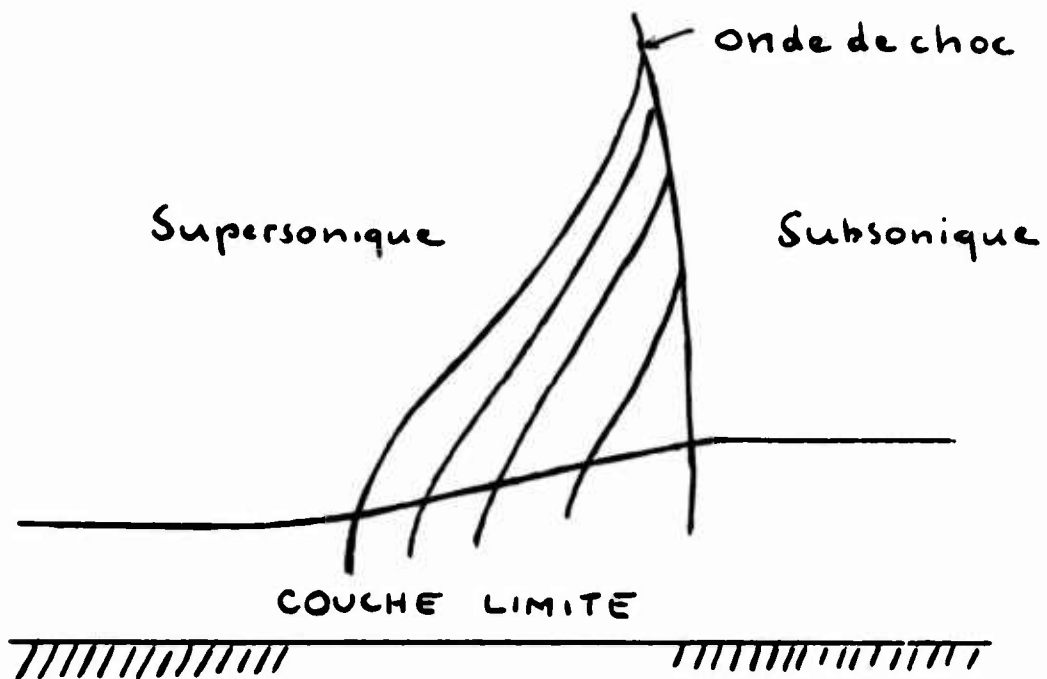


Figure 1-4

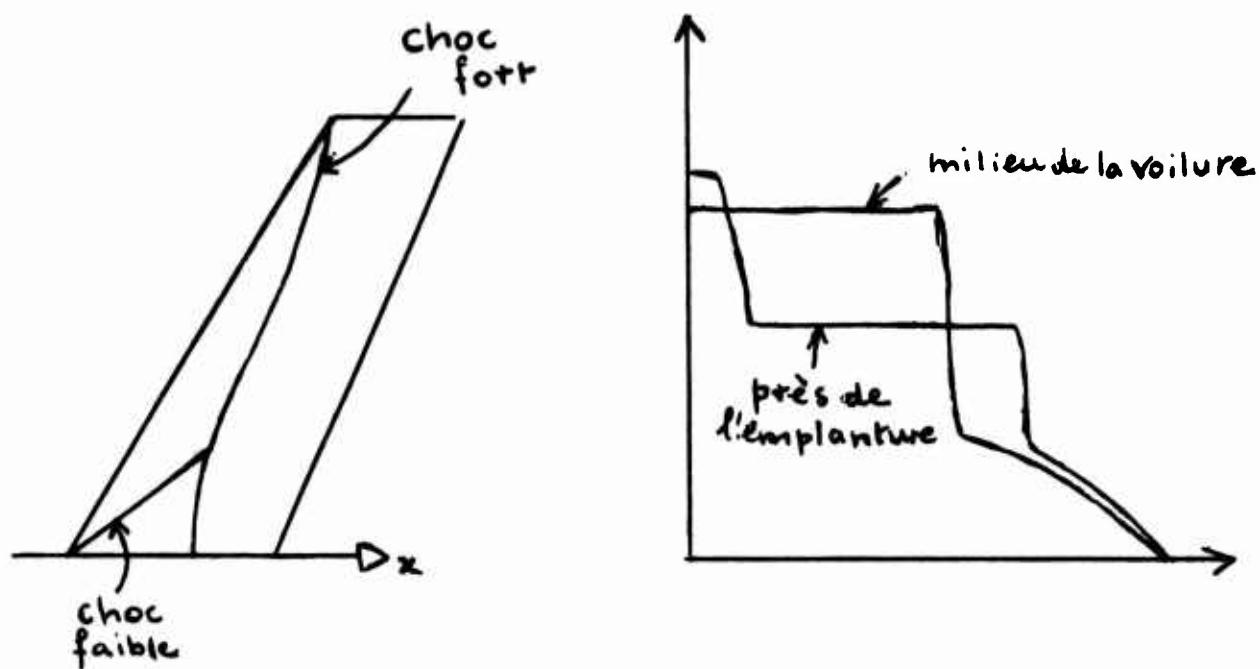
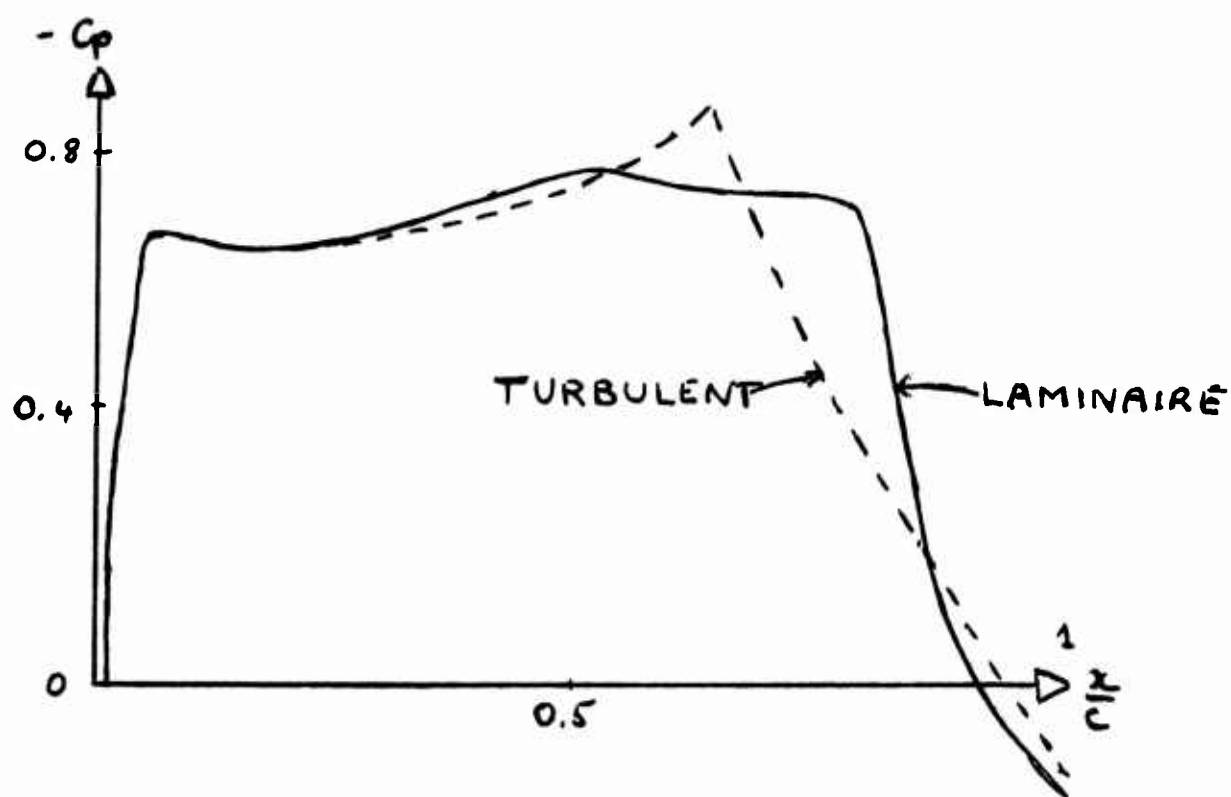


Figure I-5

Fig.I-5a Profil NLR 17(74)031450-141 RL. $M = 0,8$; $\alpha = 1,5^\circ$

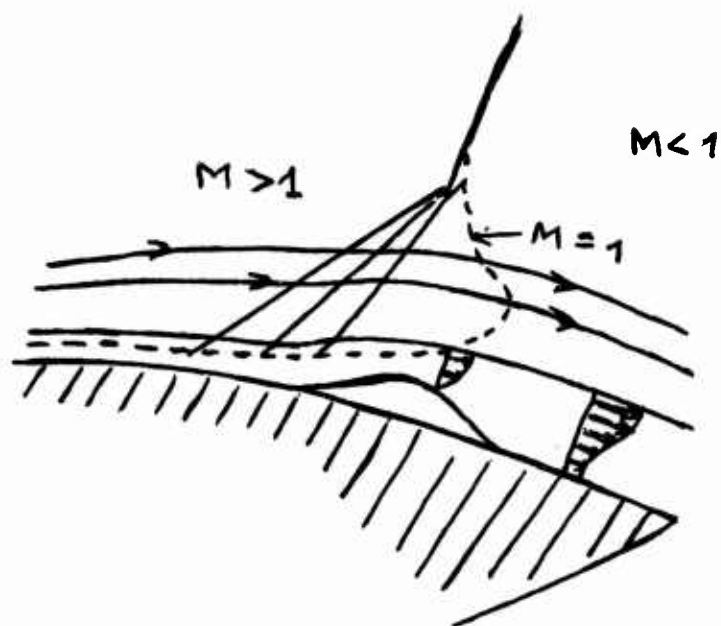


Figure I-6

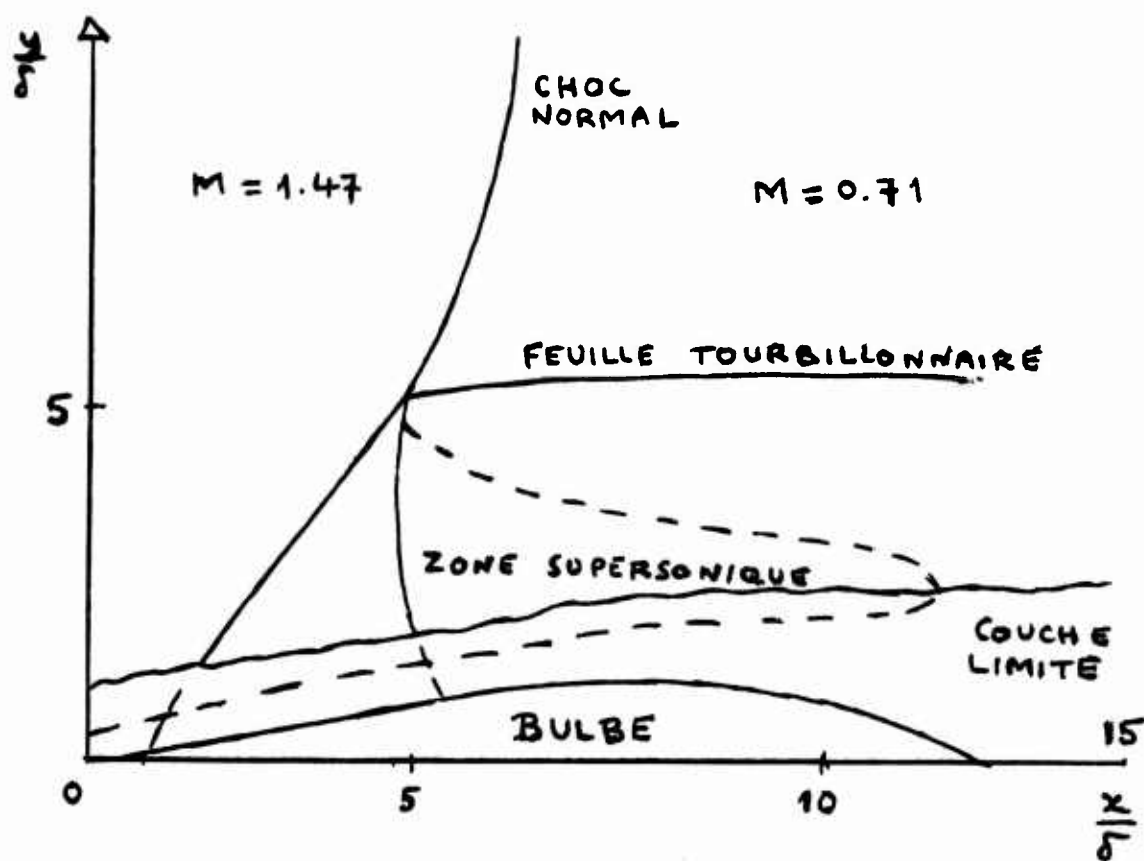


Figure I-7

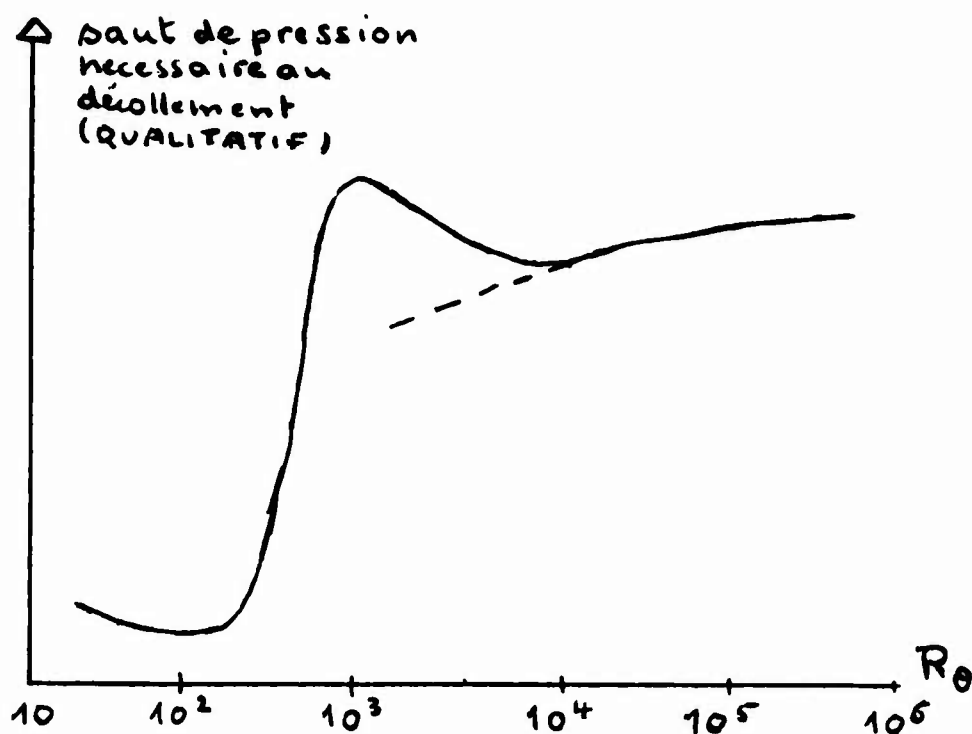


Figure I-8

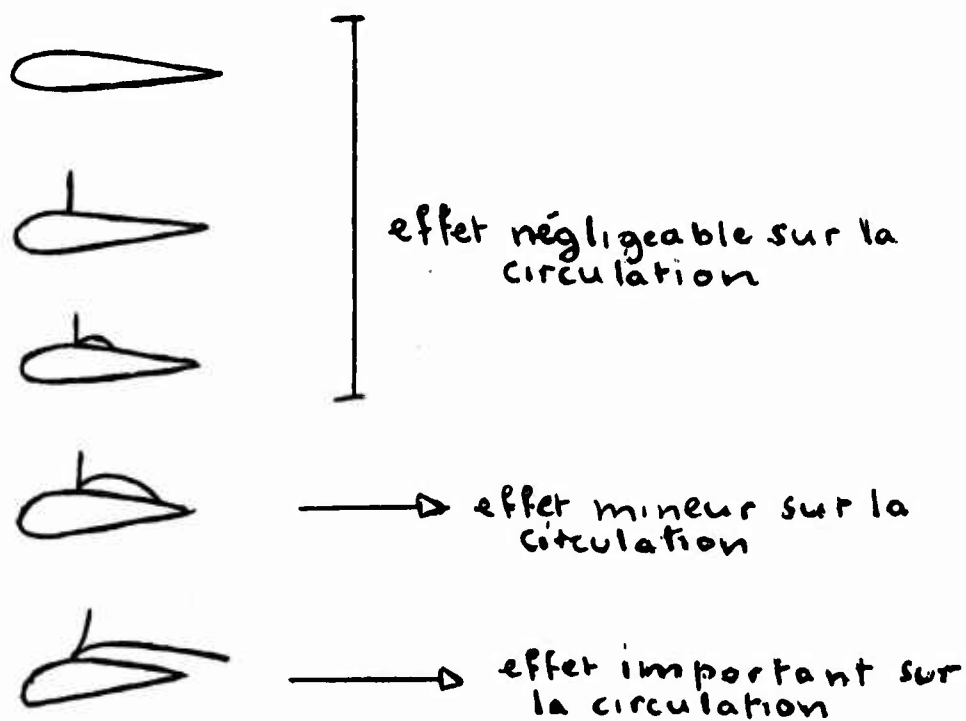


Figure I-9

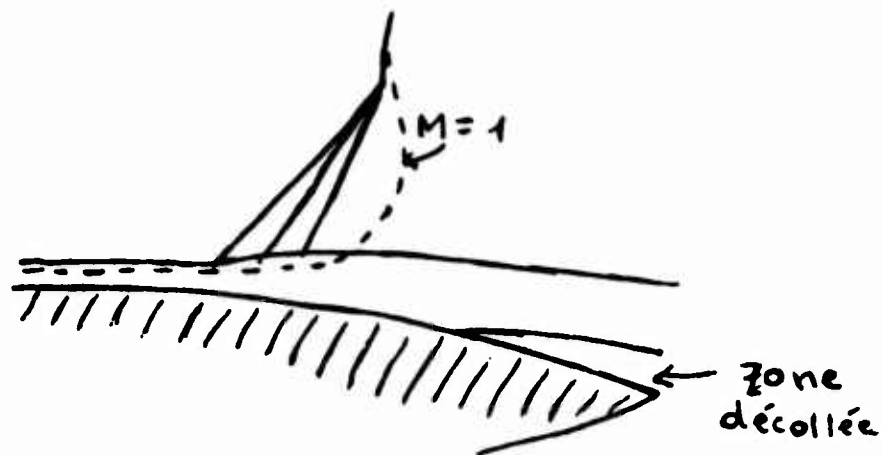


Figure I-10

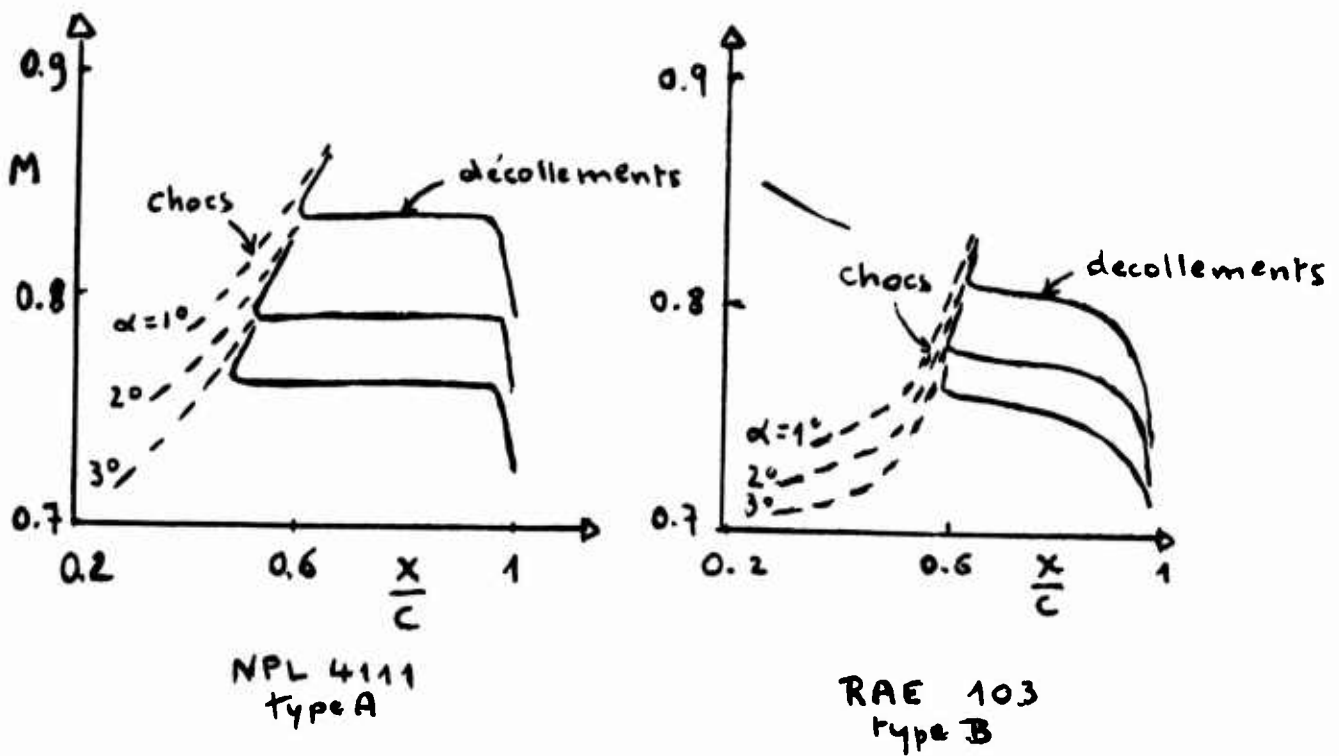


Figure I-11

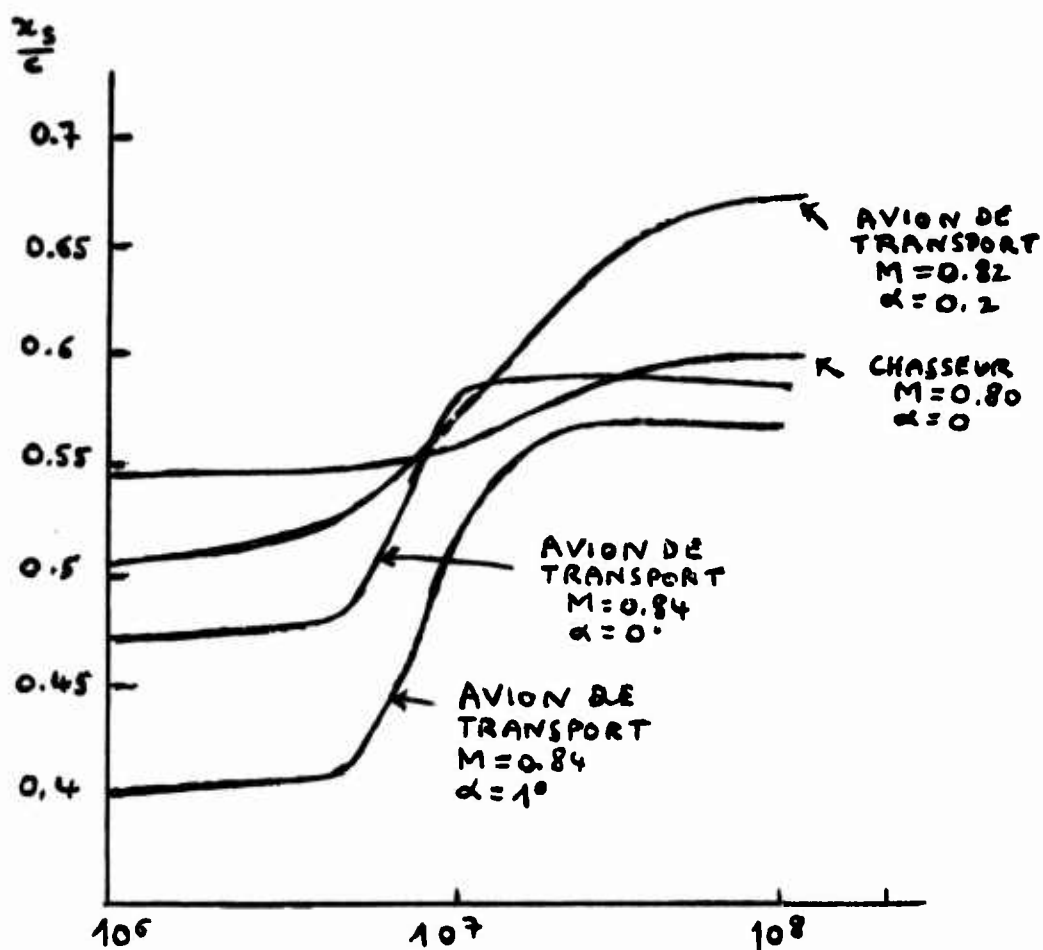


Fig. I-12 Position du choc, fonction de nombre de Reynolds. C.f. AGARD - FDP - Göttingen, 4 - 1971

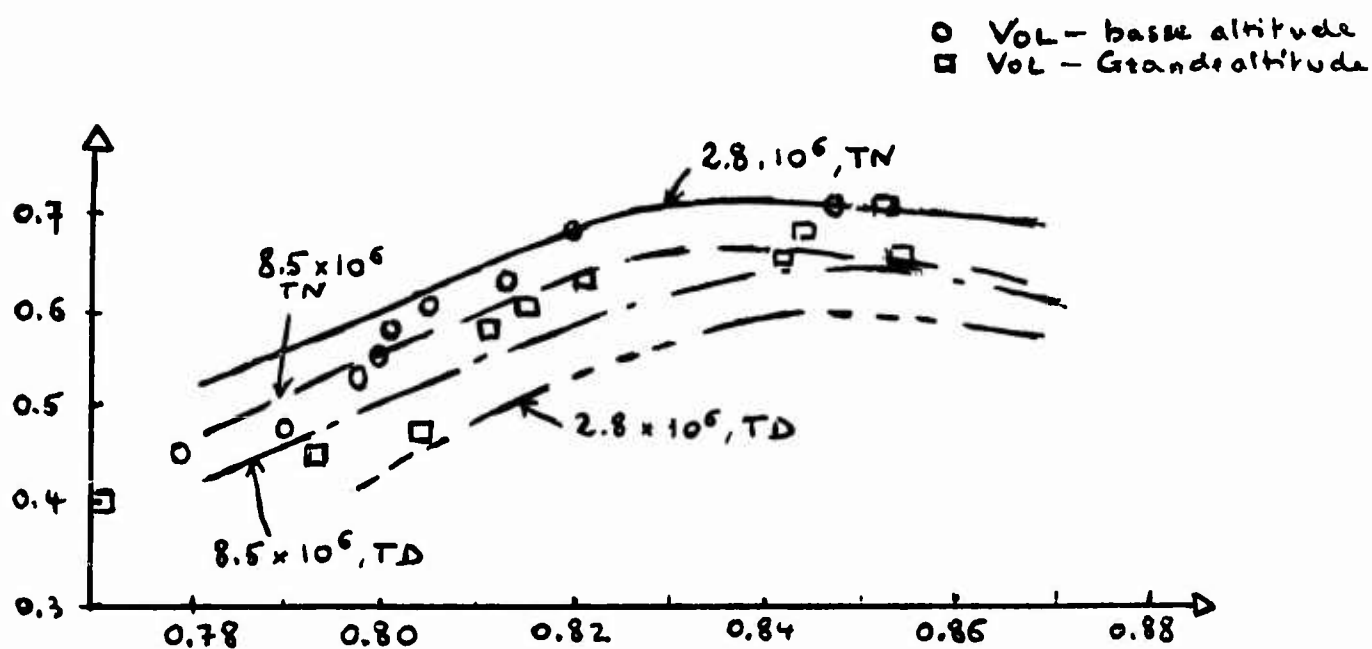


Figure I-13

Section II

FIGURATION DES FUSEAUX REACTEURS

1. INTRODUCTION

Lorsqu'on a affaire à un avion, il faut connaître les caractéristiques aérodynamiques du planeur mis en présence des tubes de courant qui servent à sa propulsion et pourraient modifier notablement les dites caractéristiques. D'où la nécessité, dès lors que la soufflerie constitue l'outil d'investigation fondamental, de réaliser des maquettes perméables où les tubes de courant traversant les fuseaux seraient homologues à ceux existant en vol.

Il est pratiquement impossible, certes, de réaliser en soufflerie dans la section de sortie des fuseaux réacteurs des conditions semblables à celles du vol (vitesses, pressions, températures). Mais, dans beaucoup de cas, il semble que ces conditions de sortie n'entraînent des interactions notables sur les caractéristiques aérodynamiques du planeur qu'à basse vitesse et grande incidence. Par exemple, la présence d'un débit plus ou moins grand localisé à l'intrados d'une aile delta près du bord de fuite n'affecte que légèrement le développement du tourbillon d'extrados. Le problème le plus important est celui de la réalisation correcte des caractéristiques du tube de courant depuis l'infini amont jusqu'à l'entrée des fuseaux.

L'évaluation de données aérodynamiques relatives aux sorties d'air constitue un problème aérodynamique important qui sera abordé au paragraphe 4. Les efforts aérodynamiques locaux sont composés d'efforts de pression p_l et d'efforts de frottements f_l respectivement perpendiculaires et tangentiels aux éléments de surface dA . Le théorème des quantités de mouvement est maintenant appliqué à trois domaines:

- (a) Tube de courant contenant le fluide qui traverse effectivement le fuseau (fluide e) et limité d'une part par la section d'entrée du canal interne du fuseau prise dans le plan des lèvres latérales (section A1); d'autre part par la section de sortie du canal interne du fuseau prise dans le plan de sortie (section A2).

$$\overrightarrow{Q_e V_2} - \overrightarrow{Q_e V_1} = - \iint_{FK,JI} \overrightarrow{p_l} dA - \iint_{FK,JI} \overrightarrow{f_l} dA - \overrightarrow{p_2 A_2} - \overrightarrow{p_1 A_1}.$$

- (b) Tube de courant contenant le fluide e et limité d'une part par la section droite prise à l'infini amont (section $A_{\infty e}$), d'autre part par la section A1

$$\overrightarrow{Q_e V_1} - \overrightarrow{Q_e V_{\infty}} = - \iint_{GF} \overrightarrow{p_l} dA - \iint_{GF} \overrightarrow{f_l} dA - \iint_{HI} \overrightarrow{p_l} dA - \overrightarrow{p_1 A_1} + \overrightarrow{p_{\infty} A_{\infty e}}.$$

- (c) Tube de courant contenant le fluide dévié par le piège à couche limite (fluide d) et limité d'une part par la section $A_{\infty d}$, d'autre part par la section de sortie du piège à couche limite (section A3)

$$\begin{aligned} \overrightarrow{Q_d V_3} - \overrightarrow{Q_d V_{\infty}} = & - \iint_{AB} \overrightarrow{p_l} dA - \iint_{BC} \overrightarrow{p_l} dA - \iint_{BC} \overrightarrow{f_l} dA - \iint_{CD,EF} \overrightarrow{p_l} dA - \\ & - \iint_{CD,EF} \overrightarrow{f_l} dA + \iint_{FG} \overrightarrow{p_l} dA + \iint_{FG} \overrightarrow{f_l} dA - \overrightarrow{p_3 A_3} + \overrightarrow{p_{\infty} A_{\infty d}}. \end{aligned}$$

Remarques sur les notations

$$\overrightarrow{Q_i V_j} = \iint_{A_{ji}} \vec{V} \rho V_n dA.$$

quantité de mouvement du fluide i traversant la section A_{ji} .

La signification des lettres est expliquée sur la Figure II-1.

$\overrightarrow{p_1 A_1}$: effort de pression agissant sur A1 dirigé vers l'intérieur du fuseau.

$\overrightarrow{p_2 A_2}$ et $\overrightarrow{p_3 A_3}$: efforts de pression agissant sur A2 et A3 et dirigés vers l'extérieur du fuseau.

Les orientations des surfaces sont précisées sur la Figure II-1.

Tenons compte de ce que l'intégrale de p_{∞} le long d'un domaine fermé est nulle; on a

— effort exercé par le fluide e sur la paroi interne des fuseaux:

$$F_{ie} = \iint_{FK,JI} \overrightarrow{p'_l} dA + \iint_{FK,JI} \overrightarrow{f'_l} dA$$

$$\vec{F}_{ie} = - \left[\overrightarrow{Q_e V_2} + \overrightarrow{p'_2 A_2} - \overrightarrow{Q_e V_1} - \overrightarrow{p'_1 A_1} \right],$$

en posant $p'_l = p_l - p_\infty$.

- effort exercé par le fluide e sur le fluide extérieur et le fluide d :

$$\vec{F}_{ee} = \iint_{GF} \overrightarrow{p'_l dA} + \iint_{GF} \overrightarrow{f_l dA} + \iint_{HI} \overrightarrow{p'_l dA}$$

$$\vec{F}_{ee} = - \left[\overrightarrow{Q_e V_1} + \overrightarrow{p'_1 A_1} - \overrightarrow{Q_e V_\infty} \right].$$

- effort exercé par le fluide d sur le fluide extérieur, le fluide e et les parois

$$\begin{aligned} \vec{F}_d = & \iint_{AB} \overrightarrow{p'_l dA} + \iint_{BC} \overrightarrow{p'_l dA} + \iint_{BC} \overrightarrow{f_l dA} - \iint_{FG} \overrightarrow{p'_l dA} - \iint_{FG} \overrightarrow{f_l dA} + \\ & + \iint_{CD,EF} \overrightarrow{p'_l dA} + \iint_{CD,EF} \overrightarrow{f_l dA} \end{aligned}$$

$$\vec{F}_d = - \left[\overrightarrow{Q_d V_3} + \overrightarrow{p'_3 A_3} - \overrightarrow{Q_d V_\infty} \right].$$

- effort exercé par le fluide extérieur sur le culot des fuseaux

$$\vec{F}_a = \iint_{JN} \overrightarrow{p'_l dA} + \iint_{JN} \overrightarrow{f_l dA}.$$

Posons alors

$$\vec{\Pi} = \text{effort de poussée}$$

$$\vec{F} = \text{effort de traînée},$$

on a

$$\begin{aligned} \vec{\Pi} + \vec{F} = & \left[\iint_{BMK} (\overrightarrow{p'_l + f_l}) dA + \iint_{ILN} (\overrightarrow{p'_l + f_l}) dA \right] + \left[\iint_{BC} (\overrightarrow{p'_l + f_l}) dA + \right. \\ & + \left. \iint_{CD,EF} (\overrightarrow{p'_l + f_l}) dA \right] + \left[\iint_{FK} (\overrightarrow{p'_l + f_l}) dA + \iint_{JI} (\overrightarrow{p'_l + f_l}) dA \right] + \\ & + \left[\iint_{JN} \overrightarrow{p'_l dA} \right]. \end{aligned}$$

On intégrera dans $\vec{\Pi}$ toutes les dynamiques entrantes et sortantes ainsi que les efforts agissant sur le culot du fuseau. Soit:

$$\vec{X}_B = - (\overrightarrow{Q_e V_2} + \overrightarrow{p'_2 A_2}) + \iint_{JN} \overrightarrow{p'_l dA} \quad (\text{effort de poussée de brute});$$

$$\vec{X}_e = - \overrightarrow{Q_e V_\infty} \quad (\text{effort de traînée de captation});$$

$$\begin{aligned} \vec{\Pi} &= \vec{X}_B - \vec{X}_e + \vec{F}_d \\ &= - (\overrightarrow{Q_e V_2} + \overrightarrow{p'_2 A_2}) + \overrightarrow{Q_e V_\infty} - (\overrightarrow{Q_d V_3} + \overrightarrow{p'_3 A_3}) + \overrightarrow{Q_d V_\infty} + \iint_{JN} \overrightarrow{p'_l dA} \\ &= \vec{F}_{ie} + \vec{F}_{ee} + \vec{F}_d + \vec{F}_a. \end{aligned}$$

On en déduit:

$$\vec{F} = \left[\iint_{BMK} (\overrightarrow{p'_l + f_l}) dA + \iint_{ILN} (\overrightarrow{p'_l + f_l}) dA \right] - \left[\iint_{IH} \overrightarrow{p'_l dA} + \iint_{AB} \overrightarrow{p'_l dA} \right].$$

Le premier terme représente les efforts classiques de pression et de frottement appliqués aux surfaces externes de l'avion; quant à la projection sur la vitesse infinie du deuxième terme, elle constitue la "traînée additive".

2. TRANSPOSITION SOUFFLERIE VOL

Ce qui précède montre clairement qu'une similitude rigoureuse est impossible; il importe néanmoins de représenter un $(\vec{\Pi} + \vec{F})$ facilement transposable au vol, les sources d'erreur ou d'indétermination étant réduites au minimum. Ainsi, après avoir déterminé l'effort $(\vec{\Pi} + \vec{F})$ en soufflerie par pesée classique sur dard ou sur mât, les opérations suivantes sont nécessaires (nous nous inspirons ici de la démarche qui a été suivie pour Concorde):-

- Mesure de \vec{X}_B soufflerie et remplacement par \vec{X}_B vol, qui n'est pas toujours facile à connaître (voir §4).
- Transposition de \vec{X}_C liée à la mesure de Q_e , d'autant plus facile que *les débits en vol et en soufflerie seront analogues* (ce qu'on supposera par la suite).
- Transposition de \vec{F}_d . Cet effort est toujours difficile à mesurer en soufflerie (surtout pour la dynalpie sortante); mais il est en partie lié à la couche limite devant le fuseau. Si donc les débits Q_e étaient peu différents, la transposition serait une question de nombre de Reynolds. En conséquence, il faut tenir compte:
 - de la modification des efforts globaux de pression;
 - de la part de couche limite prise en compte par le déviateur (si celui-ci est conçu pour absorber la couche limite en vol, il n'en absorbera qu'une petite partie en soufflerie).

Les efforts de frottement et de pression à affecter au piège seront relativement plus élevés en vol qu'en soufflerie.

- Transposition de \vec{F} , en corrigeant les efforts de frottement et les efforts de pression (liés à la forme extérieure des surfaces de courant qui traversent le fuseau); cette dernière correction est liée au choc devant le fuseau, qui dépend notamment du débit Q_e et du nombre de Reynolds.

On peut donc résumer ainsi les corrections appliquées au $(\vec{\Pi} + \vec{F})$ soufflerie:

$-\vec{X}_B$ soufflerie,	calculé à partir des mesures
$+\vec{X}_B$ vol,	donné par les caractéristiques moteur et tuyère
$+\vec{X}_C$ soufflerie,	calculé à partir des mesures
$-\vec{X}_C$ vol,	donné par les caractéristiques moteur et entrée d'air.
$+\Delta\vec{F}_d$ frottement,	déterminé théoriquement à partir des nombres de Reynolds
$+\Delta\vec{F}_d$ pression,	déterminé après essais spéciaux compte tenu des nombres de Reynolds
$+\Delta\vec{F}$ frottement,	déterminé théoriquement compte tenu des nombres de Reynolds
$+\Delta\vec{F}$ pression,	déterminé de manière théorique et empirique compte tenu des nombres de Reynolds et des débits.

En réalité toutes ces grandeurs sont à considérer sous leurs formes réduites classiques. On a à considérer:

$$\frac{P}{p} = (1 + 0,2 M^2)^{3,5} \quad (\text{pression totale et pression statique})$$

$$q = \frac{1}{2} \rho V^2$$

$$\epsilon_e = \frac{Q_e}{A_{1ref} \rho_{\infty} V_{\infty}} \quad (\text{coefficient de débit})$$

A_{1ref} est en général la projection de la section d'entrée de la prise d'air perpendiculairement à la direction moyenne de l'écoulement rentrant.

$$\frac{|\vec{X}_C|}{q_{\infty} S_{ref}}, \quad \frac{|\vec{X}_B|}{q_{\infty} S_{ref}}$$

S_{ref} aire de la section de référence avion.

$$\frac{|\vec{X}_2|}{q_{\infty} S_{ref}}, \quad \frac{|\vec{F}_d|}{q_{\infty} S_{ref}}$$

On notera les relations

$$\epsilon_a = \frac{(1 + 0,2 M_\infty^2)}{A_{1ref} M_\infty} \int_{A_m} \frac{P_m}{P_\infty} \frac{P_m}{P_m} M_m (1 + 0,2 M_m^2)^{0,5} dA_m$$

(m correspond à la section qui permet de déterminer le débit)

$$\frac{|\vec{X}_1|}{q_\infty S_{ref}} = 2\epsilon \frac{A_{1ref}}{S_{ref}}$$

$$\frac{|\vec{X}_2|}{q_\infty S_{ref}} = \frac{|\vec{X}_{02}|}{q_\infty S_{ref}} - \frac{2A_2}{1,4 M_\infty^2 S_{ref}}$$

\vec{X}_{02} est la dynalpie sortante de A_2 ou

$$\frac{|\vec{X}_2|}{q_\infty S_{ref}} = \left| \frac{2}{1,4 M_\infty^2 S_{ref}} \left[(1 + 0,2 M_\infty^2)^{3,5} \int_{A_2} (1 + 1,4 M^2) \frac{P_2}{P_2} \frac{P_2}{P_\infty} dA_2 - A_2 \right] \right|$$

$$= \left| \frac{2}{1,4 M_\infty^2 S_{ref}} \left[A_{1ref} \epsilon_e \frac{M_\infty}{M_2} \left(\frac{1 + 0,2 M_\infty^2}{1 + 0,2 M_2^2} \right)^{0,5} (1 + 1,4 M_2^2) - A_1 \right] \right|$$

3. REALISATION PRATIQUE

L'échelle de la maquette, les conditions d'essai (pression génératrice, M_∞ nombre de Reynolds . . .) sont imposées, mais l'examen des formules ci-dessus montre qu'on peut choisir M_2 correspondant à la section de sortie du fuseau et le nombre de Mach dans la section qui servira à déterminer le débit. Or on a

$$\frac{d|\vec{X}_2|}{|\vec{X}_2|} = \frac{P_\infty}{P_m} \left(\alpha' \frac{dP_m}{P_\infty} - \beta' \frac{dP_m}{P_\infty} \right) \quad \text{avec} \quad \begin{cases} \alpha' = \frac{1 + 0,4 M_m^2}{1,4 M_m^2} \\ \beta' = (1 + 0,2 M_m^2)^{3,5} \frac{1 - M_m^2}{1,4 M_m^2} \end{cases}$$

$$d|\vec{X}_2| = d|\vec{X}_{02}|$$

On trouve

$$\frac{d|\vec{X}_2|}{|\vec{X}_2|} = \frac{|\vec{X}_{02}|}{|\vec{X}_2|} \frac{P_\infty}{P_2} \left(\alpha \frac{dP_m}{P_\infty} - \beta \frac{dP_m}{P_\infty} \right)$$

avec

$$\alpha = \frac{2(1 + 0,2 M_2^2)}{1 + 1,4 M_2^2}$$

$$\beta = (1 + 0,2 M_m^2)^{3,5} \frac{1 - M_2^2}{1 + 1,4 M_m^2}$$

ou encore

$$\frac{d|\vec{X}_2|}{|\vec{X}_2|} = \frac{|\vec{X}_{02}|}{|\vec{X}_2|} \left(\frac{d\epsilon_e}{\epsilon_e} - \delta dM_2 \right)$$

avec

$$\delta = \frac{1 - M_2^2}{M_2(1 + 0,2 M_2^2)(1 + 1,4 M_2^2)}$$

L'évolution de α , β , α' , β' , δ suggère que pour un niveau d'incertitude donné sur la mesure des grandeurs en soufflerie, il est préférable pour calculer le débit et X_2 de se situer à une valeur de M_2 voisine de 1. On est néanmoins limité, M_2 étant inférieur ou du même ordre de grandeur que M_∞ , les fuseaux étant ici perméables et non motorisés.

En subsonique peu élevé, les corrections doivent être menées avec beaucoup d'attention puisque α , β , α' , β' , et δ sont nettement différents de zéro. On effectue un sondage aussi serré que possible de l'écoulement dans une section voisine de la section de sortie à l'aide d'une sonde pitot double qui donne à la fois la pression statique et la pression totale; en outre, des prises noyées donnent la répartition de pression au culot du fuseau. La connaissance de ces pressions permet de calculer par intégration ϵ_e , $\overline{X_C}$ soufflerie et $\overline{X_B}$ soufflerie.

Un examen des ordres de grandeur rencontrés sur un avion de transport supersonique montre que ces corrections sont les plus importantes. La méthode donne des résultats valables tant que les débits vol et soufflerie sont analogues; mais il est parfois difficile de simuler en même temps les vitesses et les débits. Il peut devenir nécessaire de faire appel à des dispositifs aspirant de force une partie de l'air qui traverse les fuseaux.

En supersonique, on avait initialement pensé à n'utiliser que des mesures de pression statique noyées dans la paroi. Une telle méthode supposait que l'on avait un écoulement suffisamment homogène assimilable à un écoulement par tranche. En fait si la section de sortie est ajustée de manière à ce que le choc droit ne soit pas "avalé", il s'ensuit un décollement extrêmement important de la couche limite qui risque de se prolonger sur toute la longueur du divergent du canal interne, à tel point que l'écoulement dans le convergent n'est pas homogène. On est alors conduit à utiliser des canaux internes à écoulement supersonique, mais les phénomènes de réflexions de chocs compromettent aussi l'hypothèse d'écoulement par tranche. D'où l'introduction d'une méthode plus satisfaisante de sondage de l'écoulement. C'est la somme de tous les débits élémentaires et de tous les efforts élémentaires qui permet d'aboutir à Q_e , $\overline{X_C}$, $\overline{X_2}$. Dans le cas de Concorde le procédé est mis en oeuvre avec une maquette comportant un déviateur identique à celui de l'avion et seule la première rampe doit être impérieusement figurée puisque conditionnant le débit et la configuration des chocs externes. Si on néglige la représentation de la deuxième rampe il est possible d'élargir le col, ce qui facilite l'amorçage de l'entrée d'air. Le canal interne du fuseau s'élargit pour permettre un écoulement subsonique et se termine par un col sonique dont la section doit être assez grande pour ne pas influencer le débit.

D'autres procédés doivent être envisagés pour effectuer par exemple des essais valables dans des souffleries à rafales. On peut citer:

- la mesure globale du débit permettant le calcul de $\overline{X_2}$ dans une section sonique
- la mesure globale de l'effort interne fuseau par pesée directe du canal.

4. MESURE SUR MAQUETTE DE TUYERE ISOLEE

Il n'est pas, nous l'avons dit, actuellement envisageable de réaliser et de mesurer des efforts sur une seule maquette respectant à la fois la géométrie externe, les caractéristiques d'entrée d'air et les caractéristiques de tuyère d'éjection de l'avion en vol. Cette similitude ne serait possible qu'avec certains types de simulation de motorisation d'ailleurs coûteux.

Cette considération s'est traduite jusqu'à présent en ne détaillant pas l'effort de poussée brute donné par les caractéristiques moteur et tuyère et égal à

$$\overline{X_B} = -(\overline{Q_e V_2} + \overline{p_2 A_2}) + \iint_N p_1 dA$$

et en renvoyant aux caractéristiques moteurs et tuyères.

Pour obtenir des données aérodynamiques sur les tuyères, on est amené à essayer en soufflerie deux maquettes de tuyère isolée.

- D'abord une maquette de tuyère de référence dont les formes internes et externes sont semblables à celles de la maquette complète précédemment étudiée.

La poussée du flux interne est préalablement tarée au point fixe en fonction de $P_2 A_2 / p_\infty$. La maquette est ensuite passée en soufflerie pour différentes valeurs du Mach externe; le canal interne est alimenté de telle sorte que l'on explore une plage de $P_2 A_2 / p_\infty$ qui couvre les cas rencontrés dans les essais de la maquette d'avion complet.

L'effort s'exerçant sur la maquette peut s'écrire (Figure II-2)

$$\overline{X_f} = \overline{X_{bal 0}} - \overline{X_{b0}} - p_\infty \overline{A_{mc}}$$

$\overline{X_{bal 0}}$ est l'effort mesuré sur balance

A_{mc} est la section du maître couple,

$\overline{X_{b0}}$ est la poussée brute du jet de référence.

- Ensuite une maquette de tuyère réelle, à même échelle, dont les formes internes et externes reproduisent celles de la tuyère avion. Pour chaque nombre de Mach ces maquettes sont pesées, en étant alimentées en flux primaire et secondaire par des canalisations adéquates. Les caractéristiques de ces deux flux (débit corrigé et pression totale) reproduisent celles du vol; mais leur température est celle de l'ambiance de la soufflerie. Aussi une correction de gaz chauds doit être appliquée en supersonique.

L'effort s'exerçant sur la maquette peut s'écrire ici

$$\vec{X}_T = \vec{X}_{bal} - p_{\infty} \vec{A}_{mc}.$$

- L'effort de propulsion est évalué par différence

$$\vec{X}_f - \vec{X}_T.$$

La difficulté de ce genre d'essai est liée à une incompatibilité des pressions mesurées dans la zone aval sur l'avion complet d'une part et sur le montage de tuyère de référence d'autre part. La discordance avait été initialement attribuée à une mauvaise schématisation de l'écoulement amont; mais des calculs théoriques ont montré que ce fait n'expliquait pas les divergences sur la partie aval. La cause en reviendrait plutôt à une différence d'épaisseur de couche limite et surtout à des conditions expérimentales défavorables (taux d'obstruction élevés, souffleries différentes pour les deux types d'essais, etc.).

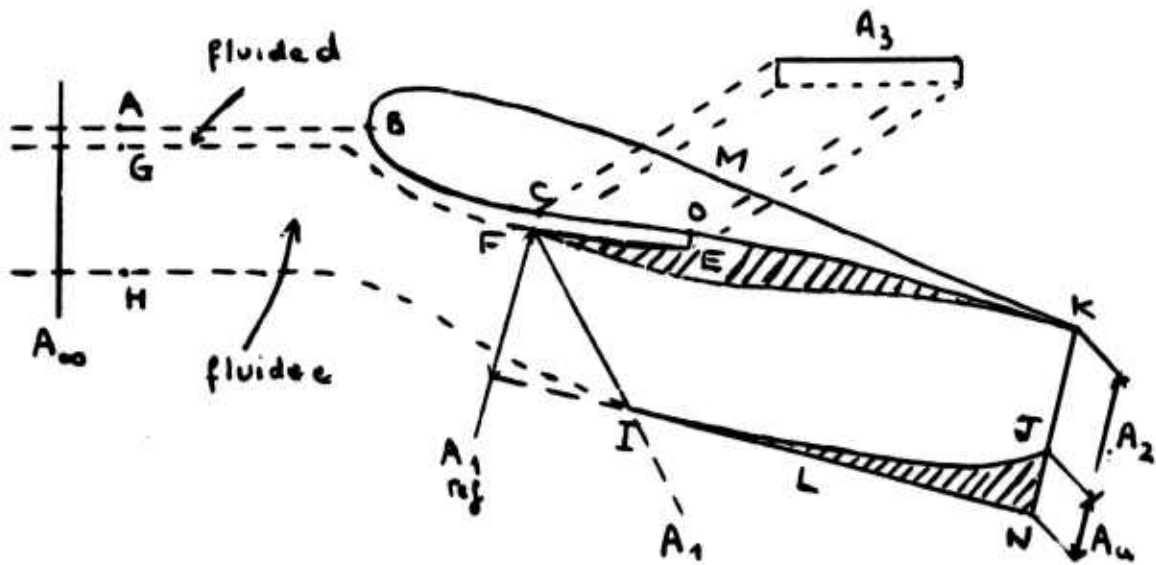


Figure II-1

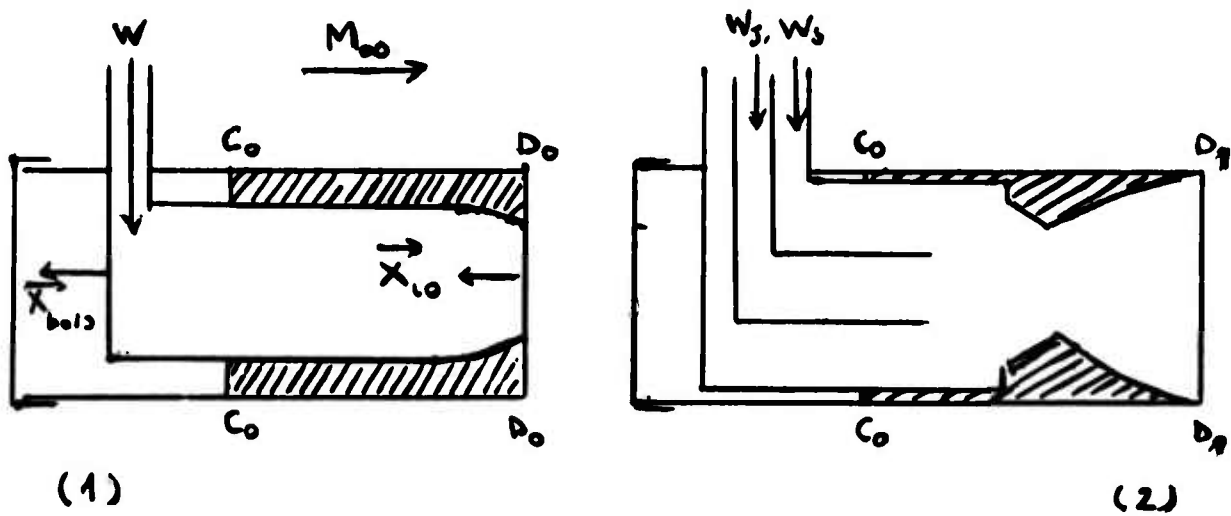


Figure II-2

Section III

L'UTILISATION DES CALCULS

1. INTRODUCTION

Nous ne détaillerons pas dans cette partie les modèles mathématiques, déjà classiques pour la partie non visqueuse et incompressible, mais moins universellement admis dès qu'il s'agit de décollements ou d'interactions. Ces domaines ne connaissent pas de méthode très générale: chaque industriel choisit les schémas de calcul et les critères qui lui paraissent le mieux correspondre à ses besoins et à son expérience.

D'une manière très générale, il faut insister sur l'extrême modularité du programme, les sous-programmes mis en oeuvre dépendant de la nature du problème traité et de la finesse de l'analyse requise. Par ailleurs, chacun des sous-programmes est susceptible d'être modifié au fur et à mesure que les connaissances fondamentales relatives aux phénomènes de base évoluent, et que les critères s'affinent. A titre d'exemple, dans les paragraphes suivants, nous penserons particulièrement à l'écoulement autour d'une ensemble voilure + fuselage.

Nous ne parlerons pas, volontairement, des calculs effectués à partir de quantités très globales avec des relations figurant dans les "Data Sheets" ou issues de l'expérience des industriels concernés. Nous pouvons dire de ces formules qu'elles donnent d'excellents résultats tant que l'écoulement n'a pas de caractéristiques nouvelles, mais qu'elles peuvent, dans le cas contraire, conduire à de très graves erreurs. Par exemple une formule de prévision du buffeting issue de l'expérience sur écoulements du type A conduira à de grossières erreurs si on l'applique à un écoulement du type B. L'applicabilité de telles formules doit être testée, dans chaque cas, par une analyse des phénomènes caractérisant l'écoulement.

2. ECOULEMENTS NON VISQUEUX

Les méthodes de calcul relatives à un écoulement tridimensionnel compressible sont dérivées des méthodes applicables à l'incompressible par l'intermédiaire d'un ensemble de corrections de compressibilité. D'après Goethert, l'analogie est obtenue par l'intermédiaire d'une affinité:

$$\left. \begin{aligned} x_a &= x \\ y_a &= \beta y \\ z_a &= \beta z \end{aligned} \right\} \quad \text{avec} \quad \beta = \sqrt{1 - M_a^2}.$$

L'expérience a montré jusqu'à présent qu'une telle correction conduit à des résultats satisfaisants jusqu'aux nombre de Mach critique.

L'écoulement incompressible sera caractérisé par une solution de l'équation de Laplace:

$$\frac{\partial^2 \phi}{\partial x_a^2} + \frac{\partial^2 \phi}{\partial y_a^2} + \frac{\partial^2 \phi}{\partial z_a^2} = 0,$$

où ϕ est le potentiel des vitesses, lui-même sujet à la condition aux limites que l'écoulement soit tangentiel le long de la surface considérée. Faisant intervenir un potentiel de perturbation φ :

$$Q = \vec{U}_\infty [x_a \vec{i} + y_a \vec{j} + z_a \vec{k}] + \varphi.$$

Les conditions aux limites peuvent s'écrire:

$$\varphi = 0 \quad \text{à l'infini amont,}$$

$$\frac{\partial \varphi}{\partial n} = - \vec{n} \cdot \vec{U}_\infty \quad \text{à la surface du corps.}$$

Dans le cas d'une aile portante l'exigence de circulation conduit à représenter le sillage par une feuille tourbillonnaire qui passe par le bord de fuite. La condition de Kutta et la condition que la feuille tourbillonnaire soit une surface de courant impliqueraient que la feuille tourbillonnaire soit tangente à l'une ou à l'autre des deux surfaces de l'aile. Mais dans le cas d'un corps portant (voilure + fuselage, par exemple) il n'y a aucune raison impérieuse qui fixe la position initiale de la feuille tourbillonnaire. L'interprétation de la condition de Kutta pour un corps qui n'est pas purement schématique est l'un des premiers problèmes qui se posent. L'une des hypothèses fréquemment faites consiste à dire que la feuille tourbillonnaire derrière le fuselage est le prolongement de celle qui apparaît après la voilure.

La forme de la feuille tourbillonnaire n'est pas connue a priori, de telle sorte que le problème des valeurs aux limites sur lequel on débouche n'est pas linéaire. On peut se débarrasser de cette difficulté en faisant l'hypothèse que la feuille tourbillonnaire est rigide et qu'elle a une direction bien déterminée au bord de fuite; sur chaque section dans le sens de l'envergure l'intensité et la direction du tourbillon sont prises constantes sans composante dans le sens de l'envergure.

Le problème de Neumann qui en résulte est résolu au moyen de la méthode des singularités. On peut représenter la surface de la voilure et du fuselage (par exemple Figure III-1) par un grand nombre de quadrilatères plans, dont chacun porte une distribution de sources d'intensité constante. On applique de plus un système de tourbillons en fer à cheval pour couvrir la surface de discontinuité derrière le corps, la surface de l'aile, avec la courbure correspondante, ainsi que sa prolongation à l'intérieur du fuselage. Les tourbillons en fer à cheval coïncident avec les bords des quadrilatères dans le sens de l'envergure et les tourbillons de bord de fuite coïncident avec les bords des quadrilatères dans le sens de l'écoulement. Les intensités des tourbillons en fer à cheval sont spécifiées a priori par segment en terme de circulation totale autour du segment. Ainsi la distribution tourbillonnaire complète est déterminée grâce à une inconnue par segment.

Le potentiel de perturbation φ en tout point qui ne coïncide pas avec les bords des quadrilatères peut s'exprimer en termes de singularités inconnues. Le problème de Neumann peut alors se résoudre en satisfaisant la condition aux limites (écoulement tangentiel) en un nombre suffisant de points de contrôle. Chaque quadrilatère porte un point de contrôle en son centre; et dans chaque segment sur la feuille tourbillonnaire on sélectionne un point de contrôle complémentaire (ce point est situé à une distance finie du bord de fuite et choisi dans le plan bissecteur du dièdre du bord de fuite).

L'application des conditions aux limites décrites ci-dessus conduit à un système d'équations linéaires de la forme

$$[M] \cdot \vec{m} = \vec{R},$$

où $[M]$ est la matrice dite des coefficients d'influence,

\vec{m} le vecteur des singularités inconnues,

\vec{R} le vecteur des conditions aux limites.

Ce qui s'écrit

$$\begin{bmatrix} S_b & | & V_b \\ \hline S_v & | & V_v \end{bmatrix} \cdot \begin{bmatrix} \sigma \\ \hline \Gamma \end{bmatrix} = \begin{bmatrix} R_b \\ \hline R_v \end{bmatrix}.$$

où S_b représente l'influence des sources sur les points de contrôle figurant dans les quadrilatères, S_v l'influence des sources sur les points de contrôle figurant sur la feuille tourbillonnaire, V_b et V_v l'influence des tourbillons.

Le système des matrices a les propriétés suivantes:

- Les termes dominants de la matrice S_b sont constitués par les blocs diagonaux qui représentent l'influence des sources situées sur le n^e segment sur les points-limites du même segment.
- Les termes dominants de la matrice V_b sont constitués par les blocs diagonaux qui représentent l'influence des tourbillons sur les points de contrôle des surfaces.
- etc.

L'importance de ces éléments prédominants permet de définir des méthodes itératives qui rendent la méthode actuellement opérationnelle.

Il reste alors éventuellement à effectuer sur le champ des vitesses les corrections de compressibilité, ce qui a été étudié par plusieurs auteurs (Goethert, Wilby, Küchemann, Weber . . .), ce qui peut présenter quelque difficulté si les corrections sont importantes.

3. ECOULEMENT VISQUEUX

- *Calcul de la couche limite laminaire:*

Le calcul peut être effectué dès que l'on connaît la distribution de pression; de nombreuses méthodes sont disponibles (Pohlhausen, Michel, etc.), qui donnent satisfaction à l'ingénieur.

— *Calcul du point de transition:*

La méthode la plus fréquemment utilisée est basée sur la théorie linéaire de la stabilité hydrodynamique. On calcule un facteur σ_a qui définit l'amplification des perturbations introduites dans la couche limite laminaire. La transition se situe à des valeurs de σ_a bien déterminées, et ce critère donne actuellement vis-à-vis des problèmes étudiés une assez bonne concordance.

— *Calcul de la couche limite turbulente:*

Les méthodes actuelles pour calculer l'évolution de la couche limite turbulente ont une assez bonne qualité. Mais il faut pour cela que l'on connaisse au point origine l'épaisseur de quantité de mouvement δ_2 et le paramètre de forme H . La valeur initiale de δ_2 pourrait être prise égale à la valeur de δ_2 obtenue grâce à la couche limite laminaire au point de transition, mais la valeur de δ_2 montre une diminution nette dans la phase transitionnelle. Il ne semble pas exister de très bonne relation permettant de prévoir une évolution correcte de H dans une couche limite turbulente.

— *Correction de la distribution de pression due à la couche limite:*

En première approximation, c'est le champ de l'écoulement non visqueux qui sert à calculer la couche limite. Une fois calculée l'épaisseur de déplacement δ_1 , le contour du corps portant peut être modifié en ajoutant localement une épaisseur δ_1 .

— *Phénomènes de décollement liés à la couche limite:*

Nous avons très longuement discuté l'ensemble de ces phénomènes dans la première partie. Nous avons souvent dit que les effets du nombre de Reynolds étaient assez mal connus, mais ce fait traduisait en réalité une ignorance théorique fondamentale. Il n'est pas étonnant, dès lors, que les calculs buttent sur les mêmes difficultés (par exemple évolution de la couche limite dans son interaction avec un choc) que l'interprétation des essais en soufflerie.

4. PERSPECTIVES

Dès lors, parmi tous les "modules" que comporte un programme d'écoulement aérodynamique autour d'un corps portant, certains n'apporteront aucune satisfaction au théoricien scrupuleux. Cela n'est pas grave si les ingénieurs peuvent mettre sur pied des méthodes approchées qui, dans un certain domaine assez bien délimité, leur donnent des résultats assez conformes à la réalité. Le praticien demandera en particulier à de tels schémas de calcul:

- qu'ils ne soient pas en opposition notoire avec les phénomènes physiques,
- qu'ils conduisent à des temps de calcul suffisamment courts,
- qu'ils fournissent, au moins dans un certain domaine, des résultats qui concordent avec la réalité.

La tendance est actuellement à l'accroissement du rôle des calculs dans l'évaluation des données aérodynamiques. On peut trouver à cette tendance trois raisons essentielles:

- d'une part, le développement des calculateurs modernes a permis d'appliquer des méthodes qui autrefois n'auraient pu être envisagées;
- d'autre part, on ne peut plus se permettre, dans l'état actuel de sophistication des projets, de modifier au fur et à mesure, à l'aide de la seule intuition, les maquettes essayées en soufflerie. Dès les premières phases d'un projet important, il faut aboutir à des configurations optimisées et seuls des moyens de calcul importants permettent d'atteindre ce but;
- enfin, les souffleries actuellement en service ne sont pas capables des nombres de Reynolds du vol. Le seul moyen raisonnable de tenir compte de l'effet d'échelle est d'effectuer à l'échelle maquette et à l'échelle vol les calculs correspondants d'évolution de la couche limite, en intégrant autant que possible les interactions et les décollements.

Le gros problème réside dans l'ignorance de critères significatifs relatifs à certains phénomènes apparaissant à des nombres de Reynolds élevés. Vis-à-vis des projets actuels, certaines de ces ignorances sont graves: elles ne pourront être vaincues que grâce à une masse suffisante de résultats d'études fines d'écoulements:

- soit dans des souffleries de recherche à grand nombre de Reynolds,
- soit en vol.

On peut penser qu'au vu de tels renseignements, les industriels seraient susceptibles d'introduire des critères ou des schémas de calcul, peut être peu "scientifiques", mais néanmoins efficaces pour résoudre les problèmes de l'ingénieur.

Pourtant, ne cachons pas que l'utilisation des calculs ne conduit pas à une diminution immédiate des coûts. A tel point que plusieurs industriels, qui disposaient pourtant de programmes très importants et assez opérationnels, ont récemment renoncé à les appliquer pour leurs projets de second ordre (avions d'affaires par exemple). De plus,

dans le passé proche, on peut remarquer que les projets ayant donné lieu à des calculs importants ont été aussi les plus gourmands en essais en soufflerie. Dans l'immédiat, il serait donc absurde de soutenir que la pratique des calculs réduira les essais en soufflerie (pas plus que les essais en soufflerie n'ont réduit les essais en vol). L'un et l'autre constituent des outils utiles mais imparfaits qu'il convient d'utiliser simultanément si on tient à éliminer les plus gros risques liés au développement d'un projet important.

Les spécialistes qui ressentent une forte propension à la science-fiction seraient parfois tentés de conclure au triomphe des calculs et à la disparition des souffleries dans un délai de, disons, 20 ans. C'est peut-être un délai au terme duquel des investigations assez fines et assez nombreuses des écoulements qui conviendront auront permis de résoudre la plupart des gros problèmes qui aujourd'hui apparaissent le plus clairement. Mais cette vision est optimiste et ne serait valable que si l'aéronautique ne devait pas pénétrer d'autres domaines que ceux explorés aujourd'hui. Mais de plus, il existe de nombreux problèmes pour lesquels l'investigation en soufflerie est à la fois moins coûteuse et aussi réaliste que des calculs, tout en permettant une "visualisation" et une "interprétation" parfois plus faciles.

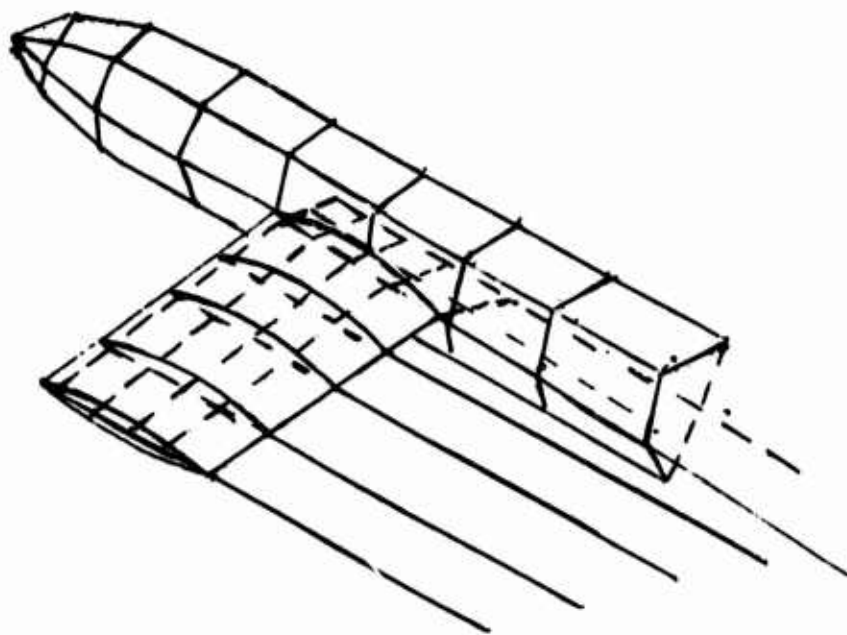


Figure III-1

MASSE D'UN AVION

(Aircraft Mass)

par

C.Vivier* et P.Cormier†

*** Ingénieur des Conventions Collectives
Section Etudes Générales
Service Technique Aéronautique
Paris, France**

**† Ingénieur de l'Armement
Section Etudes Générales
Service Technique Aéronautique
Paris, France**

TABLE DES MATIERES

	Page
<u>I – ETUDE ET PREVISION DU DEVIS DE MASSE D'UN AVION</u>	
1. INTRODUCTION	5-1
2. ETUDE DE L'EVALUATION DES MASSES	5-2
2.1 Pour le Constructeur	5-2
2.2 Le Devis de Masse	5-3
3. DERIVE DANS LE TEMPS DE LA MASSE PREVUE	5-3
4. CONCLUSION	5-5
<u>II – METHODES GENERALES</u>	
1. EVALUATION DE LA MASSE ORIGINE M_0	5-6
1.1 La Méthode	5-6
1.2 Elaboration de la Formule	5-6
1.3 Optimisation des Formules	5-7
1.4 Exemples d'Evaluations	5-7
2. DERIVE DANS LE TEMPS	5-10
3. CORRECTION DE BOULE DE NEIGE	5-11
4. OPTIMISATION	5-11
<u>III – CONCLUSION</u>	
ANNEXE 1 – MASSE – PRIX – PERFORMANCE	5-14
ANNEXE 2	5-18

MASSE D'UN AVION

C.Vivier et P.Cormier

I – ETUDE ET PREVISION DU DEVIS DE MASSE D'UN AVION

1. INTRODUCTION

1.1 L'étude et la prévision du devis de masse (M) d'un avion s'intègre dans un ensemble touchant les performances (Pf) et les prix (Px).

Les performances s'appuient essentiellement sur les caractéristiques de géométrie (aérodynamique), de propulsion et de la masse de l'avion.

Le prix, en première approximation, est proportionnel (à un coefficient de complexité près) au rapport de la masse de l'avion étudié à celle d'un avion de base, ce rapport élevé à une puissance convenable.

On constate ainsi que si la masse d'un avion donné augmente, ses performances diminuent et son prix augmente.

En raisonnant sur les paramètres Avion-Masse-Prix-Performances, on trouve une importance variable de la masse selon que l'accent est mis sur l'un ou l'autre des trois paramètres restants. L'annexe à ce texte traite cette question d'une façon détaillée.

Par exemple: la Pf est, des 4 paramètres M, Avion, Px, Pf, le plus important (par exemple un avion de transport d'une technologie avancée qui doit traverser l'Atlantique).

Le respect de cette performance impose d'abord une M maxi au-delà de laquelle on ne peut plus faire la mission. Si l'ensemble des problèmes techniques (motorisation, matériaux de structure, ...) rend le respect de cette masse difficile, il faudra chercher de nouvelles solutions: matériaux nouveaux, taux de réchauffe du moteur plus élevée, etc...

Cette recherche entrainera un Prix au kilo plus élevé, une discussion avec les Acheteurs pour le choix de leurs installations, etc....

Ainsi, il peut être important de ne pas séparer les 4 paramètres cités ci-dessus. Ce sera le cas pour une société classiquement appelée "productiviste" pour laquelle l'accent sera mis notamment sur les couples coût-rentabilité et efficacité-concurrence.

1.2 Les mathématiques ne représentent pas une arme absolue pour évaluer les masses:

- ou bien chaque pièce est calculée dès qu'il existe un assez grand nombre de dessins suffisamment précis;
- ou bien on procède par comparaison: quand il y a de nombreux renseignements, les "statistiques" sont possibles. Dix ou quinze points constituent un bon répertoire.

Quand il y a peu de renseignements, il convient d'extrapoler (ou d'interpoler).

1.3 Il y a presque toujours peu de renseignements:

- chez le constructeur la difficulté d'évaluer les masses (ou le temps dépensé pour cela) fait classer les résultats à ce sujet parmi les secrets-maison;
- chez les compagnies, le devis de masse détaillé peut être acheté avec l'avion, et seulement par les grandes compagnies: celles qui essayeront de faire des évaluations, - de même chez les militaires -;
- la concurrence entre compagnies* et la concurrence entre les constructeurs classent les masses parmi les secrets industriels - et les secrets militaires pour les militaires -. La connaissance détaillée des masses passe par la connaissance des détails de l'avion.

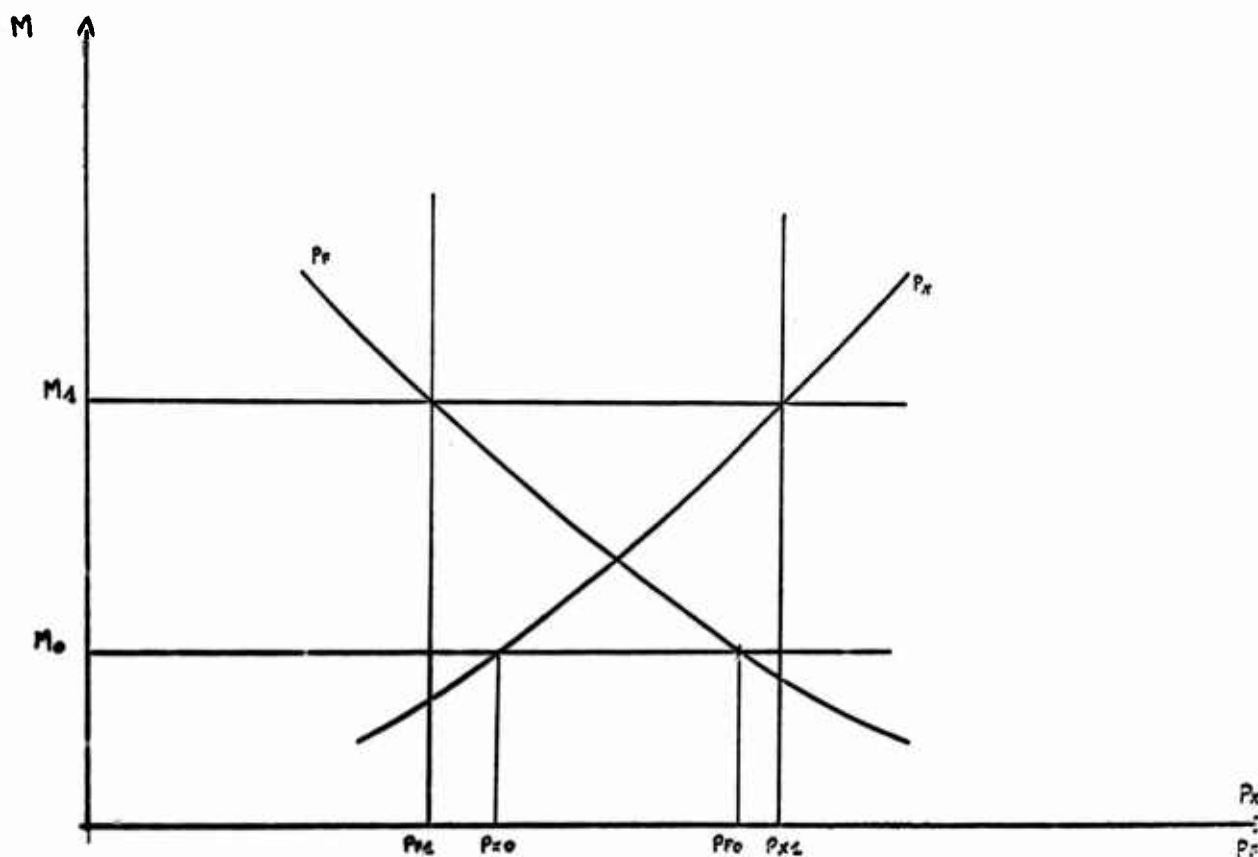
* Encore que la tendance, dans l'aviation civile, soit au groupement de techniciens des différents clients pour étudier un même avion chez le constructeur (ATLAS, KSSU).

Tout cela fait que les renseignements utilisables sur les masses des avions concurrents sont très difficiles à obtenir par un constructeur.

1.4 En plus des difficultés énumérées ci-dessus il faudra tenir compte des points suivants qui interviennent dans l'évaluation des masses:

- le constructeur: son organisation, ses méthodes et surtout son expérience;
- le type d'avion: civil, militaire et surtout si c'est une extrapolation d'un type connu (exemple Caravelle 12, Mirage F1) ou une interpolation entre plusieurs avions de types voisins (Mercure) ou bien une création ex-nihilo (Concorde, Mirage G);
- le type de l'intervention de l'Etat s'il y en a une: avion militaire ou civil, coopération internationale, appel d'offre, etc....

Quelques uns de ces points sont traités dans les chapitres suivants.



2. ETUDE DE L'EVALUATION DES MASSES

Plusieurs points sont à préciser:

- Il faut bien distinguer les différences qui existent entre l'avant-projet et le projet. L'opinion que l'on peut avoir sur la précision des résultats en dépend;
- C'est l'avion de série qui est toujours à évaluer, et non la masse d'un ou deux prototypes;
- La conclusion de l'étude aboutit à une première estimation M_0 dite "point d'origine". Les chapitres suivants traitent des modifications que peut subir ce "point" avant la délivrance du certificat de navigabilité (ou la pesée de l'avion représentatif de série) ou la réception de l'avion militaire.

2.1 Pour Le Constructeur

L'étude du devis de masse est étroitement liée à:

- son organisation:

En France, l'organisation du bureau des masses a longtemps varié considérablement avec le constructeur et le type d'avion.

Jusqu'à la construction de gros avions civils, il n'y avait pas de "bureau des masses". Ce problème était traité par les ingénieurs polyvalents du bureau d'étude, puis par ceux du bureau de calcul quand l'avion était réalisé.

Cette position, valable pour les petites affaires au regard de l'aviation moderne, est difficile à partir d'une certaine taille, soit de l'avion, soit du constructeur (nombreux types d'avions, grosses séries).

On trouve le même schéma d'organisation des masses aux USA et en Europe pour les grands constructeurs:

- Bureau des masses indépendant des bureaux d'études et des calculs;
- Ingénieur expérimenté responsable devant l'ingénieur chef du projet;
- Personnel qualifié et plus ou moins nombreux constituant le bureau;
- Emploi d'ordinateur pour la gestion des masses et le calcul.

– *son expérience:*

Les difficultés passées doivent convaincre les constructeurs de la nécessité d'une étude suivie des problèmes posés par l'évaluation des masses. Si l'avion étudié s'écarte trop des anciennes réalisations, le besoin des *données essentielles* à l'évaluation des masses apparaît, soit:

- renseignements nombreux, précis, modernes et sûrs;
- études pendant plusieurs années de l'influence sur les masses des paramètres évolutifs (vitesse de croisière, durée de vie, taille d'avion, etc...).

Si l'avion est simplement extrapolé d'une série bien connue (Mirage F1 par exemple), il ne pose pas de problèmes.

– *ses méthodes:*

Les "statistiques" de tel ou tel constructeur étranger n'ont qu'une valeur indicative: trop de raisons permettent de douter de leur exactitude. Par contre celles du constructeur dépendent essentiellement de ses réalisations antérieures.

Les méthodes du constructeur dépendent donc étroitement des deux points précédents: organisation et expérience. *

2.2 Le Devis de Masse

Il s'agit d'abord d'essayer de connaître l'avion avec le plus de détails possibles et sous tous ses aspects (structure, propulsion, systèmes). C'est le niveau du détail, ou de définition, qui classera l'avion comme avant-projet ou projet.

Comme avant-projet, aucun dessin de détail n'existe, la seule arme d'évaluation des masses est la comparaison globale, la "statistique".

Au niveau projet, les dessins se sont multipliés, les études sont devenues plus sérieuses et réalistes, la *définition* de l'avion plus précise. Les comparaisons de détails commencent à pouvoir se substituer aux "statistiques".

Le devis de masse obtenu est celui d'un avion qui dépend de la définition du moment:

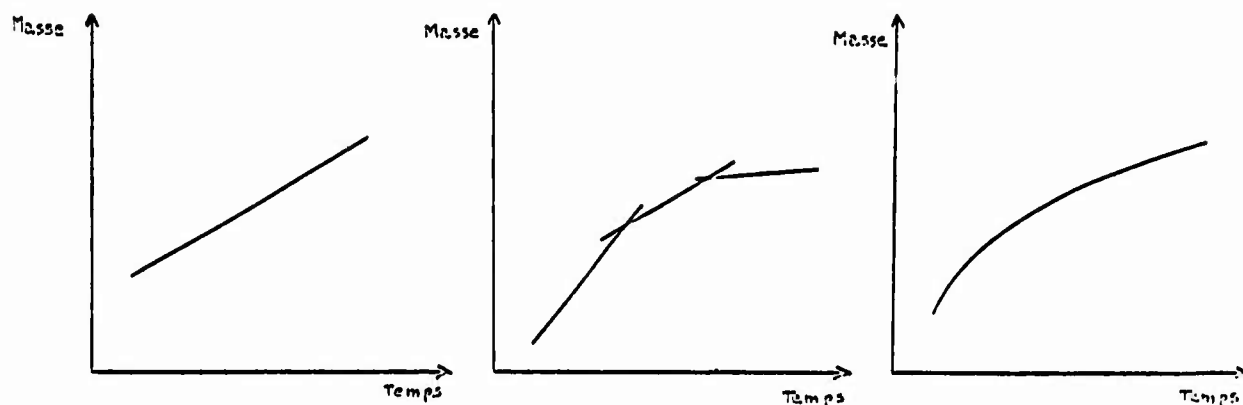
- objectif fixé pour les performances;
- options techniques pour les réaliser, et son bouclage (voir Introduction) sur l'évaluation des prix.

L'analyse constante des paramètres essentiels de l'avion donne à la masse un aspect *mouvant*. Bien des choses vont se passer *avant la pesée de l'avion de série*: cet aspect est traité au chapitre suivant. Une dérive toujours dans le sens de l'augmentation, va être enregistrée. Il est donc essentiel d'essayer de *fixer* le point M_0 à partir duquel cette augmentation, elle-même évaluée, sera applicable.

3. DERIVE DANS LE TEMPS DE LA MASSE PREVUE

3.1 L'histoire de tous les avions entre le moment où la masse est évaluée au stade de projet et la pesée du No.1 de série (ou représentatif de série) se traduit par une augmentation de la masse estimée en fonction du temps.

Comme ce sera vu ci-dessous, cette dérive peut être imagée de la façon suivante:



Les paramètres influant sur cette dérive sont très nombreux et souvent différents d'un avion à l'autre. Ce sont notamment:

- avion dérivé d'un autre avion connu ou absolument nouveau;
- précision de l'évaluation d'origine;
- qualité de la gestion des masses pendant la réalisation;
- rapidité d'intervention en cas de dépassement;
- programmes nationaux ou internationaux;
- date de sortie de l'avion de série (délai de réalisation);
- mise au point: problèmes de structure (essais), de vibration;
- demandes nouvelles (Etat-Major, compagnie ou réglementation);
- etc

3.2 Le choix de cette dérive au stade de l'évaluation est importante et délicate.

- importante parce qu'elle complète l'évaluation, quelque soit le soin apporté à définir la masse de "l'avion", dans sa définition, ses choix techniques, ses objectifs commerciaux ou opérationnels, *du moment*, les raisons du paragraphe 3.1 montrent que cette masse va augmenter.

Rappelons que la masse du premier avion de série (ou représentatif de série) est l'objectif de l'évaluation au stade du projet. Celle des avions intermédiaires (prototype et présérie) n'ont qu'une valeur indicative pour cet objectif.

- délicate parce que d'une part chaque avion construit en série a eu une dérive des masses différente, et on ne peut retenir pour les évaluations qu'une valeur moyenne. D'autre part il a été vu dans le chapitre précédent que le point à partir duquel la dérive sera appliquée est lui-même délicat à fixer.

En fait les deux opérations: évaluation de la masse à l'instant T_0 et évaluation de la dérive, sont étroitement liées.

- l'avion qui part vraiment de rien, se verra appliquer la dérive maximum compatible avec l'ensemble des paramètres *choisis* comme importants (délais, coopération internationale, par exemple).
- l'avion qui bénéficie déjà d'une expérience ou d'une longue étude ne devrait avoir qu'une faible dérive.
- enfin, cette dérive peut n'être envisagée que comme une raison de *prendre des marges*, et dans ce cas on prend des marges sur la masse M_0 , mais sans dérive. C'est ici que le terme évaluation prend tout son sens. En fait le travail du spécialiste des masses consiste à *choisir*, parmi la multitude des paramètres pouvant intervenir sur le résultat, ceux que son étude et son expérience lui suggèrent de retenir.

3.3 Un cas particulier se présente parfois. C'est l'application de cette dérive pendant la réalisation de l'avion, dans le cas d'un avion complexe et construit pendant de nombreuses années.

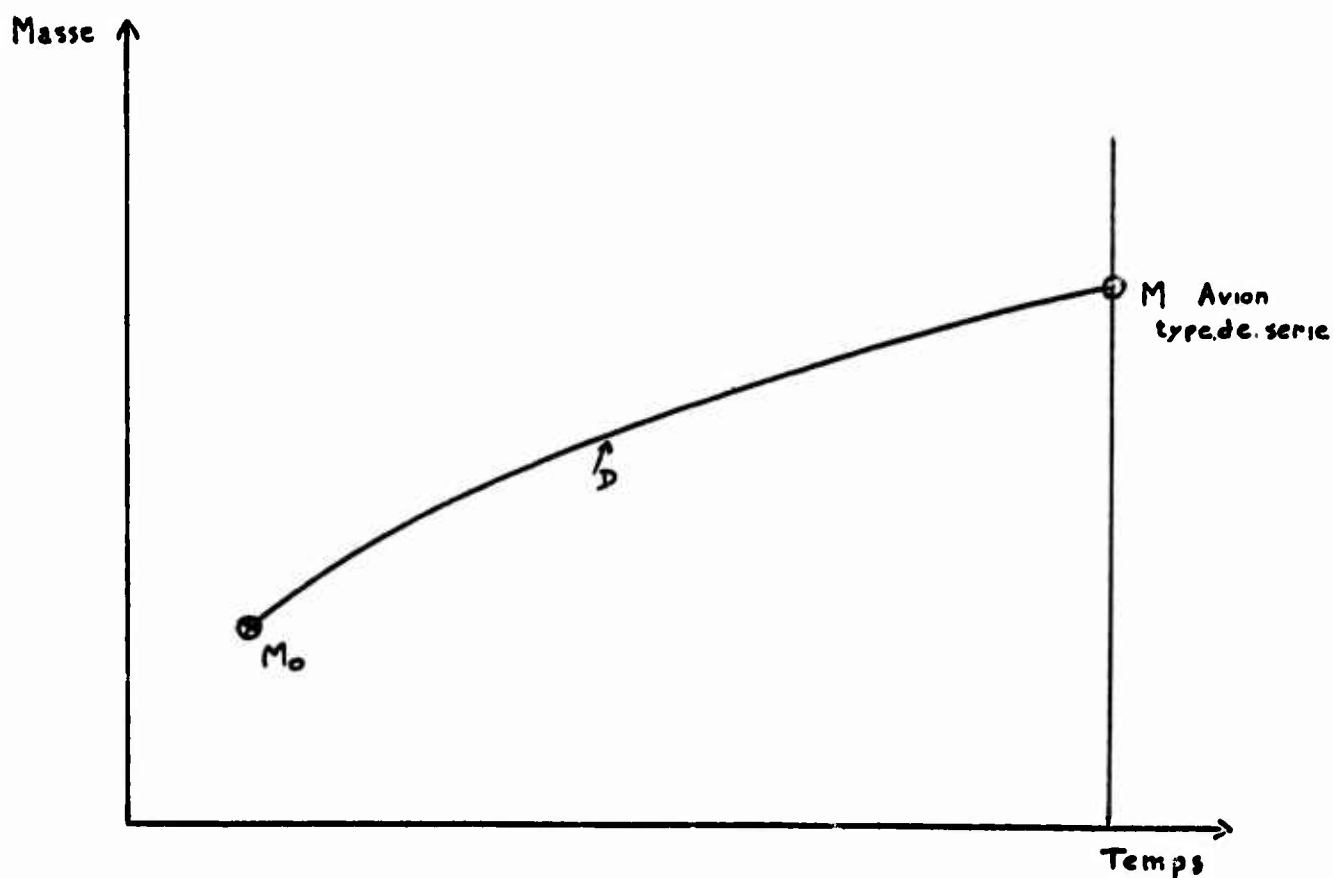
Quand l'avion n'est pas suffisamment avancé, la méthode est la même qu'au stade de l'évaluation Trop peu de données permettant d'appliquer une courbe de dérive très élaborée et très sûre.

Quand l'avion est assez avancé dans sa réalisation, il est possible et souhaitable d'extrapoler les points connus. Le problème se déplace sur les "méthodes" d'extrapolation.

4. CONCLUSION

Pratiquement on peut opérer de la façon suivante pour évaluer la masse d'un avion représentatif de la série.

1. Fixation du point origine M_0 .
2. Fixation de la dérive D . Celle-ci est appliquée à M_0 . D'où la masse M cherchée de l'avion représentatif de série à la date évaluée de son premier vol.
3. Il est possible également de transformer la courbe abstraite D en valeurs concrètes de masses réparties dans le devis. Le point M est alors obtenu par addition au point M_0 de différentes marges appliquées sur les chapitres où il y a le plus d'incertitudes.
4. Enfin, l'importance du point M , comme il a été indiqué en introduction, impose généralement une certaine discrétion. Notamment, calculateurs et dessinateurs se verront "attribuer" pour leurs pièces une masse dite "cible", inférieure à la masse évaluée réellement. La valeur psychologique de cette façon de faire semble démontrée.



II – METHODES GENERALES

1. EVALUATION DE LA MASSE ORIGINE M_0

1.1 La Méthode

La méthode de l'évaluation de la masse M_0 dépend:

- du stade d'avancement de l'avion (avant-projet, projet, développement);
- du type de l'avion (avion unique en son genre, avion comparable à d'autres).

La précision est directement liée à la méthode. Elle sera:

- médiocre au stade avant-projet, où l'on utilisera par exemple des pourcentages de masse au décollage;
- moyenne au stade projet, avec des formules de plus en plus élaborées;
- bonne pendant le développement, avec des comparaisons analytiques.

1.2 Elaboration De La Formule

Paramètres:

il faut rechercher des paramètres bien choisis et bien connus

- Il y en a peu en avant-projet.
- Il y en a trop en développement.
- Exemple de problèmes: sur la voilure.

Beaucoup de Paramètres:

$$W = k(nM)^{\alpha} s^{\beta} \lambda^{\gamma} (1 + E)^{\delta} \left(\frac{1}{e_r}\right)^{\epsilon} + \Delta M ;$$

erreurs: -23 à +33% sur 21 avions bien connus dans les 10 dernières années.

$$W = k(nM)^{\alpha} \left(\frac{b^2}{s \cos^2 \phi}\right)^{\beta} s^{\gamma} \left(\frac{1 + F}{2e_r}\right)^{\delta} (1 + V)^{\epsilon} + \Delta M ;$$

erreurs: -30 à +40%.

Paramètres Mal Connus:

$$W = k s^{\alpha} b (ZFW)^{\gamma} + \Delta M ;$$

erreurs: -65 à +60%.

••• Conclusions:

- (i) Ces formules sont sans doute bonnes pour ceux qui les ont mises au point ... mais pas pour les autres;
- (ii) La sensibilité de la formule à certains paramètres mal connus (ex. e_r et V_D) est mise en évidence;
- (iii) On remarque qu'à chaque poste il y a un $+\Delta M$: le calcul de cette "correction" de masse est souvent malaisé. De plus ce ΔM peut contenir à nouveau certains paramètres de la formule. D'où le gros danger de dériver la formule pour une optimisation.

Allure De La Formule:

la formule peut contenir autant de paramètres voulus s'ils sont bien choisis et connus.

Par contre cette formule doit avoir *peu* de coefficients.

- Etalonnage de la formule: par optimisation (sur avions bien connus). La méthode d'optimisation est limitée par le nombre d'avions et de coefficients.
- Deux objectifs sont possibles:
 - (i) soit exclure les particularités (" ΔM ") et optimiser sur le reste: avec l'espoir d'évaluer à part le ΔM ;
 - (ii) soit inclure les particularités dans la statistique: sans l'espoir d'évaluer séparément la variation de masse ΔM due aux particularités de chaque avion.

1.3 Optimisation Des Formules

L'objectif est d'évaluer l'avion étudié avec l'erreur *minimum*.

La conséquence est un *choix* parmi les paramètres qui rendent compte "exactement" de la masse.

En effet:

- Il y a toujours une *erreur*:

- si tous les paramètres sont supposés connus, l'avion se fabrique à l'intérieur de certaines "tolérances".
 - tolérances d'usinage
 - tolérances de densité des métaux
 - tolérances des tôles non usinées
 - tolérances sur les protections (peintures, PR, ...)
 - etc ...

Environ $\pm 0,5\%$.

- On se fixe une erreur acceptable au-delà de laquelle notre formule sera considérée comme mauvaise (à rattacher au stade d'avancement de l'avion).

Cette erreur comprend: tolérances

mise au point	$\left\{ \begin{array}{l} \text{essais} \\ \text{matériaux} \\ \text{maîtrise des masses} \end{array} \right.$
évolution de l'avion	$\left\{ \begin{array}{l} \text{performances} \\ \text{demandes utilisateurs} \\ \text{réglementation} \end{array} \right.$

- de nombreux paramètres sont inconnus et leur nombre varie selon le stade d'avancement d'un avion donné:

ex.: au stade projet les dessins définitifs de la structure n'existent pas;

- les charges sont approximatives;
- les calculs en statique, vibrations et avion souple comportent des inconnus;
- les calculs en fatigue sont impossibles pour l'essentiel;
- etc ...

- un choix est ainsi nécessaire parmi les paramètres accessibles.

Ce choix commence par un tri des paramètres déterminants qui se fait avec:

- le bon sens;
- des méthodes mathématiques.

1.4 Exemples D'Evaluations

1.4.1 Devis avec Pourcentages (voir le tableau à la page suivante)

1.4.2 Devis avec Formules Simples

A. Planeur

A1	$0,05 \left(\frac{nM_{hs}}{c \cos \phi} \right)^{2/3} + \Delta M_v$	base: M.Burt (RAE) n = facteur de charge extrême
A2	$0,43 (nM\phi_m L_f)^{0,44} + \Delta M_f$	ϕ_m = diamètre maxi
A3	$0,26 \left(M_v \frac{l}{L_H} \right)$ $+ 0,14 \left(M_v \frac{l}{L_v} \right) + \Delta M_E$	M_v = masse voilure l = corde de référence voilure L_H = bras de levier des empennages
A4	$0,00012 nML_f + \Delta M_{hyper}$	L_f = longueur de fuselage
A5	$0,015 v_z M_{atterrissage} + \Delta M_T$	v_z = vitesse verticale
A6	$0,06 T + \Delta M_N$	T = poussée réacteur (en N).

1.4.1

	% M _{déco}		Erreur en %		Observations
	Civils	Militaires	Civils	Militaires	
A. Planeur	33	33	±13	±25	On remarque que la grossièreté de la méthode permet tout de même d'obtenir les gros postes avec une erreur qui peut être acceptable dans un certain état d'avancement du projet. Ceci peut être obtenu extrêmement rapidement avec une liste de renseignements suffisante.
A1. Voilure	11,5	11,5	±15	±20	
A2. Fuselage	11,5	12,5	±20	±25	
A3. Empennages	2,4	2	±20	±25	
A4. Cdes de vol	1,8	2	±40	±25	
A5. Train	4,5	5	±20	±15	
A6. Nacelles	1,3	0	±20		
B. Propulsion	9	11	±30	±25	
B1. Moteurs installés	8	10	±20	±20	
B2. Circuits combustible	0,5	1	±50	±35	
B3. Inconsommables	0,2	0,2	±50	±50	
C. Aménagements toutes missions	10	10	±30	±30	
C1. Servitudes	4	4	±30	±30	
C2. Habitabilité	5	5	±20	±50	
C3. Pilotage-Nav.	1	1	±50	±50	
C4. Transmissions					
C5. Installations Opérationnelles					
C6. Lot de bord					
MASSE A VIDE	56	56	±20	±20	
D. Aménagements suivant mission					
Masse à vide équipée	59	59	±20	±20	
E. Equipage					
Masse à vide en ordre d'exploitation	60	60	±20	±20	
F. Combustibles et lubrifiants					
G. Charges variables					
MASSE TOTALE au Décollage					

1.4.2 (continué)

B. Propulsion

- B1 0,2 kg/daN de poussée + ΔM_m
 B2 0,05 kg de fuel + 0,002 T + ΔM_c
 B3 0,12 (kg de fuel)^{2/3}.

C. Aménagements

- C1 0,02 M_{décollage} + 3 kg/pax pour avion de transport
 0,04 M_{décollage} + 3 kg/pax pour avion de combat
 C2, C3, C4 Par analyse

- C5 En kg/pax pour avion de transport
 Par analyse pour avion de combat
- C6 Constante.
- D. *Aménagements* Par analyse. Par exemple: $\left[\begin{array}{l} 10 \text{ kg par siège} \\ 5 \text{ kg par passager pour} \\ \text{le commissariat} \\ \text{etc ...} \end{array} \right.$
 suivant missions
- E. *Equipage*
 M.V.O.E.

Ces formules, données en exemple, peuvent permettre un évaluation des masses moins grossière qu'un pourcentage. Elles sont cependant encore à utiliser en étroite liaison avec l'erreur obtenue sur d'autres avions de masses connues.

1.4.3 Formules plus Elaborées

Comme indiquée ci-dessus, l'évaluation du point M_0 peut se faire avec une relative bonne précision. La connaissance que l'utilisateur a de formules relativement élaborées et par lui optimisées est très importante.

Exemple:

Voilure: C'est la partie structurale la plus facile à évaluer. On peut séparer la structure;
 en parties principales (le caisson);
 en parties secondaires (bord d'attaque, bord de fuite et parties mobiles).

- (a) Pour le caisson: Une fois le tri fait pour les renforts "locaux" (renforts pour le train, pour les fixations de mâts, etc ...) afin de comparer valablement.
 les voilures de différents avions, le caisson peut être envisagé comme une poutre encastree.
 Cette poutre reprend les moments de flexion et de torsion et les efforts tranchants introduits par les charges aérodynamiques.

A partir d'une formule dans laquelle on aura retenu comme paramètres essentiels:

le facteur de charge: n ;
 la masse associée à n : M pour le cas déterminant du calcul de la voilure;
 l'envergure: b ;
 la surface plane de référence: S ;
 l'épaisseur absolue à l'emplanture: e ;
 la flèche ϕ ;
 le dièdre ψ ;

d'où la formule:

$$k_1 \left(\frac{nMbs}{e} \right)^\alpha \left(\frac{1}{\cos \phi} \right)^\beta \left(\frac{1}{\cos \psi} \right)^\gamma = M_{V_1} .$$

La masse M_{V_1} obtenue est la masse d'une voilure V_1 trapézoïdale d'épaisseur relative constante.

Une correction est nécessaire dans le cas de voilure V_2 de géométrie plus complexe, notamment d'épaisseur relative variable en envergure. Cette correction se fait en comparant les Moments de flexion de la voilure V_1 à ceux de la voilure V_2 .

Cette formule optimisée sur 15 avions de 10 à 150 tonnes au décollage aboutit à une dispersion de +3%.

- (b) Pour le reste de la voilure: une méthode identique est applicable, en tenant compte de plus de l'hypersustentation.

1.4.4 Ainsi, pour une évaluation beaucoup plus précise, chaque poste (voilure fuselage, électricité, etc ...) devra faire l'objet d'une étude particulière.

D'où sortira le point M_0 .

2. DERIVE DANS LE TEMPS

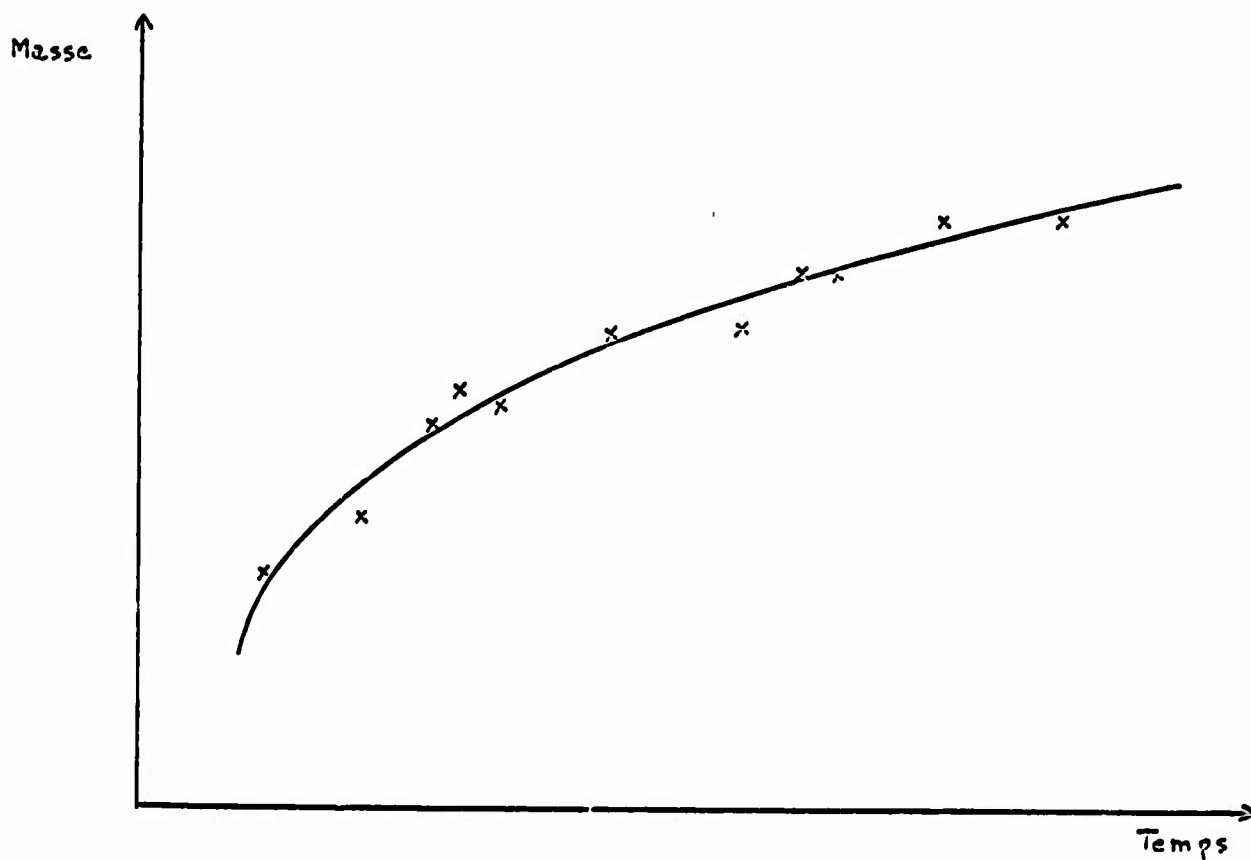
2.1 *En première approximation*, la loi de croissance peut se représenter par une droite. Voici quelques exemples de pentes notées sur les avions français bien connus du STA, pour la masse à vide équipée (MVE), à partir des devis de masse fournis par les constructeurs:

- avions militaires: 3,4% de la MVE par année de construction
 (3 exemples) 6 %
 1,3%
- avions civils: 4,25%
 (2 exemples) 6,6%

Beaucoup de dérives d'avions possèdent deux pentes: prototype et série (toujours avant la pesée du No.1 série).

- avions militaires: 5,9% entre le projet et le prototype et 0%
 (3 exemples) entre le prototype et le No.1 de série.
 7 % et 4%
 2,9% et 1%
- avions civils: 8 % et 0,7%.

Avec une analyse plus fine, l'évolution est plus complexe et présente l'aspect ci-dessous:



2.2 Le tracé à la main est souvent insuffisant. De plus, l'impartialité de cette méthode est souvent contestable.

Il convient donc d'étudier les méthodes mathématiques de lissage de courbe.

2.3 Différentes méthodes de lissage de courbes peuvent être utilisées:

1. *Moindres carrés*: on sait que cette méthode consiste à lisser une courbe de telle sorte que la somme du carré des erreurs commises soit minimum.

Malheureusement cette méthode n'est applicable qu'à des fonctions linéaires ou pouvant être mises sous cette forme.

2. *Autres méthodes*: Le problème particulier du traitement de points représentant des masses fonction du temps conduit à imaginer d'autres méthodes.

Notamment, ce problème concret doit être résolu avec des fonctions mathématiques où apparaît une asymptote (la masse de l'avion No. 1 de série).

Dans le même esprit, ces fonctions doivent pouvoir s'adapter à la forme particulière, constatée par expérience, des courbes passant au milieu des points $M =$ fonction de (t) .

Par exemple, des fonctions exponentielles semblent pouvoir répondre à ces impératifs.

3. CORRECTION DE BOULE DE NEIGE

3.1 Généralités

Au cours de l'évaluation des masses, il peut arriver qu'une masse Δm s'ajoute au Zéro Fuel Weight (ou ZFW = masse de l'avion vide de pétrole).

Cette masse Δm peut être:

- une erreur d'estimation initiale,
- une modification apportée à la structure (suite aux essais par exemple),
- une modification due à la propulsion ou aux systèmes,
- une variation de charge marchande ou des aménagements commerciaux,
- une erreur dans la gestion des masses, etc.

Quelle que soit la raison qui conduit à cette augmentation de masse Δm initiale celle-ci entraîne la plupart du temps à d'autres modifications.

La correction de boule de neige consiste à déterminer l'influence de Δm sur la masse au décollage, c'est-à-dire à calculer le ΔM_d décollage soit ΔM_d dû au Δm . Le coefficient de boule de neige est alors défini par

$$\frac{\Delta M_d}{\Delta m},$$

3.2 Mise en équation du problème

Pour fixer les idées nous supposons que le but est de respecter une performance.

Cette performance peut s'écrire comme étant une relation entre le ZFW et M_{deco} soit $g(\text{ZFW}, M_{\text{deco}}) = 0$ (1).

Différencions la relation (1)

$$\frac{\partial g}{\partial \text{ZFW}} \Delta \text{ZFW} + \frac{\partial g}{\partial M_d} \Delta M_d = 0$$

et posons

$$K = \frac{\frac{\partial g}{\partial M_d}}{\frac{\partial g}{\partial \text{ZFW}}}$$

$$\Delta \text{ZFW} = K \Delta M_d. \quad (1')$$

La définition du devis de masse nous donne la relation entre M_d , ZFW; et C masse de carburant:

$$M_d = \text{ZFW} + C \quad (2)$$

soit en différenciant

$$\Delta M_d = \Delta \text{ZFW} + \Delta C. \quad (2')$$

Le calcul du devis de masse de l'avion nous montre que le ZFW est fonction de M_{deco} , de C et de toute masse "m" pouvant varier pour une raison quelconque. On a donc la relation

$$\text{ZFW} = f(m, M_d, C). \quad (3)$$

En différence il vient:

$$ZFW = \frac{\partial f}{\partial m} \Delta m + \frac{\partial f}{\partial M_d} \Delta M_d + \frac{\partial f}{\partial C} \Delta C . \quad (3')$$

Posons

$$\frac{\partial f}{\partial m} = \lambda, \quad \frac{\partial f}{\partial M_d} = \mu, \quad \frac{\partial f}{\partial C} = \nu$$

$$\Delta ZFW = \lambda \Delta m + \mu \Delta M_d + \nu \Delta C . \quad (3'')$$

Nous avons donc le système

$$\begin{aligned} \Delta ZFW &= K \Delta M_d \\ \Delta M_d &= \Delta ZFW + \Delta C \\ \Delta ZFW &= \lambda \Delta m + \mu \Delta M_d + \nu \Delta C . \end{aligned}$$

On en déduit

$$\frac{\Delta M_d}{\Delta m} = \frac{\lambda}{K(1 + \nu) - (\mu + \nu)} \quad (R)$$

λ représente le coefficient d'influence de Δm sur le ZFW.

μ représente la répercussion structurale due à une variation de M_d .

ν donne donc les répercussions sur le ZFW d'une augmentation de carburant.

4. OPTIMISATION

4.1 Optimisation des formules d'évaluation des masses: ce qui précède a montré le danger qu'il y a d'espérer un résultat précis au stade du projet en dérivant une formule, quand cela est possible.

Il y a en effet une erreur systématique, aggravée par la nécessité de faire un choix parmi les paramètres.

4.2 Optimisation de l'avion autour du paramètre masse: l'évaluation de la masse étant supposée résolue, il se pose encore le problème de l'optimisation de l'avion.

De nombreux paramètres pouvant intervenir dans cette opération, ce sujet sera abordé à l'aide d'un exemple, (page 5.13).

Ce graphique relie les paramètres suivants:

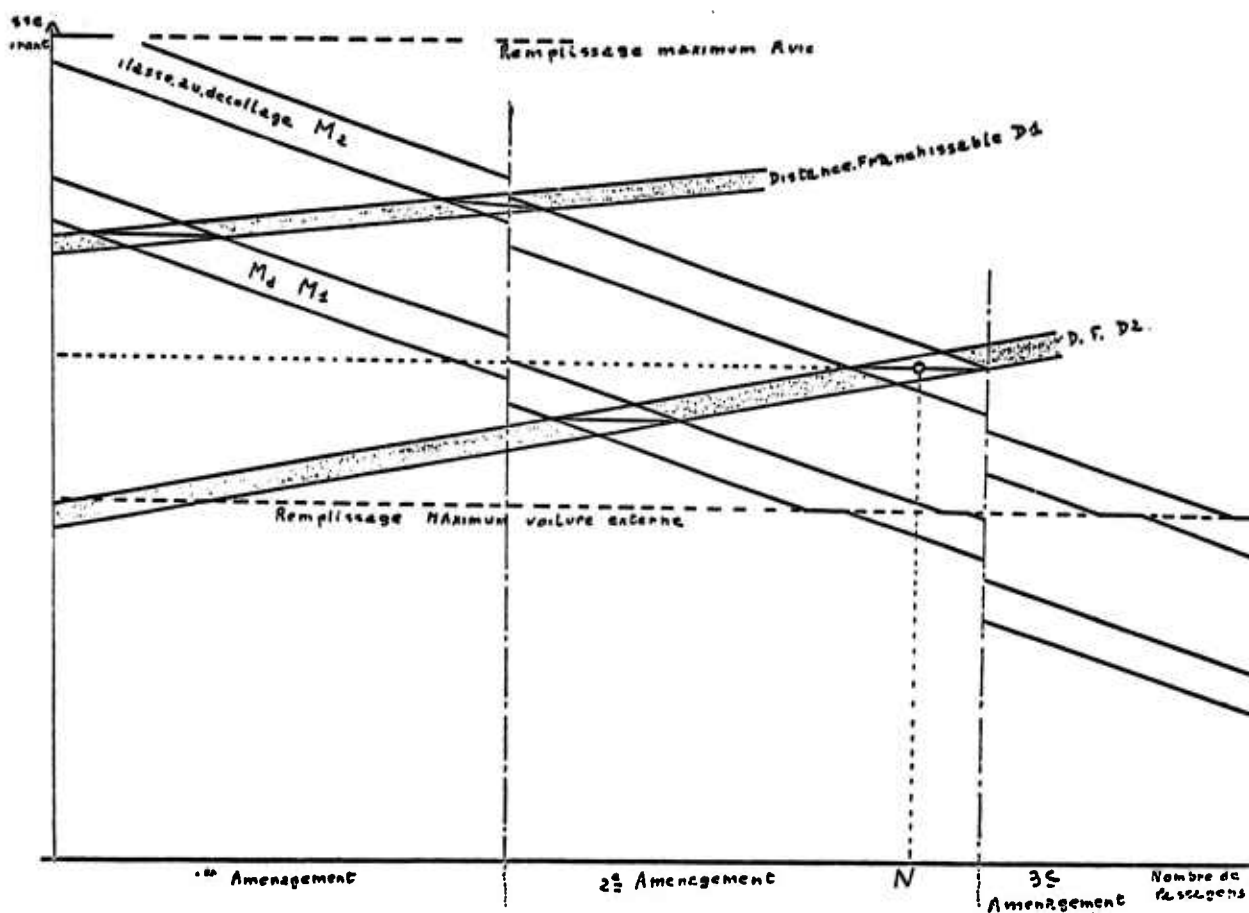
- masse de carburant;
- masse au décollage;
- aménagement: en passagers;
 en structure et aménagements de fuselage;
 en réservoirs de carburant;
- nombre de passagers;
- distance franchissable.

Cherchons par exemple la masse au décollage et l'aménagement complet (nombre de passagers maximum et modifications éventuelles du fuselage) pour obtenir un nombre de passagers maximum sur une distance franchissable choisie, toutes choses égales par ailleurs.

Pour la masse au décollage M_2 et l'aménagement No. 2 on obtient le nombre de passagers N (maximum) sur la distance franchissable D_2 .

4.3 Conclusion: il n'existe pas de méthode générale d'optimisation où la masse intervient:

- l'optimisation de la formule d'évaluation, quand elle est faisable, doit se faire avec prudence;
- l'optimisation de l'avion quand la masse intervient ne peut se faire qu'en examinant chaque cas particulier.



III - CONCLUSION

En dehors de l'important problème de l'interdépendance de la masse avec les prix et les performances, de nombreuses raisons font que la question de l'évaluation des masses d'un avion et de son optimisation se prêtent mal à l'exposé théorique.

Parmi ces raisons:

- les renseignements nombreux et précis difficiles à obtenir;
- le traitement de ces renseignements avec des méthodes exactes, paraît essentiel.

Ceci implique la *plus grande prudence* (sinon un interdit pur et simple) dans l'optimisation de formules d'évaluation des masses.

Il n'en reste pas moins que l'expérience traditionnelle, alliée à l'imagination d'un calculateur compétent, peut résoudre le problème de l'évaluation des masses d'un avion et de son optimisation avec une précision satisfaisante.

ANNEXE 1

MASSE-PRIX-PERFORMANCE

OBJET

Il s'agit d'essayer de substituer à l'étude "linéaire" des 3 critères fondamentaux masse-prix-performance une analyse "structurale", dans le sens défini ci-dessous.

METHODE

La méthode, calquée sur les principes énoncés dans "la Structure Absolue" de Raymond Abellio (voir Annexe 2), utilisera les principes suivants:

- dans le champ des critères masse-prix-performance on peut faire apparaître deux fois deux pôles;
- chaque paire de pôles se situant sur un axe, la mise en croix des deux axes schématise l'ensemble de l'analyse.

POLES ET AXES

- L'axe vertical est l'axe Avion-Masse: le mot Avion couvrant l'ensemble des caractéristiques physiques qui fait l'avion.

Par analogie avec les méthodes générales, cet axe se veut celui de l'"objet", de la quantité, de l'exécution.

- L'axe horizontal est l'axe Performances-Prix. C'est celui du "sujet", de la qualité, de la gestion.

La notion de masse dépasse déjà celle de l'objet avion mais y est physiquement liée. Passés au stade concret de la réalisation, ces deux pôles sont étroitement interdépendants.

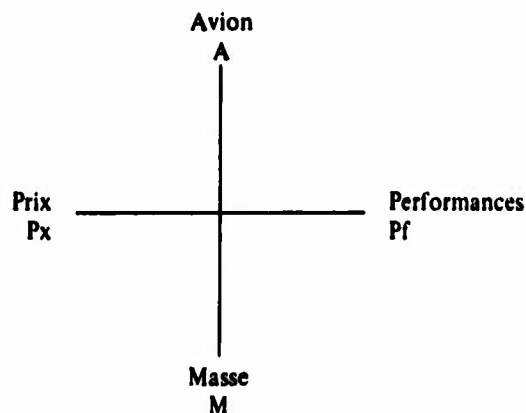
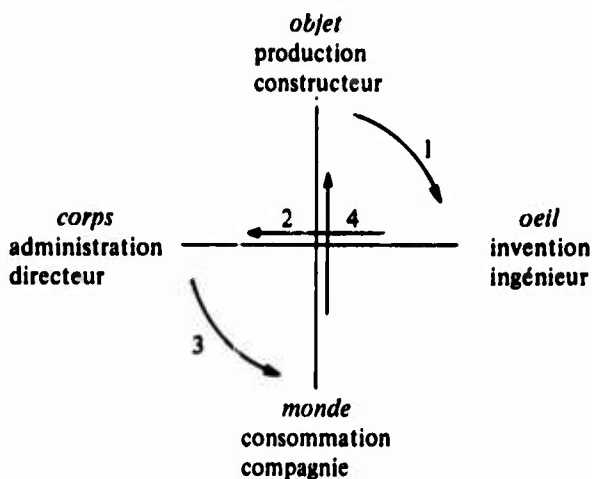
Les Performances et les Prix se situent dans un autre ordre d'idées que l'Avion et les Masses. Les premières s'attachent à la forme et à l'utilité de l'objet et dépasse donc l'objet: à charge marchande différente, on peut imaginer deux avions très différents ayant les mêmes performances. Les secondes s'attachent à la matière de l'objet, en qualité et quantité, et le dépassent aussi.

On note que les Performances s'appuient surtout sur l'Avion, tout en dépendant des masses, les Prix s'appuyant surtout sur les Masses, tout en dépendant de l'Avion. Ceci rend "préférentielle" la rotation dans le sens des aiguilles d'une montre (voir ci-après).

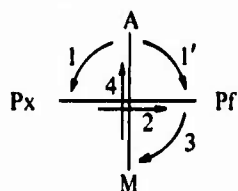
On étudiera chacun des pôles comme ayant un caractère prééminent, le caractère du pôle opposé étant récessif.

DEVELOPPEMENT

La méthode consiste à dynamiser les deux axes en quadrature en disant qu'un des pôles "active" le pôle voisin. Par exemples:



On peut ainsi envisager les cas suivants:



L'avion a le caractère prééminent. Si ce fait détermine d'abord le prix, nous avons le schéma 1: l'avion est fait, quel qu'il soit — pour des raisons non envisagées ici, par exemple parce qu'il faut produire —, mais on mettra en avant un prix compétitif. PF et M apparaissent comme des causes secondaires, sous-produits d'impératifs "supérieurs"; l'un et l'autre seront donc adaptés "à la demande" de l'avion.

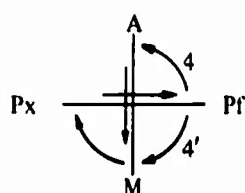
Dans le sens 1', c'est la PF qui sera présentée comme le fait important. L'A y sera provisoirement adapté après un circuit Pf-Px, Px-M, M-A. Par exemple on voudra faire un avion court-courrier, avec d'excellentes performances en croisière et à basse vitesse.

Dans les deux cas, la circulation opposée existe simultanément mais en caractère récessif. Simplement il y a toujours un caractère dominant selon le moment ou l'interlocuteur (aide pécuniaire de l'Etat, campagne commerciale, etc...).

Dans ces deux cas également, la masse n'apparaît qu'au 3ème mouvement: le bouclage sur l'avion sera ce qu'il sera. Toute modification de ce paramètre sera justifiée après coup. Le produit de ces rotations se situe sur un axe perpendiculaire aux deux autres, en ce sens qu'à la fin du mouvement 4, si la M a encore une influence sur l'A il faudra se placer dans une autre sphère, avec chacun des 4 paramètres différents. Ce seront "les différentes versions" de l'A ou ses "développements ultérieurs".

Ce schéma est du type du Mercure, Airbus et de plusieurs avions d'affaire de masse supérieure à 5,7 t (Hirondelle, Mystère XX, Mystère X).

La PF a le caractère prééminent: il s'agit par exemple de faire l'étape minimum pour laquelle l'A est fait.



Si cela détermine l'A d'abord (sens 4), tout sera fait pour agrandir les réservoirs, augmenter la finesse et diminuer la traînée, augmenter la poussée des réacteurs, etc. Mais aussi (2ème mouvement) la M prend déjà une grosse importance: la technologie sera très poussée, et la technique de connaissance des masses également.

Quant aux prix, ils seront ce qu'ils seront, comme une simple constatation.

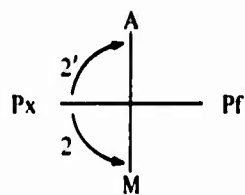
Dans le sens 4', la "guerre des masses" est directement déclenchée, dans la sphère où sera situé le problème directement après celle où l'on aura, après un bouclage complet, constaté l'insuffisance des PF (c'est-à-dire avec un certain retard). L'A sera modifié, à l'intérieur de son volume au moins, selon les choix technologiques (matériaux légers) ou commerciaux (moins de charge marchande, aménagement 1ère classe, etc...). Les Px seront regardés, en passant, avant de boucler sur les Pf.

Ce schéma est du type du Concorde et de la plupart des avions militaires (Mirages).

Là encore le sens de rotation opposé existe simultanément. On peut dire encore par exemple que si 4 est plus important que 4', c'est non seulement la constitution de l'A qui s'active mais sa "forme" apparente. En ce sens l'esthétique n'est pas indifférente, l'apparence console et est largement diffusée aux gens qui ne peuvent pas connaître la réalité. Le circuit A-M, M-Px et surtout Px-Pf (le dernier est réservé et quasi-ésotérique: c'est aussi le cas du circuit contraire 4' (choisi dans cet exemple "moins important").

Si 4' est le caractère prééminent, c'est le "fond" qui est mis en cause, ou l'éthique de l'A. On essaie de saisir la réalité dans un cercle restreint de spécialistes. L'exotisme sera l'A présenté sous une forme journalistique. Les Px annoncés comme raisonnables et nécessaires et les Pf comme révolutionnaires. Pendant ce temps 4 (caractère récessif) occupera quelques journalistes spécialisés ou des conseillers: leurs publications feront scandale et renverseront à nouveau le sens des rotations.

Le Px a le caractère prééminent. S'il attire la M (sens 2): en première approximation le prix est souvent



de la forme $[K - (M_1/M_2)]^{5\%}$, K coefficient de complexité et M, la masse d'un avion de base de prix connu. La M est donc normalement la première conséquence du souci "Px". Ce qui poussera à la révision de l'A, puis des Pf. Pendant ce temps, un courant secondaire essaiera de mettre en avant l'A: son habitabilité, sa maintenance, etc... tendant à justifier la future augmentation de masse. Ce sera le cas avec le sens 2' devenu prééminent, mais comme augmentation principale. On sera obligé d'ajouter des considérations technologiques (matériaux légers ou sandwich si leur prix est bas)

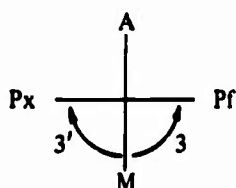
en prévision de la répercussion directe sur les M.

Ce schéma est du type de l'Alpha-Jet.

On voit que le renversement de la première réaction (2 en 2') ne peut être évité que par un certain mépris de l'A lui-même. Ce qui est bien sûr combattu (2') par les utilisateurs (Etats-Major ou Compagnies).

La M a le caractère prééminent. Dans le sens 3, on vérifié que pour cette M on peut avoir les Pf espérées.

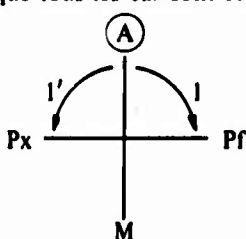
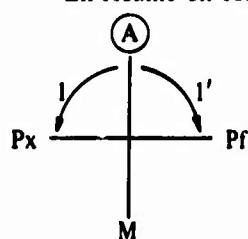
Le problème du Px devient secondaire et le bouclage se fait normalement sur l'A : tous les sacrifices seront faits pour respecter la masse (simplification du matériel, de l'armement, etc...).



Dans le sens 3', partant de la M maximale admissible, on se demande quel Px on peut mettre au projet: ce qui relègue l'A au niveau des conséquences.

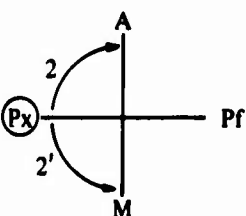
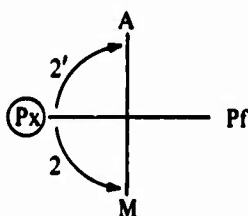
Ce schéma est du type d'un avion embarqué. Sa masse maximale sera celle que peut supporter le porte-avion pour la vitesse verticale maximale de chute. C'est aussi le cas des petits avions d'affaires qui se placent tout juste au-dessous des 5,7 t (SN 600 Diplomate).

En résumé on constate que tous les cas sont représentés dans le tableau ci-dessous.

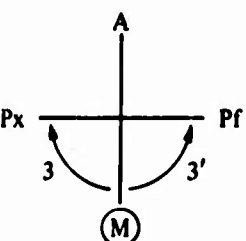
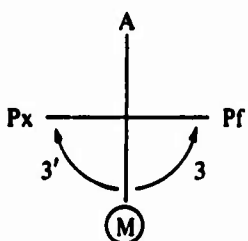


Types

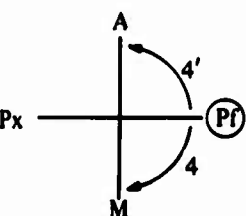
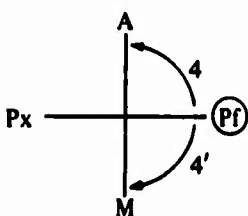
Mercure, Air-Bus, Hirondelle, Mystère XX, Mystère X.



Alpha-Jet



Avion embarqué (Jaguar marine) SN 600.



Concorde, Mirages

1, 2, 3, etc...: caractères prééminents.

1', 2', 3', etc...: caractères récessifs.

Représentation sphérique

- Pour faire de ce schéma une représentation complète, il convient de chercher quels seront les "produits" de ces rotations planes. On peut convenir de les situer dans la sphère contenant en son équateur le plan "horizontal" des rotations.

L'analyse globale est ainsi contenue dans une sphère:

- L'axe vertical vers "le bas" représente l'accumulation des outils produits par l'analyse M-Px-Pf : les bureaux de calculs s'en emparent et modèlent l'avion par une quantité de calculs.
- L'axe vertical vers "le haut" représente le sens donné à l'avion par l'analyse: le bureaux d'étude s'en inspirent pour accroître la qualité de l'appareil.

2. Les rotations notées 1 et 3 indiquent ainsi non seulement celles d'un axe "horizontal" sur l'autre, mais aussi celles des hémisphères correspondants:
 - Le sens 3 Pf → M indique la rotation de l'hémisphère "du bas" où s'incarne l'avion (de l'abstrait relatif Pf au concret relatif M);
 - Le sens 1 A → Px indique la rotation de l'hémisphère "du haut" où s'élève l'avion (du concret relatif A à l'abstrait relatif Px).
3. Cette représentation globale profite surtout au Chef, situé au centre de la sphère. Sa vision englobe à la fois le pouvoir imagé par l'hémisphère du "bas" et le savoir imagé par celle du "haut". On peut noter que cette position unique l'isole à la fois du reste de l'usine et du monde extérieur.
4. Ce schéma complet est celui d'une sphère qui "respire" (2 rotations ne sont jamais identiques) et qui est intérieurement séparée en 2 hémisphères tournant en sens inverse l'une de l'autre.

Pratiquement

On peut voir au moins deux intérêts à ce genre d'analyse:

1. La vision du Chef de l'avion (défini comme la personne concrète se trouvant dans la situation précisée ci-dessus) est la seule qui n'est pas naïve. Elle remplace les analyses linéaires par une synthèse globale constamment présente à l'esprit et aidée par une représentation relativement simple: elle peut en principe lui permettre de "figer" la sphère jugée par lui optimum*.
2. L'action de ce chef s'appuie directement sur le résultat le plus complet et le plus rapide qu'il obtient de l'analyse.

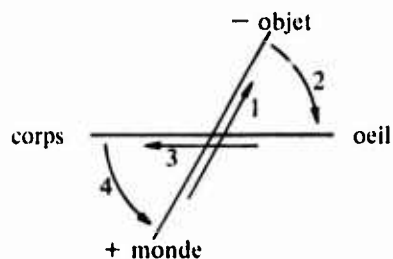
Dans l'exemple ou la Pf a le caractère prééminent ses ordres dépendront:

- de sa capacité de reconnaître le fait que c'est d'abord l'A (sens 4) qui est ensuite important compte tenu des circonstances: après avoir affiché les Pf d'une façon irréversible, certaines options primordiales (géométrie variable, aile gothique, etc...) ne peuvent plus être remises en causes;
- du fait que la M et le Px deviennent alors "secondaires": les efforts en personnel et temps de travail seront moindres dans ces secteurs. Son action intérieure et son attitude extérieure sont dictées par ce fait;
- en reconnaissant la continuelle possibilité 4' (la M devient le principal problème après les Pf) pendant que se déroule le processus 4, la sagesse sera de ne pas abandonner une gestion sérieuse des M et une étude complète de possibilités d'allègements.

* Ceci dit, l'idéogramme de la sphère (objet de cette annexe) n'est pas indispensable, comme l'exemple classique de la prose qui s'ignore l'a imagé.

ANNEXE 2

Donnons trois exemples d'application de la méthode proposée par Raymond Abellio.



I. Dans le but d'analyser la *perception* sensorielle, et les leçons à en tirer, l'auteur constate tout d'abord que, dans la vision naturelle, l'homme (ou le Je) se voit en état de *dualité simple* avec le monde. Il y a face à face le monde et moi, par exemple je vois un livre, et le simple couple de l'objet regardé et du sujet regardant.

Pourtant ce livre appartient au monde, duquel il doit se détacher pour être visible, pour tomber sous mes sens, pour *prendre un sens*, ce livre rejette ce reste du monde dans une grisaille et établit avec lui un rapport: "celui de l'objet destiné à être perçu par rapport à un reste du monde non destiné à l'être" — "Disons pour simplifier qu'un tel objet devient *actif* (+) par rapport au reste du monde considéré comme *passif* (-)".

Il est montré de la même façon que l'oeil devient actif, en s'intéressant spécialement au livre, sur le fond mis en repos de mon corps devenant passif.

La perception globale s'établit sous la forme d'une proportion:

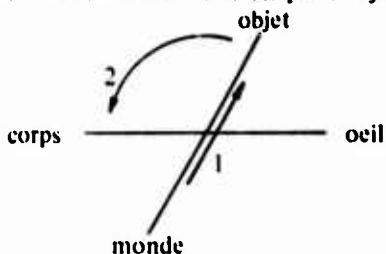
$$\frac{\text{livre}}{\text{monde}} = \frac{\text{oeil}}{\text{corps}} \quad \text{ou encore} \quad \frac{\text{objet}}{\text{monde}} = \frac{\text{organe des sens}}{\text{corps}}$$

Tout se passe comme si un *courant* (noté 1) s'établit entre le monde (d'abord actif +) et l'objet qui s'enlève sur lui. Si l'oeil "reconnait" l'objet (perception réussie), un *sens* est créé (noté 2). Sous l'influence de ce sens, un courant (noté 3) s'établit dans mon corps.

Mon corps se fait un outil de l'objet (différencié par l'oeil sur le fond du monde) et l'intègre pour s'ouvrir à nouveau au monde. Il en retirera de nouvelles émergences d'objets, après cette rotation (notée 4) en sens inverse de la première (notée 1).

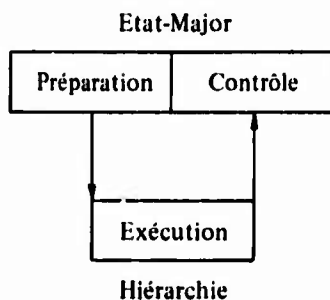
Nota:

1. Evoquant une globabilité, ce modèle devra être sphérique. Sur l'axe perpendiculaire au plan des deux axes précédents, on note les "produits" des rotations expliquées ci-dessus. Le premier, orienté par exemple vers le bas, figurera l'accumulation des *outils* par le corps (qui augmente son pouvoir sur le monde). Le second, vers le haut, figure le *sens* que prend le monde pour notre corps, (qui augmente la valeur du monde pour moi).
2. La "seconde" perception n'aura pas tout à fait le même caractère que la première bien que sur le même schéma. Cette seconde expérience sera plus *intense* que la première.
3. Si l'oeil ne reconnaît pas l'objet, la rotation s'effectue en sens inverse. L'objet est renvoyé à l'ensemble indistinct du corps. L'analyse peut être faite avec les mêmes principes, mais dans un autre champ (ici: perception "ratée").

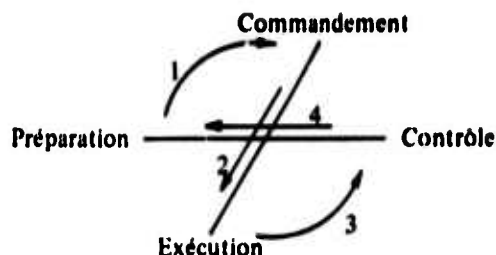


II. STRUCTURATION DES FONCTIONS DANS L'ENTREPRISE INDUSTRIELLE

Le modèle présenté par le Colonel Rimailho est le suivant:



Raymond Abellio propose:



'Au début du fonctionnement, le pôle actif de l'Etat-Major se confond avec la fonction "Préparation" et le pôle passif de ce même Etat-Major avec la fonction "contrôle"; la Hiérarchie, de son côté, est à la fois active par sa tête ("Commandement") et passive par sa base ("Exécution").'

Cette représentation plane est dynamisée par une représentation ("équatoriale" dans la sphère) à 2 rotations inverses: les 2 composantes passives devenant actives à leur tour et réciproquement.

Nota:

Les "produits" de ces rotations sur l'axe vertical, comme dans l'exemple I *l'incorporation de l'outil* (hémisphère du bas) et la *donation à sens* (hémisphère du haut), sont ici respectivement l'esprit de corps et le pouvoir du chef.

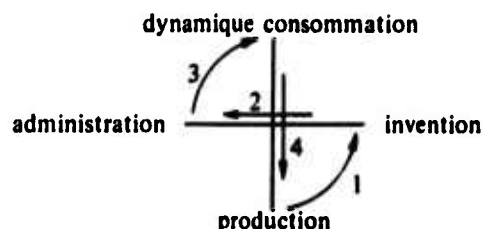
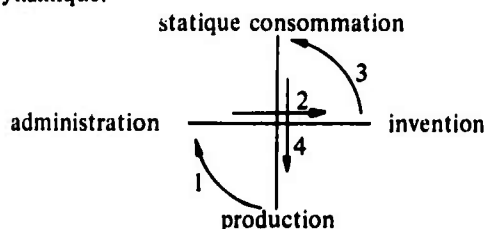
III. DYNAMIQUE DES FONCTIONS SOCIALES

'Partant d'un problème ou d'un champ donnés -- ici le champ social et son organisation fonctionnelle -- la méthode consiste à dégager les couples d'opposition "élémentaires" qui structurent ce champ 2 à 2, puis à mettre ce couple en rotation dialectique et à étudier les produits "successifs" de cette rotation.'

Ce premier couple, le plus général possible, caractérisant toute société et celui qui oppose *l'administration des choses* et le *gouvernement des hommes* (physique et politique sociales).

L'administration des choses conjoint deux fonctions: l'exécution et la gestion. La première se décompose à son tour en production et consommation, la seconde en administration et invention. "Dans l'absolu on ne pourrait désigner, au sein de ces 2 couples, une fonction plus originaire que l'autre: elles sont ensemble perpétuellement naissantes et mutantes. Simplement, l'on reconnaîtra qu'il existe, du point de vue de la physique sociale, deux grands types de sociétés selon que l'accent est mis sur la consommation ou la production."

Prenons l'exemple de la société à production prioritaire ou prééminente: cette société est productiviste ou capitaliste. De plus, selon que l'accent est mis sur l'administration ou l'invention, la société est dite statique ou dynamique.



Dans le cas statique, le producteur (originellement actif) se tourne d'abord vers l'administration pour obtenir la continuité du régime établi. En tant que consommateur (caractère récessif), il est passif et retenu par son besoin d'économie et de sécurité.

L'invention (3) et l'administration (2) se rabattent sur les consommateurs: "Dans ce cas, l'hémisphère du bas se trouvera chargé par les mesures répressives décidées par l'administration pour réduire la consommation, tandis qu'au même moment l'hémisphère du haut verra les consommateurs conduits à devenir inventifs pour se défendre".

**ENGINE SELECTION FOR TRANSPORT
AND COMBAT AIRCRAFT**

by

James F.Dugan Jr

**Head, Propulsion Section
Wind-Tunnel and Flight Division
NASA Lewis Research Center
Cleveland, Ohio, USA**

CONTENTS

	Page
1. INTRODUCTION	6-1
2. NEXT GENERATION CTOL TRANSPORT	6-1
2.1 Engine Cruise Performance	6-2
2.2 Engine Selection	6-3
2.3 Low Noise Engines for a Mach 0.98 Transport	6-3
2.4 Low Noise Engines for Mach 0.90 to Mach 0.98 Transports	6-4
3. VTOL TRANSPORT	6-6
3.1 Method of Analysis	6-7
3.2 Results and Discussion	6-9
3.3 Concluding Remarks	6-10
4. SUPERSONIC TRANSPORT	6-10
4.1 Method of Analysis	6-11
4.2 Results and Discussion	6-12
5. FIGHTER AIRPLANE	6-14
5.1 Specific Excess Power Concept	6-14
5.2 Engine Optimization	6-14
6. CONCLUDING REMARKS	6-15
REFERENCES	6-15
APPENDIX A – NOTATION AND ABBREVIATIONS	6-17
APPENDIX B – CALCULATION OF ENGINE PERFORMANCE	6-20
APPENDIX C – CALCULATION OF ENGINE WEIGHT AND DIMENSIONS	6-21
APPENDIX D – EMPIRICAL EXPRESSIONS FOR ESTIMATING LENGTH AND WEIGHT OF AXIAL FLOW COMPONENTS OF VTOL POWERPLANTS	6-25
FIGURES (1 to 39, B1 to B3, C1 to C15)	6-29

ENGINE SELECTION FOR TRANSPORT AND COMBAT AIRCRAFT

James F. Dugan Jr

1. INTRODUCTION

The purpose of this paper is to illustrate the procedures that are used to select engines for transport and combat aircraft. In general, the problem is to select the engine parameters including engine size in such a way that all constraints are satisfied and airplane performance is maximized. This is done for four different classes of aircraft: a long haul conventional takeoff and landing (CTOL) transport, a short haul vertical takeoff and landing (VTOL) transport, a long range supersonic transport (SST), and a fighter aircraft. For the commercial airplanes the critical constraints have to do with noise while, for the fighter, maneuverability requirements define the engine. Generally, the resultant airplane performance (range or payload) is far less than that achievable without these constraints and would suffer more if nonoptimum engines were selected.

2. NEXT GENERATION CTOL TRANSPORT

The next generation of CTOL transport is likely to use the supercritical wing proposed by Whitcomb¹. It offers the potential for delaying the transonic drag rise experienced by present-day jet transports as Mach 1 is approached. The supercritical wing can be exploited in several ways. A new airplane with this wing could cruise at higher speeds than current airplanes with little or no penalty in lift-drag ratio (L/D). (Symbols are listed in Appendix A.) Alternatively, at lower speed (e.g., around Mach 0.9) the supercritical wing will permit less sweepback, more thickness, and higher aspect-ratio. Used in this way, the supercritical wing would result in higher cruise L/D or less wing weight for the same L/D. In this part of the paper where design cruise speed was varied from a maximum of Mach 0.98 down to Mach 0.90, wing weight fraction remained constant but L/D increased as design speed was reduced. At Mach 0.98 the L/D was near that of the Boeing 747 cruising at Mach 0.86. At Mach 0.90, the L/D is postulated to be slightly above that obtained with the Boeing 707-320B designed to cruise at Mach 0.80. The material is taken from References 2, 3 and 4.

A sketch of a conceptual advanced tri-jet transport is shown in Figure 1. It uses the supercritical wing and has three acoustically treated turbofan engines (Fig.2). The objective of the study was to identify the engine parameters which maximized airplane performance while satisfying desired engine noise goals during takeoff and approach.

Total perceived noise has two components: jet noise from the two jet streams and fan turbomachinery noise. Jet noise, measured in PNdB, was calculated by standard methods described by the Society of Automotive Engineers in References 5 and 6. Jet noise is primarily a function of the exit velocities of the two flow streams, but is also affected by the gas flow rates and the flow areas. These variables were calculated at both Mach 0.23 (152 knots) after lift-off at full thrust and with thrust cut back to the level required during the 3° approach at Mach 0.203 (135 knots).

Fan turbomachinery noise, also measured in PNdB, is a function of spacing between rotor and stator, number of rotor and stator blades, rotor tip speed, number of stages, fan pressure ratio, thrust, and amount of nacelle acoustic treatment. It was assumed that the engines would be built in such a way as to minimize noise generation. Curves presented in Reference 7 relate machinery perceived noise level to fan pressure ratio at a fixed thrust and distance for both one- and two-stage fans. These curves were scaled from a total airplane net thrust of 400,000 newtons (90,000 lb) and a measuring-point distance of 305 meters (1000 ft) to both the sideline and approach conditions of this study. In addition to logarithmic thrust and distance-squared scaling, extra air absorption due to a change in slant range² was included. The curves which result for the sideline condition are shown in Figure 3 for a total airplane net thrust of 508,000 newtons (114,000 lb). The curves which result for the approach condition are also shown in Figure 3 for a total airplane net thrust of 160,000 newtons (36,000 lb). These thrust levels are typical for airplanes having a takeoff gross weight of 175,000 kilograms (386,000 lb), as was the case in the first part of the study where range was used as the figure of merit. At a given fan pressure ratio, the two-stage noise is about 8 dB higher than the one-stage noise. More recent investigations indicate the difference to be about 6 decibels and the matter is still under investigation.

In order to determine the total perceived noise from both the jets and the fan turbomachinery, the jet and machinery sound pressure levels (SPL) in each octave were added antilogarithmically. (This procedure is described in Reference 5 for the addition of core and fan jet noise.)

Noise calculations were made for two measuring points, both of which are specified in Federal Air Regulation Part 36. They were:

- (i) Sideline noise measured on the ground at the angle of maximum noise immediately after lift-off on a 463 meter (1520 ft) sideline for three-engine airplanes (650 m sideline for four-engine airplanes).
- (ii) Approach noise, when the airplane is 1850 meters (1 n.mi.) from the runway threshold, measured on the ground directly under the glide path at the angle of maximum noise.

The airplanes of this study were assumed to be at an altitude of 113 meters (370 ft) at this measuring station.

For airplanes with TOGW's of interest, FAR Part 36 specifies a noise limit of 106 EPNdB for both of the above measurements. A third measurement specified by this regulation should be made at a point 6.48×10^3 meters (3.5 n.mi.) from the start of takeoff roll on the extended runway centerline. If the airplane altitude at this measuring point exceeds 305 meters (1000 ft), the thrust may be reduced to that required for a 4 percent climb gradient or to maintain level flight with one engine out, whichever thrust is greater. The noise limit at this measuring station for the TOGW's considered here is 102 to 104 EPNdB. This noise measurement was ignored in this study because insufficient low-speed aerodynamic data were available to investigate the tradeoffs involved in minimizing noise at this point. The tradeoffs involved are between constant Mach number climb to maximum altitude and maximum acceleration to 305 meters (1000 ft) before thrust is reduced. For the three-engine airplanes which meet a sideline noise goal, it is felt that little difficulty will be involved in meeting the 6.48×10^3 meters (3.5 n.mi.) "takeoff" goal since the sideline noise is measured at 463 meters (1520 ft). With four-engine airplanes, the 6.48×10^3 meters (3.5 n.mi.) goal might be more difficult to meet, however, because the sideline measurement is specified at 650 meters (2126 ft) and is therefore easier to meet. The 6.48×10^3 meters (3.5 n.mi.) measurement might thus be more of a constraint for four-engine airplanes.

The noise calculations made in this study are in units of PNdB. The FAR Part 36 requirements, however, are stated in terms of EPNdB. The EPNdB scale (where E stands for effective) is a modification of the PNdB scale where a correction is made to account for subjective response to the maximum pure tone and duration of the noise heard by the observer. These modifications to the PNJB scale were not made in this study since the amount of information known about the maximum tones and directivity of the noise from the parametric engines is limited. It is thought that the error introduced by ignoring these modifications is less than the error that might occur by making further assumptions about the noise sources.

In any study of future airplanes, it is well to consider noise levels lower than those specified in FAR 36 since it is quite likely that in future years the required noise levels will be lower. Already it has been suggested that noise levels should be lowered 10 decibels every 10 years until the background noise level is reached. In this study noise levels as much as 20 decibels below the FAR Part 36 levels are considered.

2.1 Engine Cruise Performance

In any engine-airplane study it is necessary to generate engine performance over the range of important flight conditions (especially cruise, takeoff, and landing) for a family of engines whose design parameters (turbine temperature (T_4), overall pressure ratio (OPR), fan pressure ratio (FPR), and bypass ratio (BPR)) have been systematically varied.

Depending on the purpose of the study, an appropriate degree of sophistication is used to estimate engine performance (thrust, specific fuel consumption (SFC), weight, size). Of course, this presumes that we are starting from scratch with an unrestricted choice of paper engines. The approach would be different if we were limited to existing engines.

For the airplane being considered, typical cruise conditions are Mach 0.98 and 12,200 meters (40,000 ft).

A plot of cruise performance is shown in Figure 4 for an FPR of 1.50 and a cruise T_4 of 1370 K (2460°R). Although not shown, similar plots were made for other values of FPR and T_4 . Figure 4 shows that SFC can be reduced by increasing BPR with OPR fixed or by increasing OPR with BPR fixed. Unfortunately, both changes reduce cruise specific thrust which means that, if cruise sizes the engine, engine airflow must be increased to overcome the cruise drag. Higher airflow increases the engine diameter which in turn increases both drag and weight. In addition, increasing the OPR by itself tends to increase engine weight since more compressor stages are required.

Using the BPR = 4, OPR = 24 point of Figure 4 as a reference, the effects of changes in cruise T_4 , OPR, BPR, and FPR are shown in Figure 5. Increasing cruise T_4 causes an increase in both SFC and specific thrust, a mixed blessing. Increasing OPR up to about 36 causes a small decrease in SFC and only a slight reduction in specific thrust. A higher BPR decreases the SFC at a considerable drop in specific thrust. Increasing FPR, however, has a favorable effect on both SFC and specific thrust and is one of the keys to better engine performance. Since the other engine parameters improve one performance parameter at the expense of the other, an overall measure of airplane performance such as range must be examined in order to find those engine design parameters yielding an optimum balance between SFC and engine weight.

2.2 Engine Selection

In order to calculate airplane range, it is necessary to know something about the airplane and more about each engine to be considered. Starting with the cruise performance of a particular engine defined by its cruise values of T_4 , OPR, FPR, BPR, and component efficiencies, component maps are selected which are expected to characterize the engine. Using procedures such as those presented in Reference 8, engine performance at takeoff and approach is calculated. An explanation of this procedure is presented in Appendix B. There are many ways of computing engine weight. One convenient way (which was utilized in References 2 to 4) is described in Reference 9 (see Appendix C). The additional weight for installation (including inlet, nacelle, and nozzle) was assumed to be 3.13 times the total airflow at takeoff and was based on empirical data for existing high-bypass-ratio engines used in large commercial transport.

Considering now the airplane, the weight breakdown for an airplane with particular engines is shown below. Those items which remained fixed when other engines were installed are noted as "(fixed)".

Weight Statement		
	kg	lb
Airframe weight, (fixed)	81,700	180,000
Engine weight	18,100	40,000
Payload, (fixed)	27,200	60,000
Climb fuel, (fixed)	9,070	20,000
Cruise fuel	29,400	64,920
Descent fuel, (fixed)	907	2,000
Reserve fuel, (0.18 total fuel)	8,650	19,080
Takeoff gross weight, (fixed)	175,027	386,000

In this study the only other information on the airplane that was needed was its cruise L/D , which was 16.8 when engine diameter was 2.03 meters (80 in). (It rose to 17.5 for 1.52 m (60 in) engines and dropped to 15.75 for 2.79 m (110 in) engines.) The cruise L/D of course is needed to calculate cruise range

$$R = V \frac{L/D}{SFC} \log_e \left(\frac{\text{Weight at start of cruise}}{\text{Weight at end of cruise}} \right).$$

Because of the fixed weights indicated above cruise range is calculated from:

$$R_{cr} = 561 \frac{L/D}{SFC} \log_e \frac{366,000}{268,000 + 0.82 W_{eng}}.$$

The total range was assumed to be 648×10^3 meters (350 n.mi.) greater than the cruise range (370×10^3 m climb and 278×10^3 m letdown). Thus each engine defined by its cruise parameters leads to a specific value of airplane range.

Having selected design values for FPR and T_4 cruise, a "thumbprint" plot similar to the sketch of Figure 6(a) can be made for a spectrum of design values of BPR and OPR with contours of constant range. A thrust limiting line is shown below which takeoff performance will be unsatisfactory. Broken lines of constant sideline jet noise are also shown, with the lowest lines representing the highest noise levels. (Total noise is not shown as it depends on the amount of noise suppression which is defined in a later step.) Engines A, B, C, and D (selected because they produce maximum range at the selected levels of sideline jet noise) are singled out for further analysis.

In Figure 6(b), approach noise is plotted against sideline noise for lines of constant suppression and BPR. A noise goal represented by point X is postulated such that approach and sideline noise are equal. By interpolation, the noise goal can be achieved with about 16 PNdB of turbomachinery noise suppression. The range can now be found from Figure 6(c) where the ranges from Figure 6(a) have been reduced due to suppression (more suppression results in heavier engines and less fuel). In this manner then, the engine which maximizes range and the required suppression can be found for any desired noise goal.

2.3 Low Noise Engines for a Mach 0.98 Transport

Using the procedure discussed in the previous section, engines were identified which maximized airplane range when various noise constraints were imposed. Figure 7 shows the results for engines without a jet noise suppressor and with a cruise T_4 of 1150°C (2100°F). With no noise constraint, range maximizes for an FPR of 3.0. For the FAR Part 36 requirement of 106 PNdB, FPR must be 2.9 or less. At 96 PNdB, allowable FPR is about 2.1 and falls to 1.7 for 86 PNdB.

Similar results are shown in Figure 8 for engines having a 10 PNdB jet noise suppressor. The attainable range for a given noise level is higher because a higher FPR can be used.

The range/noise tradeoff for engines having a cruise T_4 of 1150°C (2100°F) is shown in Figure 9 with specific engine characteristics shown in Figure 10. Curve A is for engines having a maximum of 15 PNdB machinery noise suppression and no jet noise suppressor. Curve B is for engines without jet noise suppressors but with up to 40 PNdB of machinery noise suppression. Curve C has up to 40 PNdB of machinery noise suppression and a weightless jet noise suppressor which reduces jet noise by 10 PNdB.

The most significant comparisons to be made from Figure 9 are summarized in Figure 10. From Figures 9 and 10 it can be seen that a range penalty of 926×10^3 meters (500 n.mi.) is entailed in meeting a noise goal of 106 PNdB using curve A which represents current technology. The major reason for this is that FPR had to be reduced from 3.0 to 1.7. If curve B applies, then allowable FPR is 2.9 and the range penalty is only 139×10^3 meters (75 n.mi.). At lower noise goals, allowable FPR drops and the range penalty becomes large. At these lower noise goals, an effective lightweight jet noise suppressor would help considerably. Using curve C and a noise goal of 96 PNdB, an FPR of 2.72 can be used and the range penalty is only 167×10^3 meters (90 n.mi.).

In preliminary design work, the range and payload are fixed by route and market considerations so that airplane gross weight becomes the criteria of merit. The most commonly used economic criteria of merit is direct operating cost, DOC. It is expressed as cents per seat mile and accounts for the expenses of buying, maintaining, and insuring the airplane, paying the crew, and buying the fuel and oil. All of these expenses are dependent on the airplane design. In the preliminary design stage, DOC is a useful criteria of merit since the best designs will have the lowest DOC. DOC was calculated using the methods described in Reference 10. The results of Figure 9 were used to calculate airplane TOGW and DOC values for a fixed range of 5560×10^3 meters (3000 n.mi.). In addition some optimum engines were defined which used full coverage film cooling for cruise temperatures up to 1540°C (2800°F). These results are shown in Figure 11. Using current noise technology, a noise level 10 PNdB below FAR 36 can be achieved for a 4 percent increase in DOC. Using advanced noise technology, a noise level 20 PNdB below FAR 36 causes DOC to increase 9 percent. This penalty drops to 8 percent when both advanced noise technology and advanced turbine technology are available.

Having determined the optimum engine for a particular application based on specific input assumptions, the analyst should consider the effects of changes in the inputs. This will indicate what will happen if components do not function as expected and what benefits will accrue for various improvements in technology. The studies can also indicate the effects of lowering OPR to satisfy a pollution criterion or lowering turbine temperature to increase blade life. For the CTOL transport, a sensitivity study was done for a reference engine having a BPR of 4.8, an FPR of 1.7, an OPR of 31, and a T_4 of 1260°C (2300°F). This is the optimum engine for a noise goal of 106 PNdB if 15 PNdB of machinery noise suppression is used. The bar graph in Figure 12 shows the range increases for a 0.01 change in each of the variables. Also shown is the range increase for a 10 percent decrease in bare engine weight. By far the most sensitive of these parameters was the duct nozzle gross thrust coefficient. A one-percent change in it produced a 185×10^3 meters (100 mile) change in range. Somewhat less sensitive parameters were inlet pressure recovery and bare engine weight. It is obvious from the bar graph that care will have to be given to the inlet, duct, and duct nozzles when treating for noise since these areas are the most sensitive.

2.4 Low Noise Engines for Mach 0.90 to Mach 0.98 Transports

In this section the procedures discussed in previous sections are used to select engines for transports that cruise from Mach 0.90 to 0.98. Fan machinery noise suppression up to 20 PNdB is used. This is offered as a reasonable goal which hopefully can be met by 1978, the postulated year of first flight.

Figure 13 summarizes the results for a cruise FPR of 1.70. Range with a penalty included for the weight of the turbomachinery noise suppression is plotted against the total combined noise at either the sideline or the approach condition, whichever is greater. Three curves are shown — one for each of the cruise Mach numbers considered. The right-hand end of each curve represents the optimum cycle meeting the thrust constraint and results in a noise level of about 114 PNdB. As the noise goal is reduced, the design BPR is increasing and more acoustic treatment is being added. At the left-hand end of the curves, 27 to 30 PNdB of turbomachinery noise suppression is required. With 20 PNdB suppression, noise goals from 93 to 96 PNdB can be met at this design FPR.

Figure 14 shows the effects of various amounts of turbomachinery noise suppression for engines with a cruise FPR of 2.25. With no suppression, noise levels of about 126 PNdB are obtained. Approach noise exceeded the sideline noise at all levels of suppression considered in this plot. Unlike the case with an FPR of 1.70, BPR is not increased as the noise goal is reduced. It was found that with an FPR of 2.25 the range decreased as BPR was increased without a significant reduction in total noise. (Total noise was generally dominated by machinery noise, which is unaffected by BPR.) hence, the best tradeoff was to keep the engine cycle parameters fixed as more machinery noise treatment was added. With 20 PNdB of suppression, goals of 106 to 108 PNdB can be obtained, depending on design cruise Mach number. If the trades of FAR 36 are permitted, the goals that are met can be said to be 2 PNdB lower than these values since noise measured at the sideline station is more than 2 PNdB less than the approach noise.

In Figure 15(a) range is plotted against cruise Mach number for noise goals of 106 and 96 PNdB. Data for the 106 PNdB curve is for the two-stage fans with an FPR of 2.25 while that for the 96 PNdB curve is for the single-stage fan with an FPR of 1.70. Figure 15(a) emphasizes the increase in range possible by reducing the cruise speed from Mach 0.98 to 0.90. The range increase is 926×10^3 meters (500 n.mi.) for the 106 PNdB noise goal and 1480×10^3 meters (800 n.mi.) for the 96 PNdB noise goal. It is also apparent that there is a range penalty involved in reducing the noise from 106 to 96 PNdB. This range penalty decreases from 741×10^3 meters (400 n.mi.) at Mach 0.98 to less than 185×10^3 meters (100 n.mi.) at Mach 0.90.

The remaining parts of Figure 15 show the optimized engine parameters as a function of cruise speed and noise level. From Figure 15(b), BPR optimizes at 4 for all values of M_{cr} for the 106 PNdB noise goal and at about 6 for the 96 PNdB noise goal. In Figure 15(c) the optimum cruise overall compressor pressure ratios are shown to vary from 32 to 36 for the 106 PNdB noise goal and from 36 to 41 for the 96 PNdB noise goal. OPR is not a strong optimum and can be reduced to the vicinity of 30 without a significant adverse effect on range. This reduction may be required to curtail nitrogen oxide emissions. OPR optimized at rather high values in this study because of the advances that were assumed to occur in engine weight technology by the year 1978. Higher OPR's, therefore, did not cause great increases in engine weight. More conservative engine weight assumptions would have caused engine weight to rise faster with increasing OPR so that the optimum OPR's would have been lower.

In Figure 15(d) it is shown that the takeoff thrust-to-gross-weight ratio increases from the minimum of 0.24 for the lower cruise speeds to values as high as 0.31 for a cruise speed of Mach 0.98 and a noise goal of 96 PNdB. In this study the cruise T_4 was adjusted with the takeoff T_4 fixed at 1260°C (2300°F) to obtain an $(F_n/W_g)_{sls}$ of not less than 0.24. (The three-engine Boeing 727-200 has this value when fully loaded.) The fact that $(F_n/W_g)_{sls} > 0.24$ for the Mach 0.98 cruise case reflects that the cruise T_4 has been adjusted upward to its maximum permissible value of 1200°C (2200°F) for a takeoff T_4 of 1260°C (2300°F). To have obtained values of $(F_n/W_g)_{sls}$ closer to 0.24 would have required raising the cruise T_4 beyond 1200°C (2200°F) making the climb thrust too marginal as cruise is approached.

The cruise T_4 's that optimized performance are plotted against Mach number in Figure 15(e). For the 106 PNdB noise goal, it is seen that the cruise T_4 rises linearly from 1070°C (1965°F) at Mach 0.90 to 1200°C (2200°F) at Mach 0.98. For the 96 PNdB noise goal, the cruise T_4 optimizes at 1050°C (2100°F) at Mach 0.90 and increases linearly to 1204°C (2200°F) at Mach 0.94 where it meets the aforementioned constraint for thrust margin. Beyond Mach 0.94, the cruise T_4 is restricted to 1204°C (2200°F) although range would probably have improved if higher temperatures had been allowed.

Figure 15(f) shows the sea-level-static corrected airflow required for each of the optimized engines with airplane TOGW fixed at 175,000 kilograms (386,000 lb). For the 106 PNdB noise goal, these airflows varied from 381 to 432 kilograms per second (840 to 950 lb/sec). Airflows from 468 to 618 kilograms per second (1030 to 1360 lb/sec) were required to meet the 96 PNdB noise goal. The corresponding maximum engine diameters are shown in Figure 15(g). For the optimum engines meeting the 106 PNdB goal, the maximum diameter is about 1.78 meters (70 in). To meet the 96 PNdB goal the maximum engine diameter must be increased to 2.03 to 2.29 meters (80 to 90 in).

Figure 15(h) shows the variation of both sideline and approach noise with M_{cr} for the two noise goals. The solid curves represent sideline noise and the broken curves approach noise. The Figure shows that at the nominal 106 PNdB goal, the approach noise ranges from 106 to 108 PNdB while sideline noise varies from 100 to 102 PNdB. (As previously discussed, the ground rules of FAR Part 36 permit an excess of up to 2 PNdB at one measuring station if a corresponding reduction can be obtained at another measuring station.) For the 96 PNdB goal there was very little difference between the sideline and approach noises.

DOC is plotted against cruise Mach number in Figure 16 for noise goals of 96 and 106 PNdB. The best DOC's are obtained at cruise speeds of about Mach 0.94. At Mach 0.94 the DOC increases by only 0.00871 cents per seat-kilometer (0.014 cents per seat-statute-mile) when the noise goal is reduced from 106 to 96 PNdB. If the cruise speed is increased to Mach 0.98, the DOC increases by 0.0143 cents per seat-kilometer (0.023 cents per seat-mile) for the 96 PNdB noise goal. For the 106 PNdB noise goal, the economic penalty of increasing the cruise speed to Mach 0.98 is not nearly as great. Here, the increase in DOC is only 0.00404 cents per seat-kilometer (0.0065 cents per seat-statute-mile).

The engine cycles which were previously optimized on a range basis were re-evaluated in terms of TOGW for a fixed range of 5560 kilometers (3000 n.mi.) and a fixed payload of 300 passengers. Airframe weight was assumed to be a constant percentage of the TOGW. Engine airflows, diameters, and weights were recomputed on the basis of the different thrust levels required at the lower TOGW's. In Figure 17, TOGW is plotted against cruise Mach number for noise goals of 106 and 96 PNdB. TOGW increases markedly when cruise speed is increased from Mach 0.94 to 0.98, especially for the 96 PNdB noise goal. At the lower Mach numbers there is only a modest rise in TOGW for a noise goal of 96 PNdB as opposed to 106 PNdB. At Mach 0.98, however, the weight increase is appreciable.

In Figure 18, DOC is plotted against cruise Mach number for noise goals of 96 and 106 PNdB. These 5560 kilometer (3000 mile) DOC curves are analogous to the TOGW curves of Figure 17. For comparison, the DOC curves

for a constant TOGW and variable range (Fig.16) have been replotted in Figure 18 as the broken curves. By comparing the two sets of curves it is seen that the reduction in TOGW that was accomplished by fixing the range at 5560 kilometers (3000 n.mi.) lowered the level of DOC generally and accentuated changes resulting from increments in cruise Mach number or noise goal reduction.

The large difference between the solid curves and the broken curves at Mach 0.94 and below results from the fact that TOGW was calculated to be more than 4540 kilograms (100,000 lb) less when range was fixed at 5560 kilometers (3000 miles). The DOC's of both sets of curves appear to minimize near the middle of the range of cruise speeds studied. For the fixed range of 5560 kilometers (3000 miles), the DOC minimized at Mach 0.94 for the 106 PNdB goal and Mach 0.92 for the 96 PNdB goal. But very little increase in DOC is introduced by raising the cruise speed to Mach 0.94 for the 96 PNdB noise goal and Mach 0.95 for the 106 PNdB noise goal. At these speeds, DOC is increased by only about 0.0124 cents per seat-kilometer (0.02 cents per seat-statute-mile) when the noise goal is reduced from 106 to 96 PNdB. This does not seem to be a very large economic penalty to pay for a 10 PNdB reduction in noise. If the cruise speed is increased to Mach 0.98, the DOC increases by about 0.0497 cents per seat-kilometer (0.08 cents per seat-mile) at the 96 PNdB noise goal but by only 0.0187 cents per seat-kilometer (0.03 cents per seat-mile) for the 106 PNdB goal.

DOC, of course, does not present the entire economic picture. It does not, for instance, show how load factor might be affected by the introduction of competing airplanes designed for higher cruise speeds. Hence, although the lowest DOC's occur at design speeds between Mach 0.92 and 0.94, a faster airplane having a slightly higher DOC but a higher load factor (because of its lower block time) might be more profitable for an airline to operate. The range from New York to San Francisco, 4140 kilometers (2235 n.mi.) represents a long range domestic flight. The block time difference between Mach 0.94 and 0.98 at this range is only about 8 minutes. When block times are considered, however, it does seem worthwhile to increase the design speed to a point just to the right of the "bucket" of the DOC curves of Figure 18 since so little penalty in DOC is involved by so doing. Using this criterion, a good cruise speed selection might be Mach 0.95 for the 106 PNdB noise goal and Mach 0.94 for the 96 PNdB noise goal.

3. VTOL TRANSPORT

Vertical takeoff and landing aircraft are currently under study as a means for improving short-haul intercity air transportation. VTOL can relieve airport congestion and reduce air time delays, and can service communities currently without air transportation. A number of VTOL transports have been studied in the US and abroad. Various aircraft configurations and various means of providing vertical lift (e.g., rotors, tilting propellers, and high-bypass-ratio lift fans) were studied^{11,12,13}. None was outstandingly superior so that there is still interest in many of the concepts.

In Reference 14 the requirements and problem areas of low-pressure ratio lift fan propulsion systems are reviewed. The lift fan system has a number of features that qualify it for civilian VTOL transports. These are: (i) good potential for meeting reduced noise limitations, (ii) provision for safe management of failure of power-plant or thruster, (iii) good passenger and airline appeal for resulting aircraft, (iv) capability of high cruise speed approaching that of conventional jet transports, (v) direct use of available gas turbine technology, and (vi) elimination of mechanical transmissions. Two general types of lift-fan systems are currently being worked on, the integral system and the remote system. The integral system is similar to a high-bypass ratio turbofan in which the fan is powered by a coaxially mounted gas turbine engine. In the remote type, the fan and its drive turbine are separately located from the power-plant, and the working fluid is delivered through ducts to the turbine mounted at the tips of the fan blades. The remote system wherein hot gas from a turbojet engine is delivered to the tip turbine has been under investigation for a number of years by the General Electric Company¹⁵ and was used in the XV-5A VTOL aircraft¹⁶.

A second remote system uses a gas turbine driven fan (air generator) to supply compressed air to a burner upstream of the remote tip turbine. During cruise, the lift fans are inoperative and air from the air generator is exhausted in the conventional manner so that the air generator operates as a conventional turbofan engine. The present study is concerned solely with a particular air generator-lift fan VTOL system currently being considered at the Lewis Research Center¹⁷.

This system consists of four 66,700 newtons (15,000 lb thrust) remote lift fans and eight 33,400 newtons (7500 lb thrust) lift fans driven by gas generated just upstream of the tip turbines in auxiliary burners fed by four low bypass ratio, high fan pressure ratio air generators. Cross ducting is provided between each pair of air generators so that the thrust loss with one air generator out can be minimized. During cruise, the lift fans are inoperative and the fan exhaust is exhausted through cruise nozzles.

The objective of the study is to optimize the parameters of the air generator and remote tip-turbine lift fan. For the air generator, turbine-inlet temperature was varied from 1040° to 1370°C (1906° to 2500°F), overall pressure ratio from 12 to 21, and fan pressure ratio from 2.73 to 4.37. Bypass ratio was a dependent variable to produce the air required by the auxiliary burner which operated at 780°C (1440°F) and supplied working fluid to the 33,400

and 66,700 newtons (7500 and 1500 lb thrust) remote lift fans. Specific values of the air generator parameters were selected based on weight, dimensions, and specific fuel consumption.

The parameters of the remote tip-turbine lift fan were selected by performing a preliminary mission analysis. The propulsion systems examined were installed in a particular airplane which cruised at Mach 0.75 and 7620 meters (25,000 ft). Range was 804 kilometers (500 statute miles) and included 5 minutes of hover to account for two takeoffs and two landings. Gross weight was calculated from consideration of emergency conditions so payload varied as tip-turbine pressure ratio varied from 2.5 to 4.0, lift-fan pressure ratio varied from 1.15 to 1.35, and cruise lift to drag ratio from 8 to 12. Takeoff noise was also calculated to illustrate the payload-noise characteristics of the propulsion systems.

3.1 Method of Analysis

Propulsion system requirements – The mission selected to evaluate the propulsion system is as follows:

Stage length	804 km (500 statute miles)
Cruise Mach number	0.75
Cruise altitude	7620 m (25,000 ft)
Nominal takeoff noise goal at 152 m (500 ft), PNdB	95
Hover time for two takeoffs and two landings, min	5

The type of VTOL transport assumed in this study is shown in Figure 19. There are four large lift fans mounted in the high wing, each capable of producing 66,700 newtons (15,000 lb) of lifting thrust at sea level on a 32°C (90°F) day. At the wing tips and the forward and aft fuselage stations, there are eight half-size lift fans producing an additional 267,000 newtons (60,000 lb) of lift thrust. The four air generators are mounted in pairs on the wing. Each air generator supplies two of the full-size lift fans or four of the half-size lift fans. Air generators are interconnected so that there is no one-to-one correspondence between fans and air generators. During lift-off and landing, the core flow is deflected downward to provide additional lift thrust (the level varying slightly depending on the design of the air pump). The nominal value of total lifting thrust on a 32°C (90°F) day was 570,000 newtons (128,000 lb).

The gross weight of the VTOL transport was calculated for normal operation, operation with one air generator out, and operation with two full-size lift fans out. The least of these values was taken to be the transport gross weight for the nominal mission. For normal operation, a vertical thrust to gross weight ratio of 1.1 was assigned and a control thrust to weight ratio of 1.25, giving a gross thrust to weight ratio of 1.375. For the air generator out and full-size lift fan out cases, vertical thrust to weight ratio was 1.05 and control thrust to weight ratio 1.125. The air-generator out case was critical and resulted in a gross weight of 40,300 kilograms (88,700 lb).

Simplifying assumptions were made concerning the operating weight empty less propulsion system weight (50% of gross weight) and the transport aerodynamics (cruise L/D was varied parametrically from 8 to 12). Reserve fuel was assigned to be 3.5 percent of gross weight and fuel to accelerate and climb to cruise conditions from transition was assigned to be 3 percent of gross weight. The airplane fractional weights that varied with propulsion system design were (a) propulsion system weight, (b) fuel for two takeoffs and landings (5 min of hover), and (c) fuel to cruise the 471 kilometers (293 statute-miles) of the nominal 804 kilometers (500 statute-miles) total range (333 km (207 statute miles) were allotted for climb and letdown).

Propulsion system – The two major elements of the air generator/lift fan propulsion system are shown in Figure 20, the remote drive lift fan and the air generator.

Air enters the air generator through an acoustically treated inlet. All of the air is compressed by the low-pressure compressor, or fan. The air delivered by the low compressor is split: part of it is collected in a scroll to form the delivered air supply, the ultimate product of the air generator. The remaining air goes through the high-pressure compressor, burner, and high-pressure turbine. These three components make up the so-called high spool of the air generator which is, in reality, a gas generator for the low-pressure turbine. This turbine drives the low-pressure compressor, and these two components along with the connecting shaft constitute the low-pressure spool. The shafts for the two spools are concentric. The exhaust from the low-pressure turbine is ducted through an exhaust system which turns the flow through ninety degrees to produce a vertical thrust or lift for takeoff and landing.

The computer program of Reference 18 provides a design point configuration for the air generator. The thermodynamic performance, including the discharge thrust, is completely described, along with the dimensions and weight. Detailed thermodynamic performance, size, and weight are also calculated for the principal components (the weight and size equations are those presented in Reference 19, see Appendix D).

The length and weight of the inlet acoustic treatment and the exhaust system calculated by this computer program are appropriate for the configuration shown in Figure 20. However, the actual inlet and exhaust systems used may differ from those shown. It was assumed in this study that the sonic inlet would suppress forward propagating turbo-machinery noise to a level low enough that it would contribute a negligible amount to the total propulsion system noise.

The computer program of Reference 20 provides a preliminary design and analysis tool for an entire tip-turbine-driven lift fan assembly. This program is particularly adaptable to parametric studies of the effect of changes in the principal design variables of both the fan and turbine on the performance of the entire assembly. Considerable attention is given to the scroll which delivers the working fluid to the tip turbine. In the propulsion systems considered herein, the cold ducts that deliver the low-pressure compressor discharge air from the air generator to the lift fan are interconnected and just upstream of the scroll inlet to each lift fan is an auxiliary burner with a maximum outlet temperature of 780°C (1440°F).

The computer program for the design and performance of an air generator has considerable inherent flexibility in that no less than 44 independent parameters may be specified for any one air generator design. For all air generators, ambient pressure was 101,000 N/m² (2116 lb/ft²) and ambient temperature 32°C (90°F). Total pressure recovery of the inlet was 0.95.

For each air generator considered, the size was determined to be that required to supply two full-size lift fans each of which delivered 66,700 newtons (15,000 lb) of thrust at liftoff. The low-pressure compressor was designed with a constant hub radius and 3 to 5 stages with a corrected tip speed at the compressor inlet of 366 meters per second (1200 ft/sec) and a design point polytropic efficiency of 0.895. Average axial inlet Mach number was 0.6 and inlet hub-tip radius ratio was 0.5 for the first rotor. Diffusion through the compressor was regulated by selecting axial velocity ratio across the compressor to be 0.75. Average aspect-ratio of the first two stages (which affects both length and weight of the low compressor) was 3. The design value of low-compressor pressure ratio was varied between 2.73 and 4.37 to provide a tip-turbine pressure ratio of 2.5 to 4.0 (assuming a pressure loss through the ducts and scrolls of 8.4%).

The scroll diameter, corresponding to the maximum flow area in the scroll, was sized by the scroll Mach number of 0.3 and a selected configuration wherein the two delivery ducts are contiguous.

Most of the parameters required to describe the high compressor were used in the same manner as for the low compressor. The similar parameters are:

Flow path	constant hub
Number of stages	6 or 7
Corrected tip speed, m/sec (ft/sec)	335 (1100)
Efficiency	0.895
Axial velocity ratio	0.75
Overall pressure ratio	12 to 20

Four input parameters were required to establish the performance and geometry of the combustor. The reference burner inlet-velocity was fixed at 18.3 meters per second (60 ft/sec) so that the resultant flow area, or radial height, of the burner was a dependent variable. Burner length was determined from this height and the prescribed ratio of burner length to height. A lower heating value of 42,800 kilojoules per kilogram (184,000 Btu/lb) of JP fuel and a burner efficiency of 0.98 were used to compute fuel-air ratio.

One of the most significant parameters in the performance of the air generator is the stator inlet temperature to the high turbine. In this study it was varied from 1040° to 1370°C (1900° to 2500°F). Rotor cooling air (as a percent of high compressor discharge airflow) was scheduled to be 5.7 to 14.7 percent to reflect current technology in turbine-blade material and cooling airflow to maintain blade integrity. A high turbine loss coefficient ξ of 0.4 was used to calculate efficiency of the one-stage turbine (see Appendix D of Reference 20).

The large work extraction from the low turbine reduces the density of the working fluid so that a large flow area is required at the turbine exit. Flow area together with an assigned exit hub-tip radius ratio of 0.6 permitted turbine exit diameter to be calculated. The loss factor for the low turbine was assigned to be 0.4 and resulted in a turbine efficiency of 0.88 to 0.89.

The exhaust system on the core of the air generator includes both a duct and an adjustable nozzle which deflects the core flow to produce lift during takeoff and thrust during cruise. In order to provide control on the jet noise, the exhaust velocity from the nozzle was specified to be 198 meters per second (650 ft/sec). Exhaust system losses were accounted for through the use of a duct pressure loss coefficient of 0.125 which was multiplied by the square of the axial Mach number out of the turbine and by assigning a nozzle discharge velocity coefficient of 0.98.

During cruise, the air pump is employed as the cruise thrusting engine to overcome airplane drag. To get the required variation of specific fuel consumption with thrust setting on a standard day + 31°F (17.2°C), the procedures described in Reference 8 were employed. Maximum thrust was assigned to be that corresponding to a turbine inlet temperature 111°C (200°F) less than takeoff turbine temperature. The exhaust nozzle discharge velocity coefficient was 0.98.

Each of the full-size lift fans was sized to produce 66,700 newtons (15,000 lb) of thrust at takeoff on a 32°C (90°F) day at sea level. The program described in Reference 20 was used to compute dimensions, weight, and

performance of single-stage lift fans having design pressure ratios of 1.15 to 1.35. The single-stage tip-turbine pressure ratio was varied from 2.5 to 4.0.

The temperature into the scroll was set at 780°C (1440°F) so that the scroll could be constructed of conventional alloys. Inlet duct pressure ratio was 0.95 while fan inlet Mach number was 0.55 and fan hub-tip radius ratio was 0.4. For each tip-turbine driven lift fan, turbine exit axial Mach number was 0.3.

Some pertinent parameters are listed below:

Turbine pressure ratio	2.5	3.0	3.5	4.0
Air generator exit temperature, °C	410	427	446	463
Fan tip speed, m/sec	251	283	283	314
Fan efficiency (for fan pressure ratio of 1.25)	0.831	0.840	0.840	0.843
Tip-turbine lift fan weight (for 66,700 N thrust), kg	484	465	447	442

The total perceived noise is made up of jet noise from the fan air generators, jet noise from the twelve lift fans, and suppressed turbomachinery noise from the twelve lift fans. Turbine jet noise from the lift fans was assumed to make a negligible contribution to total noise (whether or not this can be achieved in an actual engine remains to be demonstrated). Turbomachinery noise projected out the fan inlets and air generator inlets (which contain choking devices for noise suppression) was also assumed to make a negligible contribution to total noise. The noise rating condition was assigned to be at maximum takeoff thrust.

Jet noise, measured in PNdB, was calculated by standard methods described by the Society of Automotive Engineers in References 5 and 6. At jet velocities below 1000 feet per second, there is some uncertainty as to how overall sound pressure level (OASPL) varies. In this report, the semi-log plot of the curve of OASPL against relative jet velocity shown in Figure 1 of Reference 6 was extrapolated as a straight line below 305 meters per second (1000 ft/sec). While this technique is not used exclusively throughout the industry, it does agree with recent data published in Reference 7.

Fan turbomachinery noise, also measured in PNdB, is a function of many things; for example, number of rotor blades and stator blades, tip speed, spacing between rotor and stator, fan pressure ratio, thrust, and amount of nacelle acoustic treatment. In this study, it was assumed that the engines would be built with optimum stator-rotor spacing and without inlet guide vanes in order to minimize noise generation. Curves developed by the Propulsion Systems Acoustic Branch at NASA-Lewis, and presented in Reference 7, relate fan machinery noise to fan pressure ratio for one-stage fans. These noise curves were scaled from a net thrust of 534,000 newtons (120,000 lb) and a distance of 152 meters (500 ft). According to Reference 7, acoustic treatment can reduce turbomachinery noise as much as 15 PNdB, the amount of suppression used in the noise calculations of this study. Total noise was obtained by adding anti-logarithmically, the suppressed turbomachinery and jet perceived noise, as described in Reference 5.

3.2 Results and Discussion

For a propulsion system having a lift-fan pressure ratio of 1.20, the effects of the air generator overall pressure ratio and turbine temperature on specific thrust and specific fuel consumption at SLS conditions of the complete propulsion system are shown in Figure 21. As overall pressure ratio increases from 12 to 21, specific lift thrust increases 2 percent and specific fuel consumption decreases 4 percent (Fig.21(a)). For an overall pressure ratio of 15, as turbine temperature increases from 1040° to 1370°C (1900° to 2500°F), specific lift thrust increases 2 percent and specific fuel consumption remains constant (Fig.21(b)).

On the basis of the above variations, a nominal air generator was selected with an overall pressure ratio of 15 and a turbine temperature of 1204°C (2200°F). A higher overall pressure ratio and turbine temperature offers small performance, weight, and size improvements but probably at some increase in development cost, original cost, and maintenance cost.

The weight breakdown of the dependent weight fractions is shown in Figure 22 for a cruise L/D of 10 and a lift-fan pressure ratio of 1.25. As tip-turbine pressure ratio increases, weights of the lift fans and hover fuel decrease, cruise fuel weight increases, and air generator weight stays constant above a tip-turbine pressure ratio of 3.5 (Fig.22(a)). The total of these weights decreases from 13,000 to 12,200 kilograms (28,750 to 27,000 lb) (Fig.22(b)). The weight saving can go into payload (Fig.22(a)). As tip-turbine pressure ratio increases from 2.5 to 4.0, the payload increases from 4440 to 5220 kilograms (9800 to 11,500 lb). At 93 kilograms (205 lb) per passenger and baggage, the tip turbine pressure ratio of 4.0 yields 56 passengers.

The effect of lift-fan pressure ratio on the weight breakdown is shown in Figure 23 where tip-turbine pressure ratio is 3.5 and cruise L/D is 10. As lift-fan pressure ratio increases, cruise fuel stays constant, hover fuel and air generator weight increase and lift-fan weight decreases. The summation of these weights increases (Fig.22(b)) so payload decreases as lift-fan pressure ratio increases (Fig.22(a)). For a lift-fan pressure ratio of 1.15, payload is 5720 kilograms (12,600 lb) or 62 passengers.

The tradeoff between payload and noise is shown in Figure 24. A fan pressure ratio less than 1.15 is required to achieve the noise goal of 95 PNdB. However, a lift-fan pressure ratio of 1.15 comes close: noise is 96.2 PNdB while payload for the tip-turbine pressure ratio of 4.0 is 5720 kilograms (12,600 lb). For lift fan pressure ratio less than 1.15, cruise thrust available from the four air generators falls below the drag of an airplane having a lift to drag ratio of 10.

3.3 Concluding Remarks

A simplified mission analysis was performed to evaluate the effects of lift fan pressure ratio and tip-turbine pressure ratio on the payload and noise of a remote-drive VTOL lift system. This system consisted of four 66,700 newtons (15,000 lb) thrust lift fans, eight 33,400 newtons (7500 lb) thrust lift fans and four air generators which were also used as the cruise engines.

A range of 804 kilometers (500 statute miles) was selected with a cruise Mach number of 0.75 at an altitude of 7620 meters (25,000 ft). The allowable takeoff gross weight, as dictated by the maximum available lift under emergency conditions and control requirements, was found to be about 40,300 kilograms (88,700 lb). Cruise lift-drag ratios of 8 to 12 were assumed in the study. Cruise performance calculations show that the airpump cycle can be used at cruise; with the L/D's assumed in this study, however, all four air generators would be required to provide enough cruise thrust. Cruise SFC was then used in the Breguet equation to calculate the weight of cruise fuel. Finally, payload was obtained by subtracting airframe, engine, and fuel weights from the TOGW.

For the range of tip-turbine pressure ratios and lift-fan pressure ratios examined, a near-maximum payload of 5720 kilograms (12,600 lb) was obtained with the highest tip-turbine pressure ratio considered (4) and the lowest lift-fan pressure ratio considered (1.15). At higher fan pressure ratios, noise increased and payload decreased due to an increase in hover fuel and an increase in air generator weight. Noise at 152 meters (500 ft) was calculated to be 96.2 PNdB. As advances in noise generation and suppression are made, the noise goal of 95 PNdB should be attainable.

These results are quite encouraging and suggest that the air generator lift fan remote propulsion system is an attractive candidate for V/STOL transports.

4. SUPERSONIC TRANSPORT

The Concorde and TU 144 supersonic transports use conventional kerosene fuel and cruise at about Mach 2. There is incentive to cruise at higher speed since flight efficiency continues to improve at higher speeds. The now defunct Boeing SST was designed to cruise at Mach 2.7. One of the factors that limited its cruise speed to Mach 2.7 was the heat-sink capacity of conventional kerosene-type fuel. Practically all of the heat sink available was used to absorb the heat discharged by the cabin environmental control system and the engine oil cooling system.

Studies by NASA have indicated that liquid methane may prove to be a superior fuel for SST's designed to cruise at Mach 2.7 and higher. Liquid methane has a heat-sink capacity, up to seven times as great as that of kerosene, and a heat of combustion 13 percent higher than that of kerosene. Since excess cooling capability is available, higher temperature engines may be considered. A methane-air heat exchanger can be built into the engine to cool the compressor discharge air in the turbine cooling circuit.

The purpose of this study is to determine what benefit will be obtained from the high-turbine-inlet temperature permitted by methane fuel. The data are from Reference 21. This is done with and without consideration of airport and community jet noise restrictions during airplane takeoff and climb. The method used is to determine the improvement that might be obtained in two overall airplane figures of merit, namely, (i) payload (number of passengers) and (ii) direct operating cost in cents per seat-kilometer (cents per seat-statute mile). The airframe is arbitrarily selected as a fixed-sweep, arrow-wing SCAT 15F configuration. The SCAT 15F configuration was developed by the NASA Langley Research Center to have a very high cruise lift-to-drag ratio. It is still under investigation to overcome some low-speed handling problems.

The afterburning turbojet, non-afterburning turbojet, and the duct-burning turbofan are the three engine cycles investigated. The turbine-inlet temperature is varied from 1204° to 1704°C (2200° to 3100°F). The compressor pressure ratio, bypass ratio, and the fan pressure ratio are optimized for each turbine-inlet temperature, both with and without airport and community noise restrictions.

Noise restrictions are imposed on the engines because the problem of airport and community noise during airplane takeoff and climb is of major concern to the airports and the public. Approach noise levels are also important, but these restrictions are not considered herein. If approach noise is a problem, it can be solved with a sonic inlet. The so-called airport noise is measured at the start of takeoff roll, 457 meters (1500 ft) from the centerline of the aircraft and at the angle of maximum noise. The noise level at this point should not exceed 116 PNdB. For the community noise, during airplane climb a point on the ground directly beneath the flight path and at a distance of 4.8 kilometers (3 statute miles) from the point of brake release is considered. After the engine power is reduced for a 2.53 meters per second (500 ft/min) rate of climb, the maximum noise at this point should not exceed 105 PNdB. These noise

goals were suggested by the Federal Aviation Agency at the time of the study and are less stringent than those of FAR Part 36.

Noise suppression devices of the exhaust jet are not used in order to better emphasize the influence of the primary engine parameters. It is entirely possible that the use of noise suppression devices would change the results of this study. The data presented can be considered as the two extreme cases. The best possible case assumed no airport or community noise restrictions, and the worst possible case assumed noise restrictions without suppression devices. Thus, data obtained by using various degrees of suppression would most likely occur somewhere between the extremes.

4.1 Method of Analysis

The effect of increasing turbine-inlet temperature with or without noise restrictions was calculated by analytically flying a fixed-wing airplane over a standard mission profile. The methane-fueled airplane was similar to the one shown in Figure 25 and had a ramp gross weight of 209,000 kilograms (460,000 lb). The engine parameters and engine size were optimized to maximize payload both with and without airport and community noise restrictions. The maximum cross-sectional area of the fuselage was fixed while fuselage length was varied in order to accommodate different numbers of passengers. Comparisons were made among the afterburning turbojet, non-afterburning turbojet, and duct-burning turbofan engines.

The mission requirements observed were:

Range, km; n.mi.	6482; 3500
Cruise Mach number	3
Maximum sonic boom, N/m ² ; lb/ft ²	
Climb	95.8; 2
Cruise	71.8; 1.5
Minimum climb-acceleration thrust-to-drag ratio	1.4
Minimum second-segment climb angle, deg	1.7
Maximum lift-off distance, m; ft	1460; 4450

The fuel reserve for the mission allows for (i) an additional 7 percent of the total mission fuel, (ii) an extension of 483 kilometers (261 n.mi.) to an alternate airport at cruise altitude and Mach number, and (iii) a 30 minute hold at 4570 meters (15,000 ft) altitude at Mach 0.6. An additional fuel allowance was incorporated in the mission fuel for a 25 minute idle prior to takeoff as well as a 1 minute period of maximum augmentation power application prior to takeoff roll.

The aerodynamic parameters were based on wind-tunnel data supplied by the NASA Langley Research Center for the SCAT 15F which is an advanced fixed-sweep, arrow-wing SST configuration similar to the one shown in Figure 25. The weights of the major components that comprise the empty weight were estimated by empirically established relations based on preliminary designs for similar configurations.

For each of the three types of engines considered, the performance and weight of each engine was calculated for a range of design variables. The range of variables covered in analytically finding the optimum cycle combination is shown in Figure 26. In calculating the design and off-design performance, each engine component was matched to satisfy the relations involving continuity of flow, engine rotational speed, and power balance between the compressor (or fan) and its driving turbine. The procedures used are similar to those discussed in Reference 22 (see Appendix B). Engine weight was calculated from empirical equations that relate installed engine weight to the type of engine, the design engine airflow, compressor pressure ratio, fan pressure ratio, bypass ratio, and turbine-inlet temperature. The equations are based on a composite of industry data.

The procedures for calculating jet noise are those outlined by the Society of Automotive Engineers in References 5 and 6. The method accounts for atmospheric absorption, ground attenuation, and multiple engines. The calculations are for noise produced by the jet exhaust only and do not include the noise generated by the fan or compressor.

The direct operating cost calculations were performed in the manner described in Reference 10. Airframe price, which is a function of airframe weight, was estimated with development costs included and was based on a production of 200 aircraft. The equation used to calculate the airframe price is as follows:

$$\text{Cost (dollars)} = 19 \times 10^6 + (\text{WAF} - 69,000 \text{ kg}) 147$$

$$\text{Cost (dollars)} = 19 \times 10^6 + (\text{WAF} - 150,000 \text{ lb}) 66.7$$

where WAF is weight of the airframe without engines, fuel, and passengers. A one-million dollar cost for electronics was included in the airframe price. Engine price, which is a function of engine type and size, was based on a production schedule of 1200 engines assuming each airplane would eventually require two spare engines. Engine price includes development cost. For the afterburning turbojet:

$$\text{Cost (dollars)} = 1.08 \times 10^6 + 0.00344 (w - 136 \text{ kg/sec})$$

$$\text{Cost (dollars)} = 1.08 \times 10^6 + 0.00156 (w - 300 \text{ lb/sec})$$

For the non-afterburning turbojet:

$$\text{Cost (dollars)} = 1.04 \times 10^6 + 0.00344 (w - 136 \text{ kg/sec})$$

$$\text{Cost (dollars)} = 1.04 \times 10^6 + 0.00156 (w - 300 \text{ lb/sec})$$

For the duct-burning turbofan:

$$\text{Cost (dollars)} = 1.21 \times 10^6 + 0.00280 (w - 136 \text{ kg/sec})$$

$$\text{Cost (dollars)} = 1.21 \times 10^6 + 0.00127 (w - 300 \text{ lb/sec})$$

Liquid methane fuel delivered to the airplane was assumed to cost 2.65 cents per kilogram (1.2 cents/lb).

4.2 Results and Discussion

Engine and wing sizing - Figure 27(a) is a thumbprint map for a series of SCAT 15F airplanes powered by afterburning turbojets having a turbine inlet temperature of 1050°C (2100°F). Each point on a given contour represents a combination of engine and wing size that will permit a particular number of passengers to be carried over the 6480 kilometer (3500 n.mi) range when the ramp gross weight is fixed at 209,000 kilograms (460,000 lb). The map shows that the maximum payload that can be carried is 235 passengers, which is obtained at takeoff wing and thrust loadings of approximately 3590 newtons per square meter (75 lb/ft²) and 0.27, respectively. These wing and thrust loadings correspond to a wing planform area of 569 square meters (6130 ft²) and an engine size of 180 kilograms per second (397 lb/sec). When the engine size is increased above 180 kilograms per second (397 lb/sec), payload suffers at the expense of greater engine weight. With smaller engines, payload decreases in spite of less engine weight because of excessive fuel consumption. When the engines are too small, acceleration is reduced and climb to cruise altitude takes longer. Thus, more fuel is used during climb. Cruise fuel is higher because more afterburning (higher SFC) is required to produce the required cruise thrust.

Among the performance criteria that can be critical in the design of the airplane are lift-off distance and velocity, transonic acceleration thrust margin, and sonic boom at the beginning of cruise. For the engine and wing combination that maximized payload, the required lift-off distance was 3050 meters (9000 ft) with a velocity of 104 meters per second (203 knots) (Fig. 27(b)). The angle of attack at lift-off was not allowed to exceed 11° in order to prevent the tail of the airplane from dragging on the runway. A 1370 meter (4500 ft) lift-off distance is considered to be a reasonable design criteria when hot-day conditions, one engine out performance, and clearance of a 9.14 meter (30 ft) obstacle at the end of a 305 meter (10,000 ft) runway are considered. Using takeoff lift coefficients of 0.5 and 0.6, the 1370 meter (4500 ft) lift-off distance lines are shown in Figure 27(b). Corresponding lift-off velocity scales are shown as auxiliary abscissa scales. The desired lift-off speed is 82.2 meters per second (160 knots). No firm minimum transonic thrust-drag F/D requirements exist today, but many authorities believe it should be at least 1.4 on a standard day. An F/D of 1.5 limiting line has also been superimposed on the thumbprint map. The third auxiliary abscissa scale is for initial cruise sonic boom. It decreases at lower wing loading because large wings result in higher cruise altitude and sonic boom decreases as distance increases.

With the limiting lines superimposed on the thumbprint, it is obvious that the wing and engine combination which maximized payload does not result in a satisfactory airplane. Using a takeoff lift coefficient of 0.5, a good design point would have a takeoff wing loading of 2390 newtons per square meter (50 lb/ft²), a takeoff thrust to gross weight ratio of 0.32, and a resulting payload of 201 passengers. Lift-off velocity would be about 87 meters per second (169 knots) and lift-off distance 1360 meters (4450 ft). Transonic F/D would be 1.94 and initial cruise sonic boom about 73.6 newtons per square meter (1.54 lb/ft²).

If high-lift devices allow a takeoff lift coefficient of 0.6, then a better airplane results. In this case, a good selection would be a 208 kilograms per second (460 lb/sec) engine and 2870 newtons per square meter (60 lb/ft²) wing loading. Passengers would increase 9 percent from 201 to 219 and lift-off velocity would decrease from 87 to 83.6 meters per second (169 to 163 knots). Transonic F/D would decrease slightly and cruise sonic boom would increase slightly although neither change is very significant.

Effect of engine design variables - The afterburning turbojet, the non-afterburning turbojet, and the duct-burning turbofan were considered separately to determine the engine design parameters that would enable the aircraft to carry the greatest number of passengers. The effect that design turbine-inlet temperature had on engine design parameters, payload, and DOC was considered with and without takeoff and community noise limits.

Figure 28(a) shows the passenger carrying capability of an SST as a function of design turbine-inlet temperature when the SST is powered by four afterburning turbojet engines. Without noise constraints, the number of passengers increases by 12.1 percent as turbine temperature is increased from 1204° to 1704°C (2200° to 3100°F). Overall pressure ratio increased from 10 to 19 (Fig. 28(b)). Engine airflow decreased 11.1 percent (Fig. 28(c)) but engine

weight changed only slightly (Fig.28(d)) as a result of the combined effects of overall pressure ratio, airflow, and turbine temperature.

The results obtained when takeoff noise limits were imposed are also shown in Figure 28 by the dashed lines. In meeting the noise restriction, a 10.4 percent payload penalty resulted at a design turbine-inlet temperature of 1204°C (2200°F) (Fig.28(a)). A significant increase in engine weight and size was the cause of the payload decrease. It was necessary to increase the design engine airflow by 57 percent (Fig.28(c)). This more than offset the effect of a lower overall pressure ratio (Fig.28(b)) to increase engine weight by 62.2 percent (Fig.28(d)).

In Figure 29, which uses airport sideline noise and community noise as coordinates, the 161 kilograms per second (353 lb/sec) airflow allowed the aircraft to carry maximum payload (point (a)). This engine produced sufficient thrust to meet the lift-off distance and climb-acceleration constraints for the mission. However, these engines produced 122.3 PNdB airport sideline noise and 110.3 PNdB community noise levels, which were considerably over the maximum limits.

The jet noise was reduced by operating the engine at reduced thrust without afterburning and at a reduced turbine-inlet temperature, 957°C (1755°F). To make up the thrust loss, engine size was increased to 251 kilograms per second (553 lb/sec). This engine satisfied the noise and lift-off distance constraints (point (b), Figure 29). In fact, community noise at the 4.8 kilometer (3 mile) point after power cut back was 102.5 PNdB. If engine thrust were increased until the limiting noise of 105 PNdB is reached, rate of climb at the 3-mile point would be 381 meters per second (1250 ft/min) which is well above the minimum requirement of 152 meters per second (500 ft/min).

With noise restrictions, the payload decreased by 5.6 percent (Fig.28(a)) as the turbine-inlet temperature increased to 1704°C (3100°F). Overall compressor pressure ratio increased from 8 to 12 (Fig.28(b)) and engine airflow increased 1.5 percent (Fig.28(c)). The combination of the effects of increasing turbine-inlet temperature, compressor pressure ratio, and engine size resulted in an installed engine weight increase of 13.5 percent (Fig.28(d)).

As the turbine-inlet temperature of the afterburning turbojet was increased with noise restrictions, the payload decreased because the engine weight increased faster than the fuel weight decreased. Engine performance improvement with increasing turbine-inlet temperature was offset by the engine weight as a result of the large engine size required to meet the noise and lift-off distance constraints. In fact, the over-sized engines in some cases cruised while using no afterburning and with turbine-inlet temperature reduced below design values. Therefore, little use was made of the high design turbine-inlet temperature capability.

The results for the non-afterburning turbojet are shown in Figure 30. Without noise restriction, payload increased 17.4 percent as design turbine-inlet temperature was increased from 1204° to 1704°C (2200° to 3100°F) (Fig.30(a)). Design compressor pressure ratio increased from 8.4 to 19 (Fig.30(b)) while engine airflow decreased by 27 percent. This latter trend resulted because engine size was dictated by the minimum climb acceleration thrust to drag ratio. The trends in turbine temperature, compressor pressure ratio, and engine size caused installed engine weight to decrease 13.2 percent (Fig.30(d)). The engine weight increase that normally would result as the design compressor pressure ratio is raised was offset by the large engine airflow reduction.

Imposing noise constraints lowered the payload only 1.3 percent for a turbine-inlet temperature of 1204°C (2200°F) (Fig.30(a)) because airflow had to be increased only 4.7 percent (Fig.30(b)) to meet the noise and lift-off distance requirements. As the design turbine-inlet temperature was increased from 1204° to 1704°C (2200° to 3100°F), payload decreased 4 percent. Optimum compressor pressure ratio increased from 8 to 12 (Fig.30(b)) and engine airflow increased 1.5 percent (Fig.30(c)) duplicating the trends for the afterburning turbojet. The trends in turbine temperature, compressor pressure ratio, and engine size caused installed engine weight to increase 21 percent (Fig.30(d)).

The results for the duct burning turbofan are shown in Figure 31. Without noise restrictions, payload increases 8.2 percent as turbine-inlet temperature is increased from 1204° to 1704°C (2200° to 3100°F) (Fig.31(a)). Engine noise at the airport increased from 117.9 to 121.7 PNdB. Compressor pressure ratio increased somewhat (Fig.31(b)), bypass ratio stayed constant at a value of 1.0 (Fig.31(c)), fan pressure ratio increased (Fig.31(d)), and design engine airflow decreased 11.5 percent (Fig.31(e)). The above trends resulted in an installed engine weight decrease of 8.4 percent (Fig.31(f)).

When airport and community noise limits were imposed on the duct-burning turbofan powered SST, payload decreased 2.1 percent at 1204°C (2200°F) turbine-inlet temperature. The decrease again was the result of a trade-off of a larger heavier engine that is capable of producing more thrust at maximum power, which, in turn somewhat decreased the fuel required to fly the mission. As turbine-inlet temperature increased from 1204° to 1704°C (2200° to 3100°F), payload increased 4.3 percent (Fig.31(a)). Design compressor pressure ratio increased from 9.4 to 11 (Fig.31(b)). The tendency of higher turbine-inlet temperature to increase primary stream noise was counteracted by increases in bypass ratio (Fig.31(c)) and fan pressure ratio (Fig.31(d)). Design engine airflow decreased 2 percent (Fig.31(e)). All the above trends combined to decrease installed engine weight by 4.3 percent (Fig.31(f)).

A comparison of the number of passengers the methane-fueled SST could carry when the afterburning turbojet, non-afterburning turbojet, or duct-burning turbofan engines were used is shown in Figure 32. Without noise restrictions, the number of passengers increases by 11 percent as turbine-inlet temperature is increased from 1204° to 1704°C (2200° to 3100°F). Although the effect of cycle was not great, the duct-burning turbofan was superior at lower values and the non-afterburning turbojet was superior at the higher values of turbine-inlet temperature. With takeoff and community noise restrictions, the duct-burning turbofan did significantly better than either turbojet at all temperatures considered. By increasing design turbine-inlet temperature, the number of passengers for the duct burning turbofan powered SST increased by 4 percent. Thus, the benefits of high turbine-inlet temperature were markedly affected by the takeoff noise limits. The major difference was the consequence of noise restrictions forcing the use of larger engines operating at part throttle during takeoff. The differences could be minimized (curves without noise restrictions approached) by development of effective jet noise suppressors having little thrust weight penalty.

Figure 33 shows the effect that increasing the turbine inlet temperature has on direct operating cost. Without noise restrictions, the DCC decreased by 14 percent when turbine-inlet temperature was increased from 1204° to 1704°C (2200° to 3100°F). The afterburning turbojet is superior at lower values of turbine-inlet temperature, and the non-afterburning turbojet is superior at higher values. The DCC for the duct-burning turbofan powered SST was approximately 7 percent greater than that for the afterburning turbojet powered SST because of higher duct-burning turbofan engine cost.

Figure 34 is for a different SST, the 340,000 kilogram (750,000 lb) gross weight Boeing 2707. The prototype airplane was to be powered by afterburning turbojets. Range was very adequate but sideline noise was excessive. Using a full afterburner takeoff, sideline noise was 128 PNdB or 20 PNdB above the FAR 36 requirement of 108 PNdB. Noise could have been lowered by installing larger engines and taking-off at part power but this would have resulted in a large range penalty. The other curves are for a non-afterburning turbojet, a duct-burning turbofan, and an afterburning turbofan. The afterburning turbofan gives the best results but the range penalty at FAR 36 is still excessive. The dashed curve indicates that if the afterburning turbofan engine is equipped with a jet noise suppressor that gives 6 dB of suppression for a 6 percent thrust loss, the FAR 36 noise requirement can be met with an acceptable range penalty.

5. FIGHTER AIRPLANE

A fighter pilot able to enter an engagement at a higher energy level than his opponent, and maintain this superiority, will have an offensive maneuvering advantage. The same result can be accomplished with an excess of power, for the pilot who is at a lower energy level but has the greater excess power will quickly ascend to an advantageous energy level. Energy maneuverability (EM) is the name given a process of energy management, whereby comparisons are made of energy and power of competing aircraft; manipulations are also performed to maximize each aircraft's capabilities throughout its speed-altitude envelope.

5.1 Specific Excess Power Concept

EM is based on principles of mechanics available since the time of Newton. Major John Boyd, an Air Force tactician, discovered how these relationships could be used to evaluate the maneuvering abilities of competing aircraft²³. Specific energy is the sum, per unit weight, of potential and kinetic energy. The time rate of change of specific energy is specific excess power (P_s), a quantity that characterizes a system's ability to change energy levels. The equations of flight mechanics put P_s in terms of easily measurable quantities (Fig.35).

In Figure 36(a), the 1-g specific excess power overlays compare Lockheed's CL-981 with its F104G's. The contours are lines of constant specific excess power. Note how at every point the CL-981 has some numerical specific excess power advantage over the F104G. A follow on relationship (Fig.36(b)) is then obtained by generating contours of constant differential specific excess power of the two aircraft. These contours show where each airplane has its greatest maneuvering advantage. In combat, a pilot should always attempt to fight an opponent where his differential increment in specific excess power is greatest, and avoid negative regions where his opponent would have the advantage. Even now pilots study energy maneuverability profiles of their airplane and the enemy's, learning which flight regimes give them the advantage and which do not. Simulator studies have shown time and again that the man that has this information in a fight will beat the man that does not.

5.2 Engine Optimization

For the fighter aircraft, the specific excess power requirements lead to the selection of engine design parameters including engine size much as noise requirements dictated engine design for the commercial aircraft discussed in previous sections. This is illustrated in the next three Figures for a fighter having a TOGW of 18,100 kilograms (40,000 lb) and a takeoff wing loading of 3830 newtons per square meter (80 lb/ft²).

In Figure 37, thrust loading is plotted against bypass ratio with lines of constant mission radius and various P_s requirements specified by Mach number, altitude, g condition, and thrust setting. The P_s for M0.9/30K/5g Mil

is the most demanding and if enforced would result in an unacceptable mission radius. The next most demanding P_s requirements are those for MO.9/30K/1g MII and MO.9/30K/5g Max AB. These can be satisfied if a BPR of about 0.8 is selected. Relative mission radius is seen to be 100.

In Figure 38, BPR is 0.8 and turbine-inlet temperature is 1316°C (2400°F). Discarding the MO.9/30K/5g MII P_s requirement, it appears that an overall pressure ratio of 23 or greater will satisfy the second most demanding P_s requirement at MO.9/30K/5g Max AB. Again relative mission radius is about 100.

In Figure 39, BPR is 0.8 and OPR is 23. The critical P_s requirement is again for MO.9/30K/5g Max AB and can be satisfied with a turbine-inlet temperature of 1316°C (2400°F). The proper engine size is found from the maximum thrust loading for the selected points from the last three Figures. By inspection it is 1.1, so that 196,000 newtons (44,000 lb) of thrust are required. The other parameters are: BPR is 0.8, OPR is 23, and turbine-inlet temperature is 1316°C (2400°F). If a relative mission radius less than 100 is desired, TOGW and engine size could be decreased.

6. CONCLUDING REMARKS

In this paper, the procedures that are used to select engines for transport and combat aircraft have been reviewed by illustrating the procedures for a long haul CTOL transport, a short haul VTOL transport, a long range SST, and a fighter aircraft. For the CTOL transport, it was shown that advances in noise technology and advanced turbine cooling technology will greatly reduce the airplane performance penalties associated with achieving low noise goals (as much as 20 PNdB below the FAR 36 requirement). A remote lift fan powered by a turbofan air generator was considered for the VTOL transport. In this case, the lift-fan pressure ratio which maximized payload also came closest to meeting the noise goal of 95 PNdB at 152 meters (500 ft). High-turbine temperature in three different engines was considered for the SST. Without noise constraints it led to an appreciable drop in DOC, but with noise constraints the reduction in DOC was very modest. For the fighter aircraft, it was shown how specific excess power requirements play the same role in engine selection as noise constraints for commercial airplanes.

REFERENCES

1. Thomas, B.K., Jr *New Wing Promises Design Breakthrough.* Aviation Week and Space Technology, Vol.87, No.4, 24th July 1967, pp.25-26.
2. Whitlow, J.B., Jr, et al. *Parametric Engine Study for a Mach 0.98 Commercial Air Transport.* NASA TM X-52961, 1971.
3. Kraft, G.A., Whitlow, J.B., Jr *Optimization of Engines for a Mach 0.98 Transport with Low Takeoff and Approach Noise Levels.* NASA TM X-67865, 1971.
4. Whitlow, J.B., Jr, Kraft, G.A. *Optimization of Engines for Commercial Air Transports Designed for Cruise Speeds Ranging from Mach 0.90 to 0.98.* NASA TM X-67906, 1971.
5. — *Jet Noise Prediction.* Aerospace Information Report 876, SAE, 10th July 1965.
6. — *Definitions and Procedures for Computing the Perceived Noise Level of Aircraft Noise.* Aerospace Recommended Practice 865, SAE, 15th October 1964.
7. Kramer, J.J., et al. *Noise Reduction. Aircraft Propulsion.* NASA SP-259, 1971, pp.169-209.
8. Koenig, R.W., Fishbach, L.H. *GENENG — A Program for Calculating Design and Off-Design Performance for Turbojet and Turbofan Engines.* NASA TN D-6552, 1971.
9. Gerend, R.P., Roundhill, J.P. *Correlation of Gas Turbine Engine Weights and Dimensions.* Paper 70-669, AIAA, June 1970.
10. — *Standard Methods of Estimating Direct Operating Costs of Transport Airlines.* Air Transport Association of America, August 1960.
11. — *Study on the Feasibility of V/STOL Concepts for Short Haul Transport Aircraft.* NASA CR-902, 1967.

12. Marsh, K.R. *Study on the Feasibility of V/STOL Concepts for Short-Haul Transport Aircraft.* NASA CR-670, 1967.
13. Fry, B.L.,
Zabinsky, J.M. *Feasibility of V/STOL Concepts for Short-Haul Transport Aircraft.* NASA CR-743, 1967.
14. Lieblein, S. *A Review of Lift Fan Propulsion Systems for Civil VTOL Transports.* Paper 70-670, AIAA, June 1970.
15. Kutney, J.T. *Propulsion System Development for V/STOL Transports.* Journal of Aircraft, Vol.3, No.6, November-December 1966, pp.489-497.
16. Immenschuh, W.T. *XV-5A-A Lift Fan V/STOL Research Aircraft.* Verti-Flite, Vol.11, May 1965, pp.2-9.
17. Dugan, J.F., Jr.
et al. *Preliminary Study of an Air Generator-Remote Lift Fan Propulsion System for VTOL Transports.* NASA TM X-67916, 1971.
18. Krebs, R.P. *Operational Procedure for Computer Program for Design-Point Characteristics of a Compressed-Air Generator with Through-Flow Combustor for V/STOL Applications.* NASA TM X-2422, 1971.
19. Sagerser, D.A.,
et al. *Experimental Expressions for Estimating Length and Weight of Axial-Flow Components Used in Analysis of VTOL Powerplants.* NASA TM X-2406, 1971.
20. Haller, H.C.,
et al. *Computer Program for Preliminary Design and Analysis of V/STOL Tip-Turbine Fans.* NASA TN D-6161, 1971.
21. Koenig, R.W.,
Kraft, G.A. *Influence of High-Turbine-Inlet-Temperature Engines in a Methane-Fueled SST when Takeoff Jet Noise Limits are Considered.* NASA TN D-4965, 1968.
22. Dugan, J.F., Jr. *Compressor and Turbine Matching.* Aerodynamic Design of Axial-Flow Compressors. Irving A. Johnsen and Robert O. Bullock, editors, NASA SP-36, 1965, pp.469-508.
23. London, M.P. *Tactical Air Superiority.* Space/Aeronautics, Vol.49, No.3, March 1968, pp.62-71.

APPENDIX A

NOTATION AND ABBREVIATIONS

A	area
AR	aspect ratio
BPR	bypass ratio
C	blade chord
D	drag, diameter
D_{ff}	diameter of front flange
DMOPR	diameter correction for overall pressure ratio
D_{rf}	diameter of rear flange
F	thrust
f	fuel-air ratio
FPR	fan pressure ratio
H	height, total enthalpy
IGV	inlet guide vane
KBPR	bypass ratio correction factor
KDUCT	duct correction factor
KDY	diameter correction for technology level (year)
K_{gg}	ratio of gas generator weight to total weight
KIGV	length correction for inclusion/exclusion of fan IGV
KLBPR	length correction for bypass ratio
KLIFE	life correction factor
KLOPR	length correction for overall pressure ratio
KLW_s	length correction for airflow size
KLY	length correction for technology level (year)
KM	Mach number correction factor
KOPR	overall pressure ratio correction factor
KT_s	turbine temperature correction factor
KW_s	airflow correction factor
KY	technology correction factor
L	axial length, lift
M	Mach number
N	number of stages, rings; rotational speed

OPR	overall pressure ratio
P	pressure
PNdB	perceived noise decibels
R	range, gas constant
S	axial spacing; clearance
SFC	specific fuel consumption
SLS	sea level static
SPL	sound pressure level
T	temperature
TBO	time between overhaul
TOGW	takeoff gross weight
U	wheel speed
V	velocity
W	weight
w	weight flow rate
w_a	airflow of gas generator
w_o	total fan face airflow
W_{tot}	total weight of engine
δ	corrected pressure
θ	corrected temperature
ξ	loss coefficient, energy loss to ideal energy ratio
σ	solidity

Subscripts

A	controls and accessories
a	air
B	burner
bare	bare engine
C	compressor
CMD	constant mean diameter
cr	cruise
D	fan duct
d	duct
e	engine

F	fan
f	fuel
h	hub
L	acoustic lining
M	mean
max	maximum
R	rotor
r	splitter ring
ref	reference
S	stage; structure
s	stator
T	turbine
t	tip
VMD	varying mean diameter
w	wall
x	axial
∞	free stream
1	inlet; compressor inlet
2	outlet; compressor outlet
3	turbine inlet
4	turbine outlet
<i>Superscripts</i>	
—	average

APPENDIX B

CALCULATION OF ENGINE PERFORMANCE

In order to calculate engine performance at design and off-design conditions, it is necessary to specify design point parameters (airflow, turbine temperature, pressure ratio, bypass ratio, fan pressure ratio, component efficiencies and pressure drops) and have available component performance maps.

Before the advent of computers, matching of components was done graphically to obtain off-design performance²². The example discussed here is for a simple turbojet (Fig.B1). The relations which must be satisfied deal with continuity of flow, rotational speed, and power. The relations are:

<i>Continuity</i>	<i>Speed</i>	<i>Power</i>
$w_C = w_T = w$	$N_C = N_T = N$	$w\Delta H_C = w\Delta H_T$
$\frac{w\sqrt{\theta_1}}{\delta_1} \frac{N}{\sqrt{\theta_1}} \frac{1}{(P_2/P_1)(P_3/P_2)} = \frac{wN}{\delta_3}$	$\frac{(N/\sqrt{\theta_1})^2}{(N/\sqrt{\theta_3})^2} = \frac{T_1}{T_3}$	$\frac{\Delta H_C}{N^2} = \frac{\Delta H_T}{N^2}$

To facilitate matching, the compressor and turbine performance are plotted as shown in Figure B2. When the maps are overlaid and the axes aligned, each point represents a match point satisfying the relations of continuity, speed, and power. The turbine temperature ratio can be calculated from the speed relation. The other parameters can be obtained from auxiliary plots. For example, compressor airflow can be obtained from a compressor plot of $\Delta H_C/N^2$ against $(w\sqrt{\theta}/\delta)$, for lines of constant $N/\sqrt{\theta_1}$. The information obtained from component matching yields the pumping characteristics shown in Figure B3. If an engine operating condition is specified (e.g., $T_3 = 1089^\circ\text{C}$ (2000°F) and $N = N_{\text{design}}$) and a flight condition (e.g., $M_0 = 2$ and Alt = 15,200 m (50,000 ft)), the thrust and specific fuel consumption of the engine can be calculated. Engine operation and flight condition permit T_3/T_1 and $N/\sqrt{\theta_1}$ to be calculated. The rest of the information needed to calculate thrust and specific fuel consumption is then obtained from the pumping characteristics.

The off-design performance calculations can be done much faster using digital computers. Reference 8 describes a digital computer program which is capable of running both design and off-design points for turbojet and turbofan engines. Component performance maps are reduced to tabular form to provide a base for calculating component performance. The design point is run first and map correction factors are calculated to scale the components to the desired performance. These correction factors are then applied to the component performance maps at off-design points. Initially, when the program is running at an off-design point, the components are not matched (do not satisfy the continuity, speed, and power relations), and errors (for example, work required by the compressor minus work supplied by the turbine) are generated. Small changes in each engine independent variable (for example, compressor speed) then produce small changes in the errors and these differential changes are loaded in a matrix. The matrix is then solved for the set of independent variables which result in zero errors, thus matching the components. This process may be repeated several times before matching occurs because there is a nonlinear relation between the independent variables and the errors.

APPENDIX C

CALCULATION OF ENGINE WEIGHT AND DIMENSIONS

The material in this appendix is a summary of the approach presented in Reference 9.

C1. WEIGHT

Semi-empirical correlations of engine weights and dimensions were developed using data for over 350 engines spanning the 1940 to 1980 time period. Corrections were made for parameters such as airflow, bypass ratio, pressure ratio, turbine temperature, design flight Mach number, and technology level (year) to normalize the weights and dimensions. The resulting correlations have proved to be very useful for performing engine/airplane optimization analyses.

Ratio of gas generator weight to total weight – Certain engine design variables such as overall pressure ratio and turbine-inlet temperature affect the gas generator section of the engine only and have a negligible effect on the fan section of the engine. In Reference 9, the fan section of the engine was assumed to consist of the fan and fan casing, turbines required to drive the fan, and the fan spool shafts and bearings. All remaining weight (including that of any low pressure compressor stages on the fan spool) was assigned to the gas generator section. The ratio of gas generator weight to total weight was defined as K_{gg} .

The variation of K_{gg} with bypass ratio was determined from weight breakdowns obtained for 14 different engine designs. The resulting variation of K_{gg} with bypass ratio is shown in Figure C1.

Overall compressor pressure ratio – Overall compressor pressure ratio (defined as compressor exit total pressure divided by fan face total pressure) primarily affects the weight of the compressor, burner, and high pressure turbine sections of an engine. The predominant effects of increasing compressor pressure ratio are increases in the number of compressor and turbine stages and increases in pressure and temperatures throughout most of the gas generator section of the engine. Therefore, as pressure ratio increases, casing and structural weights increase as a result of higher working pressures and necessary material substitutions in the higher temperature areas. Shafting and bearing weights also tend to increase. Figure C2 shows the pressure ratio correction factors which give the best statistical fit of the data. Straight line relations between KOPR and OPR were used over most of the pressure ratio range. However, it was found that a flattening of the slope of KOPR at the low pressure ratios gave a better fit to the statistical data. Rationalizations which could explain this are as follows: (i) As pressure ratio is reduced below a certain point, increased combustor volume (weight) begins to significantly counteract the decrease in weight due to the reduction in compressor stages, and (ii) when the point is reached where a single stage high pressure turbine can drive the compressor, further reductions in pressure ratio will not significantly reduce HP turbine weight (and may even increase it as annulus area increases). The lower slope of KOPR against OPR for low values of OPR was further confirmed by the results of several lift engines design studies by the engine manufacturers.

Turbine inlet temperature – A general trend of increasing turbine-inlet temperature (T_3) with time has been observed as shown in Figure C3. This is as would be expected since one of the main efforts of engine manufacturers is to design engines with higher values of T_3 because of the improvements this gives to several important engine characteristics. The higher thermal stresses and lower allowable stresses which accompany this temperature increase would be expected to result in increases in engine weight. However, significant advances have been made over the years in the development of materials and blade cooling techniques which have enabled T_3 to increase without penalizing weight as much as might be expected. In this correlation, a representative line was plotted through the data on the T_3 against year curve (labeled T_{3R} in Figure C3). This was taken as the reference value of T_3 for a given year at which there will be no penalty on engine weight.

However, at any given state of technological development, represented by a given year of first flight, it should be expected that as design T_3 increases, engine weight will also increase due to lowered material allowables, higher thermal stresses, and the requirement for more complex cooling schemes. A rate of change of gas generator specific weight of 3 percent per 55.6°C (100°F) increment in T_3 was found to give the best fit of the statistical data. This is represented in Figure C4 as KT_3 against $(T_3 - T_{3R})$.

Gas generator scaling – Engine weights are generally scaled by airflow (or thrust which is the same, assuming constant nozzle velocity for any thrust size). Therefore, for any given engine design, the following gas generator weight scaling expression may be applied:

$$\frac{WT}{WT_{ref}} = \left(\frac{w_a}{w_{a ref}} \right)^n$$

where "ref" relates to the airflow size at which the engine design was actually laid out. The schedule chosen for the weight correlation (Fig.C5) was influenced to a large extent by the manufacturers' data but was also adjusted to give the best fit with the statistical data. The curve for $w_a > 69 \text{ kg/sec}$ (150 lb/sec) corresponds to a scaling exponent of 1.2.

Scaling with total airflow – A survey of data from several of the engine manufacturers indicated that fans tend to scale with an exponent in the order of $n = 1.3$. This value is currently used in the correlation. For the purpose of the correlation, all engines were scaled to a primary airflow size of 68 kilograms per second (150 lb/sec), and a separate correction, KBPR, was applied to normalize the engines to a common bypass ratio of 0. Performing the airflow scaling at constant bypass ratio made it possible to represent the fan section scaling in terms of primary airflow. According to the assumed scaling law

$$\frac{(WT_{\text{fan section}})_2}{(WT_{\text{fan section}})_1} = \left(\frac{w_{02}}{w_{01}}\right)^{1.3} = \left(\frac{w_{a2}}{w_{a1}}\right)^{1.3}$$

$$KW_0 = \frac{(WT_{\text{fan section}})_2/w_{02}}{(WT_{\text{fan section}})_1/w_{01}} = \left(\frac{w_{a2}}{w_{a1}}\right)^{1.3 - 1.0} = \left(\frac{w_{a2}}{w_{a1}}\right)^{0.3}$$

Bypass ratio – Engine specific weight decreases with increasing bypass ratio. This is due to the fact that, as bypass ratio increases the portion of total fan inlet airflow which bypasses the gas generator progressively increases. Thus, the portion of the total airflow which must pass through the relatively heavy (in terms of weight per airflow) primary section of the engine decreases. The variation of engine specific weight with bypass ratio which resulted in the best fit of the statistical data is shown in Figure C6.

Year – It is well known that, due to advances in technology over the years, the engine companies have been able to design and build progressively lighter engines with equivalent cycles. Lighter, stronger materials such as titanium have replaced heavier steels in many engine components. It is now possible to aerodynamically load compressor and turbine stages to higher levels and hence to reduce the number of stages required for a given pressure ratio. Higher wheel speeds available because of improved materials and high Mach blading have also increased pressure ratio per stage. Many other advances have also contributed to the reduction in specific weight. In addition to the effect of year allowed in the turbine inlet correction, a factor KY is applied to the whole engine to account for general advances in the state-of-the-art which affect all areas of the engine design. The trend in KY which gave the best fit to the statistical data is presented in Figure C7.

Life – If all other parameters are held constant, engine weight is a function of design life, with shorter life engines weighing less than longer life engines. For the purpose of the correlation, cruise engines in the data were classified in three general categories: short, medium, or long life. Engines which were known to have been designed for relatively short life, such as drone engines, fighter engines, and lift/cruise engines, were classified as "short life". Engines which were designed for long range cruise application or which were known to have achieved very high TBO's were classified as "long life". Engines in between these two extremes, and those for which no TBO information was readily available, were classified as "medium life" engines.

The factors for life, KLIFE, which resulted in the best correlation of the statistical data are summarized below:

Engine type	Life correction KLIFE
Lift engines	0.44
Short life	0.90
Medium life	1.00
Long life	1.07.

Flight Mach number – Engines designed to operate at high supersonic flight speeds will tend to be heavier than subsonic and low supersonic designs, primarily due to the higher operating temperatures. The correction for flight Mach number is shown in Figure C8. The correction is 1.0 at Mach 2 and below since design conditions which affect engine weight tend to be equivalent between a typical SLS takeoff operating point and a typical Mach 2 operating point.

Fan duct configuration – Long duct versions of an engine weigh more than short duct versions. The following factors are used in this weight estimation procedure.

Short duct: KDUCT = 1.00

Long duct: KDUCT = 1.07.

Calculation of engine weight – The procedure for using the correlation to predict the weight of an engine with any combination of the variables w_a , BPR, T_3 , OPR, etc. is summarized below:

$$W_{tot} = 14W_a(KENG)[K_{gg}(KHP) + (1 - K_{gg})(KLP)] ,$$

where

$$KENG = (KBPR)(KY)(KLIFE)(KM)(KDUCT)$$

$$KHP = (KT_3)(KOPR)(KW_a)$$

$$KLP = KW_0 .$$

C2. DIMENSIONS

The procedures used to calculate the bare dimensions of cruise engines are as follows:

$$L_{bare} = \frac{2.16}{85} \text{ or } (KLW_a)(KLBPR)(KLY)(KLOPR)(KIGV) \quad \begin{matrix} \text{m} \\ \text{or} \\ \text{in} \end{matrix}$$

where

$KI.W_a$ correction for airflow size (Fig.C9)

$KLBPR$ correction for bypass ratio (Fig.C10)

KLY correction for technology level (Fig.C11)

$KLOPR$ correction for overall cycle pressure ratio (Fig.C12)

$KIGV$ correction for inclusion/exclusion of fan IGV

1.04 with IGV if $BPR > 2.5$

0.96 without IGV if $BPR < 2.5$

1.00 otherwise.

$$D_{ff} = D \text{ fan tip} + \frac{7.62 \times 10^{-2} \text{ m}}{\text{or}} \quad \begin{matrix} \text{m} \\ \text{3 in,} \end{matrix}$$

where

$D \text{ fan tip} = f(\text{fan face } M, \text{ hub/tip, and corrected airflow})$

$$D_{rf} = \left[(A)\sqrt{w_a} + \frac{7.62 \times 10^{-2} \text{ m}}{\text{or}} \right] \quad \begin{matrix} \text{m} \\ \text{3 in} \end{matrix} \quad \text{for turbojets and short duct turbofans,}$$

where

$A = f(BPR)$, Figure C.13,

or

$$D_{rf} = \left[(A)\sqrt{w_a} + \frac{7.62 \times 10^{-2} \text{ m}}{\text{or}} \right] + C + \frac{7.62 \times 10^{-2} \text{ m}}{\text{or}} \quad \begin{matrix} \text{m} \\ \text{3 in} \end{matrix} \quad \text{for long duct turbofans,}$$

where

$$A\sqrt{w_a} + \frac{7.62 \times 10^{-2} \text{ m}}{\text{or}} \quad \begin{matrix} \text{m} \\ \text{3 in} \end{matrix} \quad \text{duct inside diameter,}$$

C $D_{do} - D_{di}$: specified by duct corrected flow and Mach number over turbine

M 0.35 for non-duct burning turbofans

0.16 for duct burning turbofans

D_{\max} D_{ff} for short duct turbofans
 greater of D_{ff} or D_{fF} for long duct turbofans
 $(DMOPR)(KDY)\sqrt{w_a}$ for turbojets,

where

$DMOPR$ $f(OPR, w_a)$, Figure C14

KDY $f(Y)$, Figure C15.

APPENDIX D

EMPIRICAL EXPRESSIONS FOR ESTIMATING LENGTH AND WEIGHT OF AXIAL FLOW COMPONENTS OF VTOL POWERPLANTS

The expressions for estimating the length and weight of axial flow components for use in parametric analysis of powerplants suitable primarily for VTOL transport aircraft presented herein are from Reference 19. These expressions were developed from correlated lift and cruise engine data with the aid of simplified component models. Components involved include: fan, fan duct, compressor, burner, turbine, structure, and accessories. Because of differences in reported details as well as in design approaches, considerable variability was noted in the component data. However, when comparisons were made between estimated and actual total engine weight for several representative engines, good agreement was found for nearly all cases considered.

The weight of the fan is calculated from:

$$W_F = K_F (D_I)^{2.7} \frac{N}{(AR)_{X,R}^{0.5}} \left(\frac{\sigma_I}{\sigma_{I,ref}} \right)^{0.3} \left(\frac{U_I}{U_{I,ref}} \right)^{0.3} \quad (D1)$$

where $\sigma_{I,ref} = 1.25$, $U_{I,ref} = 350$ meters per second (1150 ft/sec) and $K_F = 135$ (12 for D_I in ft, W_F in lb). The fans included in the correlation primarily had solid titanium blades. Significant reductions in fan weight may be possible with hollow blade construction or the use of composite materials. In order to reflect these advanced design techniques, adjustments to the value of K_F may be made in the fan weight equations.

The weight of the duct casing was estimated by the simplified expression:

$$W_D = \pi \bar{D}_D L_D \left(\frac{W}{A} \right)_D \quad (D2)$$

where \bar{D}_D is the average diameter (between inlet and outlet) of the duct casing. Values of duct weight per unit surface area, $(W/A)_D$, from engine data varied from 2.4 kilograms per square meter (0.5 lb/ft²) to 8.3 kilograms per square meter (1.7 lb/ft²). A value of 3.5 kilograms per square meter (0.72 lb/ft²) was taken to be representative of current design practice for low pressure lift fans. This corresponds to aluminum ($\rho = 2770$ kg/m³, 173 lb/ft³) with a thickness of 0.13 centimeter (0.05 in).

Acoustic lining is generally applied to the duct walls as well as to splitter rings concentric to the duct walls. The weight of the acoustic lining is calculated from:

$$W_L = A_L \left(\frac{W}{A} \right)_L \quad (D3)$$

where the area of the acoustic lining, A_L , is a function of length, diameter, and number of splitter rings, N_I :

$$A_L = \pi \left[L_{inner,wall} \bar{D}_h + L_{outer,wall} \bar{D}_I \right] + \pi \sum_{i=1}^{N_I} L_{r,i} D_{r,i} \quad (D4)$$

and

$$\begin{aligned} \left(\frac{W}{A} \right)_w &= 2.69 \text{ kg/m}^2 \text{ (0.55 lb/ft}^2\text{) for the walls} \\ \left(\frac{W}{A} \right)_r &= 8.55 \text{ kg/m}^2 \text{ (1.75 lb/ft}^2\text{) for the splitter rings.} \end{aligned}$$

The data for the compressor were obtained from compressors with both fixed and variable angle stators, constant hub, mean and tip flow path designs, as well as both disk and drum construction. In order to estimate compressor length, the ratio of length to inlet mean diameter was correlated with the number of stages and inlet hub-tip diameter ratio to give:

$$\frac{L_c}{D_{M,I}} = 0.2 + \left[0.234 - 0.218 \left(\frac{D_h}{D_I} \right)_I \right] N \quad (D5)$$

The number of stages is related to overall compressor pressure ratio and average stage pressure ratio by:

$$\left(\frac{P_2}{P_1} \right)_s = \left[\left(\frac{P_2}{P_1} \right)_c \right]^{1/N} \quad (D6)$$

For constant blade loading, the average stage pressure ratio will be a function of the inlet corrected rotor tip speed. Because of reheat effects it will also depend on the overall compressor pressure ratio. An expression relating inlet corrected rotor tip speed to average stage pressure ratio and overall pressure ratio was deduced from simplified compressor aerodynamic considerations.

$$\left(\frac{U}{\sqrt{\theta}}\right)_{CCMD} = A \left[\left(\frac{\bar{P}_2}{P_1}\right)_s + C(P_2/P_1)^{1.8} - B \right] \quad (D7)$$

where the factor A was taken as 466 (or 1530 for $(U/\sqrt{\theta})_{CCMD}$ in ft/sec). Factor B is used to reflect blade loading level. Two levels were considered: high and moderate. Corresponding values of B were taken as 0.676 and 0.588, respectively. Factor C was taken as 0.654×10^{-3} . This relation was taken to hold for constant mean diameter compressors.

An adjustment to the average stage pressure ratio was developed to account for the effect of a varying mean diameter design. This adjustment is required because the stage rotor blade speeds (and thus the performance) will be different than for the case of a constant mean diameter compressor with the same inlet tip speed. The average stage pressure ratio for compressors with varying mean diameters was deduced as:

$$\left(\frac{\bar{P}_2}{P_1}\right)_{S,VMD} = \left[0.8 \left(\frac{D_{M,2}}{D_{M,1}}\right)_C + 0.2 \right] \left[\left(\frac{\bar{P}_2}{P_1}\right)_{SCMD} - 1 \right] + 1 \quad (D8)$$

Equations (D7) and (D8) were then combined to give a general expression for inlet corrected tip speed:

$$\left(\frac{U}{\sqrt{\theta}}\right)_C = A \left\{ \frac{\left[\left(\frac{\bar{P}_2}{P_1}\right)_s - 1 \right]}{\left[0.8 \left(\frac{D_{M,2}}{D_{M,1}}\right) + 0.2 \right]} + 1 + \frac{\left(\frac{P_2}{P_1}\right)_C^{1.8}}{C} \right\} - B \quad (D9)$$

where $(\bar{P}_2/P_1)_s$ is found from Equation (D6) and A , B , and C are given with Equation (D7).

Compressor weight is calculated from

$$W_C = K_C (D_M)^{2.2} N^{1.2} \left[\frac{U_t}{(U_t)_{ref}} \right]^C \left[1 + \frac{(L_C/D_{M,1})}{(L_C/D_{M,1})_{ref}} \right] \quad (D10)$$

where

K_C	15.5 (2.5 for D_M in ft) for lift engines
K_C	24.2 (3.9 for D_M in ft) for cruise engines
C	0.5 or less
$(U_t)_{ref}$	335 m/sec (1100 ft/sec)

The compressor weight is taken to include the rotor blades, disks (or drum), seals, stator blades, and casing.

The burners considered were annular axial-flow or reverse-flow designs. Included in this component are the diffuser (inlet transition) and the outlet transition sections. Burner length is calculated from:

$$L_B = \frac{R}{\pi V_{ref}} \left[\left(\frac{L_B}{H} \right) \left(\frac{w_{T_1}}{P_1 D_M} \right) \right] \quad (D11)$$

where

V_{ref}	18.3 m/sec (60 ft/sec) for cruise engines
V_{ref}	24.4 m/sec (80 ft/sec) for lift engines.

The burner weight includes the inner and outer casing, liner, and fuel nozzles. Burner weight is calculated from:

$$W_B = K_B \bar{D}_M^2 \left[\frac{(L_B/H)}{(L_B/H)_{ref}} \right]^{0.5 \text{ to } 1.0} \quad (D12)$$

where

$$\begin{aligned} K_B & 195 \text{ (40 for } \bar{D}_M \text{ in ft, } W_B \text{ in lb) for lift engines} \\ K_B & 390 \text{ (80 for } \bar{D}_M \text{ in ft, } W_B \text{ in lb) for cruise engines} \\ (L_B/H)_{ref} & 1.6 \text{ for lift engines and 3.2 for cruise engines.} \end{aligned}$$

Turbine data were obtained from engines with one, two, and three spools with various flowpath designs. In terms of the average axial chord length and average clearance, the turbine length (excluding possible exit straightening vanes) is given by:

$$L_T = N_T(\bar{C}_{X,R} + \bar{C}_{X,S}) + (2N_T - 1)\bar{S}_T, \quad (D13)$$

where

$$\bar{C}_X = \frac{\bar{D}_t - \bar{D}_h}{2AR_X} \quad (D14)$$

and

$$\bar{AR}_X = A + B(\bar{D}_L/\bar{D}_T). \quad (D15)$$

Values for the factors A and B are given in Table D1.

TABLE D1

Constants in Turbine Blade Aspect Ratio Equation

<i>Turbine rotor</i>	<i>A</i>	<i>B</i>
Turbofan engines (cruise and lift)		
High and intermediate pressure spool	10.45	-10.00
Low pressure spool*	13.36	-11.78
Lift jet engines		
High and low pressure spools	6.1	-5.5
Turbine stator (All engine types)	A	B
High pressure spool	6.45	-5.97
Low and intermediate pressure spool	10.95	-10.9
*Note: In this case, AR_X is limited to a maximum value of 6.		

The average clearance between blade rows was assumed to be proportional to the average rotor axial chord:

$$S_T = a_T \bar{C}_{X,R}. \quad (D16)$$

For the turbine data investigated, the proportionality constant was found to vary from 0.2 to 1.0. Since length will be critical for VTOL powerplants, a value of 0.3 or 0.4 can be considered representative for high and low pressure turbines.

The turbine weight includes the rotor disk and blades, stator blades, seals, and casing. Turbine weight is calculated from:

$$W_T = K_T(\bar{D}_M)^{2.5} N_T (\bar{U}_M)^{0.6}, \quad (D17)$$

where

$$\begin{aligned} K_T & 4.7 \text{ (0.26 for } \bar{D}_M \text{ in ft, } \bar{U}_M \text{ in ft/sec) for lift engines} \\ K_T & 7.9 \text{ (0.44 for } \bar{D}_M \text{ in ft, } \bar{U}_M \text{ in ft/sec) for cruise engines.} \end{aligned}$$

The use of lightweight materials, such as titanium rotor disks, as well as the reduced design life for lift engines seemed to account for this difference in weight.

Control and accessory weight includes the fuel and control system, oil, and starting systems. Not included are airplane power takeoffs or variable-geometry mechanisms for inlets and exhaust nozzles. The relations developed for this weight group were obtained from data for lift engines only. Control and accessory weight was calculated from:

$$W_A = K_A F [1 + A(\text{SFC})] , \quad (\text{D18})$$

where

$$\begin{aligned} K_A &= 0.0002 \text{ (0.002 for } F \text{ in lb and SFC in lb/hr lb)} \\ A &= 13.2 \text{ (1.35 for } F \text{ in lb and SFC in lb/hr lb).} \end{aligned}$$

Equation (D18) can be applied to lift system exhaust gas generators by calculating thrust and SFC assuming the exhaust gas is expanded through a nozzle to ambient conditions. Similarly, the thrust and SFC for a lift system air generator can also be found by assuming the generator air as well as the exhaust gas are expanded through a nozzle to ambient conditions. Control and accessory weight for cruise powerplants was found to vary between 9 and 30 percent of the total engine weight compared to a range of from 2 to 10 percent for lift engines.

Structure weight includes the engine mounts, bearings, bearing supports, shafts, inner wall of fan duct (for turbofan engines) and transition sections. Structure weight is calculated from:

$$W_S = K_S \sum W_{\text{components}} . \quad (\text{D19})$$

where

$$\begin{aligned} K_S &= 0.10 \text{ for lift engines} \\ K_S &= 0.18 \text{ for cruise engines.} \end{aligned}$$

Using the equations presented herein, a total powerplant weight can be determined by summing the estimated component weights including the structure weight. For example, the total weight of a lift turbofan engine may be expressed as:

$$W_{\text{total}} = W_F + (W_D + W_L) + W_C + (W_T)_{\text{high}} + (W_T)_{\text{low}} + W_A + W_S . \quad (\text{D20})$$

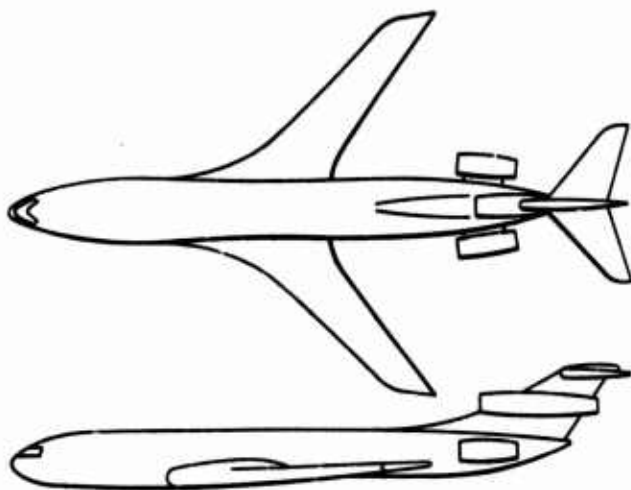


Fig.1 Conceptual Mach 0.98 transport

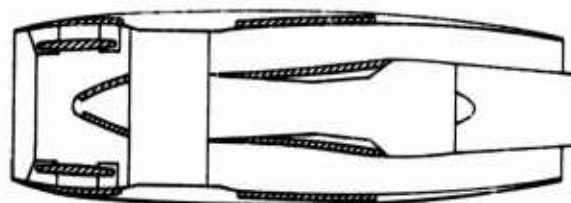


Fig.2 Turbofan engine with acoustic treatment

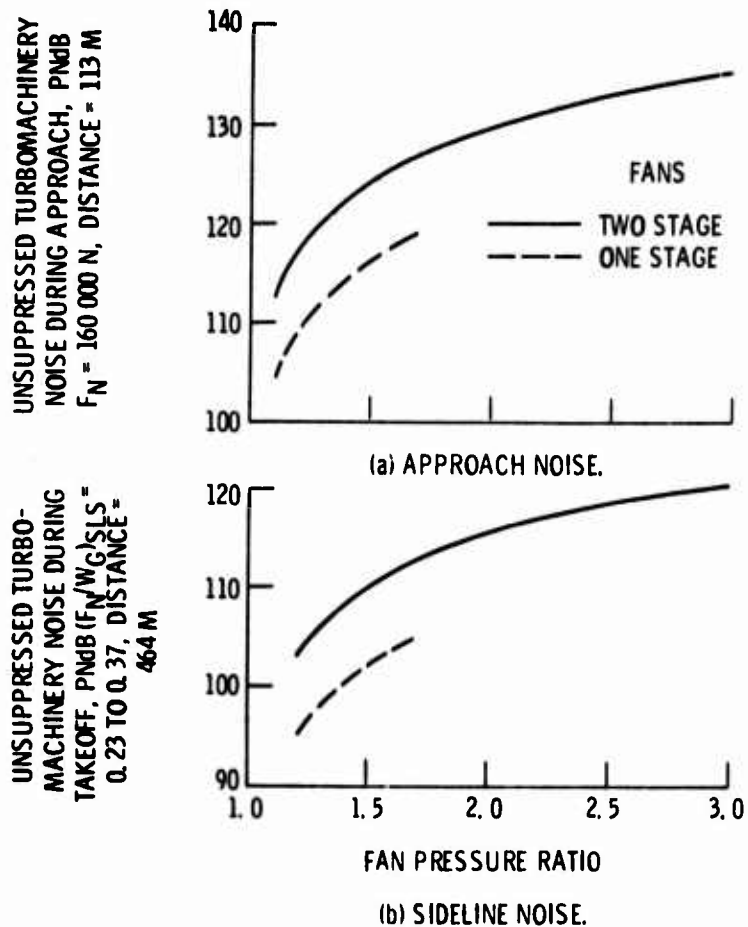


Fig.3 Unsuppressed turbomachinery noise during approach and takeoff for one- and two-stage fan engines. Airplane TOGW = 175,000 kg. Noise numbers estimated to be within ± 2 PNdB

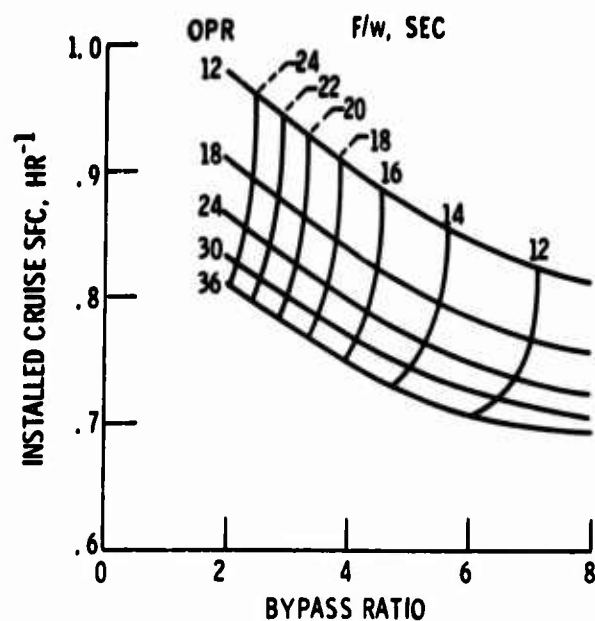


Fig.4 Performance for cruise at Mach 0.98 and 12,200 m (40,000 ft); FPR = 1.5; $T_4 = 1093^\circ\text{C}$ (2000°F)

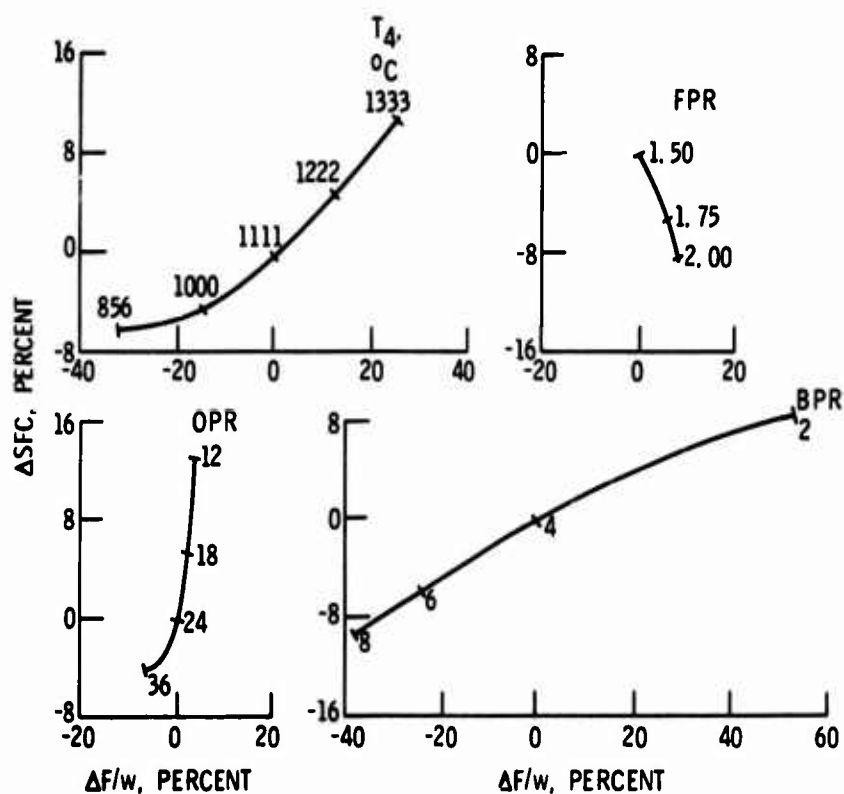
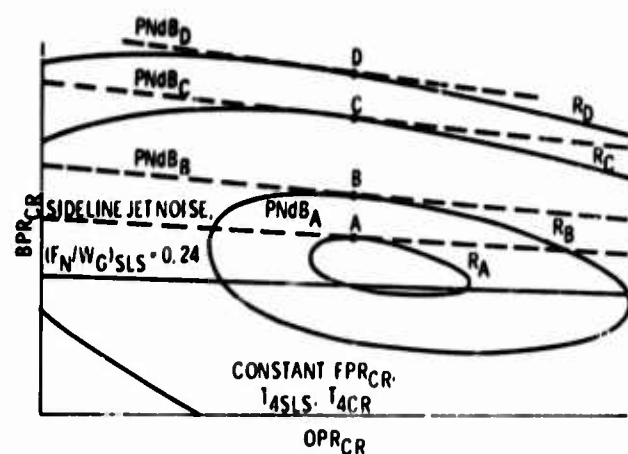
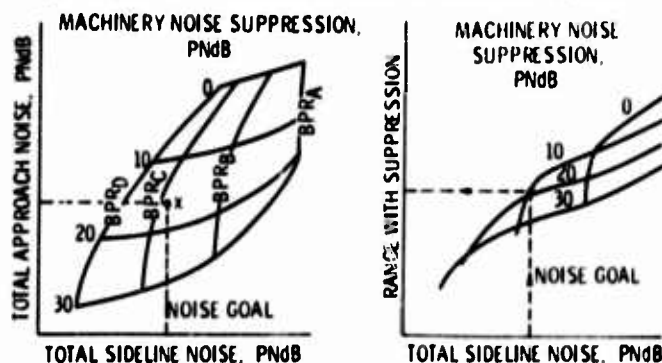


Fig.5 Effect of engine parameters on cruise performance at Mach 0.98



(a) "THUMBPRINT" PERFORMANCE PLOT. NO NOISE SUPPRESSION.



(b) TOTAL SIDELINE AND APPROACH NOISE RELATED TO AMOUNT OF FAN TURBOMACHINERY NOISE SUPPRESSION.

(c) RANGE WITH ACOUSTIC TREATMENT RELATED TO NOISE AND AMOUNT OF SUPPRESSION.

Fig.6 Illustration of method used to select engine parameters that maximize range for a given noise goal and takeoff thrust constraint. Constant TOGW, payload, FPR_{CR} , T_{4SLS} , T_{4CR}

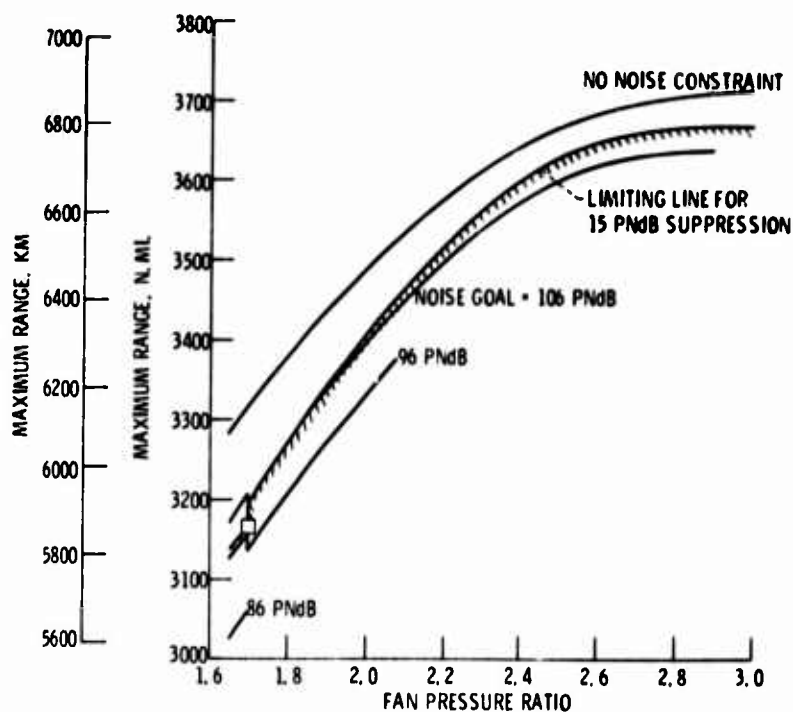


Fig.7 Maximum total range versus fan pressure ratio for several noise goals. Suppression weight penalty included. Takeoff $T_4 = 1260^\circ\text{C}$, cruise $T_4 = 1050^\circ\text{C}$, Mach number = 0.98, $\beta_{HPT} = 7.5$ percent, $\beta_{LPT} = 0$ percent, L/D varies with engine diameter

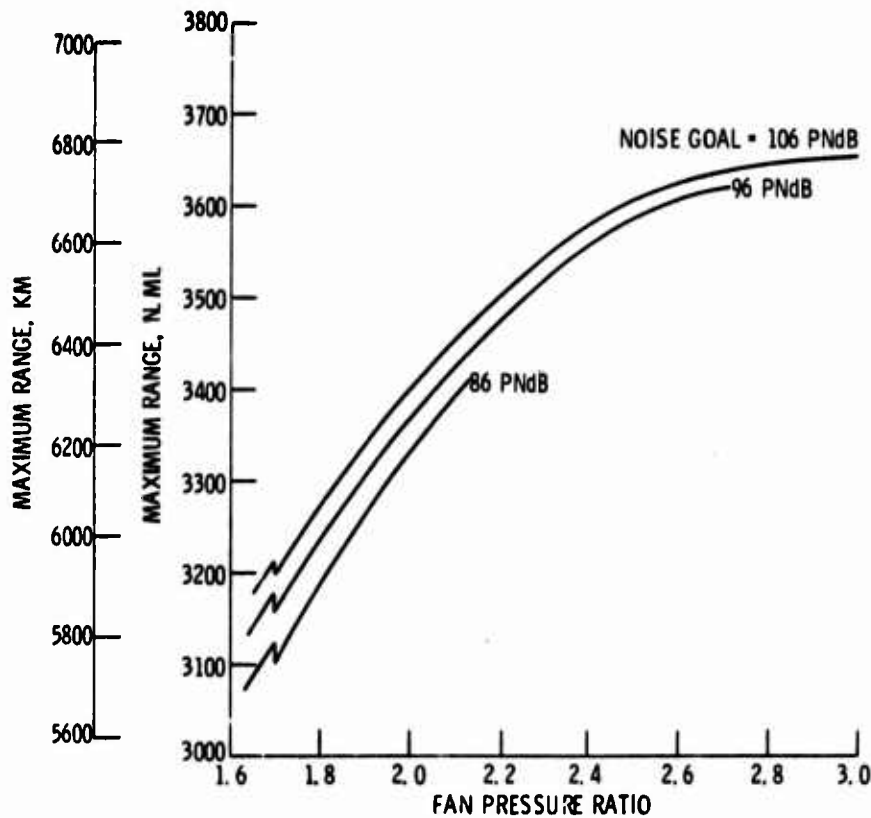


Fig.8 Maximum total range versus fan pressure ratio for several noise goals. Takeoff $T_4 = 1260^\circ\text{C}$, cruise $T_4 = 1050^\circ\text{C}$, cruise Mach number = 0.98, $\beta_{HPT} = 7.5$ percent, $\beta_{LPT} = 0$ percent, L/D varies with engine diameter, 10 PNdB jet noise suppressor assumed without weight penalty. Machinery noise suppression up to 40 PNdB assumed as necessary

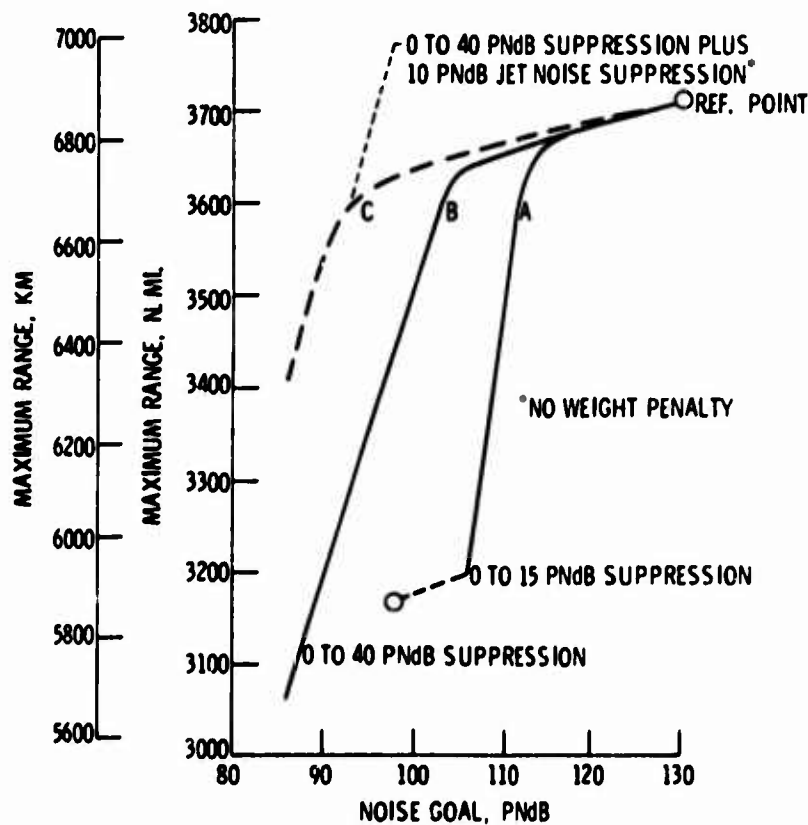


Fig.9 Range versus noise tradeoff. Takeoff $T_4 = 1260^\circ\text{C}$, cruise $T_4 = 1050^\circ\text{C}$, cruise Mach number = 0.98, $\beta_{HPT} = 7.5$ percent, $\beta_{LPT} = 0$ percent, L/D varies with engine diameter

CURVE	REFERENCE POINT	A		B			C		
NOISE GOAL, PNdB	NONE	106	98	106	96	86	106	96	86
MAXIMUM RANGE, KM	6880	5950	5880	6740	6260	5670	6760	6700	6310
RANGE PENALTY, KM	0	930	1000	139	611	1210	102	167	556
OPTIMUM FPR	3.0	1.7	1.7	2.9	2.08	1.7	3.0	2.72	2.16
OPTIMUM OPR	30.5	31.8	31.1	30.6	31.0	31.0	30.5	30.7	30.9
OPTIMUM BPR	2.4	4.8	5.5	2.45	4.1	6.5	2.4	2.7	3.9
JET NOISE SUPP.	0	0	0	0	0	0	10	10	10
MACHINERY NOISE SUPP.	0	7	15	34	28	40	25	38	40
NO. OF FAN STAGES	2 OR 3	1	1	2 OR 3	2	1	2 OR 3	2 OR 3	2
APPROACH NOISE, PNdB	130	106	98	106	96	78	106	96	86
SIDELINE NOISE, PNdB	120	106	98	106	96	86	99	94	86

Fig.10 Range-noise tradeoff, turbine rotor-inlet temperature = 1260°C

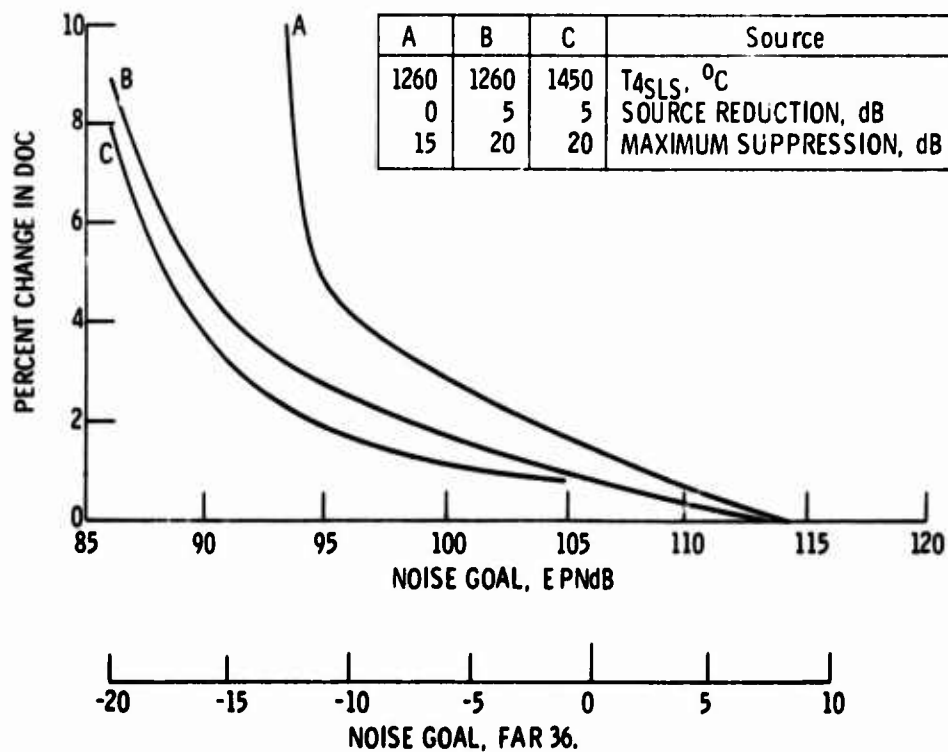


Fig. 11 Direct operating cost versus noise level

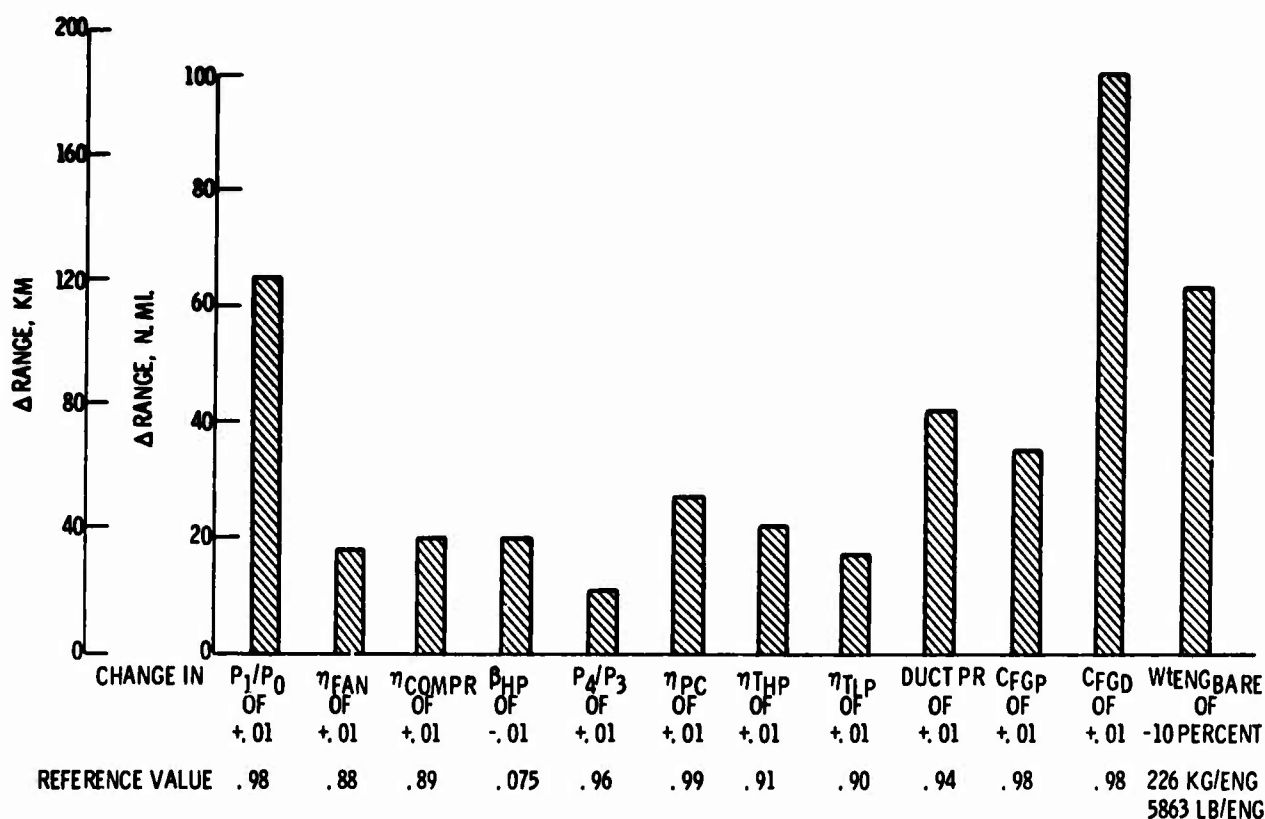


Fig.12 Change in range for a change in engine design parameter. Reference engine, takeoff $T_4 = 1260^\circ\text{C}$, cruise $T_4 = 1050^\circ\text{C}$, FPR = 1.70, OPR = 31.0, BPR = 4.8, cruise Mach number = 0.98

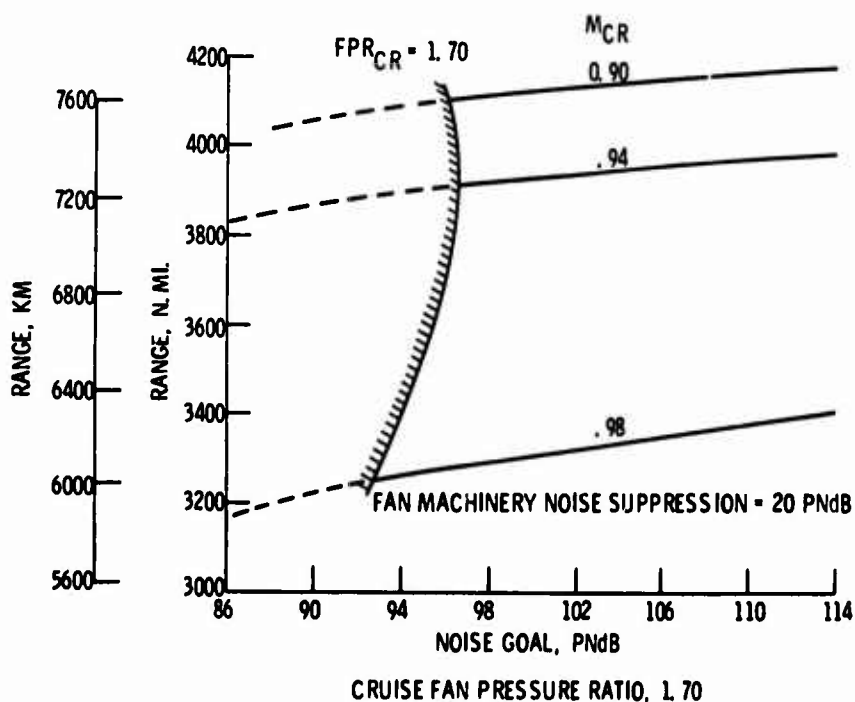
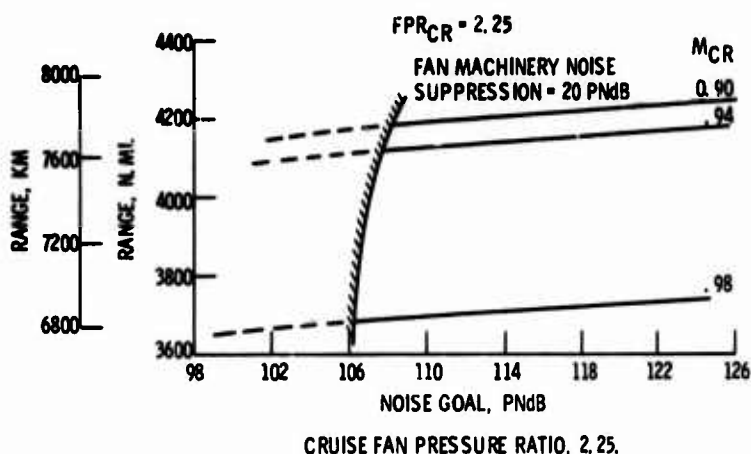


Fig.13 Range of acoustically-treated optimum airplanes as a function of desired noise goal for various design cruise Mach numbers. Takeoff gross weight, 175,000 kg; payload, 300 passengers. $T_{4SL5} = 1260^\circ\text{C}$



CRUISE FAN PRESSURE RATIO, 2.25.

Fig. 14 Range of acoustically-treated optimum airplanes as a function of desired noise goal for various design cruise Mach numbers. Takeoff gross weight, 175,000 kg; payload, 300 passengers. T_{4SLs} , 1260°C

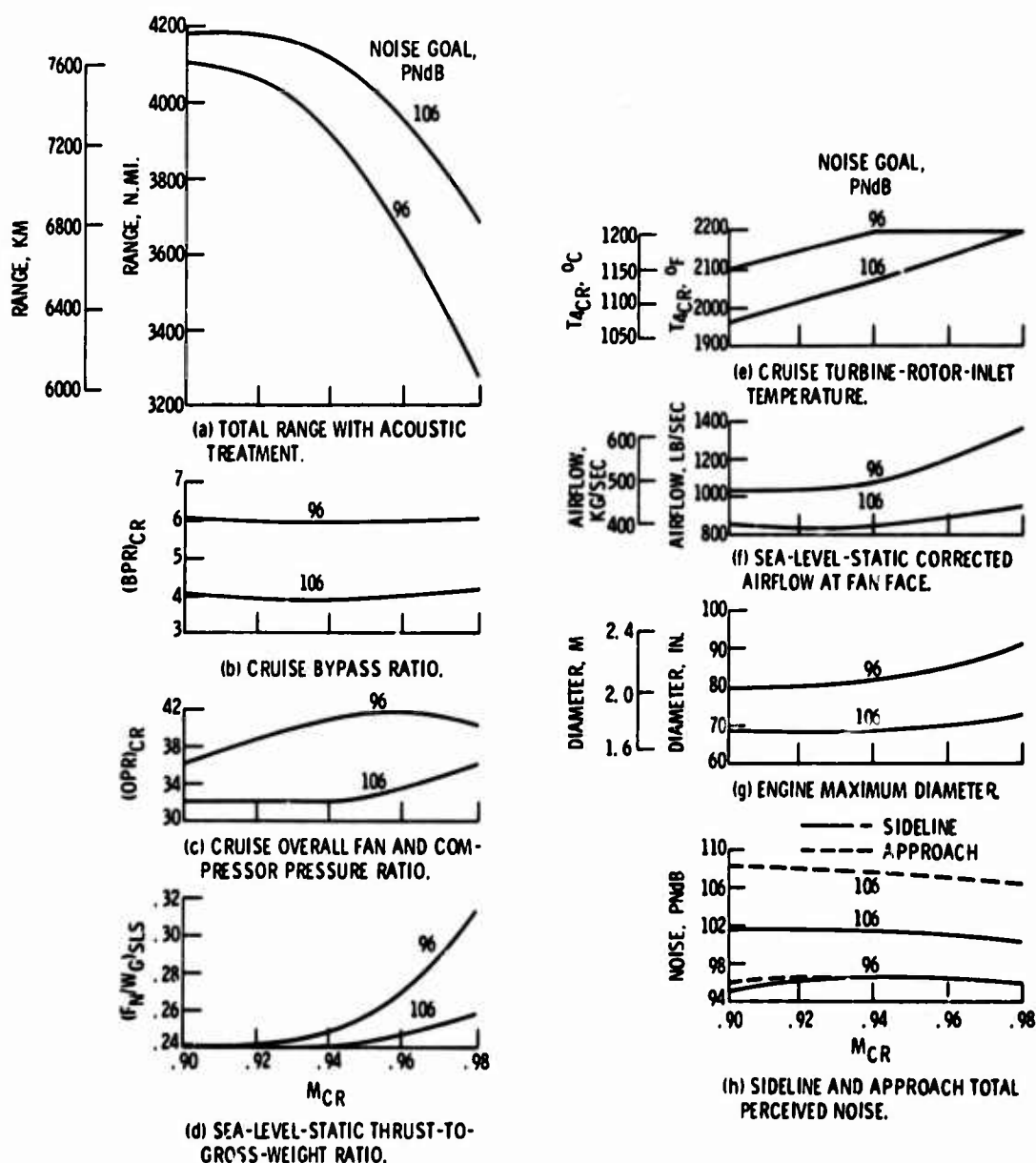


Fig. 15 Characteristics of range-optimized cycles related to design cruise Mach number at noise goals of 106 and 96 PNdB. Takeoff gross weight, 175,000 kg; payload, 300 passengers; T_{4SLs} , 1260°C

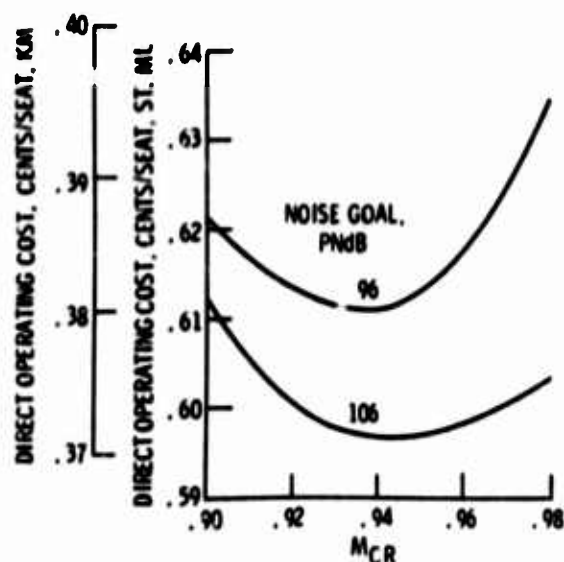


Fig. 16 Direct operating cost of range-optimized cycles related to design cruise Mach number at noise goals of 106 and 96 PNdB. Takeoff gross weight, 175,000 kg; payload, 300 passengers; T_{4SL5} , 1260°C

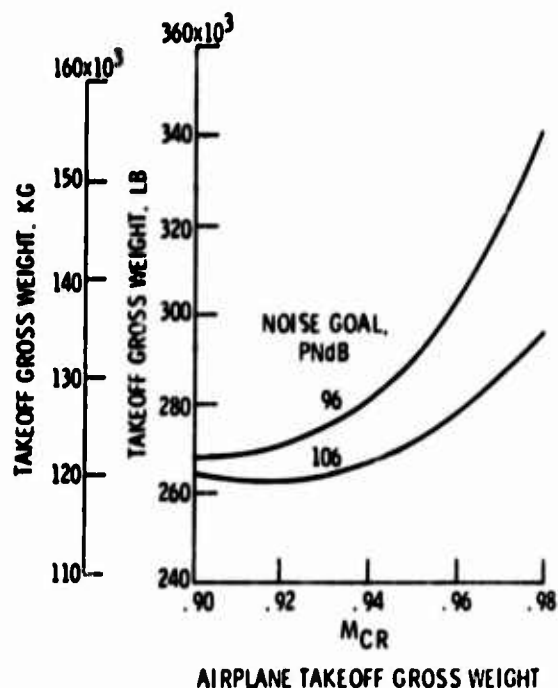
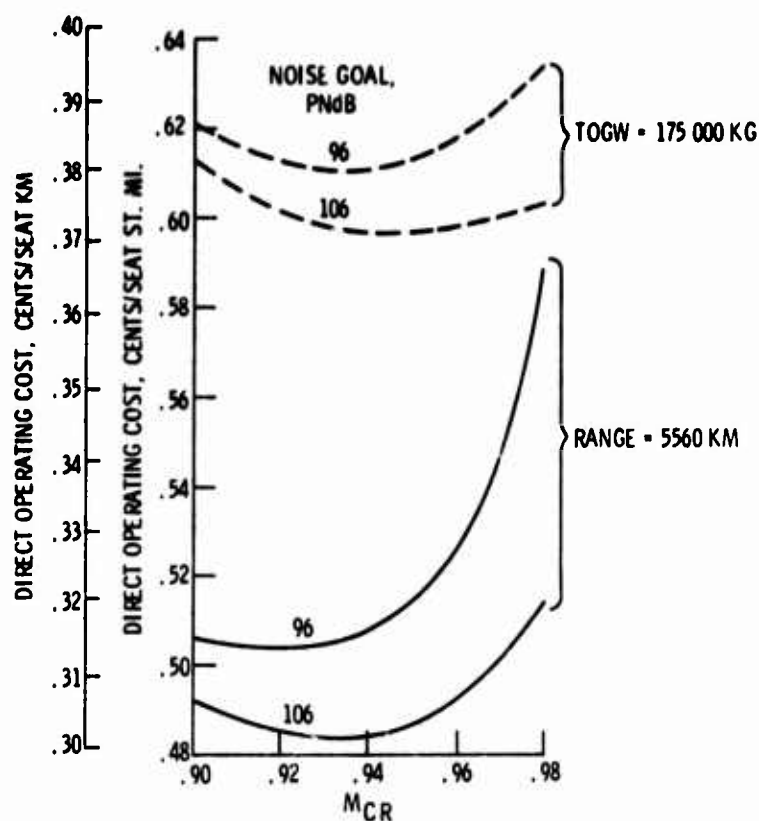


Fig. 17 Characteristics of optimized cycles related to design cruise Mach number at noise goals of 106 and 96 PNdB. Total range, 5560 km; payload, 300 passengers; T_{4SL5} , 1260°C



(a) AIRPLANE COST ESTIMATES
BASED ON CURRENT AIR-
PLANES.

Fig. 18 Direct operating cost of optimized cycles related to design cruise Mach number at noise goals of 106 and 96 PNdB. Payload, 300 passengers. T_{4SL5} , 1260°C

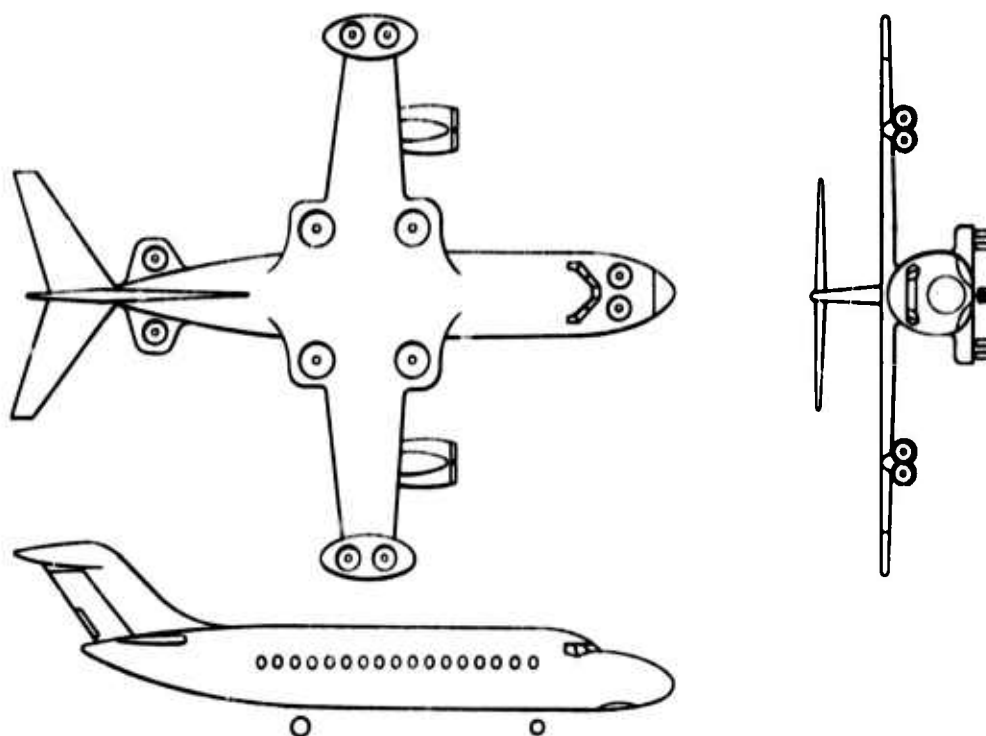


Fig. 19 VTOL transport

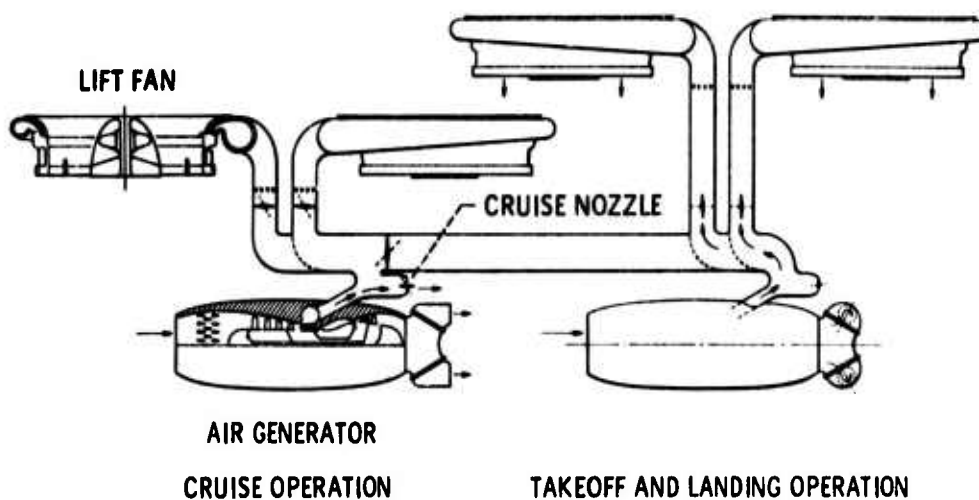
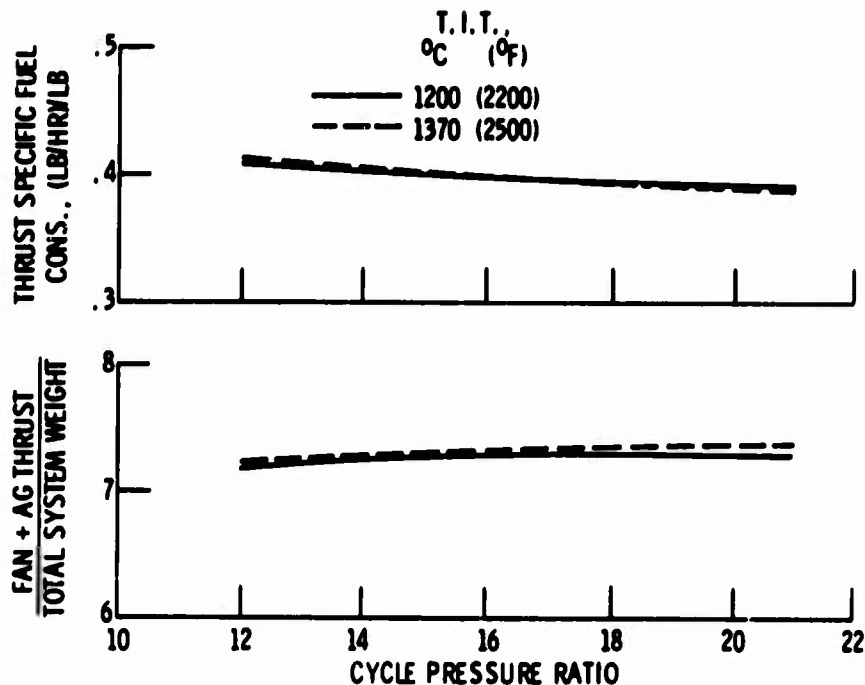
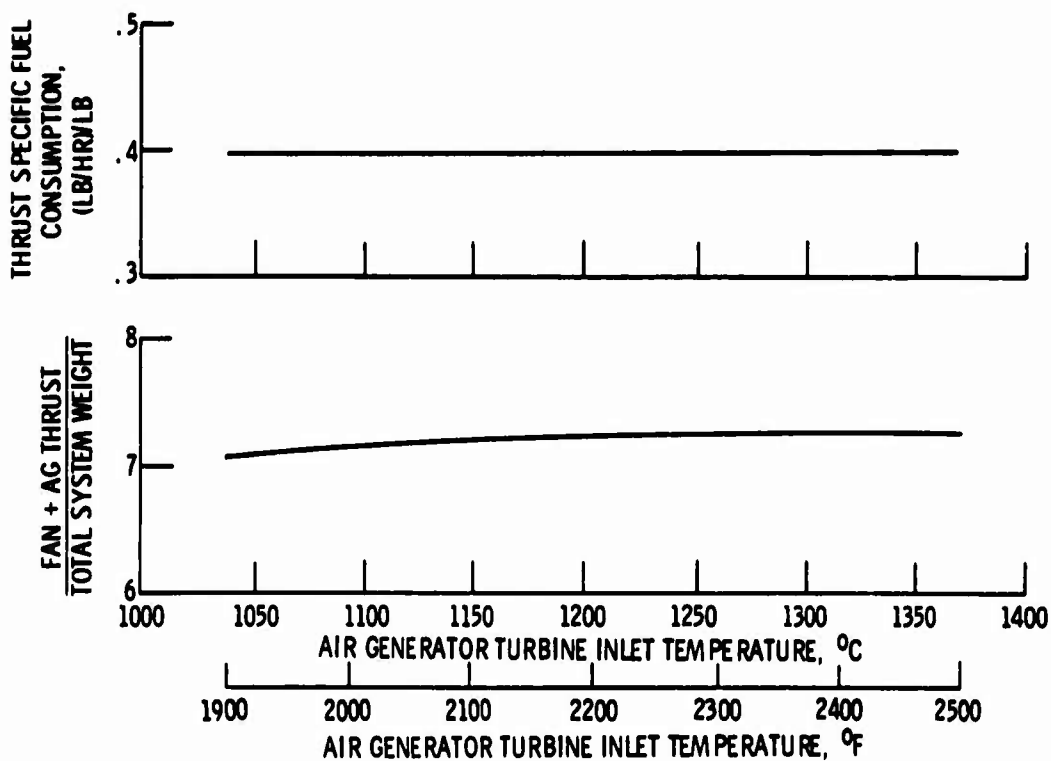


Fig. 20 Air generator remote drive lift fan propulsion system



(a) EFFECTS OF OVERALL PRESSURE RATIO ON PERFORMANCE AND WEIGHT.



(b) EFFECTS OF TURBINE TEMPERATURE ON PERFORMANCE AND WEIGHT. OVERALL PRESSURE RATIO IS 15.

Fig.21 Effects of air generator parameters on propulsion system performance, weight, and size. Lift fan pressure ratio is 1.20

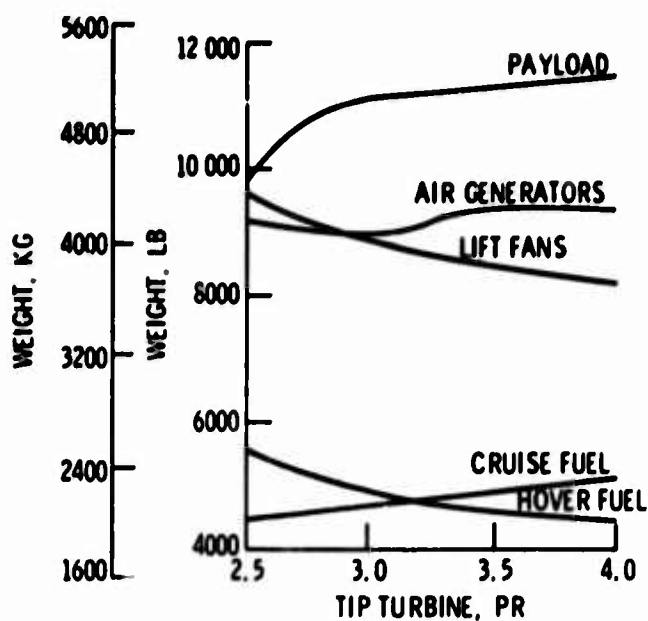


Fig. 22 Weight trends. Lift fan PR = 1.25, L/D = 10

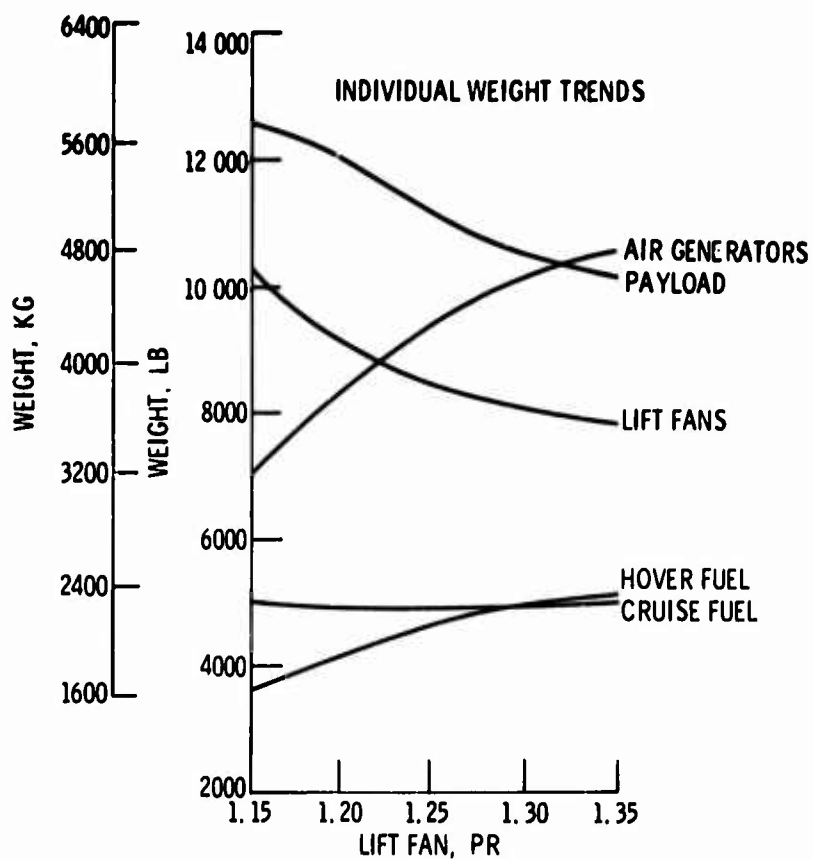


Fig. 23 Weight trends. Tip turbine PR = 3.5, $(L/D)_{CR} = 10$

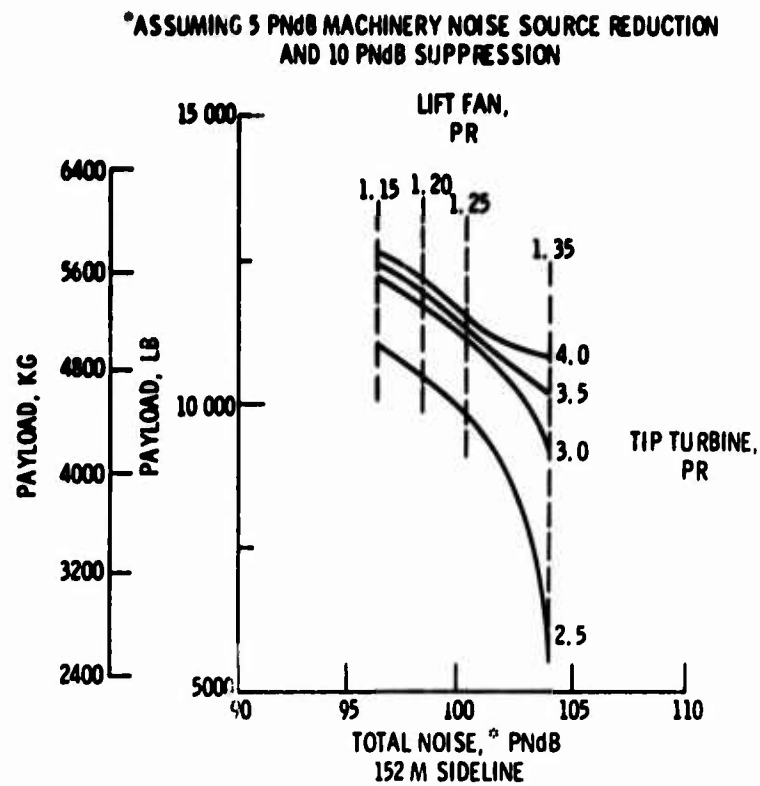
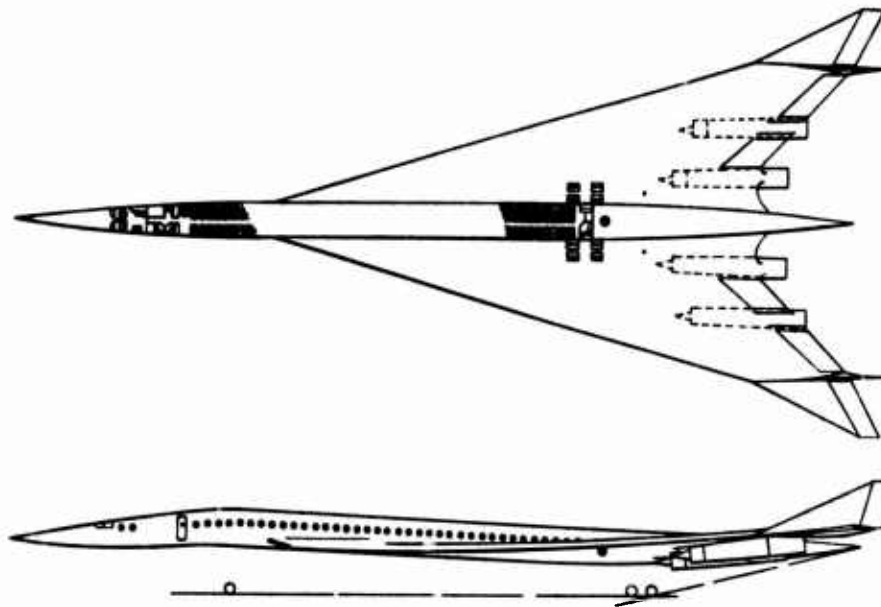
Fig. 24 Performance-noise tradeoff. $(L/D)_{CR} = 10$ 

Fig. 25 Supersonic transport

TURBINE TEMPERATURE, °C	1200 TO 1700
OVERALL PRESSURE RATIO	7 TO 19
FAN PRESSURE RATIO	1.5 TO 3.5
BYPASS RATIO	1.0 TO 3.1
MAXIMUM AUGMENTATION TEMPERATURE, °C	1700

Fig. 26 Range of engine variables

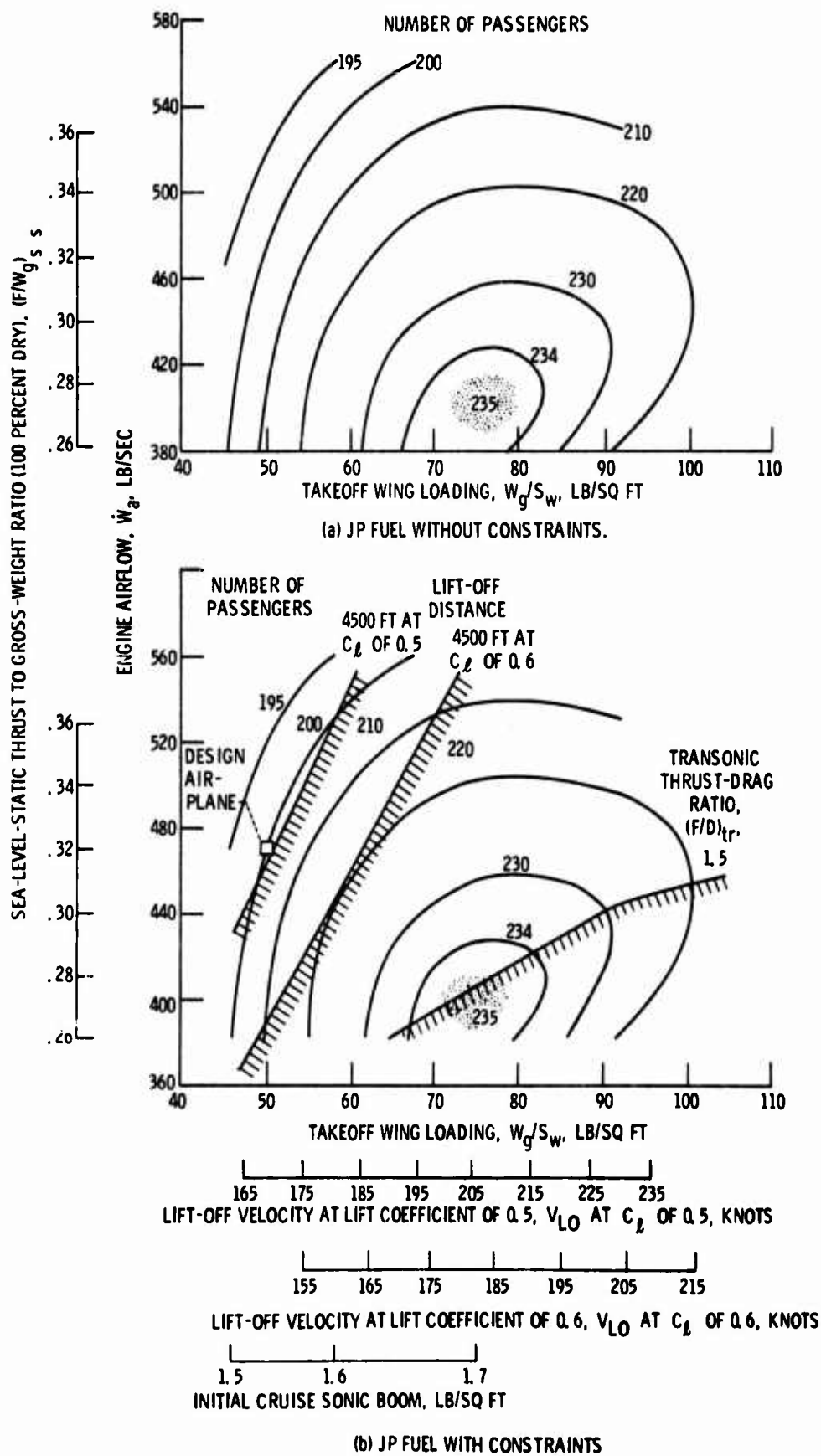


Fig. 27 Wing and engine sizing. Turbine-inlet temperature, 2100°F

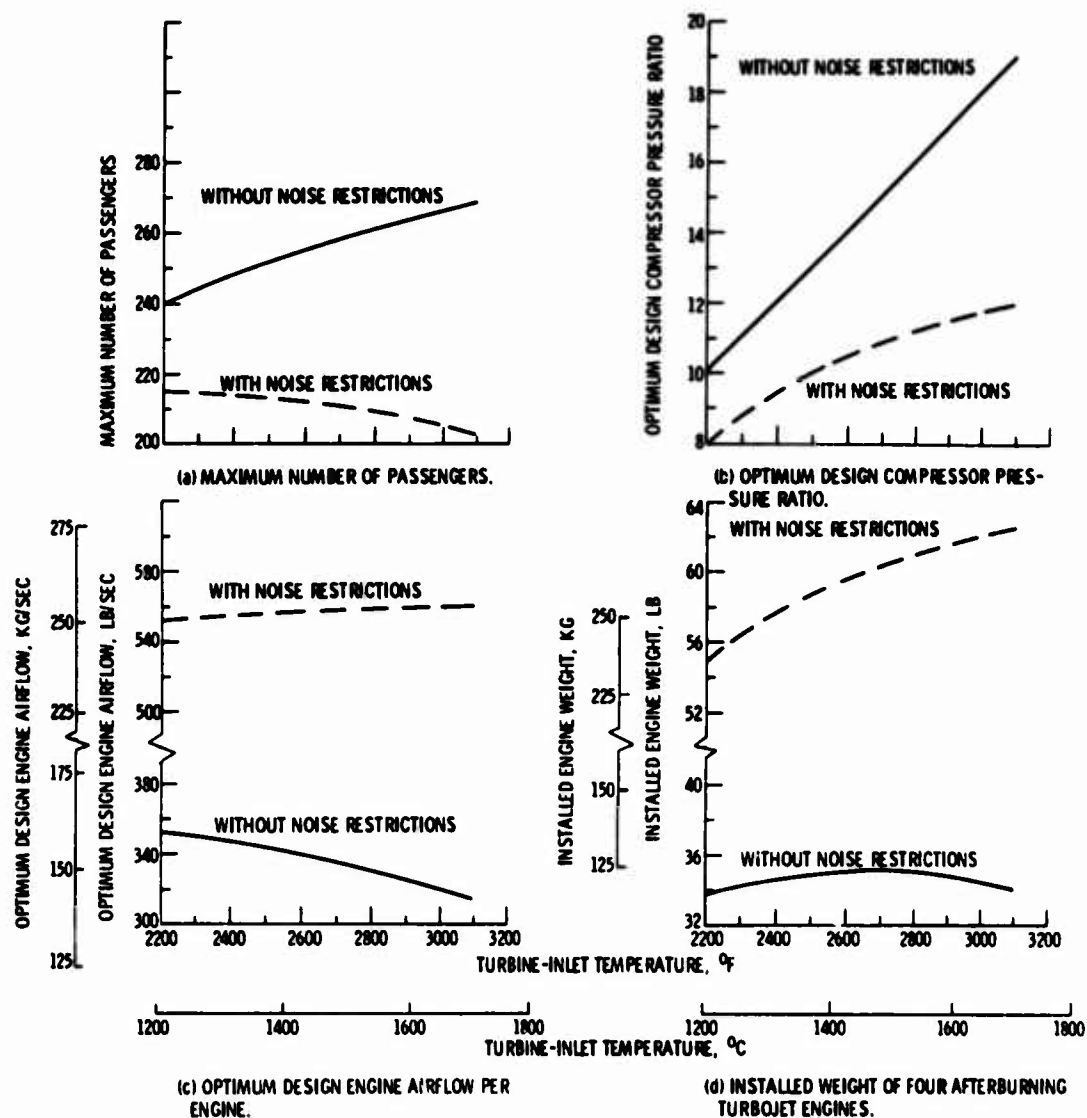


Fig. 28 Effect of design turbine-inlet temperature for afterburning turbojets; ramp gross weight, 460,000 pounds (208,652 kg); Mach 3.0 cruise

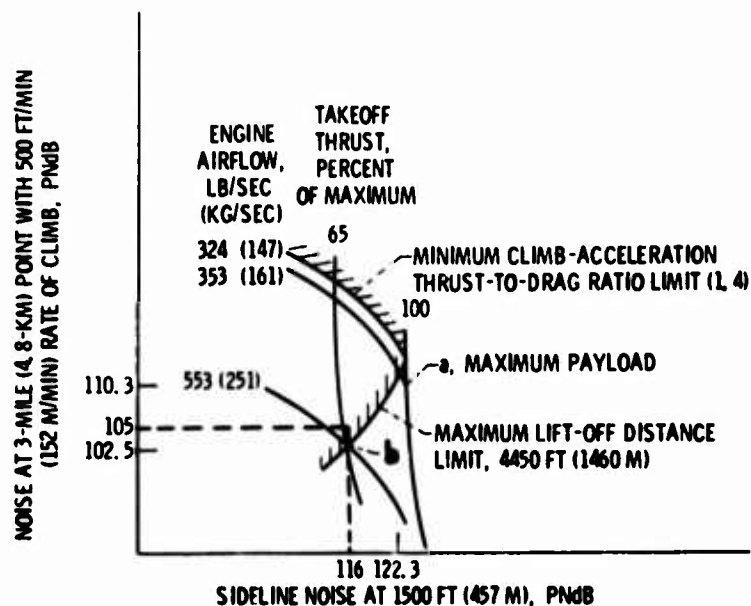


Fig. 29 Effect of engine noise goals on aircraft and engine parameters with four afterburning turbojet engines. Design turbine-inlet temperature, 2200°F (1204°C)

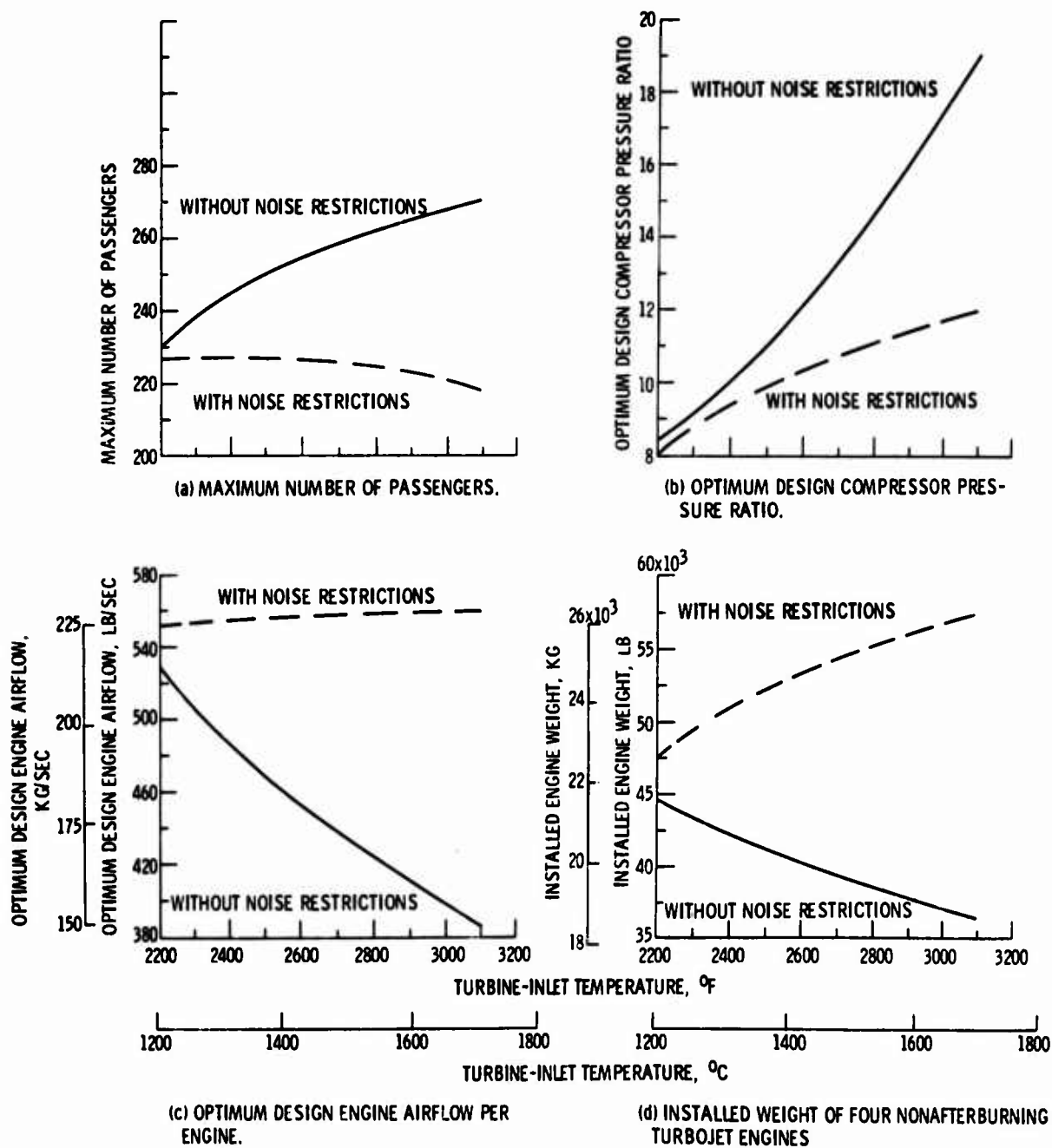


Fig.30 Effect of design turbine-inlet temperature for non-afterburning turbojets. Ramp gross weight, 460,000 pounds (208,652 kg); Mach 3.0 cruise

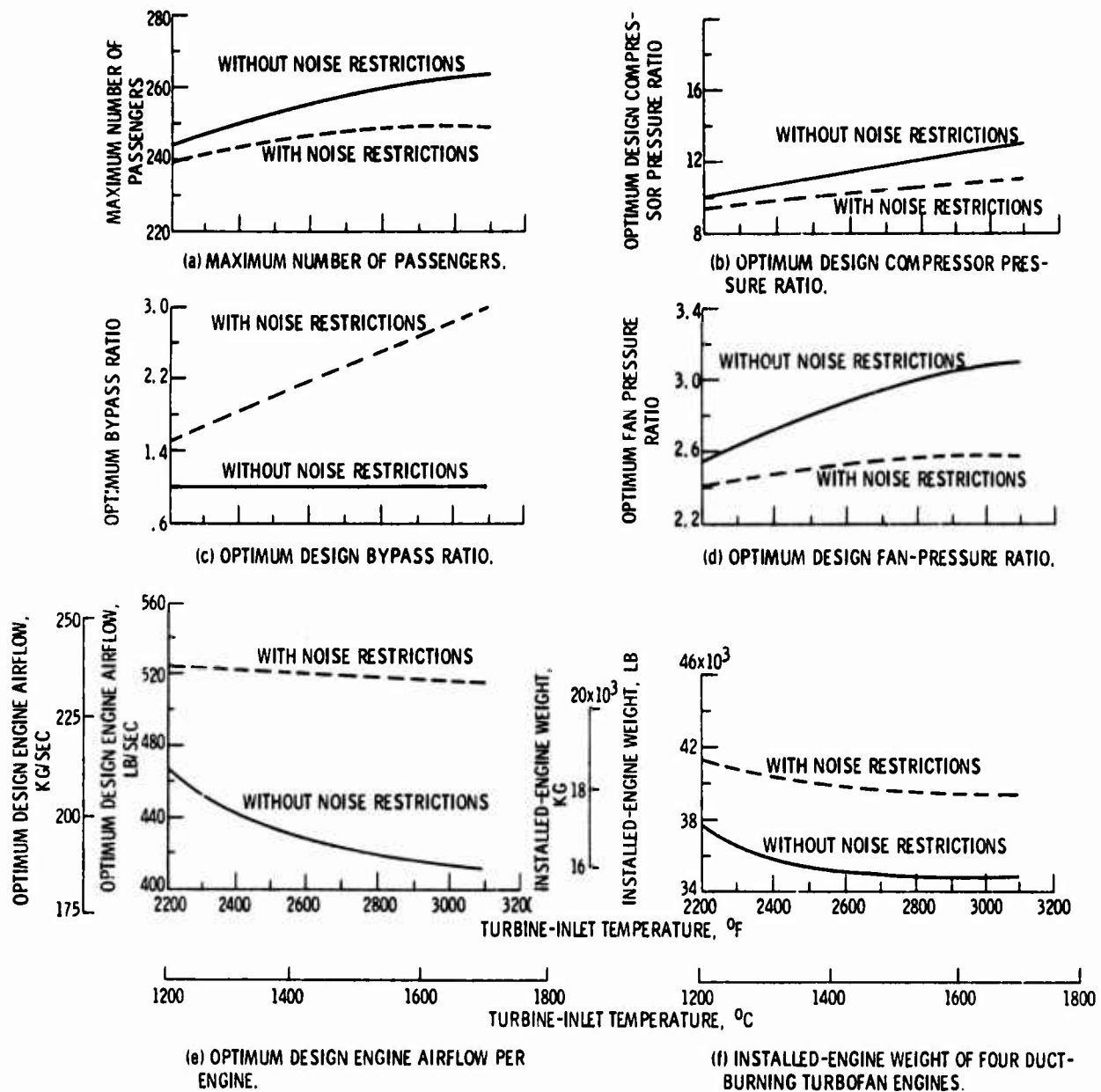


Fig.31 Effect of design turbine-inlet temperature for duct-burning engines. Ramp gross weight, 460,000 pounds (208,652 kg); Mach 3.0 cruise

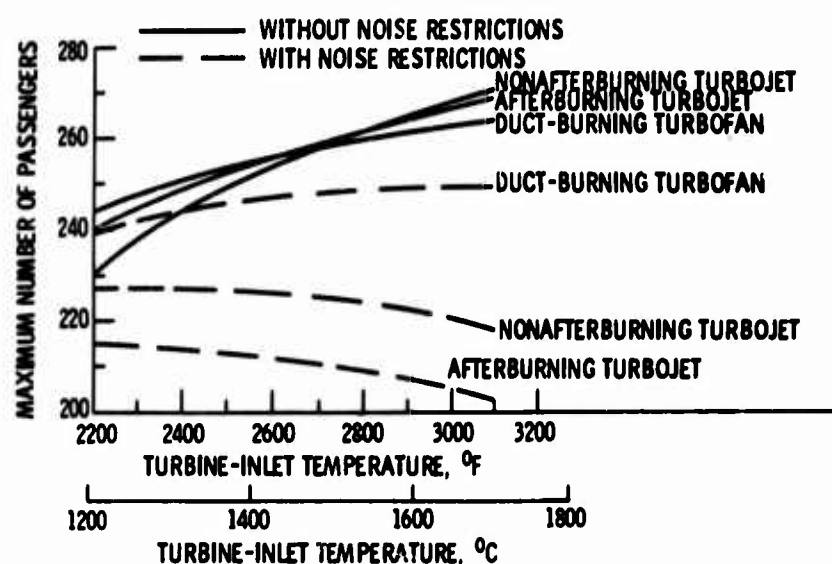


Fig. 32 Passenger carrying comparison for various turbine-inlet temperatures. Ramp gross weight, 460,000 pounds (208,652 kg); minimum sea-level-static thrust to gross weight ratio, 0.32; Mach 3.0 cruise

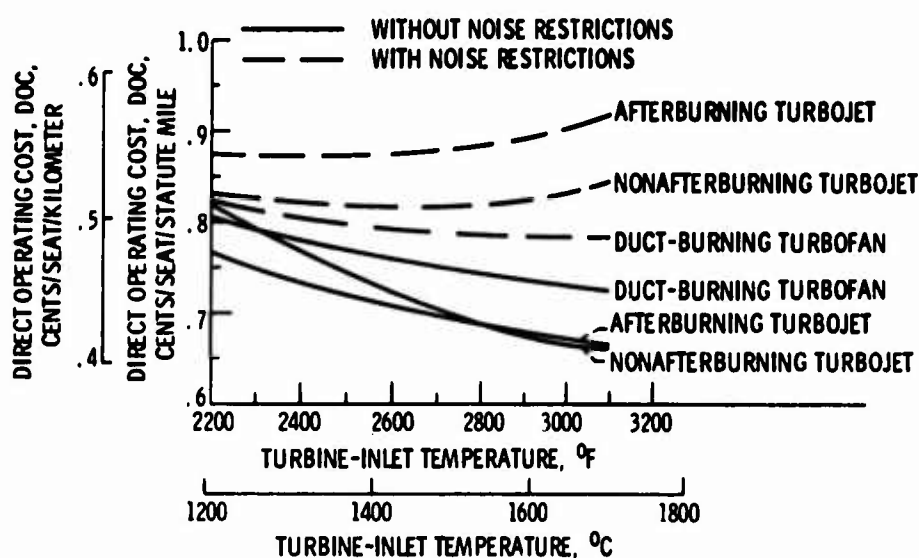


Fig. 33 Direct operating cost comparison for various turbine-inlet temperatures. Ramp gross weight, 460,000 pounds (208,652 kg); Mach 3.0 cruise

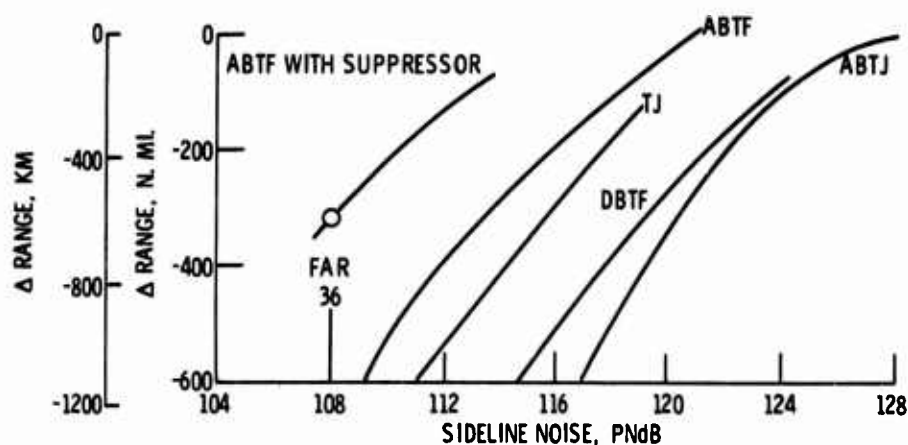


Fig. 34 Range-noise tradeoff; TOGW, 340,000 kg; Mach 2.7; payload, 22,200 kg; design turbine temperature, 1200°C

$$\Sigma F = ma$$

$$T - D - W \sin \gamma = m\dot{V}$$

$$\frac{V(T - D)}{W} = V \sin \gamma + \frac{V\dot{V}}{g}$$

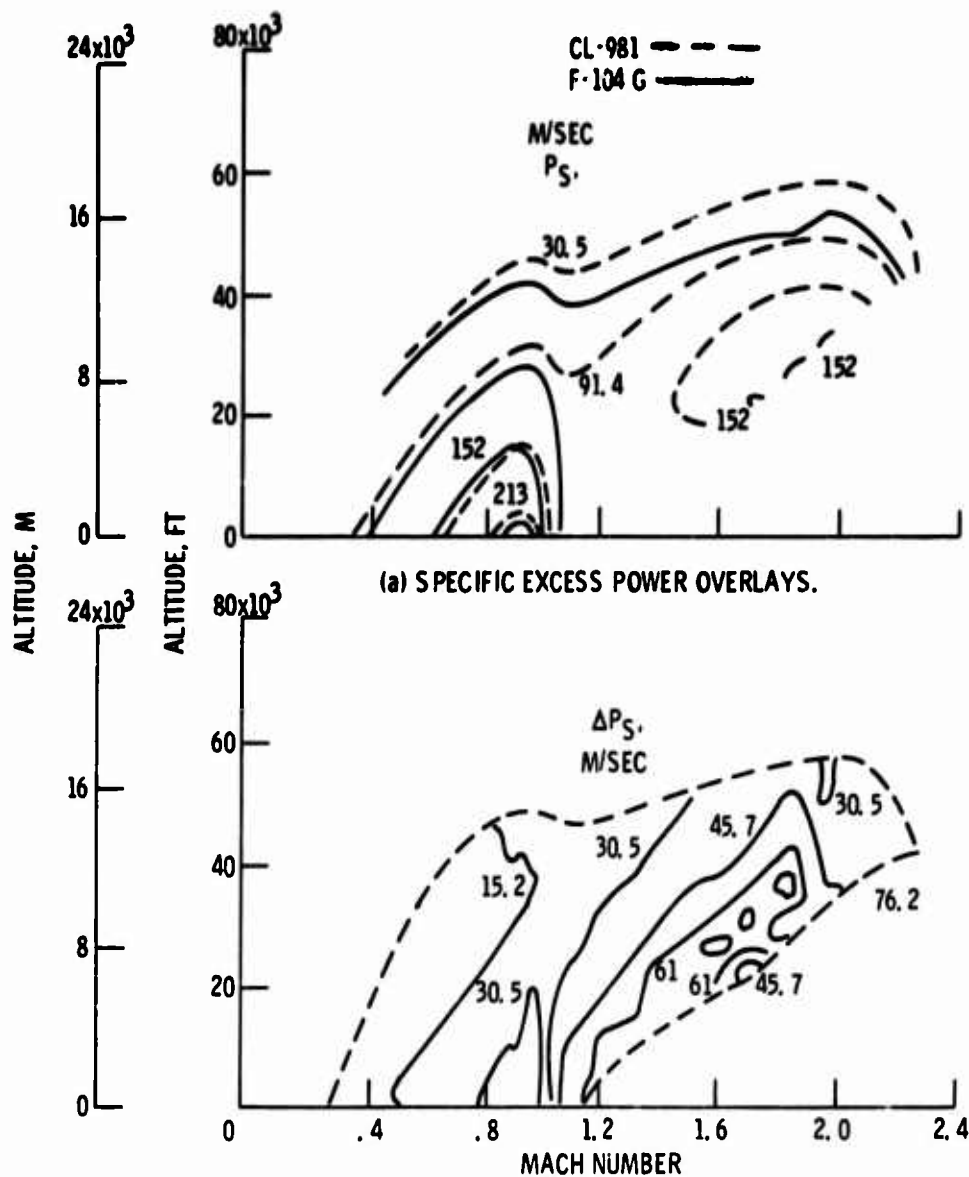
$$\frac{V(T - D)}{W} = \dot{h} + \frac{V\dot{V}}{g}$$

$$E = Wh + \frac{1}{2}mV^2$$

$$E_S = \frac{E}{W} = h + \frac{V^2}{2g}$$

$$\frac{d}{dt}(E_S) = \dot{h} + \frac{V\dot{V}}{g} = P_S$$

$$P_S = \frac{V(T - D)}{W}$$

Fig.35 Derivation of specific excess power (P_S)

(b) DIFFERENTIAL SPECIFIC EXCESS POWER CONTOURS.

Fig.36 Fighter performance comparison

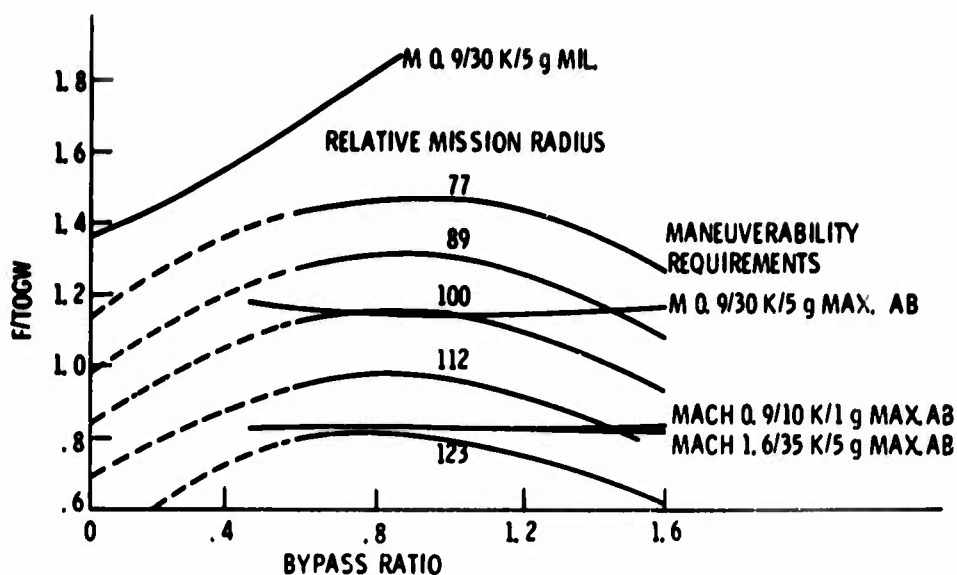


Fig. 37 Selection of bypass ratio and engine size

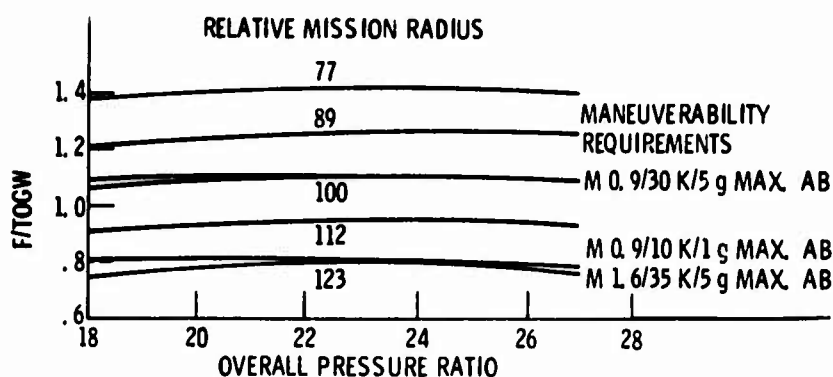


Fig. 38 Selection of overall pressure ratio; BPR = 0.8

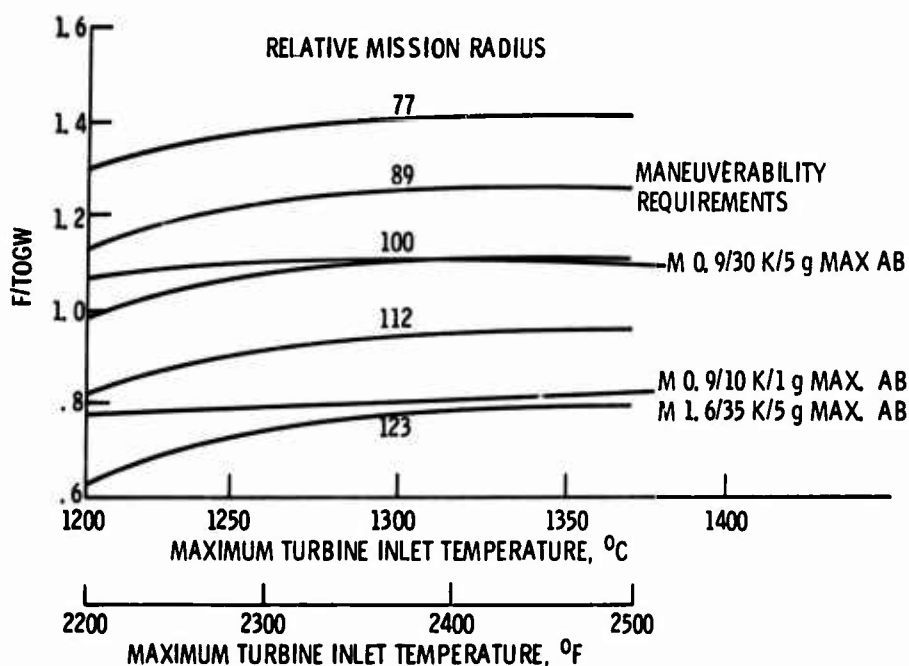


Fig. 39 Selection of turbine inlet temperature. BPR = 0.8; OPR = 23

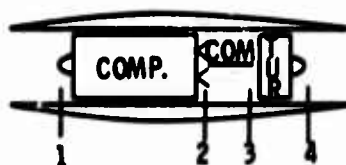


Fig.B1 Turbojet engine

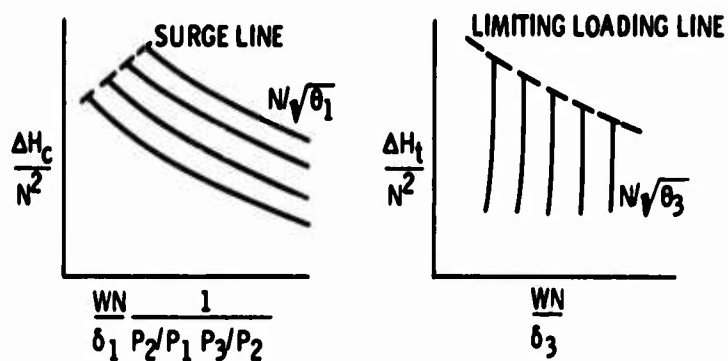


Fig.B2 Compressor and turbine matching maps

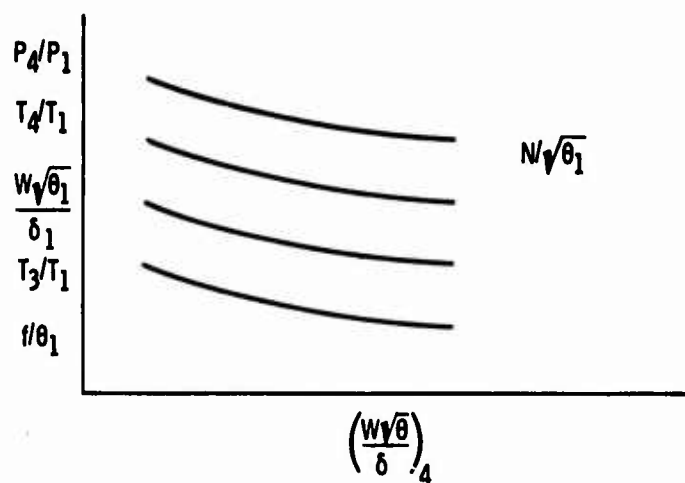


Fig.B3 Pumping characteristics

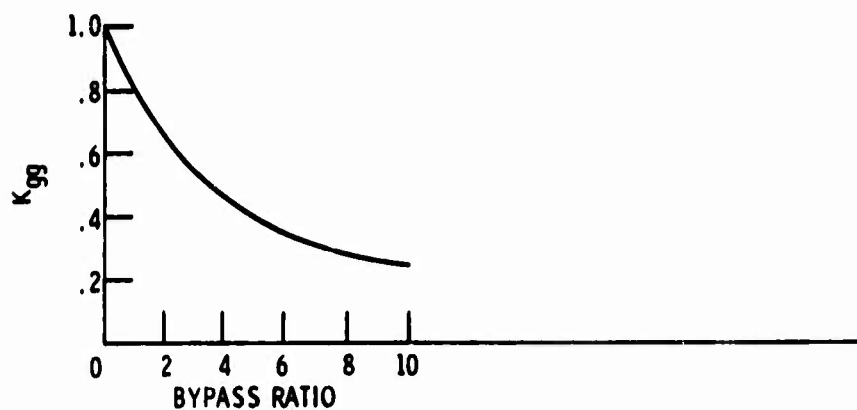
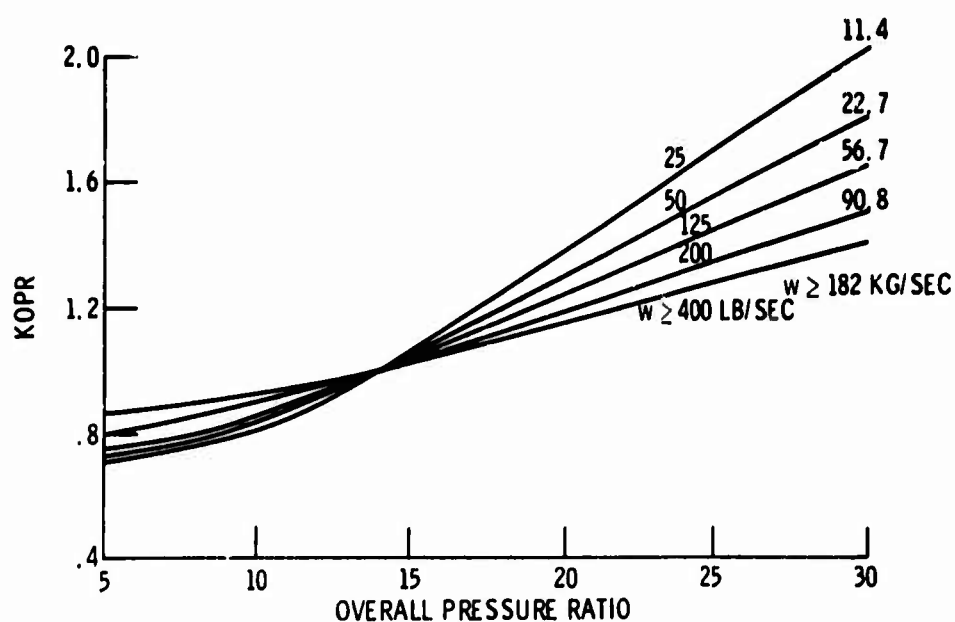
Fig.C1 Ratio of gas generator weight to total weight, K_{gg} 

Fig.C2 Correction for overall pressure ratio, KOPR

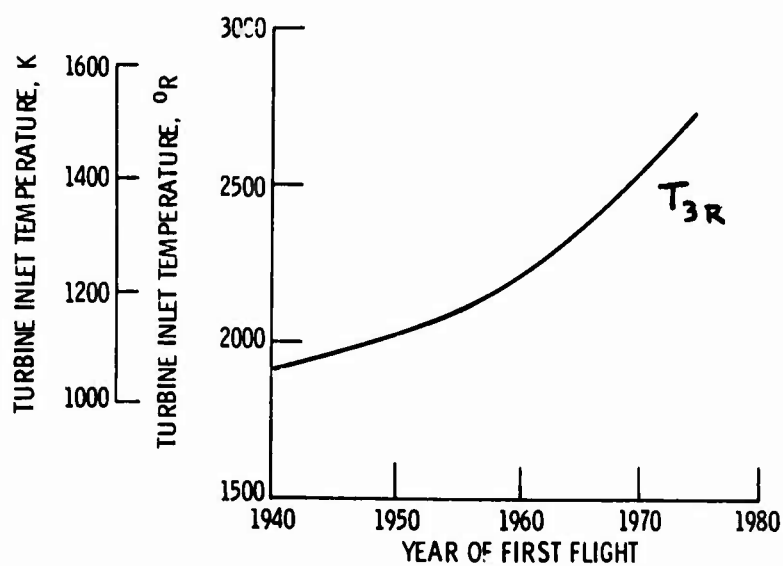


Fig.C3 Trend in turbine-inlet temperature

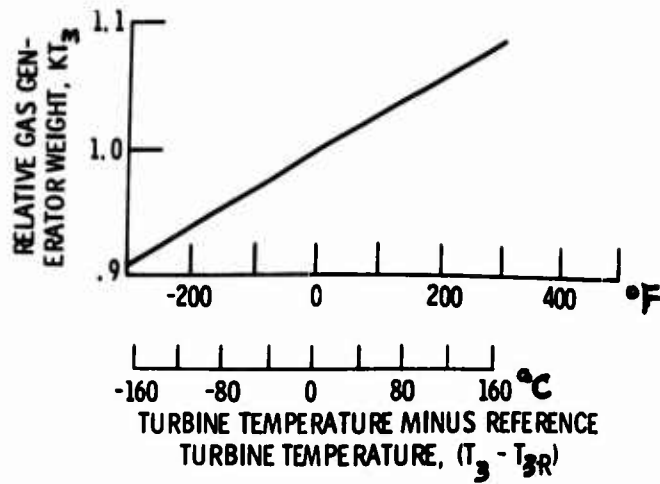
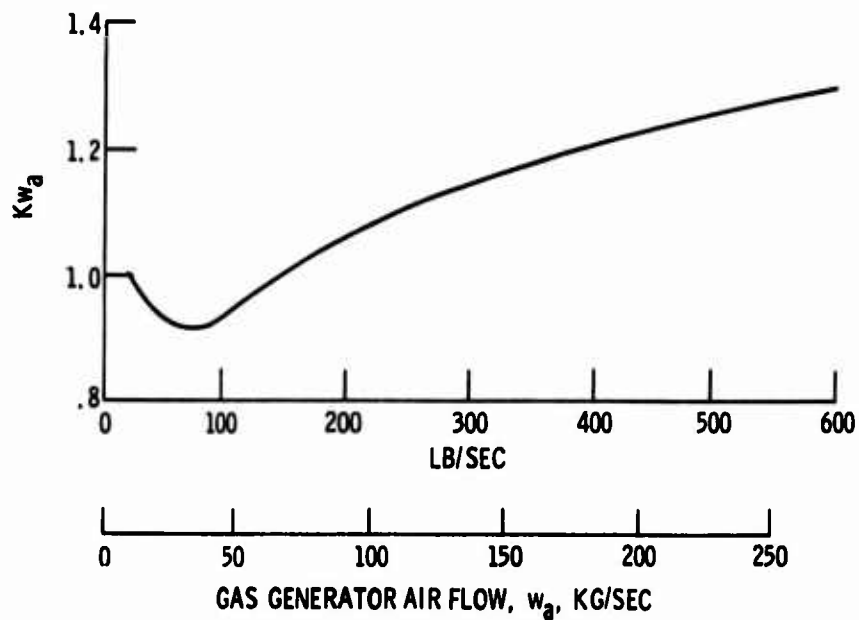
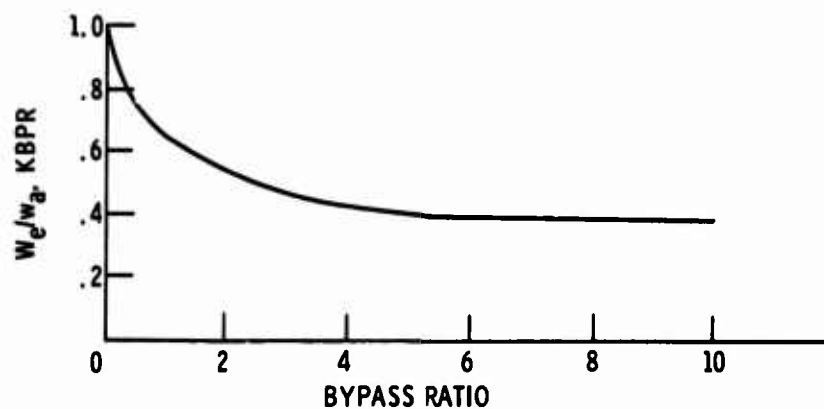
Fig.C4 Correction for turbine-inlet temperature, KT_3 Fig.C5 Correction for gas generator airflow, Kw_a 

Fig.C6 Correction for bypass ratio, KBPR

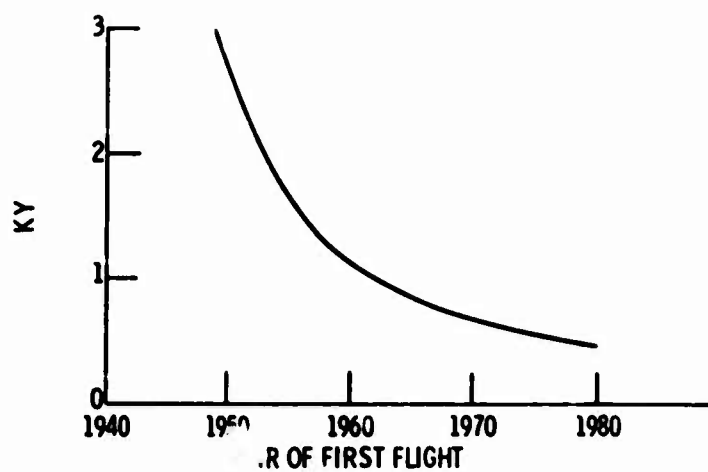


Fig.C7 Correction for year, KY

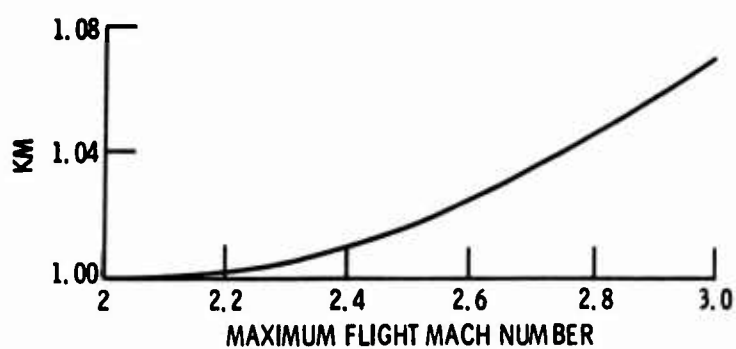


Fig.C8 Correction for Mach number, KM

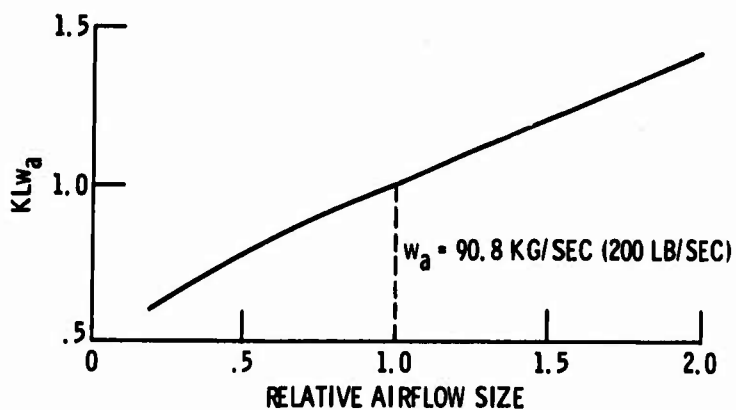


Fig.C9 Primary airflow size scaling factors for engine length

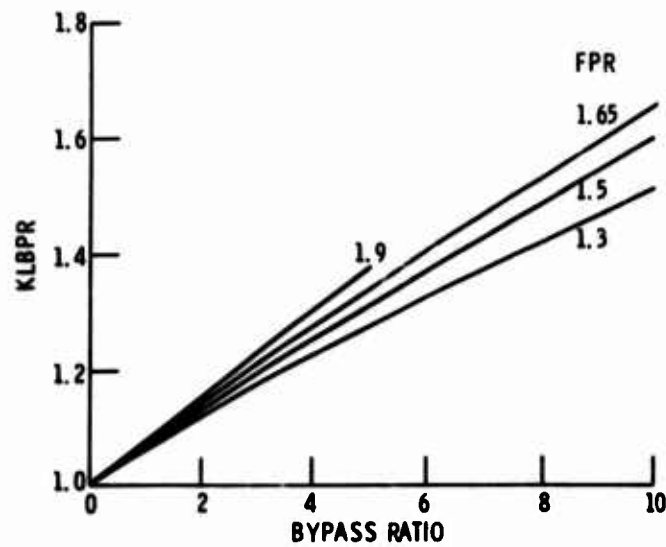


Fig.C.10 Bypass ratio-fan pressure ratio correction factor

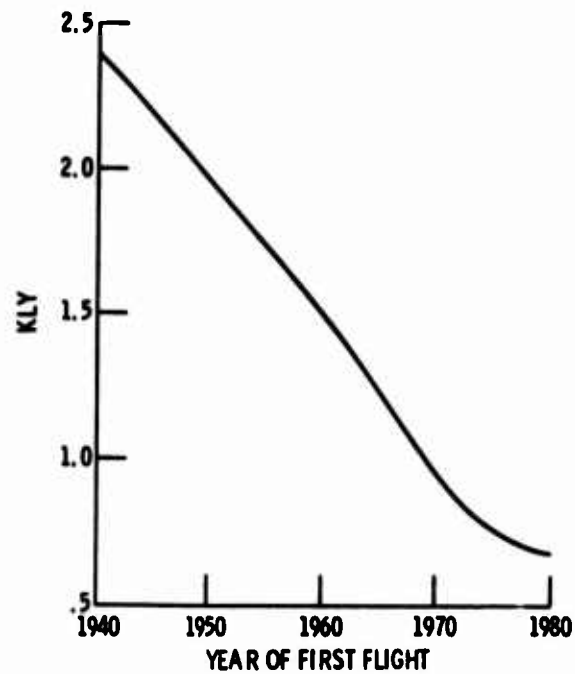


Fig.C11 Results of length correlation

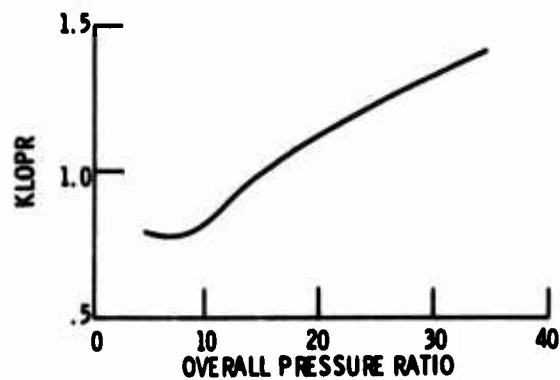


Fig.C12 Correction for overall pressure ratio

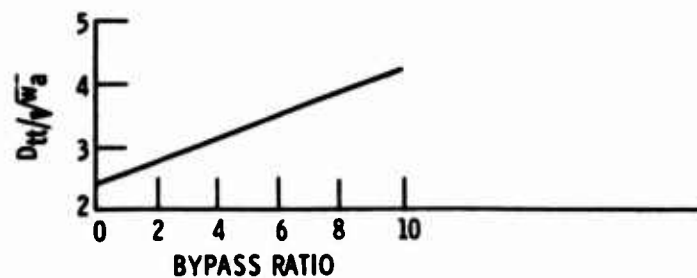


Fig.C13 Turbine tip diameter variation with bypass ratio

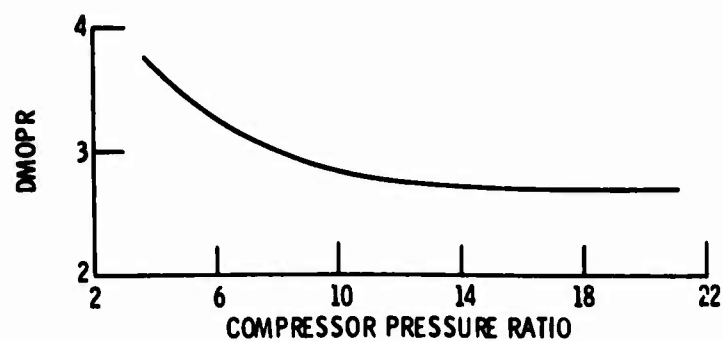


Fig.C14 Trend of normalized turbojet maximum diameter with pressure ratio

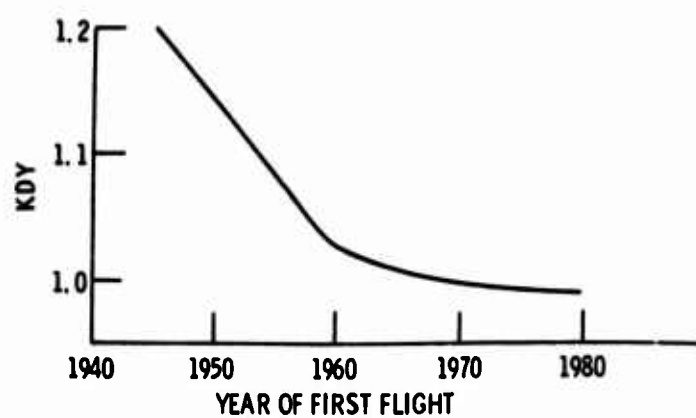


Fig.C15 Technology level (year) correction factor on turbojet maximum diameter

**PARAMETRIC AND OPTIMISATION TECHNIQUES FOR
AIRPLANE DESIGN SYNTHESIS**

by

Richard E. Wallace

**Aerodynamics Staff Product Development
Commercial Airplane Division
The Boeing Company
Seattle, Washington, USA**

CONTENTS

	Page
1. INTRODUCTION	7-1
2. DESIGN SYNTHESIS	7-3
3. PARAMETRIC EVALUATION TECHNIQUES	7-10
4. OPTIMIZATION EVALUATION TECHNIQUES	7-14
5. COMPUTERIZED AIRPLANE DESIGN SYNTHESIS	7-16
6. CONCLUDING REMARKS	7-18
REFERENCES	7-19
FIGURES	7-25

PARAMETRIC AND OPTIMISATION TECHNIQUES FOR AIRPLANE DESIGN SYNTHESIS

Richard E. Wallace

1. INTRODUCTION

Detailed methods for airplane design vary greatly between organizations, even within companies, but there are always three vital aspects for accomplishing a design and its validation. These are identified in Figure 1 as the *why*, *what*, and *whether* an airplane should be designed. The *why* statements set forth the design objectives for the airplane and must define in sufficient detail the feats that the airplane will be designed to accomplish. The *what* statements must characterize the configuration conceived to fulfill the design objectives. The configuration must contain the elements necessary for accomplishing the required mission with the specified payload. Usually, not only will a principal objective be required, but also secondary objectives may be nearly as essential to the configuration's success as the primary payload-mission objectives. Obviously, there is an extremely intimate relationship between the design objectives of an airplane and the configuration concept capable of fulfilling these objectives.

The third and equally essential aspect of an airplane design is its economic sensibility, or *whether* the design should be attempted. Without considering whether the vehicle will fit within the economic environment of the (military or commercial) user, there would be little understanding of the primary motivation for generating an airplane design for the intended user. It may be that the ultimate customer does not appreciate his need today for a given airplane. However, an airplane usually must be conceived at least a decade ahead of the time period for its fullest utilization. This crystal ball gazing into the economic sensibility of airplane design is becoming increasingly important for the design engineer to consider. Flexibility and stretchability have a very strong impact on many application alternatives and the growth potential which a good design must possess from its inception. Now it is necessary to expand a little on these three essential aspects of design.

The design objectives of an airplane include the payload to be delivered over a given range. Takeoff from an airfield may require certain performance characteristics and landing at another airfield may require, perhaps, different field performance. A wide variety of flight characteristics may be commanded from the airplane between takeoff and landing, particularly for multiple-role military missions. These can range from air-to-air combat, ground-support weapon delivery missions, bombing missions with the payload dismissed during the midpart of the mission, through to search missions which require very long flights where duration becomes nearly as important as weapon delivery effectiveness. In contrast, commercial aviation usually retains its payload throughout the flight profile. However, on shorter commuting flights it is common for many quick stops to be made with only small changes in payload and perhaps no changes in fuel to be accomplished between the origin and the final destination. During takeoff and landing there are many stringent conditions imposed on flight performance that principally involve handling qualities, safety, and the ability of the crew to accomplish the required field performance successfully.

Other design objectives that may be considered of lesser importance, must be carefully evaluated for their impact on the configuration, lest they penalize the primary objective. The primary objectives should be the key to success in the market place, so long as the resources are available to assume the risk. The airplane configuration concept must consider not only the mission requirements for efficiently delivering the payload for the specified range, but also the field performance characteristics, the climb capability, and (for military airplanes) maneuverability, dash, loiter and weapon delivery accuracy. Regardless of the airplane's purpose, its crew accommodations are very important. These would include such items as visibility from the flight deck, handling qualities, the avionics support of flight planning and execution, and the propulsion system characteristics such as the thrust response, freedom from surge, and general reliability. Another important configuration attribute is the control system on the airplane, which directly influences the handling qualities and the ability of the crew to accomplish their mission objectives.

The payload accommodations in the airplane determine its loadability and the required center of gravity travel, which in turn relates to the amount of inherent and artificial stability required for the configuration. The payload on commercial airplanes is usually passengers and their baggage as well as cargo. Military airplanes involve a wider variety of payload such as military stores, missiles, and weapon systems which are used for search and identification of the objective – whether it be an enemy airplane, surface vehicle, or other attractive military target. Additional accommodations for the crew must always include food and sanitary facilities. On commercial airplanes there is the added necessity for food and galleys needed in the preparation of the food for the passengers, as well as extensive sanitary facilities for the passengers. Also, accommodations for emergency and safety equipment on the airplane add to the empty weight requirements of the airplane.

Another important element related to the configuration concept is the ground support equipment. This equipment is roughly the same for military and commercial airplanes in that fueling, engine starting, towing, servicing, runways, and a terminal facility are required. The principal difference between military and commercial airplanes concerning the ground support equipment is associated with the payload. The commercial payload of passengers and baggage requires very rapid terminal accommodation. Loading and unloading passengers plus servicing the airplane is a critical part of commercial airplane ground support.

Technology of the propulsion and flight control systems are key to the success of a configuration, just as much as the aerodynamics and structures technologies. The delicate balance of advanced technology benefits versus the risk of unforeseen difficulties found in severe and extreme service usage can be nearly impossible to evaluate. New technology is necessary to the acceptance of a new product. However, the configuration concept must use the technology with sufficient conservatism to succeed and then capitalize on the technology for growth.

Economic sensibility of an airplane is also a very difficult and often volatile subject. Much effort during the initial stages of an airplane is given to determining the market base which can utilize the envisioned airplane. The economic picture also involves the competition airplanes under consideration by the same potential customers. The company generating a new airplane design must make a very careful evaluation of the resource requirements for producing the airplane. It may be constructed wholly in-house or partly by subcontractors. The amortization of the new production capability investment (a non-recurring cost) over the production life of the vehicle must be carefully determined, whether it is for tooling, buildings, or the engineering work of developing the design.

The economics of a mission are of primary importance, i.e., the cost of delivering a passenger a given distance, or a cargo or weapon delivered to the objective. These costs are significantly influenced by the original cost of the airplane and its expected life. The underlying reason for any airplane program is its ability to provide a profit to the company that designs and builds it as well as the customer that uses it. The airplane which accomplishes its original and subsequently imposed objectives well, will most assuredly provide a profit to the company that conceived it as well as the customer which nurtures and utilizes it during its lifetime. Also associated with an airplane design are the attributes that will open up new market opportunities, such as its operating flexibility, growth potential, and compatibility with the purchaser's fleet-wide operation. Although in the last decade dramatic airplane and engine life improvements have been achieved, the resulting increase in utilization of both commercial and military airplanes has brought added emphasis to the need for airframe, engine and system durability. Characteristics such as airframe fatigue life and system failure rates both influence airplane utilization and have become more and more the subject of initial contract negotiations. They are important ingredients of economic sensibility for the user.

The reason for this initial discussion of these three vital aspects of airplane design is to emphasize that an airplane design must be undertaken with very careful consideration of the market place and the ability of the airplane to perform competitively for a sufficient length of time to repay the investment required to initiate its production and put it into service. Each of these vital aspects, (i) design objectives, (ii) configuration concepts, and (iii) economic sensibility, have to be carefully understood and reflected in an airplane design before it has any chance of success.

In the case of the commercial airplane business the Convair 880 and the Douglas DC-9 brought their company's existence into extremely precarious circumstances. Of course, the current financial difficulty Lockheed and Rolls-Royce are experiencing with the L-1011 is another example where the economic aspects of an airplane program have dominated the project and weigh heavily on the allowable design alternatives. These examples are worth careful scrutiny.

It is the intention here to emphasize the design objectives and configuration concepts, rather than the economic sensibility (or whether). References 1 through 7 give good insight to the internal workings of an aircraft manufacturer as he attempts to be in step with his best interests and with the ideas and interests of his customers from the very earliest stages of an airplane design program. The period of time necessary to evolve an airplane concept is getting much lengthier (e.g., the SST) as airplane programs become more and more complex. Steiner¹ did a very admirable and entertaining job of describing the steps in airplane evolution (see Figure 2). These dozen steps of evolution are typical of most airplane design programs. Although the middle half-dozen steps of Figure 2 are of principal concern to this paper, it may be useful to digress for a moment and show how some typical market areas can be identified, at least for commercial airplanes.

Figure 3 shows the three major transportation gaps in the comprehensive transportation needs of man. This diagram by Smelt¹⁰ identifies the three gaps as the small-distance gap, the short-haul gap, and the long-range gap for intercontinental distances. These occur between the walking, ground transportation, and air transportation means for travel. Air transportation has always depended upon a combination of walking and ground transportation for accomplishing its initial and terminal distances, so that it incorporates a combination of all three means of movement. There has been long and extensive amounts of work associated with the gap between ground transportation and air transportation. A large number of concepts have attempted to invade this region such as rail from the ground-borne side and helicopters from the airborne side. There certainly is no universally acceptable answer to this intermediate time-and-distance market. It remains ripe for the proper answer. Similarly, supersonic and transonic airplanes have been studied extensively for over a decade to fill the long-haul gap and there are still no airplanes in service.

In the meantime, there has been an extensive growth in the subsonic airplane, or the so-called jumbo jet arena with the 747, DC-10, L1011, and next the A300 airplanes coming into service with a remarkable ability for improving the economic picture of the airlines. Current production airplanes are illustrated on the plot of Figure 4 showing the number of passengers handled for given design ranges. This chart illustrates the design applicability of a given airplane and its principal competition. These charts are familiar to designers that are setting forth to establish their company's products in a particular area of the commercial field. As illustrated, the current production airplanes cover the flight and passenger spectrums fairly uniformly from short range to long range and small to large passenger count. Any new airplane in the commercial field will face severe competition from these airplanes for the foreseeable future.

There is a new factor entering commercial airplane design that is imposing additional constraints. This is the environmental impact of airplanes on society from both the noise and the engine exhaust emissions. The noise, in particular, has produced great resentment of airports as neighbors. The procurement of land for new airports has raised objections that are nearly insurmountable, as seen in England, US and Japan recently. Ultimately, good can come from these objections, since in the engineering sense both noise and excessive emissions are wasted energy. If properly reduced, certainly greater efficiency of the propulsion systems will result.

It is necessary to utilize the engineering disciplines of aerodynamics, configuration design, flight control systems, propulsion, structures, and weights in design synthesis to produce the required airplane performance and operational economics (see Figure 5). There are many dramas of give and take between the technical disciplines. A suitable set of working relationships is necessary for the airplane design synthesis process to work with the technical team in unison. The best utilization of engineering methods in the synthesis process via parametric and optimization techniques can lead knowledgeably toward achieving the objectives sought from the resulting airplane design.

2. DESIGN SYNTHESIS

It is very important to distinguish carefully between airplane design objectives and design constraints, where both are variables in the problem. An objective is the value of a design variable (either an independent or dependent factor) that is sought from the resulting solution, i.e., an objective is the design goal for a variable. A variable is some parameter or describable factor that can be changed or does change during the design process from the initial estimate of the configuration concept to the final configuration evolved as a result of synthesizing all of the variables into an answer for the problem. A constraint is a bound placed on a variable to be recognized either as a limit (less than or equal to, or greater than or equal to) or as an assigned value (equal to). A constraint may be thought of as a *required* objective, such as range, or field length. So, in summary, all of the design factors in the synthesis process have to be considered variables, except that certain variables, which are chosen for objectives, may be constrained to specified values. Most variables are free to come out of the design process with any acceptable value. Otherwise, the problem becomes overconstrained and no solution can be found.

The word design will be used here as either a noun or a verb. When used as a noun, the word design represents an airplane which has geometry and physical components that are definitive. The word design used as a verb or adverb means to conceive and plan out, so as to devise an airplane for a specific purpose. That is, designing an airplane requires a method or a defined procedure for progressing toward its description. Therefore, the design (noun) of an airplane is the result of the design (adverb) synthesis process.

The principal lines of data flow for designing an airplane are shown schematically by Figure 6. The elemental concepts for an airplane are introduced into the technologies and the configuration design (see Figure 5). The objectives are introduced into the performance and economic evaluations. Part of the concepts introduced into the technologies are the technology "levels" or "state of the art" to be used during synthesis. In terms of aerodynamics, this could be the airfoil technology, e.g., how sophisticated the transonic airfoil concept should be. In propulsion, one of the concepts could be a definition of the hardware technology or high temperature material that influences the compression ratio, the turbine temperature, and the compactness of the machinery. These factors have a dramatic impact on the thrust-to-weight ratio of the propulsion unit. In structures, one of the concepts would define the amount of titanium or composite materials in the primary and secondary structure of the airframe, etc. In flight control systems, one concept could be the degree of artificial stability introduced to free the design for significant structural weight savings. Or, the concept could be fully-automated takeoff and landing, flight path control, etc., which would reduce the reserve fuel required to perform a given mission, because the reliability of dispatch and arrival would be significantly upgraded compared to today's operations.

The configuration design and its weights are usually very dependent upon the other technologies. However, configuration innovations are continually sought such as flying wings, sea-planes, VTOL, variable sweep, retractable landing gear, variable geometry of fuselage noses, trailing-edge and leading-edge high-lift devices, stabilizers, and other components of the airplane. Note in Figure 6 that the output from flight control systems, structures, aerodynamics, propulsion, and weights as well as configuration design must eventually go into the performance and economic evaluation block. Some of the paths are direct and other paths are indirect via weights or configuration design. Note also that the output from the evaluations feed back into all of the technology processes as a bias or guide on their contributions to the evaluations. As an example, aerodynamics will feed data such as wing area, empennage area, and

high-lift system definitions into configuration design. Complementary information on the drag polars (both for low speed and high speed) would be fed into the performance evaluation directly. The data fed from aerodynamics to the performance evaluation would be in parametric form so that the dimensioned configuration design can be used with this parametric description to generate the performance evaluation. When the configuration is defined, this transformed information gets fed back to weights so that accurate weight information can, in turn, be determined for the performance evaluation. These interactions between aerodynamics, propulsion, weights, and design are needed for generating performance evaluation input information. Note that flight systems, structures, aerodynamics, and propulsion all feed both weights and the configuration design. Only aerodynamics, propulsion, and weights feed the performance evaluation. This is because aerodynamics, propulsion, and weights provide all of the information needed to define thrust, drag, lift, and weight, which are the force vectors necessary for performance evaluation.

The design synthesis process is started with an estimate of the answer and then proceeds from this initial position to the final answer by iterative perturbation of the technology and configuration design data. Once the performance evaluation is satisfactorily accomplished, then the economic evaluation can take place with the resulting configuration design to determine its economic feasibility. This step may force additional iterative perturbations to achieve the economic design objectives.

The concept of inputs, processing of these inputs, outputs, and the analysis of these outputs must be kept in clear perspective. It is altogether too easy for an engineer in any one of the technology disciplines to become completely involved in his part of the process and lose perspective on the bigger problem of being wholly compatible with all of the other disciplines. Each participant must understand the principles of the other disciplines, because ultimately the value of one data element must be weighed very carefully against the value of the other data elements in order to determine the proper tradeoff between all factors attempting dominance. The design process is necessarily a strict hierarchy of information flow with as little artificial biasing from any one element or technology as possible.

All airplane configuration concepts are the intuitive interpretation of the various design objectives (Fig.7). These may include such items as whether the airplane is a military or commercial vehicle, whether it should fly subsonic, transonic, or supersonic, whether it should carry principally passengers or cargo, or whether it should operate from conventional fields or short takeoff and landing fields. The landing gear is particularly sensitive to the allowable field or runway bearing pressures. As an example, the 747 was constrained to takeoff and land from existing airfields. This imposed the need for a 4-post main landing gear to distribute the 400 ton landing, which was certainly an innovation on commercial airplanes. Design objectives imply careful tradeoffs between engines, wing and fuselage design arrangements and landing gear placement for a logical integrated design configuration.

There are many regulations concerning safety, handling qualities, and environmental pollution that impact the configuration with constraints. The customers desires (beyond the company chosen objectives and the Federal requirements) may strongly influence the engine choice, payload characteristics, the passenger service arrangements, and overall airplane sizing (see References 3 and 4). Ground support equipment can be a strong factor in the configuration when truck-bed-height loading, outsized cargo, containerized cargo, galley placement, and convertible airplane (passenger-to-cargo and reverse) concepts are considered. It becomes necessary to have an extremely detailed check list during the design process to make certain that an important need is not overlooked concerning either safety or customer desires.

The initial estimate of airplane size is almost always based on past experience of either other companies or members of the design team. It is always useful to compare a new design with statistical correlations of previous production examples to make certain that all aspects of the design are realistic, rather than fanciful. Each new technological improvement must be completely exploited (compatible with risk) and not lost by unintentional compromises. Mission performance, payload, and field performance are the key objectives that trigger inputs for initially estimating the airplane take-off gross weight and wing and thrust loadings. If there are unusual performance traits necessary, then there are fewer precedents to follow and less statistical information for gross checks. Choices of the aerodynamic surface shapes and sizes are always perturbed during the many design iterations. But, the better the initial estimate of their geometry, the less trading is required between the various technologies as a design unfolds.

Referring back to Figure 6, the diagram has outlined by heavier line work the relationship between aerodynamics, propulsion, and weights, with the performance and economic evaluation. These relationships can be used in a simplified way for making a preliminary estimate of the airplane regime of feasibility. When such a design process is used, the configuration is simplified into parametric equations and the weight determination is of the simplest possible nature. Such items as empennage sizing, landing gear and wing placement, engine placement, are handled by empirical relationships rather than interrelated calculations. Since it is possible to do a simple design job with these technology elements, their description will be given first and then the flight control systems and structures roles will be described.

The aerodynamic data flow is illustrated by Figure 8. Fundamental to the aerodynamics technology are the airfoil concepts, which in the fullest sense must include the wing geometry and its relationship to the airplane fuselage shape. The techniques for defining the proper shape relationships of the wing, fuselage, nacelles, and other components of the airplane so that interference effects will be minimized are also fundamental concepts of aerodynamic technology. Once the aerodynamic technology is set, then the characteristics of the geometry, the

performance, and the flight capability are determinable. The geometric aspects of aerodynamics such as wing planform, airfoil definitions across the wing span and the empennage surfaces, and the integrated area distribution of all the components can be defined for the high speed configuration. Definition of the low speed geometry of the leading-edge and trailing-edge high-lift devices is necessary for evaluation of the low-speed flight capability. Then from these clean and flapped configuration definitions the drag polars can be created for both high-speed and low-speed flight (Fig.9). This then leads directly to the definition of the flight envelopes and maneuver limits for the entire flight regime.

Information fed to weight analysis (Fig.8) includes the flight envelope, the center of gravity margins necessary for the load map, the empennage sizing criteria, and the type of high-lift devices and control surfaces on the wing and empennage. Information returned to aerodynamics are configuration design definition items such as airplane wetted areas, wing and empennage areas, nacelle size, and fuselage geometry. These items are used by the aerodynamicists for obtaining or updating the drag polars. Also needed for the drag polars are the definitions of manufacturing roughness and various protuberances, fairings, and other geometric deviations required for accommodating landing gears, air exchanger inlets, exhausts, etc. that contribute to the dirtiness of the configuration. There are always special design needs requiring doors for cargo, bumps for radomes and landing gears, or moving stabilizers, etc. These roughness elements must be evaluated carefully, so that the wetted area and profile drag (pressure or wave drag) are minimized for the volume required to contain the payload, fuel, high-lift systems, etc. The fuselage may have a high fineness ratio for low drag and long tail length, but this must be weighed against the heavier structural weight that a high fineness ratio incurs. Low fuselage fineness ratios may have excessive profile drag due to bluntness of the body closure and aft-end upsweep. Required cruising speed may control these body design factors.

The wing needs sufficient size to provide lift with adequate maneuver or buffet margins and both low profile and low induced drag. It is particularly important for the wing-body combination to have low wave drag (if supersonic) or low shock-induced pressure drag (if subsonic). At the same time, the requirements for climb, cruise, maneuver, dash, or loitering capabilities require proper compromises between airfoils, aspect ratio, area, and wing sweep. These varied flight regimes are often contradictory and may show that the best answer, particularly for a military airplane, is variable sweep to match a wide diversity of supersonic and subsonic mission requirements.

Aerodynamic considerations of the empennage center principally upon the static stability and control power desired. Airplanes with powered controls may have significantly revised stability criteria through such devices as dampers or structural load suppressors driven by suitable sensors. Usually, however, the horizontal stabilizer and elevator are sized by takeoff rotation with the center of gravity at its forward location. The aft center of gravity is based upon the inherent static longitudinal stability margin desired. Other characteristics considered for sizing the empennage include dutch roll damping, spiral dive divergence rate control, and phugoid damping. Many of these stability and control criteria have a secondary influence on the design weight and drag, but nevertheless they should be considered early enough in the design process together with aeroelastic effects to properly reflect their influence on weight and balance, which has a significant impact on the empennage sizing.

The low-speed configuration characteristics are directly related to the basic wing characteristics and the leading-edge and trailing-edge devices used. Since wing sweep decays the maximum lift available, this requires either additional wing area or more effective high-lift devices to maintain comparable takeoff and landing speeds. If high-speed characteristics make variable sweep a desirable configuration feature, then it will compensate to a great extent for high-lift device complexity and weight. As shown in Reference 16, it is very difficult to argue successfully against additional lift at low speeds, because lift has great leverage. However, the new requirements on lower noise characteristics of commercial airplanes is forcing the return of lighter wing loadings with their accompanying higher L/D for takeoff and landing. This improved L/D reduces the amount of thrust required during approach. Noise abatement procedures may require the flight paths into and out of airports to be more steep.

Leading-edge devices for wings add area and prevent leading-edge boundary layer separation, which can limit both the angle of attack and the trailing-edge flap loading. There are many passive leading-edge devices such as slats, flaps, and variable camber, slotted flaps. Active boundary layer control can be applied as suction or blowing to almost any type of these devices to extend their capability. Such powered-lift systems must be very carefully tailored to the wing loads induced by both angle of attack and trailing-edge flaps. Also, local boundary layer control can be used very effectively for overcoming interference effects from nacelle struts, slipper tanks, or close-coupled nacelles.

Trailing-edge devices are chosen to add area and provide drag control in addition to the lift needed for good field performance. There are as many or more trailing-edge flap configurations as for the leading-edge. These include split flaps, plain flaps, single or multiple-slotted flaps and may be introduced with compatible movements of spoilers and ailerons. Boundary layer control is also applicable to any of these devices to enhance their capability. The flap span is carefully controlled on swept wings to insure an improvement in trimmed lift, where the pitching moment induced by high-lift devices on the wing tip can produce large negative pitching moments that must be compensated by downloads on the tail, which, in turn, reduces the overall lift capability of the airplane. Some attempts have been made to compensate for wing trailing-edge flap negative pitching moments by using canard surfaces during takeoff and landing.

On STOL airplanes lift is very critical and maximum use must be made of such devices as powered-lift systems, drooped ailerons, boundary layer control, and wing height for establishing the maximum possible lift without adverse ground effects. It has become common practice on commercial transports to utilize spoilers in conjunction with flaps for direct lift control as well as ground lift dumping to increase braking once the vehicle has touched down. Thrust effects on trailing-edge flaps may be maximized as on STOL designs that use external blowing from the engines over the flaps to augment lift, or minimized to reduce the trim changes as on the DC-8 which has a flap segment which deflects upward out of the exhaust flow.

The data flow for propulsion in the airplane design process is illustrated by Figure 10. The input engine technology concepts include such items as the engine cycle, which is largely determined by the material technology in the combustion and the turbine sections of the engine. Compressor technology has played an increasingly important role in engine design, particularly with the higher bypass ratio fan engines used in subsonic flight.

Nacelle concepts involve both low speed and high speed considerations. At low speeds the inlet must provide good flow to the engine at very high angles of attack. This can be further complicated by local flow conditions encountered in the strong upwash near the leading-edge of a highly lifting wing (wing-mounted nacelles) or in the downwash near the trailing-edge flaps (aft-body-mounted nacelles). A very careful set of design compromises must be established between these low-speed conditions and the high-speed conditions, which require low nacelle profile and compressible interference drags. Such nacelle design technology can be nearly as complex mechanically as in fluid flow control at transonic and supersonic speeds as the engines themselves. Materials technology also has become critical to nacelles in the form of acoustic control surfaces. These surfaces are porous and must exist in extremely hot and cold environments together with fuel, oil water and dirt. Acoustic control is also influencing engine design significantly as configuration parameters are revised to reduce the generated noise intensity.

There are multiple outputs from propulsion to the configuration design, performance and economic evaluation, and weight analysis (Fig.10). Principal information fed to the configuration design includes the nacelle and engine geometry, APU geometry, and other devices supported by these primary and secondary power supplies. The principal information sent to performance evaluation includes the thrust characteristics and fuel consumption of the main propulsion engines (see Figure 11). For weights, there is a great deal of information including engine size, nacelle size, APU size, and the sizes of pneumatic and hydraulic systems. All of these sizes are determined as a result of design iterations to match the needs of the vehicle for the desired performance.

There are usually two choices of engines: (i) a current production engine or a closely related derivative and (ii) a new engine, which must be very carefully timed to the airframe production schedule (e.g., Boeing 747 and Lockheed 1011). Although a current production engine usually will not control the production schedule of a new airplane, it may significantly limit the airplane's growth potential, if the engine has been approaching its development limits, or there are no other complementary uses for a new derivative version.

It also may be important to the customer whether the engine is in his inventory. Application of an engine in service is always more attractive than introducing a new engine with its added logistics and teething problems. A current production engine also minimizes the risk associated with performance predictions, so that tighter guarantees can be made to the airplane customer.

A new engine may better match the airplane design objective and result in more attractive economics. Major factors such as fan engines versus the pure jets and high bypass ratio versus the low bypass ratio engines are very favorable factors. A new engine will be undertaken only when the engine manufacturer can be assured that broad application will ensure a long production run. Therefore, close cooperation between the airplane and engine manufacturer has become commonplace to provide the most economically competitive airplane with maximum growth potential available simultaneously from both the engine and the airframe. Only with clear technological advances is it feasible to conceive a new engine. The current pressure on pollution from noise and partially-burned fuel, as well as the craving for additional economy, are current factors that will bring new engines as rapidly as the manufacturers can accommodate the work and accumulate the capital resources. There are many aspects of the thermodynamic cycle of the engine that look attractive for the future. However, even with today's fuels and cycle concepts there is continuing improvement in thermodynamic efficiency. The design of compressors for both primary and secondary flows is a principal weight-controlling factor and the renewed emphasis on noise will bring continuing attention to their design efficiency.

The installation of engines in either podded or buried configurations is one of the most intensely studied aspects of airplane design. Podded configurations usually have the most interaction with airframe external aerodynamics, but this is an acceptable problem when compensated by the easy access for maintenance and servicing. The interference effects come from the hard nacelle surfaces, the struts, and the fluid flows exhausted from the engine. Podded configurations do have a relatively high wetted area, but this is compensated by very good inlet pressure recovery characteristics. A buried-engine configuration usually is the most acceptable aerodynamically. However, the inlet losses are usually higher and the exhaust from the buried installation usually entails very sensitive exhaust design problems. In particular, the base drag of body-mounted, multiple-engined configurations is very sensitive to design details. Compensating for these problems are the low installation weight of buried configurations (unless they are surrounded by primary structure) and a low wetted area, because the cowl surfaces are combined with other needs

such as the fuselage. Buried engines may allow more accurate area rule tailoring where ducts can be shaped internally to attain a better external shape with minimum compromise on the engine inlet flow efficiency imposed by length and changing cross-section shape. Such tailoring trades are usually very common on fighter airplanes.

The data of Figure 11 must cover the operating regime of the airplane and must be degraded from bare engine test results to recognize the installation effects imposed by the inlet and exhaust conditions, and the compressed air and power extracted for purposes other than thrust. Data must be available for standard and non-standard altitude and temperature conditions to permit performance evaluations for off-design situations. It is airports that are high and hot that can force extreme engine performance penalties.

Weight is one of the principal engineering accounting disciplines of airplane design. All of the components incorporated into a design must be recognized by the weight evaluation, whether the equipment comes from flight controls, structures, aerodynamics, or propulsion. The concepts of weight evaluation usually involve a very extensive statistical data base which is formulated by regression techniques into evaluation methods for particular types of airplanes. Also, it is extremely important that the datum base of its own company product line be properly recognized when predicting the weight of a future product. Every company tends to design its airplanes in a particular way. An extrapolation of this experience with its design personnel is the best way to reflect how future designs will be approached. The various inputs to weights from the technologies are shown by Figure 12 and typical parametric weight curves are shown by Figure 13.

Calculations must be made of the primary and secondary structure as well as the equipment and payload needed for the performance evaluation of a proposed airplane. Any new innovations or deviations from the normal design base experienced in past airplanes requires a bias on the evaluation methods to reflect the weight savings or losses from such technology deviations. It is common practice in the design process to establish a bench mark configuration which is analyzed in great detail by all of the technologies, particularly weights, for determining the accumulated effect of technology progress subsequent to the last similar product. Those weight-saving advances that can be introduced prior to the final definition of the next airplane need careful identification for risk evaluation. It is common practice to seek the lightest weight airplane to achieve the design objectives, since weight is roughly equivalent to airplane cost and directly displaces payload. As refinement is sought in the configuration design, flight control system and structure analysis must be added to the processing (Fig. 6) which makes design synthesis increasingly difficult and significantly more complex.

The flight control systems data flow is depicted in Figure 14. The input concepts are principally related to the handling qualities desired from the airplane and to the control systems required for providing these qualities. Most handling qualities of modern airplanes are enhanced significantly by powered-assist controls and systems for controlling dynamic characteristics to make the airplane feel and perform in a manner far more docile than inherently provided. Avionics has enhanced nearly every aspect of flight control systems. Also, many new innovations, such as maneuver load alleviation and structural model suppression, have become very promising ways to improve airplane flight characteristics from the piloting and structural loading viewpoints. Flight control systems relate to the configuration design and weights by control surface and empennage sizing as well as other geometric properties such as dihedral and landing gear placement. Control criteria which enter the configuration process are the nosewheel steering needed for control in cross-wind takeoff and landings as well as the directional and longitudinal control needed at lift-off or just prior to touchdown when the flight speeds are at minimum values.

The structures data flow of Figure 15 is grossly simplified. Even though the structural aspects of airplane design are not a principal point of emphasis in this paper, it is important to emphasize that the primary strength of the vehicle and the aeroelastic properties have strong interaction with the other elements of the design process. The concepts input to structures are the materials and fabrication technology utilized in construction of the airplane. It is these materials and the detailed structural design that determines the strength and weight of the airframe, its aeroelastic properties, and the ultimate life of the airplane. The material properties and the expected structural life are primary inputs to the weight evaluation of the wing, empennage, and fuselage structures. The data presented to the configuration design consists principally of where the primary structural members are located such as wing and empennage spars. The structure connecting the load paths from the empennage to the wing through the fuselage, the landing gear and nacelles into either the wing or the fuselage, must be defined. These primary structural members are an appreciable part of the airframe structural weight. Extensive definition also is needed for the secondary structure such as fairings, flight control surfaces, high-lift devices, landing gear doors, passenger and cargo doors, servicing doors and fairings for the engine as well as the inlet and exhaust nozzles and the thrust reverser. All of these structural components must be able to withstand the imposed air loads from both within and without and to accept overloaded conditions imposed by maneuver or from gusts and landing ground impact. There are also some conditions during ground handling of the airplane both during takeoff and landing with heavy fuel loads and maximum payloads that can impose maximum stress levels on the primary structure of the wing, fuselage, engine mounts, and landing gear.

Although not indicated by Figure 6, there is an extensive amount of information concerning government safety regulations that is needed for the performance evaluation concerning the field and flight performance profiles. Field performance rules are set forth in very stringent fashion for the US military (MIL-C 5011A) and the FAA civilian (FAR 25 and 36) government acceptance. These rules are based mostly on the safety requirements associated with

engine failure and adverse weather conditions such as cross winds. A simple summary of commercial airplane field performance profiles and the safety rules associated with them are shown as Figure 16. Any takeoff requires a point of decision for refusal in terms of the speed obtained at the distance down the runway so that either the acceleration can continue to a safe liftoff or the airplane can be braked to a safe stop. The rules associated with this operation are fairly conservative to allow for faulty judgement or misleading cues. There are now proposed civilian STOL rules in the US (FAR 38) which will extend these concepts to include the more difficult powered-lift airplane designs. As mentioned previously, there are new noise rules for civil and commercial airplanes to control sound energy emitted during ground roll and liftoff in the airport area (sideline noise) as well as during the climbout over adjacent communities, although engine power reduction can be used, within safe limits, to meet the designated noise levels. Airplane noise is governed as a function of gross weight in terms of EPNdB which is the equivalent perceived noise (in decibels) involving the duration and frequency spectrum characteristics of the emitted noise²⁷. The graph inset in Figure 16 shows the current maximum allowable values.

Safety is also a primary consideration when the loss of an engine is encountered and a missed approach requires that the airplane go around and try another landing. There are noise limitations imposed during the approach to the airport and many schemes are being utilized to minimize this problem. Decelerating approaches and approach paths which are significantly steeper (6 degrees) than the 3 degrees used today are being considered.

Many special problems are encountered in designing airplanes for ground-roll performance and some require special designs of the landing gear. Cross-wind landing gears have been in common use for many years and are best known for their application on the B-52 bicycle gear. A sideslipping or skewed landing angle at touchdown without a final rapid yawing for runway alignment of the bicycle landing gear necessitated a cross-wind gear. Special ground steering mechanisms of the massive main wheel trucks is increasingly common. Ground steering was required on the 747, because of the large turning radius required to keep from damaging the landing gear and the tires.

Catapult and arresting gear on the ground are becoming more prevalent for the military in addition to those used on aircraft carriers by the Navy. These field-performance augmentation installations require special automated nose gear attachment devices for launching and tail hooks for the touchdown arrest. It is standard practice to use nets for landing emergency overrun cases. The launching and arresting devices on the airplanes are a minimum penalty for the field-performance gained.

There are almost an infinite number of mission profiles possible for an airplane, and it is easy to lose perspective of the fact that a few essential performance building blocks can be used to compare almost all of this large variety. These essentials include the climb (minimum fuel, minimum time, or maximum range), cruise (either climbing or constant altitude), descent (maximum range, minimum fuel, or minimum time) and maximum thrust, level flight at any altitude, minimum fuel consumption flight for maximum duration and, in the case of fighters, high altitude maximum thrust maneuvering. With these half-dozen basic building blocks a tremendous variety of flight profiles can be composed for practically any airplane for any size payload and range. These essential profile components can be flown in any compatible sequence.

The next considerations are the rules whereby these missions are composed, i.e., principally whether civilian or military. For example, all civilian commercial airplane flight profiles (Fig. 17) in the continental US have their climb speed restricted to less than 250 knots below an altitude of 10,000 ft for flight control safety. Similarly, the cruising altitudes, headings and speeds are assigned by the flight controllers so that adequate spacing is assured laterally, vertically, and longitudinally for flight safety. For airplanes such as the SST, where the flight profiles will be significantly separated from the majority of other aircraft, there will be considerably more freedom in the choice of flight altitudes until there are a sufficient number of SST airplanes in the sky to make safety a consideration again.

Military flight profiles contain a much wider variety of climbs, cruises and maneuverings to achieve their military objectives. Refueling is a common military practice for extending the combat time, the ferry range, or for returning to the home base or carrier. In addition to the reserve rules varying significantly between the civil and military governing agencies, there are additional rules established as policy for individual airline companies or using groups. The airlines, for example, have become increasingly aware of fuel consumption during the past few years and have sought many ways for reducing these expenditures which directly impact their cash flow problems.

Now that performance evaluation has been outlined briefly, it is important to touch on the subject of operating cost analysis. Cost effectiveness as a watchword has become very prevalent in both military and commercial airplane evaluations. In commercial aviation one standard basis for comparing airplanes is the ATA Standard Method of Estimating Comparative Direct Operating Costs⁴², although these basic methods get adapted to the needs of the particular user. It is common for airlines to apply their own experience factors for their particular operation. It is similarly true that manufacturers, such as Boeing, have found it necessary to extend and modify these standard methods for transonic and supersonic airplanes. The unit cost of manufacturing a new airplane is related inversely to the anticipated number of airplanes to be produced. In turn, the user economics are related to the airplane's initial unit cost and to the recurring costs of operation on the particular route structure of that airline. Commercial airplane economics are very sensitive to the utilization of an airplane. The ability of an airline to maximize this utilization as experience with the airplane is accumulated has a strong effect on its ability to turn a profit.

Whether an airplane is for commercial or military purposes, high maintenance costs due to time and materials can rapidly encroach on everyday utilization and decrease the value of the airplane to the user. Extensive maintenance or major overhaul periods for a commercial airliner require that the airplane be taken out of service. Many airlines have been able to circumvent this problem by matching the maintenance procedures to route schedules and performing end-of-run maintenance within the limited time available during the night when load factors are a minimum. In this way maintenance procedures have the least impact on productive utilization. The result is maximum income and minimum maintenance cost per flight hour.

Turbine engines have revolutionized the reliability of commercial air transportation and have so increased the time between engine overhauls that other systems on the airplane have become more critical to on-time departure reliability. Airborne systems analysis and performance recording capability is rapidly bringing preventative maintenance based on failure anticipation into common use²¹. These airborne capabilities have replaced the former methods of statistically-determined, mean-time-between-failure maintenance. This philosophy, of letting a system operate until its monitored performance indicates by some weakness or erratic behavior that an operational failure is imminent, is significantly reducing costs of maintenance and, in general, increasing airplane dispatch reliability. Another direct saving comes from shutting a system down before it can be damaged beyond repair.

Airframe durability also has greatly reduced major airframe maintenance costs per hour of flight. The use of non-destructive testing techniques for determining structural weakness or damage has permitted most structural problems to be detected and corrected before their nature becomes critical and a catastrophic failure results. All of these maintenance subjects impact an airplane's design concept philosophy. The life of an airplane and its dispatch reliability in service are serious subjects of guarantee to the airlines and to the military.

This brief foregoing discussion of the performance and economic evaluation is intended to indicate the strong way in which all factors interplay in the determination of the "best" airplane design. It is important to appreciate the immense difficulty encountered in trying to fully recognize all of the factors influencing the design process. Another point is that very few of these factors are stationary. The design objectives, the technology, the customers, the opportunities, etc. are all changing continuously. Therefore, whatever methodology for design synthesis is evolved, it must be flexible and easily updated, open ended to admit new factors and constraints, and provide evaluation consistency between configuration alternatives and existing production airplanes.

The last three Figures (18 to 20) in this section on design synthesis show crudely the information depths that occur in the three principal technologies of aerodynamics, propulsion, and weights. The data flow of Figure 6, as amplified by Figures 7 through 17, is nearly the same, regardless of the information depth that is available about a proposed airplane design. At the initial stages of design evolution the information is usually very rudimentary or shallow. As the design alternatives are probed and the technology concepts become more firmly established, then the information moves rapidly from regression depths, based on past experience, to more extensive parametric information that also is based on past experience, but directly tailored to the configuration design being considered. Then, the next stage is to move from the parametrically evolved design data into a more detailed analysis that expands upon the description of the configuration, the composition of its aerodynamic characteristics, the establishment of the best suited propulsion characteristics, and a weight analysis of the primary and secondary structure of the airframe plus all of the systems, payload, fuel, etc.

Experimental work on components and the configuration itself in modeled form plus tests of the engines and other systems components will continue to increase the knowledge about the configuration. This biases the analyses performed and the input data. In the early stages of prototype production component and model simulation testing is continued to minimize the risk associated with putting the airplane into production. Even after prototype flight testing starts it is often necessary to continue development work in static test facilities, wind tunnels, and other laboratories to investigate problems revealed by flight test experiments. This empirical information also is assimilated via the analytical processes by evaluating its impact on airplane performance. If modifications are required to fix a problem, then these modifications will most certainly be evaluated by the same analytical processes.

This discussion of information depths leads to a point that warrants emphasis. Consistent processing of information available at all stages, from conceptual design through flight testing, should be accomplished with the utmost consistency. Such consistency is not only required of the mathematical manipulation of data, but also of the engineering methodology that is utilized in processing the data. Stepwise amplification of the various technology elements should be a simple unfolding of successively more sophisticated analysis processes. Of course the ultimate evaluation is the actual flight testing. The data determined from these flight tests must be accorded the highest respect as the final answers. Even so, the use of analytical methods for interpolating or extrapolating information obtained from flight tests is necessary to provide the complete spectrum of information needed by the customer.

There are certain extrapolations necessary from the technical information depths depicted at the various stages in Figures 18 through 20. For example, the regression information available in aerodynamics, propulsion and weights must be adapted to whatever new configuration is being considered. Usually, new configurations have some similarity to previous experience, so there is always extrapolation of existing engineering data and design analysis techniques to more adequately evaluate a new configuration. Also, the experimental testing done in the wind tunnel and in other laboratories such as engine test rigs, must be extrapolated to full-scale configuration

conditions of flight. Some full-scale testing can be accomplished before a prototype airplane is available. For example, aerodynamic components can be put on other airplanes for evaluation. It is also possible to put an engine on an existing airframe and flight test it throughout the expected flight regime, even though its installation on the production airframe may provide a different operating environment. All of the information gleaned by various analyses, experiments, and flight tests ultimately lead to answering the question of what performance an airplane manufacturer can guarantee to his customers. The tolerances required on the guarantees vary from very loose values at the early design stages of a new airplane to very tight tolerance values for an existing airplane product that has accumulated service experience. However, the subjects of design risk and guarantee tolerances are well beyond the limits of this paper. The point here is to indicate the wide variety of information that is useful to the design synthesis process. This data needs updating continually as information is accumulated during design development. Accurate and rapid dissemination of new information and its effects on the configuration design is vital to effective airplane design synthesis processes.

3. PARAMETRIC EVALUATION TECHNIQUES

Not only does the airplane manufacturer have to concern himself with the design of the optimum airframe, but he also has to be concerned with the optimum engine to match that airframe. This engine-airplane matching work is part of the engineering process needed to convince an engine manufacturer that a given type of engine will best suit their mutual customer. Much of the dialogue that takes place between an airplane manufacturer and the engine manufacturer concerning the best engine, involves parametric data interrelating engine and airplane characteristics as shown by Figures 21 through 25.

Configuration design parameters can be evaluated in the partial derivative sense to guide an airplane designer in feeling his way toward certain performance objectives. For example, it is possible to change a wing parameter such as area, or sweep, and engine parameters such as thrust or thermodynamic cycle, and thereby determine parametrically the effect of these changes on the airplane's performance. By randomly searching between the many variables so investigated, it is possible for an experienced person to quickly separate those variables that are important from those that are relatively insignificant and thereby find a best solution to a set of objectives. A proper evaluation requires recycling the chosen configuration to evaluate in detail secondary changes to the configuration from empennage sizing to meet stability and control criteria, and weight and balance, etc. In essence, the effect of changing each variable must be completely recognized on the whole to keep a design configuration from drifting away from reality through combinations of parametric trends.

It is also important to keep the question of configuration sensitivity to design objectives in clear focus. Undue penalties incurred by a particularly stringent objective or ground rule should be identified clearly. The encroachment on the versatility of a configuration by any one particular requirement must be worth the imposed compromise.

It is easy to specify a set of design objectives that cannot be met exactly and simultaneously by any airplane configuration. The more constraint conditions specified on a configuration, the less the possibility of a solution being found. Therefore, inequality objectives are usually chosen. For example, a takeoff distance less than or equal to X thousand feet, a landing distance less than or equal to X thousand feet, and a range greater than or equal to Y thousand nautical miles with Z thousand pounds of payload are all typical objectives. If a set of such (X,Y,Z) conditions are given, then a tolerance on matching these objectives should be identified, because the input and analysis methods contain inaccuracies. Even when a solution is found, it has a tolerance on its value. There is always a danger in overtrusting a calculated solution, particularly when it is produced by a complex computer program, which cannot be checked quickly and accurately by hand.

Design solutions to constrained multi-variable problems can be very difficult to fathom, because of their non-linear nature. The direct effect of many constraints are difficult to calculate simply. Most analyses are based on simplifying assumptions or approximations concerning the configuration performance limitations. For example, the maximum lift for the high-speed configuration and the low-speed configuration, the flutter speeds, the engine surge margins, the drag rise Mach number, gust load conditions, pilot response, etc. may be very difficult to evaluate accurately until the airplane is flown or, at least, extensive simulation testing has been accomplished. Parametric study is a blend of analytical evaluation and judgmental interpretation, which potentially leads to a solution that will satisfactorily meet the desired constraints. Two- or three-variable parametric studies will quickly enable an experienced engineer to develop a good feel for variable relationships when presented in suitable graphical form. Parametric design analysis techniques attempt to maximize the knowledge about the variables in a design problem for the amount of effort expended. Ultimately, only by the detailed analysis of a selected configuration through simulation, tests of hardware components, and wind tunnel tests can the real value of the answer be ascertained.

As presented in Figure 21A, one of the common graphs in airplane parametric design work is in terms of the thrust loading and wing loading required for a configuration concept to achieve given mission objectives with wing area, gross weight, and engine size as independent parameters. To these answers may be added design constraints related to field performance, noise levels, minimum cruise altitudes, maneuverability, secondary mission performance, etc. Each of these constraints can be viewed also in parametric fashion with respect to the primary variables for determining design sensitivity to and compatibility of the various constraints. A sequence of such design constraint

plots are illustrated by Figures 21B through 21E. The objectives for this particular twin-engined airplane were to carry 175 passengers a distance of 2000 miles out of a 7000 foot field length. This field performance was to be accomplished by exceeding the noise requirements set forth in FAR 36. Constraints on the design were established as an initial cruise altitude greater than 34,000 feet and a landing approach speed at design landing weight of less than 125 knots. The objective of the parametric study was to minimize the direct operating costs of this airplane for maximum economic attractiveness to the airlines. The initial cruise altitude constraint is illustrated by Figure 21B, the takeoff field length and landing approach speed constraints by Figure 21C, the noise constraints by Figure 21D, and the resulting direct operating costs by Figure 21E. A choice from this parametric family of airplanes can be obtained by the superposition of results from these various parametric plots to locate the region of those configurations which will have minimum operating cost and still meet the design constraints. Figure 21F shows a composite plot of the constraints relative to the chosen configuration, which is indicated by the bullseyes on Figures 21A through 21F. The results show that the chosen configuration is controlled principally by the takeoff field length and the relationship of the takeoff gross weight and DOC to this field length to minimize the airplane cost.

This first parametric study illustration was with a fixed payload (175 passengers), a *fixed* range (2000 nautical miles), and a *fixed* high speed design cruising number of Mach 0.84. Figure 21A shows that the resulting airplane had a wing area of 2400 square feet, an engine of 42,500 pounds of sea level static thrust, and a takeoff gross weight of about 254,000 pounds.

All of the airplanes represented by the parametric map had exactly the same wing geometry, engine geometry, engine placement, and landing gear configuration. Also, since the passenger count was fixed, the fuselage was of constant geometry. Essentially then, the wing area and engine size were either magnified or diminished with respect to the baseline airplane to create the map. The takeoff gross weight was calculated directly from these two principal variables of wing area and engine size. All of the parametric relationships for the aerodynamic, propulsion and weight characteristics used in the study were direct functions of these three variables. Obviously, second-order effects were ignored in determining the inputs (of Figures 9, 11 and 13). The accuracy of the solution map decays in regions away from the baseline configuration variables. For reference the following values were determined for the baseline airplane:

Wing Area	2,611 ft ²	Range	2,398 n.mi.
Takeoff Gross Weight	268,000 lb	Initial Cruise Alt.	37,000 ft
Engine SLST	43,000 lb	Takeoff Field Length	8,750 ft

Note that the range of this baseline airplane is greater than the 2000 n.mi. objective, it does not fall on the solution map shown by Figure 21A.

The initial cruise altitude as a function of thrust-to-weight ratio and wing loading (Fig. 21B) shows a locus of tangents between the initial cruise altitude curves, which are concave upward, and the constant-thrust engine curves, which are concave downward. These tangencies indicate the smallest size engine which can be used to obtain a particular value of initial cruise altitude. Since attaining a given performance capability with a small sized engine would provide the greatest growth potential from increased thrust, this is an important criterion to consider in choosing the configuration size. Minimum engine size also is an important factor in the airplane initial cost, because the price of engines is greater than the price of the airframe and its components.

Figure 21C shows that the takeoff field performance is one of the most significant constraints on the choice of a configuration in the range of variables considered. The approach speed of 125 knots has a considerably greater wing loading than is desirable from a cruise standpoint, as indicated by Figure 21F where the locus of L/D_{\max} conditions are shown. A better approach speed would appear to be about 118 knots from the cruise L/D viewpoint. Certainly a lower approach speed makes the airplane more attractive to an airline customer.

Noise regulations do not appear to be a particularly difficult objective to obtain with this airplane design concept. The reason is the light wing loadings and high aspect-ratio needed to enhance the single-engine-out performance of this twin-engined configuration. Of the three criteria for approach, takeoff, and sideline noise the approach noise has the smallest margin with respect to the noise regulation. The sideline and takeoff noise levels are about 6-7 EPNdB better than the specification, but the approach noise is about half this margin. Therefore, if growth versions were developed, additional work on the engine and nacelle configuration should concentrate on improving the approach noise levels.

Direct operating costs, shown parametrically by Figure 21E, indicate the usual trend that the lowest operating costs are achieved with the smallest sized airplane which will have the highest wing loading and the smallest engine. These DOC curves are directly related to the takeoff gross weight curves of Figure 21A. There is little correlation between the engine thrust curves and the direct operating cost curves of this figure.

The design point for an airplane from this parametric study (Fig. 21F) lies in the region bounded by the 7000 ft takeoff field length requirement. The L/D_{\max} locus requires the airplane to have lower wing loadings than its boundary. So the configuration should lie to the lower wing loading side (left) of these two limiting lines. Since the minimum direct operating cost airplanes lie to the right as far as possible, the lighter wing loading and smaller

engine sizes have less attractive DOC's to the left along the field length line. This made the design point choice relatively easy. The configuration size was picked at the intersection of the minimum engine size at initial cruise altitude locus juncture with the 7000 ft field length limit line. This choice provides the airplane with weight growth without exceeding the cruise L/D_{\max} criterion. As the engine grows the larger wing will assure reasonable compatibility with the initial cruise altitude objectives.

A second type of engine-airplane matching parametric study is illustrated by Figure 22 where the mission and field performance objectives are fixed and the number of passengers is allowed to vary for a *fixed* engine. This engine size of 43,000 lb of sea level static thrust is obviously compatible with the engines being utilized on the current airbus or jumbojet airplanes. Figure 22A shows that the principal variables are related a little more simply than in the previous parametric study. The lines of constant passengers are nearly orthogonal to the constant wing area lines and oblique to the takeoff gross weight lines. The initial cruise altitude relationships (Fig. 22B) provide a locus of tangents similar to the previous study where now the tangency indicates the maximum number of passengers that can be carried for a given initial cruise altitude while holding the range design constraint.

A different relationship is revealed for this fixed engine study by the field performance data (Fig. 22C) in that there is a minimum direct operating cost for a given field length. This locus of tangents was determined from superposition of the constant takeoff field length lines of Figure 22C on the DOC curves of Figure 22E. Therefore, the configuration choice should be at the intersection of this minimum DOC locus and the 7000 ft field length unless there is another incompatible constraint. The number of passengers is slightly greater than 180. The exact number of passengers, of course, is determined more precisely from an explicit layout of the cabin interior arrangement. These results would indicate that a greater number of passengers should be accommodated than the 175 chosen for the parametric study of Figure 21.

Once again the noise characteristics (Fig. 22D) of this airplane solution domain do not present a design constraint. The approach noise margin with respect to FAR 36 is less than half the margin available for takeoff and sideline conditions. Approach noise should be a target for improvement on growth versions.

Figure 22F displays the various design criteria and relationships determined by the parametric study. The design choice in this case is more explicitly defined by the crossing of the locus line for minimum DOC for a given field length and the 7000 ft field length line. This choice is conservative with respect to the locus of L/D_{\max} for cruise and is quite close to the locus for maximum passengers at initial cruise altitude. This airplane would have growth potential from increased thrust to provide increased weight with the same field performance.

These methods for portraying parametric study results by superimposing various families of curves is a good way to develop an intuitive feeling for the sensitivity of designs to the principal variables and design constraints. All of the data presented lie in the solution domain satisfying the design objectives. As mentioned before, this solution domain represents one set of configuration and technological concepts.

A very useful way of studying the variable relationships is to make each parametric family of curves on transparencies. Then each variable can be compared with any other variable simply by overlaying the respective transparencies. Although all of the transparencies overlayed simultaneously provides complete confusion, proper choices of overlays can very rapidly illustrate the most important relationships. In the examples of Figures 21 and 22 the tangential loci lead directly to the configuration choice that best suits the constrained design objectives.

Once the configuration design point has been chosen, the same engineering evaluation processes can be used to calculate off-design performance (Fig. 23). Typical results from a post-design analysis include payload range, takeoff and landing as functions of weight, and the takeoff, landing and sideline noise as functions of their respective weights. This mission and field performance data has the same accuracy as the engineering methods provide to the design synthesis process, but less accuracy than would be used for performance quoted to an airline. Usually, the parametric analysis methods are derived from more detailed engineering calculations by curve fitting and numerical simplifications to facilitate the very large number of calculations necessary to achieve the parametric solutions for the chosen matrix of independent variables. For example, the studies of fixed payload and fixed engine that were displayed by Figures 21 and 22 require rapid calculation of the airplane weight required to match the 2000 n.mi. range by interpolation of the engine performance and the fuel required for the given weight and altitude. The match between range and weight is determined iteratively by search methods for each matrix combination of wing area, takeoff gross weight, number of passengers, engine thrust, etc. Proper compromises between accuracy and speed or cost of computation are strictly a matter of judgment. Simple engineering methods should certainly be used to determine the answer to simple questions concerning trends and trades between major variables. However, as the questions become involved with a greater number of variables whose interrelationships have a strong impact on the answers, then more accurate engineering methods must be employed.

The principal reason for off-design performance is to study the usage of the chosen configuration on the route structure of various airlines. Economic studies of new airplane concepts or technological innovations are essential to determining their true value and whether the investment and/or risk of development has sufficient potential return. Each airline has peculiarities about its route system, its scheduling, and its maintenance practices that make an airplane evaluation necessary for its unique operational environment. The off-design performance is the principal

set of inputs. Other inputs include the fleet mix, competition, maintenance facilities and their locations with respect to the route structure, etc. One economic design evaluation method used by Boeing involves the following four sets of input:

Airplane Data –

- seating capacity and passenger mix
- operating empty weight
- maximum takeoff and landing weights
- fuel capacity
- fuel and time as functions of range
- reserve fuel
- takeoff and landing performance data
- taxi fuel and time allowances

Economic Data –

- airplane sale price
- number of airplanes or utilization
- flight hour costs
- block hour costs
- fuel and oil costs
- indirect operating costs
- passenger rates
- cargo rates
- insurance rates
- airplane life expectancy
- depreciation period
- cost of capital

Route Data –

- city pairs in the route system
- number and frequency of flights
- estimates of passenger demand
- estimates of cargo demand

Meteorological and Geographic Data –

- statistical winds and temperatures aloft
- random distribution of takeoff temperatures at airports
- runway lengths and altitudes.

Typical results from a route analysis study will yield the following data for the airplane being evaluated: passenger demand, cargo demand, airplane miles per week, revenue passenger miles per week, ton miles of cargo carried per week, total revenue and airplane fleet profit. It is fairly easy to analyze several potential airplane designs for several airlines modelled by the economic methods and determine the best match. Such airline business games can be treated parametrically in the same manner as the airplane design synthesis. It was stated earlier that the ultimate purpose of an airplane is to bring a profit for the customer. The manufacturer must try to understand how his product can make this profit potential larger and more probable than the product of his competitor.

The next parametric study, which is also related to engine-airplane matching, illustrates another graphical display technique called carpet plotting as an aide to envisioning multi-variable relationships. Carpet plotting gives a better intuitive feeling for the multi-dimensionality of the solution domain when curves fold over on one another.

The data of Figure 24 is taken from a parametric engine study for the 707-320B to determine the engine characteristics best suited to meet the new government noise regulations (FAR 36). This study objective is to find the optimum match between a new engine and an existing airframe that would maximize the return to the airline (minimum DOC) in compensation for the retrofitting costs. These data are plotted as a function of engine bypass ratio, which was one of the principal factors considered in controlling noise. The top two curves of Figure 24B are two other engine parameters of takeoff thrust (engine size) and turbine inlet temperature that were determined from the study. The resulting noise levels, the range improvement, and the DOC improvement are shown (Fig.24B) in relation to the empty airplane operating weight change.

The data of Figure 24 show that the best economic answer is an engine with a bypass ratio of about 4. However, the lowest noise is produced by the highest bypass ratio investigated. The break in the thrust and OEW curves at a bypass ratio of about 4.25 was the result of matching the takeoff field length second segment climb

gradient of 0.03, as indicated by Figure 24A. At bypass ratios greater than 4.25 the engine was sized by the desired initial cruise altitude of 32,500 ft for the design mission. Data for the payload-range characteristics (Fig. 24A) is shown for the bypass ratio closest to optimum ($BPR = 3.75$) for the turbine inlet temperatures studied, and for a minimum noise configuration ($BPR = 7.5$). Both payload-range curves show a considerable range improvement without a payload penalty. However, the nacelle installation of high bypass ratio engines on the -320B poses some major configurational problems that make the minimum-noise engine physical size unacceptable. Such installation problems were not resolved by the study. Although not indicated by these data, amortization for this kind of an engine retrofit to an older airframe would incur a surcharge against the flight passenger in order to pay for quieting the airplane. This is because the expected direct operating cost gains do not compensate for the short life remaining in the airframe, which has been or soon will be completely amortized. However, the carpet plot mode of presenting the parametric information generated by the study is the significant point of presenting these data, rather than an evaluation of the economic results.

The data presentations of Figure 25 are called carpet plots, because of their three-dimensional appearance which sometimes resembles imagined flying carpets. These plots are woven by plotting the relationship between two independent variables, such as bypass ratio and turbine inlet temperature used here, against a common dependent variable such as DOC, range, etc. The curves of Figure 24 correspond to the envelope generated by the range carpet plot. This range envelope or three-dimensional, upper-surface tangency corresponds to the maximum range achievable from any combination of bypass ratio and turbine inlet temperature. The DOC carpet plot minimum envelope is also very close to the locus of the maximum range points for the engine variables. The plots of takeoff thrust, OEW, and takeoff noise (Figures 25C, D and F) show the maximum range line cutting across the grid quite far from any type of envelope. In the case of the landing approach noise carpet plot (Fig. 25E) the maximum range occurs approximately one to two decibels above the minimum noise obtainable from the optimum combination of turbine inlet temperature and bypass ratio.

This is a typical study where certain parameters, not illustrated in Figures 24 and 25, were held constant on the assumption that they represented the best in the state of the art. Such factors include engine primary and secondary pressure ratio, acoustic lining of the inlet and exhaust flows, etc. Therefore, this kind of a parametric study represents the limited view of a problem where only two primary variables were studied. The airplane and the rest of the engine variables were constrained as constants.

4. OPTIMIZATION EVALUATION TECHNIQUES

Optimization techniques for airplane design synthesis use exactly the same engineering processes described for the parametric techniques. The fundamental difference between parametric and optimization techniques lies in the introduction of an iterative process control system which is capable of interpreting the analytical results and then iteratively perturbing variables to seek an optimum for some objective function. This objective function, dependent upon the perturbed design variables, is usually a performance quality such as range, weight, cost, etc. In the sense of optimization it does not matter whether the process control is for maximizing a function, such as range, or minimizing a function, such as cost or weight. This is because the maximum of a given positive function is equivalent to the minimum of its negative value.

The addition of an optimization driver to the design synthesis process is illustrated by Figure 26 as a modification of the airplane design data flow diagram shown as Figure 6. The optimization driver has two principal functions: (i) receive the evaluation results of the design synthesis process and interpret the data in light of the previous successive iterations through the process, and (ii) determine which of the variables should be perturbed and how large the perturbations should be. Then the engineering processes are repeated to determine a new configuration from these perturbed inputs. This new configuration is evaluated so the optimizer can determine whether the chosen perturbations have been successful in moving toward (or finding) the optimum answer. The iterative procedure is continued until either the objective function has been optimized or it is evident the search is fruitless.

Since the advent of the high speed digital computers, the use of optimization techniques has proliferated almost explosively. There are many excellent methods now available for use in optimizing drivers of computerized engineering problems. A good many of these are summarized in References 94 and 95 for application to constrained optimization problems such as airplane design synthesis.

Figure 27 shows the optimization methods categorized according to their mathematical sophistication and then stacked in accordance with their algorithmic complexity. The search methods are most analogous to the intuitive successive approximations used in the past for airplane design. These methods are based upon the sequential examination of attempted solutions. Then by simple comparisons of patterned or random attempted solutions, some direction is chosen to continue the search for an optimum solution. These methods require only that the design synthesis process be composed of continuous functions which can be evaluated from the chosen sets of input data. Search methods are particularly useful, because they provide information about the terrain where the optimum is found, since they interrogate the variable relationships thoroughly in arriving at the sought point. Most of the search methods seek the optimum solution rather slowly and they require very careful control to determine whether the optimum corresponds to a true minimum value. However, there are many problems where

the search methods have shown their superiority over the more sophisticated descent methods, which depend upon the mathematical interpretation of the solution domain.

The descent methods all depend upon determining a local value of first or second order derivative for explicit guidance in the direction for seeking the optimum solution. There is a great deal of literature available on these numerical optimization algorithms (see Reference Nos. 93 through 105), so no detailed description will be provided here. However, it is important to emphasize that the characteristics of the design synthesis process may have a strong influence on the suitable choice of a method for optimization. This problem was recognized years ago by Hague^{95,97} and he resolved the matter by establishing a repertoire of methods in a system of computer programs called AESOP (Automated Engineering and Scientific Optimization Program). By collecting a variety of optimization methods of both the search and descent types it was possible to choose any single method, or combinations of methods for sequentially attacking a given design problem. This optimizing driver has been adapted for use on a wide variety of computers (IBM 360, SRU 1108, CDC 6600, etc.) and has the ability to solve optimization problems involving up to 100 variables and 20 constraints. AESOP has been widely applied to performance optimization problems and to interdisciplinary design problems such as a hypersonic transport⁹⁸ and more recently the US space shuttle for NASA.

A simplified three-dimensional graphical comparison of the search and descent methods is provided by Figure 28. Search methods start at the initial guessed value of the variables and probes in the orthogonal directions of these variables to determine an appropriate direction for minimizing the performance function. The search methods simply take a step and then evaluate it for goodness. Then a decision is made whether to take another step in that direction or to look in some other direction. In this manner there are obviously a lot of false steps taken to probe the terrain which is the reason that these methods usually consume more steps and computing energy in arriving at the optimum than the descent methods. The descent methods require derivatives of the variables to be determined at the starting point before it can decide on the most beneficial direction to step. However, when a descent method does step, it is usually in a more meaningful direction than the search methods as shown in the lower diagram of Figure 28. This diagram also illustrates that the number of steps required to get from a starting point to the optimum depends upon the orientation of the local terrain orthogonal with respect to the direction of the optimum from the starting point. If the orthogonal points in the general direction of the optimum, then the solution will occur more rapidly. If, on the other hand, the orthogonal points away from the optimum direction, then more steps will be required to get the orientation corrected toward the optimum. These statements are also true, of course, for the direct search methods, although more steps generally will be required. As illustrated by these diagrams, a ridge or valley can cause a great number of changes in search direction and step size, unless the starting point is aligned reasonably well to the shallow gradient axis. Terrain characteristics like sharp ridges, bluffs, saddle points, etc. can require special techniques for finding optimum solutions or for determining if a solution is a false or real optimum.

So far this discussion of optimization has not involved the subject of constraints. Constraints can be applied as either an equality or an inequality. When an equality is imposed, then the solution will lie on the boundary containing that constraint. On the other hand, an inequality constraint will allow a solution to be found anywhere in the domain in so far as the inequality is satisfied. Figure 29 illustrates one kind of a problem associated with equality-constraint solutions. This is the type of parametric relationship shown previously by Figure 21, where a minimum weight airplane is sought with a specified takeoff and landing field performance. The constrained solution is at the juncture of the two constraint boundaries, (TOFL₂ and LDGFL₂) which is shown to be away from the locus of weight minima formed by the tangency of the takeoff field length (TOFL) lines to the takeoff gross weight (TOGW) lines. The true minimum weight, or optimized airplane, lies at the intersection of the locus of minima and the takeoff field length constraint line (TOFL₂). If this problem were posed with inequality field length constraints, then the true minimum weight of the plane would be found directly. Then the solution would tell the designer that only the takeoff field length is critical in this case.

This illustration lends emphasis to the basic tenet that all optimum solutions should be suspect. When an "optimum" answer is found, the terrain of the solution domain must be carefully examined to determine its characteristics. Most any of the direct search methods can be utilized for simple exploration locally around the answer or solution point. Such explorations should be standard practice to prevent the misinterpretation or misqualification of the solution as a true optimum.

An engine-airplane optimization study using the quadratic search method from AESOP is illustrated by Figure 30. Four engine parameters were varied: bypass ratio, turbine inlet temperature, fan pressure ratio, and compressor pressure ratio. The search limits on these respective variables are indicated by the vertical arrows in the diagrams. An initial value was chosen for the engine characteristics to be used in an engine cycle analysis program coupled with an airplane matching program to achieve the lightest takeoff gross weight for the design mission. Subordinate programs for the aerodynamics and weights were also coupled into the system.

The first 15 iterations of the design variables were required to compute all of the derivatives needed to determine the quadratic surface fit to the four-dimensional surface. Then within the next 10 steps 2 of the variables had moved to search limits and the other 2 had settled on values close to the final answers. The objective function to be minimized was the takeoff gross weight which was reduced by 10 percent during these first couple of dozen

iterations. A rhythmic pattern was set up in several of the variables after the twenty-fifth iteration as the method moved alternately between the search and derivative computations. Most of the variables established stable conditions, even though the gross weight main trend continued to diminish very slightly. The rate of gain was very small for the remaining 125 iterations, less than one-half of one percent. After the initial major weight gain the remaining reduction appeared to be false and was probably the result of randomness or noise in the engineering processes.

There are some other interesting things about these results to be mentioned. The author of AESOP⁹⁷ recommends the patterned search of any "optimum" solution to determine the nature of the answer. He also advised that it is common for the descent methods to be unable to find substantial gains in many problems where the terrain of the answer is not well suited to the nature of a quadratic surface. In fact, the large excursion just beyond the 130th iteration is probably created by the fit of derivatives calculated as the small difference between two very large numbers or some similar numerical difficulty. If this particular algorithm had a memory, it would have discarded the advice of the calculations, because the step was indeed a bad one, since the gross weight surged very high.

Current techniques in use for monitoring AESOP would have lead the observer to terminate the search iterations certainly after the second cycle of the derivative-search sequence was producing no marked reduction in weight. The great number of iterations indicated here is fairly typical of optimization techniques. This large number of calculations teaches a design team quickly that great care must be exercised in making the engineering processes as efficient as possible. Even then, considerable care must be used in choosing the solution algorithm. Many experiments are usually required to get a good match between the synthesis process and the optimization driver.

Figure 31 shows one of the several suboptimizations that are employed by an airplane design synthesis process. This plot displays the results of a search for the maximum range factor throughout the speed-altitude domain. In this case the optimum fell below the thrust limit line, so some climb margin was available. The actual speed used during the cruise was somewhat higher than the speed for maximum range factor, as indicated, to minimize the operating costs. Several constraints other than the thrust limit are considered in this kind of determination, such as the maneuver load factor to buffet, climb margin, etc.

Similar optimizations are needed for matching field performance in the sense that the best flap deflection can be found for a given wing area, but both must be optimized simultaneously. Another problem facing designers is the optimum combination of acoustic treatment and engine cycle characteristics. Tailoring new or improved engine noise characteristics output from the primary and secondary inlet and exhaust flows needs optimization for maximum suppression effectiveness. These kinds of trades involve noise, weight, thrust, external nacelle drag and interference effects with adjacent surfaces, such as the wing for wing-mounted pod installations. The treatment of any suboptimization is similar to the whole airplane problem and may require care in selecting the algorithm used to reach a solution reliably and with reasonable effort. More on this subject will be presented in the next section.

5. COMPUTERIZED AIRPLANE DESIGN SYNTHESIS

There is a broad spectrum of computerized design synthesis possibilities, ranging from simple analysis methods which use little synthesis logic to nearly full automation of the synthesis process with sophisticated optimization algorithms driving the system of computerized methods. Probably the most common type of program in use today accepts a design concept and then massages it into compatibility with performance objectives. The results discussed previously in the parametric section were of this type. In contrast, the results that will be described briefly here were produced by a computerized method that can either accept a configuration concept, or create a configuration concept from given design objectives. A range of compatible computerized methods should be available to the designer or technologist in the future, just as there has been the choice of a slide rule or desk calculator in the past.

During the last decade there has been a vast improvement in the quality of engineering design and analysis methods. Most of these methods were generated within the confines of specific disciplines for the purpose of providing more rapid or better solutions to routine engineering problems. It was very natural for the first elements to be linked for the interdisciplinary purpose of airplane configuration evaluation as indicated in Figure 6 by the dark outlined boxes. These included aerodynamics, propulsion and weights technologies coupled to performance evaluation methods. The next step was to extend the methods by simple configuration perturbation techniques for sizing wing area, engine size, etc. to meet specified performance criteria. At present, there is sufficient computing capacity and speed available on machines (CDC 6600, IBM 370, etc.) to begin a major upgrading to include *all* technical disciplines into automated design synthesis *with* optimization.

There will still be many gaps in the design synthesis processes such as flutter, viscous effects on stability, maximum lift, wave drag, etc. for the foreseeable future, but more extensive use of the computer to tie the technology methods together through explicit communication of specific interdisciplinary information flow about a design, appears to be a great step forward. It certainly is not the thesis here that all computerized methodology should be introduced into a massive computerized design/analysis system. However, current experience with interdisciplinary computerized synthesis systems has shown the following advantages:

- (i) Data consistency and method compatibility are significantly enhanced.
- (ii) Less effort and task flow time are required to attain a superior quality answer.
- (iii) The enforced design team cooperation and thinking compatibility promotes better understanding of interdisciplinary needs.
- (iv) Configuration design results are more free from fatal faults, since errors are restricted to input data, provided the methods are proven.

Pulling together a major computing system requires a significant commitment of resources and the investment is usually substantial before tangible benefits can be observed.

Keeping the computing process under control of the engineering team responsible for both the inputs and outputs to the design problem appears necessary. The use of experienced human control for monitoring via adequate summary displays can prevent loss of time and computing resources. It is impossible to set up a design problem of even moderate complexity and be absolutely sure that limits will not be exceeded, calculation instabilities will not be encountered, or that the input data have been properly chosen, keypunched, and read into the machine without error. Good use of the computer can prevent many errors by numerical input checking or data graphical displays. Then if some input data are found erroneous, the use of on-line data editing can expedite the tedious corrections. All of these techniques require time to develop, and time to acquaint users with their capabilities so the benefits are spread throughout an organization.

An evolution of the twinjet used to illustrate the parametric and optimization techniques is tabulated in Figure 32. The column labelled parametric baseline was the first approximation to the desired objectives determined from a combination of previous experience and studies. This baseline airplane was used to derive the parametric trend data (cf. Figures 9, 11 and 13) for preparation of the parametric results shown by Figures 21 and 22. Data for the fixed-engine case (Fig. 22) are shown in column 2 for comparison with the baseline. The same baseline was submitted to a computerized design synthesis program for refinement of the design with fixed wing geometry as shown by the third column. The fourth column relaxed the wing size constraint and showed a reduction in the airplane weight when sized to the 2000 n.mi. range and 7000 ft field length. Another variation was made to optimize aspect-ratio using the program to resize the wing and empennage, rebalance the configuration, and determine the best wing aspect ratio for fixed payload and performance. Although the weight gains were not as large as the previous step, good progress in reducing airplane size was made once again. These stepwise studies are not truly indicative of the optimum airplane, but point out the trends toward it. A great many more configuration variables should be freed to permit the truly minimum weight airplane to be found for a fixed engine and payload.

Many airplane concepts are input successively to parametric and optimization studies in this manner to resolve many heated discussions concerning the way an airplane should be designed. It is easy to show by examples that most airplane configurations are very sensitive to the assumptions made about the proper set of objectives and the proper set of constraints. Use of all of the methods described here have their place and can provide an effective set of synthesis tools with the computer serving simultaneously as their power source and toolbox. The designers still have to be the master craftsmen.

Figures 33 through 37 show a completely integrated computerized method for airplane design and some typical graphical results. The flow diagram (Fig. 33) indicates the various steps of the design process and the inputs necessary for the desired outputs to be obtained. The inputs describe the airplane configuration concept and the performance expected from it. Sufficient logic for generating a configuration is available to turn the inputs into a first approximation of the answer. After the configuration is weighed and balanced it is subjected to successive evaluations and perturbative iterations as the system driver seeks to satisfy the desired performance objectives. The sequence of finding the right engine size, wing, empennage, flaps, fuselage, etc. have to be altered to suit the particular problem being solved. A scheme is used for rapidly assembling basic modules to accomplish a desired task and compiling the design logic with needed data flow controls. This scheme greatly facilitates the design flexibility and opens the synthesis system to continual improvement.

A configuration two-view drawing is shown as Figure 34 with a corresponding interior deck plan of the passenger seating arrangement shown by Figure 35. This airplane is the same concept used to illustrate the parametric and optimization techniques. Use is made of rather rudimentary graphic geometry methods to reduce the configuring time on the computer to a few seconds, because it is repeated so many times. Since any significant change of a component will result in weight and balance changes that in turn force empennage resizing to maintain satisfaction with the stability criteria, the configuration is updated continuously prior to the performance evaluations. Experience has shown that precise consistency in the configurations evaluated is necessary for an optimization algorithm to accurately seek convergence on the desired solution. Even the best numerical methods involve randomness which creates "noise" that leads to algorithmic indeterminacy through contradictory information. Remember the wild gyrations of the last major excursion of Figure 30 was the result of such misguided calculations.

A dashed line in the profile view of the airplane (Fig. 34) identifies the floorline for the passenger cabin. Below this line is shown the cargo containers located fore and aft of the wing spar and landing gears. The cross mark in the topview behind the rear wing spar identifies the location of the landing gear strut. Fuel volume is contained

between the wing spars. In cases where very long range performance is desired the wing size can be controlled by the required fuel volume, unless some of the cargo space is allocated to body fuel cells. All of these factors can be controlled by inputs to the program. In fact, any piece of data flowing between modules of the system can be controlled externally, if so desired.

The floor plan is arranged automatically to accommodate the desired number of first class and tourist passengers. Additional considerations are provided for the doors, emergency exits, lavatories, galleys, etc. aft of the flight crew cabin. This capability eliminates a great amount of interior layout work, particularly for area-ruled configurations where each change in wing area, engine size, passenger count, etc. can require redistribution of the seating plan. Any of the arbitrary values assigned to an interior layout can be changed by the designer to evaluate their effect on the overall configuration. For example, the aisle width gets directly reflected in the weight, drag, and balance, just the same as the passenger class split, seat spacing, and seat width. Studies of galley location and lavatory arrangements are also feasible.

A weight diagram of the center of gravity travel for the passenger loading, the cargo loading, and the fuel loading (respectively, from left to right) is shown by Figure 36. The oblique trend of both the passenger and cargo c.g. diagrams to the MAC percent lines is common for aft-mounted engine configurations where the aft empty c.g. has to satisfy the static stability margins. Lumpiness of the passenger diagram is the result of passenger seating preference for window, aisle and then center seats, where the upper curve represents starting at the rear and loading forward in the seat-preference sequence and the lower curve starts at the front and loads aft. A similar scheme is used for the cargo, except that there is no loading preference. Cargo gets loaded either from the rear or from the front. The fuel loads by gravity from the lowest point in the tanks, but gets used from the fuselage-contained wing tank first. This is the reason for the small loop in the fuel diagram. If the wing were divided into several tanks, then it would be possible to open the fuel diagram even farther by fuel management. The complete fuel diagram is inset above the grid. This diagram can be used as an overlay on the grid to explore variations in c.g. travel as the passenger or cargo loadings change.

The last figure on the twinjet is the two diagrams showing the relationship between wing position and the horizontal tail size to match the loadability requirements to the aerodynamic stability limits. Figure 37 shows diagrammatically how the match is achieved. The upper graph is simply constructed by moving the wing back and forth along the fuselage and determining the c.g. travel of the forward and aft loaded conditions. The lower graph is constructed by varying the horizontal tail size and determining the aft c.g. stability margin and the forward c.g. control requirements. These diagrams give a very quick grasp of the way in which the c.g. travel is established. The loading map of Figure 36 makes it easy to find an average, or typical, c.g. location for determining the cruise trim condition.

Many other kinds of monitoring diagrams, data displays, drawings, etc. can be generated numerically for rapid display by the computer graphics methods available today. A great deal has been written about interactive graphics, but their use has had nowhere near the impact that was originally sought in years past. There appear to be several reasons why computer graphics should be completely subordinate to the synthesis process:

- (i) The cost burden and sophisticated hardware-software maintenance problems are significantly severe.
- (ii) The designer should only interact with the computer in the event of failure or questionable processing results, rather than continuously as a puppet answering the computer.
- (iii) Sound, consistent control logic based on accumulated experience and under automated control is more dependable than a variety of human decisions controlling a solution sequence.

There is no question that the design engineers have to control the computerized synthesis processes. However, continuously displayed summary information for the engineers to assimilate during computation makes the most of a computer's capability without compromising the decision-making authority of the human. The user must be able to continue the design process from any point of interruption without a great loss in computing resources, or he will be too hesitant to interact and evaluate the progress in detail. These bits of philosophy about computerized design are conditioned by a specific set of experiences and must be considered in the light of limited Boeing success in introducing fully interdisciplinary synthesis processes into commercial airplane design work.

6. CONCLUDING REMARKS

A brief review of parametric and optimization techniques of airplane design has been given. Considerable attention to the organization of the technology elements was required to illustrate the vast amount of interdisciplinary data that must flow in the design synthesis process. It was emphasized that several levels of methodology can be utilized for either parametric or optimization studies of configuration alternatives. As the number of independent variables is increased it falls beyond the means of parametric techniques to determine the real solution and sophisticated optimization algorithms must be employed. Regardless of which technique is used to seek a best design, there are various levels or depths of information available as a design progresses. It is important to incorporate the use of this new and more detailed information as it accumulates from analytical and experimental evaluations of the configuration and its components.

Significant progress has been made in the use of computerized engineering methods to reduce the task flow time and improve the consistency of data flow in configuration design problems. The introduction of sophisticated optimization algorithms to control large systems of interdisciplinary design synthesis systems is becoming commonplace. Some examples of digital computer graphic output shows what the designer has available to interactively monitor the output and quickly assimilate the results during computation to determine whether the solution process is progressing satisfactorily. The parametric and optimization techniques enhanced by today's powerful, high-speed, large-capacity digital computers make feasible the design process as a truly interdisciplinary design team affair.

REFERENCES

Airplane Design Synthesis

1. Steiner, J.E. *Planning a New Commercial Aircraft.* AIAA Astronautics and Aeronautics, September 1967, pp.52-60.
2. Brizendine, J.C., Strang, C.R. *The Future Transport World.* AIAA Journal of Aircraft, Vol.4, No.6, November-December 1967, pp.481-486.
3. Lloyd-Jones, D.J. *Airline Equipment Planning.* AIAA Journal of Aircraft, Vol.5, No.1, January-February 1968, pp.60-63.
4. Kolk, F.W., Blindell, D.R. *Evolution and Revolution with the Jumbo Trijet.* AIAA Astronautics and Aeronautics, October 1968, pp.64-69.
5. Orazio, F.D. *From Technology to Systems in Military Aircraft.* AIAA Astronautics and Aeronautics, July 1969, pp.48-62.
6. — *Transportation.* Space/Aeronautics, January 1970, pp.27-32.
7. Steiner, J.E. *Aircraft Development and World Aviation.* The Aeronautical Journal of the Royal Aeronautical Society, Vol.74, No.714, June 1970, pp.433-443.
8. Cleveland, F.A. *Size Effects in Conventional Aircraft Design.* AIAA Journal of Aircraft, Vol.7, No.6, November-December 1970, pp.483-512.
9. Schaefer, R.K., Velton, K.R. *Operational Constraints for STOL Aircraft.* AIAA Journal of Aircraft, Vol.8, No.8, August 1971.
10. Smelt, R. *Air Transport Boundaries for National Planning.* AIAA Astronautics and Aeronautics, November 1971, pp.27-35.
11. Worsheim, J.E. *The Design Process.* Paper No.9 in AGARD Proceedings No.62, Preliminary Design Aspects of Military Aircraft, March 1970.

Aerodynamics

12. Gardner, D. *The Drag Due to Lift of Plane Wings at Subsonic Speeds.* Journal of the Royal Aeronautical Society, Vol.70, May 1966, pp.595-598.
13. Norton, D.A. *Airplane Drag Prediction.* Published in Annals of the New York Academy of Sciences, Vol.154, Part 2, pp.245-360, presented at the International Congress on Subsonic Aeronautics, 22nd November 1968.
14. McRae, D.M. *The Aerodynamics of High Lift Devices on Conventional Aircraft.* The Aeronautical Journal of the Royal Aeronautical Society, Vol.74, June 1969, pp.535-546.
15. Baals, D.B., et al. *Aerodynamic Design Integration of Supersonic Aircraft.* AIAA Journal of Aircraft, Vol.7, No.5, September-October 1970, pp.385-394.
16. Gratzel, L.B. *Analysis of Transport Applications for High Lift Schemes.* Paper 7 in AGARD Lecture Series No.43 on Assessment of Lift Augmentation Devices, AGARD-LS-43-71, February 1971.

17. Bonner, E. *Expanding Role of Potential Theory in Supersonic Aircraft Design.* AIAA Journal of Aircraft, Vol.8, No.5, May 1971, pp.347-353.

Propulsion and Noise

18. Weir, R.H. *High Performance Turbine Engines.* The Journal of the Royal Aeronautical Society, Vol.66, No.621, September 1962, pp.541-554.
19. Halls, G.A. *Air Cooling of Turbine Blades and Vanes.* Flight International, 13th July 1967, pp.73-77.
20. Yaffee, M.L. *P & W Bases Airbus Powerplant on JT9D.* Aviation Week and Space Technology, 9th October 1967, pp.43-49.
21. Findlay, D.A. *Aids: Monitoring Aircraft Systems.* Space/Aeronautics, October 1967, pp.100-106.
22. — *The Way Ahead of the CF6.* Flight International, 31st October 1968, pp.714-717.
23. Cheney, G.H. *Aircraft Engine Noise.* Paper in Education in Creative Engineering Seminar, Massachusetts Institute of Technology, April 1969, pp.72-82.
24. Garry, F.W. *Jet Propulsion.* Space/Aeronautics, July 1969, pp.126-136.
25. Dettmering, W., Fett, F. *Methoden der Schuberrhöhung und ihre Bewertung.* Zeitschrift für Flugwissenschaften, Vol.17, No.8, August 1969, pp.257-267.
26. Orchard, P.F. *Advanced Turbine Technology.* Space/Aeronautics, March 1970, pp.29-37.
27. Cheeseman, I.C. *Noise, Its Measurement and Origin.* Flight International, 16th April 1970, pp.639-642.

Structures and Weights

28. Lackman, L.M. *Aircraft Structures.* Space/Aeronautics, July 1969, pp.158-161.
29. Kasten, H.G. (Organizer) *Fifth Weight Prediction Workshop for Advanced Aerospace Design Projects.* Sponsored by The Deputy for Development Planning, Aeronautical Systems Division, Air Force Systems Command, WPAFB, 20th-22nd October 1969.
30. Torenbeek, E. *Prediction of Wing Group Weight for Preliminary Design.* Aircraft Engineering, July 1971, pp.16-21.
31. Whinery, D.G., et al. *Composite Airframe Design.* AIAA Journal of Aircraft, Vol.8, No.11, November 1971, pp.924-929.

Flight Controls

32. Robinson, A.C. *Survey of Dynamic Analysis Methods for Flight Control Design.* AIAA Journal of Aircraft, Vol.6, No.2, March-April 1969.
33. Lorenzetti, R.C., et al. *Computerized Design of Optimal Direct Lift Controller.* AIAA Journal of Aircraft, Vol.6, No.2, March-April 1969, pp.137-143.
34. Jansen, G.R. *Flight Evaluation of Direction Lift Control on the DC8 Super 63.* SAE Paper 69270, pp.180-184.
35. Chalk, G.R., Wilson, R.K. *Airplane Flying Qualities Specification Revision.* AIAA Journal of Aircraft, Vol.6, No.3, May-June 1969, pp.232-239.
36. Lorenzetti, R.C., et al. *Direct Lift Control for Approach and Landing.* AIAA Journal of Aircraft, Vol.6, No.3, May-June 1969, pp.240-244.
37. Pasley, L.H., Kass, G.J. *Improved Airplane Performance through Advanced Flight Control System Design.* AIAA Paper No.70-875, July 1970.

38. Pinsker, W.J.G. *Direct Lift Control. The Aeronautical Journal of the Royal Aeronautical Society, Vol.74, October 1970, pp.817-825.*
39. Holloway, R.B.,
Burris, P.M. *Aircraft Performance Benefits from Modern Control Systems Technology. AIAA Journal of Aircraft, Vol.7, No.6, November-December 1970, pp.550-553.*

Economics

40. Yates, E.H. *Cost Analysis as an Aid to Aircraft Design. AIAA Journal of Aircraft, Vol.2, No.2, March-April 1965, pp.100-107.*
41. Jackes, A.M. *The Influence of Performance Characteristics on the Economic Effectiveness of Transport Vehicles. AIAA Paper No.67-802, AIAA 4th Annual Meeting and Technical Display, Anaheim, California, 23rd-27th October 1967.*
42. — *Standard Method of Estimating Comparative Direct Operating Costs of Turbine Powered Transport Airplanes. Air Transport Association of America, December 1967.*
43. Kahn, J.F. *V/STOL Airline System Simulation. AIAA Journal of Aircraft, Vol.5, No.3, May-June 1968, pp.306-311.*
44. Ormsby, R.B. *Total Airline Profit Model Program. SAE Paper 690413, presented at the National Air Transportation Meeting in New York, N.Y., 21st-24th April 1969.*
45. Morgan, M. *The Economic Impact of R & D on Aircraft Design. Aircraft Engineering, August 1970, pp.24-28.*
46. Hufford, R.D.,
et al. *The Economics of Subsonic Transport Airplane Design, Evaluation and Operation. SAE Paper 710423, presented at the National Transportation Meeting, Atlanta, Georgia, 10th-13th May 1971.*
47. Sommers, A.N.,
Jeng, D.C. *Inter-City V/STOL Service and the Businessman Traveler. AIAA Journal of Aircraft, Vol.8, No.12, December 1971, pp.976-982.*

Advanced Technology

48. Kuchemann, D. *An Aerodynamicist's Prospect of the Second Century. The Aeronautical Journal of the Royal Aeronautical Society, Vol.72, No.686, February 1968, pp.109-113.*
49. Dubey, M. *Advanced Technology Tradeoffs. Space/Aeronautics, August 1968, pp.55-62.*
50. — *North Atlantic Treaty Organization, Advisory Group for Aerospace Research and Development, "AGARD Conference Proceedings No.35, Transonic Aerodynamics", Copies of Papers Presented at a Specialists Meeting of the Fluid Dynamics Panel of AGARD, September 1968.*
51. Thring, M.W. *Power Generation for Aircraft in the Second Century. The Aeronautical Journal of the Royal Aeronautical Society, Vol.72, No.693, September 1968.*
52. Levin, S.M. *Building Blocks for the Next Subsonics. Space/Aeronautics, May 1969, pp.70-78.*
53. de Paul, M.V. *Experimental Research on Supercritical Wing Profiles. NASA TT F-12, 415, July 1969.*
54. Barnes, J.F. *Advances in Engine Technology: Cool Turbines. Aircraft Engineering, October 1969, pp.18-21.*
55. Weir, R.H. *Propulsion Prospects. The Aeronautical Journal of the Royal Aeronautical Society, Vol.73, No.707, November 1969, pp.923-934.*
56. Pearcey, H.H. *Some Problems and Features of Transonic Aerodynamics. The Seventh Congress of the International Council of the Aeronautical Sciences, ICAS Paper No.70-14, September 1970.*
57. Yaffee, M.L. *Turbine Program Sparks New Technology. Aviation Week and Space Technology, 30th November 1970, pp.53-57.*

58. Krupp, J.A.,
Murman, E.M. *The Numerical Calculation of Steady Transonic Flows Past Thin Lifting Airfoils and Slender Bodies.* AIAA Paper No.71-566, AIAA 4th Fluid and Plasma Dynamics Conference, Palo Alto, California, 21st-23rd June 1971.
59. Steger, J.L.,
Lomax, H. *Numerical Calculation of Transonic Flow About Two-Dimensional Airfoils by Relaxation Procedures.* AIAA Paper No.71-569, AIAA 4th Fluid and Plasma Dynamics Conference, Palo Alto, California, 21st-23rd June 1971.
60. Allen, J.E. *The Future of Aeronautics – Dreams and Realities.* The Aeronautical Journal of the Royal Aeronautical Society, Vol.75, September 1971, pp.587-606.
61. Schmidt, C.F. *Pointing the Way for Air Transport Technology.* AIAA Astronautics and Aeronautics, October 1971, pp.63-67.
62. Dugan, J.F., Jr *Airbreathing Propulsion System Trends.* AIAA Astronautics and Aeronautics, November 1971, pp.36-45.
63. NASA *Vehicle Technology for Civil Aviation, The Seventies and Beyond.* A Conference held at Langley Research Center, Hampton, Va., NASA SP-292, November 1971.

Parametric Techniques

64. Wimpers, J.K. *Shortening the Takeoff and Landing Distances of High Speed Aircraft.* Presented at the 26th Meeting of the AGARD Flight Mechanics Panel, June 1965, Boeing Doc. D6-16168.
65. Swan, W.C. *A Discussion of Selected Aerodynamic Problems on Integration of Propulsion Systems with the Airframe on Transport Aircraft.* Presented at the AGARD Specialists Meeting, October 1965, Boeing Doc. D6-18084.
66. Kuchemann, D. *An Analysis of Some Performance Aspects of Various Types of Aircraft Designed to Fly Over Different Ranges at Different Speeds.* Royal Aircraft Establishment Technical Report No.66188, June 1966.
67. Rockwell, R.W. *A Method for Airplane Design Trade Studies.* Boeing Doc. D6-20741, October 1967.
68. London, M.P. *Tactical Areas Superiority.* Space/Aeronautics, March 1968, pp.62-71.
69. Wharten, C.L., Jr *Unique Design Considerations for a Large T-Tail Aircraft.* SAE Paper 680204, April 1968.
70. Klees, G.W.,
Orton, H.E. *Engine Selection for Bomber Aircraft.* Proceedings of the Annual Aviation and Space Conference, Beverly Hills, California, June 1958, pp.356-364.
71. London, M.P. *VFX – The Navy's Choice.* Space/Aeronautics, November 1968, pp.50-75.
72. Perry, D.H. *Exchange Rates Between Some Design Variables for an Aircraft Just Satisfying Takeoff Distance and Climb Requirements.* Royal Aircraft Establishment Technical Report No.69167, August 1969.
73. Leavy, G.C. *Parametric Approach to Aircraft Sizing and Tradeoff Studies for Vectored Thrust Aircraft.* Paper No.1 in Reference 29, 20th-22nd October 1969.
74. Del Hagen, W.T. *Concept Development of Advanced Aircraft Systems.* Paper No.13 in Reference 29, 20th-22nd October 1969.
75. Langfelder, H. *The Use of Tradeoff Studies in Preliminary Design.* Paper No.4 in the AGARD Conference Proceedings No.62 on Preliminary Design Aspects of Military Aircraft, March 1970.
76. Klepinger, R.H.,
et al. *Future Advances in the Aerodynamics of Military Strike Aircraft.* Paper No.7 in the AGARD Conference Proceedings No.62 on Preliminary Design Aspects of Military Aircraft, March 1970.
77. Roskam, J.,
Kohlman, D.L. *An Assessment of Performance, Stability and Control Improvements for General Aviation Aircraft.* SAE Paper No.700240, March 1970.

78. Kuley, W.G.,
Donnow, A.P. *Air Transport Mission Capability Analysis.* AIAA Paper No.70-899, July 1970.
79. Kleckner, H.F. *Military/Commercial STOL Transport Commonality.* SAE Paper 710468, Presented at the National Air Transportation Meeting, Atlanta, Georgia, 10th-13th May 1971.
80. Goodmanson, L.T. *Transonic Transports.* AIAA Astronautics and Aeronautics, November 1971, pp.46-56.

Computerized Airplane Design

81. Boehm, B.W. *Keeping the Upper Hand in the Man-Computer Partnership.* AIAA Astronautics and Aeronautics, April 1967, pp.24-28.
82. Lee, V.A.,
et al. *Computerized Aircraft Synthesis.* AIAA Journal of Aircraft, Vol.4, No.5, September-October 1967, pp.402-408.
83. Klees, G.W. *Description and Operating Instructions, Boeing Engine-Airplane Matching Program (Beam).* Boeing Doc. D6-20383, July 1968.
84. Wennagel, G.J.,
et al. *IDEAS - Integrated Design and Analysis System.* SAE Paper No.680728, October 1968.
85. Wallace, R.E. *Computing Geometric Airplane Characteristics.* Paper in Education in Creative Engineering Seminar, Massachusetts Institute of Technology, April 1969, pp.163-182.
86. Milliman, P.D.,
et al. *Feasibility Study of a Computerized Preliminary Design Process.* Boeing Doc. D6-23935, June 1969.
87. Cook, D.I. *Preliminary Engineering Design System - Design Specification.* Vol.I, Boeing Doc. D1-81-0081, 8th May 1969.
88. Hurst, W.,
Ross, H. *Application of Computer Aided Design Programs for the Technical Management of Complex Fighter Development Projects.* AIAA Paper No.70-364, March 1970.
89. Przybylko, S.J.,
et al. *Advanced Integrated Diesel Engine Simulation - A Step Forward for Propulsion System Testing.* AIAA Paper No.70-633, June 1970.
90. Kondo, J. *Application of Computer Techniques to Aircraft Design Problems.* The Seventh Congress of the International Council of the Aeronautical Sciences, ICAS Paper 70-28, September 1970.
91. Greer, R.F.,
et al. *Interactive Preliminary Design System - Vol.II - Director and File Handler.* Boeing Doc. D1-62-10347-2, 11th May 1971.
92. Comisso, V. *Interactive Preliminary Design System - Vol.III - The Graphics Processor.* Boeing Doc. D1-62-10347-3, 11th May 1971.

Optimization

93. Landgraf, S.K. *Some Applications of Performance Optimization Techniques to Aircraft.* AIAA Journal of Aircraft, March-April 1965, pp.153-154.
94. Kowalik, J.,
Osborne, M.R. *Methods for Unconstrained Optimization Problems.* Elsevier, New York, 1968.
95. Hague, D.A.,
Glatt, C.R. *An Introduction to Multivariable Search Techniques for Parameter Optimization (and program AESOP).* NASA CR-703200, April 1968.
96. Schairer, G.S. *The Challenge of Optimizing Synthesis and Systems Engineering.* 1967 Daniel Guggenheim Medal Award Paper, Presented in June 1968 for the American Society of Mechanical Engineers.
97. Hague, D.A.,
Glatt, C.R. *A Guide to the Automated Engineering and Scientific Optimization Program.* Boeing Doc. D2-114271-1, September 1968.

98. Hague, D.A.,
Glatt, C.R. *Application of Multivariable Search Techniques to the Optimal Design of a Hypersonic Cruise Vehicle.* NASA CR-73202, April 1968.
99. Schmitz, F.D. *Takeoff Trajectory Optimization of a Theoretical Model of a STOL Aircraft.* AIAA Paper No.69-935, August 1969.
100. Bryson, A.E., Jr,
et al. *Energy-State Approximation in Performance Optimization of Supersonic Aircraft.* AIAA Journal of Aircraft, Vol.6, No.6, November-December 1969.
101. Silver, B.,
Ashley, H. *Optimization Techniques in Aircraft Configuration Design.* Department of Aeronautics and Astronautics, Stanford University Report, SUDAAR No.406, June 1970.
102. Peckham *A New Method for Minimizing a Sum of Squares without Calculating Gradients.* The Computer Journal, Vol.13, No.4, November 1970, pp.418-420.
103. Fox, R.L. *Unconstrained Minimization Approaches to Constrained Problems.* Chapter 6, AGARD-AG-149-71, Structural Design Applications of Mathematical Programming Techniques, edited by G.C.Pope and L.A.Schmidt, February 1971.
104. Kowalik, J.S. *Feasible Direction Methods.* Chapter 7, AGARD-AG-149-71, Structural Design Applications of Mathematical Programming Techniques, edited by G.C.Pope and L.A.Schmidt, February 1971.
105. Hedrick, J.K.,
Bryson, A.E., Jr *Minimum Time Turns for a Supersonic Airplane at Constant Altitude.* AIAA Journal of Aircraft, Vol.8, No.3, March 1971, pp.182-187.

Computer Graphics

106. Coons, S.A. *An Outline of the Requirements for a Computer Aided Design System.* Proceedings of the Spring Joint Conference, 1963, pp.299-304.
107. Chasen, S.H. *The Introduction of Man-Computer Graphics into the Aerospace Industry.* Proceedings of the Fall Joint Computer Conference, 1965, pp.883-892.
108. Gellert, G.O. *Geometric Computing - Electronic Geometry for Semi-Automated Design.* Part I - The Method and Its Application, Machine Design, 18th March 1965, pp.152-159; Part II - Fields of Application, Machine Design, 1st April 1965, pp.94-100.
109. Johnson, W.L.,
et al. *Analytical Surfaces for Computer Aided Design.* SAE Paper No.660152, January 1966.
110. Chasen, S.H.,
Seitz, R.N. *On-Line Systems and Man-Computer Graphics.* AIAA Astronautics and Aeronautics, April 1967, pp.48-55.
111. Flannagan, D.L. *Surface Molding - New Tool for The Engineer.* AIAA Astronautics and Aeronautics, April 1967, pp.58-62.
112. Bowles, R.Q. *Aircraft Design Augmented by a Man-Computer Graphics System.* AIAA Journal of Aircraft, Vol.5, No.5, September-October 1968, pp.486-497.
113. Boehm, B.W.,
et al *Developing Interactive Graphic Systems for Aerospace Applications.* AIAA Paper No. 69-954, September 1969.
114. Naraharg, R.M. *Computer Aided Design.* Space/Aeronautics, December 1969, pp.56-64.
115. Hitch, H.P.Y. *The Application of Modern Computer Techniques to Aeronautical Design Problems.* The Seventh Congress of the International Council of the Aeronautical Sciences, ICAS Paper No.70-27, September 1970.

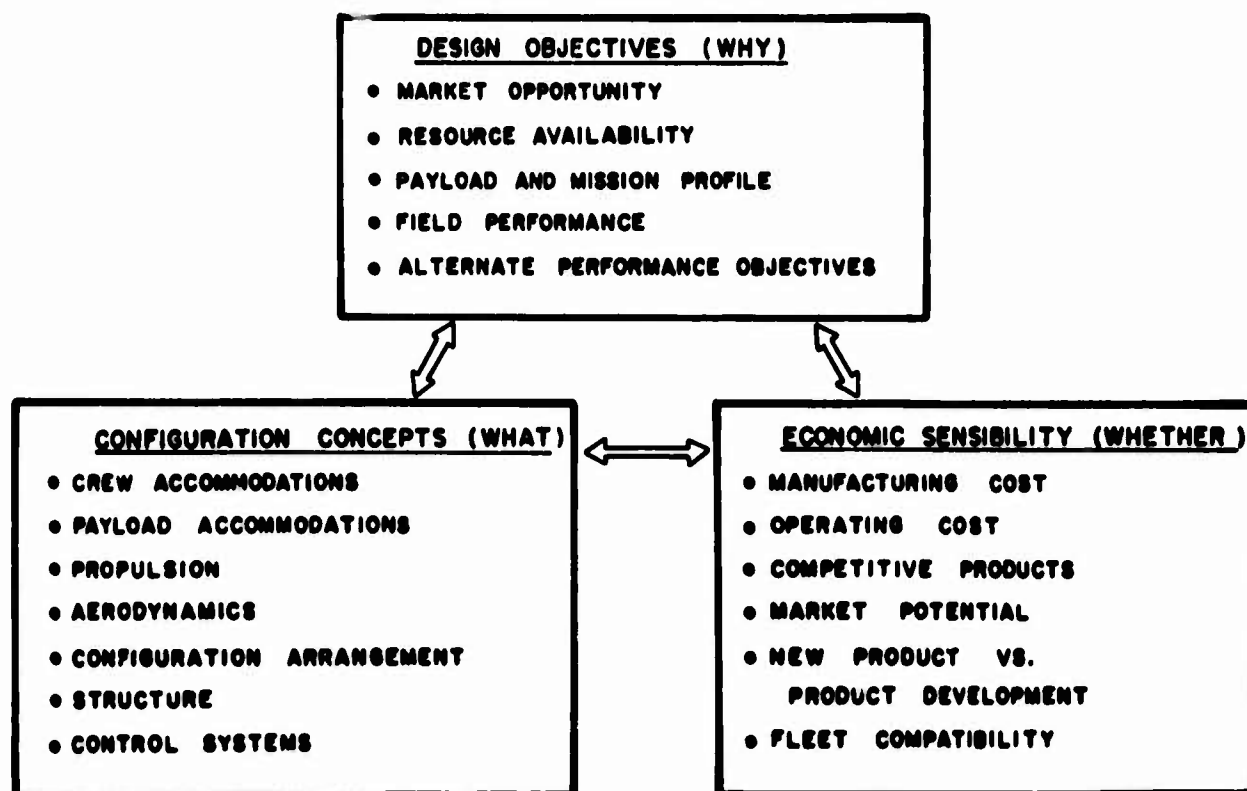


Fig.1 Vital aspects

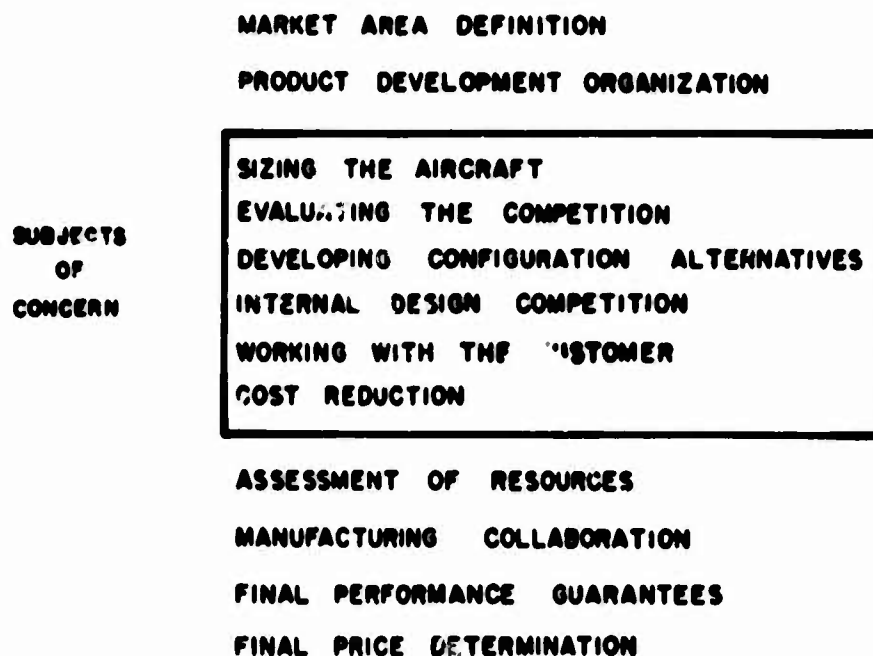


Fig.2 Steps in airplane evolution

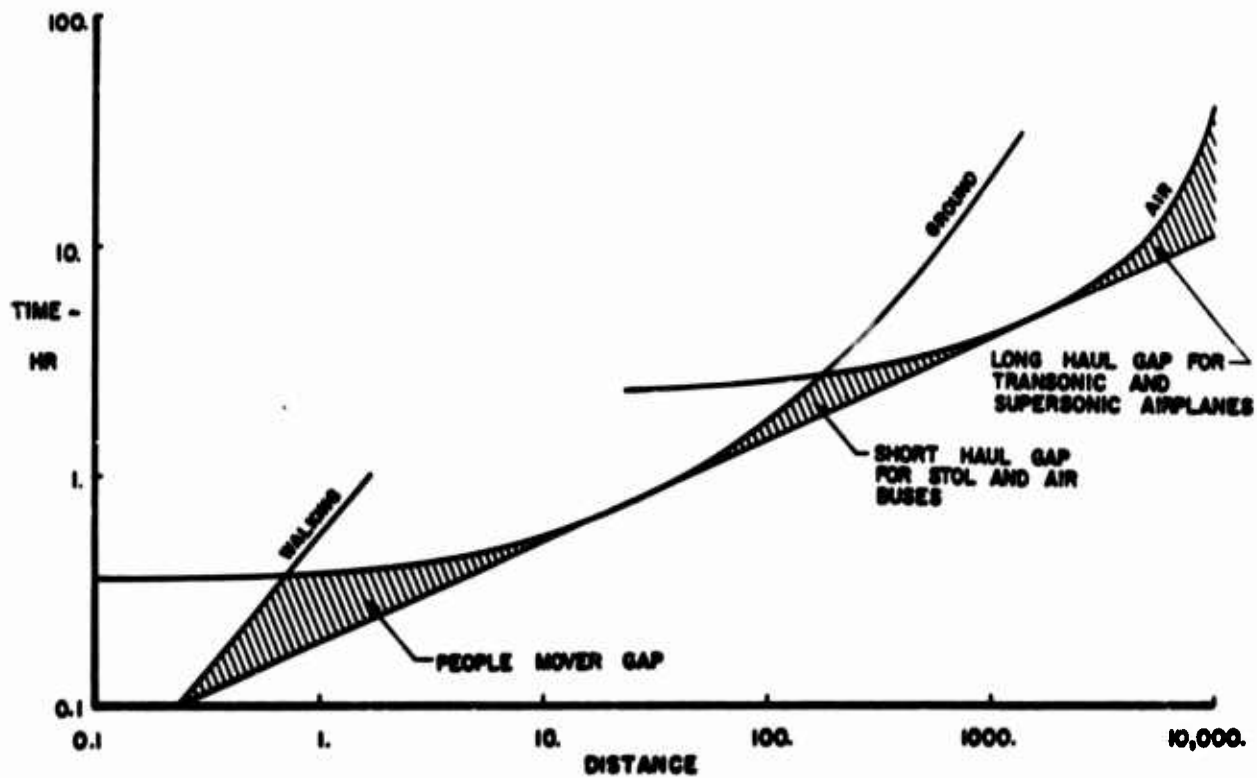
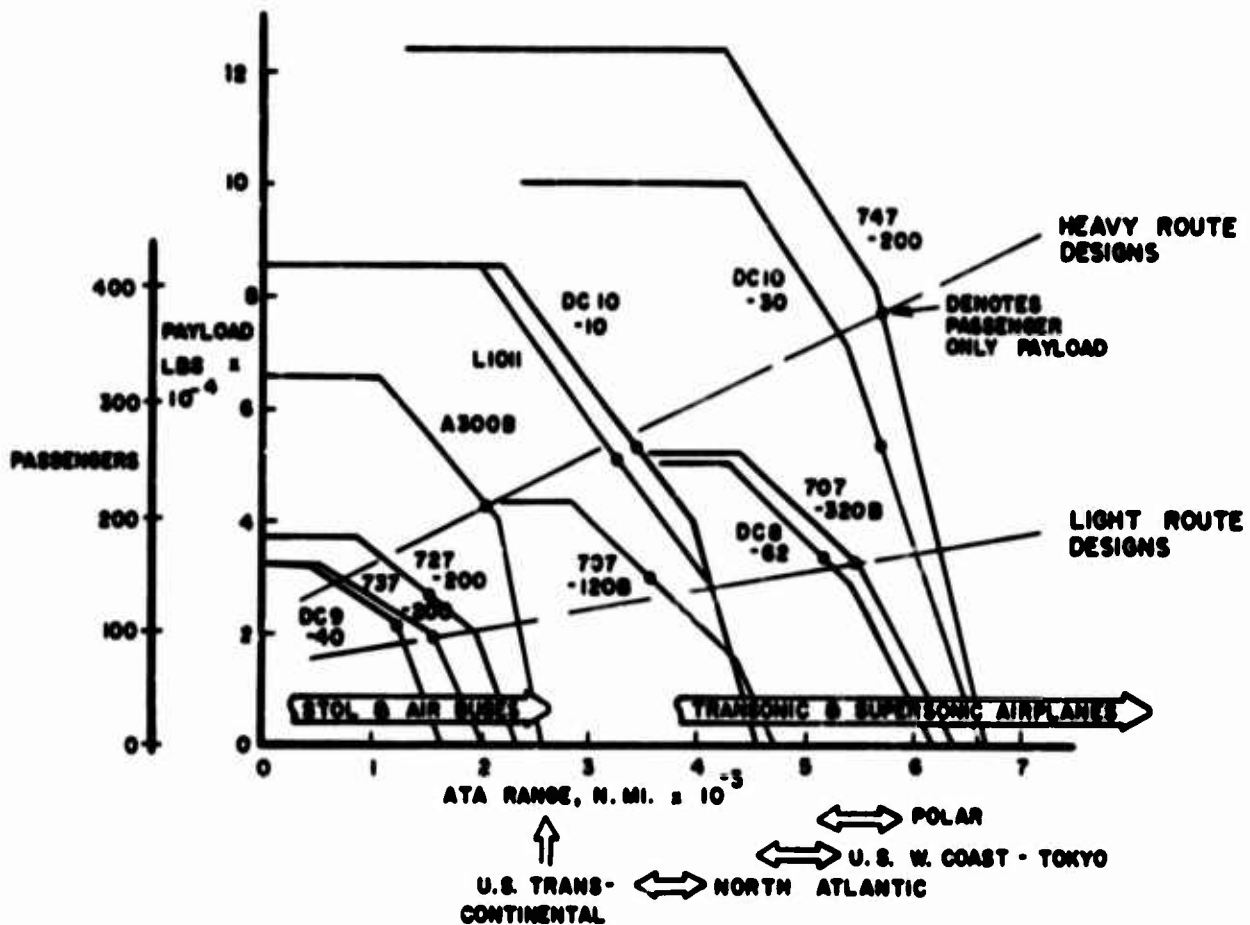


Fig. 3 Current transportation gaps



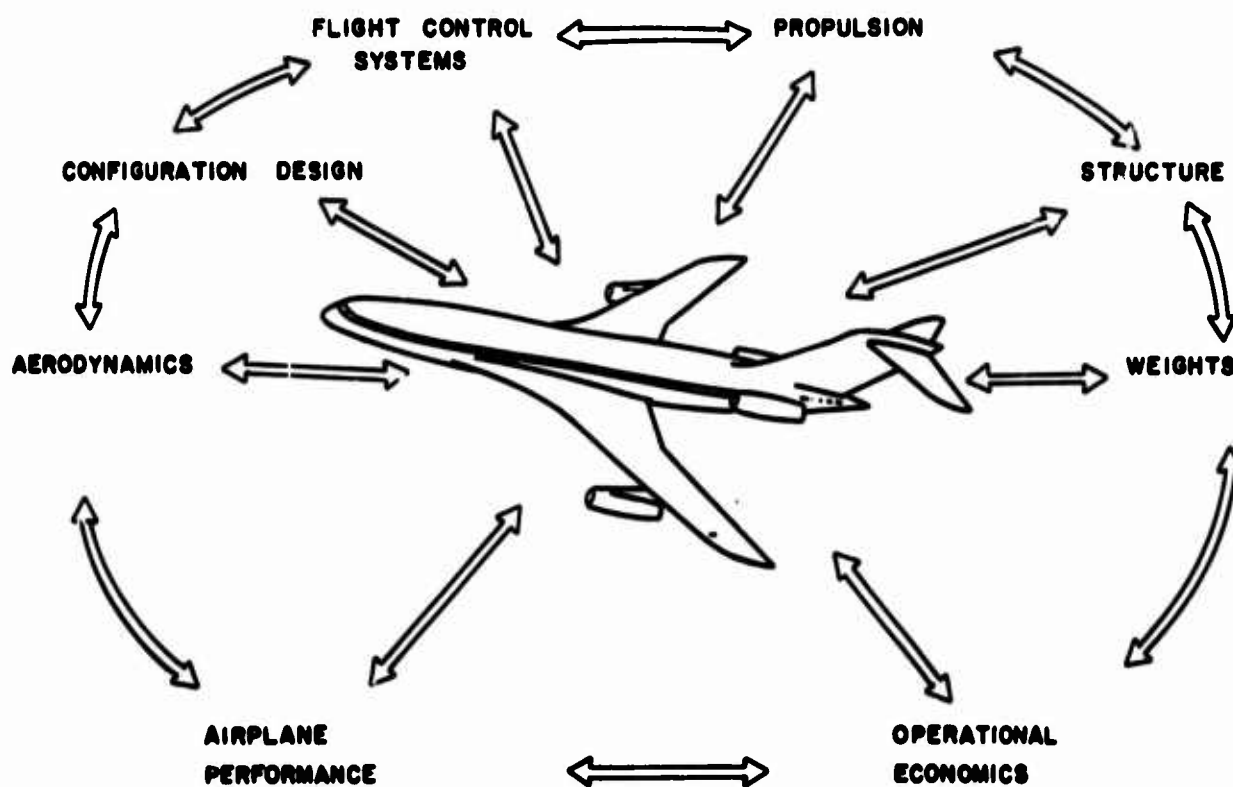


Fig.5 Elements of synthesis

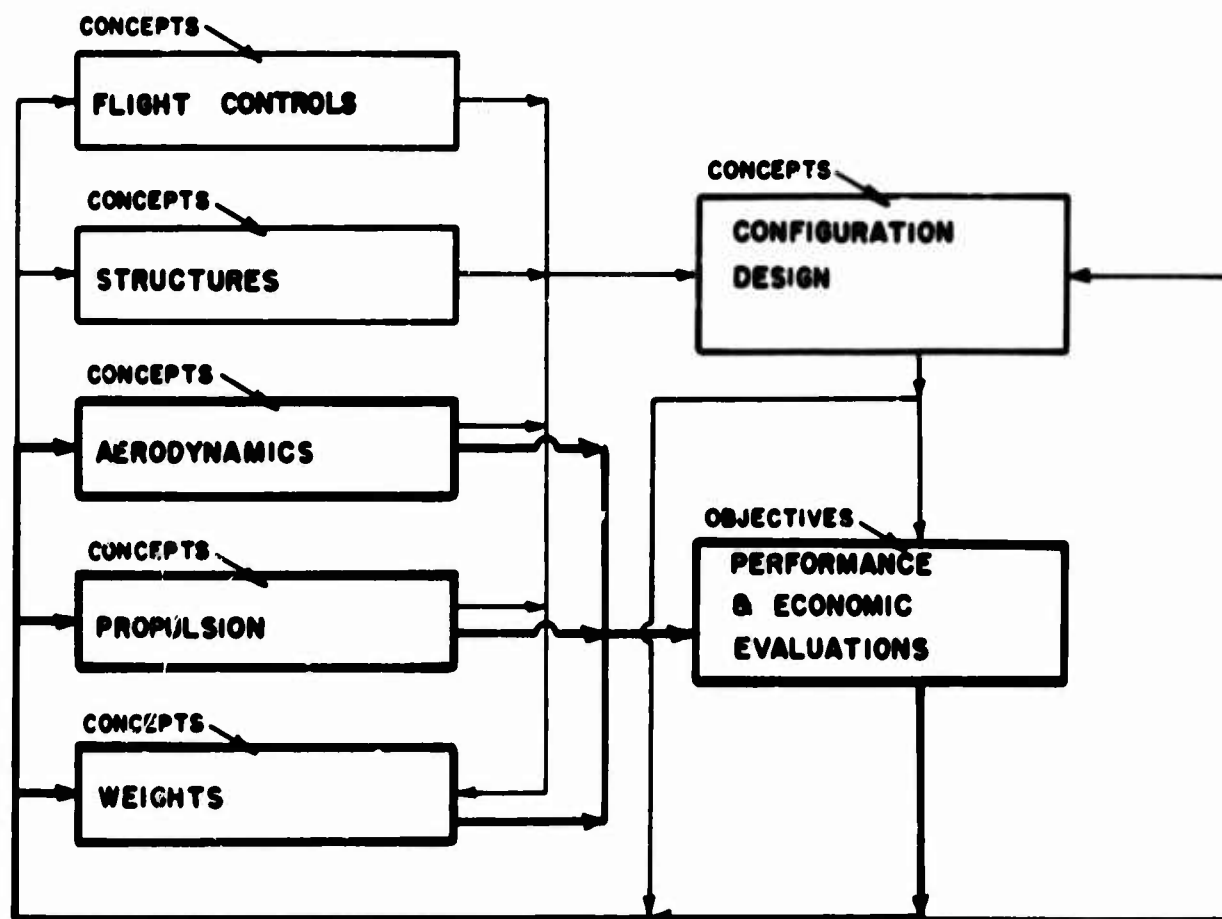


Fig.6 Principal lines of data flow for airplane design

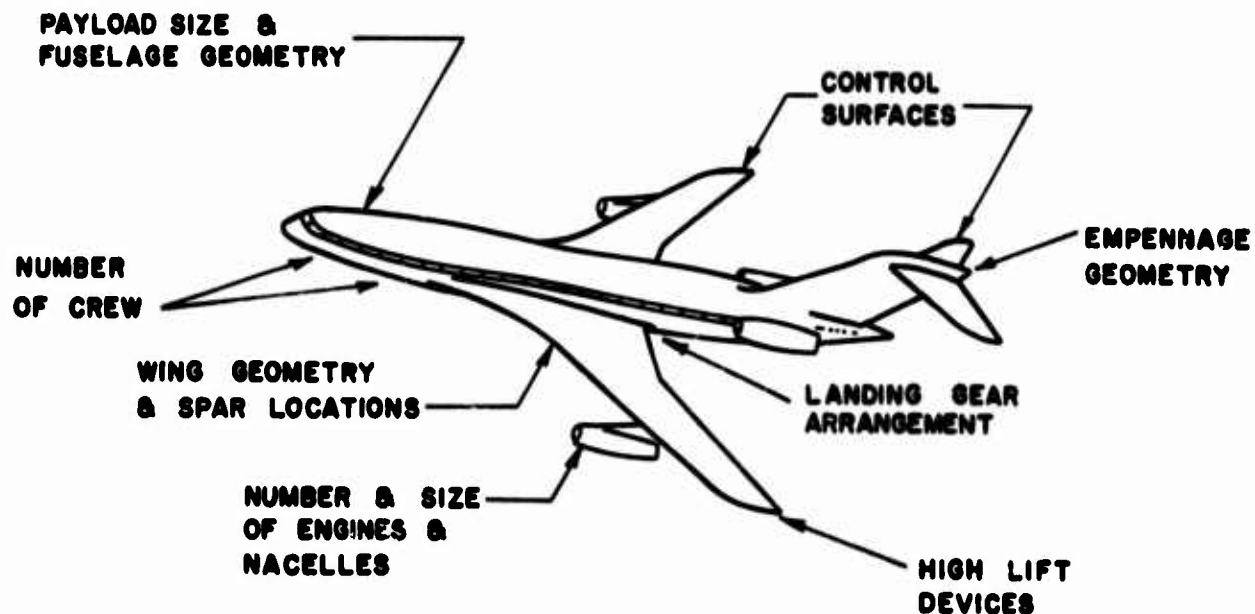


Fig.7 Configuration definition

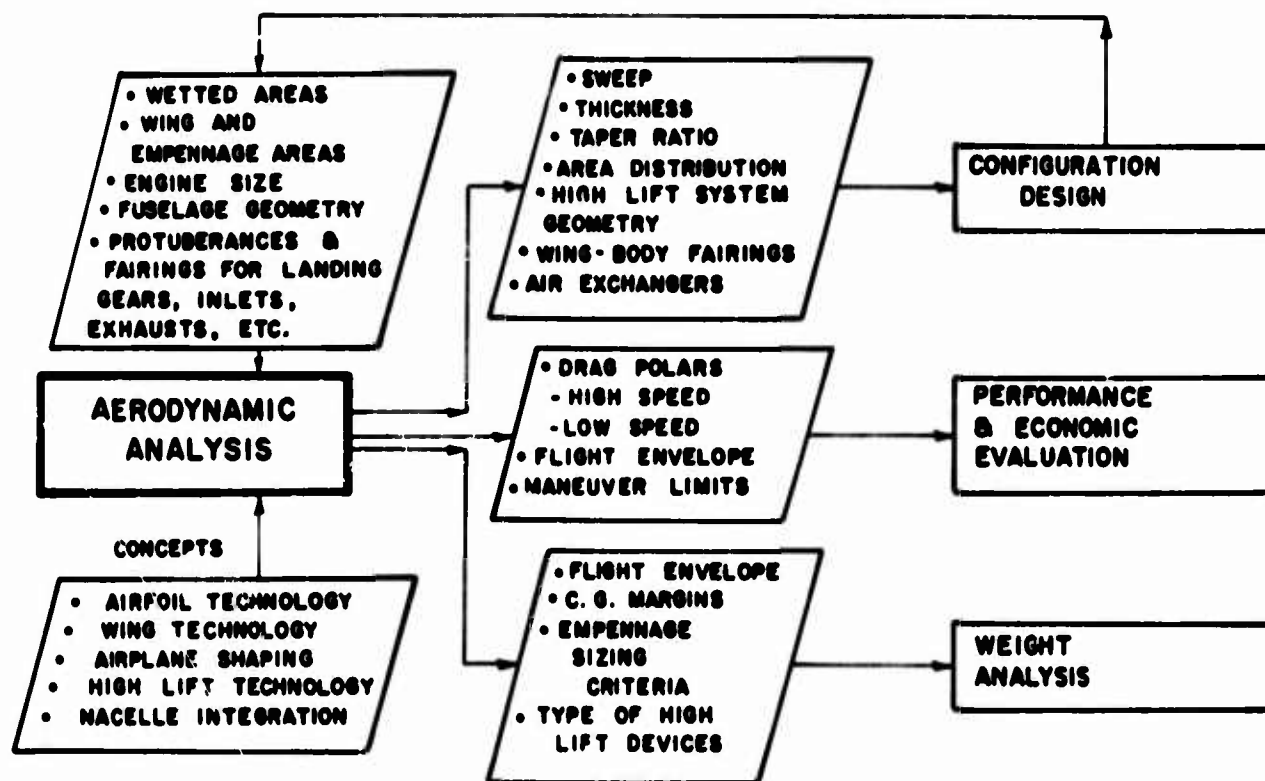


Fig.8 Aerodynamic data flow

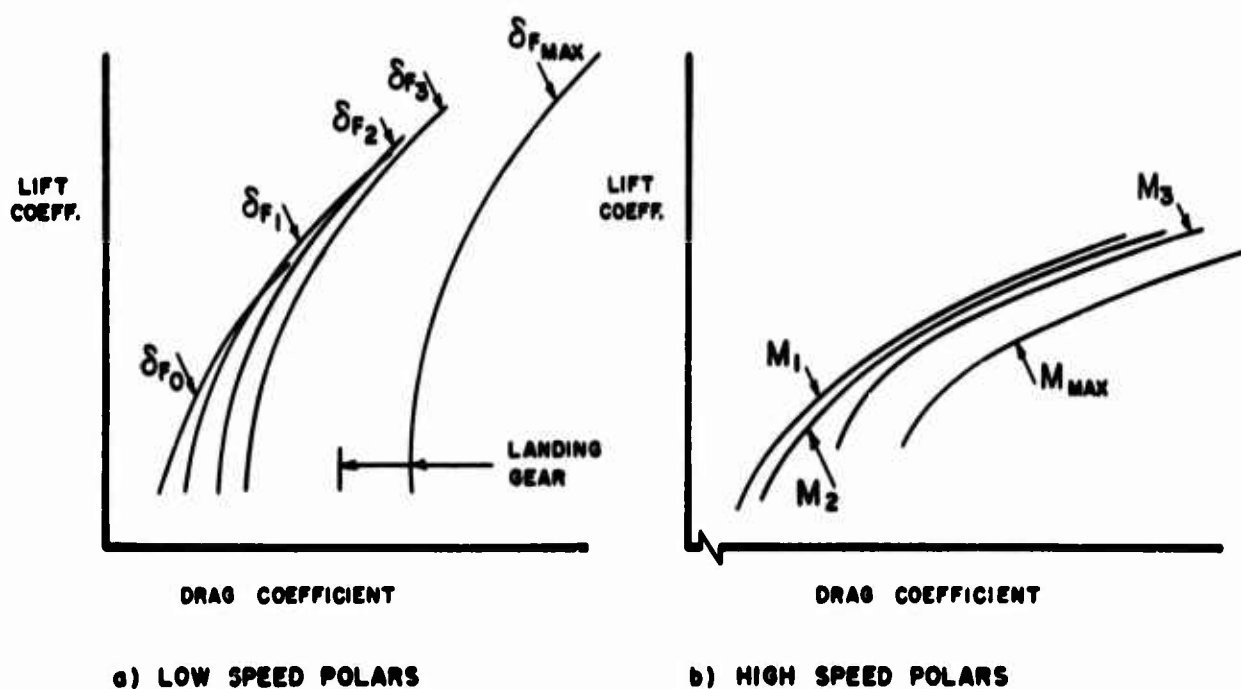


Fig.9 Aerodynamic input data

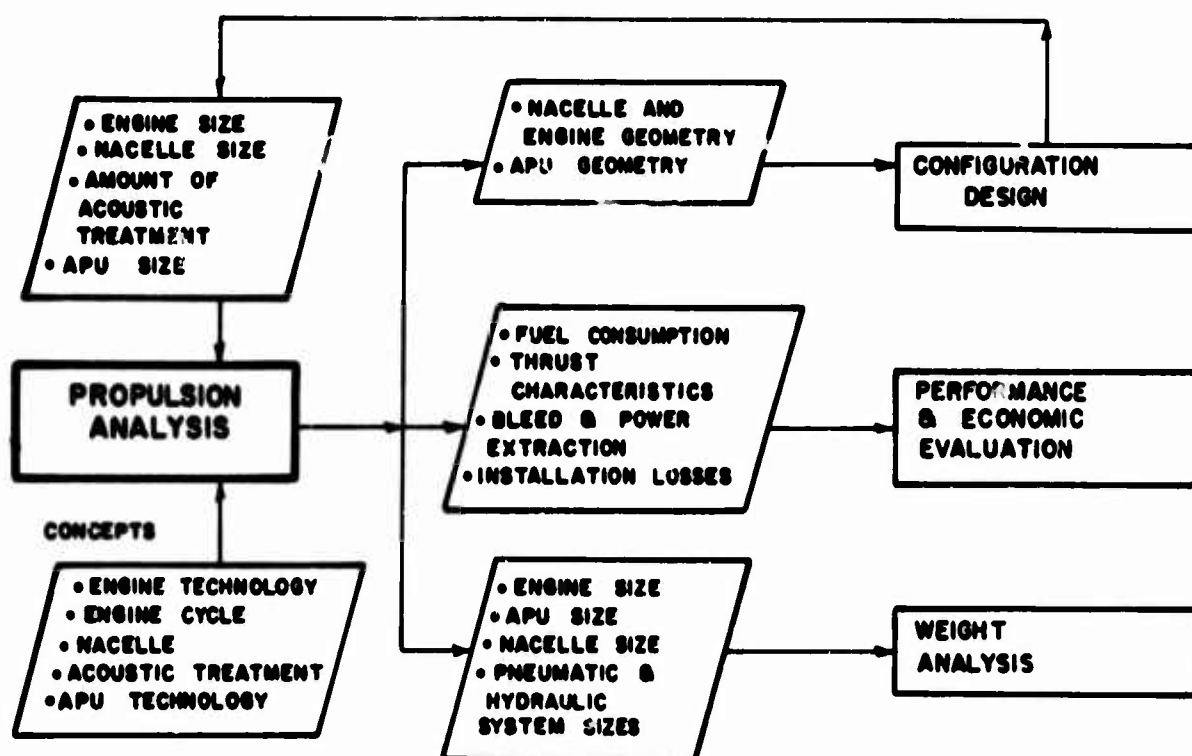


Fig.10 Propulsion data flow

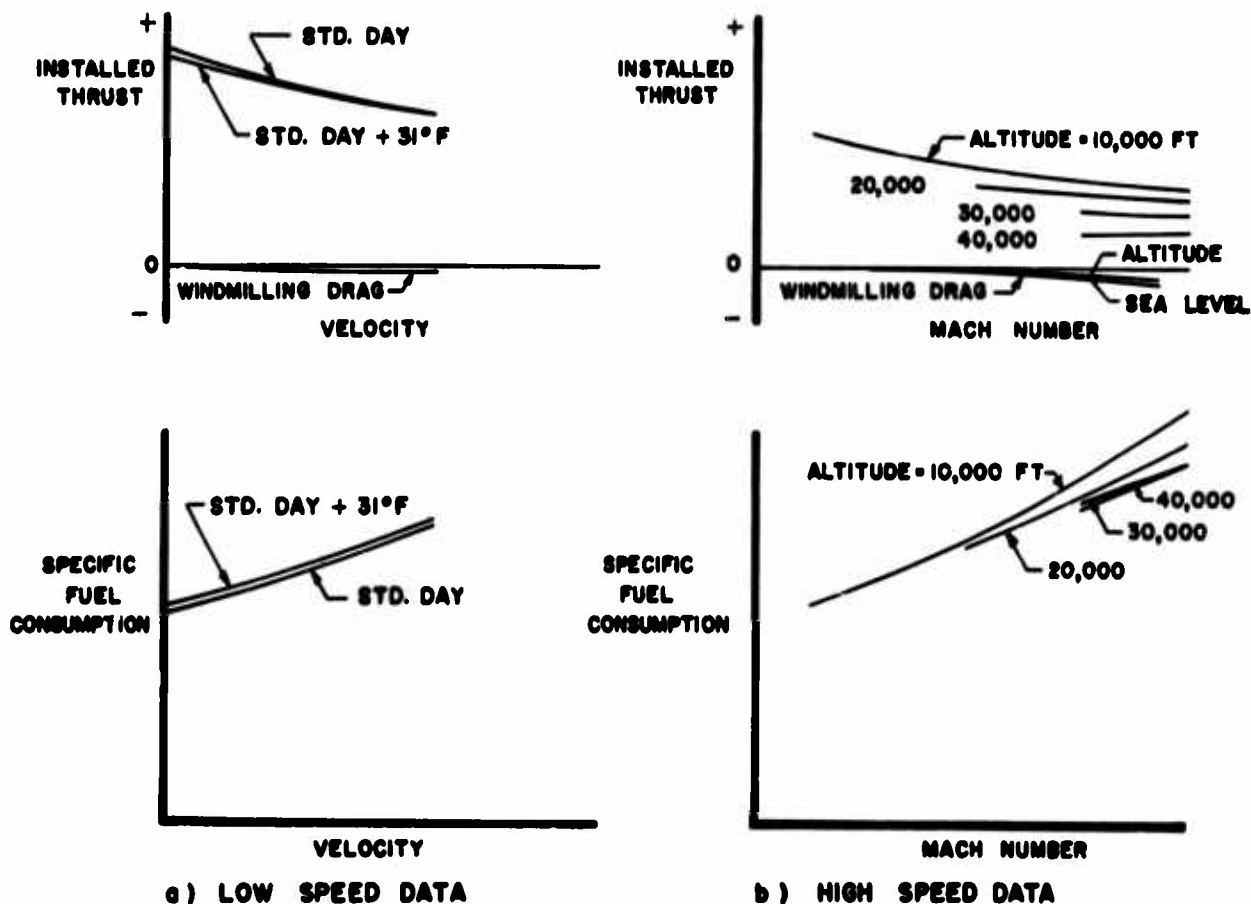


Fig.11 Propulsion input data

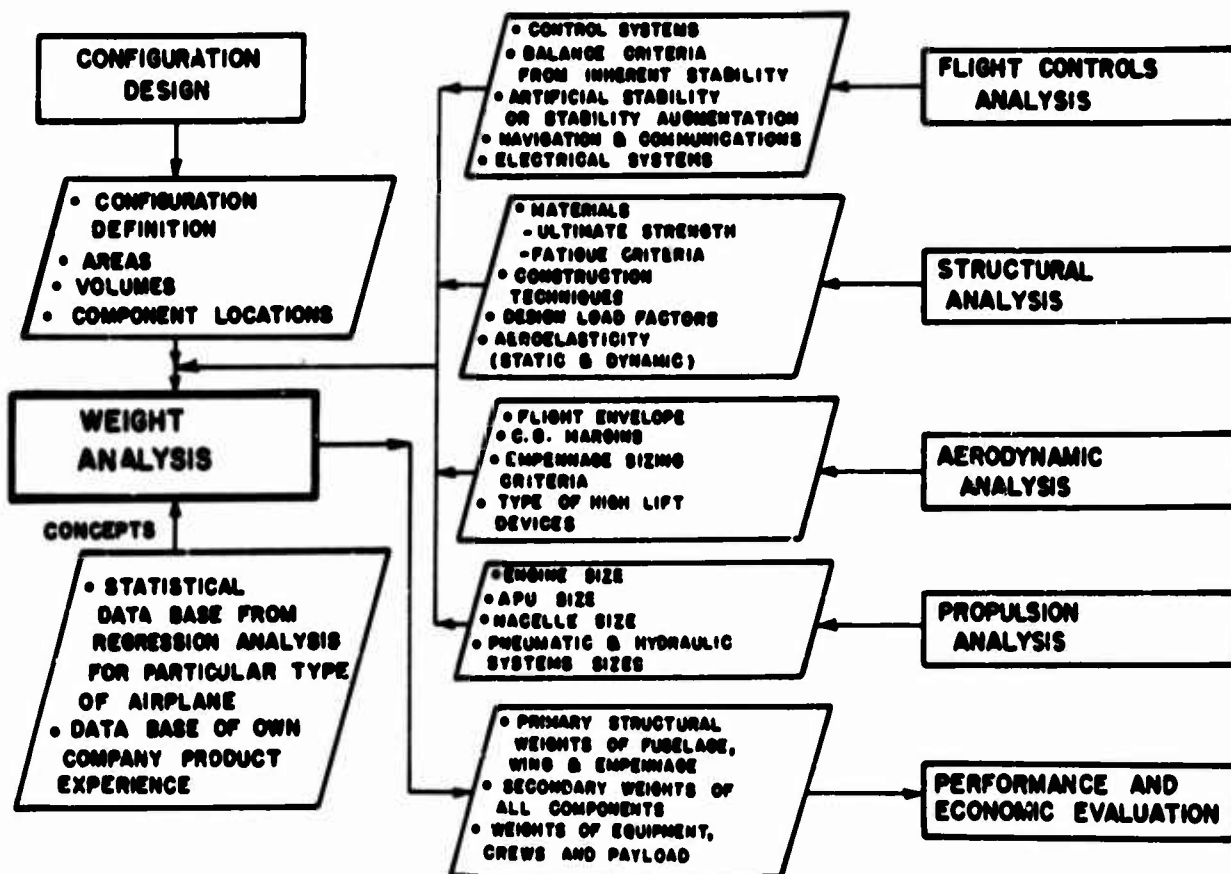


Fig.12 Weight data flow

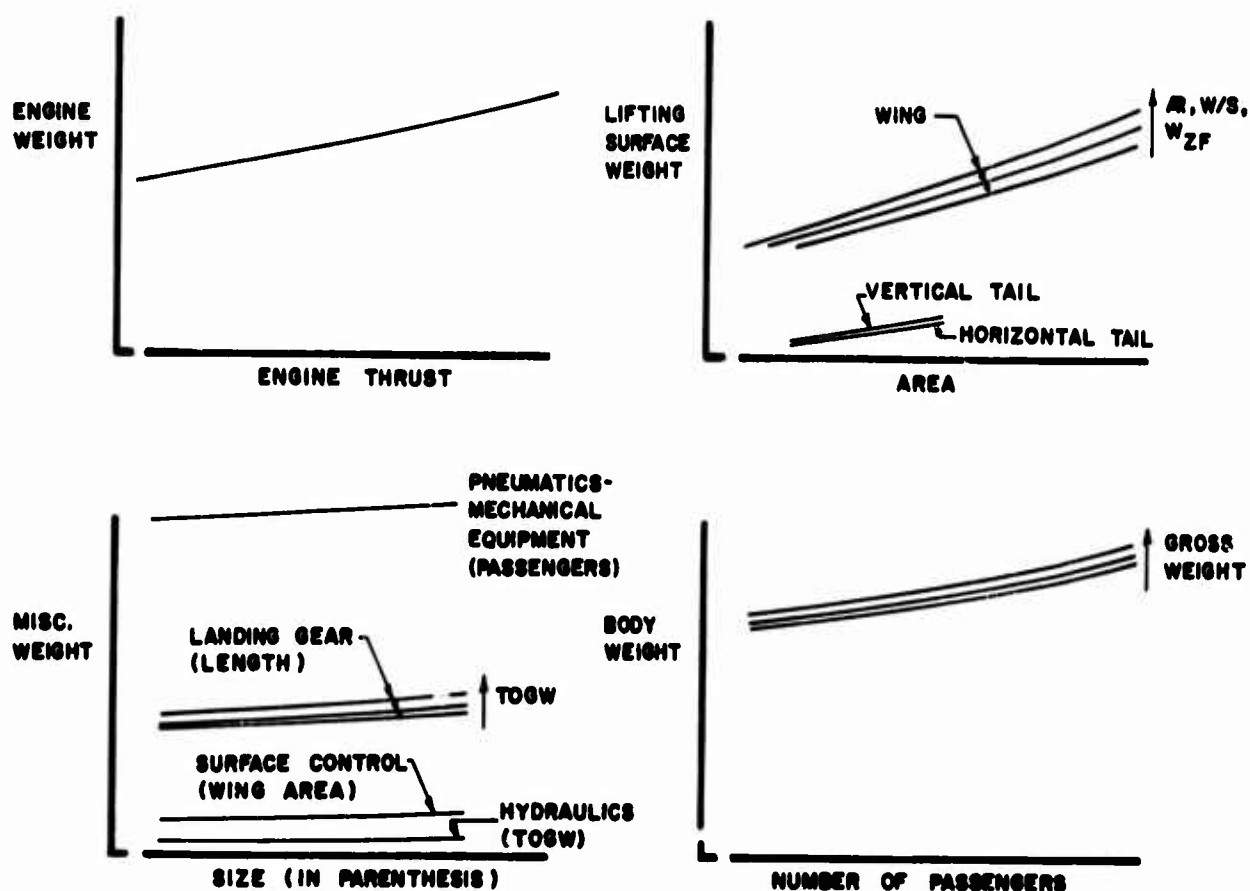


Fig.13 Weight input data

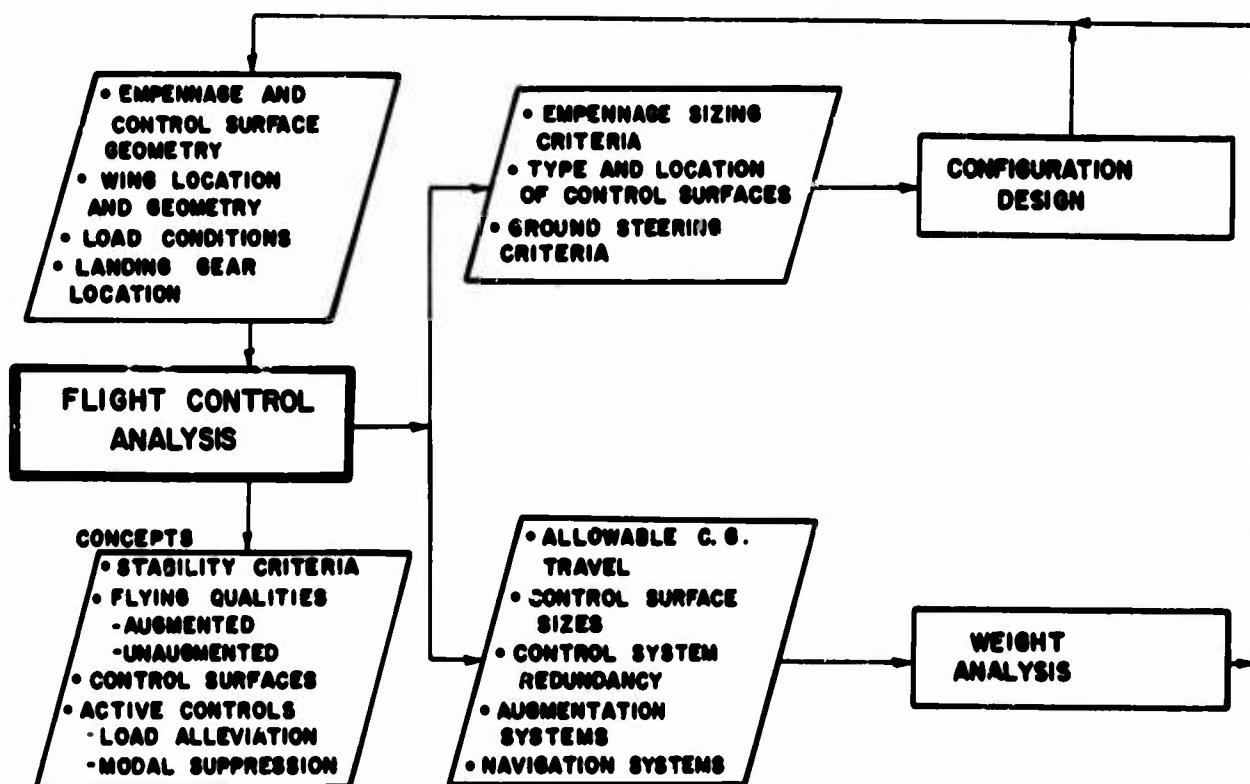


Fig.14 Flight control systems data flow

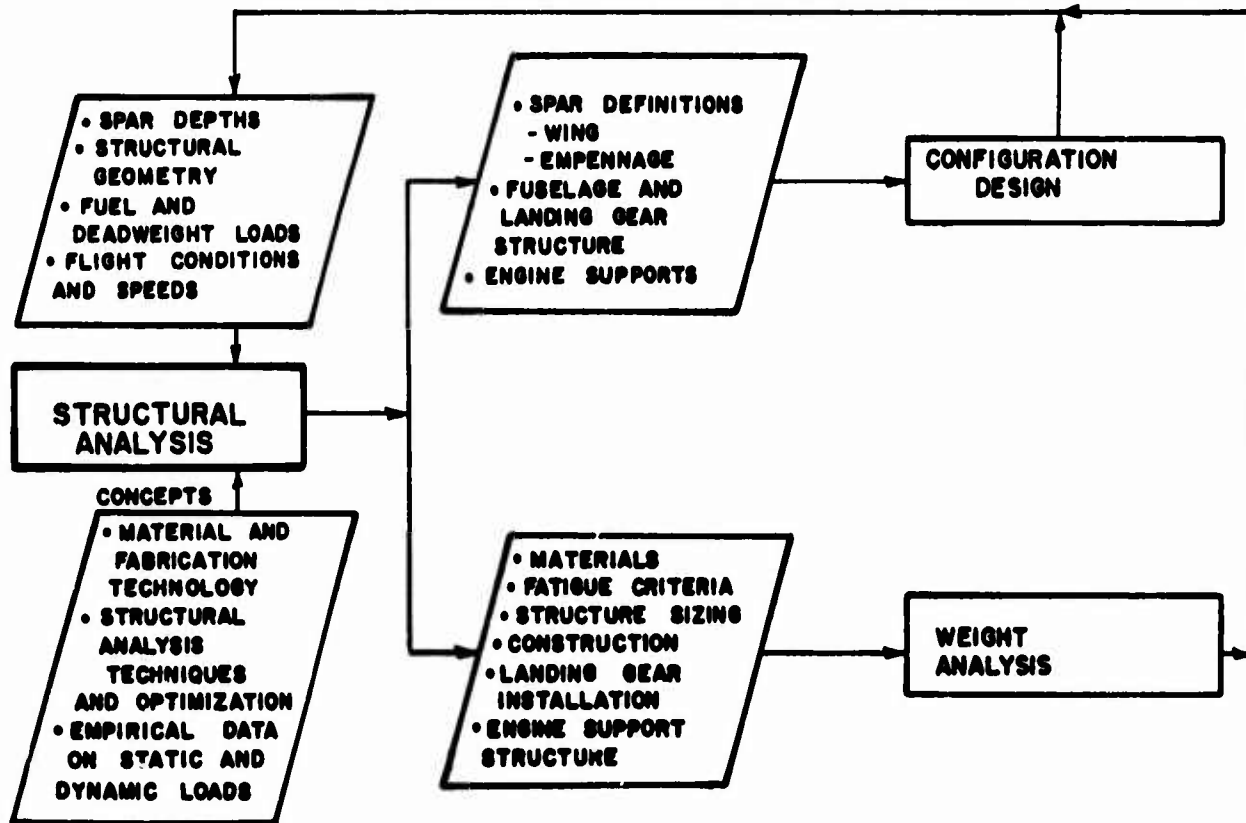


Fig.15 Structures data flow

TAKEOFF

MAXIMUM TAKEOFF
GROSS WEIGHT
SEA LEVEL, 77°F

SIDELINE

NOISE STATIONS
(.25 N. MI. FOR 3 ENGINE
CONFIGURATION &
.35 N. MI. FOR 4 ENGINE
CONFIGURATION)

$V \geq V_2 + 10 \text{ KTS}$ AT CUTBACK
(V_2 IS LEVEL FLIGHT SPEED
WITH SINGLE ENGINE
FAILURE)

NORMAL TAKEOFF

NOISE STATION
3.5 N. MI. FROM
BRAKE RELEASE

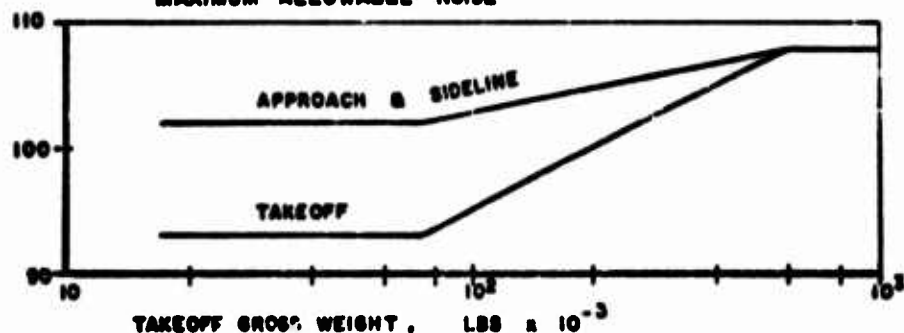
REFUSED TAKEOFF FOR
BALANCED FIELD LENGTH

SCHEDULED DISTANCE
(1.15 TIMES ACTUAL DISTANCE)

AIR DISTANCE TO CLEAR 35 FT
 $V_2 \geq 1.2 V_S$ (OR $1.1 V_{MC}$)

GROUND DISTANCE
 $V_R \geq 1.05 V_{MC}$
 $V_{LO} \geq 1.10 V_{MU}$

NOISE LIMIT
RPMdB

MAXIMUM ALLOWABLE NOISE**LANDING**

MAXIMUM LANDING WEIGHT
SEA LEVEL, MAXIMUM FLAPS

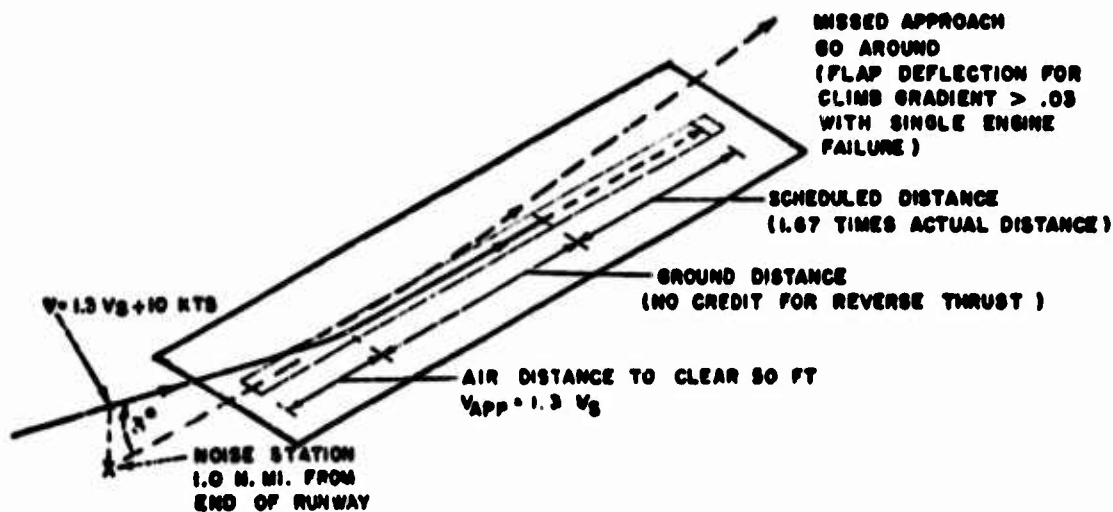


Fig.16 Field performance profiles

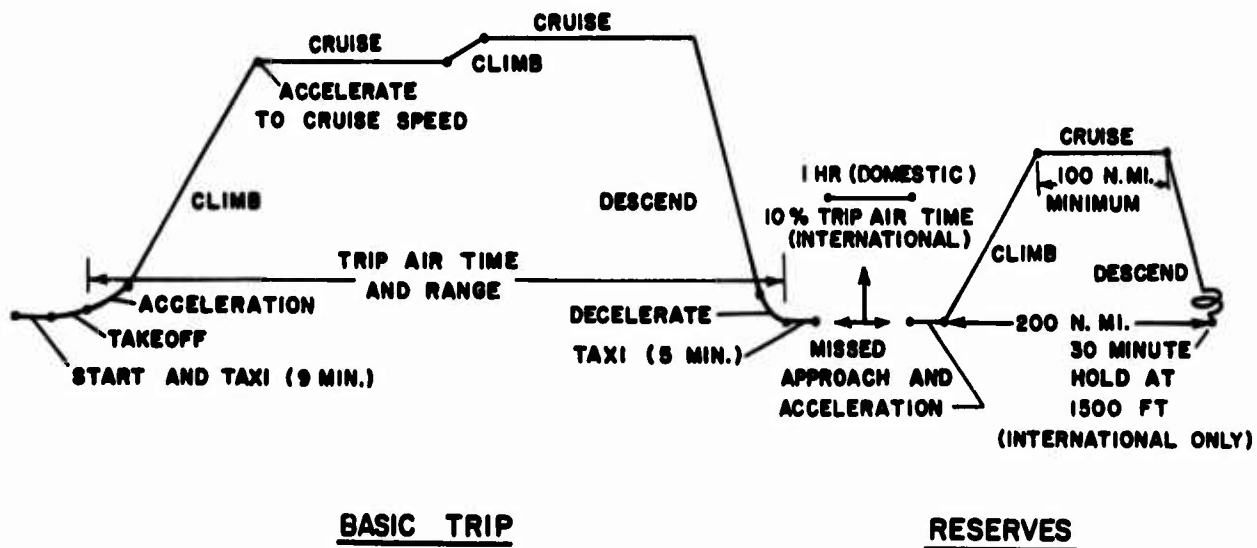


Fig.17 ATA standard mission profile

LIFT & DRAG	WING	PROFILE	→	←	COMPONENT AND CONFIGURATION DATA FROM WIND-TUNNEL OR FLIGHT TESTS
		INDUCED	→	←	
		COMPRESSIBILITY	→	←	
		HIGH LIFT	→	←	
	BODY	PROFILE	→	←	
		COMPRESSIBILITY	→	←	
	EMPENNAGE	PROFILE	→	←	
		INDUCED	→	←	
		COMPRESSIBILITY	→	←	
	NACELLES	PROFILE	→	←	
		COMPRESSIBILITY	→	←	
	REGRESSION	PARAMETRIC	ANALYTICAL	EXPERIMENTAL	

Fig.18 Aerodynamic information depths

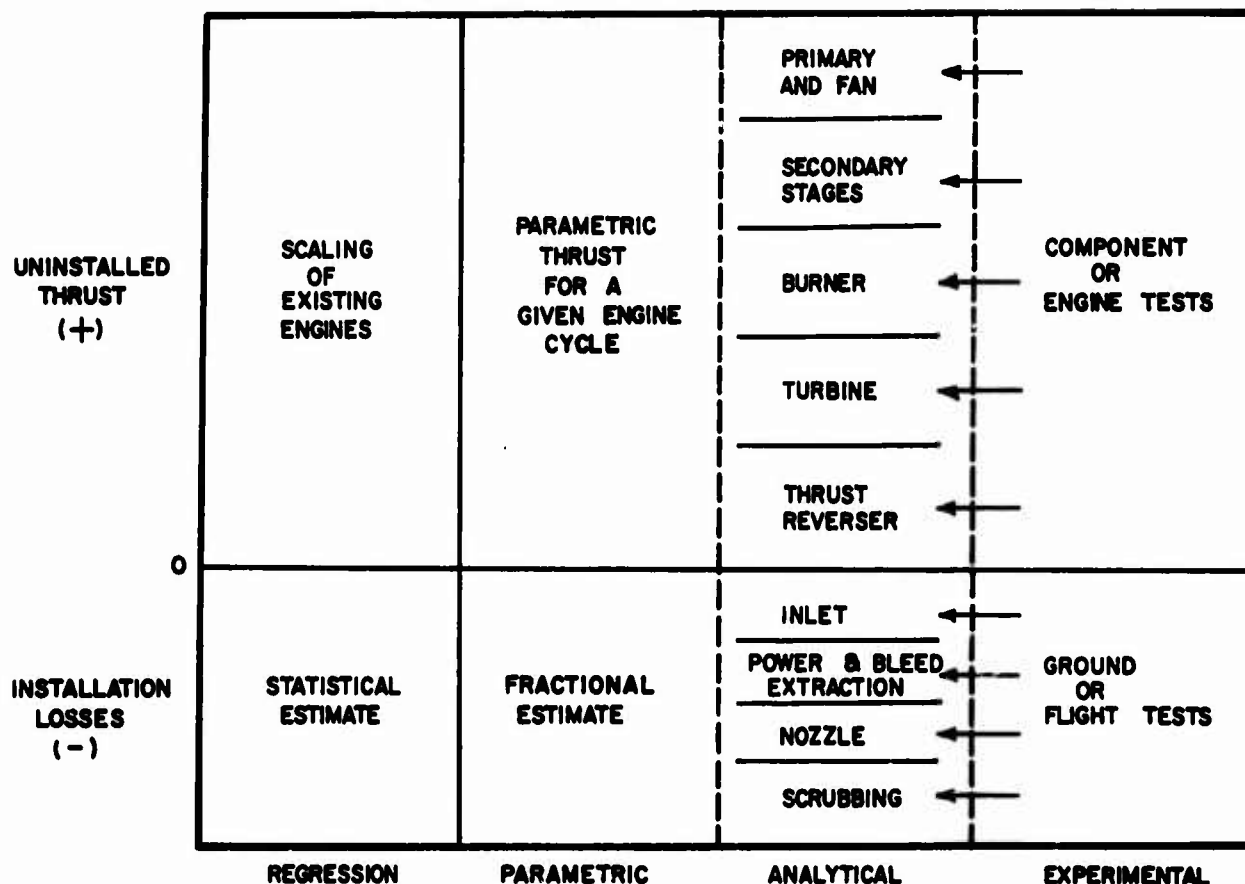


Fig.19 Propulsion information depths

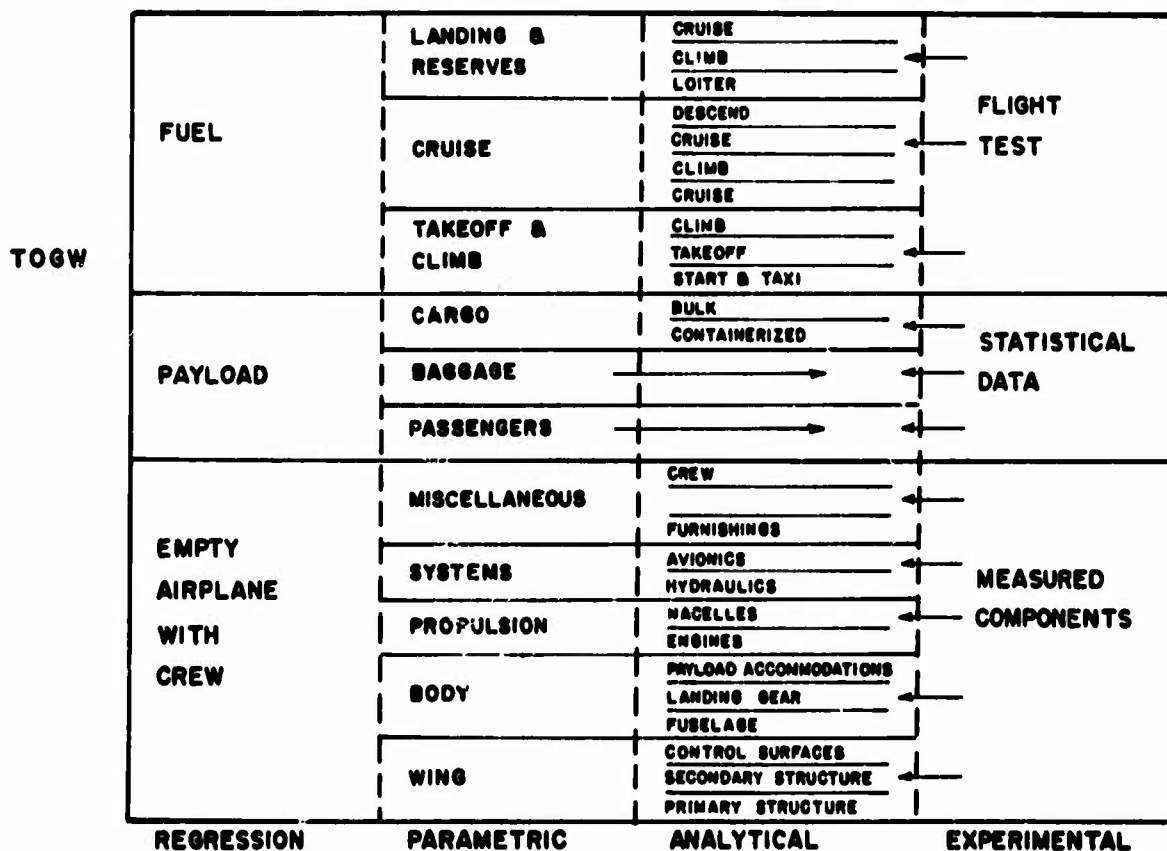
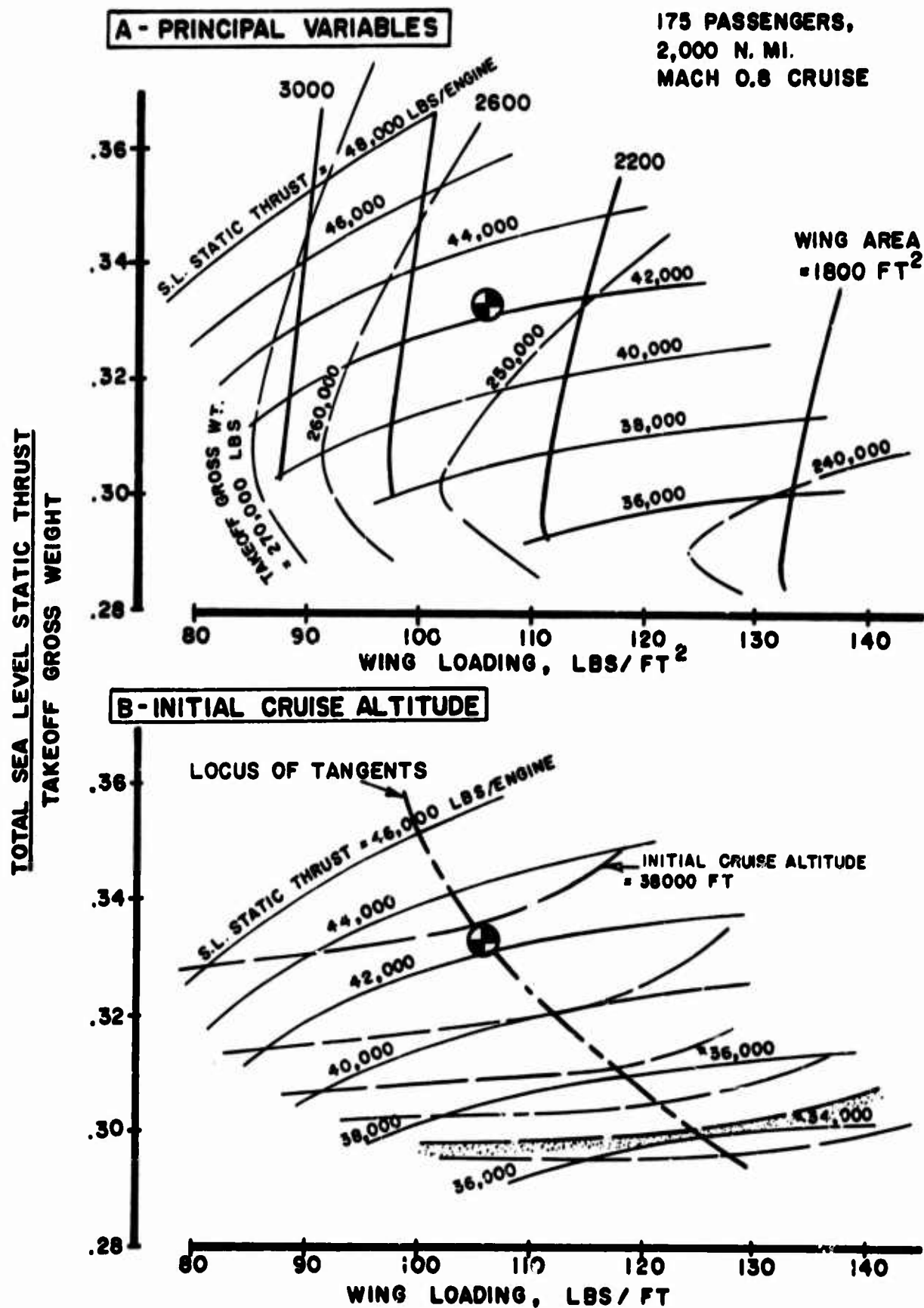


Fig.20 Weight information depths



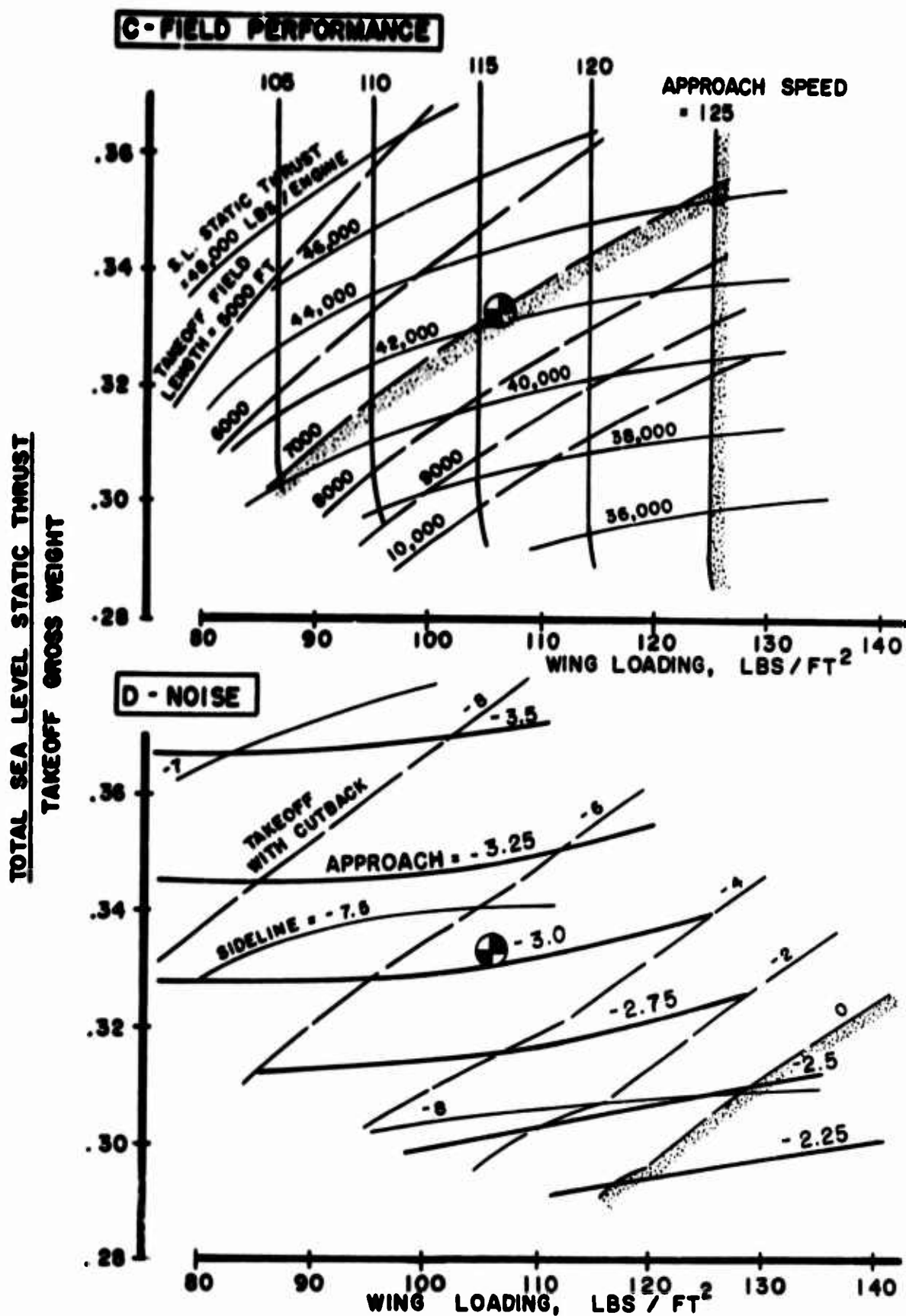
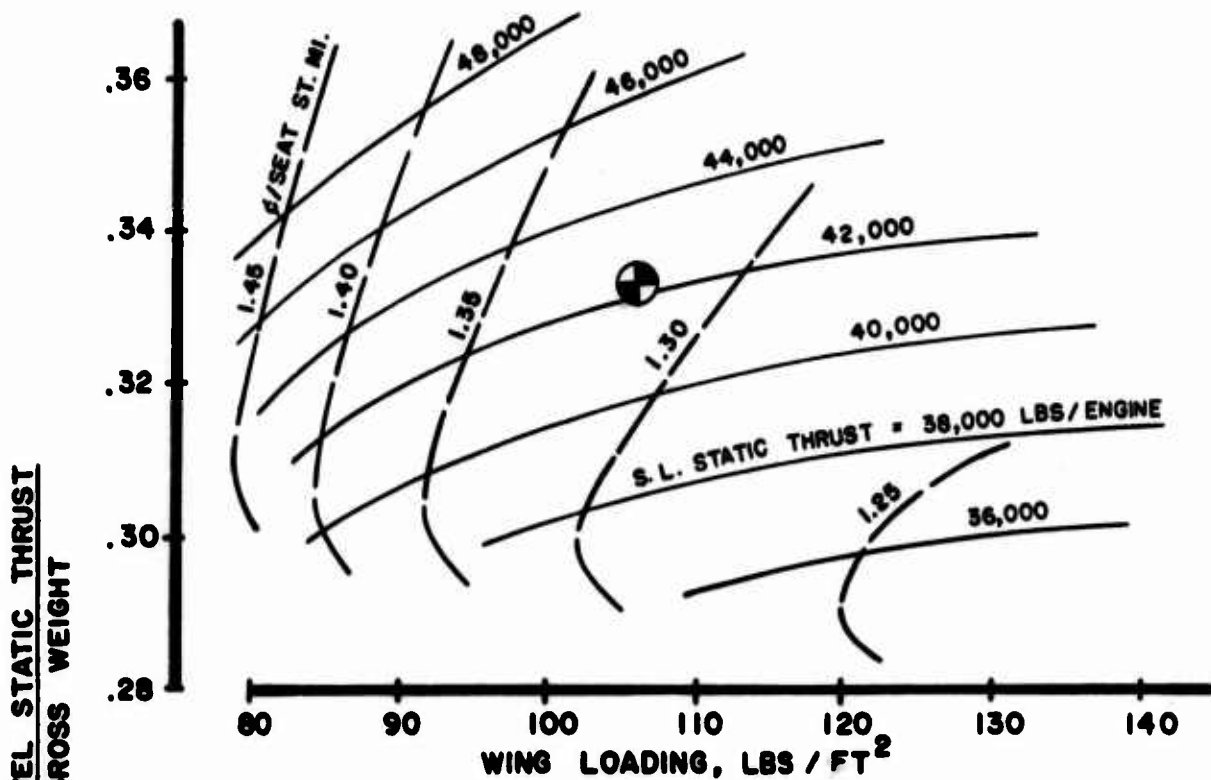


Fig.21 Fixed-payload parametric study (continued)

E - DIRECT OPERATING COSTS



F - DESIGN POINT SELECTION

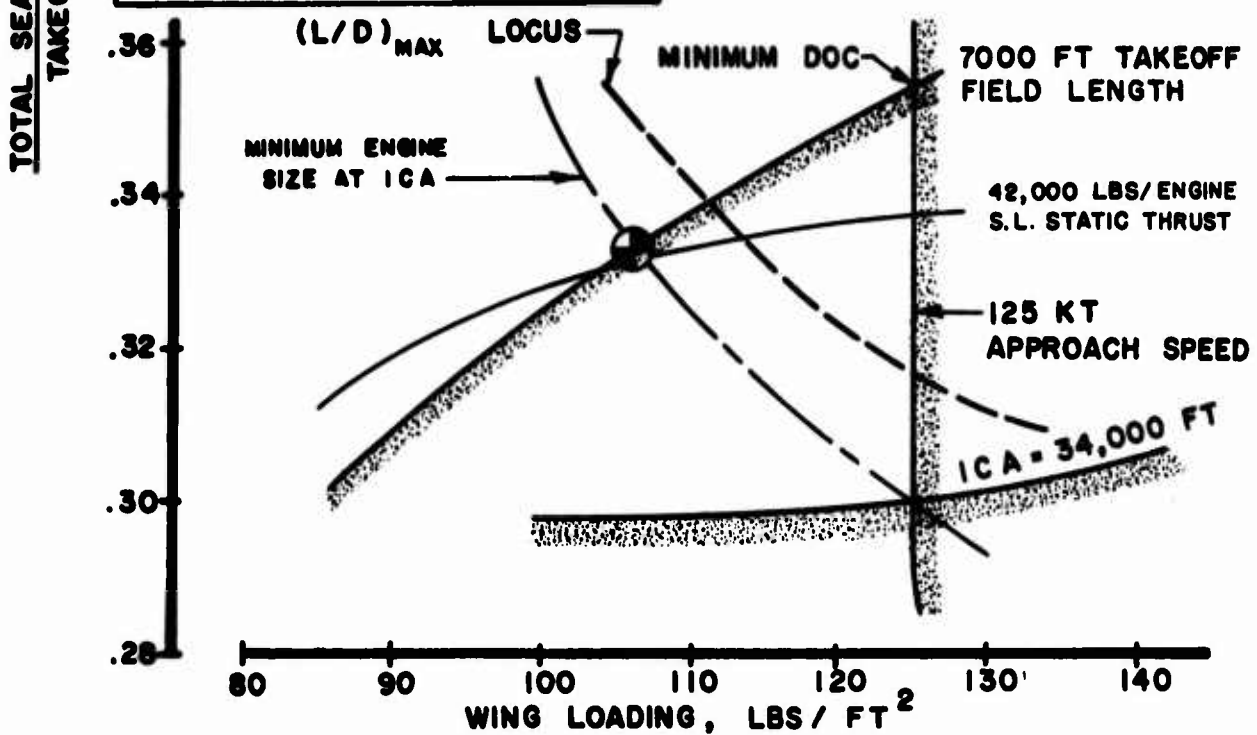


Fig.21 Fixed-payload parametric study (concluded)

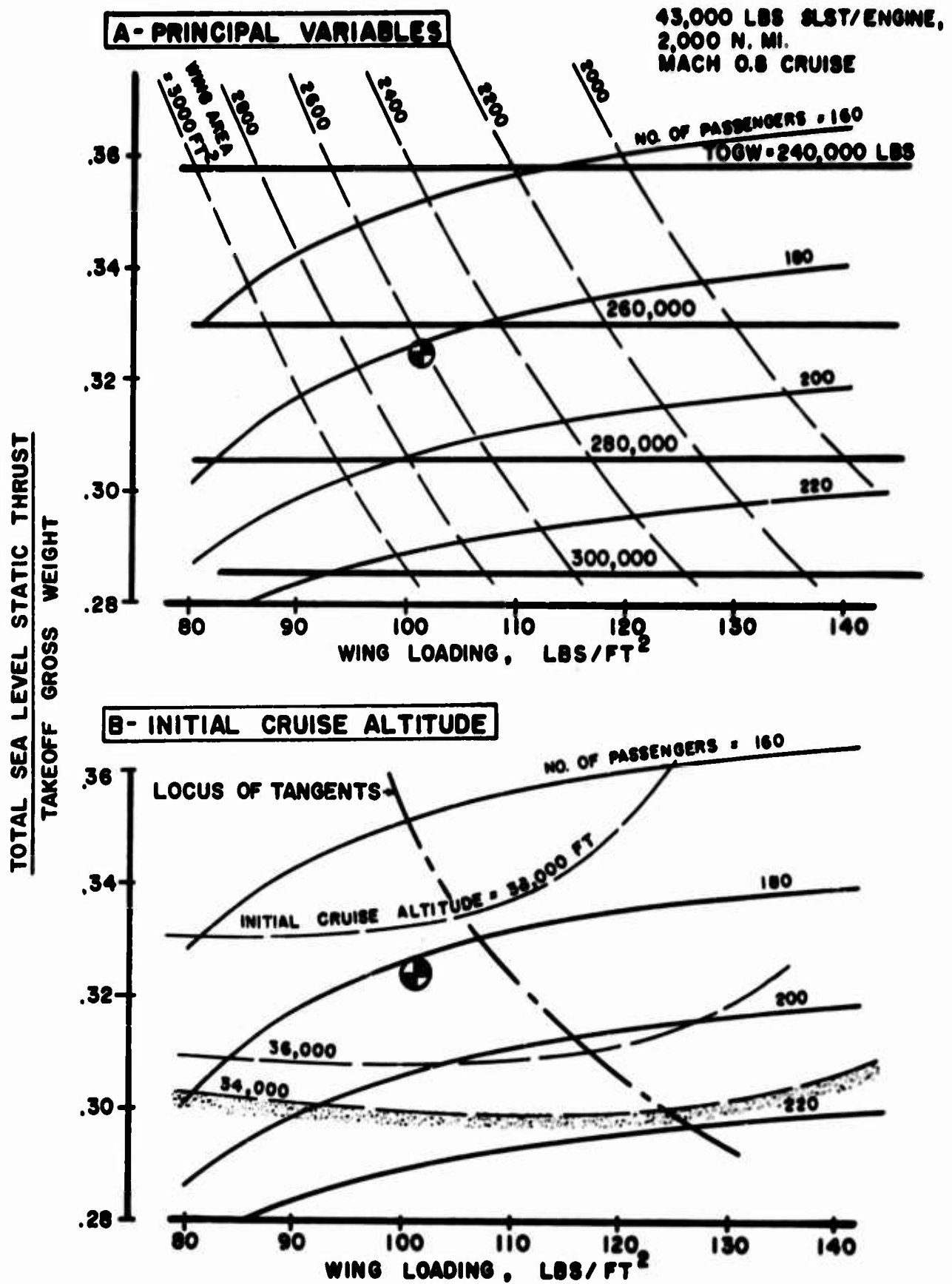


Fig.22 Fixed-engine parametric study

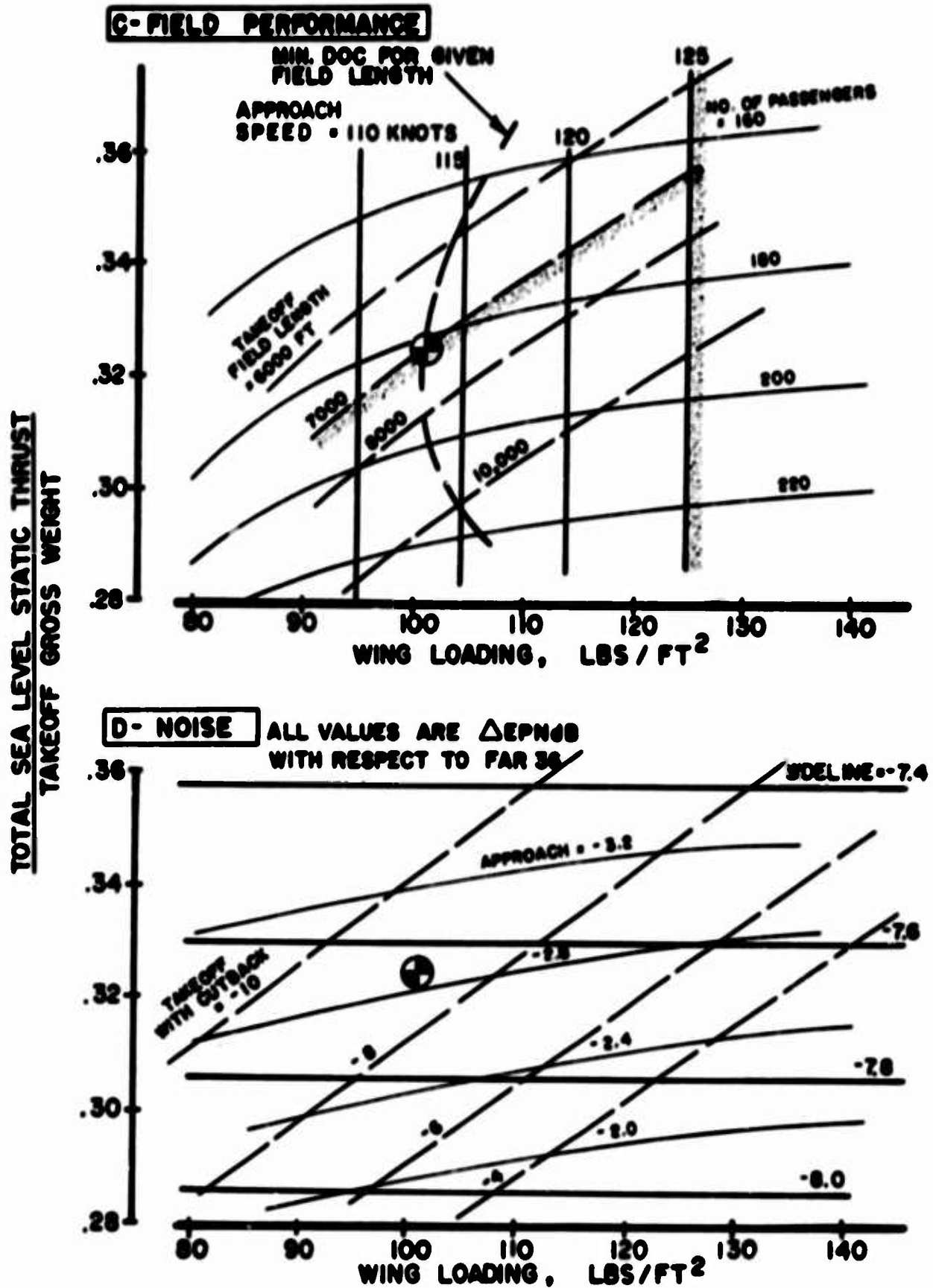


Fig.22 Fixed-engine parametric study (continued)

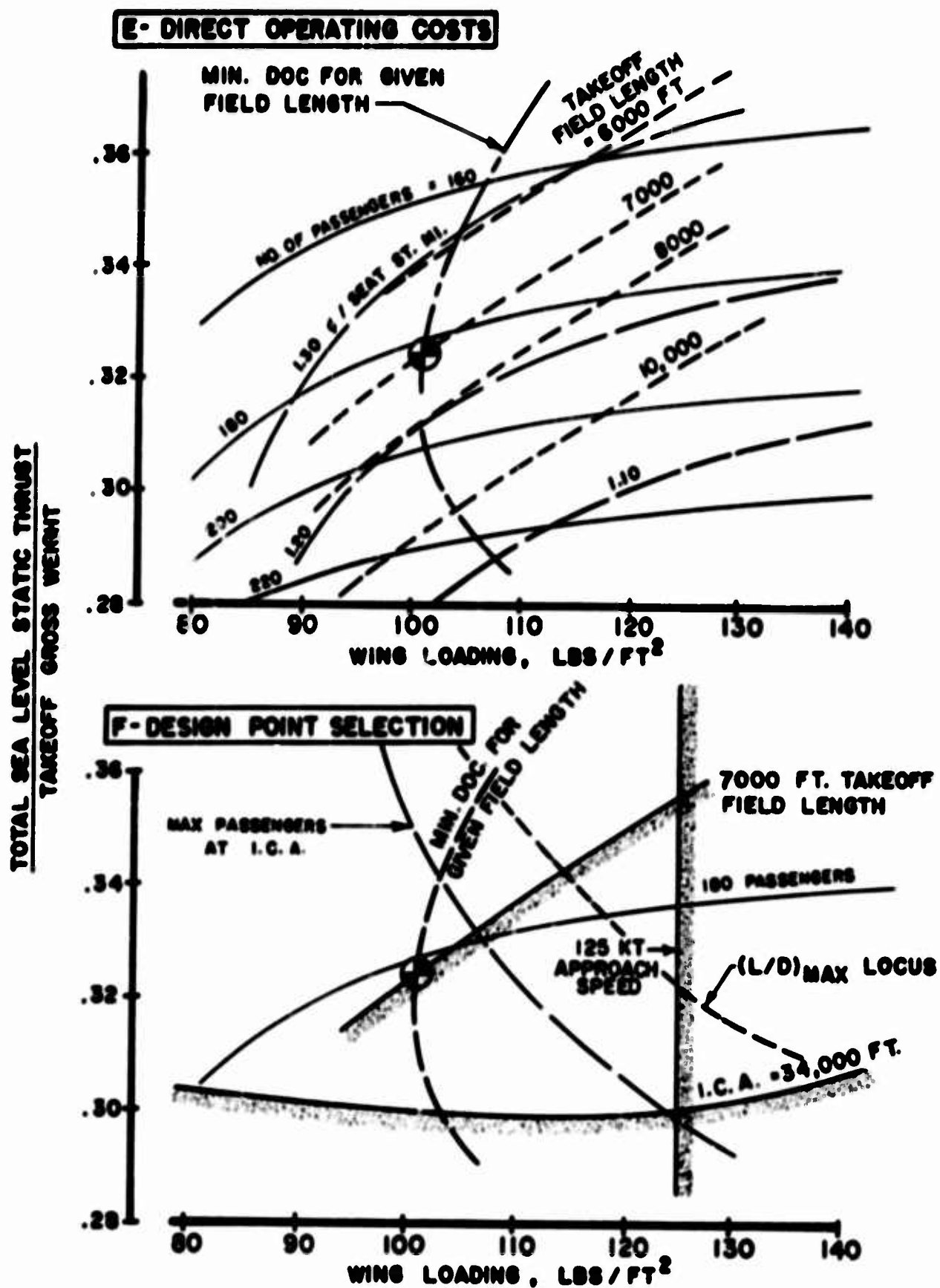


Fig.22 Fixed-engine parametric study (concluded)

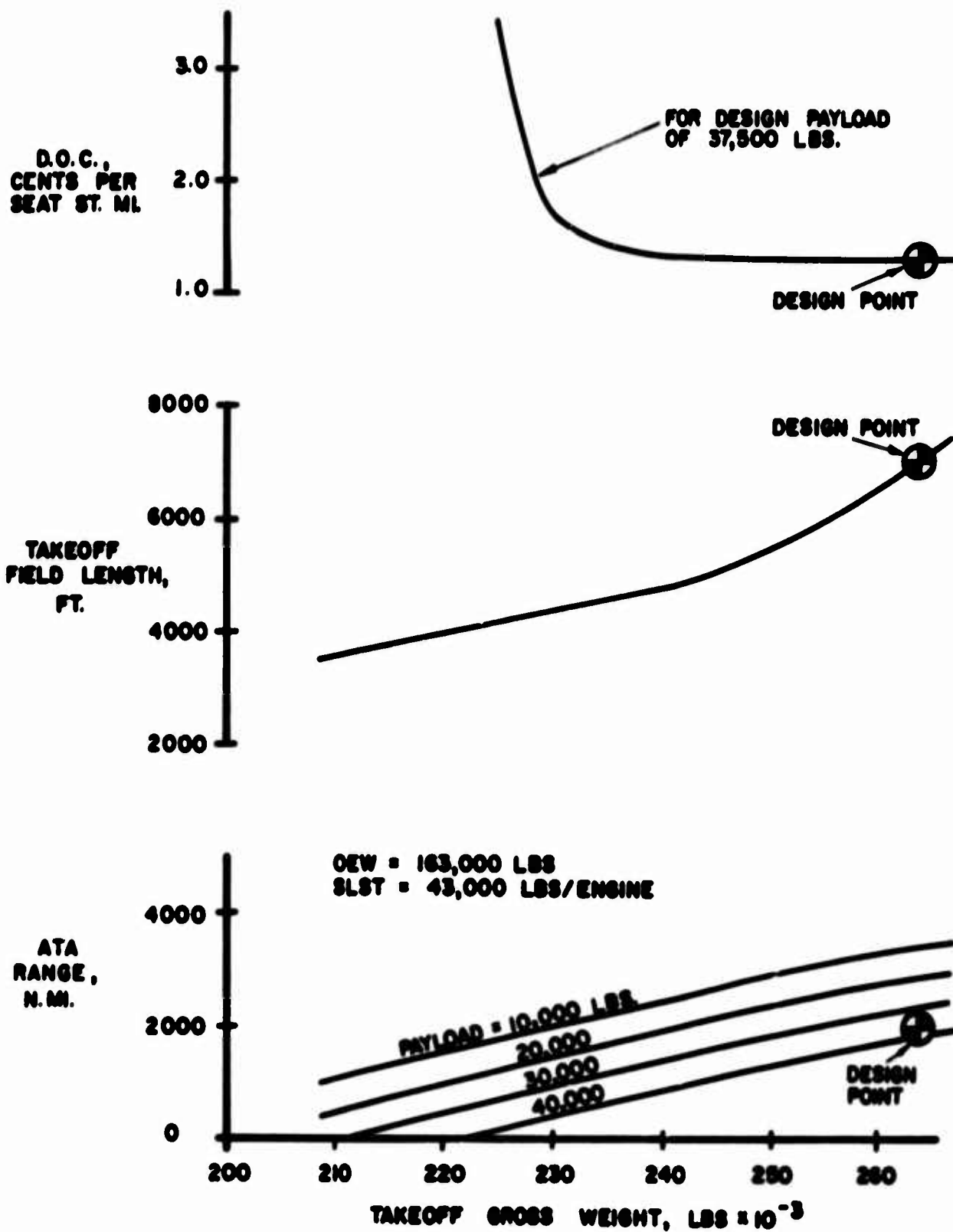


Fig.23 Off-design performance for twin-jet airplane

CRUISE MACH = 0.83
 INITIAL CRUISE ALTITUDE = 32,800 FT.
 MAX. TAXI WEIGHT = 328,000 LBS.
 TAKEOFF FIELD LENGTH
 = 10,350 FT.

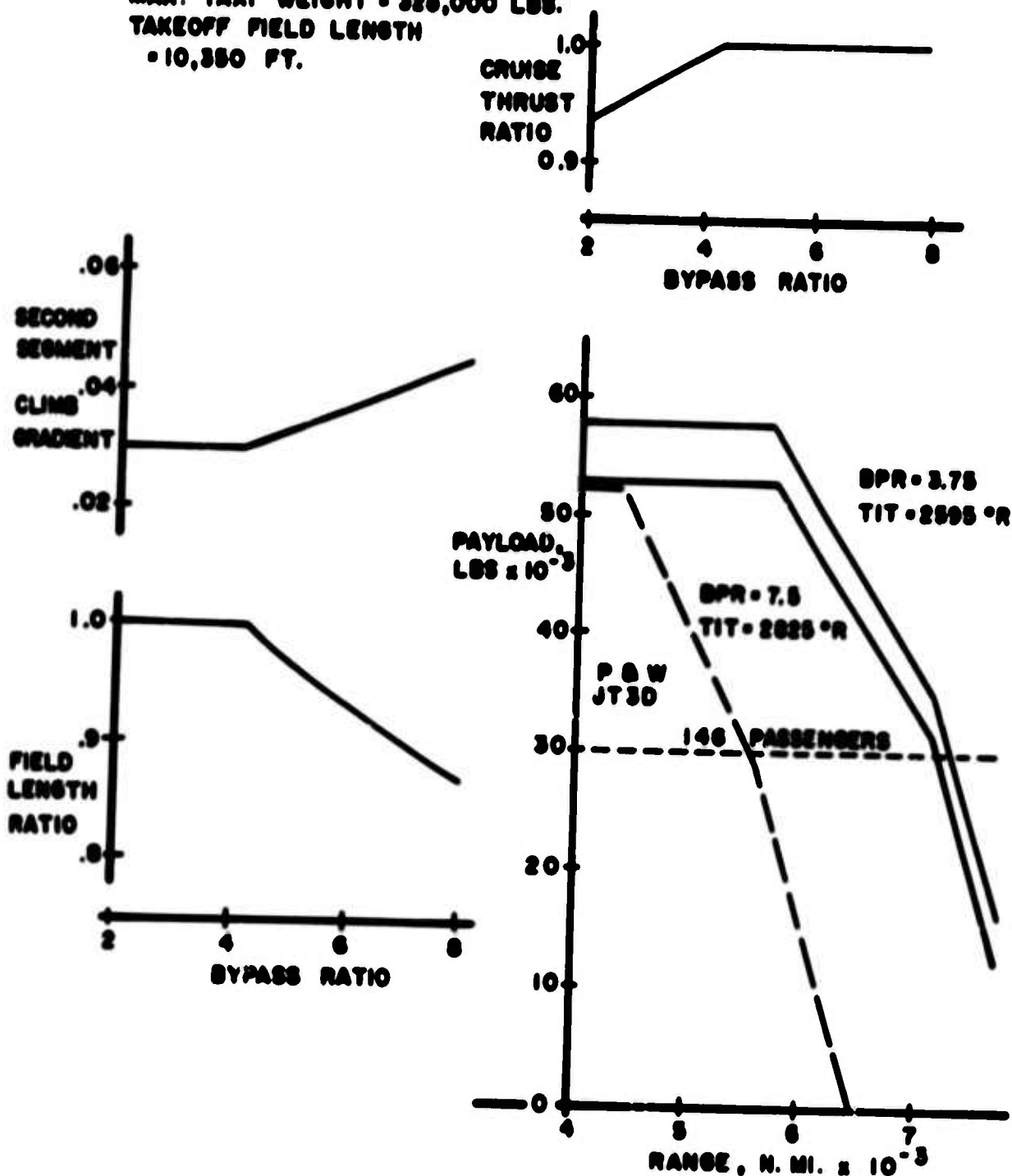


Fig. 24A Parametric retrofit engine study for 707-320N

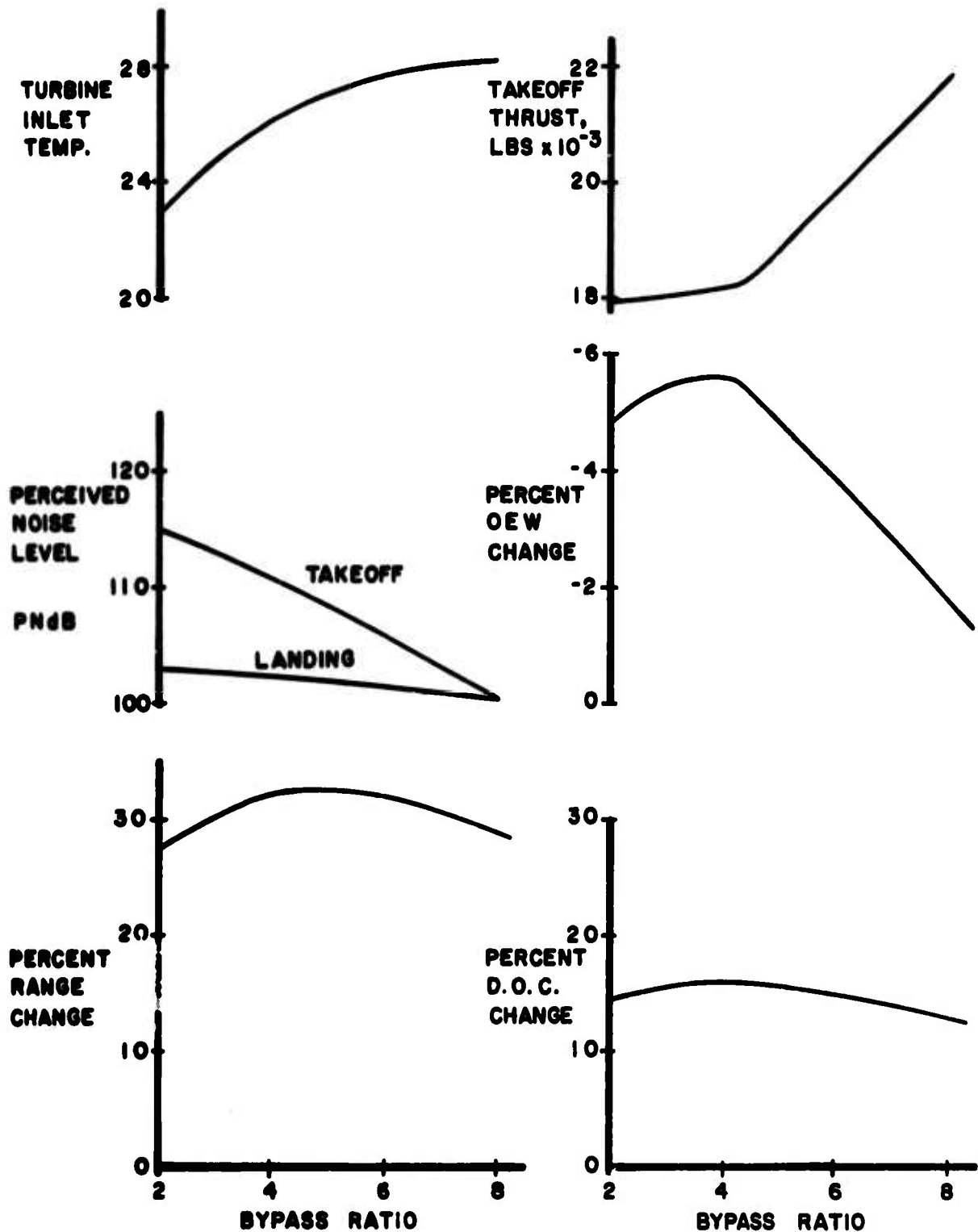


Fig.24B Parametric retrofit engine study for 707-320B (concluded)

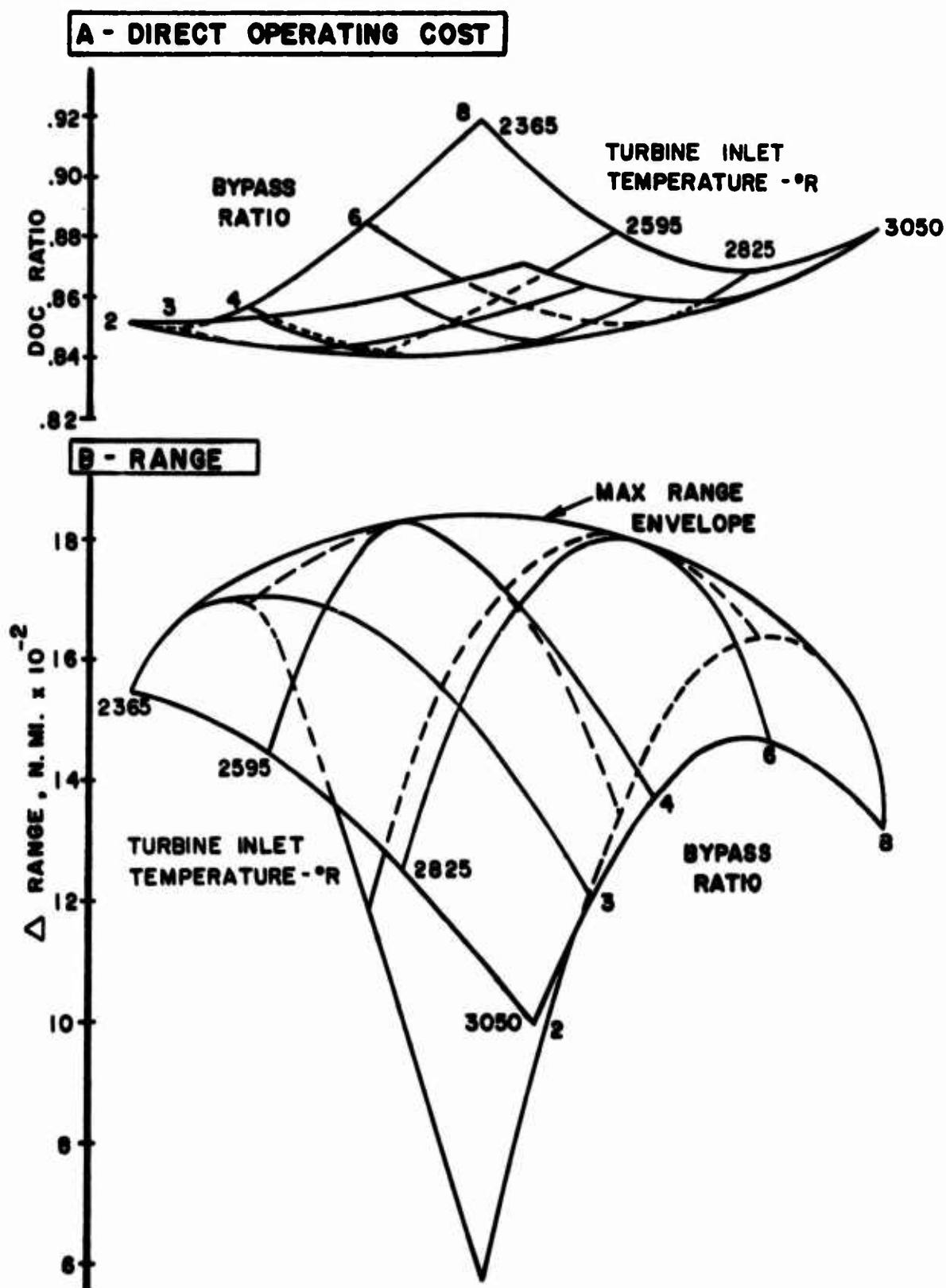


Fig.25 Parametric retrofit engine study

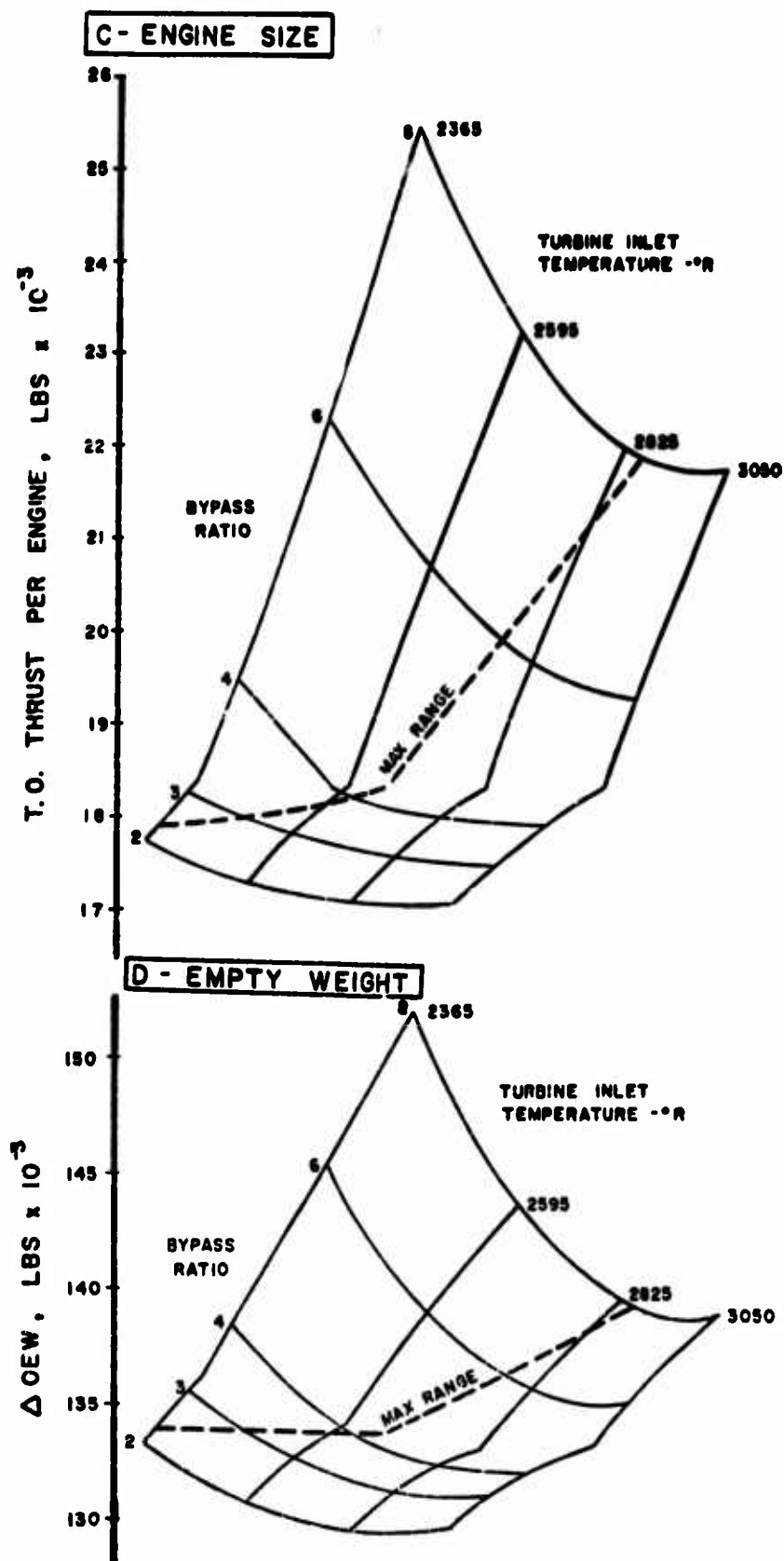


Fig.25 Parametric retrofit engine study (continued)

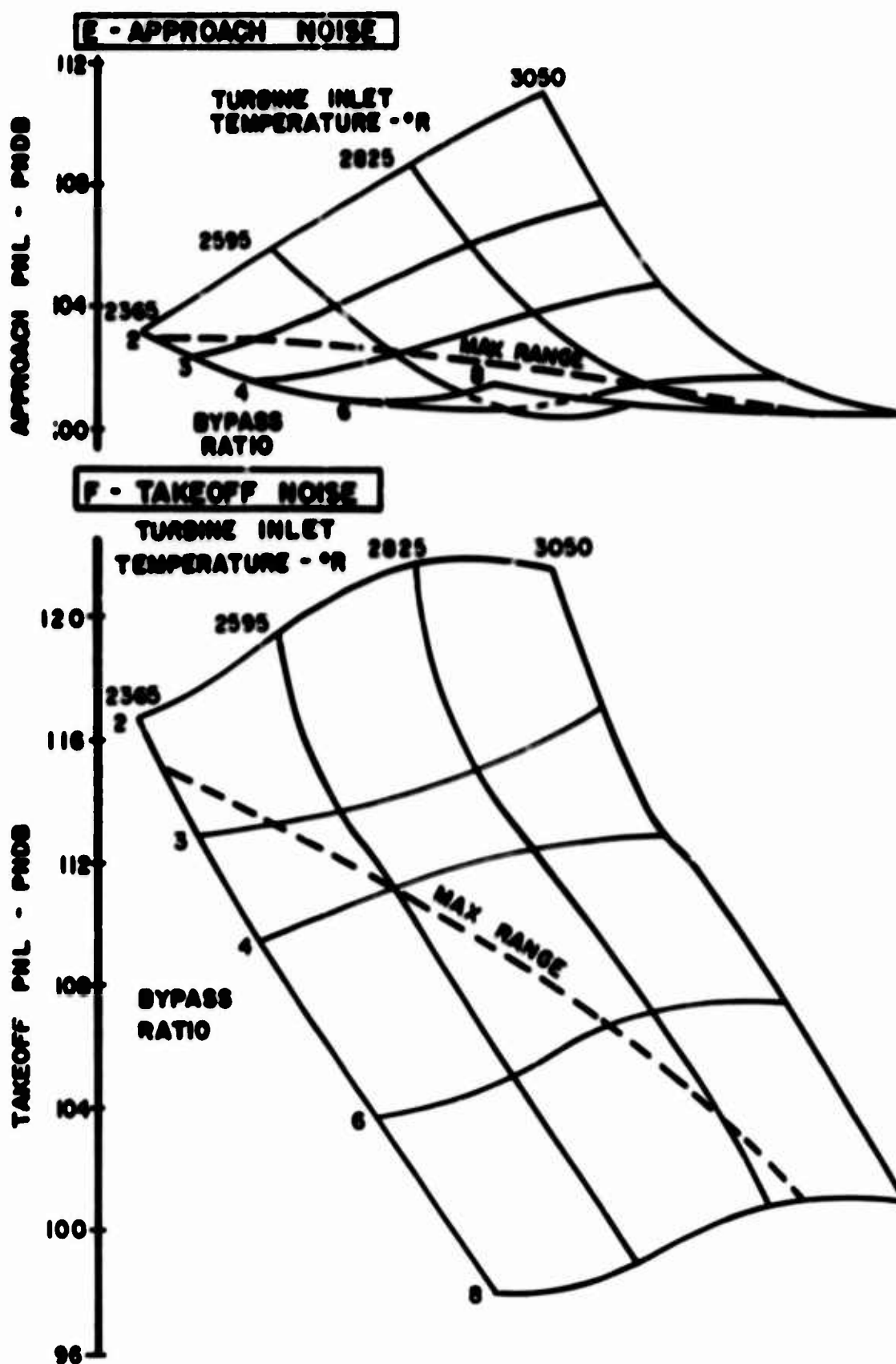


Fig.25 Parametric retrofit engine study (concluded)

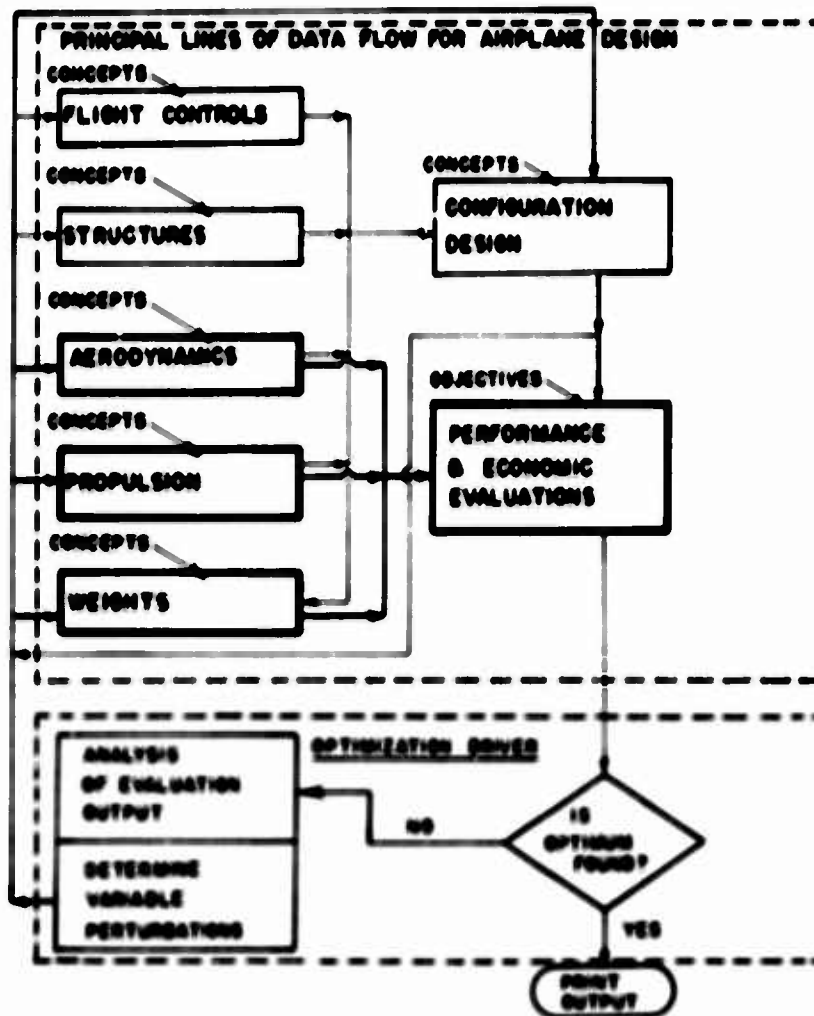


Fig. 26 Optimization schematic

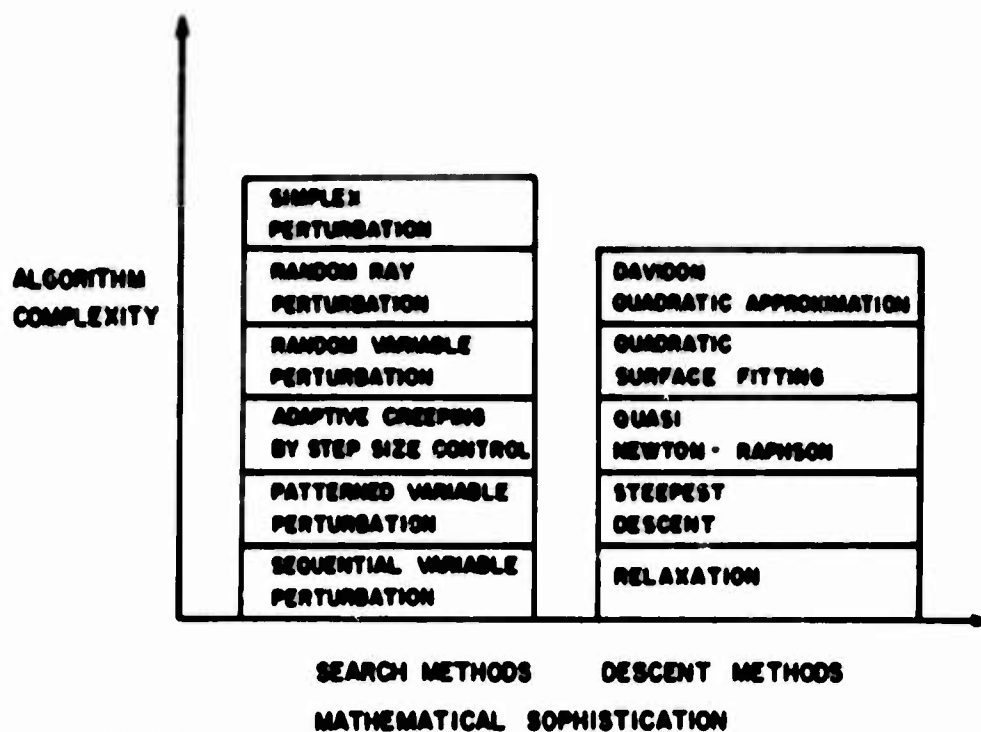


Fig. 27 Optimization methods

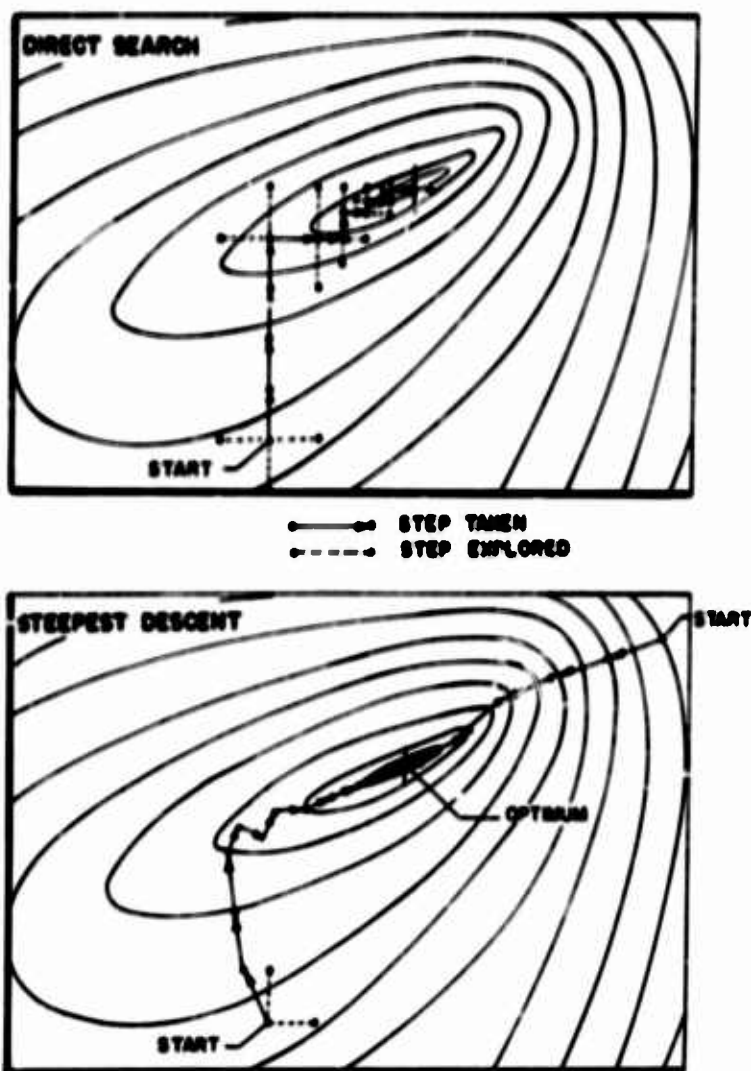


Fig.28 Search versus descent methods

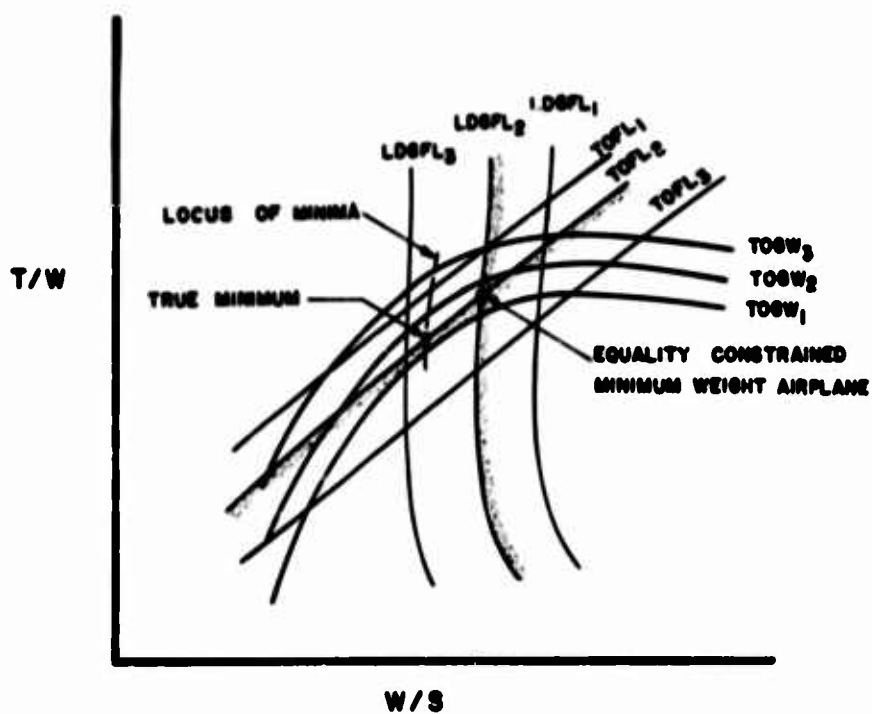


Fig.29 Equality constraint difficulty

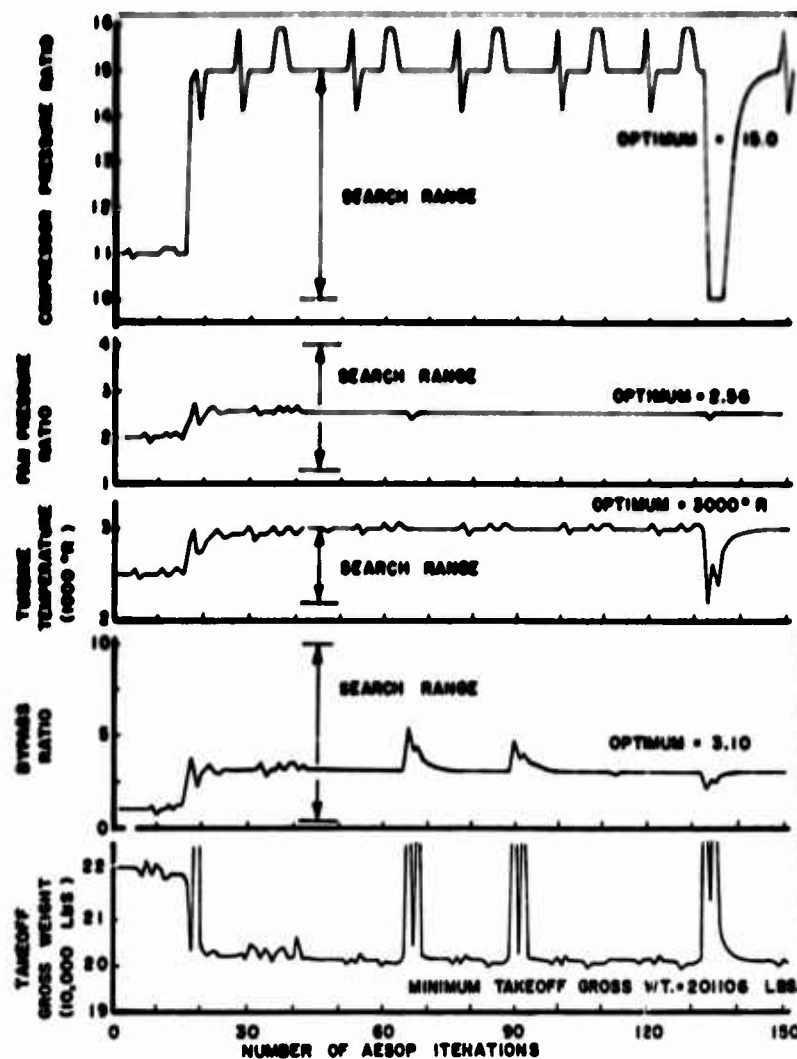


Fig.30 Engine-airplane optimization by quadratic search

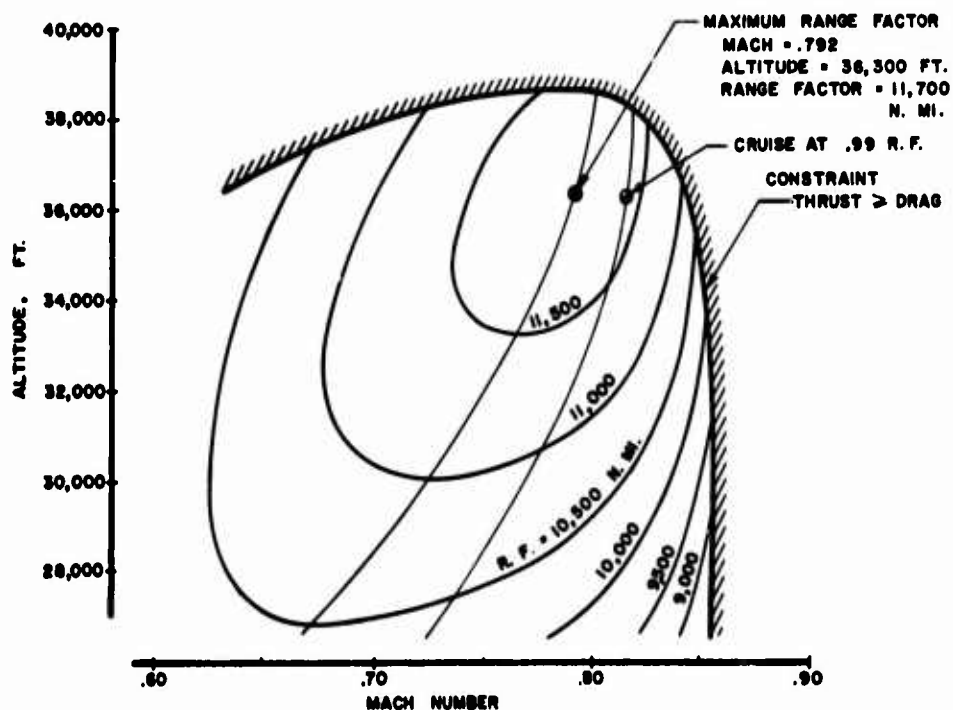


Fig.31 Cruise optimization

	PARAMETRIC BASELINE*	PARAMETRIC RESULTS	COMPUTERIZED DESIGN BASELINE	PERFORMANCE CONSTRAINTS MATCHED WITH FIXED PLANFORM	PERFORMANCE CONSTRAINTS MATCHED WITH OPTIMUM ASPECT RATIO
WING AREA, FT. ²	2611	2600	2611	2445	
WING SWEEP DEG./ OUTBOARD THICKNESS	25/.102	25/.102	25/.093	25/.093	25/.093
ASPECT RATIO	7.72	7.72	7.72	7.72	
MAX. T.O. GWT. LB.	268,000	263,400	268,000	252,600	
OEW	157,100	163,000	157,600	154,400	
OEW C.G. %MAC	13.0-47.0		7.4-49.8	7.1-50.1	
MAIN GEAR LOCATION, %MAC	53.0	-	58.8	59.7	
RANGE, N.MI.	2398	2000	2541	1991	
T.O. FIELD LENGTH, FT.	8750	7000	8772	6972	
T.O. FLAP DEFLECTION, DEG.	2	-	2	10°	
LDG. FIELD LENGTH, FT.	4370	4122	4370	4523	
MAX. LANDING WEIGHT, LB.	207,800	215,200	207,700	207,800	

* Fixed payload of 176 passengers, baggage and cargo, fixed engines, initial cruise altitude, and Mach no. The objective was 2000 N.Mi. from 7000 ft. field.

Fig.32 Comparison of successive design steps

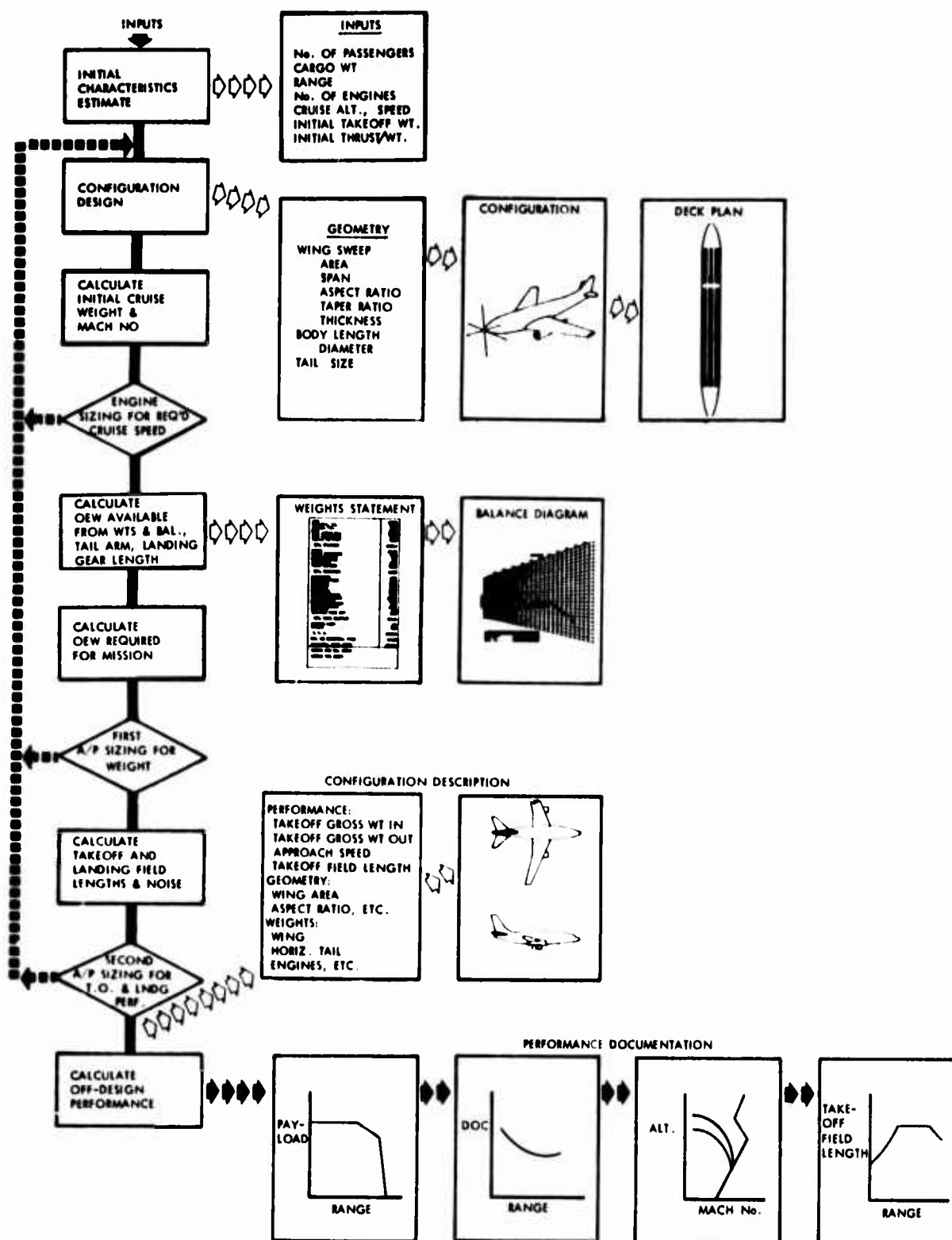


Fig.33 Computerized preliminary design level I (statistical weights)

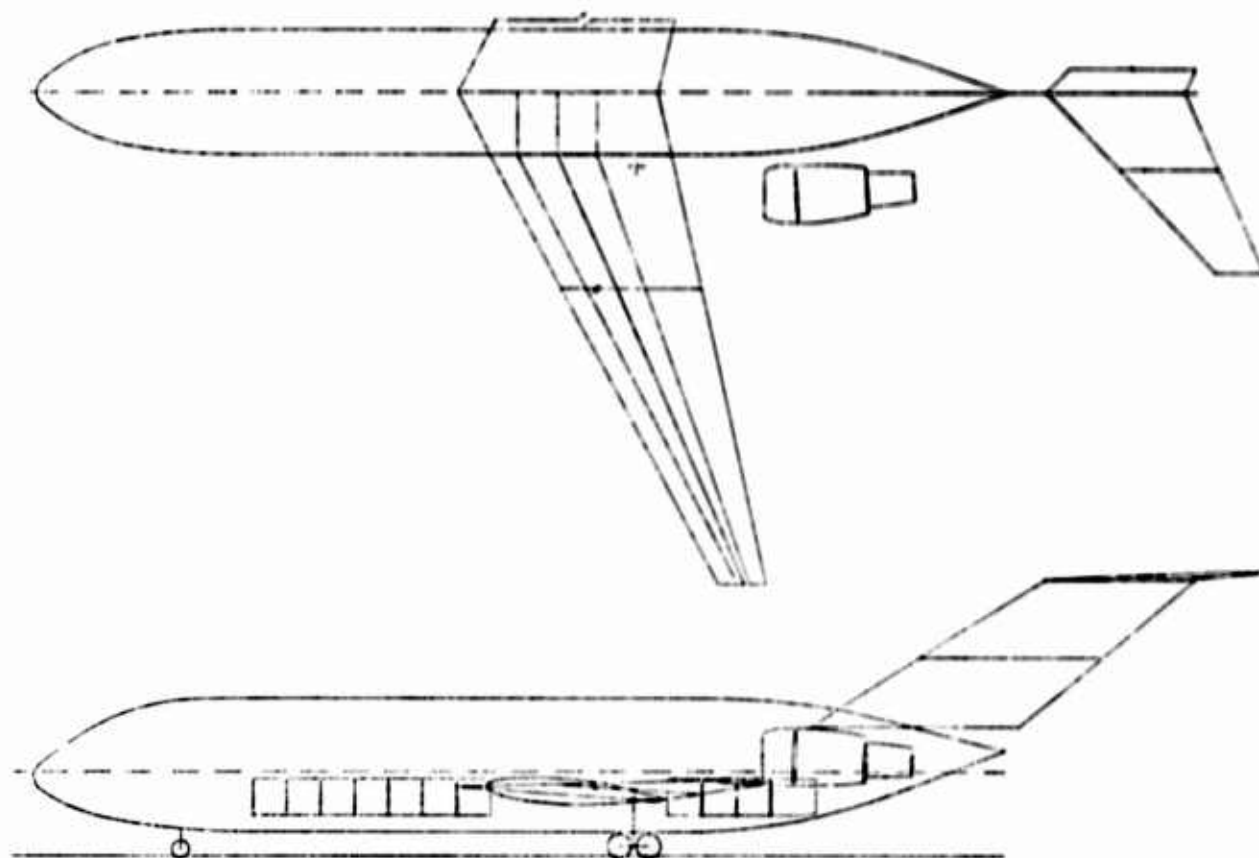


Fig.34 Machine drawing of twinjet

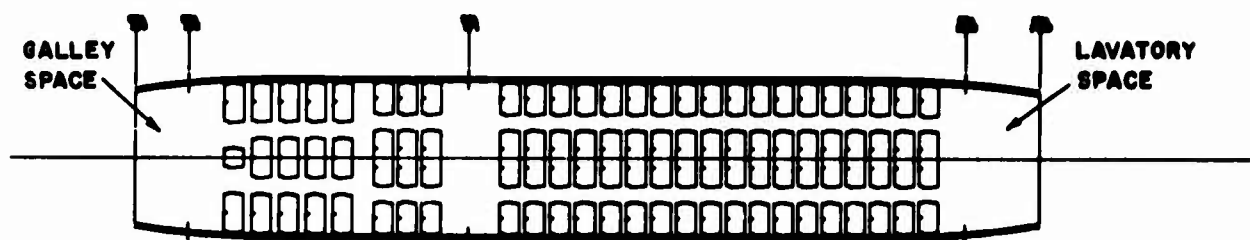


Fig.35 Deck plan

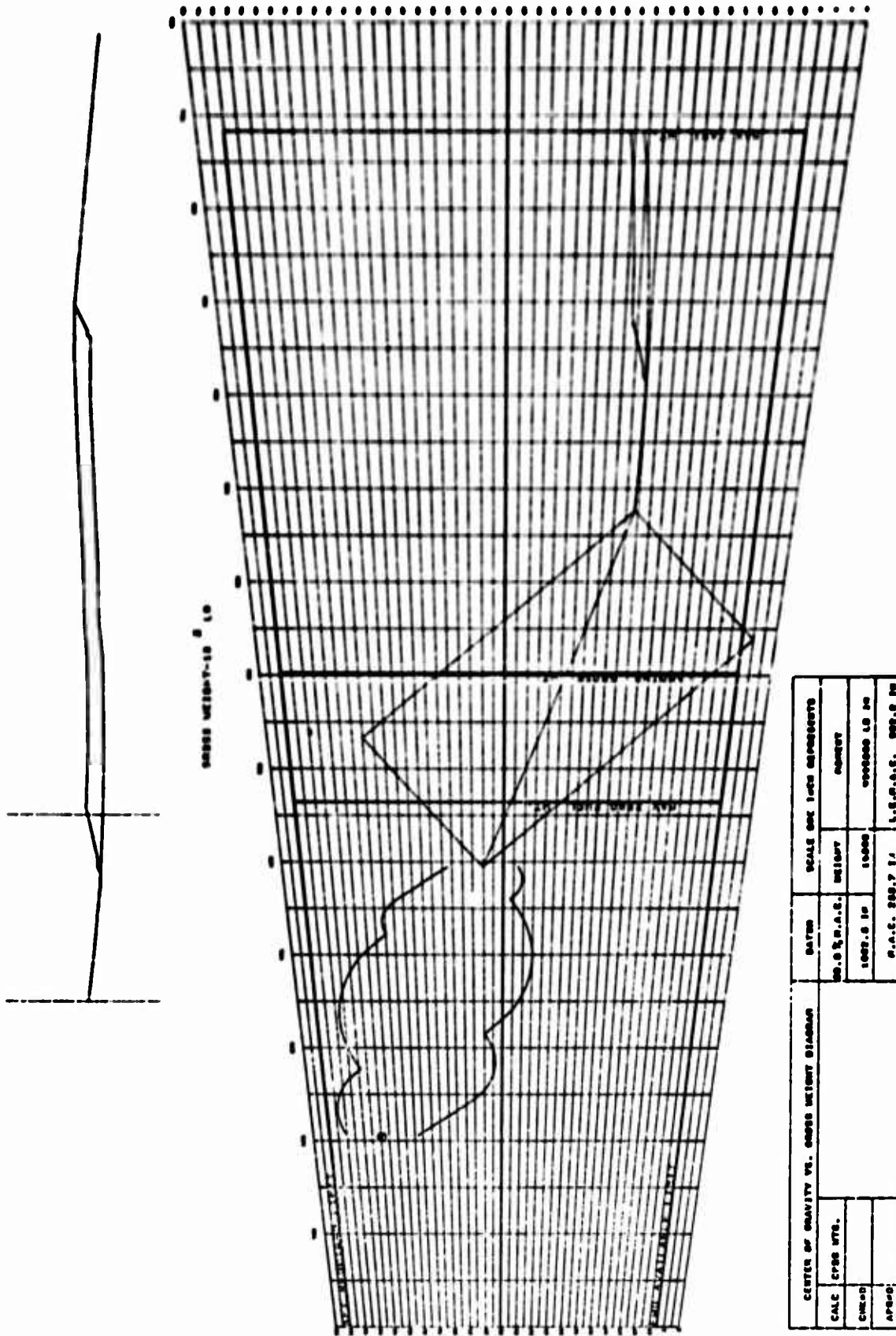
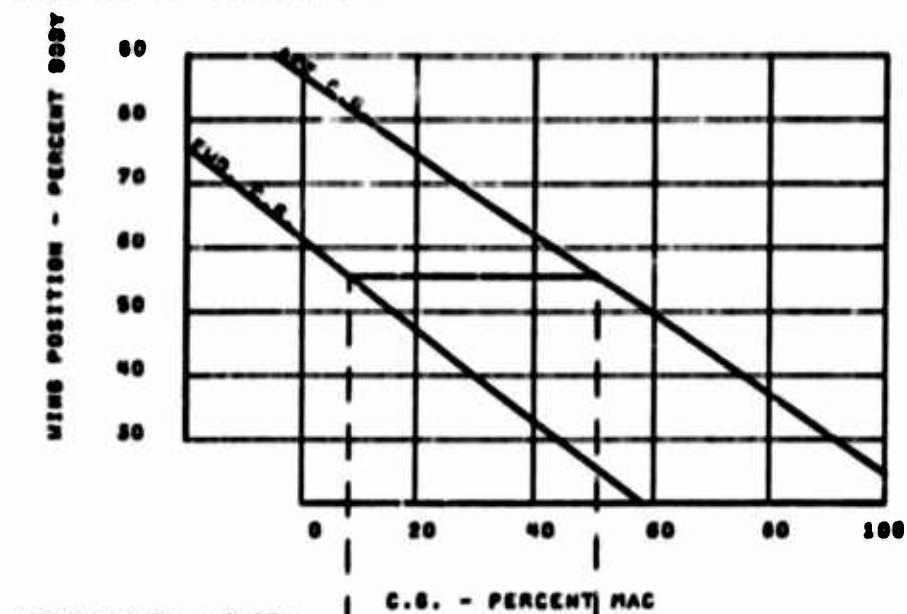
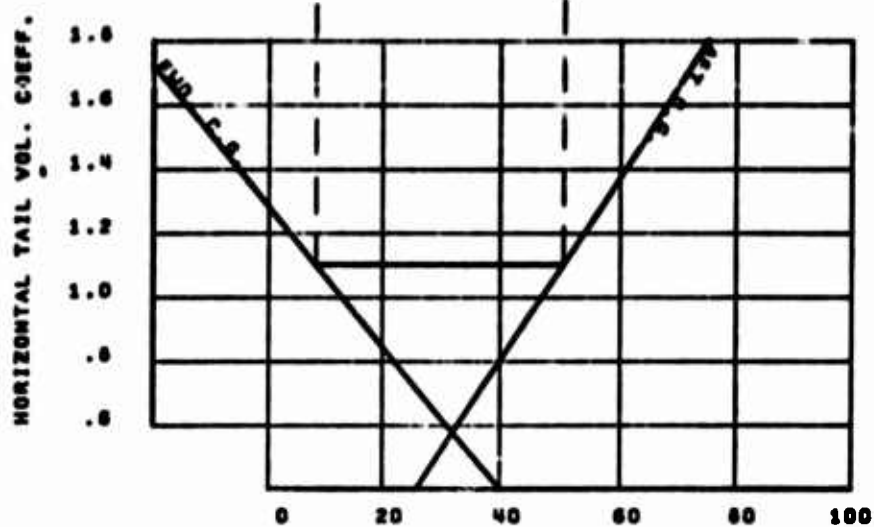


Fig.36 Weight and balance diagram

LOADABILITY REQUIREMENTS



AERODYNAMIC LIMITS



C.G. - PERCENT MAC

WING POSITION ALONG BODY AND MINIMUM REQUIRED HORIZONTAL TAIL VOLUME COEFF				
		WING POS.	55.4 PERCENT BODY	
CALC.		FWD. C.G.	6.2	REF.
CHK D		AFT C.G.	50.4	F18.
APR D		VHBAR =	1.102	PAGE

Fig.37 Tail sizing diagrams

DISCREPANCY BETWEEN APPROVAL AND MODERNISM

by

G. Dumas

Société Nationale Industrielle Aérospatiale, France

DISCREPANCY BETWEEN APPROVAL AND MODERNISM

G. Dumas

There is a problem for people who have to achieve an approved flight manual and provide any customer with what he needs to operate safely.

Let us look at what is commonly done until now, specially for a particular subject : take-off performance, and more precisely, take-off distance. The problem would be identical for 2nd segment weight, or take-off flight path.

The basis of the work :

- Engine characteristics, i.e., nowadays a magnetic tape provided by the engine manufacturer,
- Aerodynamic data, provided by flight or ground tests

are put into a computer with the appropriate deck which quickly produces plenty of results and prints them on a lot of paper.

After that, it is possible to go on "by hand" or with the aid of a new deck to "smooth" the numerous groups of curves which will be a part of the flight manual. In both cases the problem will be identical.

The take-off distance chart is generally as follows:-

At the left there is a basic carpet giving take-off distance versus temperature for a number of pressure altitudes; then, going on towards the right part of the sheet, several groups of curves, sometimes looking like a backbone of fish, each one showing the effect of a parameter such as flaps setting, weight, speed ratio, runway slope, wind, most of the time in this order.

Each curve is an average treating the various parameters independently although the influence of a runway slope is evidently different on a given take-off distance if this distance is coming from two different points as shown on the annexed diagram. Every official curve is normally drawn near to the conservative boundaries so that the overall chart is pessimistic. It is this chart which is approved by the Authorities and "is" the Flight Manual.

Now the problem arises.

The important airlines are now operating computers to establish a special Table for each of their usual airports, taking into account true runway, clearway, stopway and obstacles, and keeping only as parameters temperature, wind and atmospheric pressure. They have to put into their deck all the curves we spoke of above and they feel this work is an useless annoyance.

They demand from the aircraft manufacturer, instead of these charts, the direct results of their deck, by the way of a magnetic tape. This is more simple and cheaper for both partners of the contract.

Yes but,

When using these results the maximum take-off weights achieved by the airlines will normally be higher. To be precise, we can say that this difference may currently be, on a given runway, the equivalent of 15 passengers for a 280 seats aircraft, and in extreme cases more than 30 passengers. What does the lawyer think when the aircraft takes off at a weight higher by 6000 lb than the approved one ? Or what does the airline think when taking off 6000 lb less than it could with full respect of the requirements.

Meetings between aircraft manufacturers, airlines and authorities are necessary.

Already several solutions could be envisaged.

First, the aircraft manufacturer copies the approved curves on a tape and gives it to the airline. This method is obsolete.

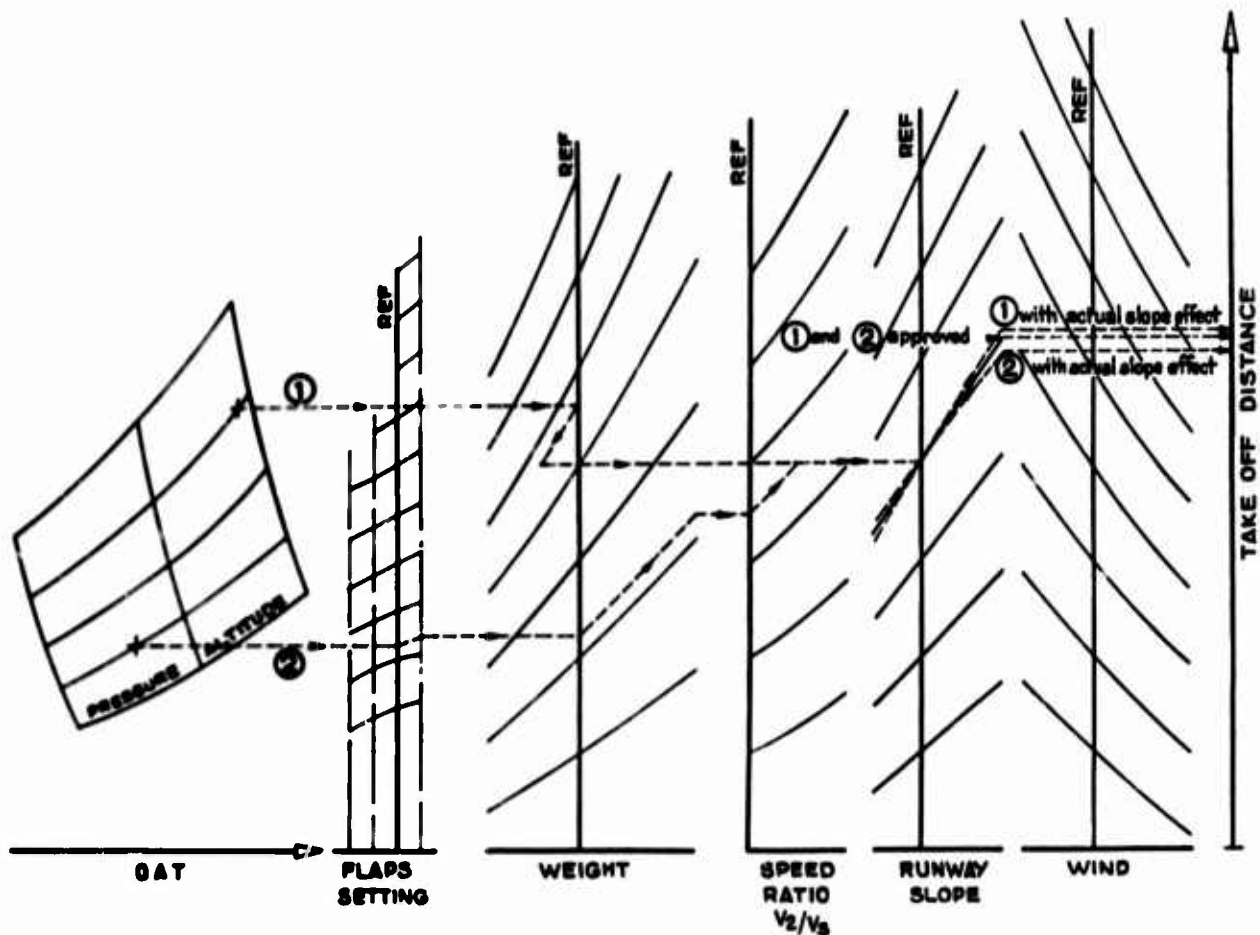
Secondly, the authorities approve the basis, the decks and consequently the direct results.

We feel it is the only reasonable way.

Lastly, the authorities approve both things, the decks and the old charts; decks for big airlines and curves for smaller ones which have no computer facilities. The small airlines would probably be obliged to have their special Tables established by the manufacturers. This is always possible.

Those charts could remain in the cockpit, as required, and used, if necessary, as a quick check in special cases.

To conclude, any change in rules or habits being long, it should be good to open discussions.



AN ANALYTICAL EXPRESSION FOR THE BALANCED FIELD LENGTH

by

E.Torenbeek

Delft University of Technology, Netherlands

CONTENTS

	Page
1. INTRODUCTION	9-1
2. DEFINITION OF THE BALANCED FIELD LENGTH (BFL)	9-1
3. CONTINUED TAKE-OFF	9-1
4. EMERGENCY STOP DISTANCE	9-3
5. DECISION POINT (V_1) AND BALANCED FIELD LENGTH (BFL)	9-3
REFERENCES	9-4
FIGURES	9-5

AN ANALYTICAL EXPRESSION FOR THE BALANCED FIELD LENGTH

E. Torenbeek

1. INTRODUCTION

The objectives of this note are:

- to derive a tractable analytical expression for the balanced field length of a civil aircraft, useful for parametric design studies (engine selection, wing sizing).
- to demonstrate that in the project design stage a detailed solution of the equations of motion and the usual graphical-numerical procedure for the definition of the decision point (V_1) can be avoided without appreciable loss of accuracy.

The condition is imposed that the result can be checked by using direct results from flight test data or flight manuals, in order to make empirical corrections, if necessary.

Some of the principles exposed in this note have been suggested by a colleague of the present author, Mr Th. van Holten, in unpublished work on parametric aircraft design studies.

2. DEFINITION OF THE BALANCED FIELD LENGTH (BFL)

Reference is made to the paper presented by Dr Williams (Ref. 1), where he states on page 2-8:

"A critical decision speed V_1 is defined so that, with a single engine failure, the total accelerate-stop distance from rest to rest becomes identical with the total take-off distance to safely reach screen height".

The following remarks are made with reference to the proposed method:

- (a) Occasionally, the factored take-off distance with all engines operating is more critical for the field length required than the emergency reference distance.
- (b) The validity of the method has not been checked for STOL aircraft and SST.

3. CONTINUED TAKE-OFF

As opposed to the usual subdivision (take-off run to lift-off, transition and climb distance), the continued take-off is split up into 2 phases (Fig. 1):

- Phase 0-1: acceleration from standstill to engine failure speed (V_x),
- Phase 1-2: the motion after engine failure, up to the moment of attaining the screen height at take-off safety speed (V_2).

The distance travelled during phase 0-1 is:

$$S_{0-1} = \frac{V_x^2}{2 \bar{a}_{0-1}} \quad (1)$$

The mean acceleration (\bar{a}_{0-1}) may be calculated accurately by numerical integration, but V_x must be known to do this. Hence, the following simplification is suggested:

(a) Jet aircraft

The mean acceleration is obtained at a velocity equal to 72% of V_x or 65% of V_2 and is approximately:

$$\bar{a}_{0-1}/g = k_T \frac{T_0}{W} - 0.04, \quad (2a)$$

where T_0 = total static (wet) thrust of all engines (kgf) and W = aircraft weight (kgf).

The thrust lapse ratio k_T represents the thrust decay with speed, taking into account bleed air and power off-takes. To compute k_T , the engine manufacturer's brochure or generalized data can be used. The factor 0.04 in Equation (2a) is a typical figure to account for ground friction and aerodynamic drag in ground effect.

(b) Propeller aircraft

The mean acceleration is obtained at a velocity equal to 70% of V_x or 63% of V_2 :

$$a_{0.1/g} = k_p \frac{76 \eta P_0}{WV} + \frac{T_j}{W} - 0.04, \quad (2b)$$

where P_0 = total static (wet) shaft horse power of all engines

W = aircraft weight (kgf)

η = effective propeller efficiency

T_j = total net jet thrust (turboprop engines, kgf)

The factor k_p takes into account the effect of speed and power off-takes.

During phase 1-2, the analysis of the motion is complicated by a number of factors (Fig. 2):

(a) Thrust

After engine failure, the thrust decays in a finite time (e.g. 4 seconds) to zero or idling thrust.

(b) Air Drag

Engine failure causes windmilling drag of the dead engine and extra drag due to the asymmetric flight condition. Additional drag is also created in the rotation and flare manoeuvres, which is considerably affected by the piloting technique. The download on the tailplane must be compensated for by extra wing lift, resulting in increased induced drag. The ground effect decreases after lift-off; hence the induced drag increases. Retraction of the undercarriage, initiated 3 seconds after lift-off, results in another drag variation.

(c) Ground friction drag is related to the lift and vanishes at lift-off.

The calculated total force component in the direction of the flight path has an irregular shape, but the variation may not be observed in practice due to the dynamic character of the motion, smoothing off the peaks.

Another complication is that, especially on large aircraft, the motion of the lowest point and not just the c.g. must be observed. On passing the screen, the total c.g. height gain in the take-off (Δh) may be considerably more than the screen height.

The energy equation is applied to Phase 1-2 (Fig. 1):

$$\frac{W}{2g} (V_2^2 - V_x^2) + W\Delta h = \int_1^2 (T - D_a - D_g) ds, \quad (3)$$

where T = thrust, D_a = air drag and D_g = ground friction d.zg.

Defining an equivalent climb gradient $\bar{\gamma}$,

$$\bar{\gamma} = \frac{\int_1^2 (T - D_a - D_g) ds}{WS_{1-2}} \quad (4)$$

the distance between V_x and V_2 is:

$$S_{1-2} = \frac{1}{\bar{\gamma}} \left(\frac{V_2^2 - V_x^2}{2g} + \Delta h \right). \quad (5)$$

4. EMERGENCY STOP DISTANCE

The velocity as a function of time after engine failure is depicted in Figure 3. Initially an appreciable velocity overshoot is observed due to the still considerable thrust immediately after the failure. Time delays are necessary for failure recognition/decision (1 second) and subsequent operation of wheel brakes, throttle closure, lift dumpers and air brakes (Ref. 2).

Integration of the velocity yields the emergency brake distance, which is approximately

$$S_{\text{stop}} = \frac{V_x^2}{2 \bar{a}_{\text{stop}}} + V_x \Delta t \quad (6)$$

where Δt may be referred to as an equivalent inertia time, affected by the thrust/weight ratio at V_x . The mean deceleration (\bar{a}_{stop}) is affected by brake design, tyre inflation pressure, runway condition, flap setting, the aerodynamic characteristics of the lift dumpers, etc.

5. DECISION POINT (V_1) AND BALANCED FIELD LENGTH (BFL)

The condition for balancing the field length is $S_{1,2} = S_{\text{stop}}$. From equations (5) and (6) the critical engine failure speed is deduced. The approximate solution of the resulting quadratic equation is, for a recognition and decision time of one second,

$$\frac{V_1}{V_2} = \sqrt{\frac{1 + 2g\Delta h/V_2^2}{1 + \gamma/(\bar{a}/g)_{\text{stop}}}} - \frac{\gamma g (\Delta t - 1)}{V_2} \quad (7)$$

The condition must be satisfied that $V_1 \leq V_R$. To check this, a more detailed analysis of the rotation and flare manoeuvre is necessary. In the case that $V_1 = V_R$, the field length is generally no longer balanced.

Substitution of V_1 according to Equation (7) into Equation (1) and (5) or (6) results in the expression

$$\text{BFL} = \frac{V_2^2}{2g\{1 + \gamma/(\bar{a}/g)_{\text{stop}}\}} \left\{ \frac{1}{(\bar{a}/g)_{0-1}} + \frac{1}{(\bar{a}/g)_{\text{stop}}} \right\} \left(1 + \frac{2g\Delta h}{V_2^2} \right) + \frac{45\Delta t}{\sqrt{\sigma}} \quad (8)$$

where σ = relative density.

The term associated with Δt (expressed in metres) is relatively small. It is an approximate solution of the exact equation, derived by substitution of typical wing and power loadings.

The result is valid for both propeller and jet aircraft. To make the expression useful for design purposes, further simplifications can be made on the basis of the following observations:

(a) Contrary to the distance $S_{1,2}$ according to Equation (5), the balanced field length appears to be insensitive to γ . For example, a 10% deviation in γ results in only 1.5% deviation in BFL.

The equivalent gradient $\bar{\gamma}$ is a linear function of the second segment climb gradient at $V_2(\gamma_2)$:

$$\bar{\gamma} = \gamma_2 + \Delta\bar{\gamma} = \gamma_{2\text{min}} + \Delta\gamma_2 + \Delta\bar{\gamma} \quad (9)$$

where $\gamma_{2\text{min}}$ is the minimum permissible climb gradient in the second segment. The excess gradient relative to the minimum is $\Delta\gamma_2$, while $\Delta\bar{\gamma}$ represents the various effects on $\bar{\gamma}$, mentioned in Section 3.

Equation (9) is illustrated on Figure 4, where the results of flight tests of a twin-engined airplane are given. Using measured values of V_x , V_2 and $S_{1,2}$, $\bar{\gamma}$ is calculated from Equation (5). The effect of the residual thrust after throttle closure is indicated separately, by calculating $\bar{\gamma}$ during phase $V_R - V_2$, assuming that negligible residual thrust is present during this phase.

On the basis of assumptions regarding undercarriage drag, ground effect, etc., it was found that almost invariably $\gamma_{2\text{min}} + \Delta\bar{\gamma} \approx 0.06$, irrespective of the number of engines.

Hence, the approximation is made:

$$\bar{\gamma} = 0.06 + \Delta\gamma_2 \quad (10)$$

(b) An average value of $\dot{a}_{\text{stop}} = 0.37g$ is established from application of the method to 15 jet transports. With optimum brake pressure control and lift dumpers, decelerations as high as 0.45 – 0.50g can be achieved on dry concrete. For very high decelerations the balancing condition (Eq. (8)) may not be satisfied.

Using an inertia time $\Delta t = 4\frac{1}{2}$ seconds and $\Delta h = 11m$, we find the following expression:

Jet Aircraft

$$BFL = \frac{0.704}{1+2.3 \Delta\gamma_2} \left(\frac{W/S}{\sigma C_{L2}} + 14 \right) \left(\frac{1}{k_T T_0/W - 0.04} + 2.7 \right) + \frac{200}{\sqrt{\sigma}} \text{ (metres),} \quad (11)$$

where

W/S = wing loading (kgf/m^2)

σ = relative air density

C_{L2} = C_L at V_2 ; $V_2 \geq 1.2V_S$, normally $V_2 = 1.2V_S$

V_S = stalling speed in accordance with the airworthiness regulations

T_0/W = total static thrust/weight (kgf/kgf)

k_T = thrust lapse factor, to be determined from the engine brochure, or approximately equal to $0.75(5 + \beta)/(4 + \beta)$

β = by-pass ratio

$\Delta\gamma_2 = \gamma_2 - \gamma_{2\min}$; γ_2 is calculated at airfield height, $\gamma_{2\min} = 0.024, 0.027$, and 0.030 for 2, 3, and 4 engines respectively. For project-design, $\Delta\gamma_2 = 0$ represents the most interesting case, as the corresponding weight is limited by the second segment climb requirement and the BFL is maximum for the particular flap setting.

Turboprop Aircraft

An interesting feature of the approximation for the thrust lapse is that for very high by-pass ratios k_T tends to 0.75, which is about the average propeller thrust in the ground run as a fraction of the static thrust. Assuming a typical value for the ratio static propeller thrust/shaft power, equation (11) can be used for propeller aircraft as well. The term $k_T T_0/W$ should be replaced by $k'_p P_0/W$, where

$$\begin{aligned} k'_p &= 1.0 \quad \text{when } P_0 \text{ is the total e.s.h.p.} \\ \text{or } k'_p &= 1.12 \quad \text{when } P_0 \text{ is the total s.h.p.} \end{aligned}$$

Equation (11) was applied to 20 civil transport aircraft. A r.m.s. deviation of 4% from the manufacturers data was found.

REFERENCES

1. Williams, J. Airfield performance prediction for transport and combat aircraft. VKI Lecture Series 49 (AGARD Lecture Series 56, paper 00 of this volume), April 1972.
2. Foxworth, T.G. Marthinsen, H.F. Another look at accelerate-stop criteria. AIAA Paper No.69-772; 1969.

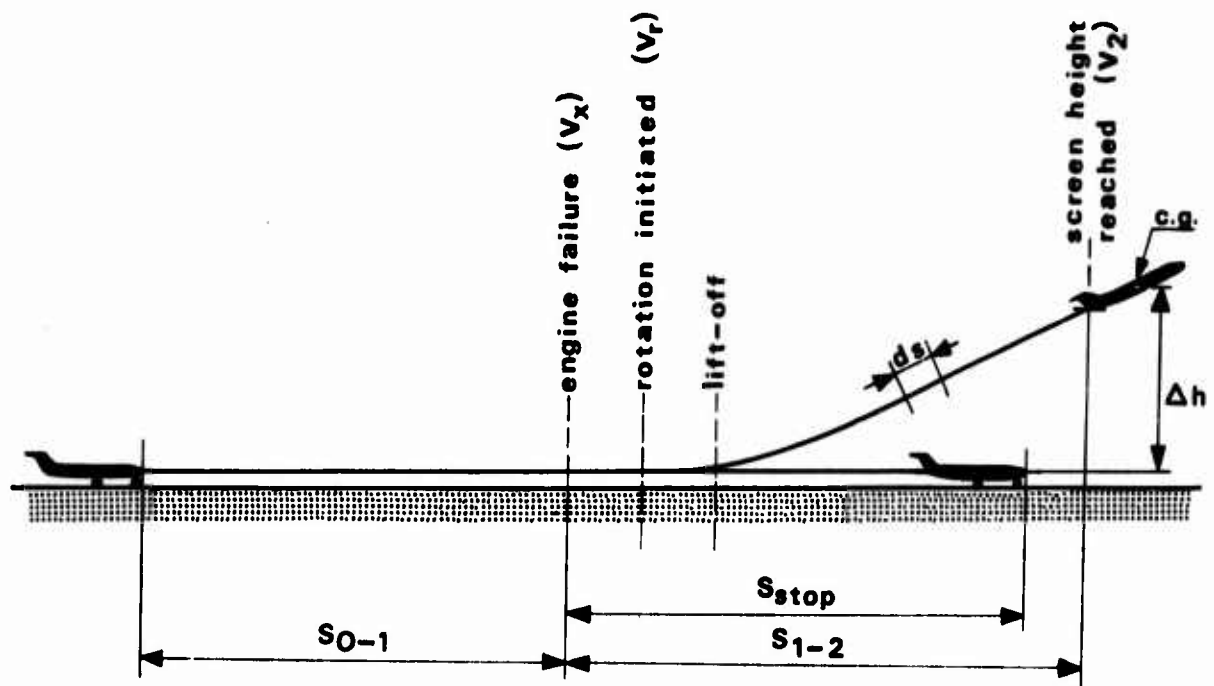


Fig.1 Phases in the take-off

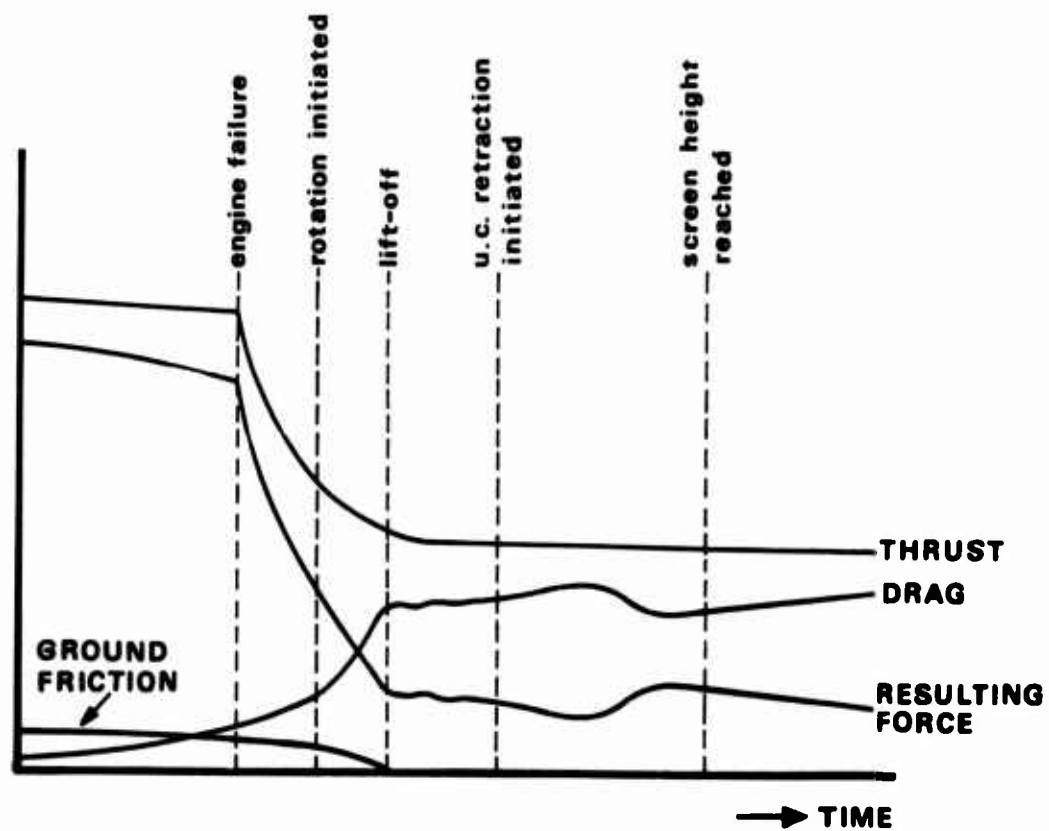


Fig.2 Forces on the aircraft

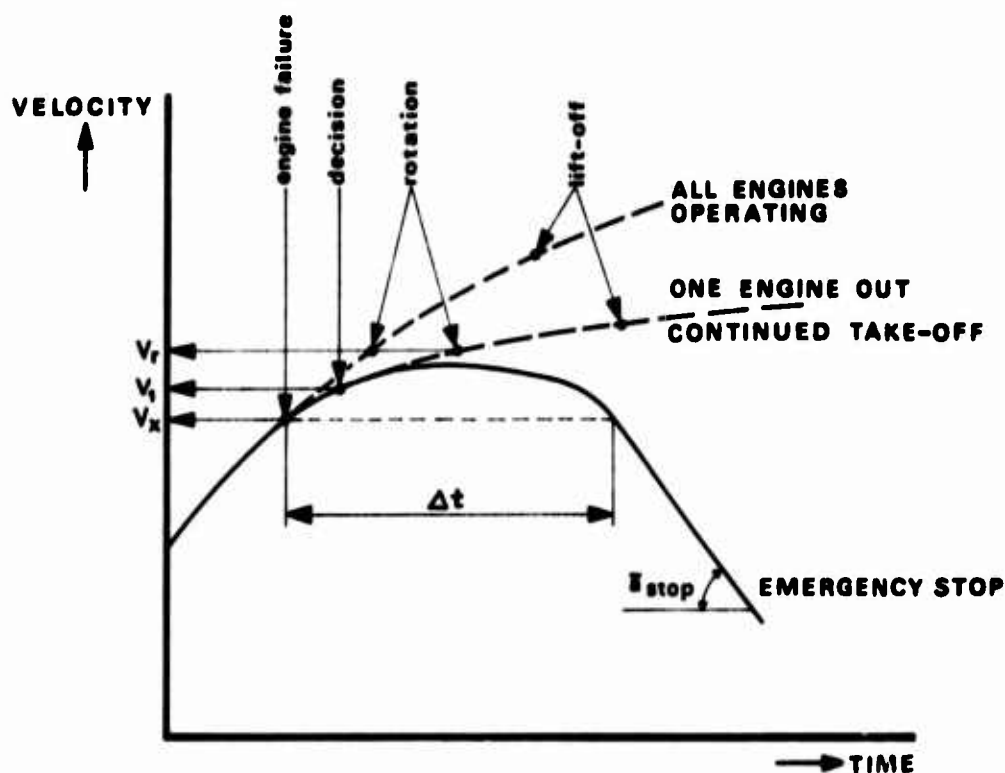


Fig.3 Velocity versus time in an aborted take-off

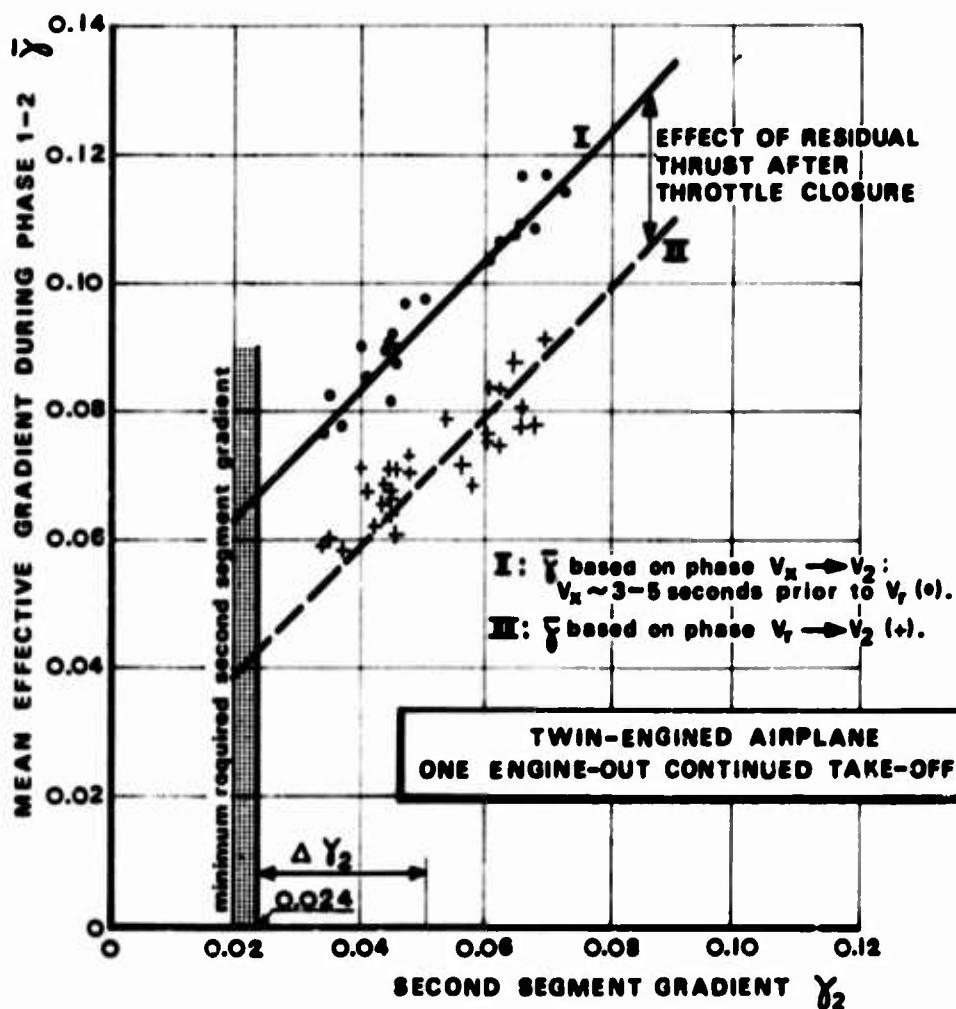


Fig.4 Effective climb gradient deduced from flight tests

**SUPPLEMENTARY NOTE TO
"FLIGHT-MANOEUVRE AND CLIMB-PERFORMANCE PREDICTION"**

by

P. Foerster

Dornier AG, Friedrichshafen, Germany

**SUPPLEMENTARY NOTE TO
"FLIGHT-MANOEUVRE AND CLIMB-PERFORMANCE PREDICTION"**

P. Foerster

In the discussion on Paper 3 of this volume, the question as to the accuracy of the optimal climb procedure (as shown by Dr Friedel) had arisen. A good idea of accuracy may be given by the following considerations.

"Elementary Theory of Energy Manoeuvrability" (E. Rutowski, H. Behrbohm, Fr. Kaiser and others) shows that the minimum-time climbing procedure is defined by the locus of all tangent points of the constant specific energy lines (E_s) and the constant specific excess power lines ($SEP = P_s$). This locus is represented in Figure 1 by the dotted line.

Similarly, the minimum-fuel climbing procedure is given in Figure 2, by the locus of all tangent points of the constant energy manoeuvrability index lines (P_{sw}) and the constant specific energy lines (E_s).

Specific excess power, energy manoeuvrability index, and specific energy are defined as follows:

$$SEP = P_s = \frac{dE_s}{dt} = V \frac{(T - D)}{W} \quad (1)$$

$$EMI = P_{sw} = \frac{P_s}{W_f} = \frac{dE_s}{dW} \quad (2)$$

$$E_s = H = h + \frac{V^2}{2g}, \quad (3)$$

where T = thrust, D = drag, W = weight, W_f = fuel flow, H = energy height, h = altitude, V = velocity, $g = 9.80665 \text{ m/s}^2 = 32.174 \text{ ft/s}^2$.

If the points of initial flight conditions ("B") and/or the points of terminated climb procedure ("A₁" or "A₂") do not coincide with a point of the minimum-time path, the aircraft must either make a dive (for example from "B" to the minimum-time path) or a zoom (for example from the minimum-time path to "A₂").

During such a climb, a series of control variables have to be changed very often. In fact, flying of any minimum-time procedure results in a pilot work load which is usually too high for most pilots.

For this reason, a more practical climb procedure is sought, which is as close to the minimum-time path as possible. Such a useful climbing procedure is as follows, especially when climb performances from brake release are to be predicted:

1. Take-off and acceleration to point "C" (see Figure 1)
2. Climb with constant calibrated airspeed CAS
3. Climb with constant Mach number
4. Acceleration or deceleration at constant altitude to desired cruise conditions.

For a typical subsonic aircraft, the two proposed climbing procedures, minimum-time path on the one hand, constant CAS – constant Mach number – climb on the other hand, differ in accuracy by about 1% with regard to time, distance and fuel consumption. Figure 3 represents on the left the two climbing procedures, treated here, and on the right the climbing performances, time, distance and consumption.

The reason for this good result is shown in Figure 4 which is valid for a typical supersonic aircraft (re-heat lit). The minimum time to climb to a given energy height is represented by the area below the envelope. In this particular case, the envelope comes very close to the line representing a constant Mach number of 0.95. For other aircraft, where the envelope is not as close to a line of constant Mach number as shown here, it will nevertheless be possible to keep the error in predicting the minimum time to climb to less than five to ten percent even if a very inaccurate procedure is used.

Another problem which had arisen during the discussion concerns the minimum-fuel climbing procedure. In equation (2), an optimal engine rating may be supposed, because thrust and fuel flow are functions of engine rpm.

An answer to this question may be given by Figure 5, where the energy manoeuvrability index P_{sw} is plotted against the engine rating. This plot is valid for a turbofan engine with low bypass ratio, and shows that there is no optimum except at maximum engine power. This tendency will probably be the stronger the higher is the bypass ratio chosen. An optimal engine rating which lies below the maximum engine rating can probably be found for turbojet engines only (re-heat unlit). In case of a maximum energy manoeuvrability (for optimal engine rating) this will be only slightly larger than the energy manoeuvrability for maximum engine rating.

◊

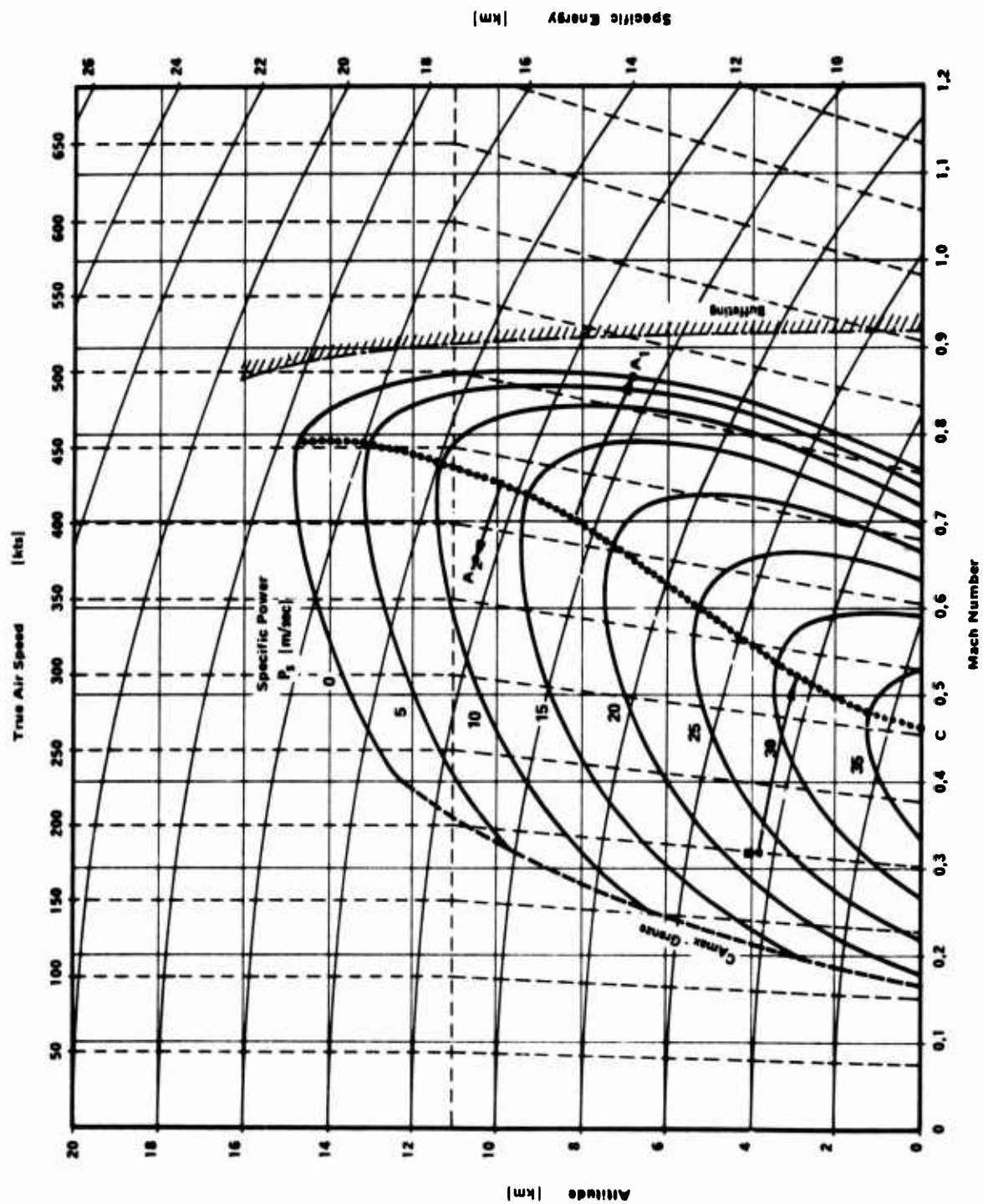


Fig.1 Kaiser plot for SEP (average aircraft weight, 100% rpm)

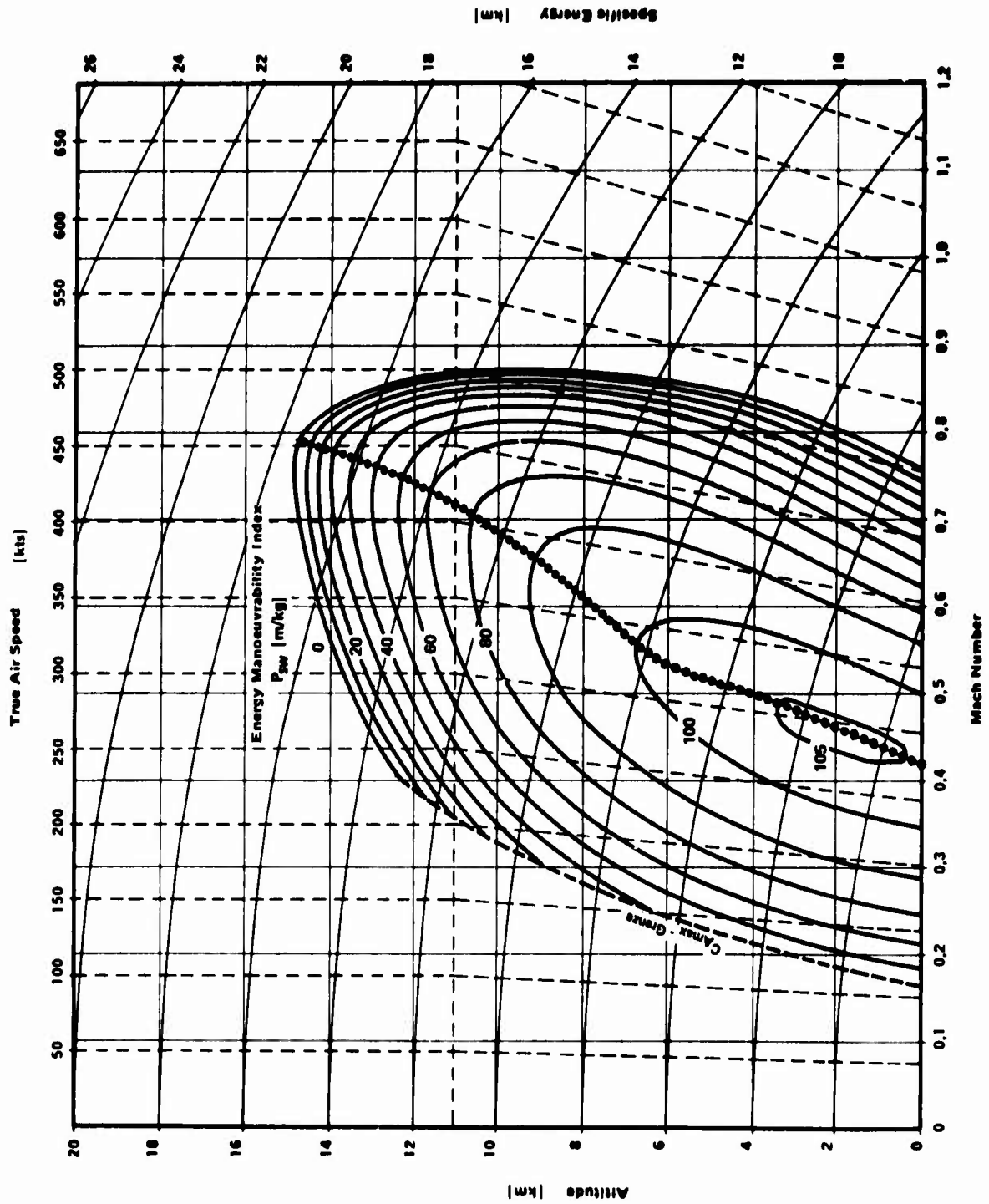


Fig.2 Kaiser plot for EMI (average aircraft weight, 100% rpm)

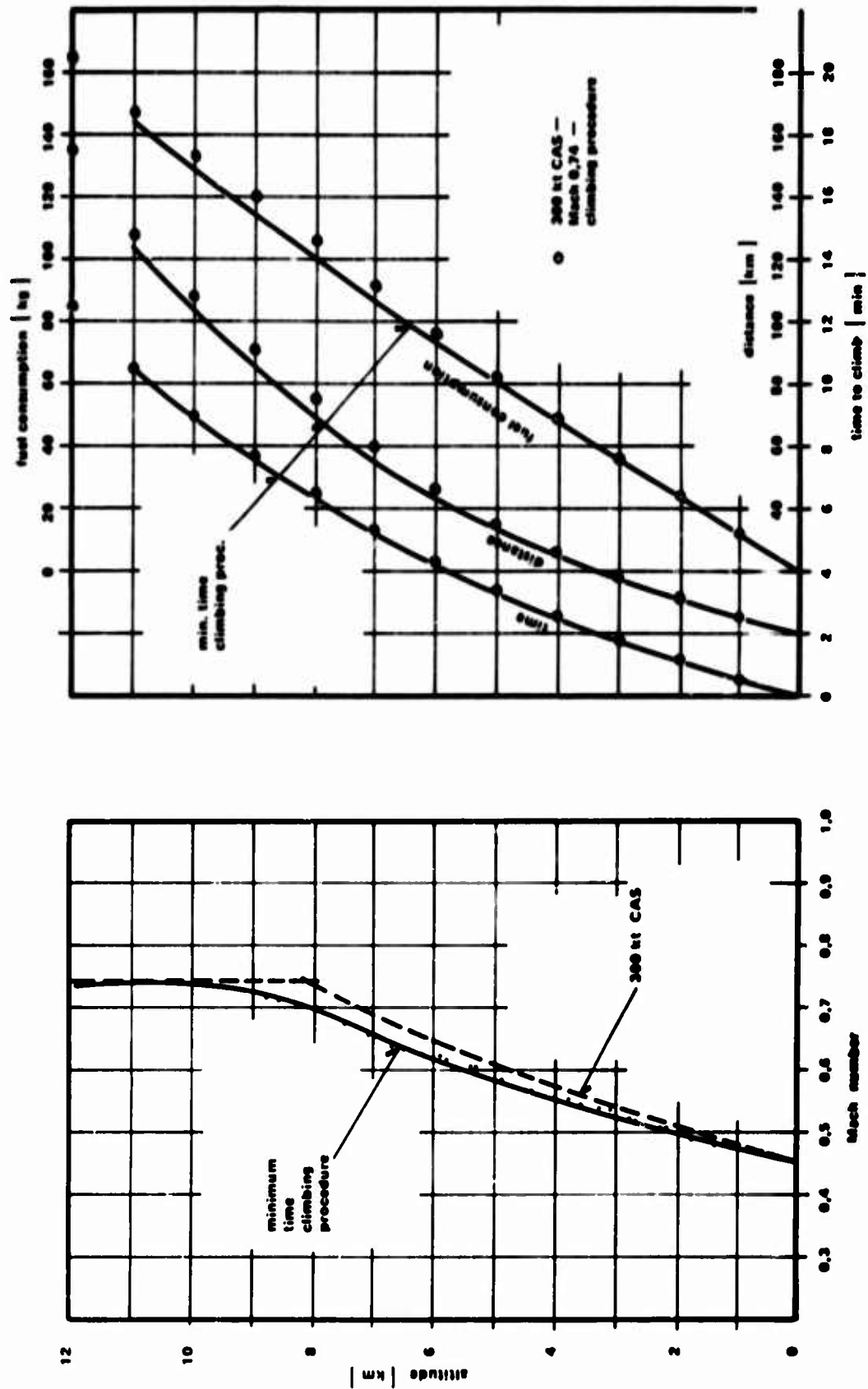


Fig.3 Comparison of climbing performances (takeoff weight, 100% rpm)

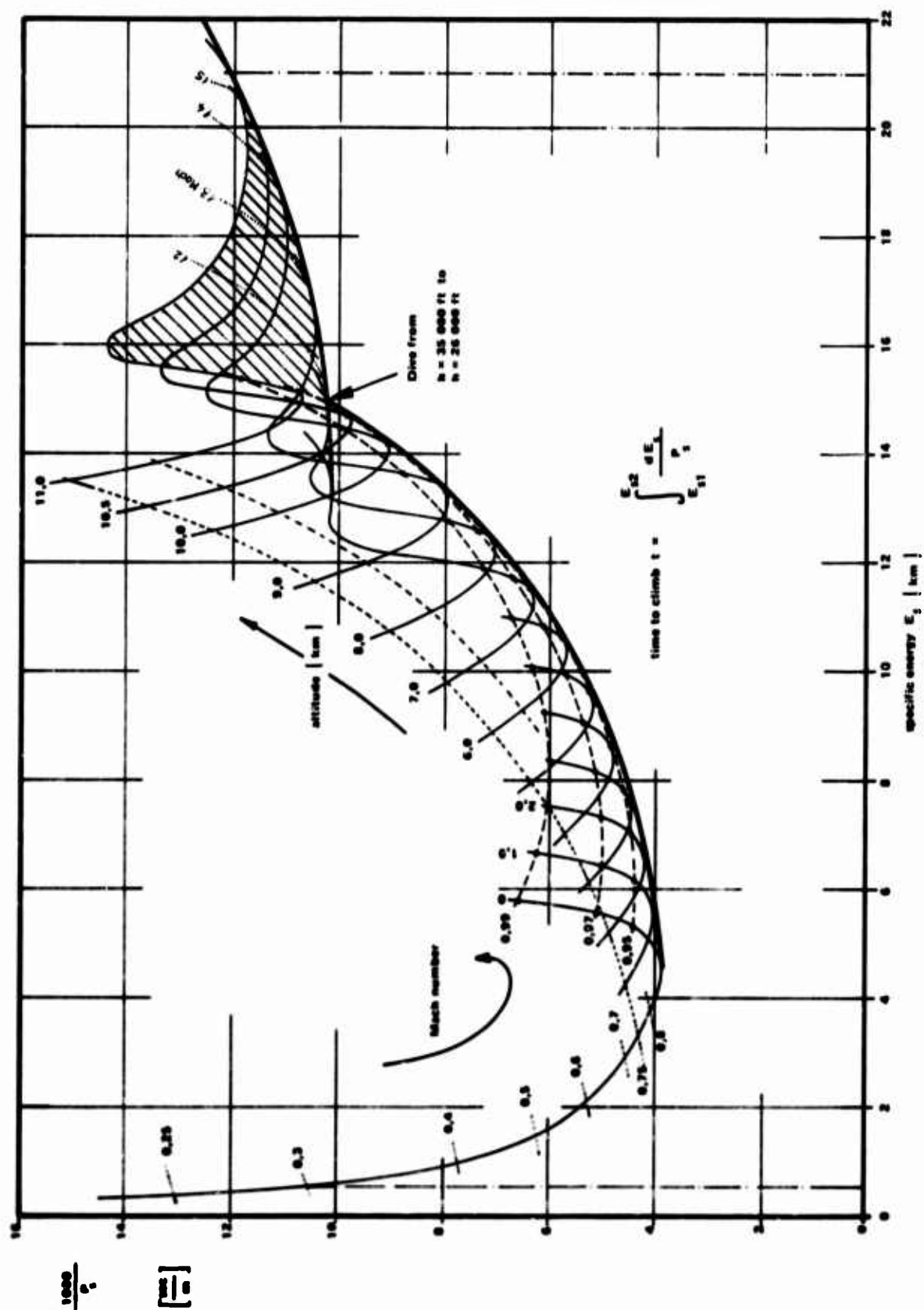


Fig.4 Graphical integration of time to climb

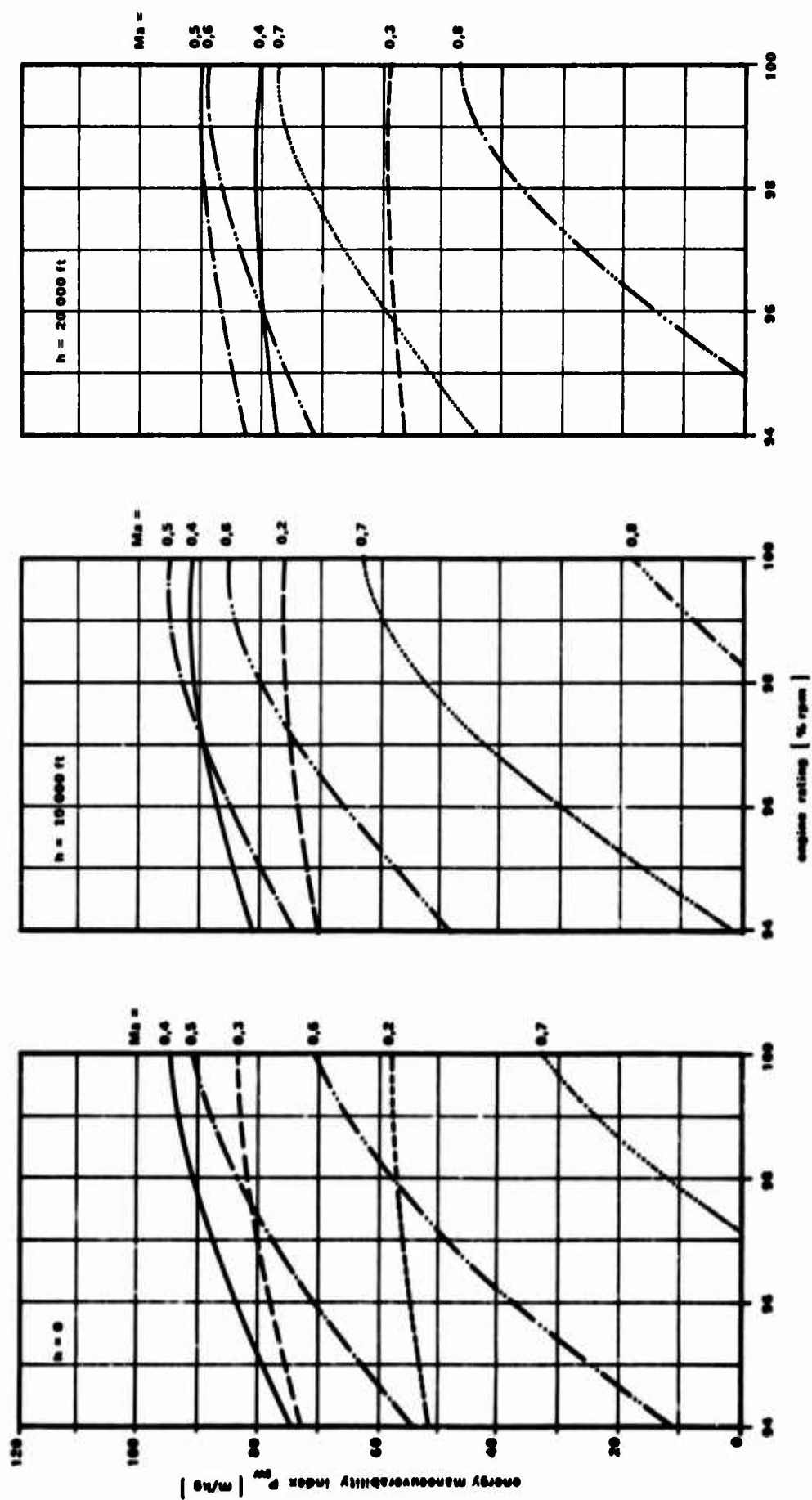


Fig.5 Energy manoeuvrability index versus engine rating

**MINIMUM TIME TRAJECTORY COMPUTATION --
DEVELOPMENT OF THE BALAKRISHNAN METHOD**

by

P. Middleton

**Hawker Siddeley Aviation,
Brough, UK**

MINIMUM TIME TRAJECTORY COMPUTATION - DEVELOPMENT OF THE BALAKRISHNAN METHOD

P. Middleton

As part of a study of interceptor systems it was decided to write a program for the computation of minimum time trajectories. At that time the method in use in our department was the energy-height method. This method has severe limitations due to several inaccuracies which arise mostly in the simplified form of the equation of motion normal to the flight path. Generally the thrust component in this equation is omitted and in certain aircraft this can lead to errors of the order of 20% of the thrust in the force sum. This term can be included at the expense of extra effort due to the necessary iteration. The acceleration normal to the flight path is also ignored and this is equally important in certain phases of the trajectory. The third source of error in this equation is the assumption of a negligibly small climb angle. With modern combat aircraft climb angles of thirty degrees are quite common and such a climb angle would cause an error of at least 25% in the induced drag calculation. These three sources of error are combined in the calculation of specific excess power. If the flight time is calculated from the change in energy-height and specific excess power then the flight time is also in error. There is a further difficulty in the calculation of the flight time since a different method is required to calculate the time necessary for ballistic climbs and dives. It was felt that the limitations of this method were too great for our study so other methods were considered.

The first to be considered was dynamic programming. In this method the state and control variables are considered at a number of discrete points and a path through the matrix of these values is computed for the solution. This method is very efficient if only a small number of discrete values are considered; however, if the number of values is increased the computation time increases very rapidly. Probably the most used modern method is the gradient method. In this method at each iteration the equations of motion are integrated. This is a costly process on a digital computer and although the results are very accurate the computation time is again very high. At about this time a Note¹ was published describing work undertaken at N.A.S.A. Flight Research Center on the use of a new method, the Balakrishnan Method, to solve this problem. Since this method seemed to offer sufficient accuracy for our needs with a small computation time it was decided to write a program using the method but including certain improvements we felt necessary.

Since this method is not well known a brief description is necessary. The basic problem as set out in Figure 1 is the minimisation of a function J of X and α , where X is an array of state variables and α an array of control variables. The state variables must satisfy a system of differential equations and also a set of terminal constraints. Dr Balakrishnan suggested that the differential equations and the function J be replaced by a function K which was to be minimised subject to the same terminal constraints. It was suggested that as ϵ tended to zero the X and α which minimised K tended to the X and α which minimised J and satisfied the differential equations. Dr Balakrishnan went on to prove that, for a certain class of problems, if the problem was soluble by the gradient method then it was also soluble by this method. In order to simplify the problem, the integrals in the function K were replaced by sums of the relevant terms at a number of intervals throughout the trajectory.

In our formulation of the minimum time problem we use five differential equations. The three shown in Figure 2 are those actually used within the Balakrishnan Method. In contrast to the N.A.S.A. team, we have included the flight path angle as a state variable and use the incidence as the control variable. This allows the inclusion of the full form of the equation of motion normal to the flight path. During each iteration of the program the mass equation is integrated using a simple form of Simpson's Rule and this has proved very satisfactory. At the output of the final trajectory the range equation is also integrated by the same method. Initial and final conditions on the speed, altitude and flight path angle are specified by the user although these constraints can be relaxed as shown later. Also on Figure 2 is the form of the optimisation function for this problem.

Figure 3 shows the manner in which the state and control variables are represented. In order to make the problem amenable to solution on a digital computer, trigonometric series are used. The state variables are represented by a linear term plus a sine series, thus ensuring that the terminal constraints are satisfied. For the control variable it is assumed that the terminal conditions are not known, so a constant term plus a cosine series is used. Because the method has very satisfactory convergence properties it is possible for the initial guess to set the coefficients of the trigonometric series to zero. This is in direct contrast to the gradient method where a very accurate first guess is necessary. The method of optimisation used is a first order Newton-Raphson method. Initially only the flight time was used as a convergence criterion but, since this occasionally caused false convergence, the value of the optimisation function is also checked now. One possible limitation is the lack of an engine control parameter.

This is of no significance in climb and acceleration cases but could be important in descents. Since these latter cases are very rare, it was decided this facility should not be included. It is possible to include time, speed or height dependent limitations on engine ratings however.

At this point the program seemed to be at the same stage of development as the N.A.S.A. program. Unfortunately, although convergence was achieved for some cases, the solution was obviously incorrect. On examining the results it became obvious that this was due to a problem in the optimisation function. Because the terms from the errors in the differential equations all carry the same weighting in this function, the errors in the equations tend to be of the same order. Since the derivatives themselves are of vastly different orders, this causes very large errors in some derivatives. To remedy this problem the optimisation function was changed from the first form shown in Figure 4 to the second and this solution has proved successful.

During their studies the N.A.S.A. team had stability problems with the optimisation process and, on the advice of Dr Balakrishnan, inserted a constant in the Newton-Raphson method to remedy this. We found that this was insufficient as the constant required was problem dependent. From a study of the constant required for convergence in several cases, we produced a function of the initial and final conditions of a case which gave a constant almost always ensuring convergence.

Figure 5 shows typical results produced by the program at this stage of development for a project aircraft. These appear similar to the general type of curves generated by minimum time processes. On closer inspection however of the flight path numbered three, it is seen that the climb angle in the later portions of the flight was very great. In order to check more easily the accuracy of the program in these areas, a level acceleration case was considered. This showed that at very low specific excess power quite substantial errors were present in our solution. Since the method depends on the minimisation of a sum of error terms, it is inevitable that errors are present in the final solution; and since only the numerical value of the error is considered, the relative value of the error will be greater at low SEP. In order to remove this source of error, a correction procedure was used when the final trajectory was computed. In this process the time for a portion of the trajectory is factored by the ratio of the demanded and available SEP during that portion. Although this process inevitably moves the solution slightly away from the optimum, it is felt that its inclusion is necessary. Figure 6 shows a comparison of the trajectories for a particular case before and after correction. It is interesting to note that in this case of a climb to 50000 ft. the change in time is of the order of 25%, whereas in a climb to 36000 ft. the change is less than 1%. There is still a problem with this procedure if the demanded and available SEP have different signs, since a negative factor cannot be used.

We have a large amount of work which we would like to do in the future in connection with this project. It is always very difficult to check that a supposed optimum calculated numerically is in fact a true optimum. As a first stage in checking this program, we intend to write a program to integrate the equations of motion to check the consistency of the output trajectory. This integration would probably be controlled by the Mach number altitude relationship and the other variables such as flight path angle and range would be compared with those output from the optimisation program. A further use of such a program would be to study the use of non-optimum trajectories since it is usually impossible in practice to fly optimum trajectories. Work is also now going on in certain countries on the use of inflight computation of near optimum trajectories and this also would be a profitable field of study. The obvious check on results from such a program as this is to physically fly them and it is hoped to do this shortly. For this purpose accurate input data is obviously necessary and, when this is available, trajectories will be computed and flown. Mathematically we are now looking at the possibility of writing a minimum fuel trajectory program. A program has been written to calculate both minimum time and minimum fuel trajectories, but no development of the latter facility has taken place. In Figure 7 the changes necessary to the method for this purpose are summarised. Firstly, the mass equation must be included within the Balakrishnan process and hence the mass must be represented by a trigonometric series. This creates difficulties since the initial but not the final value is known. In order to overcome this problem the mass is represented in the same way as the other state variables, but the final mass is treated as a variable in the optimisation. This points the way as mentioned previously to the solution of cases with one or more end constraints removed. Finally, Figure 7 shows the new optimisation function for both time and fuel cases with a new weighting factor for the mass equation term.

REFERENCE

1. Taylor, L.W.
et al. Experience using Balakrishnan's Epsilon Technique to compute optimum flight profiles. AIAA Paper 69-75; 1969.

$$\begin{aligned}\frac{dx_i}{dt} &= f(x, \alpha) \quad x(0) = x_0 \quad x(T) = x_T \\ J &= \int_0^T g(x, \alpha) dt \\ K &= \frac{1}{2} \int_0^T \sum_i \left(\frac{dx_i}{dt} - f(x, \alpha) \right)^2 dt + \int_0^T g(x, \alpha) dt \\ K &= \frac{1}{2} \sum_i^N \sum_i \left(\frac{dx_i}{dt} - f(x, \alpha) \right)^2 \Delta t + \sum_i^N g(x, \alpha) \Delta t\end{aligned}$$

Fig.1 Balakrishnan Method

$$\begin{aligned}\frac{dv}{dt} &= \frac{T \cos(\alpha + \phi) - D}{m} - g \sin(\gamma) \\ \frac{dh}{dt} &= v \sin(\gamma) \\ \frac{d\gamma}{dt} &= \frac{T \sin(\alpha + \phi) + L}{mv} - \frac{g \cos(\gamma)}{v} \\ K &= \frac{1}{2} \sum_i^N \left[\left(\frac{dv}{dt} - \frac{T \cos(\alpha + \phi) - D}{m} + g \sin(\gamma) \right)^2 \right. \\ &\quad \left. + \left(\frac{dh}{dt} - v \sin(\gamma) \right)^2 \right. \\ &\quad \left. + \left(\frac{d\gamma}{dt} - \frac{T \sin(\alpha + \phi) + L}{mv} + \frac{g \cos(\gamma)}{v} \right)^2 \right] \Delta t \\ &\quad + \sum_i^N \Delta t\end{aligned}$$

Fig.2 Minimum time trajectory problem

$$\begin{aligned}v &= v_0 + (v_T - v_0) \frac{t}{T} + \sum_i^M a_J \sin\left(\frac{J\pi t}{T}\right) \\ \alpha &= \alpha_0 + \sum_i^M b_J \cos\left(\frac{J\pi t}{T}\right)\end{aligned}$$

Fig.3 Representation of variables

$$K = \frac{1}{\varepsilon} \sum_i^N \left[\left(\frac{dv}{dt} - \frac{T \cos(\alpha + \phi) - D}{m} + g \sin(\gamma) \right)^2 \right. \\
+ \left(\frac{dh}{dt} - v \sin(\gamma) \right)^2 \\
+ \left. \left(\frac{d\gamma}{dt} - \frac{T \sin(\alpha + \phi) + L}{mv} + \frac{g \cos(\gamma)}{v} \right)^2 \right] \Delta t \\
+ \sum_i^N \Delta t$$

$$K = \sum_i^N \left[\frac{1}{\varepsilon_1} \left(\frac{dv}{dt} - \frac{T \cos(\alpha + \phi) - D}{m} + g \sin(\gamma) \right)^2 \right. \\
+ \frac{1}{\varepsilon_2} \left(\frac{dh}{dt} - v \sin(\gamma) \right)^2 \\
+ \left. \frac{1}{\varepsilon_3} \left(\frac{d\gamma}{dt} - \frac{T \sin(\alpha + \phi) + L}{mv} + \frac{g \cos(\gamma)}{v} \right)^2 \right] \Delta t \\
+ \sum_i^N \Delta t$$

Fig.4 Revised optimisation function

TIME/FUEL USED						
CASE	INITIAL		FINAL		TIME SEC	FUEL USED LB
	MACH NO.	ALTITUDE	MACH NO.	ALTITUDE		
1	.4	0	.9	36,089	123	945
2	.4	0	1.5	36,089	254	1,870
3	.4	0	1.5	50,000	340	2,375
4	.4	0	.9	10,000	50	500

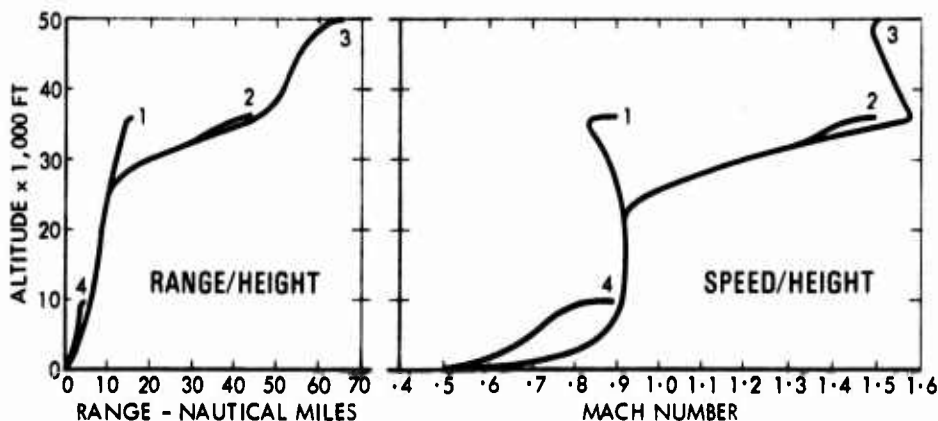


Fig.5 Typical program output

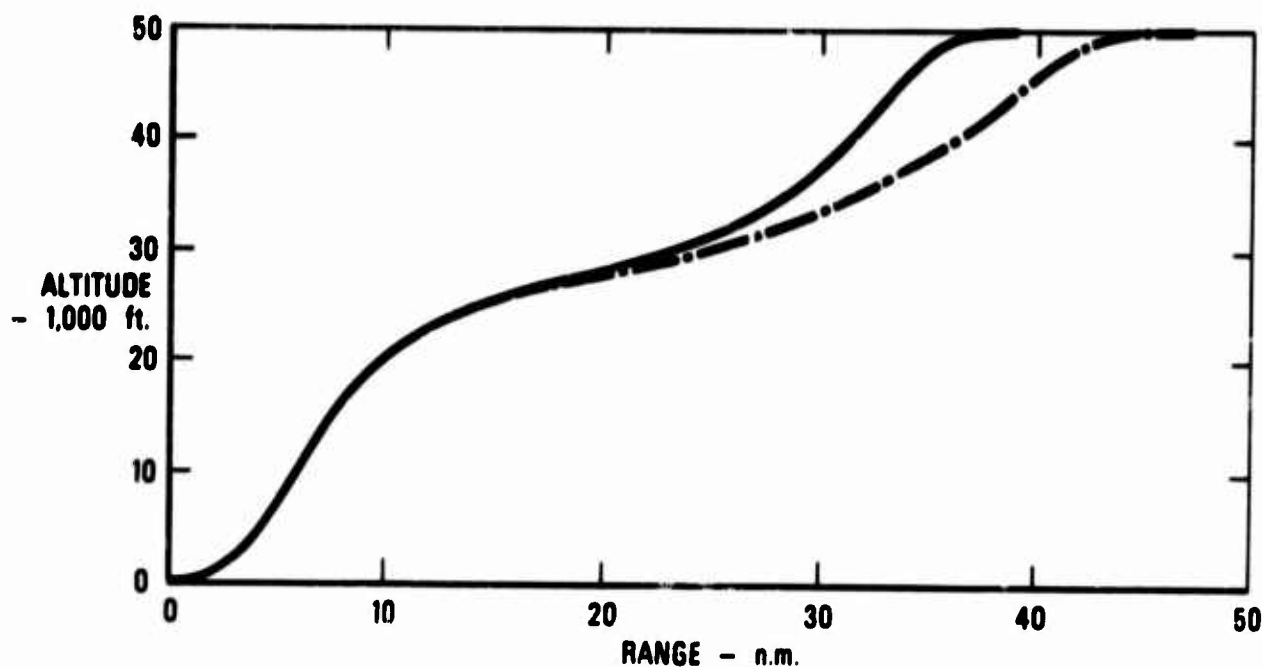


Fig.6 Effect of error correction procedure

$$\frac{dm}{dt} = -F_e$$

$$m = m_c + (m_T - m_0) \frac{t}{T} + \sum_1^M a_J \sin\left(\frac{J \pi t}{T}\right)$$

$$K = \sum_1^N \left[\frac{1}{\varepsilon_1} \left(\frac{dv}{dt} - \frac{T \cos(\alpha + \phi) - D}{m} + g \sin(\gamma) \right)^2 \right. \\ + \frac{1}{\varepsilon_2} \left(\frac{dh}{dt} - v \sin(\gamma) \right)^2 \\ + \frac{1}{\varepsilon_3} \left(\frac{d\delta}{dt} - \frac{T \sin(\alpha + \phi) + L}{mv} + \frac{g \cos(\gamma)}{v} \right)^2 \\ \left. + \frac{1}{\varepsilon_4} \left(\frac{dm}{dt} + F_e \right)^2 \right] \Delta t \\ + \left\{ \begin{array}{l} \sum_1^N \Delta t \\ \sum_1^N F_e \Delta t \end{array} \right\} \begin{array}{l} \text{minimum time} \\ \text{minimum fuel} \end{array}$$

Fig.7 Minimum fuel problem

REVIEW OF TWO METHODS OF OPTIMISING AIRCRAFT DESIGN

by

D.L.I. Kirkpatrick

**Royal Aircraft Establishment,
Farnborough, Hampshire, UK**

SUMMARY

This paper outlines two methods of optimising aircraft design which have been developed at the RAE. One of these is an analytical method of optimising three of the principal design variables of a subsonic swept-wing jet transport aircraft, and demonstrates broadly how the optimum design is affected by changes in the mission requirements, the operational constraints and the assumed design standards. The second method uses an aircraft design program coupled with the multivariate analysis technique to optimise 15 aircraft design variables, using complex and detailed equations to represent the aerodynamic characteristics of the wing and high-lift devices, the masses of all the various aircraft components and the engine performance. This method yields rapid and accurate assessments of the effects on the optimum aircraft design of changes in requirements, constraints and design standards, including, for example, advanced wing design, take-off and landing distance requirements and various noise-reduction techniques.

CONTENTS

	Page
SUMMARY	12
1. INTRODUCTION	12-1
2. ANALYTICAL OPTIMISATION	12-1
2.1 Assumptions	12-1
2.2 Discussion of Results	12-4
3. MULTIVARIATE ANALYSIS	12-5
4. CONCLUDING REMARKS	12-6
TABLES	12-7
FIGURES	12-8

REVIEW OF TWO METHODS OF OPTIMISING AIRCRAFT DESIGN

D.L.I.Kirkpatrick

1. INTRODUCTION

One of the purposes of Projects Division of Aerodynamics Department at the Royal Aircraft Establishment is to assess the effect on aircraft design of advances in aeronautical research, such as the development of supercritical aerofoil sections, carbon-fibre-reinforced plastics or high-bypass-ratio engines, and also to identify those areas in which successful research would lead to a significant increase in the operating efficiency of one or all of the ever-changing array of aircraft projects. To enable this purpose to be achieved efficiently, a group within Projects Division has during the last few years developed two methods of optimising the design of swept-wing jet transport aircraft to meet a chosen range/payload specification.

One of these is a simple analytical method of optimising three of the principal aircraft design variables, the wing loading, the aspect ratio and the engine-weight fraction, to give the maximum value of the payload fraction. This method uses simple empirical expressions for the aerodynamic characteristics, structure weight and engine performance so the results are not absolutely accurate; but they do provide a useful insight into the complex interactions between the aircraft design variables and the assumed values of aerodynamic, structural and engine coefficients and into the effects on the optimum design of operational constraints, such as the need to carry fuel reserves and to limit the approach speed.

The other method uses an aircraft design program coupled with the multi-variate analysis technique to find the optimum values of 15 design variables which yield the minimum value of the direct operating cost, or of some other criterion of efficiency, and simultaneously satisfy several design constraints. This method uses a more detailed flight plan and much more complex expressions for the aerodynamic characteristics of wings, flaps and slats, for the engine performance and for the weights of the various components of the optimum aircraft. Because multi-variate analysis can successfully optimise a large number of design variables, this method provides rapid and accurate estimates of the effect on the optimum design of an aircraft project of changing the specified mission or the design constraints or of advances in aeronautical technology.

2. ANALYTICAL OPTIMISATION

2.1 Assumptions

In the analytical optimisation, it is assumed that the weights of certain components of an aircraft, such as the undercarriage, the tail unit and the systems, are proportional to the take-off weight W and that the weights of other components, such as the fuselage and furnishings, are proportional to the payload W_p , as presented in the table below:

<i>Symbol</i>	<i>Estimate</i>	<i>Component</i>
W_{UC}	0.05 W	undercarriage
W_T	0.02 W	tail unit
W_S	0.05 W	systems
W_P		payload
W_{FUS}	0.75 W_p	fuselage
W_{FUR}	0.60 W_p	furnishings
W_W		wing
W_E		engine
W_F		fuel

The payload fraction W_P/W may then be written as a function of the wing-weights, engine-weight and fuel-weight fractions,

$$W = a_1 W + a_2 W_P + W_W + W_E + W_F;$$

therefore

$$\frac{W_P}{W} = \frac{1}{a_2} \left[1 - a_1 - \frac{W_W}{W} - \frac{W_E}{W} - \frac{W_F}{W} \right].$$

Using the assumptions presented below, these three fractions can be written in terms of the design variables, viz. the wing loading, aspect-ratio and engine-weight fraction, and of the design parameters which define the assumed aerodynamic drag, structure weight, engine performance and the specified mission.

Design variables

Wing loading W/S

Aspect-ratio A

Engine - weight fraction W_E/W .

Design parameters

Wing profile drag

Fuselage and nacelle drag

Induced drag factor

} Aerodynamics

Engine thrust/weight ratio

Cruise specific fuel consumption

Hold specific fuel consumption

} Powerplant

Wing-box weight parameter

High-lift devices weight parameters

} Structures

Cruise speed

Take-off weight

Range

} Mission

For chosen values of the design parameters, the maximum value of the payload fraction occurs when the design variables satisfy the three equations which form the optimisation criterion:

$$0 = \frac{\partial}{\partial A} \left(\frac{W_P}{W} \right) = \frac{\partial}{\partial W/S} \left(\frac{W_P}{W} \right) = \frac{\partial}{\partial W_E/W} \left(\frac{W_P}{W} \right).$$

The analytical optimisation method depends on assumptions which permit the profile drag of an aircraft and its wing-weight, engine-weight and fuel-weight fractions to be expressed as functions of the three design variables. It is assumed that the profile drag coefficient C_{DO} of the aircraft is given by the sum of the drag coefficients of the wing, fuselage and nacelles and that the drag of the fuselage and nacelles can be rewritten as the product of the wing loading and a parameter C which depends on the fuselage area/unit payload, the payload fraction, the nacelle wetted area/unit thrust, the thrust/weight ratio and the coefficients C_1 and C_2 which include the appropriate skin friction coefficients, form factors and interference factors.

$$\begin{aligned} C_{DO} &= C_{DW} + C_{D/FUS} + C_{D/NAC} \\ &= C_{DW} + C_1 \frac{S_{FUS}}{W_P} \frac{W_P}{W} \frac{W}{S} + C_2 \frac{S_{NAC}}{T} \frac{T}{W} \frac{W}{S} \\ &= C_{DW} + C \frac{W}{S}. \end{aligned}$$

The net thrust T from a given engine at a chosen cruise speed is assumed to be proportional to the air density so that T/ρ is constant. It is also assumed that the installed weight W_E of an engine is directly proportional to the cruise thrust at a given altitude,

$$W_E = E(T/\rho).$$

If the aircraft does not carry fuel reserves, its fuel fraction is given by the Breguet range equation

$$\frac{W_F}{W} = 1 - e^{-r},$$

where

$$r = \frac{c}{V} \left(\frac{D}{L} \right)_{\alpha} R = \frac{2c}{Vn} \sqrt{\frac{KC_{DO}}{\pi A}} R$$

and c is the specific fuel consumption, V is the cruise speed and R is the range. If the aircraft does carry fuel reserves, the fuel fraction is made up of cruise fuel, diversion fuel and hold fuel so that

$$\frac{W_F}{W} = \frac{W_{FC}}{W} + \frac{W_{FD}}{W} + \frac{W_{FH}}{W}.$$

Assuming that the aircraft is flown at cruising speed for the specified diversion distance R_{div} and at minimum drag speed for the specified holding time t_H , the fuel fraction is given by an expression including the specific fuel consumption in cruise and in hold, the profile drag coefficient C_{DO} , the lift-dependent drag factor K and the aspect ratio A :

$$\begin{aligned} \frac{W_F}{W} &= \frac{W_{FC}}{W} + \frac{W_{FD}}{W} + c_H t_H \left(\frac{D}{L} \right)_{\min} \left(1 - \frac{W_{FC}}{W} - \frac{W_{FD}}{W} \right) \\ &= 1 - e^{-r} \left(1 - 2c_H t_H \sqrt{\frac{KC_{DO}}{\pi A}} \right). \end{aligned}$$

where

$$r = \frac{2c}{Vn} \sqrt{\frac{KC_{DO}}{\pi A}} (R + R_{div}).$$

Gabrielli's formula for wing weight,

$$W_w = k_1 W A b + k_2 S,$$

therefore

$$\frac{W_w}{W} = k_1 \sqrt{SA^3} + k_2 S/W,$$

provides an estimate of the wing-weight fraction for a wing box with structural efficiency k_1 and a specified set of high-lift devices whose weight/unit area is k_2 . The presence of the wing area S in the wing-box term introduces the square-cube law into the analysis so that the wing-weight fraction increases with aircraft size. An alternative, and more realistic, formula assumes that the complexity and weight of the high-lift devices is proportional to the approach lift coefficient; then, for a given approach speed, k_2 is proportional to the approach wing loading

$$k_2 = k_3 \frac{W}{S} \left(1 - \frac{W_{FC}}{W} \right)$$

and the wing-weight fraction is given by an equation which includes the cruise fuel fraction

$$\frac{W_w}{W} = k_1 \sqrt{SA^3} + k_3 \left(1 - \frac{W_{FC}}{W} \right).$$

In practice the value C_{La} of the approach lift coefficient which can be achieved at any point in time is limited by the state of aerodynamic knowledge and structural technology at that time, so for a given approach speed the approach wing loading is limited,

$$\frac{W}{S} \left(1 - \frac{W_{FC}}{W} \right) \leq q_a C_{La}.$$

If the approach wing loading is set equal to its limiting value, the wing-weight fraction is given by an equation which includes the cruise fuel fraction in both terms,

$$\frac{W_w}{W} = k_1 \sqrt{WA^3} \left[\left(1 - \frac{W_{FC}}{W} \right) / q_a C_{La} \right]^{1/2} + k_3 \left(1 - \frac{W_{FC}}{W} \right).$$

2.2 Discussion of Results

These assumptions can now be used, in conjunction with a typical set of design parameters, to discover the optimum aircraft configurations for different ranges and how these optimum configurations are affected by limitations on the approach speed or on the approach wing loading, or by the need to carry fuel reserves.

If it is assumed that the aircraft carries no fuel reserves and the high-lift devices governing the approach lift coefficient are specified (method I), then the wing-weight, engine-weight and fuel-weight fractions which give the maximum payload fraction for given ranges can be calculated. Figure 1 shows that the optimum aircraft, calculated using the assumptions of method I, has high wing loading and low aspect-ratio at short ranges to give low wing-box weight, whereas at long ranges where the fuel fraction is more important the optimum aircraft has a large wing and higher aspect-ratio to give good cruise efficiency at high altitudes. But since the approach lift coefficient is fixed by the choice of high-lift devices, the high values of wing loading are accompanied by unacceptably high approach speeds, in excess of 250 knots at the shorter ranges.

In method II it is assumed that the approach speed is fixed at an acceptably low value, and that the complexity and weight of the high-lift devices are directly proportional to the approach lift coefficient required, as discussed above. Figure 1 shows that the optimum aircraft design calculated using this set of assumptions has lower wing loading to avoid the need for very large and heavy high-lift devices, lower aspect-ratio to prevent the increased wing area leading to an excessive increase in wing-box weight, and larger engines to drive the larger wing along at the same cruise speed. The payload fraction is slightly smaller at short ranges.

It is now assumed in method III that the aircraft must carry standard fuel reserves so that the fuel-weight fraction is given by an equation including the specified diversion distance and holding time. Figure 1 shows that the optimum aircraft design variables calculated using the third set of assumptions have lower wing loading to reduce the profile drag coefficient and higher aspect-ratio to reduce the induced drag coefficient; both these effects lead to a higher maximum lift/drag ratio and reduced fuel consumption in the holding phase. The need for fuel reserves has more effect at short ranges where the reserves form a considerable proportion of the total fuel carried.

In calculations based on the second and third set of assumptions, the approach lift coefficient was allowed to assume its optimum value, however large this value might be. In method IV it is assumed that the approach lift coefficient is limited so that the take-off wing loading is a function of the approach lift coefficient, the approach speed and the cruise fuel fraction. The optimum design variables calculated using the fourth set of assumptions were plotted in Figure 1 and suggest that long-range aircraft can be designed with the optimum wing loading but short-range aircraft must have a lower than optimum wing loading because of the limitation on the approach lift coefficient.

Figure 1 shows the effects on the optimum values of the design variables of limited approach speed, of fuel reserves and of limited approach lift coefficient, but it does not provide a realistic estimate of how the optimum design variables for aircraft projects vary with range because *these* curves have been calculated using *fixed* values of the design parameters whereas in fact some of these parameters vary with range.

To discover whether this simple analytical optimisation method accurately reflects the fundamental features of the design of swept-wing transport aircraft, a set of design parameters were chosen to represent the situation around 1960, and the variation with range of the optimum values of the design variables was calculated by method III, assuming fixed approach speed, and by method IV, assuming fixed approach wing loading. In this calculation the fuselage and nacelle drag parameter C was related to the payload fraction W_p/W , and the payload W_p was related to the range by the two equations

$$C = 0.0006 + 0.0096W_p/W$$

$$W_p \propto \sqrt[3]{R}.$$

The first equation takes account of the fact that aircraft with large fuselages also have large values of profile drag coefficient, and the second of the fact that aircraft designed for long ranges must be large to reduce their operating cost/seat mile whereas at short ranges frequency of service, which leads to smaller aircraft, is comparatively more important. Figure 2 compares the design characteristics predicted using methods III and IV with those of real aircraft, and suggests that the aircraft which entered service around 1960 were designed by method IV, assuming fixed approach wing loading, so that their wing loading increases with range. The predicted optimum aspect-ratio and the aspect-ratios of real aircraft do not vary significantly with range because at long ranges, where high aspect-ratios with good aerodynamic efficiency are desirable, the aircraft are large and their aspect-ratio is reduced by the square-cube law. The predicted optimum engine-weight fraction and the engine weight fractions of real aircraft tend to decrease with increasing range because the higher wing loading of long-range aircraft reduces the cruise thrust required. This figure suggests that, despite the comparative simplicity of its assumptions, the analytical method gives reasonably accurate estimates of the optimum values of the design variables.

Having demonstrated that this analysis does include the principal factors in the aircraft design procedure, it is interesting to look some years into the future and to calculate the optimum variables for an aircraft which might enter service about 1980. For this calculation a new set of design parameters was chosen to represent the situation around 1980, assuming increases in the required cruise speed and payload, decreases in the structure weight coefficients and in the specific fuel consumption, and improvements in the design of aerofoil sections and high-lift devices. Figure 3 shows the optimum design variables for 1980 and compares them with the 1960 values. This comparison suggests that by 1980 improved high-lift devices will permit aircraft for most ranges to be designed with their optimum wing loading and only ultra-short range aircraft will have designs constrained by limits on approach wing loading. The assumed payloads of the 1980 aircraft were greater by a factor of about 5 than those of the 1960 aircraft, but the optimum aspect-ratios predicted for the 1980 aircraft are not very different from those of 1960 aircraft, because the effects of the square-cube law are partially counterbalanced by the assumed improvements in structural materials and design. The static thrust/weight ratio of the predicted 1980 aircraft is considerably higher than the values for 1960, because the higher cruise speed assumed for 1980 requires higher cruise thrust and because the high-bypass-ratio engines chosen for the 1980 aircraft have a larger static thrust/cruise thrust ratio than 1960 engines. The payload fraction is predicted to improve by about 7% at short ranges and 30% at long ranges.

The analytical optimisation method thus provides a simple method of assessing the effects of operational constraints, estimating the effects of changes in the design parameters, of correlating the characteristics of existing aircraft and of predicting the probable optimum characteristics of future aircraft.

3. MULTIVARIATE ANALYSIS

The second method of aircraft optimisation which has been developed in Projects Division at RAE uses the multivariate analysis technique to optimise 15 design variables to give the minimum value of the direct operating cost or some other chosen objective function. Figure 4 shows the configuration of a typical short-range jet transport and presents the 15 design variables (wing area, aspect-ratio, taper-ratio, sweep and thickness, engine size, tail size, flap chord and span, slat chord and span, flap and slat deflections at take-off and landing, speed, altitude, design C_L , and design Mach number) used in the multivariate analysis. Because the multivariate analysis program is at present directed principally towards optimising the geometry of the wing and high-lift devices, this geometry is specified in more detail than other parts of the aircraft; for example only the size of the engine is varied in the optimisation while its bypass ratio, fan pressure ratio, etc. are fixed. However there is no fundamental reason why a future version of the program should not include optimisation of the engine design, provided that the appropriate equations linking engine performance, size and weight can be formulated.

Figure 5 presents the layout of the program and shows that the optimisation program must be supplied with a chosen objective function (the aircraft all-up mass, the first cost and the direct operating cost have all been used) and that the design program must be supplied with chosen mission requirements and operational constraints, as well as with information on the aerodynamic, structural and engine design standards. This information must include sufficient data for the design program to calculate the performance, weight and cost of the various aircraft designs. Using coefficients in the input data, the design program calculates the aircraft cruise drag as a function of the wing geometry, i.e. aspect-ratio, sweepback, thickness, aerofoil section and design Mach number, and the cruise conditions, i.e. the cruise Mach number, the Reynolds number and the lift coefficient. The lift and drag coefficients at take-off and landing are calculated as functions of the geometry of the wing, i.e. aspect-ratio, sweepback, thickness and taper-ratio, and of the geometry of the high-lift devices, i.e. flap chord, flap span and flap deflection, slat chord and slat deflection. It would take a long time to describe in detail either these performance calculations or the weight break-down used in the multivariate analysis, but some idea of the complexity of the latter can be obtained by considering, as an example, the weight of the wing-box structure. In the analytical optimisation the wing-box weight is estimated from one term including only the wing area, the aspect-ratio and an empirical coefficient, but in the multivariate analysis optimisation the wing-box weight is given by the sum of the weights of the box covers, the spar webs, the ribs, the joints, the wing tip and the undercarriage support structure and the weights of these 6 components are calculated independently as functions of the wing-box chord, the wing area, aspect-ratio, thickness, sweepback, taper-ratio, load factor and eleven empirical coefficients.

The optimum aircraft design calculated by the multivariate analysis program must satisfy several design constraints as well as meeting the payload/range specification. These constraints include:—

- approach speed \leq a specified value related to the landing distance
- take-off distance \leq specified take-off distance
- engine-failed climb gradient \geq value given in airworthiness regulations
- volume in the wing-box \geq volume of fuel carried.

To test the multivariate optimisation program, it was used to design a 100 seat short-range jet transport aircraft similar to the BAC 111, DC 9 and Boeing 737. Typical values, for this class of aircraft, of the payload, range, fuel reserves, take-off distance, approach speed and cruise conditions were chosen and the optimum aircraft configurations were calculated using three alternative objective functions. Table 1 shows that the predicted values of some of the design variables, of the empty weight and of the all-up weight are not significantly affected by the choice of the objective function and are close to the values for real aircraft. One noticeable feature of this table is that the wing areas of real aircraft are about 10% greater, and the aspect-ratios correspondingly smaller, than the calculated optimum values. Half of this discrepancy can be attributed to the fact that the calculated values quoted are trapezoidal areas whereas the tabulated areas for real aircraft are gross areas, which include extra areas inboard of the trailing-edge crank; the other half arises because the optimum with respect to wing area is fairly flat and in practice it is sensible to choose a wing area slightly greater than optimum in order to provide an adequate buffet margin and to allow for future stretch to a higher all-up weight.

As an example of the results from the multivariate analysis program, Table 2 shows the effects on the optimum aircraft design of changing the cruise speed at a given altitude. As the specified cruise speed increases, the wings become thinner and more highly swept; this reduces their maximum lift coefficient at low speed so the wing area must be increased to maintain the same landing speed; the span is kept approximately constant to maintain the climb performance after take-off; the fuel used rises as the cruise lift/drag ratio deteriorates, and the operating cost rises with speed.

As another example of the results from the multivariate analysis, Table 3 shows the effect of fuel price on the optimum aircraft configuration, for fixed values of cruise speed and altitude. The current price of fuel is about 0.014 £/kg, and halving and doubling of this price were considered. The main effect of increasing fuel price is to increase the wing aspect-ratio giving a better value of lift/drag ratio in cruise and reducing the fuel mass at the expense of an increase in wing mass.

After formulating the equations in the aircraft design program and choosing the coefficients which specify design standards in the input data, the most difficult problem lies in the choice of the objective functions. In the early stages of program development, the minimum all-up mass and the minimum first cost were used as optimising functions, but these functions do not accurately reflect the operating efficiency of the aircraft. The direct operating cost, which includes depreciation, maintenance, fuel, crew costs and landing fees, was then used as an optimising function but this does not fully recognise the importance of speed and yields an aircraft with a low cruise speed. Using minimum passenger cost, equal to the fare paid by the passenger plus the value of the time of his journey, as the optimising function gives a much faster aircraft with only a small increase in operating costs. The optimising function of principal interest to an airline is its profits, which are revenue minus costs, and the revenue is proportional to the load factor which is affected by block time, ride comfort, cabin noise, etc. Another plausible optimising function is the 'social benefit', which is composed of operating costs and the value of the aircraft's noise footprint. Systematic and detailed comparison of the aircraft designs optimised using these different functions is revealing the essential features underlying the design of a successful aircraft.

4. CONCLUDING REMARKS

The two optimisation methods I have described perform two complementary functions. The analytical optimisation, with simple equations defining the optimum aircraft configuration in terms of the design parameters, provides some physical insight into the fundamental features of aircraft design. It may be used either to correlate the designs of current aircraft or to predict the designs of future aircraft, and also to help interpret the results of the more complex multivariate optimisation process.

The studies using the multivariate analysis technique have demonstrated that the design equations normally used in project studies can, when cast in the right form, be put together to form an aircraft design program and that an optimisation technique can be successfully applied to such a program. This technique provides a rapid means of calculating an optimum aircraft design for a given set of mission requirements, operating constraints and design standards and of evaluating the effects on this design of change in the requirements, constraints or standards. At present the program is being used to assess the effects of advanced wing designs, of take-off and landing distance requirements and of various noise reduction techniques.

Table 1

		Minimum operating cost	Minimum first cost	Minimum all-up mass	A	Aircraft B	C
Wing area	m ²	83.9	83.6	80.8	95.8	93.0	91.1
Wing span	m	30.2	27.5	28.8	28.8	28.5	28.4
Aspect-ratio		10.8	9.0	10.3	8.5	8.7	8.8
Sweepback	deg	26.3	23.1	28.0	20.0	24.0	25.0
Thickness/chord		0.119	0.113	0.134	0.110	0.116	0.129
Empty mass	kg	24150	23651	23780	~24450	~24500	~25400
All-up mass	kg	44218	44262	44095	45200	44450	45575
First cost	M£	1.852	1.837	1.845	~2	~2	~2
Operating cost	p/seat km	0.2765	0.2789	0.2776			

Table 2

Cruise Mach Number		0.75	0.80	0.85
Wing area	m ²	75.9	83.9	98.5
Wing span	m	30.8	30.2	29.9
Aspect-ratio		12.5	10.8	9.1
Sweepback	deg	15.0	26.3	32.4
Thickness/chord ratio		0.126	0.119	0.109
Approach lift coefficient		1.82	1.73	1.59
Cruise lift/drag ratio		14.2	13.1	11.9
Powerplant mass	kg	2950	3299	3909
Fuel mass	kg	8046	8758	9913
All-up mass	kg	41770	44220	47900
Operating cost	p/seat km	0.2682	0.2765	0.2933

Table 3

Fuel price		£/kg	0.007	0.014	0.028
Wing area	m ²		83.1	83.9	84.0
Wing span	m		29.4	30.2	31.4
Aspect-ratio			10.4	10.8	11.7
Sweepback	deg		26.1	26.3	28.1
Thickness/chord ratio			0.121	0.119	0.124
Cruise lift/drag ratio			12.88	13.13	13.51
Wing mass	kg		4972	5229	5627
Fuel mass	kg		8881	8758	8581
All-up mass	kg		44140	44220	44380
Operating cost	p/seat km		0.2536	0.2765	0.3216

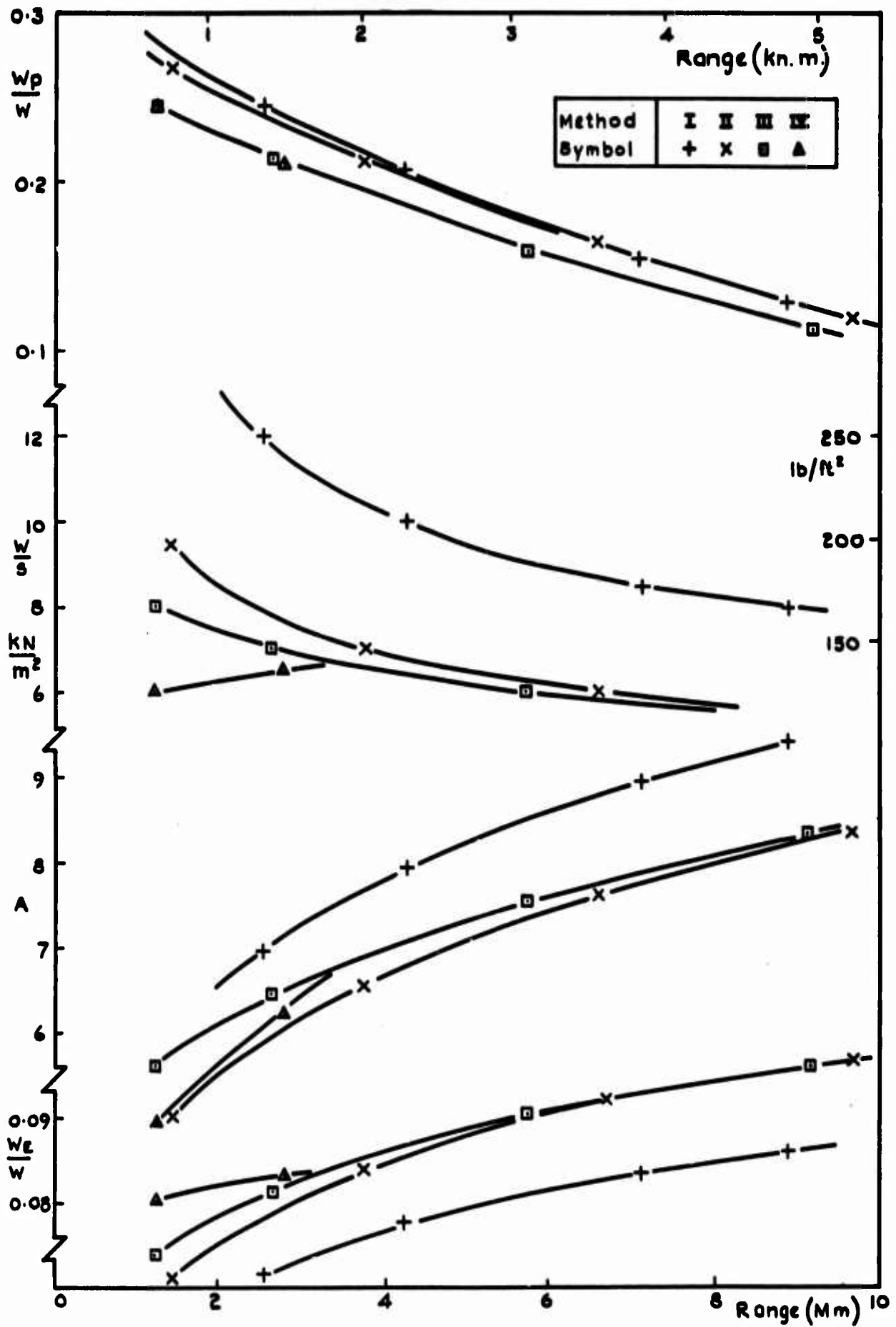


Fig.1 Predicted design characteristics of datum aircraft.

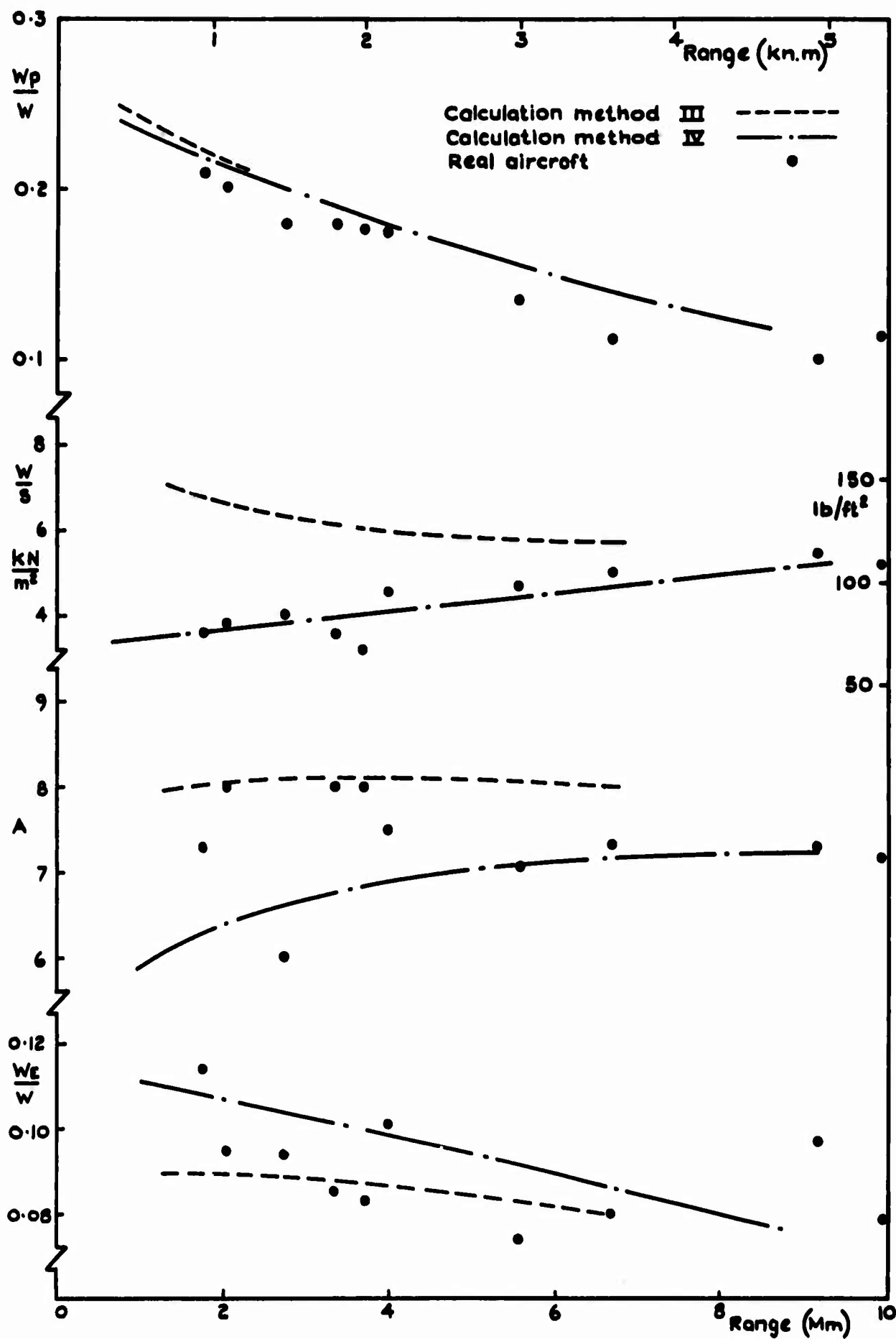


Fig.2 Predicted and actual characteristics of 1960 aircraft.

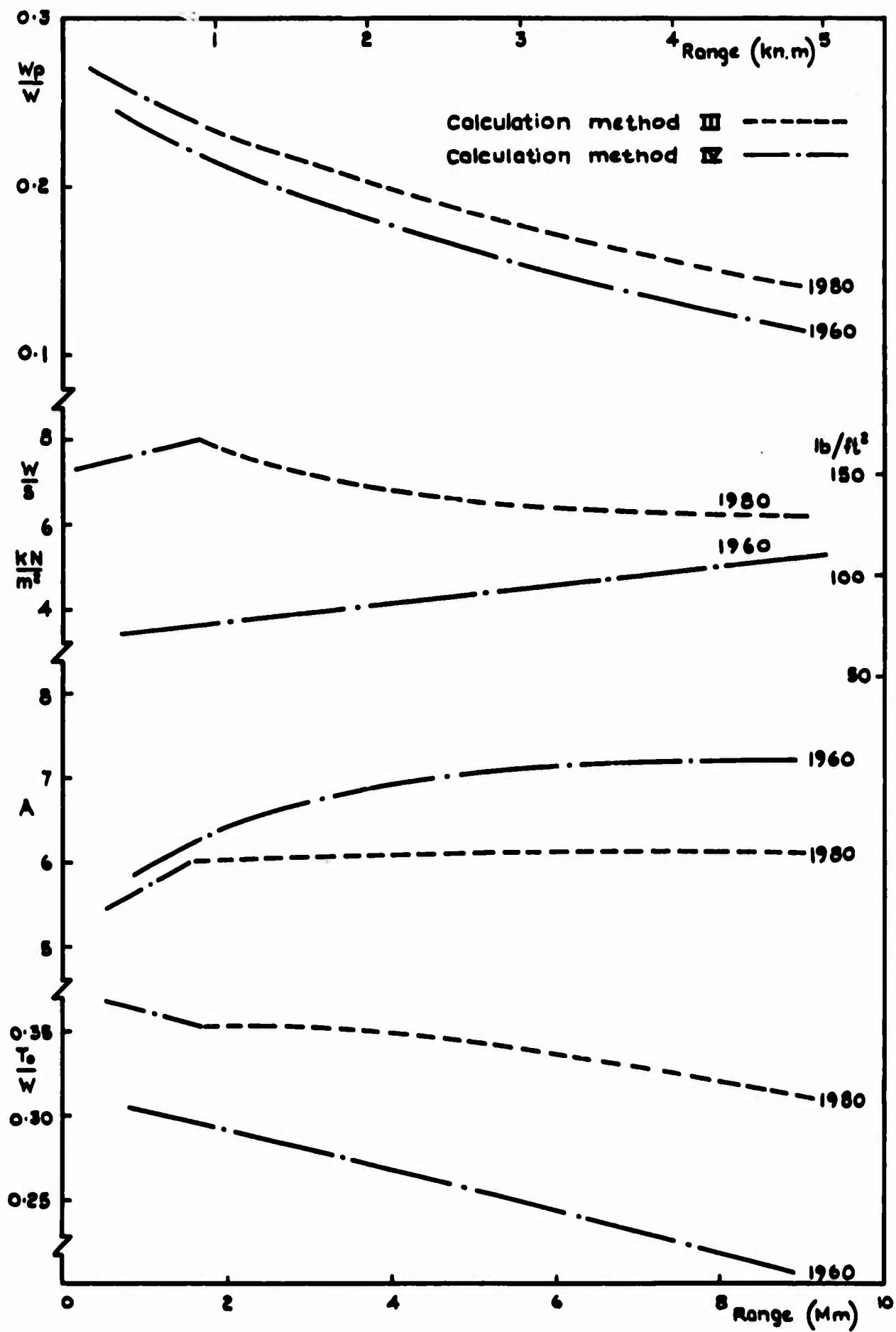


Fig.3 Predicted designs of 1960 and 1980 aircraft.

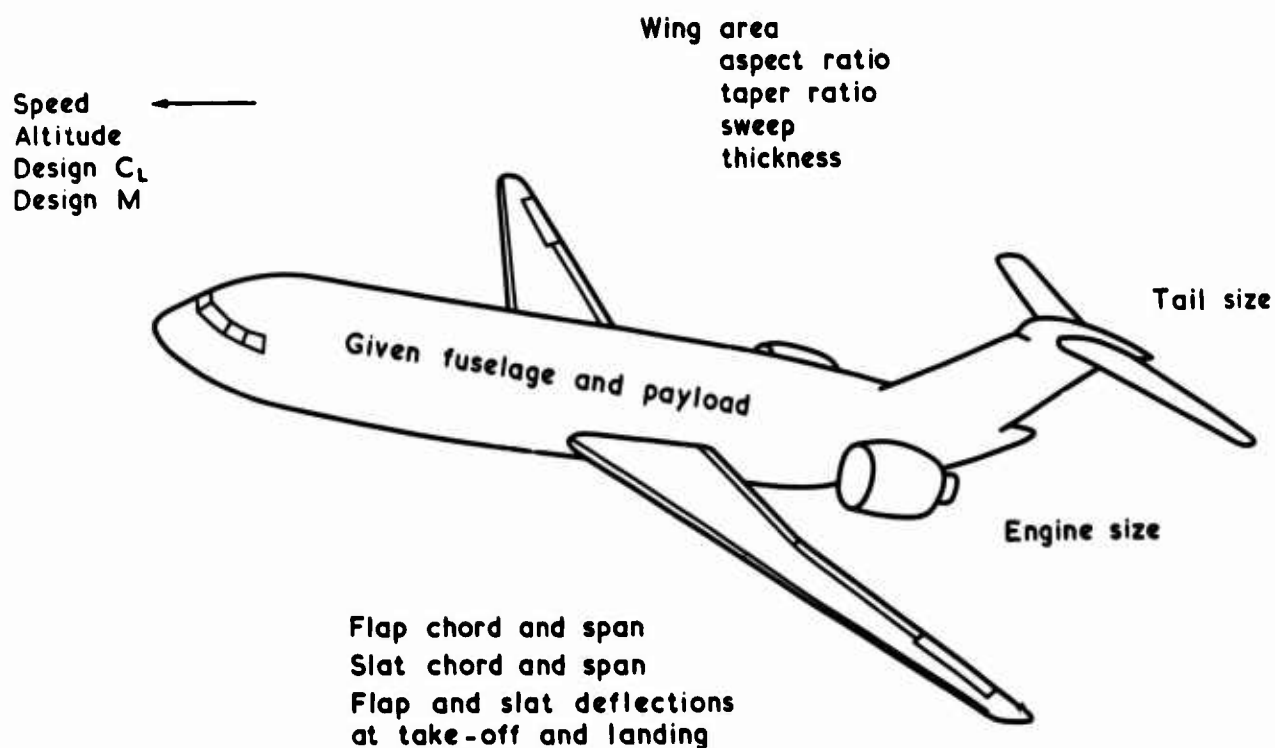


Fig.4 Variables to be optimised.

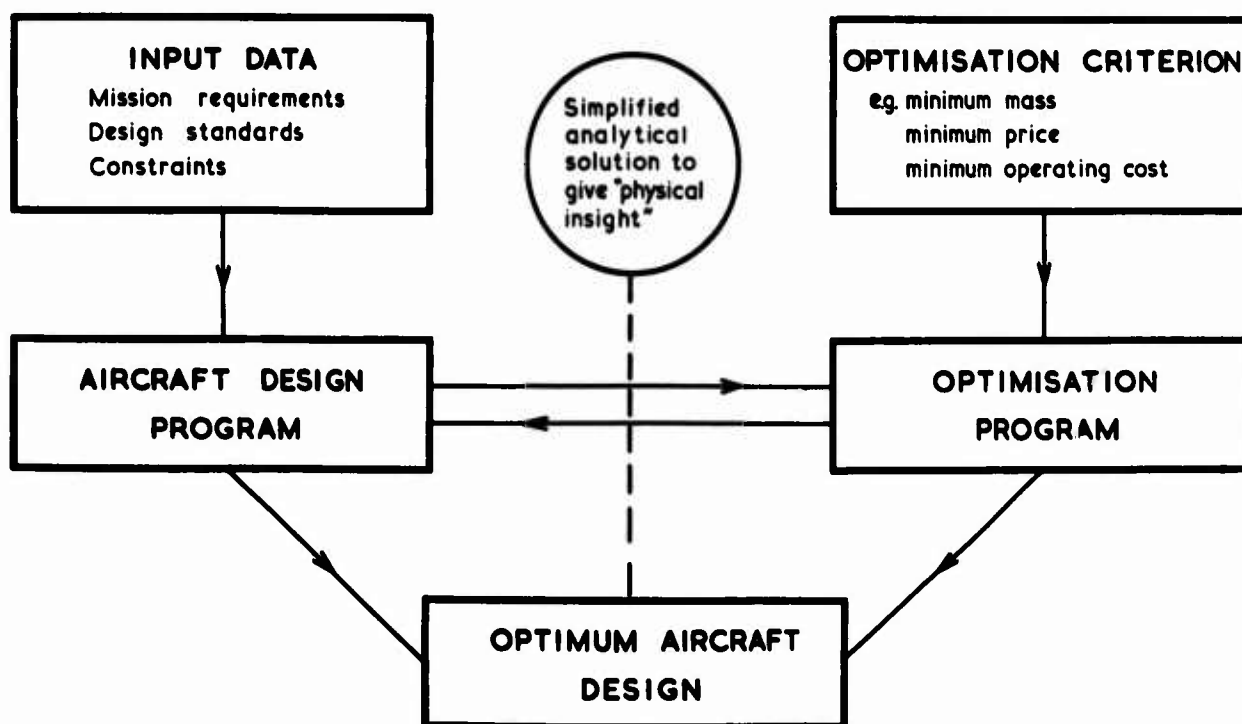


Fig.5 Organisation of optimum aircraft design study.